ISSN 0424-7116 | DOI 10.3285/eg.60.1
Edited by the German Quaternary Association
Editor-in-Chief: Holger Freund

E&G

Eiszeitalter und Gegenwart
Quaternary Science Journal

Vol. 60
No 1
2011

LOESS IN EUROPE

GUEST EDITOR Manfred Frechen

GEOZON

E&G

Eiszeitalter und Gegenwart
Quaternary Science Journal

Volume 60 / Number 1 / 2011 / DOI: 10.3285/eg.60.1 / ISSN 0424-7116 / www.quaternary-science.net / Founded in 1951

AIMS & SCOPE
The *Quaternary Science Journal* publishes original articles of quaternary geology, geography, palaeontology, soil science, archaeology, climatology etc.; special issues with main topics and articles of lectures of several scientific events.
MANUSCRIPT SUBMISSION
Please upload your manuscript at the online submission system at our journal site www.quaternary-science.net. Please note the instructions for authors before.
FREQUENCY
Four numbers at volume

SUBSCRIPTION
Free for DEUQUA-Members! Prices for standing order: single number 27,– Euro; double number 54,– Euro; plus shipping costs. We offer discounts for libraries and bookstores. Please subscribe to the journal at the publisher *Geozon Science Media*.
JOURNAL EXCHANGE
If you are interested in exchange your journal with the *Quaternary Science Journal*, please contact: Universitätsbibliothek Halle
Tauschstelle, Frau Winther
August-Bebel-Straße 13
D-06108 Halle (Saale), Germany
Tel. +49 (0)345-55 22 183
E-Mail: tausch (at) bibliothek.uni-halle.de
REORDER
Reorders are possible at the publishing house. See full list and special prices of available numbers on page 207.
PUBLISHING HOUSE
Geozon Science Media UG (haftungsbeschränkt)
Postfach 3245
D-17462 Greifswald
Germany
Tel. +49 (0)3834-80 40 80
E-Mail: info (at) geozon.net
www.geozon.net

PRINT
Printed in Germany on 100% recycled paper climate neutral produced
COVER PHOTO
Juliane Herrmann (LIAG)
Aufschluß Süttö in Nordungarn

E&G Quaternary Science Journal
Volume 60 / Number 1 / 2011 / 3–5 / DOI 10.3285/eg.60.1.00
www.quaternary-science.net

GEOZON SCIENCE MEDIA
ISSN 0424-7116

Loess in Europe

Guest Editorial

Manfred Frechen

Address of author: **M. Frechen**, Leibniz Institute for Applied Geophysics (LIAG), Geochronology & Isotope Hydrology, Stilleweg 2, 30655 Hannover, Germany. E-Mail: Manfred.Frechen@liag-hannover.de

The papers of this Special Issue give remarkable new results and conclusions on loess from Europe underlining the excellence of loess archives for past climate and environment reconstructions from a local and regional perspective and their relationship to a more global interpretation (Frechen 2011 a, b). Loess is a clastic predominantly silt-sized sediment, which is formed by the accumulation of wind-blown dust. According to Pye (1995) four fundamental requirements are necessary for it formation: a dust source, adequate wind energy to transport the dust, a suitable accumulation area, and a sufficient amount of time. During the Quaternary, loess and loess-like sediments were formed in periglacial environments on mid-continental shield areas in Europe and Siberia, on the margins of high mountain ranges like in Tajikistan and on semi-arid margins of some lowland deserts like in China.

The term "Löß" was first described in Central Europe by Karl Cäsar von Leonhard (1823/24) who reported yellowish brown, silty deposits along the Rhine valley near Heidelberg. Charles Lyell (1834) brought this term into widespread usage by observing similarities between loess and loess derivatives along the loess bluffs in the Rhine and Mississippi. At that time it was thought that the yellowish brown silt-rich sediment was of fluvial origin being deposited by the large rivers. It took until the end of the 19th century until the aeolian origin of loess was recognized (Virlet D'Aoust 1857), especially the convincing observations of loess in China by Ferdinand von Richthofen's (1878). A tremendous number of papers have been published since then, focusing on the formation of loess and on loess/palaeosol sequences as archives of climate and environment change (e.g. Pye 1995; Smalley 1995; Pécsi & Richter 1996).

Much effort was put into the setting up of regional and local loess stratigraphies and their correlation (Kukla 1970, 1975, 1977). But even the chronostratigraphical position of the last interglacial soil correlating to marine isotope substage 5e has been a matter of debate, owing to the lack of robust and reliable numerical dating, as summarized for example in Zöller et al. (1994) and Frechen, Horváth & Gábris (1997) for the Austrian and Hungarian loess stratigraphy, respectively.

Since the 1980s, thermoluminescence (TL), optically stimulated luminescence (OSL) and infrared stimulated luminescence (IRSL) dating are available providing the possibility for dating the time of loess (dust) deposition, i.e. the time elapsed since the last exposure of the mineral grains to daylight. During the past decade luminescence dating has significantly improved by new methodological improvements, especially the development of single aliquot regenerative (SAR) protocols (Murray & Wintle 2000) resulting in reliable ages (or age estimates) with an accuracy of up to 5 and 10% for the last glacial record. More recently luminescence dating has also become a robust dating technique for penultimate and antepenultimate glacial loess (e.g. Thiel et al. this issue; Schmidt et al. this issue) allowing for a reliable correlation of loess/palaeosol sequences for at least the last two interglacial/glacial cycles throughout Europe and the Northern Hemisphere (Frechen 2011a). Furthermore, the numerical dating provides the basis for quantitative loess research applying more sophisticated methods to determine and understand high-resolution proxy data, such as the palaeodust content of the atmosphere, variations of the atmospheric circulation patterns and wind systems, palaeoprecipitation and palaeotemperature.

The papers of this Special Issue on Loess in Europe give the basis for substantial further challenging developments in loess research and are summarised geographically from north to south.

Little is known about the timing of loess accumulation and soil formation as well as the settlement history in the "Altmoränengebiet" in northern Germany. Urban, Kunz & Gehrt (this issue) provide some evidence for the human impact on soil development since the late Neolithic by means of sedimentology, pedology and palynology as well as OSL and radiocarbon dating.

Wagner (this issue) carried out a spatial compilation and visualisation of loess parameters for loess and loess-like sediments in the Weser-Aller catchment, including parts of southern Lower Saxony and northern Hesse in Northwest Germany. In this study, very detailed maps of loess property patterns including loess thickness, granulometry and stratigraphy were collected from publications and historically maps published between 1876 and 2007 resulting in more than 600 loess locations providing the base information for the area under study.

The loess/palaeosol sequences from Saxony were re-investigated by Meszner, Fuchs & Faust (this issue), who

present a new composite profile including new stratigraphic marker horizons and palaeosols. They identified three palaeosols for the so far poorly differentiated Weichselian Pleniglacial record in Saxony.

In the Lower Rhine Embayment, detailed loess/palaeosol sequences have been described from the km-wide exposures of the brown coal open-cast mines and from many brickyards, e.g. Grafenberg, Rheindahlen and Erkelenz. Most of the studied sections give evidence for rich Palaeolithic (and younger periods) artefacts and settlement structures. Pawlik & Thissen (this issue) present results from a Middle Palaeolithic archaeological layer in the open cast brown coal mine Inden, which they correlate to the Eemian interglacial. The studied artefacts give evidence for birch pitch fixed tools, either as hafted impliments fixed with birch pitch onto shafts or being used for successive hafting-and-retroling activities. Pawlik & Thissen (this issue) point out that birch pitch residues evidence human use of adhesive and multicomponent tool making already in the Middle Palaeolithic.

At the Schwalbenberg section, a very detailed Weichselian Middle Pleniglacial loess record is exposed (Frechen & Schirmer this issue). Eight weak interstadial palaeosols including Ah and Bcv (calcic cambisol) horizons are intercalated in loess and reworked loess. The chronostratigraphical units show little or no age increase with depth indicating fast accumulation of sediment and fast formation of the soils; similar observations were made for the Early Weichselian record at the Tönchesberg section (Boenigk & Frechen 2001).

Maar lakes and dry maars of the West Eifel Volcanic Field are excellent sediment traps and provide sediment records with the possibility to archive event-laminated sediments. Dietrich & Sirocko (this issue) describe the potential of micro X-ray fluorescence (μXRF) scanning to study bulk sediment chemical data for major and trace elements in maar lake sediments to determine the elemental stratification within sediment cores. The cores under study from the Dehner dry maar and the Schalkenmehren maar show both fully glacial as well as warm and wet climate conditions and give evidence for the major dust deposition events. Dietrich & Sirocko (this issue) show evidence that a combination of the Ca content and the grayscale values correlates best with the signal of aeolian sediment input.

Reliable dating of maar sediments is a real challenge. Schmidt et al. (this issue) studied sediments from the Jungfernweiher located in the West Eifel Volcanic Field using luminescence dating. The IRSL dating study indicates that the sediments from 16 m below surface have luminescence age of 250 ka and increase up to 400 ka for the oldest sampled sediments about 94 m below modern surface. However, one of the co-authors (F. Sirocko, see appendix of Schmidt et al. this issue a) has a different interpretation based on radiocarbon dating and further relative dating methods, such as sediment magnetisation, tuning of greyscale variations with Greenland ice core and intercalated tephra horizons indicating a last glacial record. The different opinions show that chronological approaches are very challenging.

At the gravel quarry Gaul located near Weilbach in the southern foreland of the Taunus Mountains, a Middle to Upper Pleistocene loess/palaleosol sequence is exposed correlating with the last three glacial cycles. The oldest loess gave post-IR IRSL at 225°C age estimates of at least 350 ka (MIS 10) ago (Schmidt, Semmel & Frechen this issue). A humic-rich horizon ("Weilbacher Humuszone") correlates to the late phase of the penultimate interglacial (MIS 7). The uppermost loess correlates to the Upper Würmian.

Thiel et al. (this issue) investigated three important Pleistocene key loess sections in Lower Austria, these are Joching, Paudorf and Göttweig. The post-IR IRSL age estimates allow for a correlation of the pedocomplex "Paudorfer Bodenbildung" with the last interglacial (MIS 5), which is in agreement with previous TL age estimates of Zöller et al. (1994). However, the pedocomplex "Göttweiger Verlehmungszone" is signifiacantly older (≥350 ka) than the last interglacial soil. Thiel et al. (this issue) found out that discontinuities in loess/palaeosol records observed in Lower Austria are significant making a simple counting from the top approach unreliable. Thus, the Lower Austrian loess stratigraphy including the timing of the intercalated palaeosols remains under discussion and requires further luminescence based age determination.

Loess deposits from the Hagenbach Klamm located in the northern Vienna Forest were dated using luminescence dating by Frank et al. (this issue). The mollusc assemblages indicate very humid and cool climatic conditions for the Upper Pleniglacial (Upper Würmian). Frank et al. (this issue) observed good agreement between malcalogical results and those of numerical dating including ^{14}C and IRSL ages. The dating results make a loess accumulation prior to the Last Glacial Maximum most likely.

Zech et al. (this issue) give an overview on the most recent proxy developments concerning biomarkers and compound-specific stable isotopes. The aim of these novel methodological approaches is to determine more quantitative palaeoclimate proxies for reconstruction of vegetation history, palaeotemperature and palaeoclimate/aridity.

Wacha et al. (this issue) investigated a very detailed loess/palaeosol sequence on Susak. Radiocarbon ages and luminescence age estimates indicate an Upper Pleistocene record including a very detailed and thick Middle Pleniglacial record (MIS 3) including numerous intercalated palaleosols and at least three tephra layers, most likely from the Italian Volcanic provinces. The island of Susak is unique in the North Adriatic Sea because the geomorphology of the island has all characteristics of a loess plateau dissected by numerous gorges, steep bluffs and gullies (Wacha et al. this issue).

The Late Pleistocene/Holocene morphological and geological history of the Paraguayan Chaco and the Argentine Pampa Plain (Chaco-Pampa Plain) was studied by Kruck et al. (this issue). Satellite images were used to synthesise previous and new multidisciplinary results of this vast-extended area. Kruck et al. (this issue) localised source regions of loess, loess-like sediments and sandy deposits in the southwestern Pampa and the neighbouring Andean slopes and the Altiplano, thus indicating a sediment transport towards east and later northeast.

References

Boenigk, W. & Frechen, M. (2001): The loess record in sections at Koblenz-Metternich and Tönchesberg in the Middle Rhine Area. – Quaternary International, 76/77: 201–209.

Dietrich, S. & Sirocko, F. (this issue): The potential of dust detection by means of !XRF scanning in Eifel maar lake sediments. – Quaternary Science Journal (EuG), 60 (1).

Frank, C., Terhorst, B., Damm, B., Thiel, C., Frechen, M. & Peticzka, R. (this issue): Pleistocene loess deposits and mollusc assemblages in the Eastern Pre-Alps. – Quaternary Science Journal (EuG), 60 (1).

Frechen, M. (2011a): Loess in Eurasia. – Quaternary International, xyxy, 1–3.

Frechen, M. (2011b): Timing and Vegetation History of Interglacials in northern Eurasia. – Quaternary International, 141: 1–2.

Frechen, M., Horváth, E. & Gábris, G. (1997): Geochronology of Middle and Upper Pleistocene loess sections in Hungary. – Quaternary Research, 48: 291–312.

Frechen, M. & Schirmer, W. (this issue): Luminescence Chronology of the Schwalbenberg II Loess in the Middle Rhine Valley. – Quaternary Science Journal (EuG), 60 (1).

Kruck, W., Helms, F., Geyh, M.A., Suriano, J.M., Marengo, H.G. & Pereyra, F. (this issue): Late Pleistocene-Holocene History of Chaco-Pampa Sediments in Argentina and Paraguay. – Quaternary Science Journal (EuG), 60 (1).

Kukla, G. (1970): Correlation between loesses and deep-sea sediments. – Geologiske Foreningen Foerhandlingar, 92: 148–180; Stockholm.

Kukla, G.J. (1975): Loess stratigraphy of Central Europe. – In K.W. Butzer and G.L. Isaac, Eds., After the Australopithecus, pp. 99–188; Mouton, The Hague.

Kukla, G.J. (1977): Pleistocene Land-Sea Correlations I. Europe. Earth Science Reviews, 13: 307–374.

Leonhard, K.C. von (1823/24): Charakteristik der Felsarten. – 3 Vols., J. Engelmann Verlag Heidelberg, pp. 772.

Lyell, C. (1834): Observations on the loamy deposits called "loess" of the basin of the Rhine. – Edinburgh New Philosophical Journal, 17: 110–113, 118–120.

Meszner, S., Fuchs, M. & Faust, D. (this issue): Loess-Palaeosol-Sequences from the loess area of Saxony (Germany). – Quaternary Science Journal (EuG), 60 (1).

Murray, A. S. & Wintle, A. G. (2000): Luminescence dating of quartz using an improved single aliquot regenerative-dose protocol. Radiation Measurements 32: 57–73.

Novothny, A., Horvath, E. & Frechen, M. (2002): The loess profile at Albertirsa, Hungary – improvements in loess stratigraphy by luminescence dating. – Quaternary International, 95–96: 155–163.

Pawlik, A.F. & Thissen, J. (this issue): The 'Palaeolithic Prospection in the Inde Valley' Project. – Quaternary Science Journal (EuG), 60 (1).

Pécsi, M. (1990): Loess is not just the accumulation of dust. – Quaternary International, 7/8: 1–21.

Pécsi, M. & Richter, G. (1996): Löss: Herkunft – Gliederung – Landschaften. – Zeitschrift für Geomorphologie, Neu Folge Supplementband 98, Berlin.

Pye, K. (1995): The nature, origin and accumulation of loess.- Quaternary Science Reviews, 14: 653–667.

Richthofen, F. von (1878): Bemerkungen zur Lößbildung. – Verh Geol Reichsanst, Berlin, pp 1–13.

Schmidt, E.D., Semmel, A. & Frechen, M. (this issue): Luminescence dating of the loess/palaeosol sequence at the gravel quarry Gaul/Weilbach, Southern Hesse (Germany). – Quaternary Science Journal (EuG), 60 (1).

Schmidt, E.D., Murray, A.S., Sirocko, F., Tsukamoto, S. & Frechen, M. (this issue): IRSL Signals from Maar Lake Sediments Stimulated at Various Temperatures. – Quaternary Science Journal (EuG), 60 (1).

Smalley, I. (1995): Making the material: the formation of silt-sized promary mineral paricles for loess deposits. – Quaternary Science Reviews, 14: 645–651.

Thiel, C., Buylaert, J.P., Murray, A.S., Terhorst, B., Tsukamoto, S., Frechen, M. & Sprafke, T. (this issue): Investigating the chronostratigraphy of prominent palaeosols in Lower Austria using post-IR IRSL dating. – Quaternary Science Journal (EuG), 60 (1).

Urban, B., Kunz, A., Gehrt, E. (this issue): Genesis and dating of Late Pleistocene-Holocene soil sediment sequences from the Lüneburg Heath, Northern Germany. – Quaternary Science Journal (EuG), 60 (1).

Virlet D'Aoust, P.T. (1857): Observations sur un terrain d`origine météorique ou de transport aerien qui existe au Mexique et sur le phénomène des trombes de poussière auquel il doit principalement son origine. – Geol. Soc. France, Full., 2d, Ser. 2, 129–139.

Wacha, L., Mikulcic Pavlakovic, S., Frechen, M., Crnjakovic, M. (this issue): The Loess Chronology of the Island of Susak, Croatia. – Quaternary Science Journal (EuG), 60 (1).

Wagner, B. (this issue): Spatial analysis of loess and loess-like sediments in the Weser-Aller catchment (Lower Saxony and Northern Hesse, NW Germany). – Quaternary Science Journal (EuG), 60 (1).

Zech, M., Zech, R., Buggle, B., Zöller, L. (this issue): Novel methodological approaches in loess research – interrogating biomarkers and compound-specific stable isotopes. – Quaternary Science Journal (EuG), 60 (1).

Zöller, L., Oches, E.A.. & McCoy, W.D. (1994): Towards a revised chronostratigraphy of loess in Austria with respect to key sections in the Czech Republic and in Hungary. – Quaternary Geochronology (Quaternary Science Reviews), 13: 465–472.

E&G Quaternary Science Journal
Volume 60 / Number 1 / 2011 / 6–26 / DOI 10.3285/eg.60.1.01
www.quaternary-science.net

GEOZON SCIENCE MEDIA
ISSN 0424-7116

Genesis and dating of Late Pleistocene-Holocene soil sediment sequences from the Lüneburg Heath, Northern Germany

Brigitte Urban, Alexander Kunz, Ernst Gehrt

Abstract: The stratigraphy and settlement history of the loess-areas in Central Europe is well known for the glacial periods and the Holocene. In contrast there are no recent investigations in the sandy loess areas of the so called "Altmoränengebiet" in northern Germany on the age of the sediments, timing of soil formation and settlement history. In this study two soil profiles in the Lüneburg Heath are investigated. The soils have been studied by means of sedimentology, pedology and palynology. Dating was done by optically stimulated luminescence (OSL) and radiocarbon. The results give the first evidence from the Altmoränengebiet for human impact on soil development as early as the late Neolithic. In the soil profiles, periods of erosion and accumulation with enrichment in organic rich material are indicated.

(Genese und Datierung spätpleistozän-holozäner Paläobodensequenzen in der Lüneburger Heide, Norddeutschland)

Kurzfassung: Während in den Lössgebieten Mitteleuropas die Lössstratigraphie und die menschliche Besiedlung der Lössgebiete sowohl eiszeitlich wie auch im Holozän gut bekannt sind, liegen zu den Sandlössgebieten der Altmoränengebiete keine neueren Erkenntnisse zur zeitlichen Stellung der Sedimente oder zur Siedlungsgeschichte und zum Einfluss auf die Bodenentwicklung vor. In der Arbeit werden aus einem Sandlössgebiet in der Lüneburger Heide zwei Bodenprofile vorgestellt deren Gliederung einen Einblick in die Genese der vergangenen 10 000 Jahre erlaubt. Die Profile wurden sedimentologisch, pedologisch und palynologisch untersucht und charakterisiert. Die Datierung der Profile erfolgte mittels optisch stimulierter Lumineszenz (OSL) und Radiokarbondatierung. Die Ergebnisse legen einen menschlichen Einfluss auf die Böden ab dem späten Neolithikum nahe. Darunter sind Erosions- und Akkumulationsprozesse und insbesondere eine Anreicherung mit organischem Material zu fassen. Erstmals können mit dieser Studie Datierungen von Sedimenten und Böden des Altmoränengebietes präsentiert werden.

Keywords: *loess, palaeosols, luminescence dating, pollen analysis, palaeoenvironment, human impact*

Addresses of authors: **B. Urban**, Institute of Ecology, Leuphana University Lüneburg, Herbert-Meyer-Str. 7, 29556 Suderburg, Germany. E-Mail: b.urban@uni.leuphana.de; **A. Kunz**, Section S3: Geochronology and Isotope Hydrology, Leibniz Institute for Applied Geophysics, Hannover, Germany (present address: Department of Geosciences, National Taiwan University, Taipeh, Taiwan (R.O.C.). E-Mail: a.kunz96@yahoo.com; **E. Gehrt**, State Authority for Mining, Energy and Geology of Lower Saxony (LBEG), Stilleweg 2, 30655 Hannover, Germany. E-Mail: e.gerth@lbeg.niedersachsen.de

1 Introduction

The present morphology of the Lüneburg Heath was mainly formed by the Saalian glaciation (Oxygen Isotope Stage 6–8), when the area was covered at least three times by ice. Weichselian glaciers (Oxygen Isotope Stage 2–5d) did not reach the area which was strongly influenced by periglacial processes, like erosion and solifluction. The landscape of the Lüneburg Heath is hence characterised by ground moraines, terminal moraines, outwash plains, glaciofluvial deposits and, in some limited areas, by loess deposits (Fig. 1) (Hagedorn 1964, Caspers et al. 1995).

From soil mapping it is known that 70 to 90 cm thick humic horizons in the soils of the sandy loess areas are common. These horizons occur in depressions but also on topographic highs. The formation of typical Plaggic Anthrosols (Blume & Leineweber 2004) is not known for the Lüneburg Heath. There are still questions about the age of these humic horizons and about their formation processes.

Our investigations concentrate on an area south of Lüneburg, near the village of Seedorf (Figs. 1 and 2) that is well-known for its highly fertile soils, which have developed on sandy loess ("Sandlöss") (Gehrt 2000). The sandy loess was deposited during the Upper Weichselian (Geological Map GK 25 2929) and is generally overlying Saalian and Lower and Middle Weichselian sediments. The prevailing soil types developed on sandy loess in the Lüneburg Heath were described by Roeschmann in Kuntze et al. (1995) and by Gehrt (2000). They range from Luvisols, stagnic Luvisols, Cambisols and Podzols to Fluvisols and Gleysols in the small brook valleys (Soil Map BK50 L2928, Bad Bevensen) (Fig. 3). Figure 4 shows the distribution of the characteristic deep humic horizons in the study area, which are classified as colluvium and generally overly the diagnostic B horizons. There is archaeological evidence of an Iron Age cultural stage of the Jastorf culture (Seedorf-Stufe, Schwantes 1952, Hässler 1991) though as well as of Neolithic settlements (Sprockhoff 1975, Heege & Maier 1991, Geebers 1995, Richter 2002) in the area and of a number of archaeobotanical investigations from prehistoric sites. The few data available from peat bogs though provide background information on landscape development (Becker 1995, Kirleis 2003, Becker & Urban 2006). This study of a Gleysol/Colluvisol developed in a brook valley and of a Colluvisol/stagnic Luvisol sequence developed on sandy loess at higher topographic elevation near the vil-

Fig. 1: Location of Seedorf, county of Uelzen, Lower Saxony and distribution of loess and sandy loess in northern Germany. Grey shaded area shows the location of the Luenburg Heath. Hatched area marks the northern most distribution of loess. Sandy loess areas are marked by cross-hatches. 1 = Lower Rhine Area; 2 = Recklinghausen; 3, 4 = Soester Börde; 5 = Münster; 6 = Bersenbrück; 7 = Damme; 8 = Wehden; 9 = Wunstorf, Rehurg; 10 = Goldenstedt; 11 = Syke; 12 = Apensen; 13 = Harburg; 14 = Garlsdorf; 15 = Uelzen, Bevensen; 16 = Clenze; 17 = Bergen, Jettebruch; 18 = Wittingen; 19 = Klötze; 20 = Peine, Braunschweig; 21 = Helmstedt; 22 = Haldensleben; 23 = Magdeburg.

Abb. 1: Lage von Seedorf (Landkreis Uelzen) in Niedersachsen und Verbreitung von Löss und Sandlöss in Nord-Deutschland. Die graue Fläche zeigt die Lage der Lüneburger Heide. Die schraffierte Fläche markiert die nördlichste Verbreitung von Löss in Deutschland. Sandlössgebiete sind durch Kreuzschraffur markiert. 1 = Niederrhein; 2 = Recklinghausen; 3, 4 = Soester Börde; 5 = Münster; 6 = Bersenbrück; 7 = Damme; 8 = Wehden; 9 = Wunstorf, Rehurg; 10 = Goldenstedt; 11 = Syke; 12 = Apensen; 13 = Harburg; 14 = Garlsdorf; 15 = Uelzen, Bevensen; 16 = Clenze; 17 = Bergen, Jettebruch; 18 = Wittingen; 19 = Klötze; 20 = Peine, Braunschweig; 21 = Helmstedt; 22 = Haldensleben; 23 = Magdeburg

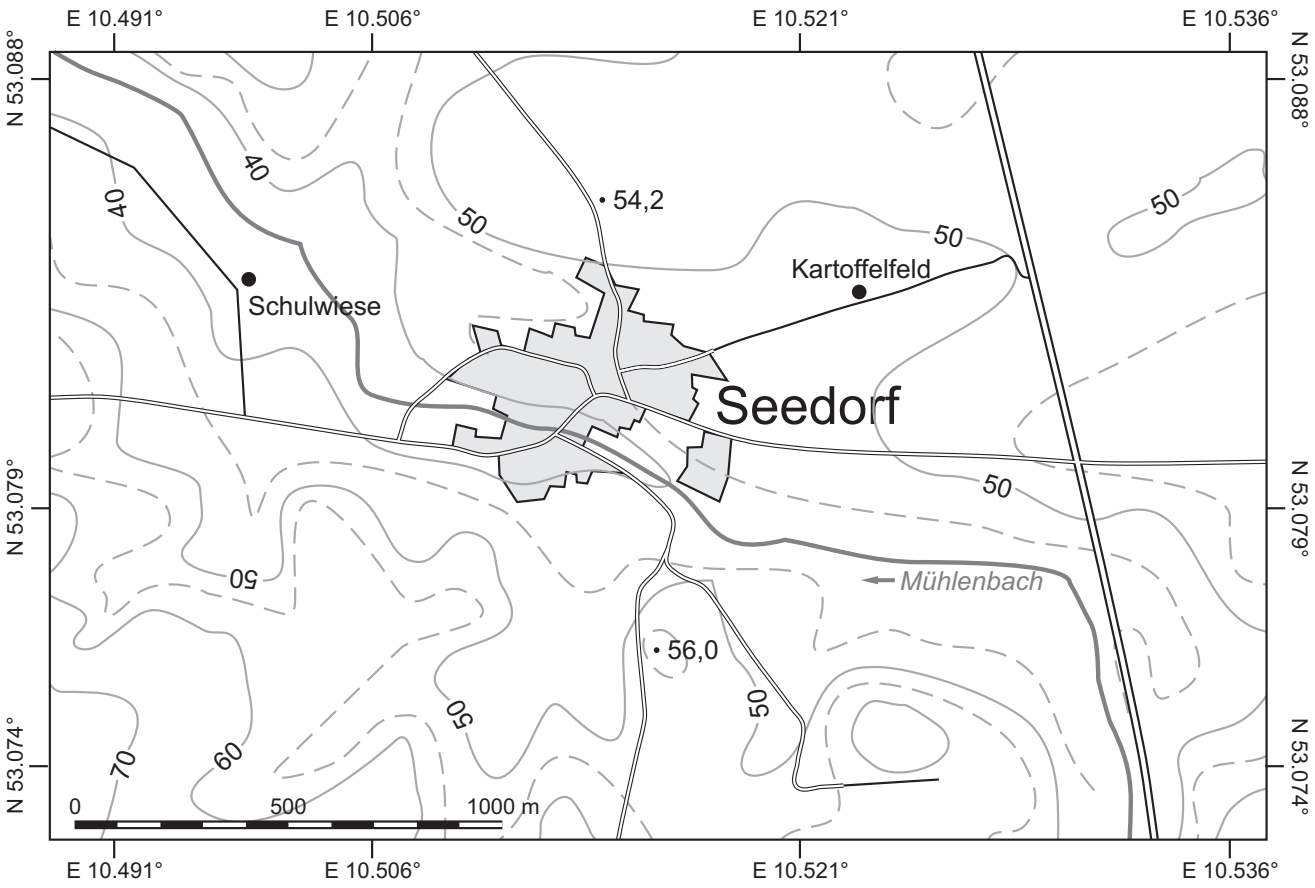

Fig. 2: Location of soil profiles Schulwiese and Kartoffelfeld near the village of Seedorf, county of Uelzen.

Abb. 2: Lage der untersuchten Profile Schulwiese und Kartoffelfeld in Seedorf (Landkreis Uelzen).

lage of Seedorf (Figs. 2 and 4) aims at dating and reconstructing (palaeo) environmental conditions of soil genesis and human impact on landscape evolution in the northernmost patchy sand loess region at the margin of the Western European contiguous loess belt.

2 Materials and methods

2.1 Description of the soils of the studied sites

Two sites have been selected for in-depth studies of their genetic development, which differ strongly in topography and hydrological conditions as well as in the type of land use. The prevailing soil types in the floodplains are Gleysols developed on alluvial deposits and Histosols that are mainly used as pasture, and stagnic Luvisols that are widespread at higher elevations and support arable agriculture (Fig. 3). The upper layers/horizons of the soils in both topographic positions are characterized by colluvial cover deposits.

The profiles of the two sites, *Schulwiese* and *Kartoffelfeld,* have been described in the field using the German soil mapping instructions (KA5 2005) (Tabs. 1 and 2), soil colour was determined by Munsell soil colour charts.

The investigated section *Schulwiese* (Figs. 2 and 4) (53.08°N, 10.52°E, 38 m a.s.l.) is located on a slip-off slope in a floodplain of a small watercourse close to the village of Seedorf in the western part of the Lüneburg Heath. The sequence consists of 1.75 m thick silty, clayey soil-sediment with fluvic and gleyic features. The uppermost 46 cm are made up of a colluvial cover layer. The entire sequence has a silty texture, which is moderately clayey to medium clayey from the middle part of the profile downwards (Tab. 1, Fig. 5). The profile is carbonate-free and the organic content ranges between weak to strong humic. The profile *Schulwiese* has been subdivided vertically using the international nomenclature (IUSS 2006) (Fig. 5). By applying the German soil classification system (KA5 2005), the vertical sequence was subdivided into Ap (0–14 cm) /M-Go (14–46 cm) /aGo (46–72 cm) /fAa+Gr (72–104 cm) /aGr (104–114 cm) /fAa+aGr (114–130 cm) /aGr (130–156 cm) /aGr (156–175 cm) (Kucz 2006). The Ap and the Bg1 horizon are developed in a loess colluvium (M-Go).

The profile *Kartoffelfeld* (53.08°N, 10.52°E) is located northeast of the village of Seedorf at 47.80 m a.s.l on an elevated plateau (Figs. 2 and 4). The basal part of the 1.70 m thick profile is made up by Saalian glacial till underlain by glaciofluvial sands; the soil type developed on the silty sands is a stagnic Luvisol. From 133 cm upwards the stagnic Luvisol is overlain by a (sandy) loess colluvium showing weak cambic properties (Tab. 2). The organic content assessed ranges from weak to very weak humic. The profile *Kartoffelfeld* is vertically subdivided (IUSS 2006) into the horizons Ap-Bw1-Bw2-Bw3-2Btb/Bgb1-2Bwb1/Bgb1-3Bwb2/Bgb2/C (Fig. 6). By applying the German soil classification system (KA5 2005) the sequence of horizons can be described as Ap (0–30 cm) /M (30–54 cm) /M (54–82 cm) /M (82–110 cm) / Swd-Bt (110–133 cm) /Swd-Bv (133–138 cm) /Swd-Bv (138–

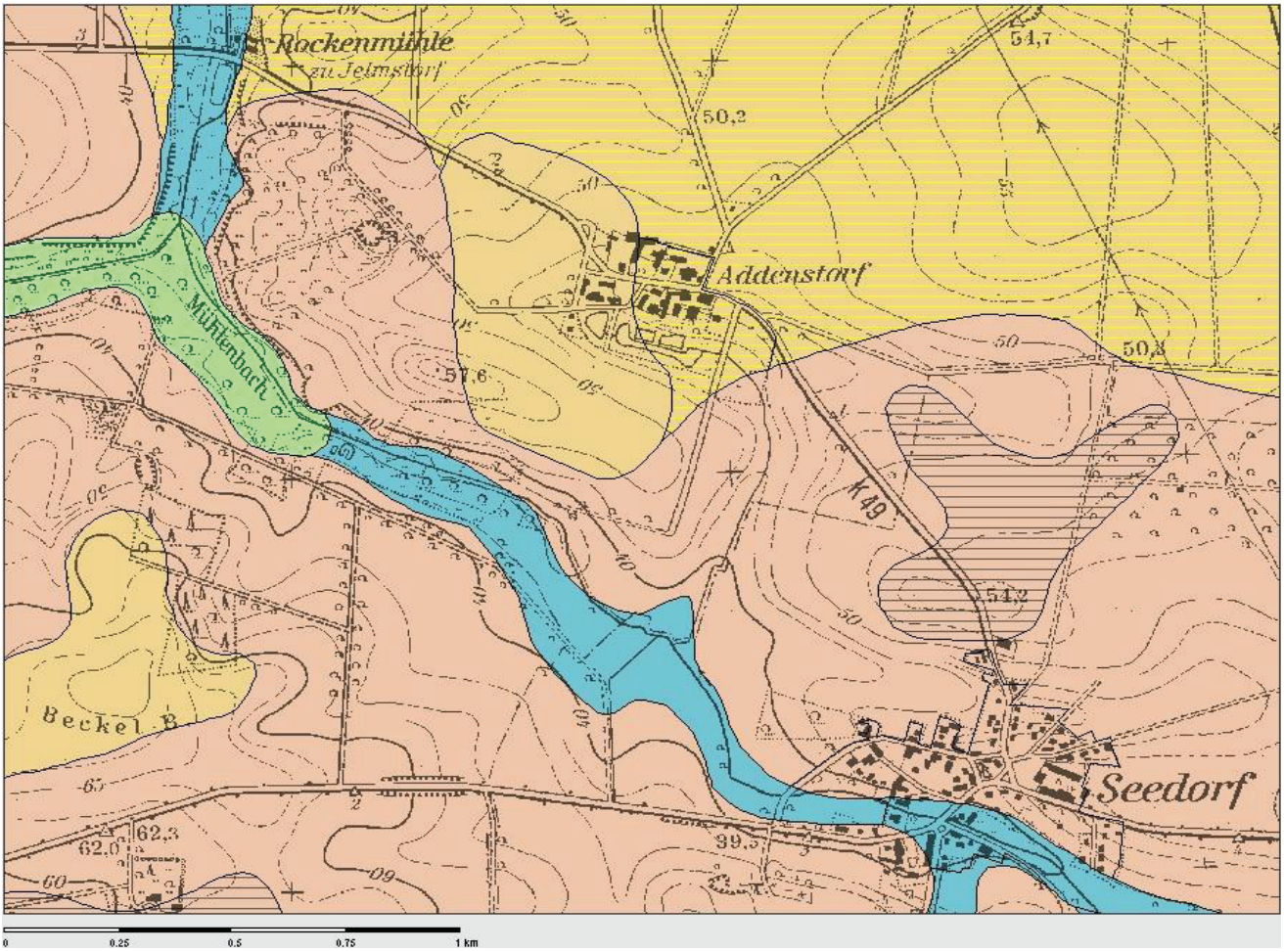

Fig. 3: Soil map of Uelzen (BK50 L2928, Bad Bevensen).
Abb. 3: Bodenkarte von Uelzen (BK50 L2928, Bad Bevensen).

162 cm) /Cv (162–170 cm) (Kucz 2006). The Ap and Bw1, Bw2, Bw3 horizons developed within the loess colluvium (M 30–110 cm).

2.2 Sedimentological and pedological analysis

The texture of the horizons was determined by the hydrometer method (van Reeuwijk 1992). For physico-chemical analysis, the same samples were taken and analyzed for their pH in a 1:2.5 0.01 M $CaCl_2$-suspension, for organic carbon (C_{org}) according to the Walkley-Black procedure (Page et al. 1982) and organic nitrogen using the *Kjeldahl* procedure. Major (Al, Fe, and Mn) and trace (S, Cr, Cu, Pb, Zn, Co, Ni, Cd, Sr, Hg, V) elements were determined using an X-ray fluorescence (XRF) spectrometer (SpectroXepos-Benchtop-Roentgenfluoreszenz-Spektrometer) equipped with a Rh tube (Chen et al. 2001). Quality control of the analytical procedure was established using three internationally recognized standard reference materials (SRMs) viz., ISE, BCSS-1, and MESS-1. Based on these standards, the accuracy and precision of the analysis were within 1% for major elements and within 5% for trace elements. Oxalate Fe_o and dithionite Fe_d extractable iron (Holmgren 1967) were measured by inductively coupled plasma spectrometry (ICP). The soil organic matter (SOM) has been calculated as C% * 1.72. All analyses were carried out at Leuphana University Lüneburg, Germany.

2.3 Age determination

The depositional ages of the sediments were determined mainly by optically stimulated luminescence (OSL) with one sample for radiocarbon dating taken from the profile *Schulwiese*. The sampling positions are shown in Tabs. 7 and 8.

2.3.1 Optically stimulated luminescence (OSL) dating

OSL is one of the dosimetric dating methods and is an excellent tool for determining the depositional time of sediments. The method is based on the accumulation of electrons in defects of the crystal lattice induced by the natural radioactivity in the surrounding sediment. Due to the physical mechanism of the OSL method, reliable and precise results

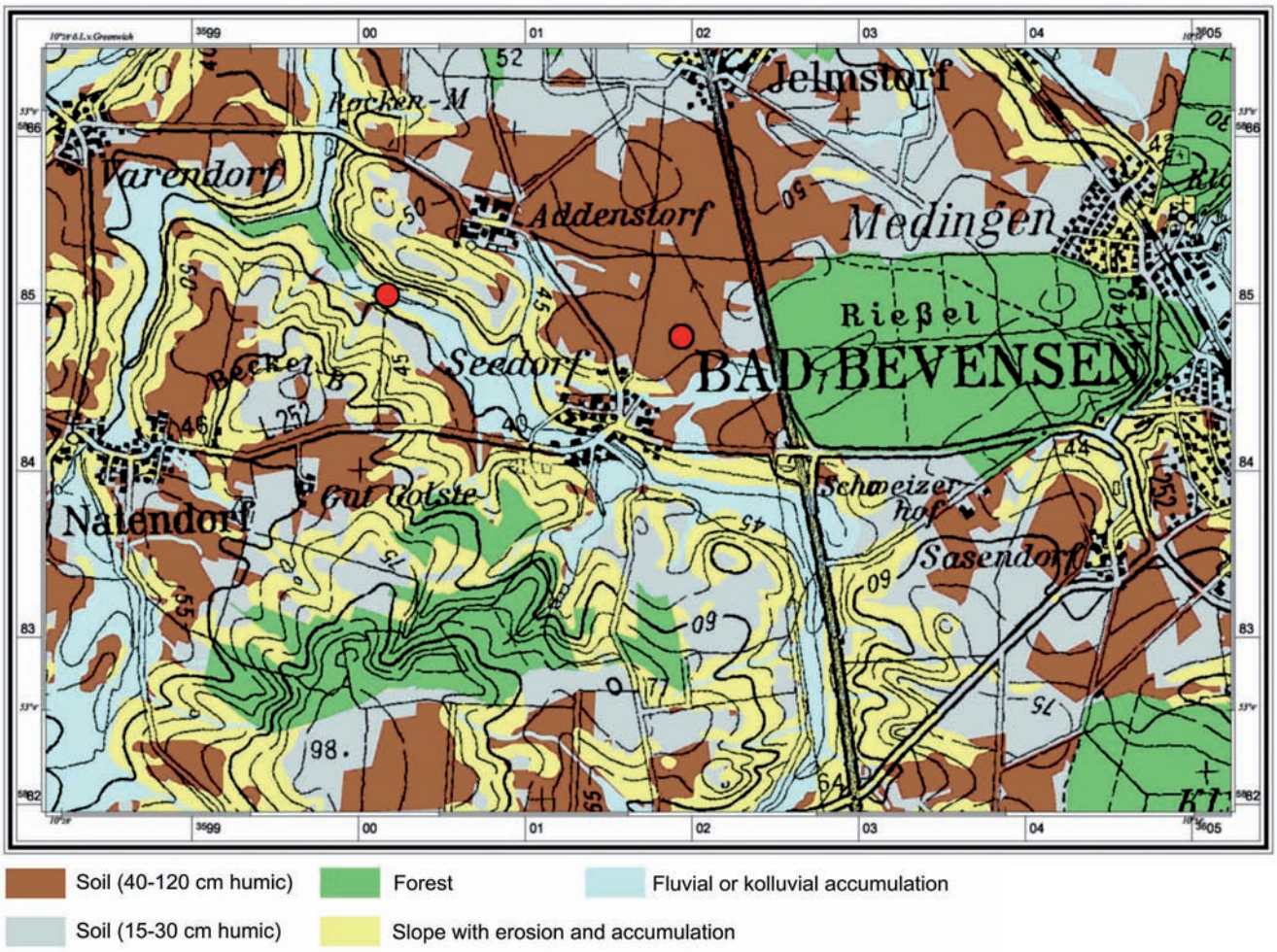

Fig. 4: Distribution of deep humic horizons, fluvial and colluvial layers and forest cover in the area of Seedorf/Bad Bevensen, county of Uelzen.

Abb. 4: Verbreitung von tief-humosen Böden, fluvialen und colluvialen Lagen und Waldbedeckung in der Umgebung von Seedorf/Bad Bevensen (Landkreis Uelzen).

for well-bleached aeolian sediments like loess or dunes can be determined. Therefore, OSL has been applied successfully to these deposits. Loess and loess like sediments have been investigated and dated with OSL in many studies (Roberts 2008). Loess research in Germany has a more than 175 year tradition with sections in the loess areas in the Rhineland (western Germany) and in southern Germany having been investigated in detail. The geochronological studies with thermoluminescence and OSL dating are summarized in Frechen et al. (2003). For loess and loess like sediments in northwest Germany geochronological studies are still missing. There are detailed sedimentological investigations done by Dewers (1932), Fiedler & Altermann (1964) and Lang (1974, 1990). This study will provide the first OSL ages for the sandy loess area in northwest Germany.

Samples for OSL dating were collected in steel tubes hammered into vertical sediment exposures after cleaning the wall. The cylinders were sealed to protect the samples from light exposure. Preparation of fine grained material was done following the description from Frechen et al. (1996). For the OSL measurement, the grain size fraction between 4–11 µm was taken.

A Risø Reader TL/OSL-DA-15 was used for the measurement of the luminescence signal. The polymineral fine grain samples were stimulated with infrared LEDs with a wavelength of 875 nm and a maximum power of 135 mW cm^{-2}. The emitted light was detected with a bialkali EMI 9235QA photomultiplier tube. For the measurement of the feldspar emission a combination of a Schott BG 39 and a Corning 7–59 filter was used. Irradiation of the samples was done by an attached $^{90}Sr/^{90}Y$ beta source with a dose rate of 0.16 Gy s^{-1}. According to studies from Mauz & Lang (2004) and Mauz et al. (2006), the dose rate has to be reduced for the calculation of the equivalent dose obtained with aluminium discs. Our experiments showed that the dose rate for our reader using fine grains on aluminium discs has to be 16% lower than for coarse grains (quartz) on stainless steel discs.

Feldspars suffer from an effect called anomalous fading. This is a non-thermal loss of charge from kinetically stable traps due to quantum mechanical tunnelling which results in age underestimation (Spooner 1994, Visocekas 2002, Visocekas et al. 1994, Wintle 1973). A quantitative correction method for samples younger than 20 ka was proposed by Huntley & Lamothe (2001). This method for fading correction was applied to correct the ages for all samples in this study.

The natural luminescence signal is mainly the result of the natural radioactivity from uranium and thorium chains and ^{40}K and a minor portion of some other radioisotopes and cosmic radiation. For the age calculation it is essential to know the annual dose rate of the surrounding sediment. In this study the dose rate was measured by gamma spectrome-

Table 1: Field soil description of soil profile Schulwiese (Gleysol/Colluvisol).

Tabelle 1: Beschreibung der Bodenhorizonte des Profils Schulwiese ((Kolluvisol-)Gley).

Horizon (KA5 2005)	Horizon (IUSS 2006)	Depth [cm]	Texture	Munsell Color
Ap	Ap	0–14	Silt	2.5Y5/4
M-Go	Bg1	14–46	Silt	2.5Y5/4
aGo	Bg2	46–72	Moderate clayey Silt	2.5Y4/4
fAa+Gr	2Ahb/Crb	72–104	Medium clayey Silt	2.5Y4/3
aGr	2Crb	104–114	Medium clayey Silt	2.5Y4/3
fAa+Gr	3Ahb/Crb	114–130	Moderate clayey Silt	2.5Y2.5/1
aGr	3Crb1	130–156	Moderate clayey Silt	2.5Y4/2
aGr	3Crb2	156–175	Moderate clayey Silt	Not determined

Table 2: Field soil description of soil profile Kartoffelfeld (Stagnic Luvisol/Colluvisol).

Tabelle 2: Beschreibung der Bodenhorizonte des Profils Kartoffelfeld (Kolluvisol, Pseudogley-Parabraunerde).

Horizon (KA5 2005)	Horizon (IUSS 2006)	Depth [cm]	Texture	Munsell Color
Ap	Ap	0–30	Silt	2.5Y5/4
M	Bw1	30–54	Silt	2.5Y6/4
M	Bw2	54–82	Moderate sandy Silt	2.5Y5/4
M	Bw3	82–110	Moderate sandy Silt	2.5Y5/6
Swd-Bt	2Btb/Bgb1	110–133	Strong silty Sand	2.5Y6/8
Swd-Bv	2Bwb1/Bgb1	133–138	Medium silty Sand	2.5Y6/6
Swd-Bv	3Bwb2/Bgb2	138–162	Weak silty Sand	2.5Y6/6
Cv	C	162–170	Weak silty Sand	2.5Y5/6

try with an HPGe (High-Purity Germanium) N-type coaxial detector in the laboratory. The results of the gamma spectrometry are shown in Table 3. For the dosimetry the infinite matrix approach is assumed (Aitken 1998). This means for a volume having dimensions greater than the range of radiation, that the rate of energy absorption is equal to the rate of energy emission. The gamma spectrometry allows the monitoring for any radioactive disequilibrium. For all samples radioactive equilibrium could be observed. For potassium-rich feldspar the alpha contribution has to be corrected by a factor: the a-value (alpha efficiency). In this study an a-value of 0.08 ± 0.01 was used, as proposed by Rees-Jones (1995) for polymineral fine grain samples. The contribution of the cosmic radiation, which depends on latitude, longitude, altitude and thickness of the sediment cover, was calculated using the approach of Prescott & Hutton (1994) and Prescott & Stephan (1982). The values for the cosmic radiation are shown in Table 3.

The intensity of the natural radioactivity in the sediment is attenuated by the water in the sediment. Therefore the annual dose rate has to be corrected. For the samples from the profile *Schulwiese* the water content was measured in the lab from additional samples taken during the OSL sampling. The water content for the upper samples is around 12 %. This is a typical value for European loess (Pécsi 1990). The samples at lower positions are within the influence of the ground water. Here the water content is between 19 and 25 %. To take seasonal fluctuations of the water content into account, the error was set quite large. For the upper samples it is 5 % and for the lower samples 10 % (Tab. 3). For the samples from the profile *Kartoffelfeld* (Tab. 3) no water content was measured because there was not enough sampling material collected to measure the water content in the lab. In this case the water content had to be estimated using the values from the higher part of the nearby profile *Schulwiese*.

The OSL-ages are calculated by dividing the equivalent dose (D_e) by the dose rate of the sediment including the contribution of the cosmic rays and the attenuation by the water content. The obtained ages were fading corrected with the g-value by the method described in Huntley & Lamothe (2001). The equivalent doses are calculated using the weighted mean. The results of the age calculation are shown in Tab. 4. The distribution of the equivalent doses was checked using the Kolmogorov-Smirnov-Test (K-S-test) which shows if there is a normal distribution or not. For a normal distribution the obtained K-S-value from this test should be lower than the critical test value. The results of the K-S-test are shown in Tab. 4. All samples show a normal distribution. Based on these results an incomplete bleaching of the samples is unlikely.

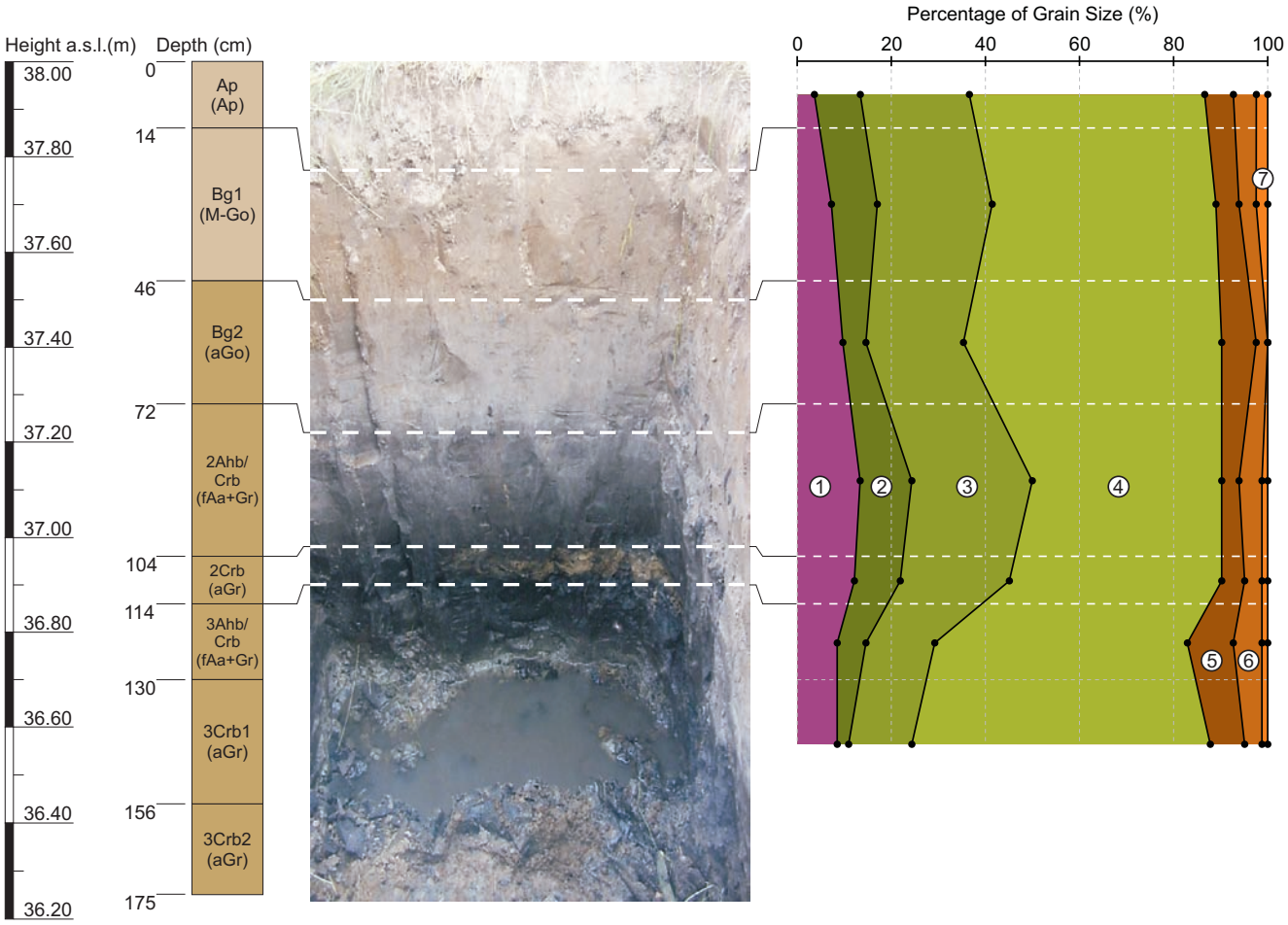

Fig. 5: Profile Schulwiese (Gleysol/Colluvisol) and grain size distribution. Soil description based on IUSS (2006) and in brackets on KA 5 (2005). 1 = clay (<0.002 mm), 2 = fine grained silt (0.002–0.006 mm), 3 = middle grained silt (0.006–0.02 mm), 4 = coarse grained silt (0.02–0.063 mm), 5 = fine grained sand (0.063–0.2 mm), 6 = middle grained sand (0.2–0.63 mm), 7 = coarse grained sand (0.63–2 mm).

Abb. 5: Profil Schulwiese ((Kolluvisol-)Gley) und Korngrössenverteilung. Bodenbeschreibung nach IUS (2006) und in Klammern nach KA 5 (2005). 1 = Ton (<0,002 mm), 2 = Feinschluff (0,002–0,006 mm), 3 = Mittelschluff (0,006–0,02 mm), 4 = Grobschluff (0,02–0,063 mm), 5 = Feinsand (0,063–0,2 mm), 6 = Mittelsand (0,2–0,63 mm), 7 = Grobsand (0,63–2 mm).

2.3.2 OSL measurements and experimental details

Before starting the OSL measurements with a single aliquot regenerative dose (SAR) protocol, several tests were performed to check the suitability of the material for dating. The SAR protocol based on Murray & Wintle (2000) was used in this study. The protocol was modified by inserting a hot-bleach step and the cutheat temperature was chosen equivalent to the preheat temperature (Wallinga et al. 2007). Preheat tests, dose recovery tests and fading tests were performed. The tests were made for the top-most samples and the bottom-most samples in the profiles. Samples SEE 1-A and SEE 1-F from profile *Schulwiese* and samples SEE 2-A and SEE 2-C from profile *Kartoffelfeld* were used for preheat tests. Samples SEE 1-C and SEE 2-A were used for a dose recovery test. The fading tests were done for all samples using fresh aliquots.

The results of the preheat plateau test are shown in Fig. 7. For the samples from profile *Schulwiese,* the D_e show a plateau in the temperature range of 160°C to 240°C (SEE 1-A) and 180°C to 240°C (SEE 1-F). For higher preheat temperatures the D_e are increasing significantly. The recycling ratios are in the range of acceptance of 1.0 ± 0.1 for preheat temperatures up to 240°C. For higher preheat temperatures the recycling ratios are decreasing. The recuperation is increasing for preheat temperatures higher than 240°C. Based on these results a preheat temperature of 200°C for all the samples from profile *Schulwiese* was used.

The behaviour for the samples from profile *Kartoffelfeld* differs. There is no clear preheat plateau visible for the samples SEE 2-A and SEE 2-C. The D_e are slightly increasing with increasing preheat temperature. The recycling ratios are decreasing and scattering for preheat temperatures higher than 220°C. The recuperation is increasing exponentially for preheat temperatures higher than 200°C. Based on the behaviour of the recycling ratios and recuperation, a preheat temperature of 180°C was used for all samples from the profile *Kartoffelfeld.*

After determination of the appropriate preheat tempe-rature, dose-recovery tests based on the protocol described by Murray & Wintle (2003) were carried out. This test determines whether an artificially applied dose can be recovered by the SAR protocol. For the profile *Schulwiese* 15 aliquots from sample SEE 1-C and 10 aliquots from sample SEE 2-A (profile *Kartoffelfeld*) were bleached in a Dr. Hönle SOL 2 solar simulator for 2 hours. The bleached samples are irradiated in the Risø Reader with a fixed beta-dose which is close to the expected equivalent dose. This dose was measured us-

Table 3: Results of the gamma spectrometry, cosmic dose and water content for the samples from section Schulwiese (SEE 1) and section Kartoffelfeld (SEE 2). Depth is below surface. The dose rate is the sum of the dose rates from the alpha, beta, gamma and cosmic radiation. For the calculation of the total dose rate the conversion factors published by Adamiec & Aitken (1998) were used. An a-value of 0.08 ± 0.01 (Rees-Jones 1995) for the alpha-efficiency was used for all samples. A systematic error of 8 % is included for the calculation of the dose rate including uncertainties from beta-attenuation, conversion factors, calibration of the gamma detector and effects of past disequilibrium. An error of 10 % is estimated for the cosmic dose.

Tabelle 3: Ergebnisse der Gammaspektrometrie, kosmischen Strahlung und Wassergehalt für die Proben aus dem Profil Schulwiese (SEE 1) und Profil Kartoffelfeld (SEE 2). Tiefe ist unter Geländeoberkante. Die Dosisleistung des Sediments ist die Summe aus den Dosisleistungen der alpha-, beta-, gamma- und kosmischen Strahlung. Für die Berechnung der gesamten Dosisleistung wurden die Umrechnungsfaktoren von Adamiec & Aitken (1998) verwendet. Zur Berechnung der alpha-Effizienz wurde der a-Wert von 0,08 ± 0,01 für alle Proben verwendet (Rees-Jones 1995). Ein systematischer Fehler von 8% wurde bei der Berechnung der Dosisleistung einbezogen. Dieser Fehler beinhaltet Unsicherheiten durch die beta-Abschwächung, der Umrechnungsfaktoren, der Kalibrierung des Gammaspektrometers und Effekte durch frühere radioaktive Ungleichgewichte. Für die kosmische Strahlung wurde ein Fehler von 10% angenommen.

Sample	depth [m]	water content [%]	K [%]	U [ppm]	Th [ppm]	cosmic dose [mGy a^{-1}]	dose rate [mGy a^{-1}]
SEE 1-A	0.30	12 ± 5	1.48 ± 0.07	2.02 ± 0.10	6.45 ± 0.32	0.20 ± 0.02	2.78 ± 0.17
SEE 1-B	0.45	11 ± 5	1.56 ± 0.08	2.34 ± 0.12	7.09 ± 0.35	0.20 ± 0.02	3.04 ± 0.17
SEE 1-C	0.60	13 ± 5	1.63 ± 0.08	2.27 ± 0.11	7.54 ± 0.38	0.19 ± 0.02	3.05 ± 0.17
SEE 1-D	0.85	19 ± 10	1.55 ± 0.08	2.50 ± 0.13	8.06 ± 0.40	0.18 ± 0.02	2.92 ± 0.20
SEE 1-E	0.97	25 ± 10	1.31 ± 0.07	2.51 ± 0.13	7.13 ± 0.36	0.18 ± 0.02	2.49 ± 0.18
SEE 1-F	1.15	17 ± 10	1.41 ± 0.07	2.25 ± 0.11	6.94 ± 0.35	0.17 ± 0.02	2.67 ± 0.20
SEE 2-A	0.80	12 ± 5	1.70 ± 0.09	2.28 ± 0.11	6.90 ± 0.35	0.18 ± 0.02	3.08 ± 0.17
SEE 2-B	0.82	12 ± 5	1.71 ± 0.09	2.21 ± 0.11	6.79 ± 0.34	0.18 ± 0.02	3.06 ± 0.17
SEE 2-C	1.38	12 ± 5	1.20 ± 0.06	2.45 ± 0.12	8.91 ± 0.45	0.17 ± 0.02	2.86 ± 0.17

ing the SAR protocol applied for the samples. The ratio of applied dose to recovered dose for sample SEE 1-C is 0.94 ± 0.03 and for sample SEE 2-A is 1.03 ± 0.01. Based on the results of the performance tests a SAR protocol (Tab. 5) was developed and the D_e values of the samples are measured with this protocol. The IR-stimulation time for the samples from profile *Schulwiese* are reduced from 300 s to 100 s to save measuring time. The IRSL-signal is reduced after 50 s to background-level. Longer IR-stimulation time gives no better behaviour concerning fully bleaching and recuperation.

2.4 Palynological investigations

For palynological, including charcoal particle, analysis, about 10 g sampled at intervals of 2–5 cm of the OSL dated layers were treated by standard palynological methods. The procedures included dispersion with 10% NaOH, carbonate removal by 10% HCl, flotation to separate organics from the inorganic matrix using sodium metatungstate ($3NaWO_4 \cdot 9WO_3 \cdot H_2O$) and acetolysis to dissolve cellulose and to darken the palynomorphs for ease of recognition (Faegri & Iversen 1989, Moore et al. 1991). Prepared residues were embedded in glycerine over which coverslips of 24 x 32 mm were sealed with Entellan® and samples subsequently counted mostly at x400 magnification. Three slides of 24 x 32 mm per sample were analyzed for pollen and non-pollen palynomorphs except for micro charcoal, which was counted in 1 slide and then calculated for 3 slides as well. For detailed morphological studies a x100 oil immersion lens was used. Pollen and spores were identified from the atlases of Moore et al. (1991), Beug (2004), Faegri & Iversen (1989) and a reference collection of the Laboratory of the Division of Soil Science and Biology at Leuphana University of Lüneburg. The guide and reference literature of van Geel (1978, 2001) was used to identify fungal remains and other non-pollen palynomorphs. The pollen sum (100%) is based on terrestrial pollen exclusive of Cyperaceae and Ericaceae as well as fern and moss spores. Pollen calculation and diagram construction were performed with the software package TILIA, TILIA GRAPH and TILIA VIEW (Grimm 1990).

3 Results

3.1 Sediment and soil properties

3.1.1 Profile Schulwiese

The Ap and Bg1 horizons (colluvium) of the Gleysol/Colluvisol *Schulwiese* (Tab. 1, Figs. 5 and 8) are characterized by pure silt, the underlying buried Ahb and Crb horizons are composed of moderate clayey silt, and the 2Ahb/Crb horizon has the highest clay content. The pH [$CaCl_2$] of the entire profile ranges from 5.6 to 5.8 except for the Bg2 horizon, which has a pH of slightly above 6. Organic carbon and Soil Organic Matter (SOM) respectively reach highest values in the buried A horizons 2Ahb/Crb (2.66 % C) and 3Ahb/Crb (2.25% C) and in the Ap (2.03 % C) and Bg1 (1.87% C) horizons which developed on the colluvium. The 2Crb horizon has still a carbon content of 1.15 % whereas the Bg2 (0.5%) and the 3Crb1 (0.44%) horizons are low in carbon. Similar results were found for organic nitrogen with highest amounts in the buried A horizons and in the horizons developed within the colluvium (Fig. 8). Total (Fe_t) as well as free iron (Fe_d) have highest values in the uppermost colluvial horizons Ap and Bg1 (Fig. 9 and 10) pointing to supply with fresh loess-soil borne material. Among the trace and major elements the

Table 4: Results of the OSL measurements, age calculation and statistical parameters for the samples from section Schulwiese (SEE 1) and the section Kartoffelfeld (SEE 2). The grain size for all samples is 4–11 µm. Equivalent doses are calculated using weighted mean including an error of 3 % for the calibration of the beta source in the OSL reader. Fading corrected ages are calculated using the approach from Huntley & Lamothe (2001). Number of aliquots shows the amount of aliquots used for the age calculation. The K-S-value shows the results of the Kolmogorov-Smirnoff-Test which tests for a normal distribution. Distributions of equivalent doses with K-S-values lower than the critical K-S-value are regarded as normal distributions.

Tabelle 4: Ergebnisse der OSL-Messung, der Altersberechnung und statistische Parameter für die Proben aus dem Profil Schulwiese (SEE 1) und Kartoffelfeld (SEE 2). Alle Proben sind polymineralische Feinkornproben mit einer Korngrösse zwischen 4 µm und 11 µm. Die Äquivalenzdosen wurden über das gewichtete Mittel berechnet. Die Fehlerberechnung beinhaltet einen Fehler für die Kalibrierung der beta-Quelle im OSL-Reader von 3%, Die Fadingkorrektur wurde nach der Methode von Huntley & Lamothe (2001) durchgeführt. Anzahl der Aliquots zeigt die Zahl der für die Altersberechnung verwendeten Aliquots an. Mit Hilfe des Kolmogorov-Smirnoff-Test wurden die Verteilungen der Äquivalenzdosen auf Normalverteilung getestet. Verteilungen mit einem K-S-Wert niedriger als der kritische K-S-Wert wurden als Normalverteilung angesehen.

Sample	equivalent dose [Gy]	g-value [% per decade]	fading uncorrected age [ka]	fading corrected age [ka]	number of aliquots	K-S-value	critical K-S-value
SEE 1-A	2.18 ± 0.02	5.4 ± 0.3	0.79 ± 0.05	1.2 ± 0.1	18	0.142	0.309
SEE 1-B	2.10 ± 0.03	5.1 ± 0.2	0.69 ± 0.04	1.0 ± 0.1	18	0.115	0.309
SEE 1-C	5.47 ± 0.06	4.4 ± 0.2	1.8 ± 0.1	2.5 ± 0.1	19	0.161	0.301
SEE 1-D	5.50 ± 0.06	4.5 ± 0.2	1.9 ± 0.1	2.6 ± 0.2	20	0.138	0.294
SEE 1-E	7.28 ± 0.08	3.9 ± 0.3	2.9 ± 0.2	3.9 ± 0.3	20	0.089	0.294
SEE 1-F	19.16 ± 0.28	2.9 ± 0.3	7.2 ± 0.6	9.0 ± 0.7	20	0.106	0.294
SEE 2-A	10.78 ± 0.10	3.5 ± 0.3	3.5 ± 0.2	4.6 ± 0.3	20	0.101	0.294
SEE 2-B	6.04 ± 0.06	3.8 ± 0.2	2.0 ± 0.1	2.6 ± 0.1	20	0.171	0.294
SEE 2-C	138.99 ± 2.00	3.5 ± 0.3	48.5 ± 2.9	66.9 ± 4.5	17	0.087	0.318

Table 5: Single aliquot regenerative (SAR) protocol used for the measurement of the samples from sections Schulwiese and Kartoffelfeld.

Tabelle 5: Für die Messung der Proben aus den Profilen Schulwiese und Kartoffelfeld benutztes Single Aliquot Regenerative (SAR) Protokoll.

Step	Treatment	Schulwiese	Kartoffelfeld	Observed
1	give regenerative dose D_i	1.6–48 Gy	9.6–160 Gy	
2	preheat [5°C/s heating rate]	200°C for 10 s	180°C for 10 s	
3	IRSL	100 s @ 50°C	300 s @ 50°C	L_i
4	give test dose D_t	0.8 Gy	1.6 Gy	
5	cutheat [5°C/s heating rate]	200°C for 10 s	180°C for 10 s	
6	IRSL	100 s @ 50°C	300 s @ 50°C	T_i
7	IRSL [hotbleach]	100 s @ 290°C	100 s @ 290°C	

For the natural sample i=0 and D_0=0. The whole sequence is repeated for several regenerative doses, including a zero dose and a repeat dose. Regenerative doses D_i depending on the expected age of the sample. Doses are chosen in that way, that they bracket the natural dose. In this table the range of all given doses for all samples is given. The ratio between L_i/T_i is used for the calculation of the equivalent dose. The IRSL-signal from step 7 (hotbleach) is not used.

amounts of phosphorous, manganese as well as of chlorine are increasing in the Ap and Bg1 horizon (Fig. 10), whereas calcium and sulfur are predominant in fossil horizons 2Ahb/Crb and 3Ahb/Crb. The sulfur enrichment might be explained as a result of anaerobic processes under (ground) water saturated conditions, which is as well supported by the high amounts of still preserved SOM.

3.1.2 Profile Kartoffelfeld

The Ap, Bw1, Bw2 and Bw3 horizons, which are developed on the loess-soil colluvium, are characterized by a silty (0–54 cm) to moderate sandy silty texture (54–110 cm) (Fig. 6, Tab. 2). The texture of 2Btb/Bgb1 (110–133 cm) is a strong silty sand and that of 2Bwb1/Bgb1 (133–138 cm) a medium silty sand while the 3Bwb2/Bgb2 and C horizons are of a weak silty sand texture. 2Btb/Bgb1 (110–133 cm) and 2Bwb1/Bgb1 (133–138 cm) horizons developed on Weichselian periglacial silty sand, whereas the basal 3Bwb2/Bgb2 and C horizons formed on Saalian (Drenthe Stadium) sandy till. The uppermost four horizons show a steady increase of organic Carbon, total Nitrogen as well as of pH [$CaCl_3$] (Fig. 11) from about 100 cm to the top of the profile. Total (Fe_t) as well as free Iron (Fe_d) in particular Fe_o-oxides have highest values in the uppermost colluvial horizons (Fig. 12) pointing to recent rejuvenation of the sequence with loess-soil borne parent material. The Fe_o/Fe_t ratio of the underlying buried stagnic luvic and C horizons is very low reflecting old pedogenic weathering processes. A major erosive hiatus between the basic horizons and the colluvial cover pediment is assumed as a buried Ahb horizon is missing in the sequence of profile *Kartoffelfeld*.

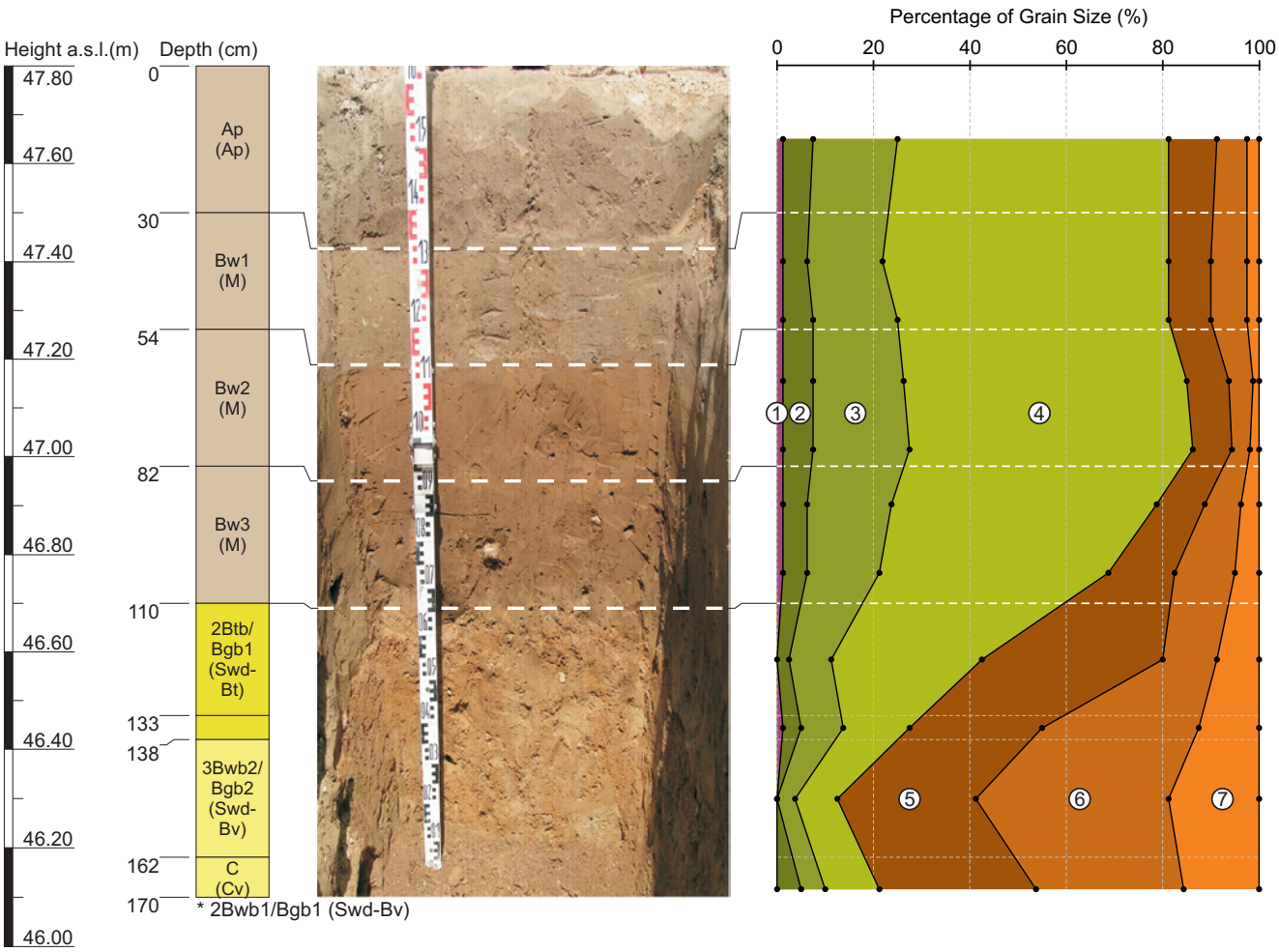

Fig. 6: Profile Kartoffelfeld (Colluvisol/Stagnic Luvisol) (Seedorf, Lower Saxony) and grain size distribution. Soil description based on IUSS (2006) and in brackets on KA 5 (2005). 1 = clay (<0.002 mm), 2 = fine grained silt (0.002–0.006 mm), 3 = middle grained silt (0.006–0.02 mm), 4 = coarse grained silt (0.02–0.063 mm), 5 = fine grained sand (0.063–0.2 mm), 6 = middle grained sand (0.2–0.63 mm), 7 = coarse grained sand (0.63–2 mm).

Abb. 6: Profil Kartoffelfeld (Kolluvisol, Pseudogley-Parabraunerde) und Korngrössenverteilung. Bodenbeschreibung nach IUS (2006) und in Klammern nach KA 5 (2005). 1 = Ton (<0,002 mm), 2 = Feinschluff (0,002–0,006 mm), 3 = Mittelschluff (0,006–0,02 mm), 4 = Grobschluff (0,02–0,063 mm), 5 = Feinsand (0,063–0,2 mm), 6 = Mittelsand (0,2–0,63 mm), 7 = Grobsand (0,63–2 mm).

3.2 OSL dating

The results of the dosimetry, the OSL measurements and the age calculation for profiles *Schulwiese* and *Kartoffelfeld* are summarized in Tables 3 and 4. The equivalent doses and calculated ages, fading uncorrected and fading corrected ones, show an increase of D_e and of age with depth. Sample SEE 1-B has a slightly lower D_e and lower age than the sample from above. The 1-sigma standard deviation makes an equal deposition age likely for SEE 1-A and SEE 1-B. Based on the geochronology, four periods of increased accumulation of sediment can be identified in the profile *Schulwiese*. The first one took place 9.0 ± 0.7 ka while a second period is indicated at 3.9 ± 0.3 ka. Samples SEE 1-C and SEE 1-D show a third period of deposition at around 2.5 ka and the fourth period of deposition is shown by samples SEE 1-A and SEE 1-B at around 1.0 ka before present.

In profile *Kartoffelfeld* there is an increase of D_e and age with depth. The sample SEE 2-A was taken from a parallel profile a few meters from the main profile. It could be expected, that the ages of SEE 2-A and SEE 2-B should be nearly the same. The difference can be explained by the palaeo-topographic situation at this site which was not evident during sampling.

Due to the colluvial deposition of the sediment, incomplete bleaching of the samples could be expected. In the case of incomplete bleaching the distributions of the equivalent doses obtained during the SAR-measurement should show a large scatter. But all investigated OSL samples show very low scatter and a normal distribution indicating fully bleached samples. The obtained OSL-ages (Tab. 7 and 8) are in agreement with radiocarbon dating, pollenanalysis and archeological investigations in that area.

3.3 Radiocarbon dating

In this study humic-rich material from a depth of 108 cm below surface was taken for radiocarbon dating. The specific activity of ^{14}C was measured radiometrically by proportional counters (Geyh 2005). The conventional age is given with a 2-sigma standard deviation and was calculated into calibrated age using Calib 5.0.1 based on Stuiver & Reimer (1993). For terrestrial material the dataset intcal04 (Reimer et al. 2004) was used and the calibrated ^{14}C-age is in the 2-sigma range. The ^{14}C-age of sample Hv25552 is 5960 ± 60 years BP ($\delta^{13}C$ = -28.7) and the calibrated age is cal BC 5081 - 4551 (Early Neolithic, Linear Pottery culture) (Tab.7).

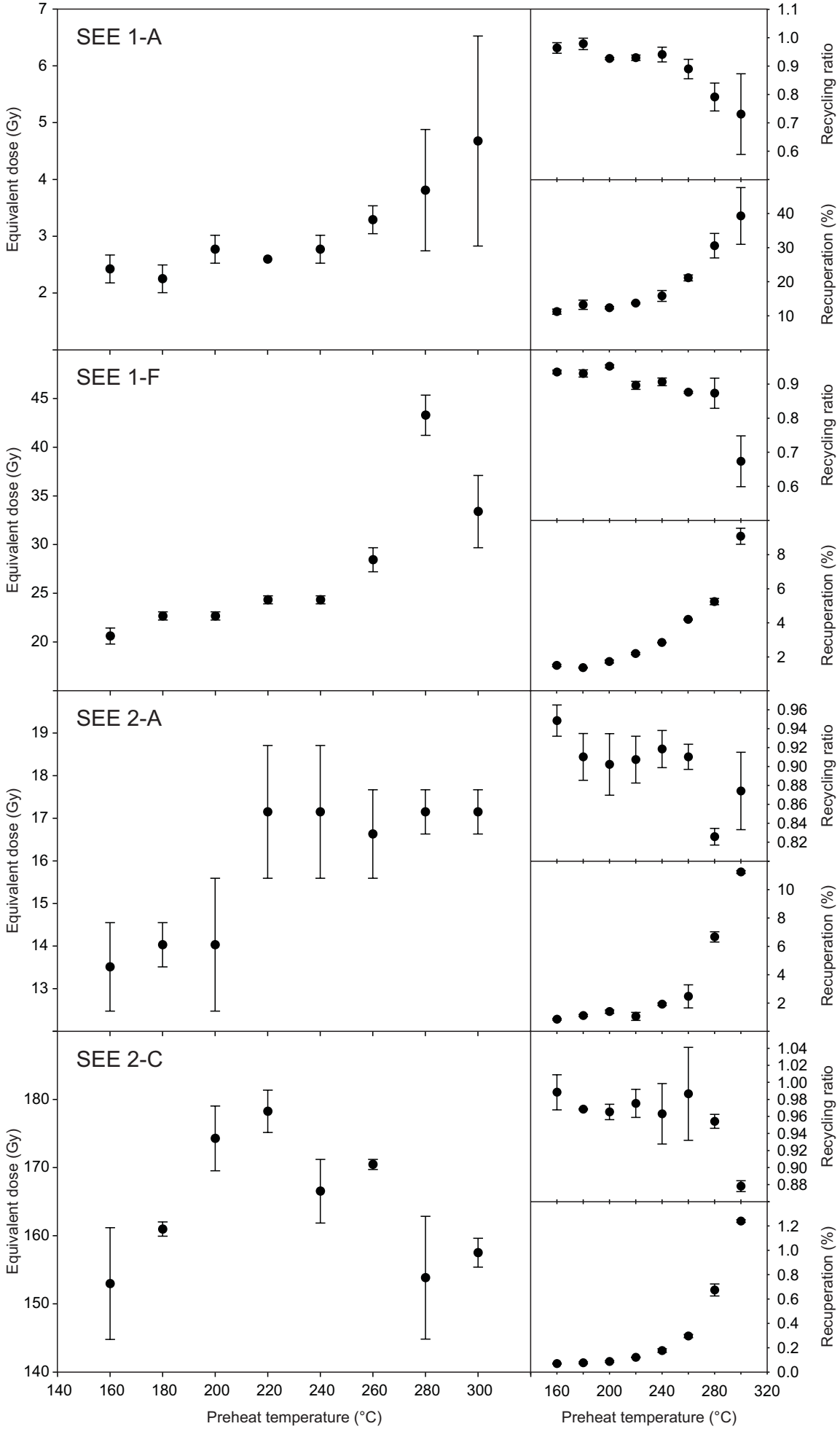

Fig. 7: Results of the preheat plateau test for the samples from profile Schulwiese (SEE 1-A and SEE 1-F) and from profile Kartoffelfeld (SEE 2-A and SEE 2-C). For each temperature the mean value and the standard deviation from three aliquots is shown. On the right side the recycling ratios and the recuperation for each temperature is shown.

Abb. 7: Ergebniss des preheat-Plateau-Tests für die Proben aus dem Profil Schulwiese (SEE 1-A und SEE 1-F) und aus dem Profil Kartoffelfeld (SEE 2-A und SEE 2-C). Für jede Temperatur ist der Mittelwert und die Standardabweichung aus drei Aliquots angegeben. Auf der rechten Seite sind die recycling ratios und die recuperation für jede Temperatur angegeben.

E&G / Vol. 60 / No. 1 / 2011 / 6–26 / DOI 10.3285/eg.60.1.01 / © Authors / Creative Commons Attribution License

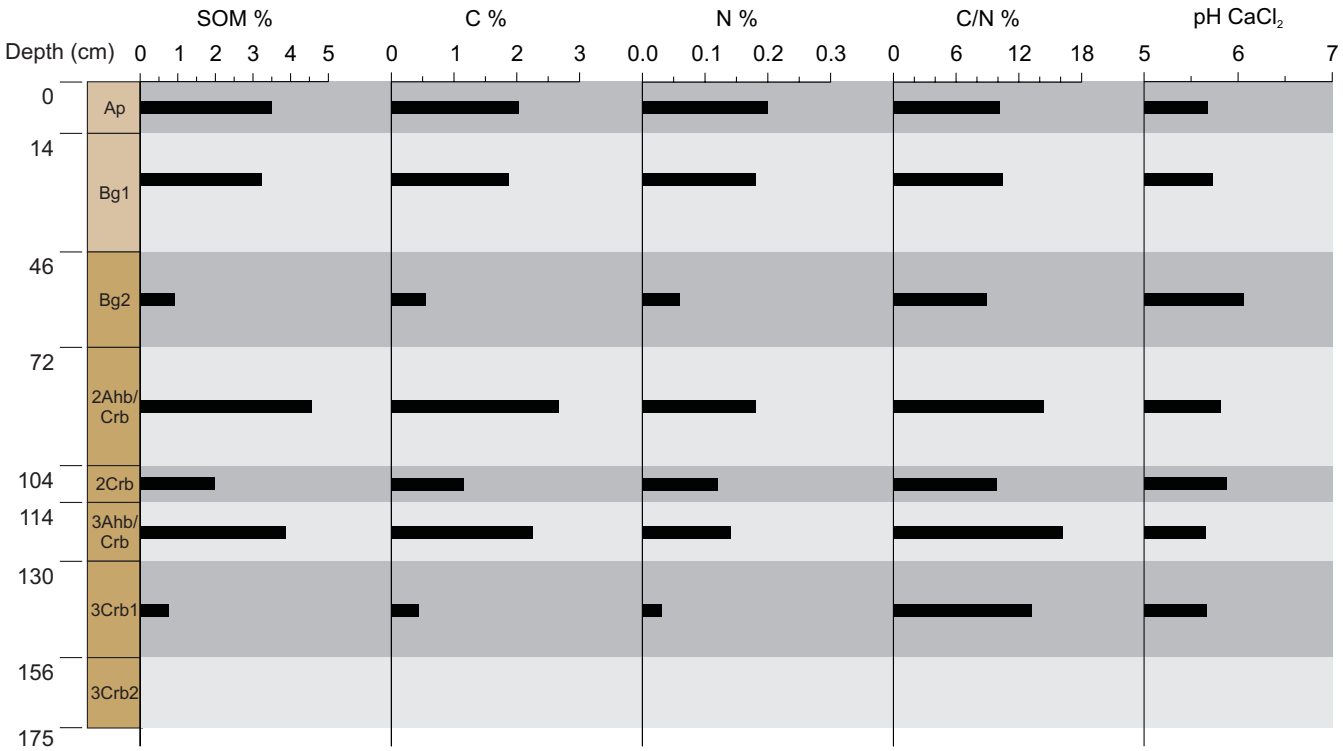

Fig. 8: Soil properties of profile Schulwiese (Seedorf, Lower Saxony).

Abb. 8: Bodeneigenschaften des Profils Schulwiese (Seedorf, Niedersachsen).

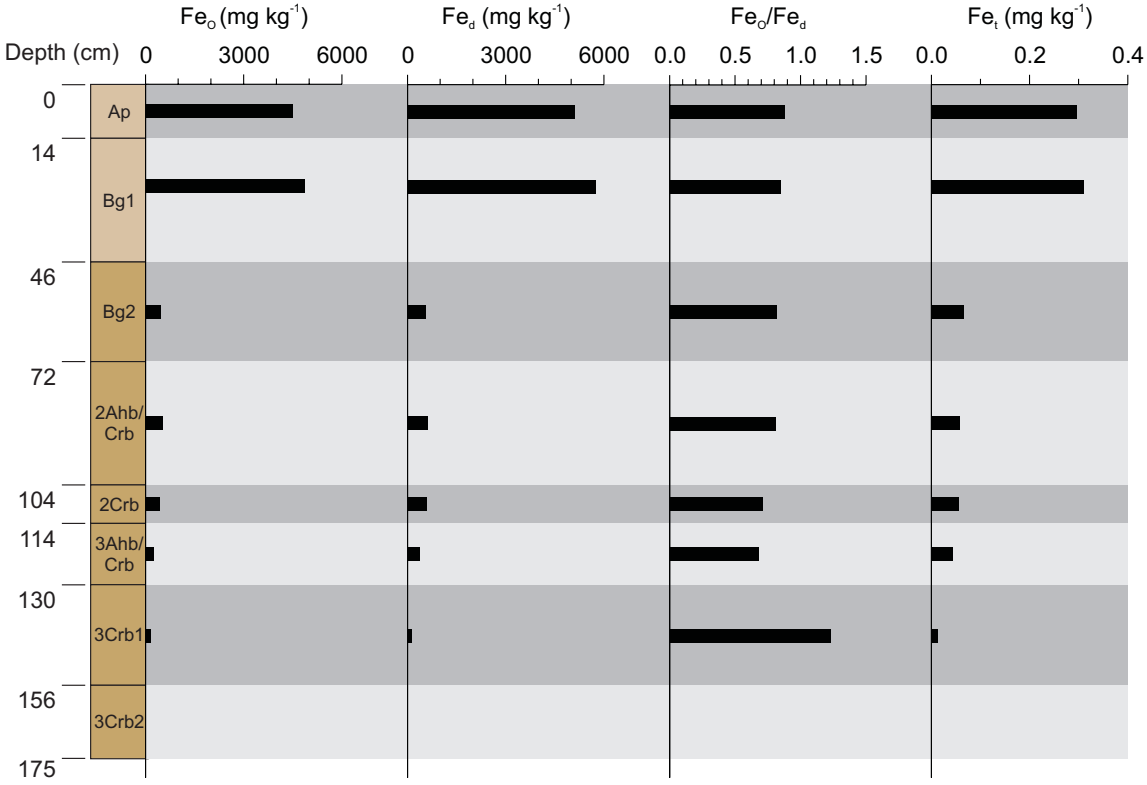

Fig. 9: Total Fe and pedogenic F_e-oxides of profile Schulwiese (Seedorf, Lower Saxony).

Abb. 9: Verteilung von Eisen (F_e) und pedogenen Eisenoxiden im Profil Schulwiese (Seedorf, Niedersachsen).

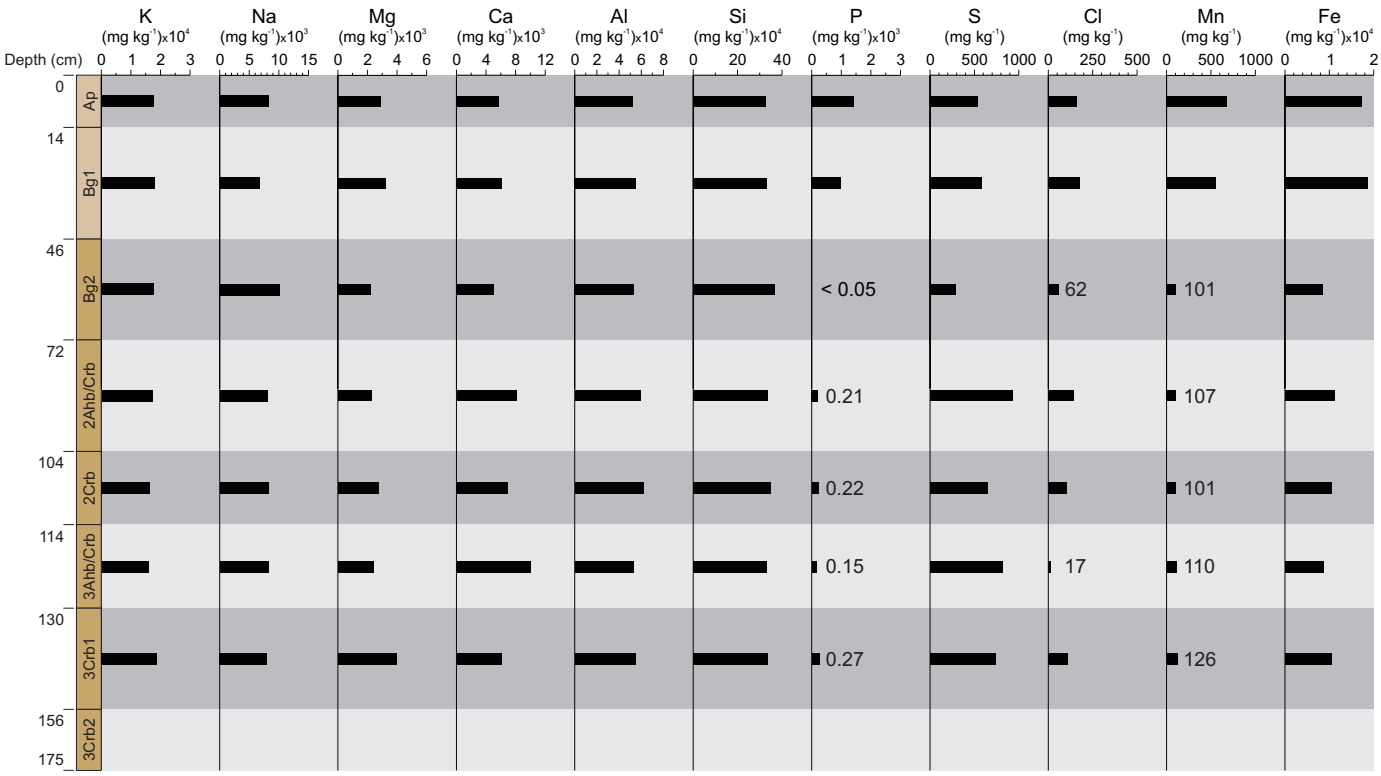

Fig. 10: Major and trace element analysis of profile Schulwiese (Seedorf, Lower Saxony).

Abb. 10: Verteilung von Haupt- und Spurenelementen im Profil Schulwiese (Seedorf, Niedersachsen).

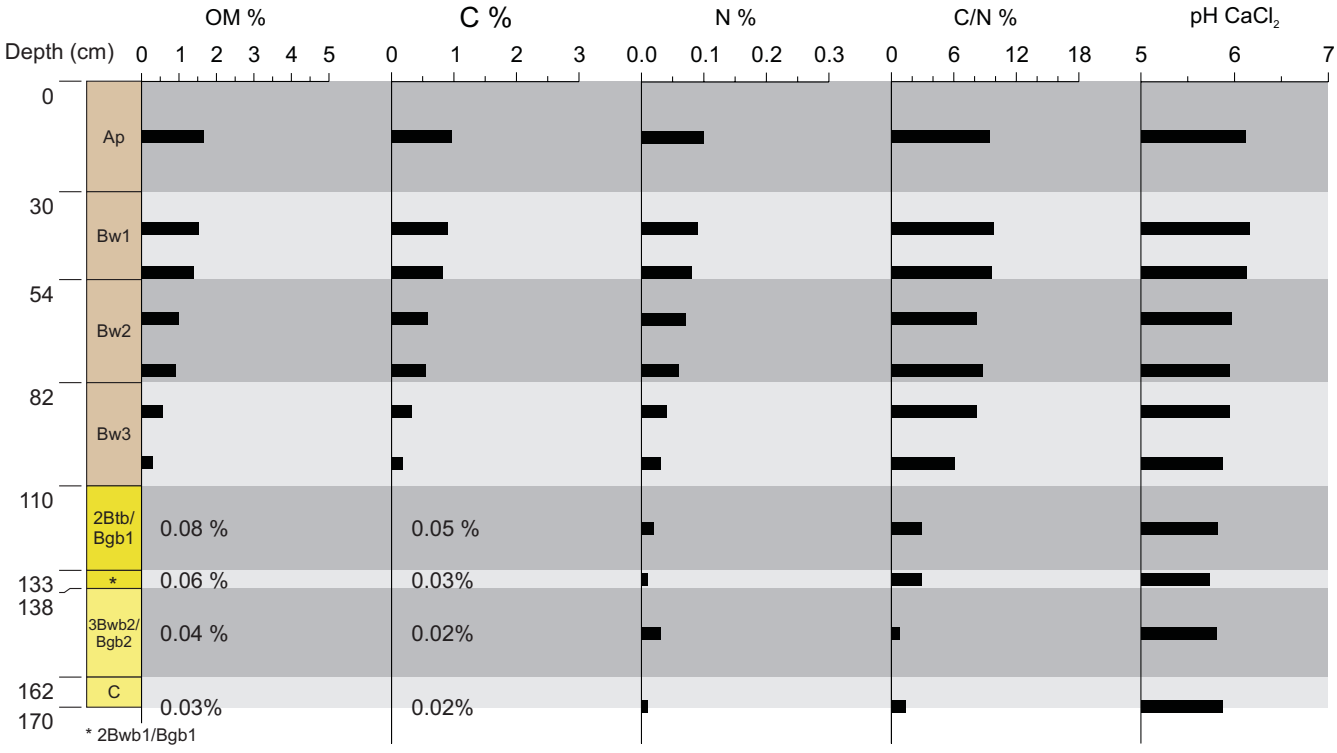

Figure 11: Soil properties of profile Kartoffelfeld (Seedorf, Lower Saxony).

Abbildung 11: Bodeneigenschaften des Profils Kartoffelfeld (Seedorf, Niedersachsen).

E&G / Vol. 60 / No. 1 / 2011 / 6–26 / DOI 10.3285/eg.60.1.01 / © Authors / Creative Commons Attribution License

Table 6: Pollen assemblages and Holocene climatic zones of profile Schulwiese (Seedorf, Lower Saxony).

Tabelle 6: Pollenzonen und klimatische Gliederung des Holozän für das Profil Schulwiese (Seedorf, Niedersachsen).

Local pollen assemblage Zone, LPAZ	Soil horizons	Pollen, Vegetation	Climatic Zones
S5	Bg1	Quercus increasing, Alnus, terrestrial herbs, Cerealia	Late Subatlantic
S4	Bg2	Alnus, dominance of Poaceae and terrestrial herbs, Cichoriaceae, Cerealia and Secale [reye]	Early Subatlantic
S3b	Bg2	Decrease of Alnus, strong increase of heliophytes and Poaceae, continuous curve of Cereals	Subboreal
S3a	2Ahb/Crb	Alnus, Quercus, Poaceae, slight increase of Cyperaceae	
S2	2Crb	Alnus, Quercus, Tilia, Ulmus, Betula, Pinus, Polypodiaceae, Poaceae increasing	Atlantic
S1	3Ahb/Crb	Betula, Pinus, Selaginella selaginoides	Boreal Preboreal

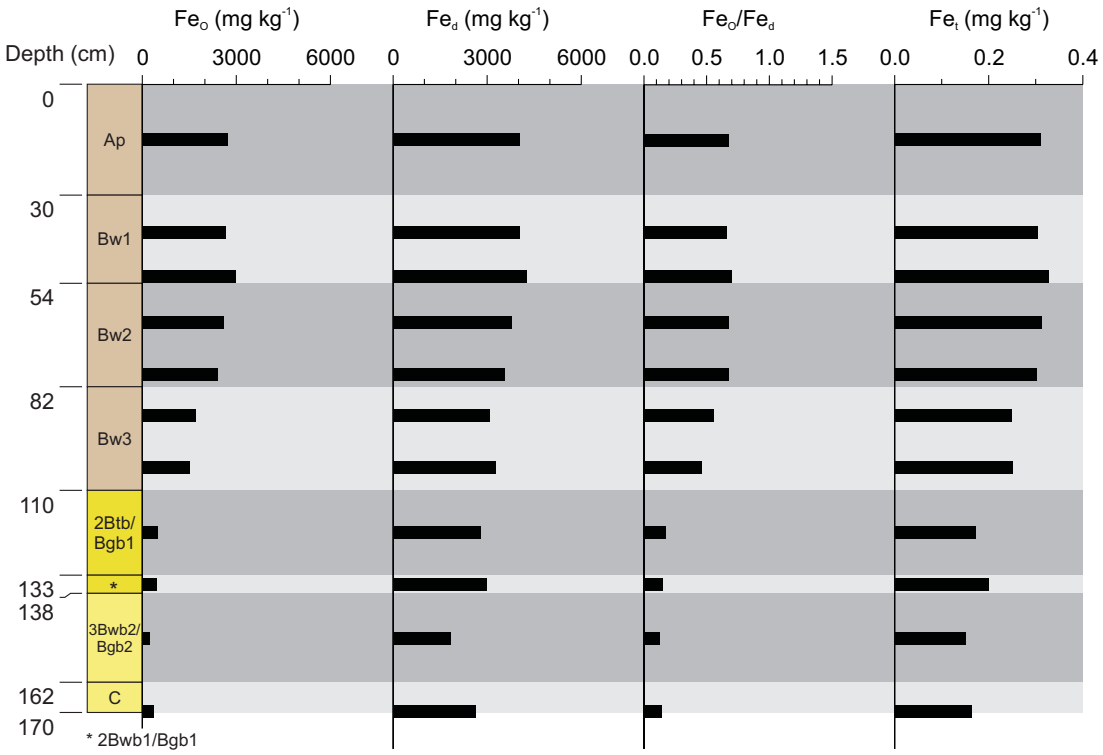

Fig. 12: Total F_e and pedogenic F_e-oxides of profile Kartoffelfeld (Seedorf, Lower Saxony).

Abb. 12: Verteilung von Eisen (F_e) und pedogenen Eisenoxiden im Profil Kartoffelfeld (Seedorf, Niedersachsen).

Table 7: Late Glacial and Holocene climate, dating, archaeological periods and soil development (profile Schulwiese, Seedorf, Lower Saxony). Sampling points for OSL dating are marked by black crosses. White cross marks the sampling position for radiocarbon dating. Soil description is based on IUSS (2006) and in brackets on KA 5 (2005). Soil horizons 3Crb1 and 3Crb2 are covered by groundwater and not visible in the picture.

Tabelle 7: Spätglaziale und holozäne Klimaentwicklung, Datierungsergebnisse, archäologische Perioden und Bodenentwicklung für das Profil Schulwiese in Seedorf (Niedersachsen). Probennahmepunkte für die OSL-Datierung sind mit schwarzen Kreuzen markiert. Weisse Kreuze markieren den Probennahmepunkt für die Radiokarbondatierung. Die Beschreibung der Bodenhorizonte ist nach IUSS (2006) und in Klammern nach KA 5 (2005). Bodenhorizonte aGr im Liegenden sind durch Grundwasser bedeckt und im Foto nicht sichtbar.

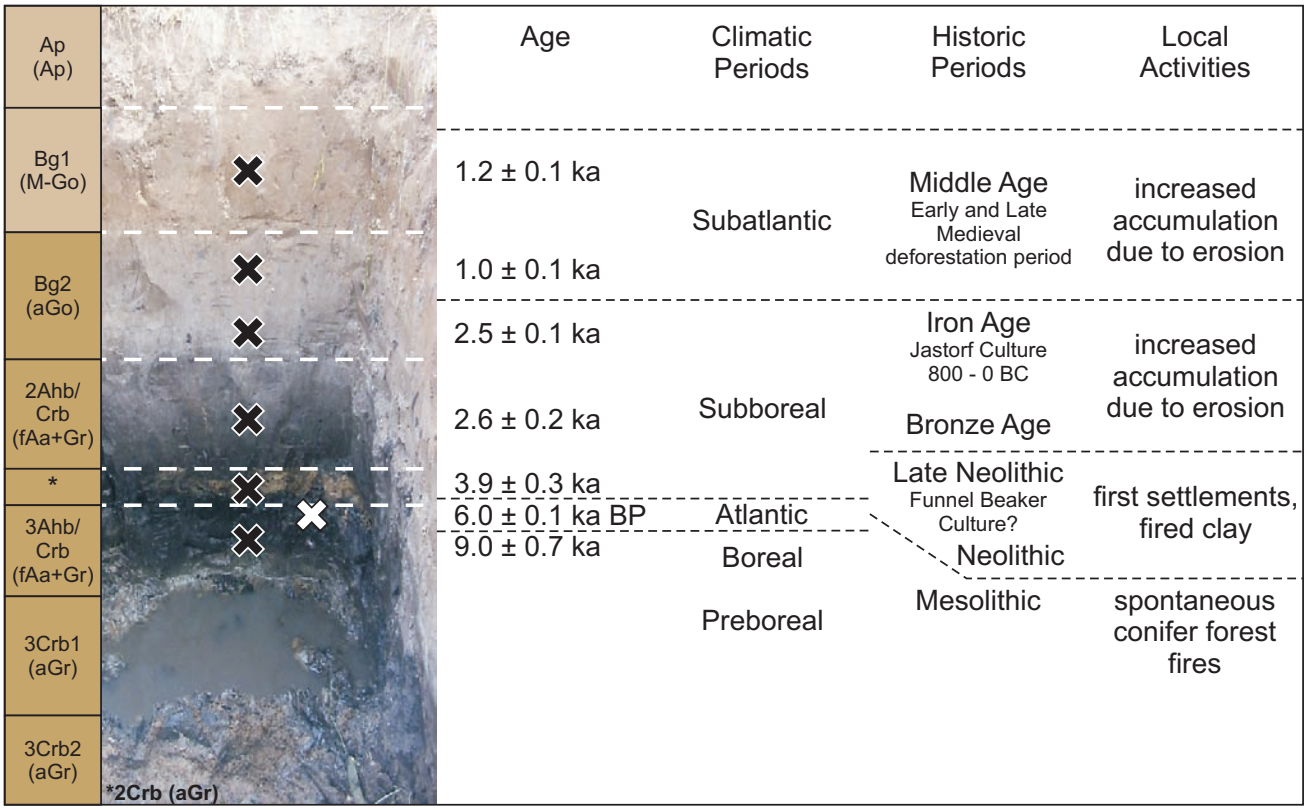

3.4 Palynology

The results of 23 samples of profile *Schulwiese* (130 cm–37 cm) containing between 200 and 580 palynomorphs per count and abundant in micro charcoal are presented in a pollen diagram (Fig. 13). The diagram is subdivided into 5 local pollen assemblage zones (LPAZ) S1–S5, while one zone, LPAZ S3, is further divided into subzones 3a and 3b.

LPAZ S1 (130–117.5 cm; horizon 3Ahb/Crb) is characterized by high values for *Betula, Alnus* and *Pinus;* pollen of *Ephedra fragilis* and spores of *Selaginella selaginoides* indicate relatively open stands characteristic for early Holocene conditions. Pollen of *Quercus, Corylus* and *Ulmus* at the base of the pollen zone might be reworked. The micro charcoal curve peaks in the lower most sample which is probably due to lightning or spontaneous combustion of the conifer (*Pinus*) dominated woodland rather than pointing to human activities (Kalis et al. 2003). Based on the pollen assemblage the parent material and horizon 3Ahb/Crb most probably developed during the Preboreal-Boreal transition.

The pollen assemblage of **LPAZ S2** (117.5–102.5 cm; upper part of horizon 3Ahb/Crb, horizon 2Crb, lowest part of 2Ahb/Crb) is dominated by *Alnus* whereas *Betula* has decreased, followed by *Pinus* and *Corylus*, *Quercus, Ulmus* and *Tilia* among the arboreal taxa (AP). Fern spores as well as pollen of *Alnus* and *Betula* and of herbs like *Filipendula* point to a swampy temporarily flooded environment and a high groundwater level. Pollen of other terrestrial heliophilous herbs like Asteraceae, Apiaceae, Caryophyllaceae, Cichoriaceae and Rosaceae are indicative of local open meadows at site *Schulwiese*. The increasing curve of grass pollen (Poaceae) and a peak in the generally high charcoal curve observed in horizon 2Crb, might point to human activity although anthropogenic indicators are still lacking in this pollen zone. From the pollen assemblage of the woody plants a local back swamp forest with predominantly *Alnus* and *Betula* can be concluded whereas *Quercus-Ulmus-Tilia-Corylus woodland* was distributed on higher elevated loess stands. Summarizing the pollen assemblage of woody plants of pollen zone S2 (horizon 2Crb) points to an Atlantic age.

This conclusion is supported by a ^{14}C-age of cal BC 5081–4551 obtained from humic material of the 2Crb (108 cm) pointing to a younger Atlantic age for upper parts of LPAZ S2 (Tab. 6)

LPAZ S3 is divided into subzone S3a (102.5–92.5 cm) representative of the lower part of 2Ahb/Crb horizon and subzone S3b (92.5 cm–62.5 cm) which characterizes the upper part of the 2Ahb/Crb and the lower part of Bg2 horizons. LPAZ 3a is still characterized by high amounts of AP, mainly of *Alnus, Quercus, Pinus, Tilia* and *Corylus*. The Poaceae curve increases towards the boundary with subzone S3b and a slight increase of Cyperaceae is observed as well as

E&G / Vol. 60 / No. 1 / 2011 / 6–26 / DOI 10.3285/eg.60.1.01 / © Authors / Creative Commons Attribution License

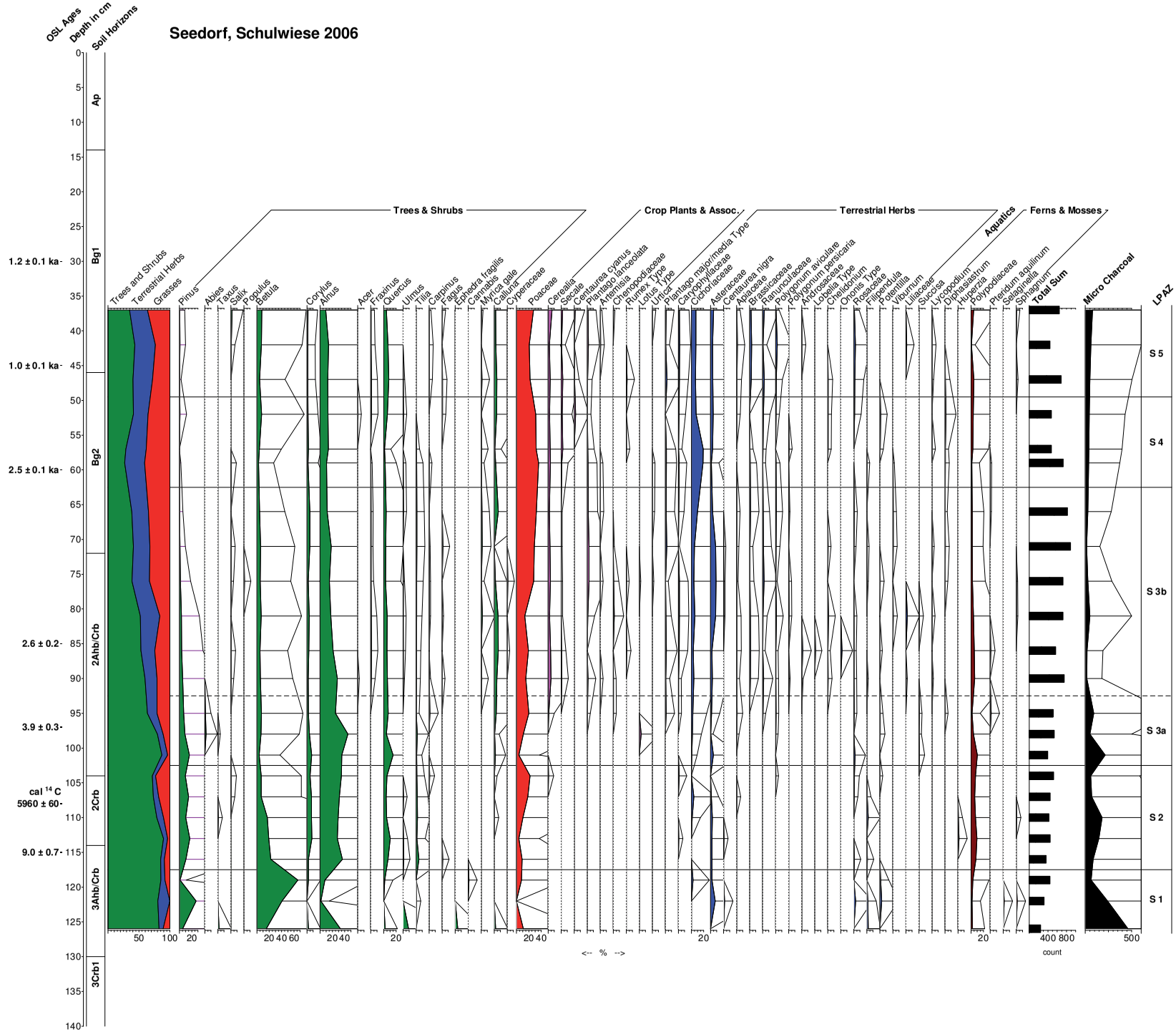

Fig. 13: Pollen diagram of profile Schulwiese (Seedorf, Lower Saxony).

Abb. 13: Pollendiagramm vom Profil Schulwiese (Seedorf, Niedersachsen).

Table 8: Late Weichselian and Holocene climate, dating, archaeological periods and soil development (profile Kartoffelfeld, Seedorf, Lower Saxony). Sampling points for OSL dating are marked by black crosses. Soil description is based on IUSS (2006) and in brackets on KA 5 (2005).

Tabelle 8: Spätweichselzeitliche und holozäne Klimaentwicklung, Datierungsergebnisse, archäologische Perioden und Bodenentwicklung für das Profil Kartoffelfeld in Seedorf (Niedersachsen). Probennahmepunkte für OSL-Datierung sind mit schwarzen Kreuzen markiert. Die Beschreibung der Bodenhorizonte ist nach IUSS (2006) und in Klammern nach KA 5 (2005).

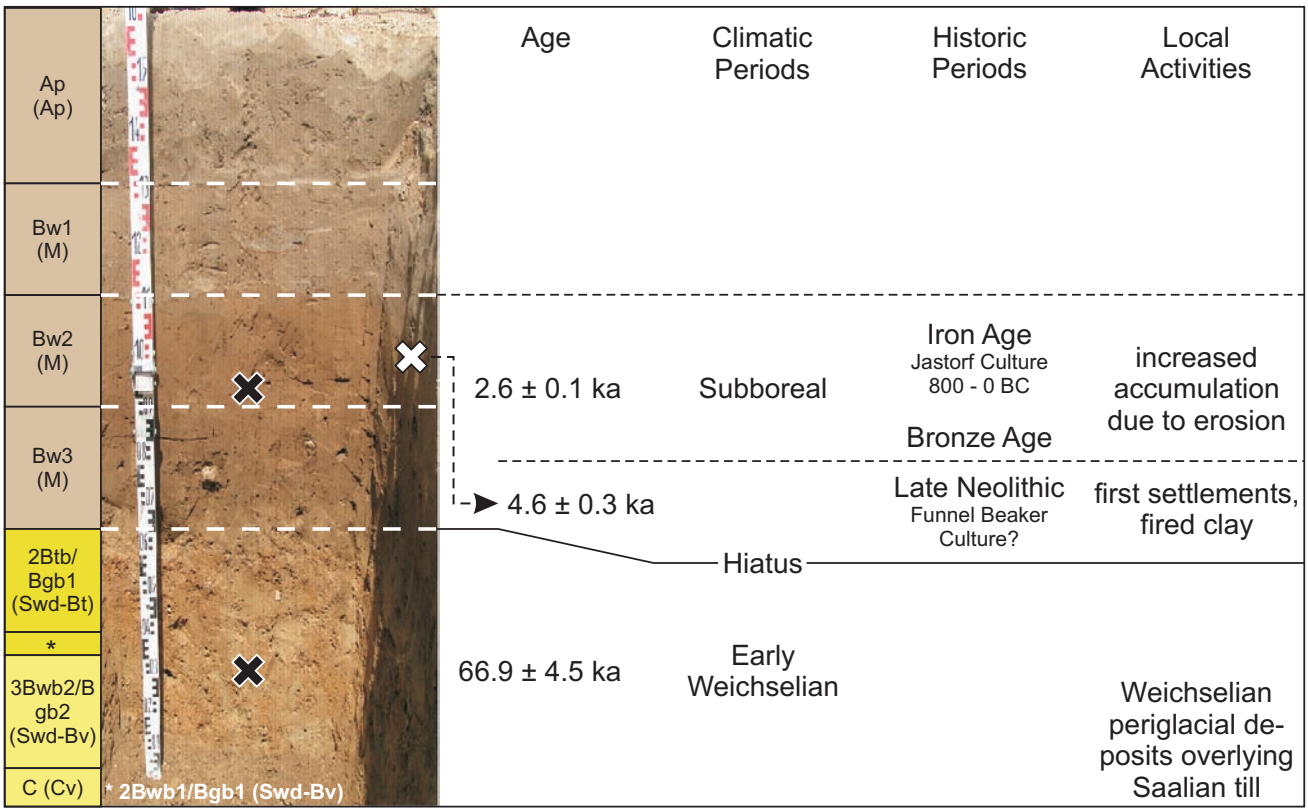

an increase of the heath *Calluna*. In the same levels (lower part of LPAZ 3a and 2Ahb/Crb horizon) a fresh thin alluvial loess layer with fired clay and two peaks in the charcoal curve point to earliest human environmental impact in the study area.

During LPAZ S3b a decrease in arboreal pollen in particular of *Pinus* and a strong increase of heliophytes and Poaceae is observed accompanied by the continuous presence of *Cerealia* pollen and frequent occurrence of other anthropogenic indicators like *Plantago lanceolata, Plantago major/media* Type, *Artemisia, Rumex* and Chenopodiaceae (Behre 1981) and a further increase of *Calluna*. A Subboreal age can be concluded from the pollenspectra for LPAZ S3a whereas LPAZ S3b reveals a phase of intensive land use activities of late Subboreal, early Subatlantic times.

The OSL age of 3.9 ± 0.3 ka at the layer of fired clay in 97 cm, most probably indicates Late Neolithic cultural activities in the area of Seedorf during pollen subzone S3a (Tabs. 6, 7 and 8). The OSL age obtained from sample SEE 1-C (85 cm) (Tab. 3) of LPAZ S3b is around 2.6 ka and indicates a Late Subboreal age (Tab. 6) with evidence for Late Bronze Age to Iron Age settlement activities.

LPAZ S4 (62.5–49 cm) comprises the middle and upper part of the Bg2 horizon. It is characterized by a nearly total lack of *Pinus*, the dominance of Poaceae and terrestrial herbs, Cichoriaceae, Cerealia and the first occurrence of *Secale* (rye) pollen. Summer rye cultivation on sandy soils of Northern Germany since the Roman Iron Age has been demonstrated repeatedly by Behre (2000). Its regular cultivation in the study area since the 2nd century after Christ (AC) is known from archaeobotanical investigations of excavated sites by Kirleis (2003) and from peat bog pollen studies for northeast Lower Saxony (Kirleis 2003, Becker & Urban 2006). The OSL age of 2.5 ± 0.1 ka from 60 cm depth is in agreement with the Early Subatlantic pollenspectra indicative for ongoing land use activities and early rye cultivation.

LPAZ S5 (49–36.5 cm) is the youngest pollen zone describing the uppermost part of Bg2 and the lower and middle parts of the colluvial horizon Bg1. The upper part of this horizon as well as the Ap horizon have not been sampled for pollen and age determination because of ploughing and other land use activities in the valley. The local pollen assemblages are similar to those of LPAZ S4 except for increasing *Quercus* values and a richer heliophilous herb flora. The OSL ages for LPAZ S5 of 1.2 ± 0.1 ka and 1.0 ± 0.1 ka from 45 cm and 60 cm depth for the colluvium and the underlying Bg2 horizon (Tabs. 6, 7 and 8) are indicating another intensive accumulation phase which can be related to the Middle Age deforestation period (Tab. 9).

4 Discussion and Conclusion

In contrast to the loess areas in Germany (summarised in Gehrt 2000 and Eckmeier et al. 2007) little is known on the environmental history and role of people in soil-sediment genesis of the particular sand loess study area in the central Lüneburg Heathland.

E&G / Vol. 60 / No. 1 / 2011 / 6–26 / DOI 10.3285/eg.60.1.01

Subdivision of Holocene in Lower Saxony (Northern Germany)

Timescale (years BP)		Zonation Central Europe		Climate	Vegetation	Palynological evidence (Northern German lowland)	LPAZ Seedorf	Archaeology	cal. years BC/AD
		X	Late Subatlantikum	present climate	Intensive forest use and heath culture	plantation of pine forests cultivation of buckwheat cultivation of winter rye	S5	Present Time	+1950
1150				cool-humid	Fagus phase	increase of anthropogenic indicators and non-arboral pollen		Medieval	+1500 +1200 +1000
		IX	Early Subatlantikum					Migration Period	+700
								Roman Period	+400
2400				atlantic-oceanic	Quercus phase	rye	S4 S3b	Iron Age	0
		VIII	Subboreal	cooler dryer more continental	Corylus-Alnus phase	immigration of beech and hornbeam	S3a	Bronze Age	-800
5660	Holocene					elmfall		Neolithic	-2200
		VII	Atlantikum	humid atlantic-oceanic climate optimum	Quercetum mixtum phase (Quercus, Ulmus, Tilia, Corylus, Alnus)	first appearance of anthropogenic indicators	S2		-4000
9220		VI				increase of alder, oak, elm decrease of pine		Mesolithic	
		V	Boreal	dry continental	Corylus phase	first increase of hazel	S1		
10640									
		IV	Preboreal	temperate continental	Betula-Pinus phase	increase of birch and pine			-9000
11560									
12680	Weichselian Late Glacial	III	Dryas 3	cold	subarctic steppe, tundra			Paleolithic	
13500		II	Allerød	temperate	betula-pine forests (salix, populus)				
13540		Ic	Dryas 2	cold	herbs, open betula forests				
13670		Ib	Bølling	temperate	betula forests				
13800		Ia	Dryas 1	cold	steppe, tundra				

Based on LBEG (2004)

Table 9: Late Glacial and Holocene climate, vegetation, archaeological periods and local pollen assemblage zones of soil-sediment profile Schulwiese (Seedorf, Lower Saxony) (after Firbas, 1949, Iversen 1954, Litt et al., 2003).

Tabelle 9: Spätglaziale und holozäne Klimazonen, Vegetationszonen, archäologische Perioden und lokale Pollenzonen für das Profil Schulwiese in Seedorf (Niedersachsen) (nach Firbas, 1949, Iversen 1954, Litt et al., 2003)

By comparing textures of the loess colluvials of the investigated profiles with other sand loess deposits in Northern Germany and proximal areas (Fig. 14), it can be shown that the texture of Gleysol/Colluvisol *Schulwiese* reveals clayey, sandy silt whereas the Colluvisol/Stagnic Luvisol *Kartoffelfeld* has slightly higher sand content. Those differences are most probably due to the different depositional environments of site *Schulwiese* in a small flood plain and of the second higher elevated gently sloping plateau site *Kartoffelfeld* (Figs. 2 and 4). All horizons developed on colluvium as well as the buried A horizons situated in the valley bottom, are rich in organic Carbon and Nitrogen as well as in free Iron, which is indicative of the loess-soil borne younger material. Profile *Schulwiese* situated at the valley bottom at the margin of a small flood plain experienced at least three phases of relative unstable land surface and accumulation phases respectively.

The pollen assemblage zones do not reflect a continuously deposited sediment record, but the analysed pollen and spore assemblages derive from periods of temporary flooding, phases of pedogenetic processes under stable land surface as well as reflecting hiatuses caused by erosion. OSL ages and palynological data refer to Preboreal-Boreal times for the development of horizon 3Ahb/Crb and its parent material (Tab. 7). The radiocarbon age of cal BC 5081–4551 for horizon Crb2 and palynological results indicate a middle-younger Atlantic age. The OSL age of 3.9 ± 0.3 ka at the slightly higher level of 97 cm (horizon 2Ahb/Crb and 2Crb) suggests an early Subboreal age for the accumulation and soil development phase and dates the palynological evidence of Late Neolithic land use activities in the area of Seedorf (Fig. 13, Tabs. 6, 7 and 8). Roeschmann (in Kuntze et al. 1994) described soil development, erosion and accumulation of colluvium in the Northern German scattered sand loess areas as a product of initial Neolithic anthropogenically induced environmental changes. There is evidence of the Late Neolithic Funnel Beaker culture (3300–2700 BC, Hege & Maier 1991) for the area southwest and east of Lüneburg (Sprockhoff 1975, Schirnig 1979, Assendorp 1999) in the close vicinity to the study sites of Seedorf. *Calluna* (heather) is recorded from local pollen assemblage zone S3a as well as Cerealia pollen. Becker & Urban (2006) demonstrated temporary expansion of heathland as a consequence of agricultural land use and woodland pasture occurring during the latest Neolithic period at the beginning of the Bronze Age and in Medievel times for the southern part of the County of Uelzen.

The two OSL ages obtained from 85 cm and 60 cm (Tabs. 3 and 7) of around 2.6 ka date the local pollen assemblage zone S3b, which reveals a phase of intensive land use and consequently sediment accumulation due to erosion from settlement activities of Late Bronze and Iron Age cultural groups

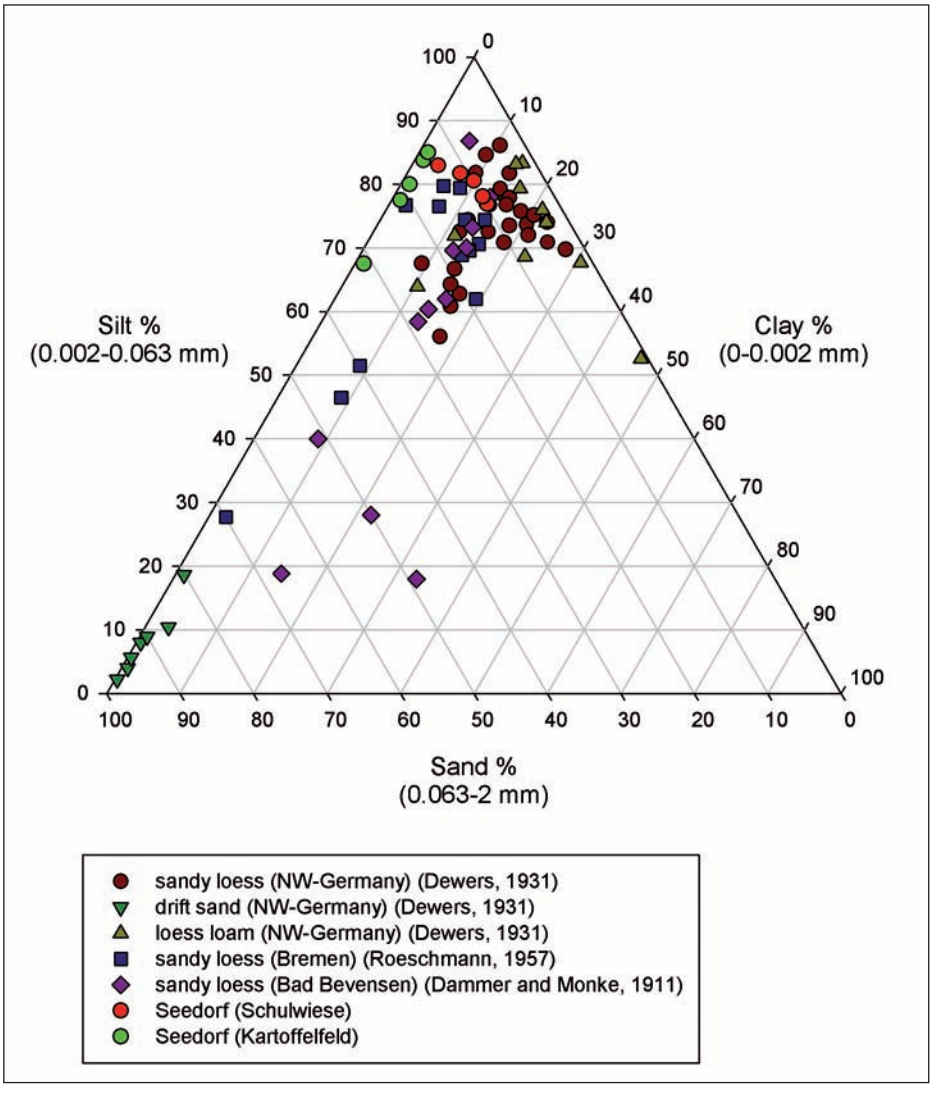

Fig. 14: Soil texture triangle showing different sand and loess sites in Northern Germany in relation to texture characteristics of profiles Schulwiese and Kartoffelfeld (Seedorf, Lower Saxony).

Abb. 14: Zusammenstellung verschiedener Proben aus Sand- und Sandlössgebieten in Norddeutschland und vergleich mit den Korngrössenuntersuchungen aus den Profilen Schulwiese und Kartoffelfeld (Seedorf, Niedersachsen).

E&G / Vol. 60 / No. 1 / 2011 / 6–26 / DOI 10.3285/eg.60.1.01 /

(Tabs. 6, 7 and 9). As there is local (Seedorf Cultural Stage, Schwantes 1952) and regional archaeological evidence of widespread Iron Age settlements attributed to the Jastorf culture (600–0 BC, Hässler 1991), this part of the profile *Schulwiese* clearly derives from a phase of intensive anthropogenic impact on the Late Subboreal/Early Subatlantic landscape, which is as well recorded from pollen diagrams of peat bogs and archaeobotanical investigations of sites close by (Kirleis 2003). Unexpected observations were made for the colluvial accumulation of Bw3 and Bw2 horizons of profile *Kartoffelfeld* (Tab. 8), which have been OSL dated to 4.6 ka and 2.6 ka corresponding most probably to the same Late Neolithic and Iron Age cultural periods, the latter one attributed to the Jastorf culture, found as well in profile *Schulwiese* (Tab. 7).

The latest severe erosional phase which resulted in the colluvium of profile *Schulwiese* (Tabs. 7 and 9, Fig. 12) was OSL dated to around 1 ka and corresponds with the Early and Late Medieval deforestation period, which is not recorded in the pollen diagram but well known from other research. Bork et al. (1998) describe a reduction of forest cover in Germany up to 17% at the time of 1300 AD due to extensive expansion of arable land.

The OSL age of 66.9 ± 4.5 ka for the parent material of horizons 2Bwb1/Bgb1and 2Btb/Bgb1 of sequence *Kartoffelfeld* points to an Early Weichselian depositional phase of sandy silty material and gives additional information about erosion processes since that time.

The results show evidence of human impact on soil development since the Neolithic which is shown by the black horizon in the *Schulwiese* profile. However, organic horizons are not mandatory for anthropogenic activities. Based on this study human impact on the widely distributed humic soils in the sandy loess area has to be accepted since the late Neolithic Bronze Age transition. Zolitschka et al. (2003) demonstrated that the first spread of Neolithic cultures in the loess areas of southern Germany was guided by soil quality. Their observations point to a change of that pattern towards the late Neolithic, when agriculture expanded all over and across central Europe, which coincides with the start of cooler and moister climatic conditions. Our results deduced from soil sediment archives suggesting four post-Neolithic main periods, the early Bronze Age, the pre-Roman and the Roman Iron Age and the early to late Medieval of increasing human environmental impact and settlement in the sandy loess region of the Lüneburg Heathland (Tabs. 7, 8 and 9), which are in good accordance with findings made in colluvial, fluvial and lacustrine archives of other reference areas in Germany described by Zolitschka et al. (2003).

More work on other sites of the Lüneburg Heathland is required to prove and refine our results and furthermore to separate the humic horizons from modern Plaggen soils.

5 Acknowledgements

We thank Christiane Hilmer, Suderburg for valuable help with laboratory treatment of the samples and soil analyses and Katrin Becker for her assistance with the palynological work. We are very thankful to Mario Tucci, Suderburg who helped draft graphs and figures. We finally like to thank Professor Peter Kershaw, Monash University, Australia for correcting the English manuscript and the two reviewers for their valuable advice.

6 References

Adamiec, G. & Aitken, M. (1998): Dose-rate conversion factors: update. – Anc. TL, 16: 37–50; Aberystwyth.

Aitken, M. J. (1998): An introduction to optical dating. – 267 S.; Oxford (Oxford University Press).

Assendorp, J.J. (1999): Die Häuser der Trichterbecherkultur in Nordostniedersachsen. – Ber. Denkmalpfl. Niedersachs., 19: 180–185; Hameln.

Becker, K. (1995): Paläoökologische Untersuchungen in Kleinmooren zur Vegetations- und Siedlungsgeschichte der zentralen Lüneburger Heide. – 159 S.; Diss. Univ. Hannover.

Becker, K. & Urban, B. (2006): Jungholozäne Umweltentwicklung und Landnutzungsgeschichte im Hardautal, Ldkr. Uelzen (südliche Lüneburger Heide). – TELMA, 36: 11–38; Hannover.

Behre, K.-E. (1981): The interpretation of anthropogenic indicators in pollen diagrams. – Pollen et Spores, 23: 225–245; Paris.

Behre, K.-E. (2000): Frühe Ackersysteme, Düngemethoden und die Entstehung der nordwestdeutschen Heiden. – Arch. Korrbl., 30: 135–151; Mainz.

Beug, H.-J. (2004): Leitfaden der Pollenbestimmung für Mitteleuropa und angrenzende Gebiete. – 542 S.; München (Pfeil-Verlag).

Blume, H.-P. & Leinweber, P. (2004): Plaggen Soils: landscape history, properties, and classification. – J. Plant Nutr. Soil Sci., 167: 319–327.

Bork, H.-R., Bork, H., Dalchow, C., Faust, B., Piorr, H.-P. & Schatz, T. (1998): Landschaftsentwicklung in Mitteleuropa. – 328 S.; Gotha (Klett-Perthes).

Caspers, G., Jordan, H., Merkt, J., Meyer, K.-D., Müller, H. & Streif, H. (1995): Niedersachsen. In: Benda, L. (Hrsg.): Das Quartär Deutschlands: 23–58; Stuttgart (Borntraeger).

Chen, C.-T. A., Wann, J.-K. & Lou, J.-Y. (2001): Aeolian flux of metals in Taiwan in the past 2600 years. – Chemosph., 43: 287–294; Amsterdam.

Dammer, B. & Monke, H. (1911): Erläuterungen zur Geologischen Karte von Preußen und benachbarten Bundesstaaten – Blatt Bienenbüttel. – 67 p.; Berlin (Königlich Preußische Geologische Landesanstalt).

Dewers, F. (1932): Flottsandgebiete in Nordwest-Deutschland, Ein Beitrag zum Lössproblem. – Abh. Naturwiss. Ver. Bremen, 28: 131–204; Bremen

Eckmeier, E., Gerlach, R., Gehrt, E. & Schmidt, M.W.I. (2007): Pedogenesis of Chernozems in Central Europe – a review. Geoderma, 139: 288–299; Amsterdam.

Faegri, K. & Iversen, I. (1989): Textbook of pollen analysis. – 338 p.; London (John Wiley & Sons).

Fiedler, H. J. & Altermann, M. (1964): Verbreitung, Entstehung und Eigenschaften von Sandlöss (Flottsand) im norddeutschen Flachland und angrenzenden Gebieten. – Geologie, 13: 1199–1226; BerliFirbas, F. (1949/52): Spät- und nacheiszeitliche Waldgeschichte Mitteleuropas nördlich der Alpen (2 Bde.). – 480+256 p.; Jena (Fischer).

Frechen, M., Oches, E. A. & Kohlfeld, K. E. (2003): Loess in Europe – mass accumulation rates during the Last Glacial Period. – Quat. Sci. Rev., 22: 1835–1857; Amsterdam.

Frechen, M., Schweitzer, U. & Zander, A. (1996): Improvements in sample preparation for the fine grain technique. – Anc. TL, 14: 15–17; Aberystwyth.

Geebers, W. (1995): Fünfzehn Jahre Grabung Rullstorf, eine Bilanz. – Ber. Denkmalpfl. Niedersachs., 6: 65–60; Hameln.

Gehrt, E. (2000): Nord- und mitteldeutsche Lössbörden und Sandlössgebiete. – In: Blume et al. (1995): Handbuch der Bodenkunde, 9. Erg.-Lfg. 10/2000; Weinheim (Wiley-VCH).

Geyh, M. A. (2005): 14C dating - still a challenge for users? – Z. Geomorph. N.F. Suppl., 139: 63–85; Berlin.

Grimm, E. (1990): TILIA, TILIAGRAPH & TILIAVIEW. PC spreadsheet and graphics software for pollen data. Illinois State Museum, IL, USA. (http://www.geo.arizona.edu/palynology/geos581/tiliaview.html)

Hässler, H.-J. (1991): Vorrömische Eisenzeit. – In: Häßler, H.-J. (Ed.):Ur- und Frühgeschichte in Niedersachsen: 193–237; Stuttgart (Theiss).

Hagedorn, J. (1964): *Geomorphologie des Uelzener Beckens.* – Göttinger geogr. Abh., 31: 200 p. Göttingen.

Heege, E. & Maier, R. (1991): Jungsteinzeit. – In: Häßler, H.-J. (Ed.): Ur- und Frühgeschichte in Niedersachsen: 109–154; Stuttgart (Theiss).

Holmgren, G.G. (1967): A rapid citrate-dithionite extractable iron procedure. – Soil Sci. Soc. Am. Proc., 31: 210–211; Madison.

Huntley, D. J. & Lamothe, M. (2001): Ubiquity of anomalous fading in K-feldspars and the measurement and correction for it in optical dating. – Can. J. Earth Sci., 38: 1093–1106; Ottawa.

IUSS Working Group WRB (2006): World Reference Base for Soil World Resources 2006. – World Soil Resources Report, 103; Rome (FAO).

Iversen, J. (1954): Late-Glacial Flora of Denmark and its relation to climate and soil. – Danmarks Geologiske UndersØgelske, II. Række, 80: 87–119; Kopenhagen.

KA5 (2005): AG Boden – Bodenkundliche Kartieranleitung. – 438 S.; Stuttgart (Schweizerbart).

Kalis, A. J., Merkt, J. & Wunderlich, J. (2003): Environmental changes during the Holocene climatic optimum in central Europe – human impact and natural causes. – Quat. Sci. Rev., 22: 33–79; Amsterdam.

Kirleis, W. (2003): Vegetationsgeschichtliche und archäobotanische Untersuchungen zur Landwirtschaft und Umwelt im Bereich der prähistorischen Siedlungen bei Rullstorf, Ldkr. Lüneburg. – Probl. Küstenforsch. südl. Nordseegeb., 28: 65–132; Oldenburg.

Kucz, V. (2006): Erstellung einer bodenkundlichen Bestandsanalyse und Berechnung der Bodenerosion mithilfe der allgemeinen Bodenabtragsgleichung (ABAG) im nördlichen Teil des Landkreises Uelzen, Gemeinde Seedorf. – Diploma Thesis, LEUPHANA University Lüneburg; unpublished.

Kuntze, H., Roeschmann, G. & Schwerdtfeger, G. (1994): Bodenkunde. – 424 S.; Stuttgart (Ulmer).

Lang, H. D. (1974): Über Verbreitung, Zusammensetzung und Alter des Sandlösses im Raum Wittingen-Hankensbüttel. – Z. Dtsch. Geol. Gesellsch., 125: 269–276; Hannover

Lang, H. D. (1990): Der Sandlöss in der Umgebung von Bergen Krs. Celle – Verbreitung, Zusammensetzung und Entstehung. – Eiszeitalter und Gegenwart, 40: 97–106; Öhringen/Württ.

Litt, T., Schmincke, H.-U. & Kromer, B. (2003): Environmental response to climate and volcanic events in central Europe during the Weichselian Lateglacial. – Quaternary Science Reviews, 22: 7–32; Oxford.

Mauz, B. & Lang, A. (2004): The dose rate of beta sources for optical dating applications: a comparison between fine silt and fine sand quartz. – Anc. TL, 22: 45–48; Aberystwyth.

Mauz, B., Packman, S. & Lang, A. (2006): The alpha effectiveness in silt-sized quartz: new data obtained by single and multiple aliquot protocols. – Anc. TL, 24: 47–52; Aberystwyth.

Moore, P.D.; Webb, J.A. & Collins, M.E. (1991): Pollen analysis. – 224 S.; Oxford (Blackwell Scientific Publications). Munsell Soil Color Charts. Baltimore, U.S.A.

Murray, A. S. & Wintle, A. G. (2000): Luminescence dating of quartz using an improved single-aliquot regenerative-dose protocol. – Radiat. Meas., 32: 57–73; Oxford.

Murray, A. S. & Wintle, A. G. (2003): The single aliquot regenerative dose protocol: potential for improvements in reliability. – Radiat. Meas., 37: 377–381, Oxford.

Page, A. L., Miller, R. H., Kennedy, D. R., Baker, D. E., Ellis, R. & Rhoades, J. D. (Hrsg.) (1982): Methods of Soil analysis. Part 2. chemical and microbiological properties. – 1159 S., Madison (Soil Science Society of America).

Pécsi, M. (1990): Loess is not just the accumulation of dust. – Quat. Int., 7/8: 1–21; Amsterdam.

Prescott, J. R. & Hutton, J. T. (1994): Cosmic ray contributions to dose rates for luminescence and ESR dating: large depths and long-term time variations. – Radiat. Meas., 23: 497–500, Oxford.

Prescott, J. R. & Stephan, L. G. (1982): The contribution of cosmic radiation to the environmental dose for thermoluminescent dating – Latitude, altitude and depth dependences. – PACT, 6: 17–25; Strasbourg.

Rees-Jones, J. (1995): Optical dating of young sediments using fine-grain quartz. – Anc. TL, 13: 9–14, Aberystwyth.

Reimer, P. J., Baillie, M. G. L., Bard, E., Bayliss, A., Beck, W. J., Bertrand, C. J. H., Blackwell, P. G., Buck, C. E., Burr, G. S., Cutler, K. B., Damon, P. E., Edwards, R. L., Fairbanks, R. G., Friedrich, M., Guilderson, T. P., Hogg, A. G., Hughen, K. A., Kromer, B., McCormac, G., Manning, S., Bronk Ramsey, C., Reimer, R. W., Remmele, S., Southon, J. R., Stuiver, M., Talamo, S., Taylor, F. W., van der Plicht, J. & Weyhenmeyer, C. E. (2004): Intcal04 terrestrial radiocarbon age calibration, 0–26 cal kyr BP. – Radiocarbon, 46: 1029–1058; Tuscon.

Richter, P. B. (2002): Das neolithische Erdwerk von Walmstorf, Ldkr. Uelzen: Studien zur Besiedlungsgeschichte der Trichterbecherkultur im südlichen Ilmenautal. – Veröff. d. Urgesch. Samml. Landesmus. Hannover, 49: 90 S.; Oldenburg (Isensee).

Roberts, H. M. (2008): The development and application of luminescence dating to loess deposits: a perspective on the past, present and future. – Boreas, 37: 483–507.

Roeschmann, G. (1957): Die Bodenbildung auf dem Flottsand im Bereich des Großblattes Bremen 1:100 000. 53 p.; Hannover (Amt für Bodenforschung).

Schirnig, H. (1979): Die Siedlung auf dem schwarzen Berg bei Wittenwater, Kreis Uelzen. H. Schirnig (Ed.), Großsteingräber in Niedersachsen. – Veröff. d. Urgeschich. Samml. Landesmus. Hannover, 24: 244–246; Oldenburg (Isensee).

Schwantes, G. (1952): Die Seedorf-Stufe. – In: Kivikoski, E. (Hrsg..): Corolla archaeologica in honorem C.A. Nordman. 68–76 S., Helsinki.

Spooner, N. A. (1994): The anomalous fading of infrared-stimulated luminescence from feldspars. – Radiat. Meas., 23: 625–632; Oxford.

Sprockhoff, E. (1975): Atlas der Megalithgräber Deutschlands 3. Niedersachsen – Westfalen. Textband. Bonn (Habelt).

Stuiver, M. & Reimer, P. J. (1993): Extended 14C data base and revised Calib 3.0 14C age calibration program. – Radiocarbon, 35: 215–230; Tuscon.

van Geel, B. (1978): A palaeoecological study of Holocene peat bog sections in Germany and the Netherlands. – Rev. Palaeobot. Palynol., 25: 1–120; Amsterdam.

van Geel, B. (2001): Non-pollen palynomorphs. In: Smol, J.P., Birks, H.J.B. & Last, W.M. (Hrsg.): Tracking Environmental Change Using Lake Sediments, Volume 3: Terrestrial, Algal, and Siliceous Indicators. 99–119 S.; Dordrecht (Kluwer Academic Publishers).

van Reeuwijk, L.P. (Ed.), (1992): Procedures for Soil Analysis. Wageningen (ISRIC).

Visocekas, R. (2002): Tunnelling in afterglow, its coexistence and interweaving with thermally stimulated luminescence. – Radiat. Prot. Dosim., 100: 45–54; Oxford.

Visocekas, R., Spooner, N. A., Zink, A. & Blanc, P. (1994): Tunnel afterglow, fading and infrared emission in thermoluminescence of feldspars. – Radiat. Meas., 23: 377–385; Oxford.

Wallinga, J., Bos, A. J. J., Dorenbos, P., Murray, A. S. & Schokker, J. (2007): A test case for anomalous fading correction in IRSL dating. – Quat. Geochronol., 2: 216–221; Amsterdam.

Wintle, A. G. (1973): Anomalous fading of thermoluminescence in mineral samples. – Nature, 245: 143–144; London.

Zolitschka, B., Behre, K.-E., Schneider, J. (2003): Human and climatic impact on the environment as derived from colluvial, fluvial and lacustrine archives – examples from the Bronze Age to the Migration period, Germany. – Quat. Sci. Rev., 22: 81–100.

E&G Quaternary Science Journal
Volume 60 / Number 1 / 2011 / 27–46 / DOI 10.3285/eg.60.1.02
www.quaternary-science.net

GEOZON SCIENCE MEDIA
ISSN 0424-7116

Spatial analysis of loess and loess-like sediments in the Weser-Aller catchment (Lower Saxony and Northern Hesse, NW Germany)

Bianca Wagner

Abstract: A spatial compilation and visualization of loess parameters was carried out for the Pleistocene loess and loess-like sediments in the Weser-Aller catchment (southern Lower Saxony and northern Hesse, NW Germany), one of the loess regions of Central Europe. As far as available, data about main loess characteristics like thickness, granulometry and stratigraphy were combined for the first time with spatial information extracted from maps. Data storage and analysis in a geographical information system (GIS) permitted creation of large-scale thematic loess maps.
The loess thickness map displays an increase of the thickness in valleys and basins and from north to south. The granulometry map presents main granulometrical facies types of the loess cover. Furthermore, several loess locations with unusual thickness were identified and their special geological and geomorphological conditions are discussed.
In summary, the loessic sediments in the northern part of the study area are of Upper Weichselian age, whereas in the southern upland regions incomplete or detailed Weichselian loess sequences were identified. In conclusion, highly detailed maps of regional loess-property patterns can be created even if only heterogeneous historically published data are taken into account.

[Räumliche Analyse von Lössen und löss-ähnlichen Sedimenten im Weser-Aller-Einzugsgebiet (Süd-Niedersachsen und Nord-Hessen, NW-Deutschland)]

Kurzfassung: Eine räumliche Kompilation und Darstellung von Löss-Parametern wurde für die pleistozänen Lösse und löss-ähnlichen Sedimente im Weser-Aller-Einzugsgebiet (Süd-Niedersachsen und Nordhessen, NW-Deutschland), einer der Lössregionen in Mitteleuropa, durchgeführt. Erstmals wurden Daten, soweit verfügbar, über die wichtigsten Lösseigenschaften, wie Mächtigkeit, Granulometrie und Stratigraphie mit räumlichen Informationen von Karten kombiniert und ausgewertet. Die Datenerfassung und – analyse in einem Geographischen Informationssystem (GIS) ermöglichte die Ableitung großformatiger thematischer Lösskarten.
Daten über Lössmächtigkeiten wurden analysiert und zu einer regionalen Mächtigkeitskarte kompiliert. Zusätzlich dazu wurden zahlreiche Lössvorkommen mit anormaler Mächtigkeit aufgrund spezieller geologischer und geomorphologischer Bedingungen abgegrenzt. Mehrere Lössregionen mit unterschiedlicher granulometrischer Fazies wurden ausgeschieden. Zudem konnten regionale Lössdecken unterschiedlichen Alters kartiert werden. Die Lössdecken im nördlichen Teil des Untersuchungsgebietes haben jungweichselzeitliches Alter, dagegen wurden im Bergland Regionen mit unvollständigen und gut gegliederten weichselzeitlichen Lössabfolgen nachgewiesen. Die Ergebnisse der Untersuchung zeigen, dass auf der Grundlage veröffentlichter, heterogener Daten neue Aspekte und regionale Muster abgeleitet werden können.

Keywords: *loess, loess-like deposits, Pleistocene, Weichselian, spatial analysis, NW Germany*

Address of author: **B. Wagner**, Department of Applied Geology, Geoscience Centre Göttingen, University of Göttingen, Goldschmidtstr. D-37077 Göttingen, Germany. E-Mail: bwagner1@gwdg.de

1 Introduction

Loess and loess related sediments cover wide parts of Europe. In North-Western and Central Europe they form a continuous loess belt, trending roughly in ESE-WNW direction. The belt is limited by a northern and southern boundary (Haase et al. 2007). In Germany, the northern boundary of the loess belt runs north of the Rhenish Massif, the Harz Mountains and the Ore Mountains and separates the loess and loess-like sediments from cover sands and drift sands (Eissmann 2002, Haase et al. 2007). Five main loess regions adjoin to the northern boundary. These are from west to east the lower Rhine area, southern parts of the Weser-Aller catchment (southern Lower Saxony and northern Hesse), the loess region northeast of the Harz Mountains (Saxony-Anhalt) and the loess region north of the Ore Mountains (Saxony).

The loess and loess related sediments in the Weser-Aller catchment were the subject of many mapping campaigns and studies. Grupe (1916a) and Seltzer (1936a, 1936b) recognized different layers, paleosols and ice-wedge pseudomorphs in the loess outcrops and tried to distinguish loessic sediments of different ages. Schönhals, Rohdenburg & Semmel (1964) published a detailed stratigraphy of the loesses in Hesse that is based on paleosols and tephra. Rohdenburg & Meyer (1966) extended the Eemian and Weichselian part of the pedostratigraphy to southern Lower Saxony and northern Hesse. Rohdenburg (1966) added ice-wedge pseudomorphs. Subsequently, new facies types (Breinum soil, Hattorf soil, Alversdorf soil) of the Middle Weichselian Lohne soil were described by Bartels & Rohdenburg (1968), Ricken & Meyer (1982), Ricken (1983) and Brosche & Walther (1978, 1991).

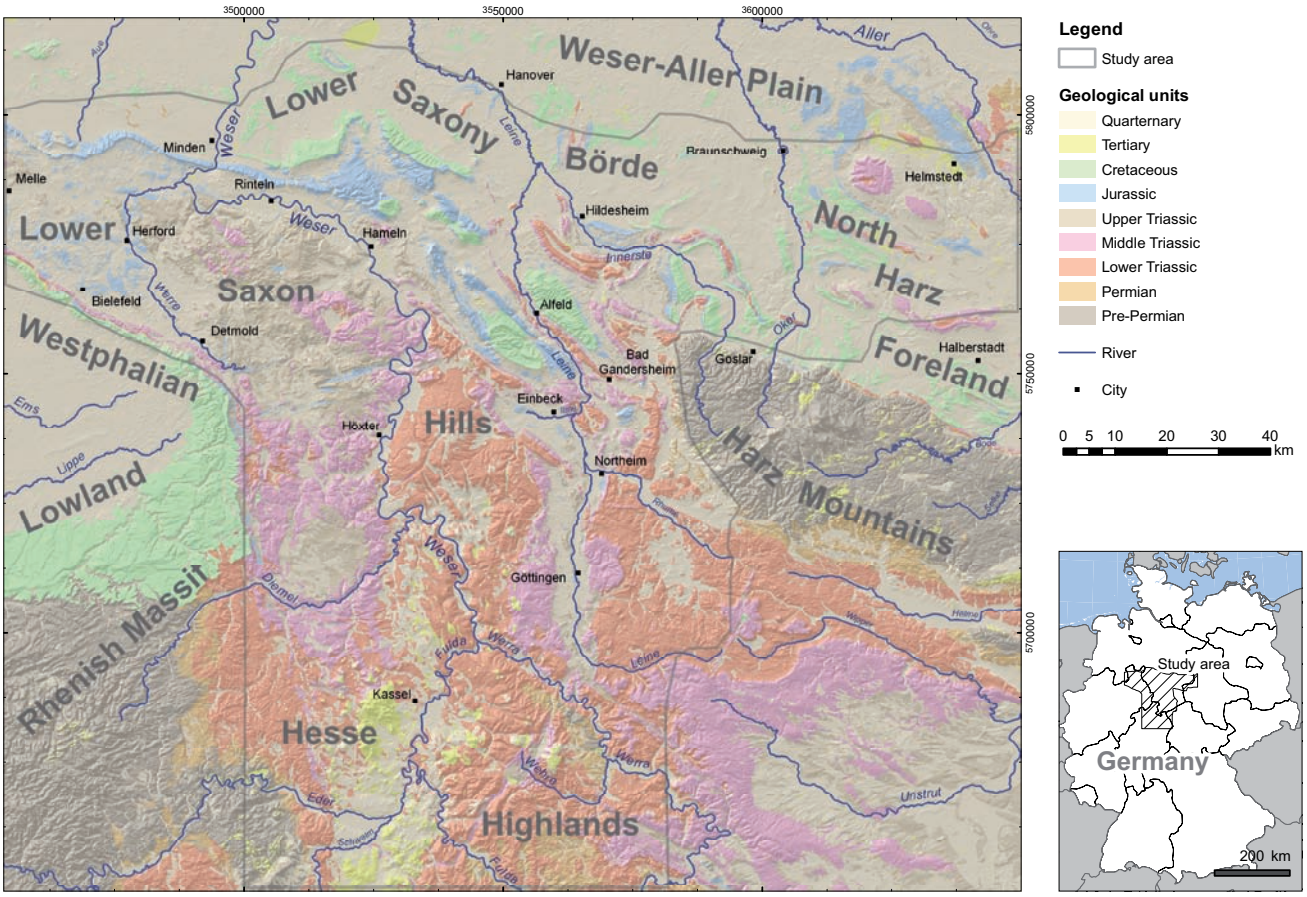

Fig. 1: Outline, main geological units and shaded relief of the study area. (DEM: ASTER GDEM is a product of METI and NASA; river network: OpenStreetMap, published under CC-BY-SA 2.0)

Abb. 1: Umriss, geologische Haupteinheiten und beleuchtetes Geländemodell des Untersuchungsgebietes. (DGM: Globales ASTER-DGM ist ein Produkt von METI und NASA, Flussnetzwerk: OpenStreetMap, veröffentlicht unter CC-BY-SA 2.0)

Ricken & Grüger (1988) verified the age of the oldest palaeosols based on a transition between dated lake sediments and paleosols of Eemian and Early Weichselian age. Roeschmann et al. (1982) published a compiled overview of the paleosols in Lower Saxony and Bremen. This loess stratigraphy was proven and correlated with other regions (e.g. Ricken 1983).

In the following years scientists mapped and published a lot of detailed individual loess sections or outcrops in smaller areas based on the above mentioned pedostratigraphy. Brosche & Walther (1978) examined and correlated sections in the brown-coal opencast pits near the northern loess boundary. Jauhiainen & Brunotte (1978), Schwartau (1978, 1979) and Brunotte & Jauhiainen (1979) described a complete Upper Weichselian section in the Leine valley. Ricken & Meyer (1982) and Ricken (1983) studied the loess cover and paleosols in the Southwest Harz Foreland and the Eichsfeld.

In northern Hesse Jacobshagen, Huckriede & Jacobshagen (1963), Bosinski (1969), Kulick & Semmel (1968) and Bosinski & Kulick (1973) analyzed archeological and paleontological findings in loess sections. Semmel (1967) reported new findings of Eltville tephra in Hesse and he published a summary of the loess sections in Hesse in 1968. Brosche & Walther (1980) studied loess outcrops in the Weser valley.

Furthermore, some isolated deposits of Lower or Middle Pleistocene age, not included by the pedostratigraphy of Rohdenburg & Meyer (1966), were examined. Most of the loess remnants survived due to special conditions, e.g. in grabens or subrosive sediment traps. Moreover, they contain paleosols or are intercalated with interglacial sediments. Lüttig (1960a), Jordan & Schwartau (1993) and Grüger et al. (1994) investigated such deposits in the Leine valley. Lüttig & Rein (1955), Lüttig (1965) and Bittmann & Müller (1996) analyzed the interglacial sediments and loesses in the Bilshausen clay pit in the Southwest Harz Foreland. Sabelberg et al. (1976) and Mahaney, Andres & Barendregt (1993) studied the stratigraphically important Dreihausen paleosol sequence in northern Hesse.

The loess and loess related sediments along the northern boundary contain no Eltville tephra and no paleosols of Weichselian age. Therefore, the pedostratigraphical scheme of Rohdenburg & Meyer (1966) can not be applied on these sediments. Gehrt (1989, 1992, 1994) mapped the loess near the boundary between the Leine and Oker valley. He found vertical and horizontal zones of different lithology and age. As a result, he defined a lithostratigraphy of this marginal facies. Hilgers et al. (2001) carried out luminescence dating in order to establish a chronostratigraphy for these loess and sandy-loess sediments.

Beside these stratigraphic investigations the authors tried to analyze the spatial properties of loess and to subdivide the loess region into subregions. Wortmann (1942) published the first loess map of Lower Saxony based on small-scale soil maps displaying sediment lithology and thick-

ness. Merkt (1968) published a new version of a loess distribution map of southern Lower Saxony and adjacent regions. In contrast to Wortmann (1942), he exploited small-scale geological maps and unpublished material.

Müller (1961), Niederbudde (1976) and Siebertz (1988) analyzed loess properties (e.g. grain size distribution, mineral composition) to outline regional zones within the loess cover. Beside this, scientist tried to distinguish regions that show differences in paleosols, lithology or sequences. They aimed to determine climatic differences and trends. For example, Rohdenburg & Meyer (1966) published outcrop maps, maps of the Lohne soil distribution and described wet and dry loess provinces based on paleosols facies. Furthermore, Walther & Brosche (1983) gave an extended compilation of stratigraphical columns including climatic interpretation near the northern loess boundary. Brosche & Walther (1991) mapped a large number of loess sections in Lower Saxony and north-eastern North Rhine-Westphalia. They provided many details for the regional loess stratigraphy and to the geomorphological periods during the Weichselian. Correlation of loessic, solifluction deposits, fluvial and glaciofluvial sediments in the North Harz Foreland combined with luminescence dating was published by Reinecke (2006).

In spite of the huge dataset only few regional graphical presentations, e.g. location maps, distribution maps, facies maps (Rohdenburg & Meyer 1966, Walther & Brosche 1983, Brosche & Walther 1991), or maps, displaying the distribution of marker horizons like the Lohne soil or the Eltville tephra, were compiled. The available geological or loess maps give only limited information about the third dimension (e.g. thickness, loess sequences or the age of the loess deposits). In contrast to the regional overview of the loess properties in Eastern Germany by Eissmann (2002), there is no recent compilation of such data for Northwestern Germany.

The aim of this study is a regional overview of the main loess characteristics (granulometry, thickness and stratigraphy) in the Weser-Aller catchment which is based on all available descriptive or graphical data. The second objective of the investigation is a spatial analysis of the existing data in order to recognize spatial patterns of regional scale. The following questions are addressed:

- May spatial information be extracted from published data?
- To which level of spatial and qualitative accuracy can the data be extracted over the extended area?
- Can regional ages of the loess cover be estimated, if there are only few numerical ages available?

2 Background

Study area

The study area is located in Northwest Germany covering an area of about 17,800 km² (Fig. 1). It comprises the southern part of the Northwest German Plain and the northern part of the Northwest Central Uplands. The study area is bordered by the Harz Mountains, the Thuringian Basin, the Vogelsberg Mountains, the Rhenish Massif and the Westphalian Lowlands. The rivers Weser and Aller and their tributaries drain wide parts of the study area. The elevation ranges from 30 m a.s.l. in the North to 730 m a.s.l in the South.

The area is subdivided into the northern lowland and the southern mountainous region. The northern part comprises the Weser-Aller Plain, the Lower Saxony Börde and parts of the northern Harz Foreland. The region is covered by extended Pleistocene and Holocene sediments. The underlying Tertiary to Mesozoic sedimentary rocks are exposed in a few ridges or hills only (Fig. 1).

The southern mountainous area is subdivided into the Lower Saxon Hills including Weser and Leine Hills (or Weser-Leine Uplands) and the northern Hesse Highlands. In the higher parts, ridges or hills with marine to terrestrial sedimentary rocks of Upper Palaeozoic to Tertiary age are exposed. In the South mainly Triassic rocks crop out, whereas to the North mainly Jurassic to Cretaceous rocks are exposed. Weak to strong tectonic overprint of the pre-Quaternary rocks is evidenced by normal faults and grabens, inverse faults, thrusts and folds. The tectonic pattern is also influenced and complicated by strong halokinetic processes like salt movements, salt dissolution, and salt intrusion in relation to the various salt-bearing Permian to Mesozoic strata. These processes are still ongoing. The main tectonic directions, visible in the orientation of the large folds, faults, ridges and valleys are NW-SE, N-S and NE-SW. This complex geology of the pre-Quaternary bedrock results in a heterogeneous, small-scale regional pattern of valleys, hills, basins and grabens. Quaternary sediments were mainly accumulated in the valleys, on slopes and in upland basins or marginal basins.

The distribution of the Pleistocene sediments is characterized by three important boundaries (Fig. 2). The northern boundary of the loess belt runs along the line Melle – Minden – Hanover – Braunschweig – Helmstedt. It separates the almost continuous cover of loess and loess-like sediments in the South from regions in the North, where predominantly cover sands and drift sands were deposited. The southern boundaries of the Elsterian and Saalian glaciation cross the study area along a line Rinteln – Alfeld – Seesen – Goslar (Kaltwang 1992). They separate the periglacial Pleistocene sediments in the South from the glacial, glaciofluvial, periglacial and fluvial deposits in the North. The ice-shield of the Weichselian glaciation did not extend to the study area.

Aeolian sediments

The aeolian sediments of the study area can be subdivided by their grain-size distribution into aeolian loess, sand-banded loess, sandy loess, and cover sand (Vierhuff 1967, Weise 1983). In general, the light-coloured, calcareous, unstratified, loess contains more than 15 % of silt (medium to coarse silt), less than 15 % sand (0,063–2 mm), and clay. The sandy loess consists of more than 15 % sand and more than 15 % silt (maxima in medium to coarse silt). The sand-banded loess is a stratified mixture of loess and sandy-loess. During the last century local German names, like "Flottsand" and "Flottlehm" were used for sandy loess. These terms are not exactly defined and used by different authors for different aeolian sediments (Wortmann 1942, Siebertz 1982, Siebertz 1992). Generally "Flottlehm" is a silt-rich sandy loess and "Flottsand" a sand-rich sandy loess (Gehrt 1994). Cover sand has an even higher sand content.

Apart from these, some more loess-like deposits are rel-

evant, which were originated from loess by different processes. Loamy loess or loess loam is loess which was decalcified during weathering and soil genesis. Soliflucted reworked loess was generated by downslope movement during gelifluction or solifluction, which results in a mixed, banded or chaotic structure with possible higher amounts of clay, sand, or blocky gravel from over- or underlying material. The colour is strongly influenced by the amount of these contaminants. When aeolian loess is eroded and transported by water, fluvially reworked loess with a striated structure and gravel or sand intercalations will be deposited.

A special type of aeolian deposition is represented by mixed layers of glacial loam, sand, and silt on top of unweathered glacial till. Many authors interpret their fine sand and silt content as aeolian relics, reworked and incorporated in these layers. This "Geschiebedecksand" may have a basal stone layer, fluvial structures and cryoturbation features.

Loess regions

The northernmost part of the loess belt investigated comprises the "Börde" – a loess-rich region between the northern loess boundary and the slopes of the Lower Saxon Hills and the Harz Mountains (Fig. 2). The almost flat plain ascends slightly to the South. It is underlain by thick glacial, glacio-fluvial and periglacial sediments. The region is structured only by few ridges or swells of Mesozoic bedrock (Fig. 1).

The Börde is 6 to 30 km wide in North-South direction and separated by the Weser, Leine, Innerste, and Oker valleys into different segments: the narrow Lübbecke Löss Börde, the A-shaped Calenberg Löss Börde and the Braunschweig-Hildesheim-Börde. The Börde zone merges east of Helmstedt into the Magdeburg Börde. The loess accumulated all over the lowland and on most slopes, only dissected by drainage networks.

The Elm-Asse-Helmstedt region east of the Hildesheim-Braunschweig-Börde also borders to the northern boundary of the loess belt. This region is characterized by a quite different morphology more similar to the upland dominated by several NW-SE-trending anticlines and synclines of folded Mesozoic to Tertiary sedimentary rocks, where the Elm and the Asse are the largest domes. Due to the undulating morphology the loess cover is not continuously, loess is enriched in valleys and slopes, basins and lower ridges (Merkt 1968). According to Wortmann (1942) there is also loess on the higher parts of the slopes, even on the hills and ridges, e.g. parts of the Elm.

Some areas, which are separated from the loess boundary by ridges and small uplands or those located in the Lower Saxon Hills, have a Börde-like appearance. This includes a huge, extended loess cover and wide, flat areas with smooth or undulating morphology. The loess cover is only dissected by the recent drainage network or influenced by some steeper ridges or slopes. There is the wide region between the Harz Mountains and the anticlines in its foreland and the Ravensburg Hills, a long stripe between the Wiehen Hills, the Tecklenburg-Osning and the Wehre valley in the easternmost part of the study area.

In contrast, the uplands south of the Calenberg Börde and the Hildesheim-Braunschweig Börde, the so called Leine Uplands, show a more pronounced morphology which is caused by synclines, anticlines, and thrusts of folded Mesozoic rocks. The Leine Uplands are subdivided by the narrow Leine and Innerste valley into the Calenberg Uplands, Alfeld Uplands and Innerste Uplands. According to Merkt (1968) loess covers the flat regions, the north-eastern and northern slopes and few south-western slopes of the elongated valleys and hills up to 200 to 250 m altitude and is accumulated in some grabens and subrosion-related structures.

The morphology of the above mentioned long and narrow valleys and basins is quite different from the more irregular and diverse loess accumulation sites in the central parts of the upland. The deposition structures of various sizes and shapes occur mainly within plateaus of Triassic sedimentary rocks, which are dissected by several faults and influenced by subrosion activities. The loess was accumulated in the shallow basins, in sinks, tectonic grabens, and mainly on eastern, north-eastern, and northern slopes up to 230 to 270 m altitude, and in drainage features. The higher ridges, hills, and steep slopes are free of loess. The situation is typical for the Lower Eichsfeld Basin, the Uslar Basin, and the Warburg Börde but is also found within the Lippe Upland, the Pyrmont Uplands and Oberwälder Land, and the Waldeck Uplands and Plains.

Apart from these small-scale irregular and shallow loess accumulation structures wide and extended depressions occur within the Uplands. They were filled with Tertiary and Quaternary sediments during long-lasting periods of subsidence caused by tectonic or halokinetic processes. Loess accumulated within the depressions mainly on the eastern slopes. Large depressions are located in the Leine-Ilme Basin and the West Hessian Depression.

Southwest of the Harz Mountains there are marginal basins with Tertiary fillings and strong subsidence. The basins are smaller and show a small-scale pattern of valleys and ridges. Typical for this type is the triangular Southwest Harz Foreland between the Alfeld Uplands and the Harz Mountains. Common subrosion and karst features are related to highly soluble Permian sulphate and carbonate rocks. Loessic sediments cover the plains, the basins, the valleys and the slopes up to 200 to 300 m in elevation.

The main river valleys within the Lower Saxon Hills and the Hesse Highlands are also distinct, morphological traps for loess deposition. They are treated as separate loess regions in this study. The valleys of the rivers Weser, Fulda, Werra and Leine are rich in loess compared to the adjacent regions.

The upper Leine valley between Göttingen and Einbeck, South of the Leine-Ilme Basin, is mainly influenced by the complex structure of the N-S-striking Leine valley Graben. The wide valley with the distinct, fault-related slopes has a closed loess cover, quite different from the adjacent hills. The valleys of the rivers Fulda, Werra and Werre in the Southeast of the study area follow tectonic structures in a small-scale pattern of NW-SE-trending faults and fractures. The loess accumulated in the narrow and steep valleys, especially on the western or north-western side up to 250 m in elevation. The bedrock consists of Lower Triassic sandstones and subordinate Paleozoic rocks.

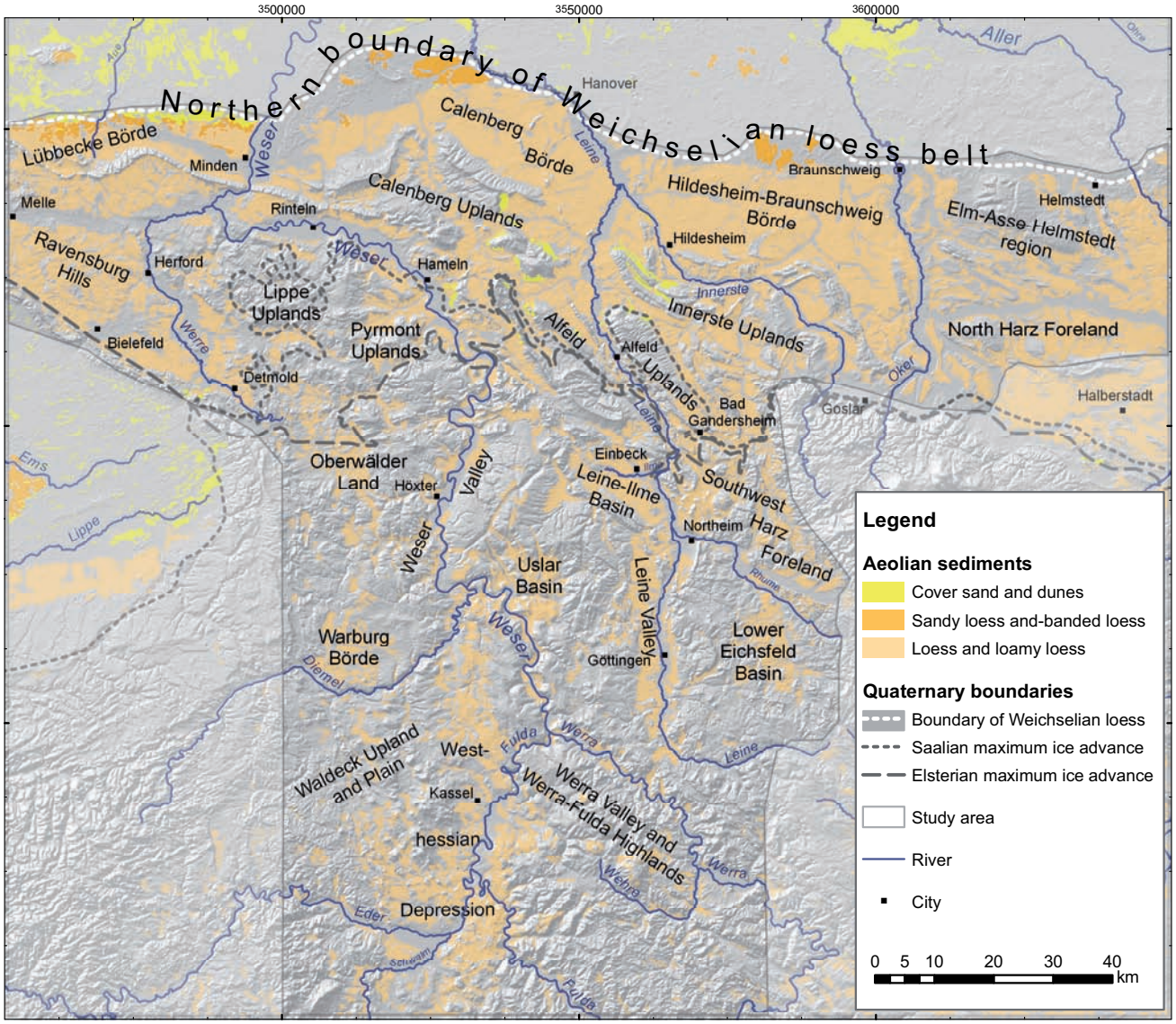

Fig. 2: Aeolian sediments, loess regions and main boundaries of Quarternary age. (DEM: ASTER GDEM is a product of METI and NASA; river network: OpenStreetMap, published under CC-BY-SA 2.0; maximum ice advance: Kaltwang 1992)

Abb. 2: Äolische Sedimente, Löss-Regionen und wichtige quartäre Verbreitungsgrenzen. (DGM: Globales ASTER-DGM ist ein Produkt von METI und NASA; Flussnetzwerk: OpenStreetMap, veröffentlicht unter CC-BY-SA 2.0; Maximale Eisausdehung: Kaltwang 1992)

The upper Weser flows in a narrow, meandering valley deeply incised in Lower Triassic sandstone through the so-called Upper Weser Uplands. North of Hameln the river flows in a NW-SE-trending valley through Middle to Upper Triassic and Jurassic to Cretaceous rocks of the Lower Weser Uplands. The river leaves the Lower Saxony Hills through Porta Westphalica and enters the loess Börde of the Northwest German Plain. Along the river loess was mapped on the valley slopes on one or both sides, favourably on northeast-, north- and east-facing sides up to 200 to 300 m altitude. Graupner (1970) and Brosche & Walther (1991) already noted that the region south of Hameln is richer in loess. Single loess deposits were mapped in abandoned lobes, incoming valleys, or subrosive sinks. With increasing distance from the main valley the loess cover thins out and is only found in some patches. Wortmann (1942) mapped some parts of the Weser valley. His loess patches are a bit larger and more connected than on the other maps.

Loess stratigraphy

The loess stratigraphy of the study area comprises Upper Pleistocene loessic sediments and paleosols (Tab. 1). The stratigraphically lowest part of the Upper Pleistocene is the Eemian interglacial soil, a typical brown haplic luvisol (WRB). The Lower Weichselian is composed of loess, which is in most cases decalcified, and has a strong pedogenetic overprint. Besides loess a lot of other sediments are typical for this unit, like pedosediments of Lower Weichselian or Eemian soil horizons, glaciofluvial and glacial sediments, or weathered bedrock. In the stratigraphically upper part of the Lower Weichselian sequence the loess amount increases. The most prominent pedogenetic features are Ah, Al and Bt horizons and features related to stagnic conditions. These soil horizons are relics of haplic chernozem, rendzic leptosol, haplic luvisol and stagnic gleysol. Ricken (1983) mentioned cycles from dry to wet conditions inferred from these palaeosols. The main important marker horizons are up to four Ah horizons includ-

Table 1: Pedostratigraphy of the loess- and loess-like sediments in southern Lower Saxony and northern Hesse (after: Rohdenburg & Meyer 1966, Ricken & Meyer 1982, Brosche & Walther 1991, Pouclet & Juvigne 2009).

Tabelle 1: Pedostratigraphie der Löss und löss-ähnlichen Sedimente in Süd-Niedersachsen und Nordhessen (nach: Rohdenburg & Meyer 1966, Ricken & Meyer 1982, Brosche & Walther 1991, Pouclet & Juvigne 2009).

Period	Loess and loess-related sediments	**Marker horizons** southern Lower Saxony	northern Hesse	Age (ka)
Late Weichselian		Laacher See Tephra		12.900
Upper Weichselian	wj5 alpha loess wj4 alpha loess wj3 gamma loess wj3 alpha loess wj2 alpha loess wj1 beta loess wj1 alpha loess	wj4 beta soil wj3 delta soil wj3 beta soil wj2 beta soil wj1 gamma soil	Eltville Tephra E4 E3 E2 E1	20.000
Middle Weichselian	wm	Lohne soil & equivalents Kirchberg soil Herzberg soil	Hahnstatt soil Gräselberg soil	30.000
Lower Weichselian	wa2	Ah horizon Ah horizon	Niedervellmar soil complex	
	wa1	Ah horizon Ah horizon	Bilshausen soil complex	
Eemian		Eemian soil	Erbach soil	117.000

ing one typical Al horizon (bleached zone), disconformities (stone layer), a basal solifluction layer, enrichments in Mn-Fe concretions and charcoal. Due to the wide range of sediments, the influence of local material and the possible soil horizons the Lower Weichselian sections show a high heterogeneity. Without the prominent Ah horizons a clear correlation of different sections is quite difficult.

The Lower Weichselian in the study area was subdivided by Rohdenburg & Meyer (1966) and Ricken & Meyer (1982) into a lower unit (wa1) and an upper unit (wa2). Generally, the base of wa1 is a solifluction deposit of reworked Eemian soil material, the stratigraphically youngest Ah horizon is the boundary to the Middle Weichselian. In some locations a loamy soil complex (Niedervellmar soil complex) was formed instead of typical soil horizons. If it is overlain by Middle Weichselian arctic brown soils or loamy loess, no clear boundary can be drawn. The authors dated the Niedervellmar soil complex as a part of the wa2 and wm (Tab. 1).

The Middle Weichselian is characterized by calcified or partly decalcified loess, a high amount of fluvially reworked loess, and intercalations of gravel and sand. In the loess sequence, artic brown soils and arctic soils are found, e.g. the Herzberg soil and the Kirchberg soil. Reinecke (2006) described very detailed Middle Weichselian loess sequences with several intercalated soils east of the study area. The most prominent marker horizon is the Lohne soil, which is correlated with the Denekamp interstadial. Bartels & Rohdenburg (1968) described a greyish brown soil equivalent called Breinum soil, Ricken (1983) found a stagnic palaeosol of the same age termed Hattorf soil, and Brosche & Walther (1991) located an arctic paleosol equivalent termed Alversdorf soil. The Lohne soil and its equivalents correlate to the top of the Middle Weichselian record.

The Upper Weichselian is the most homogeneous unit of the study area (Rohdenburg & Meyer 1966). It is composed mainly of loess. Up to five arctic palaeosols are found in the loess sequence (wj1gamma, wj2beta, wj3beta, wj3delta, wj4beta), generally the wj3delta soil is the most prominent one. Besides the soils the Eltville tephra, ice-wedge pseudomorphs of various sizes, and frost fissures are important marker horizons. The uppermost arctic paleosol (w4beta) was found very seldom, sometimes in sinks of ice-wedge pseudomorphs, normally but masked by the Holocene soil formation.

E&G / Vol. 60 / No. 1 / 2011 / 27–46 / DOI 10.3285/eg.60.1.02

3 Data

The available published data about loess in the study area can be subdivided into three different types (Fig. 3).

- The first, most important data type includes descriptions of loess sections, outcrops, or drill-holes. The information is provided mainly as text, sketches or pictures, and few tables.
- In contrast, the second type of data comprises descriptions about loess properties in a limited area, such as local thickness, granulometry, age, or facies of loessic sediments.
- The third type compiles data about loess properties that are already published in a two dimensional way. These can be hard-copies of maps or digital maps. They cover more or less the whole study area, because of the large-scale.

The main data sources used are publications, maps and digital data. Most of the articles, mentioned in the previous chapter, contain extensive descriptions and sketches of loess sections, outcrops and drill-holes. Furthermore, they comprise comments about the local and regional loess properties. These papers are the essential data source of the study.

Additionally, publications about Holocene and Pleistocene sediments were examined, as well as palaeobotanical, geomorphological, archaeological or paleontological topics including supplementary details about loess and loess-like sediments. Furthermore, releases like excursion guides or general publications about the occurrences of unconsolidated construction material or brown coal deposits were included.

Other important input sources are explanatory notes on the geological map sheets. The German geological map sheets on a scale of 1: 25,000 (GK25) have been mapped since the late 19th century by the regional Geological Surveys (Fig. 4). Together with every completed map sheet, the Geological Surveys published an explanatory report of varying extent. In these explanatory notes the authors described every geological unit in detail and added further

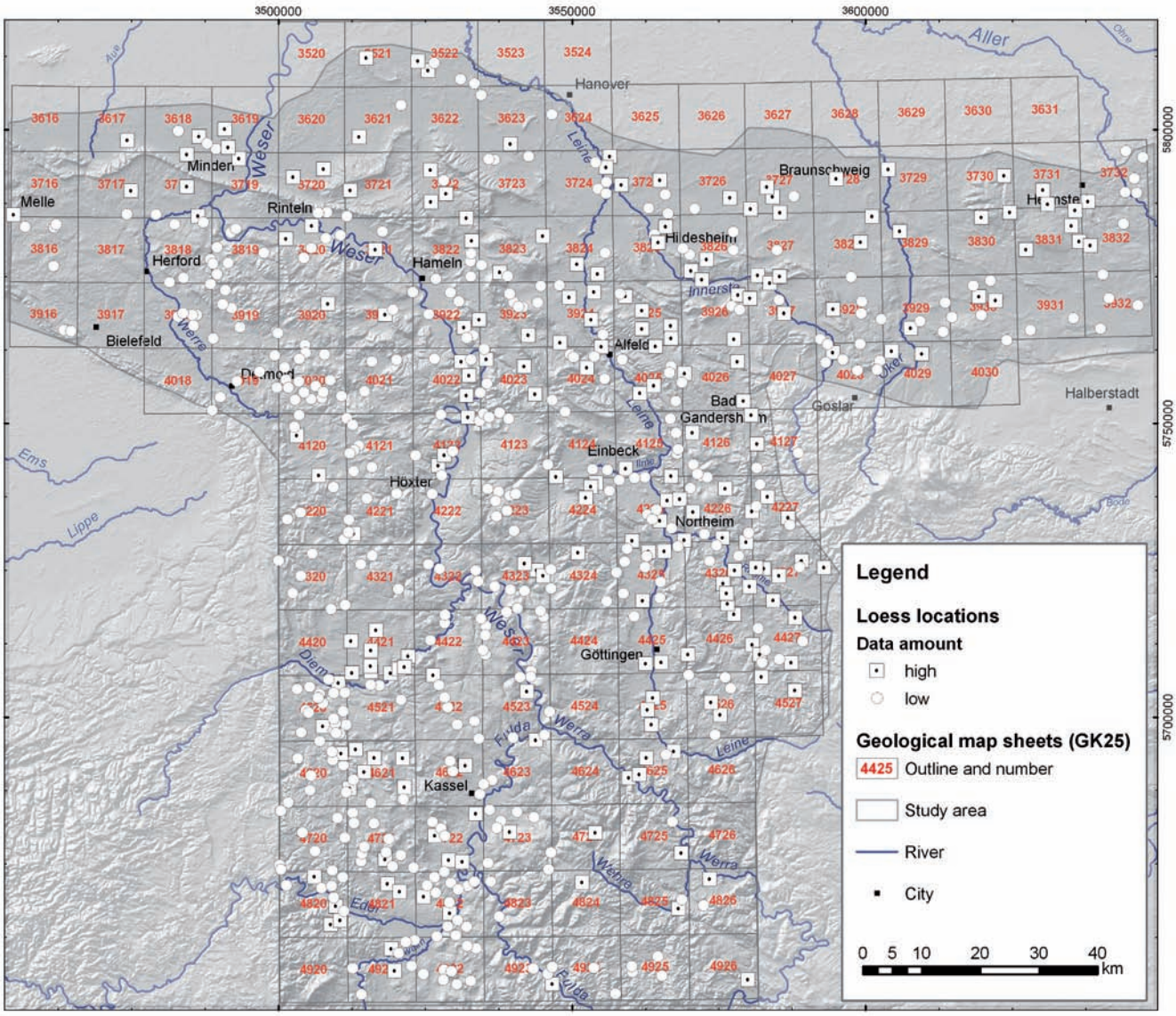

Fig. 3: Loess locations and outline of geological map sheets (1: 25,000 – GK25). (DEM: ASTER GDEM is a product of METI and NASA; river network: OpenStreetMap, published under CC-BY-SA 2.0)

Abb. 3: Lösslokationen und Umrisse der geologischen Kartenblätter (1: 25.000 – GK25). (DGM: Globales ASTER-DGM ist ein Produkt von METI und NASA; Flussnetzwerk: OpenStreetMap, veröffentlicht unter CC-BY-SA 2.0)

descriptions that are not presented on the associated geological map. For that reason, in most explanations some loess sections or drill-holes have been described in detail and some outcrops with remarkable thickness were cited. Furthermore, the authors released short or extended descriptions of the properties of the loess and loess-like deposits in the particular area covered by the map sheet.

Moreover, different thematic maps, either as hard copies or as digital data, were used for the study. The following three thematic loess maps, available as hard copies, were analyzed.

- The loess map of Wortmann (1942) on a scale of 1: 700,000 is based on small-scale soil maps. On the map the units of the aeolian sediments are classified according to granulometry (loess, "Flottlehm", "Flottsand" and sandy loess) and thickness (0.2 to 0.5 m; 0.5 to 2 m and more than 2 m). Cover sands and drift sands were not considered, because the author could not infer them from the soil maps. The map covers southern Lower Saxony and small areas of Saxony-Anhalt and Thuringia.
- The loess map of Merkt (1968) is based on published geological maps and unpublished drafts from the Geological Survey of Lower Saxony on a scale of 1: 25,000 and a 1: 200,000 general map. The scale of the loess map is 1: 300,000, covering southern Lower Saxony and small parts of North Rhine-Westphalia, Hesse and Saxony-Anhalt. Merkt (1968) distinguished loess, sand-banded loess as well as sandy loess and separated two thickness classes. Additionally, he illustrated the heterogeneous data level of each input map as a small figure.
- Müller (1961) outlined loess, sandy loess, cover sands and drift sands, weathered soils and recent deflation areas on the loess map of North Rhine-Westphalia on a scale of 1: 1,000,000. The latter author distinguished four loess regions according to their grain size values and mineral composition, but without thickness data. Only region IV (Lower Weser Upland) of Müller (1961) belongs to the recent study area.

Furthermore, a geological map of the whole study area was incorporated. The geological map of Germany on a scale of 1: 200,000 (GÜK200) is a digital and generalized compilation of all German geological maps sheets on a scale of 1: 25,000 (GK25). The part of the GÜK200 that covers the study area was used in this study. In contrast to the above maps, this digital map has an attached database containing properties of all mapped units. Aeolian sediments are subdivided in loess and loamy loess, sandy loess and cover sands. But there are no thickness values. A digital elevation model based on ASTER satellite data with horizontal resolution of 25 m x 25 m was inserted. These data are distributed by the Land Processes Distributed Active Archive Center (LP DAAC), located at the U.S. Geological Survey (USGS) Earth Resources Observation and Science (EROS) Center (lpdaac.usgs.gov). ASTER GDEM is a product of METI and NASA.

4 Methods

GIS

The database of this study consists of a huge, heterogeneous data set of point data, local descriptions and regional information. All types of data contain spatial references (information about location or coordinates). For spatial analysis the GIS software ArcGIS was used which permits storage, display and analysis of spatial data in so called layers. The graphical part of the data (the map content) is represented in vector format as points, polylines or polygons, or in raster format as images or grids. The individual layers can be superimposed exactly above each other according to accurate coordinates, comparable to a traditional stack of maps or transparent papers. In contrast to a traditional

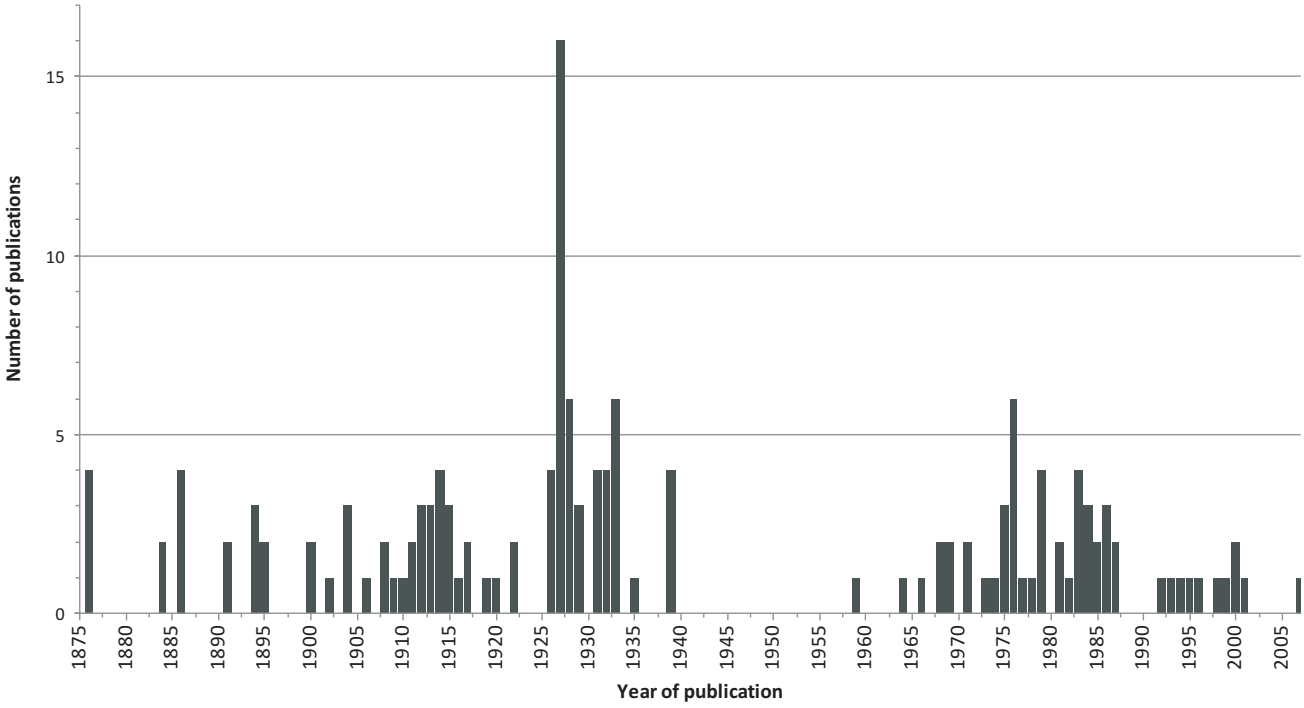

Fig. 4: Year of publishing and number of published explanations on the geological map sheets on a scale of 1: 25,000 (GK25) of the study area.

Abb. 4: Jahr der Veröffentlichung und Anzahl der veröffentlichten Erläuterungen zur Geologischen Karte 1: 25.000 (GK25) des Untersuchungsgebietes.

E&G / Vol. 60 / No. 1 / 2011 / 27–46 / DOI 10.3285/eg.60.1.02 / © Authors / Creative Commons Attribution License

stack of maps or image processing in graphical software packages the GIS software stores attribute data of each object in a connected table or database. For further analysis objects with relevant attribute data can be extracted based on logical queries, displayed, labelled, and overlain.

A new GIS-project in ArcGIS with the coordinate system Gauß Krüger Zone 3 was created. Firstly, the digital data (GÜK200 files, ASTER DEM files) were imported and prepared for further analysis. The single tiles were merged to create mosaics, the part of the mosaic, covering the study area was clipped. The clipped files were transformed from geographic coordinates to the projected coordinate system Gauß Krüger Zone 3. Afterwards the hard copies of the analogue loess maps were scanned, added to the GIS project, and geo-referenced. Finally, different shaded relief images on the basis of the DEM were calculated.

In contrast to processing of the digital input data most of the spatial information about loess properties is expressed in texts, tables, or sketches in loess-related publications. For use in the GIS program they have to be transformed into GIS layers. Hence, two types of layers for the different data types were created.

The first one is a point layer representing loess outcrops, drill-holes, or sections. All points, independent from outcrop type, were named as "loess locations". These loess locations were digitized as points according to their coordinates or position details or copied from geo-referenced location maps.

Sometimes several single descriptions of loess sections had to be generalized and combined to one loess location. The reasons for that may be that

- different sections were mapped in one outcrop or clay pit,
- several descriptions on one outcrop were made by different authors, or
- several loess outcrops are located close to each other in one region.

These "summary" locations were named after the nearest village, town or natural region. In the connected attribute table the following data, if available, of each loess location were stored:

- name of the loess location
- description of geographical location
- coordinates
- data source
- structural type
- granulometry of sediments
- thickness
- marker horizons
- stratigraphical ages
- fossil content

Hereby, as much information as possible, preferring the latest published data, were extracted and stored. Additional data from older publications were added to create complete description. Unsure and inaccurate descriptions and sections that could not be located were excluded.

In summary, 639 loess locations were created (Fig. 3). Their available attribute data are very heterogeneous, because of large differences in quantity and quality of the outcrop descriptions. They range from few hints about loess outcrops to detailed descriptions with a lot of parameters. The reasons are the different publishing dates of the papers and the context, in which the outcrops were examined (loess, fluvial sediments, deposits, paleontological or archeological investigations). In many loess locations some parameters or details are missing. Most information was available about thickness, less information about the other parameters. Sometimes the description is based on incomplete stratigraphy. The loess locations were classified in a group of very detailed data (421 locations) and in a group of general data (218 locations).

Secondarily, a polygon layer in the GIS project was created to store the data extracted from the explanations on the geological map sheets in scale 1: 25,000. The outline of each map sheet was digitized as rectangle (Fig. 3). All loess-related information was stored in the related attribute table, including:

- number of explanatory note
- publishing year
- author(s)
- loess distribution
- accumulation zones
- horizontal zones and granulometric boundaries
- granulometry and vertical sequences
- morphology of loess cover
- thickness
- stratigraphic age
- fossils
- cryoturbation features

From the notes as much information as possible was extracted, more recently published explanatory notes were preferred. Older notes were checked, additional facts and descriptions were added, if available.

In summary, all available notes were examined and data of 152 of them were stored. The notes were published between 1876 and 2007 (Fig. 4), therefore amount and quality of loess-related data are very heterogeneous. Most publications were released in the 1920s and 1930s or between 1960 and 1985. The older notes released before 1940 give only few details on loessic sediments. Aeolian loess and loess derivates are not differentiated. Moreover, in the oldest prints there is no differentiation between loess and floodplain deposits. Sometimes one note describes two or three map sheets. Few map sheets were published without explanatory note.

In addition to the layers "loess locations" and "explanatory notes", other layers in the GIS project including digitized main topographic features (e.g. rivers, cities, geological boundaries) were created.

Selection of base map

The accurate distribution of loess and loess-like sediments in the study area is a fundamental base for further analysis of the parameters thickness, granulometry and age. The study is not a mapping campaign, so a base map showing a realistic loess distribution to work with had to be selected. The already mentioned loess maps of Wortmann (1942), Müller (1959) and Merkt (1968) and the digital geological map (GÜK200) were evaluated based on the parameters: scale, units, coverage, accuracy and publishing age. The result shows that none of them displays a realistic distribution of loess and loess-like sediments. Reasons are the difference in the map coverage and the inaccuracy due to

the combination of aeolian loess, loamy loess, soliflucted or fluvial reworked loess to one „loess unit". Sometimes even younger colluvial or slope sediments were included.

It is also obvious that the maps based on geological surveys display a smaller, fragmented loess cover, which was caused by the mapping policy before 1960s. Field geologists drilled only few 1-m drill-holes per map sheet. They focused on the mapping of the bedrock to visualize the complex geological and tectonic situation, especially in the Lower Saxon Hills and the Hesse Highlands. Even when the bedrock was only visible in boulders or referred from morphological bends, they mapped the bedrock unit instead of the overlying loose material.

Lüttig (1968) compared the results of different geological surveys in 1890–1891, 1948 and 1956/1961 on the the geological map sheet 4325 (GK25). He proved that a more accurate distribution of loess is displayed in the latest map only, covering much larger areas than in the older maps. From the 1960s on field geologists drilled much more drill-holes (2 m) and tried to map the uppermost geological unit. Most GK 25 sheets, which are the database of the map of Merkt (1968) and GÜK200, were mapped before 1960; some are younger reprints or revision maps with only little changes. Field geologist had no general rule how to map the minimal thickness of loess. Therefore, the loess distribution based on the geological maps show a minimum loess distribution representing a loess cover thicker than 0.5 m, 1 m or 2 m.

The loess unit of the GÜK200 and the loess map of Merkt (1968) show a lot of similarities. In few regions, the GÜK200 shows smaller loess patches. The map of Merkt (1968) displays locally a more realistic distribution. The author examined not only the published GK25 map sheets, but also drafts of modern, unpublished mapping campaigns from the archive of the Geological Survey of Lower Saxony, resulting in some differences and sharp edges between adjacent regions.

The loess map of Wortmann (1942) displays a larger, but also inaccurate loess distribution. The map is based on soil survey campaigns. The uppermost geological unit has a high influence on the resulting soil. Hence, the soil map reflects much more information about the loess and loess-related sediments than the underlying hard rocks. Comparing this map with the map of Merkt (1968) and the GÜK200, a much larger area of loess cover becomes obvious especially in the uplands. However, the map contains loess patches close to the main rivers, where no real loess can be found. Possibly Wortmann (1942) combined loess and loess derivates with younger flood plain deposits (colluvial loess).

Although none of the maps shows a realistic loess distribution, each of them inhibits important details. Therefore, the comparison between the geology based maps and the soil based map can give additional information. This applies especially to thin loess covers in the uplands as recorded by Wortmann (1942).

However, the GÜK200 was selected as main base map for the following analysing steps of the study. The map shows smaller loess patches than the other maps and is based on an unclear minimal loess thickness to be mapped. Nevertheless, the map covers the whole investigation area and is the most detailed because of its small scale. The map is in a digital format, representing the loess and loess-related sediments as polygons, to which new information can be added.

Thickness

In the GIS project all objects of the layers "loess locations" and "explanations" that contain thickness values or thickness ranges were displayed. Each object was labelled with these values or ranges. The loess map of Merkt (1968) was used as background. Then all available thickness values were explored for their minima, their maxima and their typical ranges.

To define thickness classes for a compiled thickness map, some limitations of the data set had to take into account. In general, a loess cover has a very wide range of thickness values in one area depending on the local morphology. There is no or only few loess on steep slopes, but very much loess on E-facing slopes or in other accumulation positions. And there are a lot of transitions between these extremes.

For that reason, wide thickness classes covering the typical ranges of loess thickness were defined. The main focus laid on the maximum values.

> 0.5 to > 2 m (few data)
≤ 3 m
≤ 5 m
≤ 6 m
2 – 8 m
3 – 10 m
3 – 20 m

The thickness values of all input sources were compared and new patches of the same thickness class were outlined. The new thickness classes were added to the polygons of GÜK200.

The following rules were set for this procedure:

- If the area was not covered by the map of Merkt (1968) and no further information (loess locations, descriptions) were available, the class "> 0.5 to > 2 m (few data)" was selected.
- The thickness data of the loess map of Merkt (1968) were copied, if no further information (loess locations, descriptions) were available.
- The same was done, if the loess locations and the thickness in the loess map were similar.
- New thickness patches were outlined, when the loess locations showed higher values, than the loess map of Merkt (1968).

The advantage of the method is the combination of different input data. Basal map information from the loess map of Merkt (1968) was used and regions with higher loess thickness were added. Nevertheless, the loess locations with thickness values are not distributed equally. In some regions no or few loess locations were reported in the literature. Additionally, authors mentioned minimal thickness values or combined thickness values of loessic sediments and other material in their publications.

Granulometry

In the GIS project a query was applied to display all objects ("loess locations" and "explanations") with data about petrography, grain sizes, and typical sediment sequences. The granulometric descriptions of the loess maps of

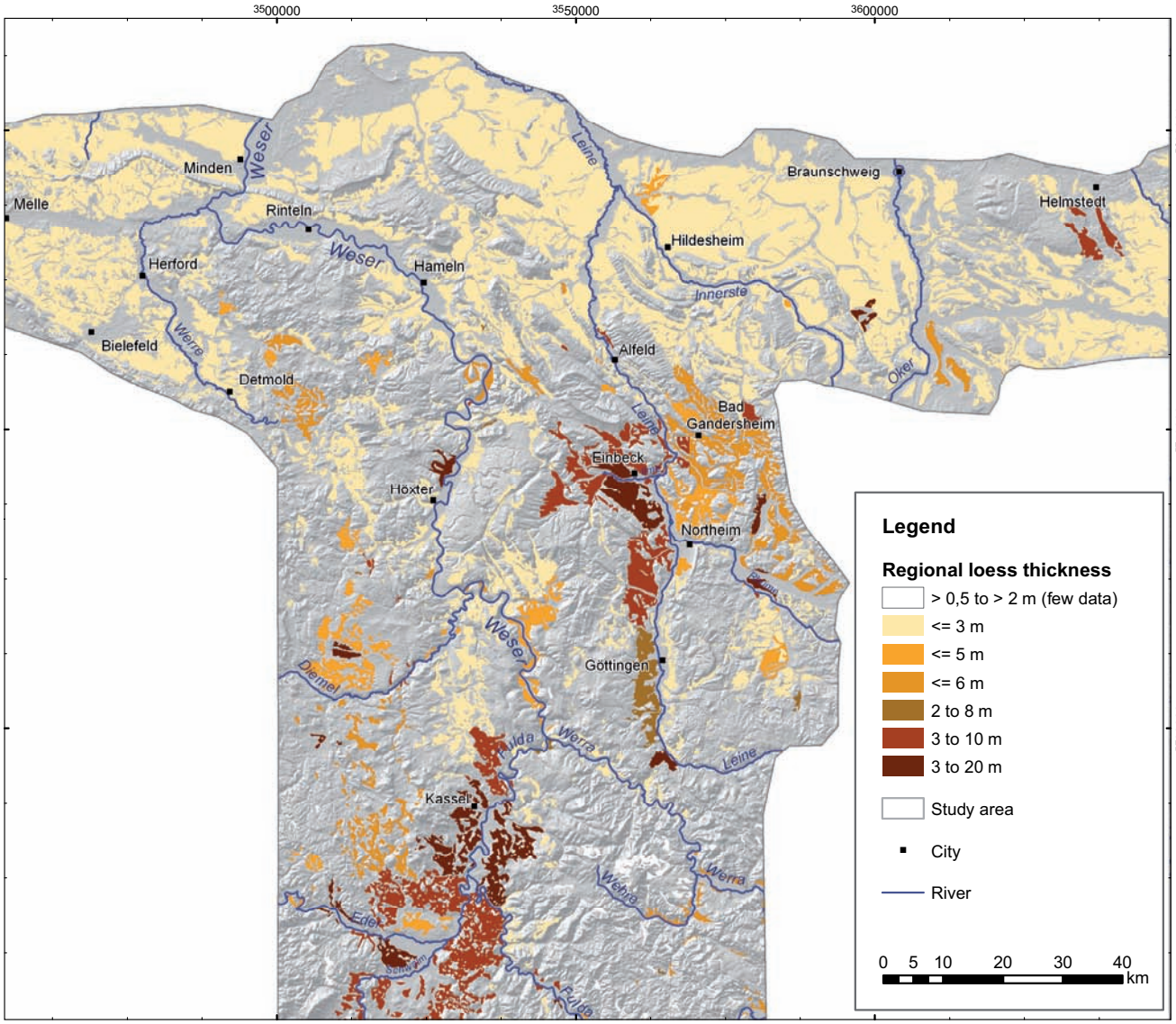

Fig. 5: Thickness map displaying regional thickness ranges of loess and loess-like sediments (including loamy loess, reworked loess, sandy loess, sand-banded loess and cover sand). (DEM: ASTER GDEM is a product of METI and NASA; river network: OpenStreetMap, published under CC-BY-SA 2.0)

Abb. 5: Mächtigkeitskarte der regionalen Mächtigkeitsbereiche von Lössen und löss-ähnlichen Sedimenten (Lösslhem, Schwemmlöss, Sandlöss, Sandstreifenlöss, Decksand). (DGM: Globales ASTER-DGM ist ein Produkt von METI und NASA; Flussnetzwerk: OpenStreetMap, veröffentlicht unter CC-BY-SA 2.0)

Merkt (1968), Wortmann (1942), and the geological map (GÜK200) were visualized. These input data vary in quality and quantity. Some loess locations have detailed grain size measurements and grain size curves. In contrast, many others have only rough descriptions, the loess maps displaying only the uppermost loessic sediment in one region. As a result, small-scale details were not separated, but a general subdivision in a loess cover layer and a basal layer was carried out. The cover layer represents the homogeneous upper part of the loess deposits. The underlying basal layer can vary widely in thickness, granulometry, pedogenetic overprint, intercalations, and distribution. The cover layer was separated into:

- sandy facies (sandy loess, sand-stripped loess and derivates)
- loessic facies
- thin or no sandy facies (very thin cover with gaps)
- thin or no loessic facies (very thin cover with gaps)

The lower part (base layer) of the loess cover was subdivided into:

- unknown base layer
- mixed layer or stone layer
- reworked loess

All regions with the same cover layer and the same base layer were outlined. Then, the following combinations of these two layers were generated:

- sandy facies on unknown base layer
- sandy facies on mixed/ stone layer
- sandy facies on reworked loess
- thin or no sandy facies on reworked loess
- loessic facies on unknown base layer
- loessic facies on mixed/ stone layer
- loessic facies on reworked loess
- thin or no loessic facies over reworked loess

These granulometric types were attached to the GÜK200 polygons. During the analysis the outline of the new regions followed the boundaries of the map sheets. In case that a map sheet had no information about the base layer, the class "unknown base layer" was selected.

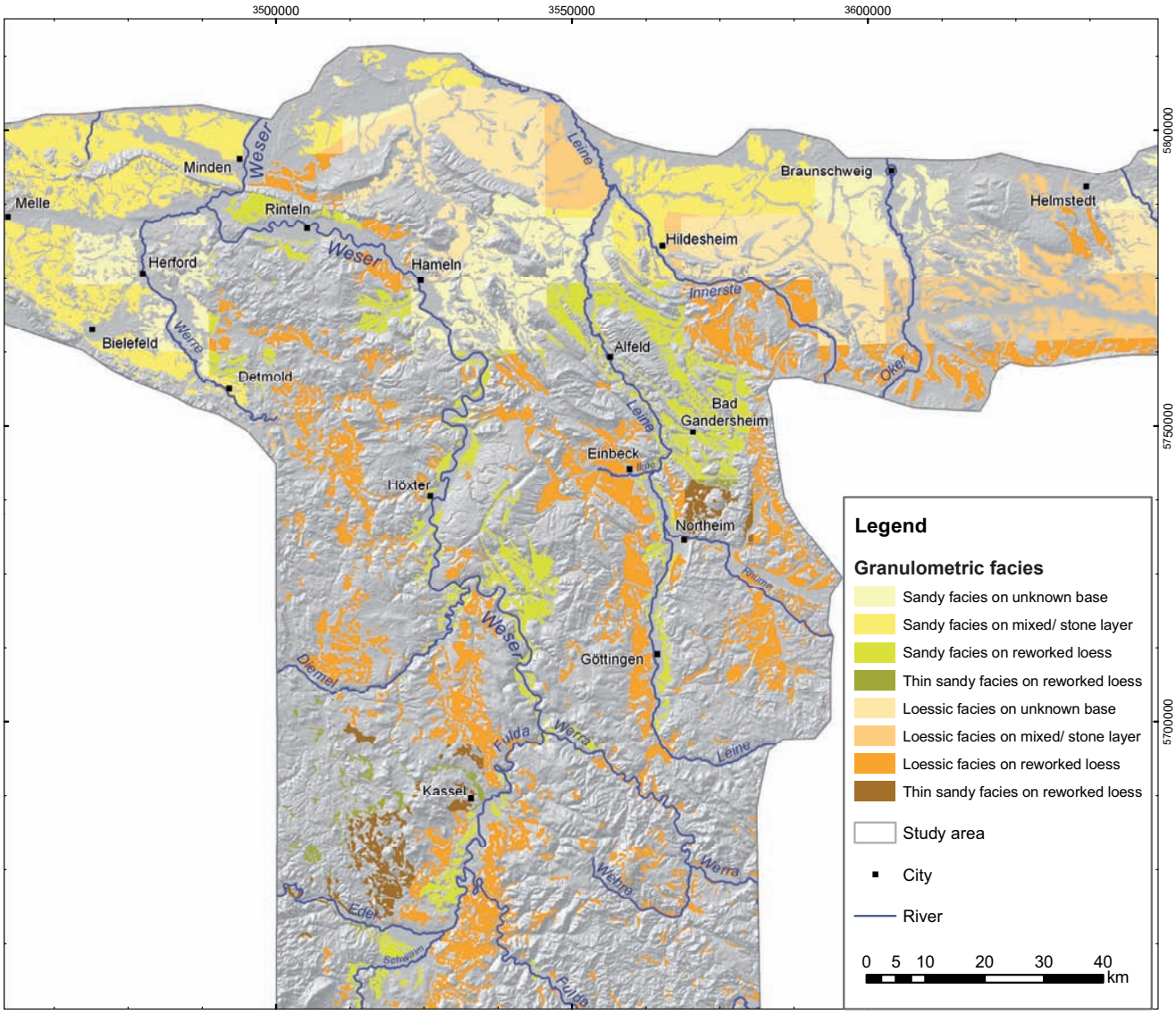

Fig. 6: Granulometric map of the regional types of cover and base layers. (DEM: ASTER GDEM is a product of METI and NASA; river network: OpenStreetMap, published under CC-BY-SA 2.0)

Abb. 6: Granulometrische Karte der regionalen Typen von Deck- und Basislagen. (DGM: Globales ASTER-DGM ist ein Produkt von METI und NASA; Flussnetzwerk: OpenStreetMap, veröffentlicht unter CC-BY-SA 2.0)

Stratigraphy

In the GIS project all loess locations with loess age data were extracted. The loess age can be estmated on marker horizons like paleosols or tephra, archaeological or paleontological findings, numerical dating or ages assumed by the author. The loess ages were displayed as combinations of the following symbols representing all horizons that were found in the locations:

- Eltville tephra
- wj: Upper Weichselian loess
- wm: Middle Weichselian loess
- wa: Lower Weichselian loess
- pW: pre-Weichselian loess

155 of 639 loess locations contain age information based on paleosols or tephra, but they are distributed very irregularly over the study area. The data reflect ages of the regional loess cover and of single loess deposits in special sediment traps. Thus, all latter locations were marked to differentiate between two accumulation types. The resulting map distribution of dated outcrops was compared with the thickness map (Fig. 5) and the granulometry map (Fig. 6) to outline regional loess cover areas of the same age (Fig. 7).

5 Results and discussion

Thickness

The resulting thickness map (Fig. 5) permits a more detailed view on loess thickness than the maps of Merkt (1968) or Wortmann (1942). Regions with thicknesses below 2.5 m are very similar, but a lot of new information about thicker loess covers appears.

The thickness of the loess and loess-related sediments ranges between few centimeters and twenty meters. Along the northern boundary of the loess belt and in the Börde region the loess cover is quite homogeneous with slight thickness variations due to exposition. Thickness values range from 0.5 to 2.5 m, sometimes up to 3 m. Thicker layers of sandy loess, sand-banded loess, or loess were found only in some locations with a specific accumulation situation as boundary dunes or in cryoturbation structures.

In the Elm-Asse-Helmstedt region and in the northern

E&G / Vol. 60 / No. 1 / 2011 / 27–46 / DOI 10.3285/eg.60.1.02 / © Authors / Creative Commons Attribution License

parts of the Leine Uplands comparable thickness ranges were found. However, morphological ridges clearly influence the thickness resulting in an apparent heterogeneity between loess-free regions and loess accumulation sites.

In the central and southern parts of the study area thickness values show much larger variations. On plateaus or plains the loess cover varies between few centimeter and 3 meters. In shallow depressions and in valleys the regional loess thickness can reach up to 4, 5 or 6 m. Loess thickness up to 10 or even 20 m occurs only in the large depressions (Leine-Ilme Basins and the Westhessian Depression) and in some smaller areas along the Werra Valley, the southernmost tip of the Leine Valley, and in the Southwest Harz Foreland. All these regions are influenced by subrosive activities.

In the uplands loess thickness is strongly influenced by the elevation, the steepness, and the aspect of the slopes. The thickest loess covers were found on slopes facing to E, NE or NW. Slopes in the opposite directions are normally bare or have a thinner loess cover.

Several loess sections with thickness values clearly above those of the surrounding regions were found. Most of them are trapped in karstification as sinks or dolines. Other extreme or untypical thick sections are caused by cryoturbation or glacial structures. Some other locations like abandoned meanders also have higher thickness values. Most likely they contain fluvial reworked loess.

The highest density of small-scale subrosion features were found in the Waldeck Upland, Warburg Börde und western part of the Lower Weser Upland. The thickest loess deposit (up to 20 m) was found at Albaxen in the Weser valley.

In general, loessic sediments thicker than 3 m occur only in valleys, basins, and special sediment-traps related to karstification, subrosion or cryoturbation. In all other regions, the loess thickness varies mainly between few centimetres and 2.5 or 3 m.

Granulometry

The resulting granulometry map (Fig. 6) is quite heterogeneous, due to some missing data, but general trends can be deduced. Several regions have a sandy cover layer with varying amounts of sandy loess, sand-striped loess and aeolian loess.

The main loess region is located along the northern boundary of the sandy belt, as visible on the GÜK200 and described in detail by Gehrt (1989, 1992, 1994, 1998) from the Hildesheim-Braunschweig Börde. Authors of the explanatory notes on the geological map sheets described either a sharp boundary between this zone and the aeolian sediments north of the loess belt or a wide mixing- or transition-zone from loess to sandy loess into cover sands and drift sands.

Additionally, a sequence of the sandy facies was mapped in the long and narrow upland stripe between the Wiehen Hills and the Ravensburg Hills in the north-eastern study area. Here the northern boundary of the loess belts bends between the upland and the Westphalian Lowland to the Southeast. In regions, where this facies was mapped, mostly loess and sand-banded loess were overlain by sandy loess.

Furthermore, the granulometry map (Fig. 6) shows large areas covered with sandy loess, sand-banded loess and loess within the upland. Most of these deposits with a dominant sand content and a more reddish colour were found on wide plateaus of Lower Triassic red sandstones (Bunter Sandstone) in the South of the study area.

In contrast to the northern regions, where coarser sediments increase to the top, the loess sequences in the uplands have higher sand contents at the base and a fining upward trend.

In some regions with large sandstone outcrops, as Fulda Highlands and the Lower Eichsfeld, sandy loess is assumed, but only rare data were available from the literature. Most significant sources of sandy loess are the river valleys that are cut into sandstones. There are many locations where sandy loess or even cover sand makes up the main unit. The sandy loess facies was also found in the central part of the Leine Uplands, the so-called Alfeld Upland. All other regions are covered by the typical loess, as evidenced by the recent available outcrop descriptions.

Beside this, the map shows a zoning of the basal layer types, although less data about this lower part of the sections was found. Along the northern boundary of the loess belt, in large parts of the adjacent Börde regions, and in the Northwest of the study area a mixed layer or a prominent stone layer forms the base of the aeolian sediments.

In the southern part of the study area the loess facies or sandy loess facies is underlain mainly by fluvial or soliflucted, reworked loess. In the Southwest Harz Foreland (around Seesen) and in the Waldeck Uplands and Plains the reworked loess of the basal layer forms the main part of the loess cover. The cover layer is very thin or not existing due to the climatic conditions. Already Brosche & Walther (1991) mentioned the "wet facies" of the Seesen region.

Stratigraphy

The stratigraphic map (Fig. 7) shows a variety of different loess ages. Lower and Middle Pleistocene loess-related sediments occur in some locations all over the study area. However, most loess deposits are of Weichselian age.

The distribution of the loess ages seems to be quite irregular, because of the mixture of different accumulation sites. One group of loess locations belongs to the typical loess cover, e.g. on slopes, on plateaus, in wide basins. The other group are the special locations found in different sedimentary traps. In most of these traps pre-Weichselian sediments were preserved.

On the contrary, if the dated loess locations are examined without these special cases, a zoning of the loess ages becomes obvious. Complete Weichselian sequences, containing Lower, Middle and Upper Weichselian loess occur in the southernmost parts of the study area. Incomplete Weichselian sequences, whether Lower and Upper Weichselian loess or Middle and Upper Weichselian loess, were reported in some valleys or basins in the central and southern parts of the study area. Upper Weichselian sequences were described all over the study area, but mainly in the northern parts. The most complete Upper Weichselian sequences were exposed in the outcrops Elvershausen and Einbeck.

Between the northern boundary of the loess belt and the

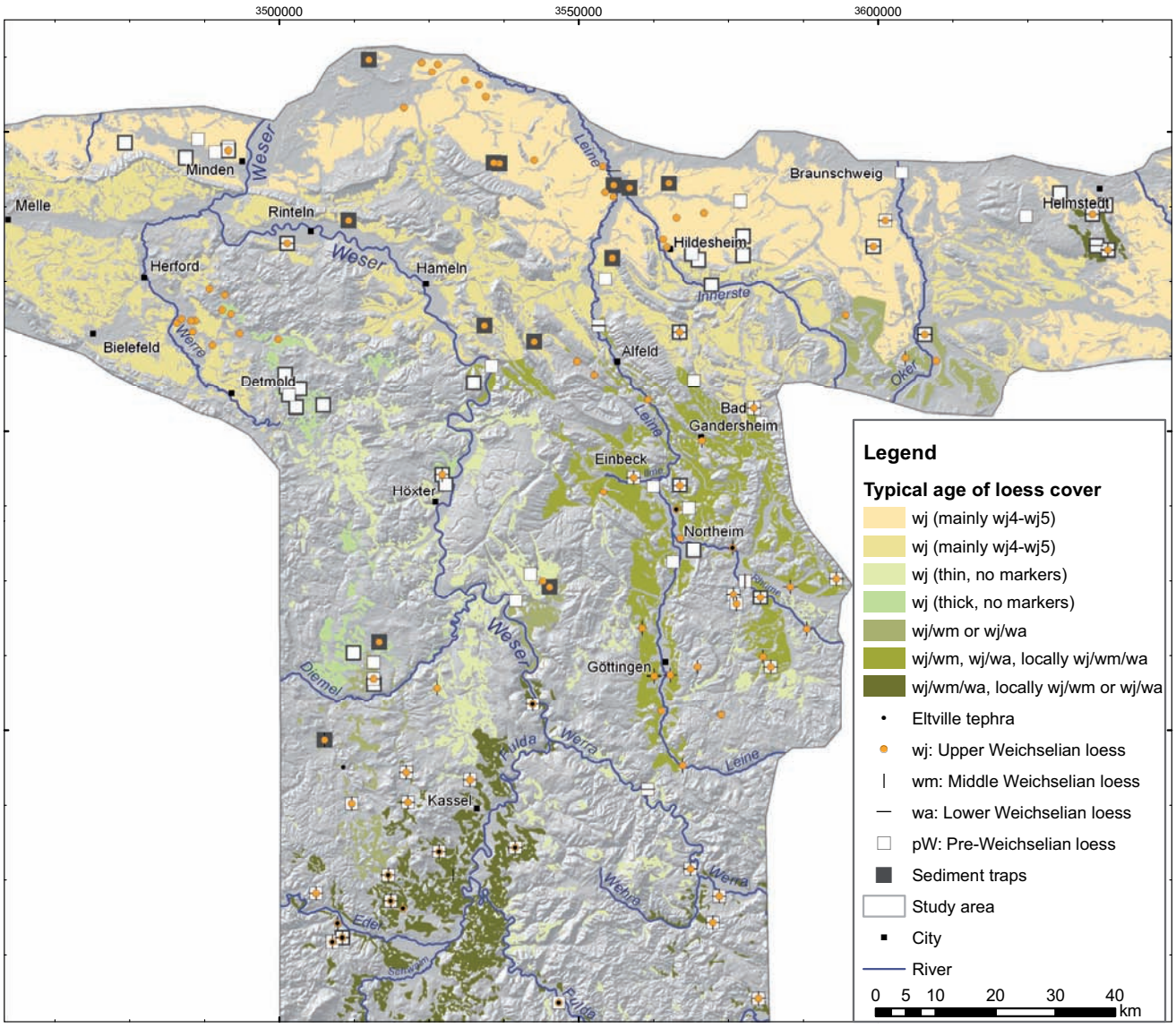

Fig. 7: Stratigraphic map displaying dated loess locations and typical ages of the regional loess cover (including loess-like sediments). (DEM: ASTER GDEM is a product of METI and NASA; river network: OpenStreetMap, published under CC-BY-SA 2.0)

Abb: 7: Stratigraphische Karte der datierten Lössvorkommen und der typischen Alter der regionalen Lössdecke (mit löss-ähnlichen Sedimenten). (DGM: Globales ASTER-DGM ist ein Produkt von METI und NASA; Flussnetzwerk: OpenStreetMap, veröffentlicht unter CC-BY-SA 2.0)

northern slopes of the Lower Saxon Hills, predominantly Upper Weichselian loess and loess-related sediments were preserved. The cover layer consists mainly of sandy or loessic sediments without prominent intercalations of other sediments, gaps or zones of strong pedogenetic or erosional overprint. Moreover, in this area the loess thickness ranges between few centimetres and 2.5 or 3 m. In wide parts, the cover layer is underlain by a distinctive stone or mixed layer over periglacial, glacial or fluvioglacial sediments. This layer was found in several places and can be called a marker horizon. In its fine-grained matrix it may contain remnants of older aeolian sediments. However, a clear or thick basal layer of reworked aeolian sediment, representing older loessic sediments, was not found. In conclusion, the regional loess cover in this area was accumulated after strong periods of fluvial or solifluidal reworking in the Upper Weichselian, because most of the older loessic sediments were eroded.

Similar observations were made by other scientists. Vierhuff (1967) postulated that the age of the sandy-loess north of the loess belt is of Upper Weichselian age. Rohdenburg & Meyer (1966) visualized on their location map a lot of outcrops without marker horizons in the northern part of southern Lower Saxony. They interpreted the regional loess cover as an Upper Weichselian deposit. Gehrt (1989, 1992, 1994) examined a lot of loess sequences in the Braunschweig-Hildesheim Börde, along the northern boundary of the loess belt. He postulated that the sandy and loessic sediments on top of a mixed or stone layer are of Upper Weichselian age. Gehrt (1998) specified the age of these sediments as upper Upper Weichselian (wj4 to wj5). Lower Upper Weichselian sediments (wj1 to wj3) were conserved in the base layer. He mentioned that units of the same age were mapped west of Hanover in the Calenberg Börde.

Reinecke (2006) determined the age of the loess and loess-like sediments of the North Harz Foreland based on palaepedological analysis and OSL dating. Moreover, he separated the regional loess cover into a lower facies (wj1 to wj3), which is only accumulated on Northeast-, East- or

Northwest-facing slopes, and an overlying regional loess unit of wj4 to wj5 age.

Not only the Börde loess, but also the thin loess cover (less than 3 m, containing no marker horizons) in the upland region of the study area may be of similar age. When the loess thickness exceeds 2.5 or 3 m in valleys or basins, incomplete Weichselian loess sequences become more frequent. In summary, if the loess is thicker than 2.5 or 3 m, it becomes more likely to find loess and loess-like sediments of Upper Weichselian and of Middle or Lower Weichelian age.

Complete loess sequences containing Lower, Middle and Upper Weichselian loess are more common in the southernmost part of the study area in the Westhessian Depression, due to the geomorphological situation in the wide-ranging basin und the weaker erosional overprint.

Moreover, to the Southwest of the study area an increasing number of findings of mammal fossils like *Equus, Cervus elaphus, Rangifer tarandus, Mammuthus primigenius* (Beyrich & Moesta 1876, Grupe 1916b, Horn 1982, Becker & Kulick 1999) and loess snails *Succinea oblonga, Helix bispida, Helix obvoluta, Helix hortensis, Helix pulchella, Pupa muscorum* (Moesta 1876a, Moesta 1891, Moesta & Beyschlag 1886D, Grupe 1916B, Lang & Blanckenhorn 1920, Blanckenhorn 1926, Becker & Kulick 1999) were recorded. It can be concluded that the West Hessian Depression has the best conditions for loess preservation in the study area.

Various authors gave some remarks about the regional ages of the loess cover in the upland (Lower Saxon Hills and Hesse Highlands). Ricken & Meyer (1982) wrote that in the South Harz Foreland the Eemian soil is quite seldom, loess cover starts with Lower Weichselian deposits (soils) on Middle Terrace gravel. Feldmann (2002) mentioned that the Eemian soil is mainly eroded in the Aller catchment area. The age of the loess cover in the Alfeld region was estimated by Lüttig (1960b) mainly postdating the main glacial period. Thus, a Upper Weichselian loess deposition is most likely due to the larger deflation area.

Jordan (1984) found only few relicts of the Eemian soil in the Leine valley in sheltered positions. Brosche & Walther (1991) postulated that the loess in the Northern Harz Foreland is 3 to 5 m thick and of Upper Weichselian or Lower Weichselian age. In the Borgentreich region, west of the Hessian Depression no Lower or Middle Weichselian loess was found, only at the Daseburg and Hofgeismar sections.

Beside this local concepts about loess stratigraphy, Gehrt (1998) established a model of regional loess ages in the lowlands and uplands. He postulated a regional age of the aeolian sediments in the Börde region and along the northern loess boundary of wj4 to wj5. On the slopes of the southerly adjacent upland also patches of older Weichselian loess (Lower Weichselian to wj3) can be conserved above remants of the Eemian soil. These local relicts are overlain by the regional Upper Weichselian loess (wj4 to wj5). The most complete sections of Weichselian loess can be preserved according to his model in upland basins or in subrosion basins.

Based on the local observations and the regional model, typical ages of the regional loess ages in the study area were outlined (Fig. 7). The resulting map represents large-scale zones of loess ages, which are maximum ages and do not show local variations. Therefore, the stratigraphic map gives an orientation where which type of loess sequences might occur.

Conclusions

Based on spatial data, which are quite different in publishing age, amount of information, spatial resolution and data type, loess parameters were analyzed.

A detailed thickness map (Fig. 5), a granulometry map (Fig. 6) and a stratigraphy map, displaying dated loess locations and regional loess ages (Fig. 7), were compiled. By means of this new spatial representation of loess characteristics, large-scale differences and trends become obvious.

The local variations of the loess parameters that are not displayed on the large-scale maps may be the object of future investigations. In such studies limited areas should be selected, which represent different geomorphological regions (Börde, plateau, plain, valley, basin) and loess cover types. There, the local variablility of the loess parameters (thickness, granulometry and stratigraphy) can be examined in detail. Furthermore, the results might be integrated in the regional maps to improve their accuracy.

Acknowledgements

The author gratefully acknowledge Brunk Meyer (†) for the guided tours through the construction sites and clay pits of Göttingen, the interesting explanations and discussions. I also owe sincere gratitude to Manfred Frechen for the positive reinforcement and the field trip to the overwhelming outcrops in the Eifel and Rhine region.

References

Bartels, G. (1967): Stratigraphische und geomorphologische Auswertung von Schuttdecken vor Muschelkalkschichtkämmen und -schichtstufen im niedersächsichen Bergland – Eiszeitalter und Gegenwart, Band 18, S. 76–81.

Bartels, G. & Rohdenburg, H. (1968): Fossile Böden und Eiskeilhorizonte in der Ziegeleigrube Breinum (Niedersächsisches Bergland) und ihre Auswertung für die Reliefentwicklung im Jungquartär – Göttinger Bodenkundl. Ber., 6, 109–126; Göttingen.

Becker, R. E. & Kulick, J. (1999): Erläuterungen zur Geologischen Karte von Hessen 1: 25 000 Blatt Nr. 4923 Altmorschen – Hessisches Landesamt für Bodenforschung, Wiesbaden; 394 S., 66 Abb., 34 Tab., 1 Beibl., 1 Beil.

Behrend, F. (1927A): Erläuterungen zur Geologischen Karte von Preußen und benachbarten deutschen Ländern Blatt Hamersleben – Preußische Geologische Landesanstalt, Berlin N 4, 32 S.

Behrend, F. (1927B): Erläuterungen zur Geologischen Karte von Preußen und benachbarten deutschen Ländern Blatt Schöningen Nr. 2096. Preußische Geologische Landesanstalt; 1 Fig.

Behrend, F. (1927C): Erläuterungen zur Geologischen Karte von Preußen und benachbarten deutschen Ländern Blatt Hornburg Nr. 2161. Preußische Geologische Landesanstalt.

Behrend, F. (1927D): Erläuterungen zur Geologischen Karte von Preußen und benachbarten deutschen Ländern Blatt Hessen Nr. 2162 – Preußische Geologische Landesanstalt.

Behrend, F. (1927E): Erläuterungen zur Geologischen Karte von Preußen und benachbarten deutschen Ländern Blatt Jerxheim – Preußisch Geologische Landesanstalt, Berlin N 4, 44 S.

Behrend, F. & Kühne, F. (1932): Erläuterungen zur Geologischen Karte von Preußen und benachbarten deutschen Ländern Blatt Barum – Preußische Geologische Landesanstalt, Berlin N 4, 53 S.

Beyrich, E. & Moesta, F. (1876): Erläuterungen zur geologischen Specialkarte von Preussen und den Thüringischen Staaten Blatt Sontra – Königlich Geologische Landesanstalt u. Bergakademie, Berlin N. 4, 35 S.

Beyschlag, F. (1906): Erläuterungen zur Geologischen Karte von Preußen und benachbarten Bundesstaaten Blatt Cassel – Königlich Preußische Geologische Landesanstalt.

Beyschlag, F. & Zeise, O. (1909): Erläuterungen zur Geologischen Karte von Preußen und benachbarten Bundesstaaten Blatt Besse – Königlich Geologische Landesanstalt, Berlin N. 4, 29 S.

Bittmann, F. & Müller, H. (1996): The Kärlich interglacial site and ist correlation with the Bilshausen sequence – In: Turner, Ch. (ed.), The early middle Pleistocene in Europe: 187–193, Rotterdam.

Blanckenhorn, M. (1926): Erläuterungen zur Geologischen Karte von Preußen und benachbarten deutschen Ländern Blatt Borken – Preußische Geologische Landesanstalt.

Bode, A. & Schroeder, H. (1913): Erläuterungen zur Geologischen Karte von Preußen und benachbarten Bundesstaaten Blatt Goslar – Königlich Geologische Landesanstalt, Berlin, N. 4, 188 S.

Bork, H.-R. (1983): Die holozäne Relief- und Bodenentwicklung in Lössgebieten; Beispiele aus dem südöstlichen Niedersachsen – Catena Supplement 3, S. 2–93; Tübingen.

Bork, H.-R. & Rohdenburg, H. (1979): Beispiele für jungholozäne Bodenerosion und Bodenbildung im Untereichsfeld und Randgebiete – Landschaftsgenese und Landschaftsökologie, Heft 3, S. 115–134.

Bosinski, G. (1969): Eine Variante der Micoque-Technik am Fundplatz Buhlen, Kreis Waldeck – Jahresschrift mitteldeutscher Vorgeschichte, S. 59–74; Halle (Saale).

Bosinski, G. & Kulick, J. (1973): Der mittelpaläolithische Fundplatz Buhlen, Kr. Waldeck. Vorbericht über die Grabungen 1966–1969 – Germania, 51, S. 1–41.

Brosche, K.-U. (1996): Wirkungen des pleistozänen kaltzeitlichen Klimas, insbesondere des Bodenfrostes, in den Sedimenten des östlichen Ostfalen (Raum Hannover – Wolfsburg – Helmstedt – Bad Harzburg – Salzgitter Bad – Hannover). Teil 1 – Eiszeitalter und Gegenwart, 46, S. 1–17, 16 Abb.; Hannover.

Brosche, K.-U. & Walther, M. (1978): Die jungpleistozänen Löß-Deckschichten der Braunkohlentagebaue der Braunschweigischen Kohlenbergwerke (BKB) zwischen Helmstedt und Schöningen – Eiszeitalter und Gegenwart, Band 28, p. 51–67, 5 fig.

Brosche, K.-U. & Walther, M. (1980): Lößprofile von Vaake (Bl. 4523, Münden) und Albungen (Bl. 4725, Bad Sooden-Allendorf) in Nordhessen – Geologisches Jahrbuch Hessen, 10, S. 143–150, Wiesbaden.

Brosche, K.-U. & Walther, M. (1991): Untersuchungen zur Lößstratigraphie und jungpleistozänen Formung in Südniedersachsen und östlichen Westfalen – Geographica-Oekologica, 2, S. 1–52, Berlin.

Brunotte, E. & Jauhiainen, E. (1979): Bodenstratigraphische und geomorphologische Untersuchung eines Lössprofils bei Einbeck, Bundesrepublik Deutschland – Terra Suomen Maantieteellisen Seuran aikakauskirja, 91/3, S. 141–146.

Bücking, H., Pröscholdt, H. & Zeise, O. (1904): Erläuterungen zur Geologischen Karte von Preußen und benachbarten Bundesstaaten Blatt Kella – Königlich Geologische Landesanstalt u. Bergakademie, Berlin N. 4, 21 S. [GK]

Burre, O. (1926): Erläuterungen zur Geologischen Karte von Preußen und benachbarten Ländern Blatt Herford West Nr. 2082 – Preußische Geologische Landesanstalt, Berlin N4, 1926. [GK]

Dahlgrün, F. (1939): Erläuterungen zur Geologischen Karte von Preußen und benachbarten deutschen Ländern Blatt Salzgitter Nr. 2160 – Preußische Geologische Landesanstalt; 1 Taf.

Denckmann, A. (1902): Erläuterungen zur geologischen Specialkarte von Preussen und benachbarten Bundesstaaten Blatt Kellerwald – Königlich Geologische Landesanstalt u. Bergakademie, Berlin N. 4, 84 S.

Deutloff, O. (1995): Erläuterungen zu Blatt 3818 Herford. Geologisches Landesamt Nordrhein-Westfalen, Krefeld, 182 S., 13 Abb., 17 Tab., 2 Taf.

Dienemann, W. (1926): Erläuterungen zur Geologischen Karte von Preußen und benachbarten deutschen Ländern Blatt Neuenkirchen – Preußisch Geologische Landesanstalt, Berlin N 4, 24 S.

Dienemann, W., Koert, W. & Stach, E. (1939): Erläuterungen zu den Blättern Melle, Querheim, Oeynhausen, Nr. 3716, 3717, 3718 – Preussische Geologische Landesanstalt, Berlin, 145 S.

Dietz, C. (1959): Erläuterungen zur Geologischen Karte von Niedersachsen 1: 25000 Blatt Hannover Nr. 3624 – Niedersächsisches Landesamt für Bodenforschung; Hannover, 177 S., 1 Kt., 3 Taf., 13 Abb., 5 Tab.

Dietz, C. (1973): Erläuterungen zu Blatt Lehrte Nr. 3625 – Niedersächsisches Landesamt für Bodenforschung; Hannover, 83 S., 7 Abb., 7 Tab., 2 Taf., 1 Kt. [GK]

Ebert, A. & Grupe, O. (1928): Erläuterungen zur Geologischen Karte von Preußen und benachbarten Ländern Blatt Gerden Nr. 1953 (3623). – Preußische Geologische Landesanstalt, 78 S.; Berlin. [GK]

Ebert, T. (1894): Erläuterungen zur geologischen Specialkarte von Preussen und den Thüringischen Staaten Blatt Gelliehausen – Simon Schropp´sche Hof-Landkartenhandlung, Berlin, 14 S.

Ebert, T. & Koenen, A. v. (1895): Erläuterungen zur geologischen Specialkarte von Preussen und den Thüringischen Staaten Blatt Lindau. – Simon Schropp´sche Hof-Landkartenhandlung (J. H. Neumann), Berlin W., 15 S.

Eissmann, L. (2002): Quaternary geology of eastern Germany (Saxony, Saxon-Anhalt, South Brandenburg, Thüringia), type area of the Elsterian and Saalian Stages in Europe – Quaternary Science Reviews, 21, S. 1275–1346.

Fabian, H.-J. (1957): Die Bohrung "Northeim 1" - Ergebnisse eines regionalgeologisch interessanten Aufschlusses am Leinetalgraben – N. Jb. Geol. Paläont., Abh., 105, S. 113–122; Stuttgart.

Farrenschon, J. (1986): Geologische Karte von Nordrhein-Westfalen 1 : 25 000 Erläuterungen zu Blatt 4019 Detmold – Geologisches Landesamt Nordrhein-Westfalen, 172 S., 13 Abb., 15 Tab., 3 Taf.; Krefeld.

Farrenschon, J. (1995): Erläuterungen zu Blatt 4020 Blomberg – Geologisches Landesamt Nordrhein-Westfalen, Krefeld, 9 Abb., 13 Tab., 1 Taf., 155 S.

Farrenschon, J. (1998): Erläuterungen zu Blatt 3919 Lemgo – Geologisches Landesamt Nordrhein-Westfalen, Krefeld, 189 S., 8 Abb., 10 Tab., 2 Taf.

Feldmann, L. (2002): Das Quartär zwischen Harz und Allertal mit einem Beitrag zur Landschaftsgeschichte im Tertiär – Habilitationsschrift der Uni Clausthal.

Fröhlich, H. (1990): Weichsezeitliche Periglazialseidment und Böden in einer feuchten Liasmulde bei Göttingen – Stratigraphie und Landschaftsgenetische Auswertung – Unveröffentlichte Diplomarbeit, Geographisches Institut der Unviersität Göttingen, 85 S.

Gaertner, v. H.-R. & Herrmann, A. (1968): Erläuterungen zu Blatt Hardegsen Nr. 4324. Niedersächs – Landesamt f. Bodenforschung, Hannover; 271 S., 16 Abb., 16 Tab., 10 Taf., 1 Kt.

Gehrt, E. (1989): Verbreitung und Stratigraphie der äolischen Sedimente im Bereich der Lößgrenze westlich Braunschweigs – Mitt. Dt. Bodenkundl. Ges., 59/II, S. 887–890, 1 Abb., Göttingen.

Gehrt, E. (1992): Verbreitung und Stratigraphie der äolischen Sedimente zwischen Leine und Oker – DEUQUA `92, 12.9. – 21.9.1992 in Kiel, Tagungsprogramm und Kurzfassungen, 41.

Gehrt, E. (1994): Die äolischen Sedimente im Bereich der nördlichen Lössgrenze zwischen Leine und Oker und deren Einflüsse auf die Bodenentwicklung – Dissertation, Universität Göttingen, 217 S.

Gehrt, E. (Ed.) (1998): Äolische Sedimente und Bodenentwicklung im nördlichen Harzvorland – Exkursionsführer zur 17. Sitzung des Arbeitskreises Paläopedologie der Dt. Bodenkundl. Ges. am 21. bis 23.5.1998 in Braunschweig, Hannover.

Gehrt, E. & Hagedorn, J. (1996): Zur Entstehung der äolischen Sedimente im Bereich der nördlichen Lößgrenze in Mitteleuropa – Böden als Zeugen der Landschaftsentwicklung, Festschrift zum 80. Geburtstag von Prof. Dr. H. E. Stremme, Landesamt f. Natur u. Umwelt des Landes Schleswig-Holstein, Kiel, S. 59–66

Graupner, A. (1970): Steine und Erden – Tone (einschließlich Tonsteine), Lehme und Schluffe, Sande und Kiese, sonstige Lockergesteine, Industrieminerale – Geologie und Lagerstätten Niedersachsens, Fünfter Band, Kommissionsverlag Gebr. Wurm KG, Göttingen.

Grüger, E., Jordan, H., Meischner, D. & Schlie, P. (1994): Mittelpleistozäne Warmzeiten in Göttingen, Bohrungen Ottostraße und Akazienweg – Geologisches Jahrbuch, A 134, S. 9–69, 29 Abb., 1 Tab.; Hannover.

Grupe, O. (1910): Erläuterungen zur Geologischen Karte von Preußen und benachbarten Bundesstaaten Blatt Stadtoldendorf – Königlich Geologische Landesanstalt, Berlin, N. 4, 28 S.

Grupe, O. (1912): Erläuterungen zur Geologischen Karte von Preußen und benachbarten Bundesstaaten Blatt Holzminden – Königlich Preußische Geologische Landesanstalt.

Grupe, O. (1916A): Über jüngeren und älteren Löß im Flußgebiet der Weser. Jahrb. F. 1916, 37/1, S. 144–163.

Grupe, O. (1916B): Erläuterungen zur Geologischen Karte von Preußen und benachbarten Bundesstaaten Blatt Kirchohsen (3922) – Königliche Geologische Landesanstalt, Berlin N. 4, 59 S.

Grupe, O. (1927A): Erläuterungen zur Geologischen Karte von Preußen und benachbarten deutschen Ländern Blatt Schwalenberg – Preußische Geologische Landesanstalt, Berlin, N 4, 47 S.

Grupe, O. (1927B): Erläuterungen zur Geologischen Karte von Preußen und benachbarten Bundesstaaten Blatt Aerzen (3921) – Königliche Geologische Landesanstalt, Berlin N. 4, 35 S.

Grupe, O. (1927C): Erläuterungen zur Geologischen Karte von Preußen und benachbarten deutschen Ländern Blatt Pyrmont – Preußische Geologische Landesanstalt, Berlin N 4, 49 S.

Grupe, O. (1929A): Erläuterungen zur Geologischen Karte von Preußen und benachbarten deutschen Ländern Blatt Holzminden – Preußische Geologische Landesanstalt, Berlin, N 4, 71 S.

Grupe, O. (1929B): Erläuterungen zur Geologischen Karte von Preußen und benachbarten deutschen Ländern Blatt Höxter Nr. 2371 – Preußische Geologische Landesanstalt. [GK]

Grupe, O. (1929C): Erläuterungen zur Geologischen Karte von Preußen und benachbarten Bundesstaaten Blatt Ottenstein – Königliche Geologische Landesanstalt, Berlin N. 4, 85 S.

Grupe, O. (1933A): Erläuterungen zu Blatt Kathrinhagen Nr. 2018 (Auetal, Nr. 3721) – Preußische Geologische Landesanstalt, Berlin N4, 1933, 56 S.

Grupe, O. (1933B): Erläuterungen zur Geologischen Karte von Preußen und benachbarten deutschen Ländern Blatt Bückeburg – Preußische Geologische Landesanstalt, Berlin N 4, 69 S.

Grupe, O. & Ebert, A. (1927A): Erläuterungen zur Geologischen Karte von Preußen und benachbarten deutschen Ländern Blatt Rodenberg (Barsinghausen) – Preußische Geologische Landesanstalt, 33 S.; Berlin. [GK]

Grupe, O. & Ebert, A. (1927B): Erläuterungen zur Geologischen Karte von Preußen und benachbarten deutschen Ländern Blatt Springe – Preußische Geologische Landesanstalt, Berlin N4, 1927, 52 S. [GK]

Grupe, O.& Ebert, A. (1927C): Erläuterungen zur Geologischen Karte von Preußen und benachbarten deutschen Ländern Blatt Lauenau – Preußische Geologische Landesanstalt, Berlin N4, 1927, 47 S.

Grupe, O. & Stach, E. (1933): Erläuterungen zur Geologischen Karte von Preußen und benachbarten deutschen Ländern Blatt Stadthagen Nr. 1951 – Preußische Geologische Landesanstalt, Berlin. [GK]

Grupe, O., Haack, W. & Schucht, F. (1915): Erläuterungen zur Geologischen Karte von Preußen und benachbarten Bundesstaaten Blatt Bockenem – Königlich Preußische Geologische Landesanstalt. [GK]

Grupe, O., Koert, W. & Stach, E. (1933): Erläuterungen zur Geologischen Karte von Preußen und benachbarten deutschen Ländern Blatt Minden – Preußische Geologische Landesanstalt, Berlin N 4, 67 S. [GK]

Habort, E. (1913): Erläuterungen zur Geologischen Karte von Preußen und benachbarten Bundesstaaten Blatt Königslutter (3730) – Königl. Geologische Landesanstalt, Berlin, 102 S. [GK]

Harbort, E. (1914): Erläuterungen zur Geologischen Karte von Preußen und benachbarten Bundesstaaten Blatt Süpplingen (3731) – Königl. Geologische Landesanstalt, Berlin, 142 S.

Harbort, E., Herrmann, F. & Woldstedt, P. (1931): Erläuterungen zur Geologischen Karte von Preußen und benachbarten deutschen Ländern Blatt Braunschweig (3729) – Preußische Geologische Landesanstalt, Berlin N4, 1931, 58 S. [GK]

Harbort, E., Woldstedt, P. & Görz, G. (1931): Erläuterungen zur Geologischen Karte von Preußen und benachbarten deutschen Ländern Blatt Wolfenbüttel Nr 2094 – Preußische Geologische Landesanstalt.

Harms, F.- J. (1984): Erläuterungen zu Blatt Nr. 4025 Freden – Niedersächs. Landesamt f. Bodenforschung, Hannover; 168 S., 20 Abb., 18 Tab., 7 Kt.

Held, G. (1987): Jungpleistozäne Paläoböden aus Löß im südlichen Niedersachsen und ihre räumliche Anordnung im Kartiergebiet Rosdorf bei Göttingen – Unveröffentlichte Diplomarbeit, Institut für Bodenwissenschaften der Universität Göttingen.

Herrmann, A. (1974): Erläuterungen zu Blatt Sievershausen Nr. 4223 (Neuhaus am Solling) – Niedersächsisches Landesamt für Bodenforschung, 82 S., 8 Abb., 8 Tab., 1 Taf., 1 Kt; Hannover.

Herrmann, R. (1958): Eisrandablagerungen und Fließerden am Nordrand des Leineberglandes – Geologisches Jahrbuch, 76, S. 309–320. [GK]

Herrmann, R. (1964): Erläuterungen zu Blatt Salzhemmendorf Nr. 3923 – Niedersächsisches Landesamt für Bodenforschung, Hannover, 1 Kt., 3 Taf., 5 Tab., 10 Abb., 133 S.

Hilgers, A., Gehrt, E., Janotta, A. & Radtke, U. (2001): A contribution to the dating of the northern boundary of the Weichselian Loess Belt in Northern Germany by luminescence dating and pedological analysis – Quaternary International, 76/77, S. 191–200.

Hinze, C. (1976): Erläuterungen zu Blatt Seesen Nr. 4127 – Niedersächsisches Landesamt für Bodenforschung; Hannover, 161 S., 18 Abb., 8 Tab., 4 Taf., 6 Kt.

Hinze, C. (1983): Erläuterungen zu Blatt Nr. 3616 Preußisch Oldendorf – Niedersächsisches Landesamt für Bodenforschung; Hannover, 100 S., 13 Abb., 3 Tab., 7 Kt. [GK]

Hinze, C., Jerz, H., Menke, B. & Staude, H. (1989): Geogenetische Definitionen quartärer Lockergesteine für die Geologische Karte 1: 25 000 (GK25) – Geologisches Jahrbuch, A112, Hannover. [GK]

Hoffmann, A. (1927): Erläuterungen zur Geologischen Karte von Preußen und benachbarten deutschen Ländern Blatt Elze Nr. 2089 – Preußische Geologische Landesanstalt. [GK]

Hofrichter, E. (1976): Erläuterungen zu Blatt Lauenberg Nr. 4224 – Niedersächsisches Landesamt für Bodenforschung; 113 S., 6 Abb., 8 Tab., 3 Taf., 1 Kt.

Horn, M. (1971): Erläuterungen zur Geologischen Karte von Hessen 1: 25 000 Blatt Nr. 4721 Naumburg – Hessisches Landesamt für Bodenforschung, Wiesbaden, 285 S., 29 Abb., 10 Tab., 1 Taf., 1 Beil.

Horn, M. (1976): Erläuterungen zur Geologischen Karte von Hessen 1: 25000 Blatt Nr. 4620 Arolsen – Hess. Landesamt f. Bodenforschung, Wiesbaden, 225 S. 35 Abb., 9 Tab., 1 Taf., 1 Beibl.

Horn, M. (1982): Erläuterungen zur Geologischen Karte von Hessen 1:25.000 Blatt Nr. 4520 Warburg – Hess. Landesamt f. Bodenforschung, Wiesbaden, 238 S., 28 Abb., 32 Tab., 1 Taf., 1 Beil.

Horn, M. & Kulick, J. (1969): Erläuterungen zur Geologischen Karte von Hessen 1: 25 000 Blatt Nr. 4720 Waldeck – Hessisches Landesamt für Bodenforschung, Wiesbaden, 227 S., 25 Abb., 8 Diagr., 15 Tab., 1 Beil.

Horn, M., Kulick, J. & Meischner, D. (1973A): Erläuterungen zur Geologischen Karte von Hessen 1: 25000 Blatt Nr. 4820 Bad Wildungen – Hess. Landesamt f. Bodenforschung, Wiesbaden, 386 S. 69 Abb., 20 Tab., 2 Taf., 3 Beibl.

Horn, M., Kulick, J. & Meischner, D. (1973B): Erläuterungen zur Geologischen Karte von Hessen 1:25000, Blatt Nr. 4820 Bad Wildungen – Hessisches Geologisches Landesamt für Bodenforschung, Wiesbaden, 386 S.

Jacobshagen, E., Huckriede, R. & Jacobshagen, V. (1963): Eine Faunenfolge aus dem jungpleistozänen Löß bei Bad Wildungen – Abhandlungen des Hessischen Landesamtes für Bodenforschung, 44, 105 pp.

Jauhiainen, E. & Brunotte, E. (1978): Stratigraphische Gliederung und – Material des Lößprofils bei Einbeck, BRD. Commentationes Physico-Mathematical, 48, 1, S. 1–10; Helsinki.

Jordan, H. (1976): Erläuterungen zu Blatt Osterode Nr. 4227 – Niedersächsisches Landesamt für Bodenforschung, 148 S., 14 Abb., 12 Tab., 5 Kt; Hannover.

Jordan, H. (1979): Erläuterungen zu Blatt Nr. 3521 Rehburg – Niedersächsisches Landesamt für Bodenforschung, 134 S., 14 Abb., 8 Tab., 1 Taf., 7 Kt.; Hannover.

Jordan, H. (1984): Erläuterungen zu Blatt Nr. 4325 Nörten-Hardenberg – Niedersächs. Landesamt f. Bodenforschung, Hannover; 148 S., 12 Abb., 13 Tab., 8 Kt.

Jordan, H. (1986): Erläuterungen zu Blatt Nr. 4225 Northeim West – Niedersächs. Landesamt f. Bodenforschung, Hannover; 144 S., 13 Abb., 13 Tab., 7 Kt.

Jordan, H. (1987): Erläuterungen zu Blatt Nr. 3924 Gronau – Niedersächsisches Landesamt f. Bodenforschung, 181 S., 22 Abb., 21 Tab., 7 Kt.

Jordan, H. (1993): Erläuterungen zu Blatt Nr. 4125 Einbeck – Niedersächs. Landesamt f. Bodenforschung, Hannover; 107 S., 12 Abb., 18 Tab., 6 Kt.

Jordan, H. (1994): Erläuterungen zu Blatt Nr. 4024 Alfeld – Niedersächs. Landesamt f. Bodenforschung, Hannover; 126 S., 17 Abb., 13 Tab., 7 Kt.

Jordan, H. (1996): Erläuterungen zu Blatt Nr. 4226 Northeim Ost – Niedersächs. Landesamt f. Bodenforschung, Hannover; 111 S., 10 Abb., 14 Tab., 6 Kt.

Jordan, H. (2001): Erläuterungen zu Blatt Nr. 4124 Dassel – Niedersächsisches Landesamt für Bodenforschung, 93 S., 14 Abb., 11 Tab., 2 Kt.; Hannover.

Jordan, H. & Schwartau, W. (1993): Das Lößprofil von Ahlshausen und weitere tiefe Quartäraufschlüsse entlang der Bundesbahn-Neubaustrecke bei Northeim, Südniedersachsen – Eiszeitalter und Gegenwart, 43, S. 110-122, 9 Abb., 3 Tab.; Hannover.

Kaltwang, J. (1992): Die pleistozäne Vereisungsgrenze im südlichen Niedersachsen und im östlichen Westfalen. Mitteilungen aus dem Geologischen Institut der Universität Hannover, 33, 161 S., 7 Abb., 38 Tab., 49 Karten.

Keilhack, K., Kraiss, A. & Renner, O. (1917): Erläuterungen zur Geologischen Karte von Preußen und benachbarten Bundesstaaten Blatt Lage – Königlich Geologische Landesanstalt, Berlin, N. 4, 57 S. [GK]

Knapp, G. (1983): Erläuterungen zu Blatt 4321 Borgholz – Geologisches Landesamt Nordrhein-Westfalen; Krefeld, 160 S., 17 Abb., 8 Tab., 1 Taf.

Knapp, G. (1986): Erläuterungen zu Blatt 4421 Borgentreich – Geol. Landesamt NRW, Krefeld, 172 S., 13 Abb., 11 Tab, 1 Taf.

Knauff, W. (1978): Erläuterungen zu Blatt 3918 Bad Salzuflen – Geologisches Landesamt Nordrhein-Westfalen, Krefeld, 143 S., 17 Abb., 18 Tab., 5 Taf.

Koenen, A. v. (1894): Erläuterungen zur geologischen Specialkarte von Preussen und den Thüringischen Staaten Blatt Reinhausen – Simon Schropp´sche Hof-Landkartenhandlung, Berlin, 21 S.

Koenen, A. v. (1895): Erläuterungen zur geologischen Specialkarte von Preussen und den Thüringischen Staaten Blatt Bad Gandersheim – Simon Schropp´sche Hof-Landkartenhandlung (J. H. Neumann), Berlin W., 24 S.

Koenen, A. v. (1900A): Erläuterungen zur geologischen Specialkarte von Preussen und den Thüringischen Staaten Blatt Jühnde – Simon Schropp´sche Hof-Landkartenhandlung, Berlin, 19 S. [GK]

Koenen, A. v. (1900B): Erläuterungen zur geologischen Specialkarte von Preussen und den Thüringischen Staaten Blatt Dransfeld – Simon Schropp´sche Hof-Landkartenhandlung, Berlin, 15 S. [GK]

Koenen, A. v. & Ebert, T. (1894): Erläuterungen zur geologischen Specialkarte von Preussen und den Thüringischen Staaten Blatt Waake – Simon Schropp´sche Hof-Landkartenhandlung, Berlin, 22 S. [GK]

Koenen, A. v. & Linstow, O. v. (1928): Erläuterungen zur Geologischen Karte von Preußen und benachbarten deutschen Ländern Blatt Hann. Münden – Preußische Geologische Landesanstalt, Berlin N 4, 46 S.

Koenen, A. v., Schlunck, J. & Menzel, H. (1911): Erläuterungen zur Geologischen Karte von Preußen und benachbarten Bundesstaaten Blatt Salzhemmendorf – Königlich Geologische Landesanstalt, Berlin, N. 4, 42 S.

Koenen, A. v., Schucht, F., Grupe, O. & Seidl, E. (1915A): Erläuterungen zur Geologischen Karte von Preußen und benachbarten Bundesstaaten Blatt Hildesheim – Königlich Preußische Geologische Landesanstalt.

Koenen, A. v., Schucht, F., Grupe, O. & Seidl, E. (1915B): Erläuterungen zur Geologischen Karte von Preußen und benachbarten Bundesstaaten Blatt Sibbesse – Königliche Geologische Landesanstalt, Berlin N. 4, 53 S.

Koert, W. & Dienemann, W. (1927): Erläuterungen zur Geologischen Karte von Preußen und benachbarten deutschen Ländern Blatt Hötensleben Nr. 2097 (3832) – Geologische Landesanstalt, Berlin, 1927.

Kraiss, A., Renner, O. & Mestwerdt, A. (1915): Erläuterungen zur Geologischen Karte von Preußen und benachbarten Bundesstaaten Blatt Bösingfeld (3920) – Königliche Geologische Landesanstalt, Berlin N. 4, 69 S.

Kulick, J. & Semmel, A. (1968): Die geomorphologische und quartärgeologische Bedeutung des paläolithischen Fundplatzes Buhlen (Waldeck) – Notizbl. hess. L.-Amt Bodenforsch., 95: 347-351, Wiesbaden.

Kupfahl, H.-G. (1975): Erläuterungen zur Geologischen Karte von Hessen 1: 25 000 Blatt Nr. 4823 Melsungen – Hessisches Landesamt für Bodenforschung, Wiesbaden, 195 S., 27 Abb., 22 Tab., 1 Taf., 1 Beibl.

Kupfahl, H.-G. (1981): Erläuterungen zur Geologischen Karte von Hessen 1: 25000 Blatt Nr. 4723 Oberkaufungen – Hess. Landesamt f. Bodenforschung, Wiesbaden, 212 S. 15 Abb., 17 Tab., 3 Taf., 1 Beibl.

Lang, H. D. (1962): Erläuterungen zu Blatt Isernhagen Nr. 3524 (Hannover N) – Niedersächsisches Landesamt für Bodenforschung, 130 S., 1 Kt., 5 Taf., 24 Abb., 6 Tab.; Hannover. [GK]

Lang, O. & Blanckenhorn, M. (1919): Erläuterungen zur Geologischen Karte von Preußen und benachbarten Bundesstaaten Blatt Gudensberg – Preußische Geologische Landesanstalt.

Lang, O. & Blanckenhorn, M. (1920): Erläuterungen zur geologischen Karte von Preussen und benachbarten Bundesstaaten Blatt Homberg a. d. Efze – Preußische Geologische Landesanstalt, Berlin N 4, 128 S.

Lepper, J. (1976): Erläuterungen zu Blatt 4322 Karlshafen. – Geol. Landesamt Nordrhein-Westfalen, Krefeld, 190 S., 14 Abb., 11 Tab., 6 Taf.

Lepper, J. (1977): Erläuterungen zu Blatt Uslar Nr. 4323 – Niedersächs. Landesamt f. Bodenforschung, Hannover; 129 S., 14 Abb., 13 Tab., 10 Taf., 7 Kt.

Lepper, J. (1984): Erläuterungen zu Blatt Nr. 3725 Sarstedt – Niedersächsisches Landesamt für Bodenforschung; Hannover, 177 S., 24 Abb., 13 Tab., 4 Kt.

Linstow, O. v. (1928A): Erläuterungen zur Geologischen Karte von Preußen und benachbarten deutschen Ländern Blatt Ödelsheim Nr. 2518 – Preußische Geologische Landesanstalt.

Linstow, O. v. (1928B): Erläuterungen zur Geologischen Karte von Preußen und benachbarten deutschen Ländern Blatt Trendelburg Nr. 2517 – Preußische Geologische Landesanstalt, Berlin N 4, 36 S.

Linstow, O. v. & Breddin, H. (1928): Erläuterungen zur Geologischen Karte von Preußen und benachbarten deutschen Ländern Blatt Hofgeismar – Preußische Geologische Landesanstalt, Berlin N 4, 38 S.

Look, E.-R. (1968): Geologisch-stratigraphische Untersuchungen in Sedimenten der Elster- und Saale-Eiszeit (Pleistozän) am Elm, östlich von Braunschweig – Mitt. Geol. Inst. Techn. Univ. Hannover, 6, 108 S., 27 Beilagen; Hannover.

Lüttig, G. (1960A): Elster-Löß und Holstein-Ton von Northeim (Hann.) – Eiszeitalter und Gegenwart, 11, S. 206–210; Öhringen/Württ.

Lüttig, G. (1960B): Neue Ergebnisse quartärgeologischer Forschung im Raum Alfeld-Hameln-Elze – Geologisches Jahrbuch, 77, 337–390, 11 Abb., 5 Tab.; Hannover.

Lüttig, G. (1962): Das Braunkohlenbecken von Bornhausen am Harz – Geologisches Jahrbuch, 79, S. 565–662, 1 Beil.; Hannover.

Lüttig, G. (1965): The Bilshausen Type Section, West Germany – The Geological Society of America, Special Paper, 84, S. 159–178. [553]

Lüttig, G. (1968): Probleme und Möglichkeiten der geologischen Kartierung und der Darstellung von Loess und ähnlichen Sedimenten in Niedersachsen (Zur Geologie, Geokartographie und Sedimentologie der periglaziären Sedimente in Niedersachsen 2) – Naturhist. Ges. Hannover, Ber., Beiheft 5, S. 285–298.

Lüttig, G. & Rein, U. (1955): Das Cromer- (Günz/Mindel-) Interglazial von Bilshausen (Unter-Eichsfeld) – Geologisches Jahrbuch, 70, S. 159–166; Hannover.

Mahaney, W. C., Andres, W. & Barendregt, R. W. (1993): Quaternary Paleosol Stratigraphy and Paleomagnetic Record Near Dreihausen, Central Germany – Catena, 20, S. 161–177.

Meiburg, P. (1983): Erläuterungen zur Geologischen Karte von Hessen 1:25.000 Blatt Nr. 4521 Liebenau – Hess. Landesamt f. Bodenforschung, Wiesbaden, 175 S., 27 Abb., 13 Tab., 2 Beil.

Merkt, J. (1968): Erläuterungen zur Karte der Lößverbreitung in Südniedersachsen – Geologisches Jahrbuch, 86, S. 107–112; Hannover.

Mestwerdt, A. (1914A): Erläuterungen zur Geologischen Karte von Preußen und benachbarten Bundesstaaten Blatt Heiligendorf – Königlich Geologische Landesanstalt, Berlin, N. 4, 77 S. [GK]

Mestwerdt, A. (1914B): Erläuterungen zur Geologischen Karte von Preußen und benachbarten Bundesstaaten Blatt Groß-Twülpstedt – Königlich Geologische Landesanstalt, Berlin, N. 4, 66 S. [GK]

Mestwerdt, A. (1922): Erläuterungen zur Geologischen Karte von Preußen und benachbarten Bundesstaaten Blatt Herford-Ost – Geologische Landesanstalt Berlin. [GK]

Mestwerdt, A. (1926): Erläuterungen zur Geologischen Karte von Preußen und benachbarten deutschen Ländern Blatt Halle i. W. – Preußisch Geologische Landesanstalt, Berlin N 4, 41 S.

Mestwerdt, A. & Burre, O. (1926): Erläuterungen zu Blatt 3917 Bielefeld – Geologisches Landesamt Nordrhein-Westfalen, Krefeld, 2 Abb., 1 Tab., 39 S. [GK]

Mestwerdt, A. & Stille, H. (1911): Erläuterungen zur Geologischen Karte von Preußen und benachbarten Bundesstaaten Blatt Steinheim – Königlich Geologische Landesanstalt, Berlin, N. 4, 41 S.

Moesta, F. (1876A): Erläuterungen zur geologischen Specialkarte von Preussen und den Thüringischen Staaten Blatt Waldkappel – Neumann´sche Kartenhandlung, Berlin, 24 S.

Moesta, F. (1876B): Erläuterungen zur geologischen Specialkarte von Preussen und den Thüringischen Staaten Blatt Eschwege – Neumann´sche Kartenhandlung, Berlin, 24 S.

Moesta, F. (1876C): Erläuterungen zur geologischen Specialkarte von Preussen und den Thüringischen Staaten Blatt Netra – Königlich Geologische Landesanstalt u. Bergakademie, Berlin, N. 4, 28 S. [GK]

Moesta, F. (1891): Erläuterungen zur geologischen Specialkarte von Preussen und den Thüringischen Staaten Blatt Lichtenau – Simon Schropp´sche Hof-Landkartenhandlung, Berlin, 23 S. [GK]

Moesta, F. & Beyschlag, F. (1886A): Erläuterungen zur geologischen Specialkarte von Preussen und den Thüringischen Staaten Blatt Ermschwerd – Simon Schropp'sche Hof-Landkartenhandlung, Berlin, 17 S.

Moesta, F. & Beyschlag, F. (1886B): Erläuterungen zur geologischen Specialkarte von Preussen und den Thüringischen Staaten Blatt Witzenhausen – Simon Schropp'sche Hof-Landkartenhandlung, Berlin, 37 S.

Moesta, F. & Beyschlag, F. (1886C): Erläuterungen zur geologischen Specialkarte von Preussen und den Thüringischen Staaten Blatt Großalmerode – Simon Schropp'sche Hof-Landkartenhandlung, Berlin, 55 S. [GK]

Moesta, F. & Beyschlag, F. (1886D): Erläuterungen zur geologischen Specialkarte von Preussen und den Thüringischen Staaten Blatt Bad Sooden-Allendorf – Simon Schropp'sche Hof-Landkartenhandlung, Berlin, 66 S.

Moesta, F. & Beyschlag, F. (1891): Erläuterungen zur geologischen Specialkarte von Preussen und den Thüringischen Staaten Blatt Seifertshausen – Simon Schropp'sche Hof-Landkartenhandlung, Berlin, 14 S.

Motzka-Nöring, R. (1987): Erläuterungen zur Geologischen Karte von Hessen 1: 25.000 Blatt 4925 Sontra – Hessisches Landesamt für Bodenforschung, Wiesbaden; 296 S., 91 Abb., 14 Tab., 1 Beibl., 6 Taf.

Müller, E.H. (1961): Art und Herkunft des Lösses und Bodenbildungen in den äolischen Ablagerungen Nordrhein-Westfalens unter beson-

derer Berücksichtigung der Nachbargebiete – Fortschr. Geol. Rheinld. Westf., 4, S. 255–265; Krefeld.

Müller, H. (1965): Eine pollenanalytische Neubearbeitung des Interglazial-Profils von Bilshausen (Unter-Eichsfeld) – Geologisches Jahrbuch, 83, S. 327–352; Hannover.

Naumann, E. (1922): Erläuterungen zur Geologischen Karte von Preußen und benachbarten deutschen Ländern Blatt Rinteln – Geologische Anstalt, Berlnin N. 4, 46 S.

Naumann, E. (1925): Erläuterungen zur Geologischen Karte von Preußen und benachbarten deutschen Ländern Blatt Vlotho – Geologische Anstalt, Berlnin N. 4, 54 S.

Naumann, E. (1927A): Erläuterungen zur Geologischen Karte von Preußen und benachbarten deutschen Ländern Blatt Eldagsen Nr. 2088 – Preußische Geologische Landesanstalt.

Naumann, E. (1927B): Erläuterungen zur Geologischen Karte von Preußen und benachbarten deutschen Ländern Blatt Hessisch-Oldendorf. – Preußische Geologische Landesanstalt, Berlin N 4, 43 S.

Naumann, E. & Burre, O. (1927): Erläuterungen zur Geologischen Karte von Preußen und benachbarten deutschen Ländern Blatt Hameln Nr. 2087 – Preußische Geologische Landesanstalt, 1 Tafel.

Niederbudde, E.-A. (1976): Die regionale Unterscheidung von Lössen des Jungwürms durch Körnung und Tonmineraleigenschaften unter Anwendung multivariater Methoden – Eiszeitalter und Gegenwart, 27, S. 121–133; Öhringen.

Pouclet, A. & Juvigne, E. (2009): The eltville tephra, a late pleistocene widespread tephra layer in germany, belgium and the netherlands; symptomatic compositons of the minerals – Geologica Belgica, 12/1–2, p. 93–103.

Pröscholdt, H. & Zeise, O. (1902): Erläuterungen zur Geologischen Karte von Preußen und benachbarten Bundesstaaten Blatt Heiligenstadt – Königlich Geologische Landesanstalt u. Bergakademie, Berlin N. 4, 13 S. [GK]

Reinecke, V. (2006): Untersuchungen zur jungpleistozänen Reliefentwicklung und Morphodynamik im nördlichen Harzvorland – Sonderdruck der Aachener Geogr. Arbeiten, 2006.

Ricken, W. (1983): Mittel- und jungpleistozäne Lössdecken im südwestlichen Harzvorland; Stratigraphie, Paläopedologie, fazielle Differenzieung und Konnektierungen in Flussterrassen – Catena Supplement 3, S. 95–138; Tübingen.

Ricken, W. & Grüger, E. (1988): Vegetationsentwicklung, Paläoböden, Seespiegelschwankungen: Untersuchungen an eem- und weichselzeitlichen Sedimenten vom Südrand des Harzes – Eiszeitalter & Gegenwart, 38, S. 37–51, 8 Abb., 1 Tab.

Ricken, W. & Meyer, B. (1982): Lößbürtige Böden des Jungquartärs zwischen Harz und Leine – Beziehungen zur Quartär-Chronostratigraphie, Relief-Geschichte der Landschaft, fluvialen Sedimentation, Paläoklimakunde und Variation der holozänen Prozesse der Bodenbildung – Ber. ü, d. Exk. d. AK "Paläoböden" d. Dt. Bodenkl. Ges. am 16. u. 17.10.1982, Mitt. Dt. Bodenkdl. Ges., 34, S. 249–263.

Roeschmann, G., Ehlers, J., Meyer, B., Rohdenburg, H. & Benzler, J.H. (1982): Paläoböden in Niedersachsen, Bremen und Hamburg – Geologisches Jahrbuch, Reihe F, 14, S. 253–307.

Rohde, P. (1978): Erläuterungen zu Blatt 3523 Garbsen – Niedersächsisches Landesamt für Bodenforschung, 135 S., 18 Abb., 8 Tab., 7 Kt.; Hannover. [GK]

Rohde, P. (1983): Erläuterungen zu Blatt Nr. 3724 Pattensen – Niedersächsisches Landesamt für Bodenforschung; Hannover, 192 S., 43 Abb., 31 Tab., 2 Taf., 8 Kt.

Rohde, P. (1985): Erläuterungen zu Blatt Nr. 3620 Niedernwöhren – Niedersächsisches Landesamt für Bodenforschung; Hannover, 145 S., 38 Abb., 15 Tab., 8 Kt. [GK]

Rohde, P. (1992): Erläuterungen zu Blatt Nr. 3520 Loccum – Niedersächsisches Landesamt für Bodenforschung, 144 S., 28 Abb., 21 Tab., 8 Kt.; Hannover. [GK]

Rohdenburg, H. (1965A): Untersuchungen zur pleistozänen Formung am Beispiel der Westabdachung des Göttinger Waldes – Giessener Geographische Schriften, H. 7, S. 5–83.

Rohdenburg, H. (1965B): Die Muschelkalkschichtstufe am Ostrand des Sollings und Bramwalds – Göttinger Geograph. Abhandl., 33

Rohdenburg, H. (1966): Eiskeilhorizonte in südniedersächsischen und nordhessischen Lössprofilen – Mitt. d. Dtsch. Bodenkdl. Ges., 5, S. 138–160.

Rohdenburg, H. (1968): Jungpleistozäne Hangformung in Mitteleuropa – Beiträge zur Kenntnis, Deutung und Bedeutung ihrer räumlichen und zeitlichen Differenzierung – Göttinger Bodenkundl. Ber., 6, 3–107; Göttingen.

Rohdenburg, H. & Meyer, B. (1966): Zur Feinstratigraphie und Paläopedologie des Jungpleistozäns nach Untersuchungen an südniedersächsischen und nordhessischen Lößprofilen – Mitt. d. Dtsch. Bodenkdl. Ges., 5, S. 1–137.

Rösing, F. (1966): Erläuterungen zur Geologischen Karte von Hessen 1:25.000 Blatt Nr. 4621 Wolfhagen – Hess. Landesamt f. Bodenforschung, Wiesbaden, 246 S., 13 Abb., 8 Tab., 2 Diagr.

Rösing, F. (1969): Erläuterungen zur Geologischen Karte von Hessen 1:25.000 Blatt Nr. 4622 Kassel-West – Hess. Landesamt f. Bodenforschung, Wiesbaden, 205 S., 9 Abb., 4 Tab.

Sabelberg, U., Mavrocordat, G., Rohdenburg, H. & Schönhals, E. (1976): Quartärgliederung und Aufbau von Warmzeit-Kaltzeit-Zyklen in Bereichen mit Dominanz periglazialer Hangsedimente, dargestellt am Quartärprofil Dreihausen/Hessen – Eiszeitalter & Gegenwart, 27. p. 93–120, 7 fig. , 3 tab.

Schmierer, T. (1914): Erläuterungen zur Geologischen Karte von Preußen und benachbarten Bundesstaaten Blatt Helmstedt – Königlich Preußische Geologische Landesanstalt; 113 S.

Schönhals, E., Rohdenburg, H. & Semmel, A. (1964): Ergebnisse neuerer Untersuchungen zur Würmlöß-Gliederung in Hessen – Eiszeitalter und Gegenwart, Band 15, S. 199–206; Öhringen.

Schroeder, H. (1912A): Erläuterungen zur Geologischen Karte von Preußen und benachbarten Bundesstaaten Blatt Salzgitter (3928) – Königl. Geologische Landesanstalt, Berlin, 195 S. [GK]

Schroeder, H. (1912B): Erläuterungen zur Geologischen Karte von Preußen und benachbarten Bundesstaaten Blatt Ringelheim – Königlich Preußische Geologische Landesanstalt.

Schwartau, W. (1978): Lößuntersuchungen bei Einbeck (Südhannover) – Vortrag auf der Jahrestagung der Dt. Quartärvereinigung in Wien.

Schwartau, W. (1979): Stratigraphische Untersuchungen im Löß bei Einbeck – Mitteilungsbl. d. Arbeitsgem. Südniedersächs. Heimatfr., 7, 1, S. 7–8; Einbeck.

Selzer, G. (1936A): Diluviale Lößkeile und Lößkeilnetze aus der Umgebung Göttingens – Geol. Rundschau, 27: 255–293; Stuttgart.

Selzer, G. (1936B): Die Gliederung des Lößes im westlichen Eichsfeld und im Talgebiet der oberen Leine – Stille-Festschrift, Stuttgart, S. 212–222.

Semmel, A. (1966): Erläuterungen zur Geologischen Karte von Hessen 1: 25.000 Blatt 5124 Bad Hersfeld – Hessisches Landesamt für Bodenforschung, Wiesbaden, 209 S. [GK]

Semmel, A. (1967): Neue Fundstellen von vulkanischem Material in hessischen Lößen – Notizbl. hess. L.-Amt Bodenforsch., 95, S. 104–108; Wiesbaden.

Semmel, A. (1968): Studien über den Verlauf jungpleistozäner Formung in Hessen – Frankfurter Geographische Hefte, 45, S. 4–58.

Siebertz, H. (1982): Die Bedeutung des Feinheitsgrades als geomorphologische Auswertungsmethode – Eiszeitalter & Gegenwart, 32, S. 81–91, 4 Abb., 5 Tab.

Siebertz, H. (1988): Die Beziehung der äolischen Decksedimente in Nordwestdeutschland zur nördlichen Lößgrenze – Eiszeitalter und Gegenwart, 38, S. 106–114.

Siebertz, H. (1992): Neue Befunde zu den sedimentologisch-stratigraphischen Lagerungsverhältnissen und zur Alterszuordnung der äolischen Decksedimente auf dem Niederrheinischen Höhenzug – Eiszeitalter und Gegenwart, 42, S. 72–79.

Speyer, O. & Zeise, O. (1904): Erläuterungen zur Geologischen Karte von Preußen und benachbarten Bundesstaaten Blatt Berlingerode – Königlich Geologische Landesanstalt u. Bergakademie, Berlin N. 4, 8 S.

Speyer, O. (1884A): Erläuterungen zur geologischen Specialkarte von Preussen und den Thüringischen Staaten Blatt Gieboldehausen – Simon Schropp'sche Hof-Landkartenhandlung (J. H. Neumann), Berlin W., 12 S.

Speyer, O. (1884B): Erläuterungen zur geologischen Specialkarte von Preussen und den Thüringischen Staaten Blatt Duderstadt – Simon Schropp'sche Hof-Landkartenhandlung, Berlin, 6 S.

Stille, H. (1908A): Erläuterungen zur Geologischen Karte von Preußen und benachbarten Bundesstaaten Blatt Willebadessen – Königlich Preußische Geologische Landesanstalt, Berlin N. 4, 72 S.

Stille, H. (1908B): Erläuterungen zur geologischen Specialkarte von Preussen und den Thüringischen Staaten Blatt Driburg – Königlich Geologische Landesanstalt, Berlin N. 4, 81 S.

Stille, H. (1935): Geologische Karte von Preussen und benachbarten deutschen Ländern Erläuterungen zu Blatt Willebadessen – Preussische Geologische Landesanstalt, Berlin N 4, 26 S. [GK]

Stille, H. & Lotze, F. (1933): Erläuterungen zur Geologischen Übersichtskarte der Umgebung von Göttingen. Hochschulexkursionskarte Nr. 3, 1:100.000 – Preuß. Geol. L. Anst.; Berlin.

Stille, H. & Mestwerdt, A. (1908): Erläuterungen zur Geologischen Karte von Preußen und benachbarten Bundesstaaten Blatt Peckelsheim – Königliche Geologische Landesanstalt, Berlin N. 4, 85 S. [GK]

Stille, H. & Mestwerdt, A. (1935): Erläuterungen zur Geologischen Karte von Preußen und benachbarten deutschen Ländern Blatt Peckelsheim – Preußische Geologische Landesanstalt, Berlin, N 4, 29 S. [GK]

Stoller, J. (1931): Geologische Karte von Preussen – Erläuterungen zu Blatt 3627 [1957] Peine – Preußische Geologische Landesanstalt, Berlin N4, 100 S. [GK]

Stottmeister, L., Jordan, H. & Röhling, H.-G. (2007): Erläuterungen zur Geologischen Karte 1:25.000 von Sachsen-Anhalt (GK25) Blatt Helmstedt 3732 – Landesamt für Geologie und Bergwesen Sachsen-Anhalt; 260 S., 49 Abb., 22 Tab., 3 Kart., 6 Beikart.; Halle.

Thiem, W. (1988): Das Oberwesertal im Raume Polle-Bodenwerder-Hehlen; Zu aktuellen Problemen der Talgeschichte der Oberweser im Quartär. Ausgewählte Exkursionen zu Landeskunde von Niedersachsen und Bremen – Festschrift zum 65. Geb. von Prof. Dr. H. H. Seedorf H. H. Meyer, Hannover, Geogr. Ges. Hannover, 14, S. 273–326.

Urban, B, Elsner, H., Hölzer, A., Mania, D. & Albrecht, B. (1991A): Eine eem- und frühweichselzeitliche Abfolge im Tagebau Schöningen, Landkreis Helmstedt – Eiszeitalter und Gegenwart, Band 41. p. 85–99, 7 fig. , 2 pl. [465]

Urban, B. (1991): Zusammenfassung biostratigraphischer Ergebnisse holstein- und saalezeitlicher Vorkommen im Tagebau Schöningen, Ldkrs. Helmstedt – Sonderveröff. Geol. Inst. Univ. Köln, 82, S. 329–342; Köln [Brunnacker-Festschrift]. [578]

Urban, B. (1993): Mittelpleistozäne Interglaziale im Tagebau Schöningen – EAZ Ethnographisch-archäologische Zeitschrift, 34, S. 620–622; Heidelberg.

Urban, B. (1995A): Vegetations- und Klimaentwicklung des Quartärs im Tagebau Schöningen – In: Thieme, H. & Maier, R. (Hrsg.): Archäologische Ausgrabungen im Braunkohlentagebau Schöningen, Landkreis Helmstedt; S.44–56; Hannover.

Urban, B: (1995B): Palynological evidence of younger Middle Pleistocene Interglacials (Holsteinien, Reinsdorf, Schöningen) in the Schöningen open cast lignite mine (eastern Lower Saxony/Germany) – Meded. Rijks geol. Dienst, 52, S. 175–186; Amsterdam.

Urban, B. (1996): Zur Paläoökologie und Stratigraphie des Mittelpleistozäns im Tagebau Schöningen/NO Niedersachsen – Böden als Zeugen der Landschaftsentwicklung, Festschrift zum 80. Geburtstag von Prof. Dr. H. E. Stremme, Landesamt f. Natur u. Umwelt des Landes Schleswig-Holstein, Kiel, S. 127–139.

Urban, B., Lenhard, R., Mania, D. & Albrecht, B. (1991B): Mittelpleistozän im Tagebau Schöningen, Ldkr. Helmstedt – Z. dt. geol. Ges., 142, S. 351–372, 6 Abb., 2 Tab., 1 Taf.; Hannover.

Urban, B., Thieme, H. & Elsner, H. (1988): Biostratigraphische, quartärgeologische und urgeschichtliche Befunde aus dem Tagebau „Schöningen", Ldkr. Helmstedt – Z. dt. geol. Ges., 139, S. 123–154; Hannover.

Urban, B., Thieme, H., Mania, D. & Kolfschoten, T. van (1995): Mittel- und jungpleistozäne Abfolgen im Tagebau Schöningen (Niedersachsen) – Archäologie, Geologie, Biostratigraphie – In: Schirmer, W. (Hrsg.): Quaternary Field Trips in Central Europe, 4: Exkursionen in Berlin und Umgebung, S. 1253–1255; München.

v. Koenen, A. (1894): Erläuterungen zur geologischen Specialkarte von Preussen und den Thüringischen Staaten, Blatt Göttingen – Veröff. d. Königl. Preussischen geol. Landesanstalt, 1894, 58 S. [GK]

Vierhuff, H. (1967): Untersuchungen zur Stratigraphie und Genese der Sandlöß-Vorkommen in Niedersachsen – Mitt. Geol. Inst., TH Hannover, 5, S. 1–95, 35 Abb.

Vinken, R. (1971): Erläuterungen zu Blatt Dingelbe Nr. 3826 – Niedersächsisches Landesamt für Bodenforschung; Hannover, 225 S., 31 Abb., 23 Tab., 1 Taf. 2 Kt.

Vinken, R. (1975): Erläuterungen zu Blatt Hohenhameln Nr. 3726 – Niedersächsisches Landesamt für Bodenforschung; Hannover, 104 S., 5 Abb., 8 Tab., 3 Kt.

Vinken, R. (1977): Erläuterungen zu Blatt Hämelerwald Nr. 3626 – Niedersächsisches Landesamt für Bodenforschung; Hannover, 142 S., 3 Abb., 12 Tab., 4 Taf., 2 Kt. [GK]

Voss, H.-H. (1979): Erläuterungen zu Blatt Nr. 3522 Wunstorf – Niedersächsisches Landesamt für Bodenforschung, 102 S., 14 Abb., 8 Tab., 6 Kt.

Waldeck, H. (1975): Erläuterungen zu Blatt Eschershausen Nr. 4023 – Niedersächsisches Landesamt für Bodenforschung, 189 S., 8 Abb., 20 Tab., 1 Kt.; Hannover.

Walther, M. & Brosche, K.-U. (1983): Zur Bedeutung der Lößstratigraphie für die Rekonstruktion des jungpleistozänen Klimas im nördlichen Mitteleuropa am Beispiel norddeutscher Lößprofile – Ber. Naturhist. Ges. Hannover, 125, S. 97–159; Hannover.

Weise, O. R. (1983): Das Periglazial Geomorphologie und Klima in gletscherfreien, kalten Regionen – Gebr. Bornträger, Berlin , Stuttgart, 199 S., 97 Abb., 6 Tab.

Weissermel, W. (1929): Erläuterungen zur Geologischen Karte von Preußen und benachbarten deutschen Ländern Blatt Brakel Nr. 2370 – Preußische Geologische Landesanstalt, Berlin N 4, 40 S.

Woldstedt, P. (1928): Erläuterungen zur Geologischen Karte von Preußen und benachbarten deutschen Ländern Blatt Meine (3629) – Preußische Geologische Landesanstalt, Berlin N4, 72 S. [GK]

Woldstedt, P. & Beschoren, B. (1932): Erläuterungen zur Geologischen Karte von Preußen und benachbarten deutschen Ländern Blatt Gr. Ilsede (3727) – Preußische Geologische Landesanstalt, Berlin N4, 1932, 55 S.

Woldstedt, P. & Harbort, E. (1931): Erläuterungen zur Geologischen Karte von Preußen und benachbarten deutschen Ländern Blatt Schöppenstedt Nr. 2095 – Preußische Geologische Landesanstalt.

Woldstedt, P. & Hausbrand, O. (1932): Erläuterungen zur Geologischen Karte von Preußen und benachbarten deutschen Ländern Blatt Vechelde (3728) – Preußische Geologische Landesanstalt, Berlin N4, 1932, 39 S. [GK]

Woldstedt, P., Schmierer, T., Dahlgrün, F., Görz, G. & Ihnen, K. (1933): Erläuterungen zur Geologischen Karte von Preußen und benachbarten deutschen Ländern Blatt Lesse Nr. 2092 – Preußische Geologische Landesanstalt. [GK]

Woldstedt, P., Stach, E., Cramer, R. & Assmann, P. (1932): Erläuterungen zur Geologischen Karte von Preußen und benachbarten deutschen Ländern Blatt Wendeburg (3628) – Preußische Geologische Landesanstalt, Berlin N4, 38 S. [GK]

Wortmann, H. (1942): Bemerkungen zu einer Karte der Lössverbreitung in Niedersachsen. Archiv für Landes- und Volkskunde von Niedersachsen. – Oldenburg, ZDB-ID 5017579, Bd. 12.1942, S. 192–200 Archiv für Landes- und Volkskunde von Niedersachsen – Oldenburg, ZDB-ID 5017579, Bd. 12.1942, S. 192–200.

Wortmann, H. (1968): Erläuterung zu Blatt 3619 Petershagen – Geologisches Landesamt Nordrhein-Westfalen, Krefeld, 122 S., 7 Taf., 30 Abb., 9 Tab.

Wortmann, H. (1971): Erläuterungen zu den Blättern 3617 Lübbecke und 3618 Hartum – Geologisches Landesamt Nordrhein-Westfalen, 214 S., 3 Taf., 24 Abb., 13 Tab.; Krefeld. [GK]

E&G Quaternary Science Journal
Volume 60 / Number 1 / 2011 / 47–65 / DOI 10.3285/eg.60.1.03
www.quaternary-science.net

GEOZON SCIENCE MEDIA
ISSN 0424-7116

Loess-Palaeosol-Sequences from the loess area of Saxony (Germany)

Sascha Meszner, Markus Fuchs, Dominik Faust

Abstract: Based on new descriptions of loess-palaeosol profiles, we present a new composite profile for the loess region of Saxony, Germany. In addition to former studies of Lieberoth & Haase new stratigraphic marker horizons and palaeosols were added. Concerning the so far poorly differentiated Weichselian pleniglacial we identified three palaeosols. A palaeoclimatic interpretation for the last glacial (Weichselian) is presented and discussed.

[Löss-Paläobodenprofile aus dem Sächsischen Lösshügelland (Deutschland)]

Kurzfassung: Auf der Grundlage von neu aufgenommenen Lössprofilen im sächsischen Lösshügelland wird ein Standardprofil für die Region vorgestellt. Den früheren Arbeiten von Lieberoth & Haase konnten neue stratigraphische Markerhorizonte und Paläoböden hinzugefügt werden. Besonders im bisher kaum differenzierten Hochweichsel konnten 3 Paläobodenhorizonte detektiert werden. Aus den neuen Befunden zu den Löss-Paläobodensequenzen Sachsens wird eine Klimarekonstruktion abgeleitet und zur Diskussion gestellt.

Keywords: *loess, palaeosol, palaeoclimate, Weichselian, Saxony, Germany*

Addresses of authors: **S. Meszner***, **D. Faust**, Institute of Geography, Dresden University of Technology, 01062 Dresden, Germany. E-Mail: sascha.meszner@tu-dresden.de; **M. Fuchs**, Geographical Institute, University of Bayreuth, 95440 Bayreuth, Germany.
*corresponding author

1 Introduction

The Saxonian Loess Region is situated in the center of Saxony, East Germany (Fig. 1) and represents the transition zone between the North European Plain and the Central Upland (Erzgebirge). In this area of gently rolling hills, a loess cover of up to 20 m was accumulated during the last glacial cycle (Weichselian), intercalated by a number of palaeosols. These loess-palaeosol sequences represent an excellent sediment archive for reconstructing environmental and climate change of the last glacial cycle.

The first study of loess sediments in Saxony was carried out by Pietzsch (1922), dividing the sedimentary record into two main parts; one lower part with reworked sandy loess sediments and an upper one composed of more or less pure loess. In the following years, studies were focused on loess distribution and on the general composition of loess and loess-like sediments (Grahmann, 1925). In a first approach Gallwitz (1937) described a section close to the Elbe river, where he was able to distinguish several loess layers with intercalated levels of ice wedges and reworked loess. Grahmann (1932) published the first map of loess distribution in Europe.

Since 1950 the loess in Saxony was subject of intense palaeopedologic and stratigraphic investigation. Based on several sections Lieberoth built up a stratigraphy, which is accepted until now (Lieberoth 1959, 1962a, 1963, 1964a, 1964b). Later on Haase (1963, 1968) and Neumeister (1966) worked on geomorphic features of the northern loess boundary (Lössrandstufe). At this time, the loess research of Eastern Germany was summarized by Gellert (1965) and Richter et al. (1970). Since then, only a few articles were published (Altermann et al. 1978; Biering & Frühauf 1999; Meng 2003; Zoeller et al. 2004; Koch & Neumeister 2005). A systematic approach with further results is still lacking.

In the present study the existing results are summarized in respect to the Saxonian loess stratigraphy and improved by new findings to broaden our knowledge of loess-palaeosol sequences in Saxony. As most sections mentioned before are inaccessible today, new sections had to bee opened for this study. Due to the fact that loess-palaeosol sequences of Saxony represent an important link between the Western European loess records formed under moister conditions and the Bohemian loess records formed under more continental conditions, the Saxonian Loess Region provides valuable information about the palaeoclimate change in this transitional zone.

1.2 Geographical setting

The Saxonian Loess Region is situated in East Germany, west of the city of Dresden and characterized by gently rolling hills, covered by up to 20 m thick loess accumulations (Fig 1). The landscape is dissected by small rivers incised into the loess cover down to the bedrock (Granite of Meissen). The loess was deposited in the foreland of the Erzgebirge, forming a plateau-like topography, representing the so-called "Saxonian Loess Plateau". Surrounded by deep incised valleys of the Elbe and the Mulde River the landscape is and was endangered by soil erosion processes even in former times.

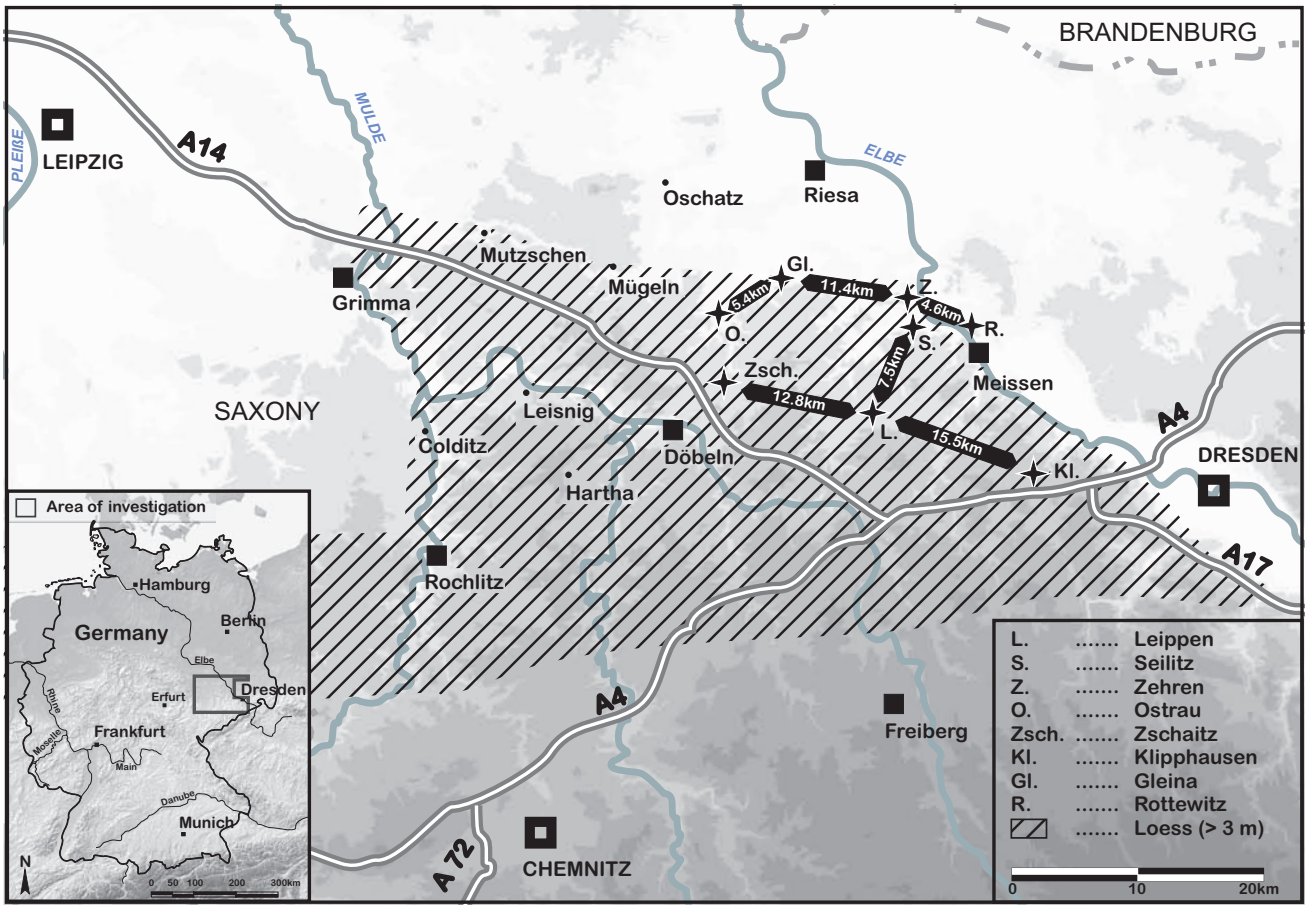

Fig. 1: Map showing study area and distribution of loess (>3 m thickness).

Abb. 1: Die Karte zeigt die untersuchten Profile und Lössverbreitung (mächtiger als 3 m) im Arbeitsgebiet.

In the Early to Middle Pleistocene the study area was covered by the ice shield of the "Elster Glaciation". From the First Saalian Glaciation glacial deposits are described by Eissmann (1994). These deposits were reworked and enriched by loess deposits of the Late Saalian Glaciation (Warthe), which evidence that the Late Saalian ice advance stopped some kilometres further north. The last period of loess accumulation took place during the Weichselian Glaciation.

The fertile soils, formed during late Pleistocene and Holocene, were cultivated by early farmers around 7500 BP (cf. Oexle 2000). Today the landscape is characterized by varying soil patterns showing a mosaic of truncated luvisols of different stages owing to extended agricultural activity. The valley bottoms are filled by colluvial material up to 4 m thick. Some strongly eroded hill slopes show that the underlying calcareous loess is already at the surface and is mixed into the soil by modern ploughing. In positions of little erosion we assume a deepness of decalcified loess due to soil formation of about 1.8 m. We conclude that at some places more than 2 m of soil was eroded.

Today the mean annual temperature is about 8.8°C, as determined in a nearby climate station (Döbeln). The mean annual precipitation is about 600 mm with it's maximum in summer.

2 Methods

Field Work

In order to select the locations for detailed field work and profile description, the study area was investigated using aerial and satellite images. After deciding to open seven new sections, field work included cleaning, drawings, and sampling of each profile. The samples were taken in respect to the layering of the section. Some sections were sampled equidistant with a 2 cm resolution. Standard sedimentological and pedological analyses like granulometry, pH value, carbonate content, soil organic matter, and content of several iron compounds were conducted in the laboratory of the Institute of Geography (Dresden University of Technology). During field work we already established a preliminary litho- and pedostratigraphy with focus on the identification of loess-palaeosol complexes. Magnetic susceptibility was measured in SI units in the field with a portable Bartington MS2 susceptibility meter. For this purpose we chose an interval of less than 5 cm. Commonly, three measurements were averaged (cf. Dearing, 1999).

Sedimentology

At the Institute of Geography (Dresden), soil textures were analysed. Bulk sample (10 g) was mixed with 25 ml dispersing solution (sodium hexametaphosphate: $(NaPO_3)_6$ – 39 g/l H_2O) and 200 ml H_2O. After rotating the suspension for at

E&G / Vol. 60 / No. 1 / 2011 / 47–65 / DOI 10.3285/eg.60.1.03 / © Authors / Creative Commons Attribution License

least 2 h it was stored for 12 h for complete dispersion. The grain-size measurements of the sand fraction were carried out by means of the wet sieve technique (2.0–0.63 mm: coarse sand; 0.63–0.2 mm: medium sand; 0.2–0.125 mm: fine sand; 0.125–0.063 mm: finest sand). Coarse silt (0.063–0.02 mm), medium silt (0.02–0.0063 mm), fine silt (0.0063–0.002 mm) and clay (<0.002 mm) were measured by pipette analyses (Schlichting et al., 1995).

The carbonate content was determined by CO_2 gas volume. Soil samples were added with hydrochloric acid in a closed system, and the resulting CO_2 gas volume was measured by a Scheibler apparatus (cf. Schlichting et al., 1995). The soil organic matter (SOM) was determined by oxidation with $K_2Cr_2O_7$ in a concentrated H_2SO_4 medium and measurement of absorbance at 590 nm (cf. Schlichting et al., 1995). The pH value was determined in a 1:2.5 soil/solution ratio in 25 ml 0.01 M $CaCl_2$ (cf. Schlichting et al.). After 30 min stirring the suspension, the pH value was measured.

For extracting the pedogenic iron compound (Fe_d), soil samples were deferrated by the bicarbonate-buffered dithionite–citrate procedure (cf. Schlichting et al., 1995). To determine the total iron content (Fe_t), 100 mg soil material was digested with 2 ml concentrated nitric acid (HNO_3) and 2 ml concentrated hydrofluoric acid (HF) using steam autoclaves. The amounts of pedogenic (Fe_d) and total (Fe_t) iron were measured using an atomic absorption spectrometer.

Mollusk analyses

The mollusk analyses were carried out by Hamann (2010 unpub.). Samples of about 10 to 15 kg were taken, sieved (200 or 400 µm mesh size) and washed to extract the mollusk shells, which were counted and identified. The species were classified according to Ložek (1964).

IRSL Dating

Samples for IRSL dating were taken using steel cylinders, hammered into the cleaned loess section to avoid any contamination of the samples with light-exposed material. Sample preparation was performed under subdued red light (640 ± 20 nm), using the polymineral fine-grain fraction (4–11 µm) for luminescence measurements.

The equivalent dose (De) was determined applying a multiple aliquot additive dose protocol. To construct a saturating exponential growth curve for De determination, 10 natural aliquots and six groups of artificially irradiated aliquots (five each) were used. Artificial irradiation was carried out with a $^{90}S/^{90}Y$ b-source (9.9 Gy/min). During IR stimulation (880 nm ± 80 nm), the shine-down curves were measured for 60 s at room temperature after a preheat at 220°C for 300 s and using a detection filter combination of BG39, 2 x BG3 and GG400 (390–450 nm). Before IRSL measurements, the samples were stored (room temperature) for a minimum of one month after artificial irradiation. Finally, the Dewas calculated from the 0–40 s signal integral after subtracting the 'late light' signal of the 55–60 s integral (Aitken & Xie 1992). In addition, an extra set of aliquots was used to test for anomalous fading and to determine the α-efficiency (a-value) of the measured material. No anomalous fading was detected. Dose rates were obtained using low-level γ-spectrometry and conversion factors given by Adamiec & Aitken (1998).

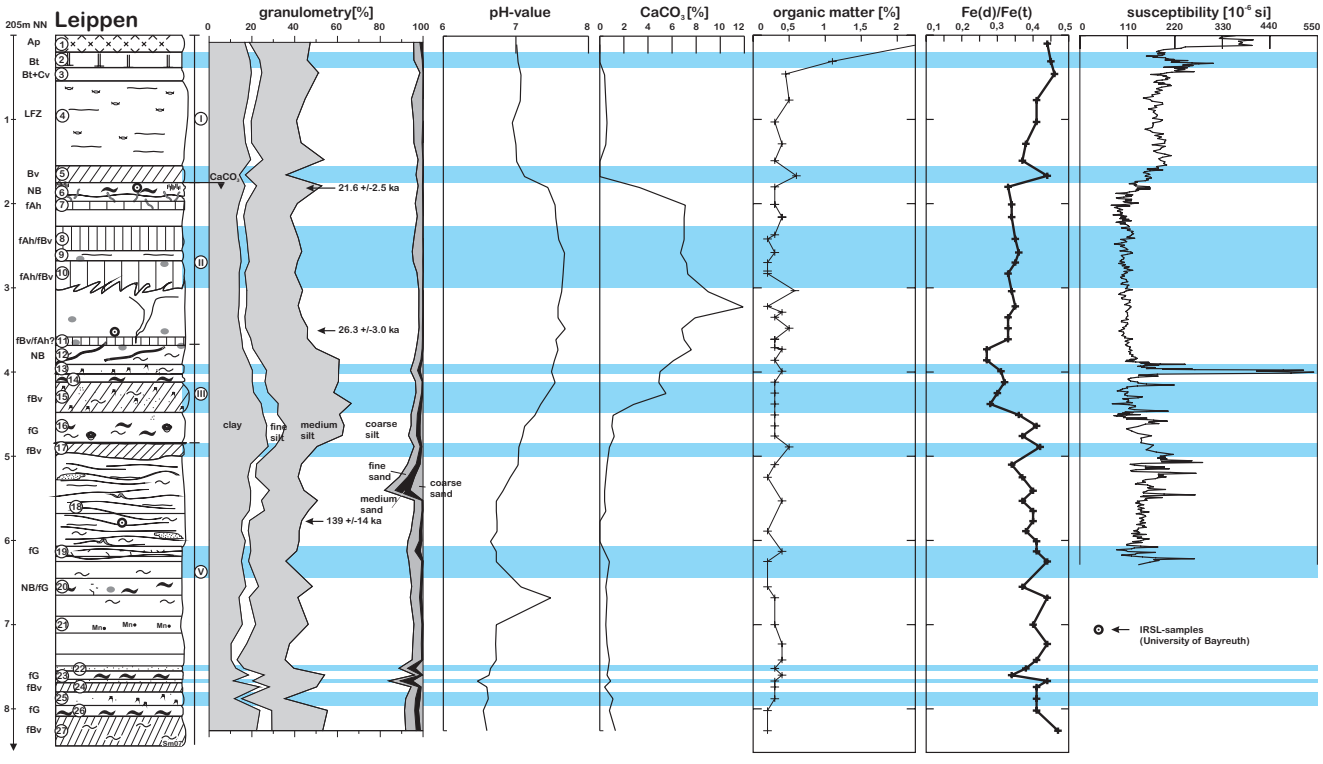

Fig. 2: Profile Leippen with geochemical results.

Abb. 2: Profil Leippen mit den dazugehörigen geochemichen Analyseergebnissen.

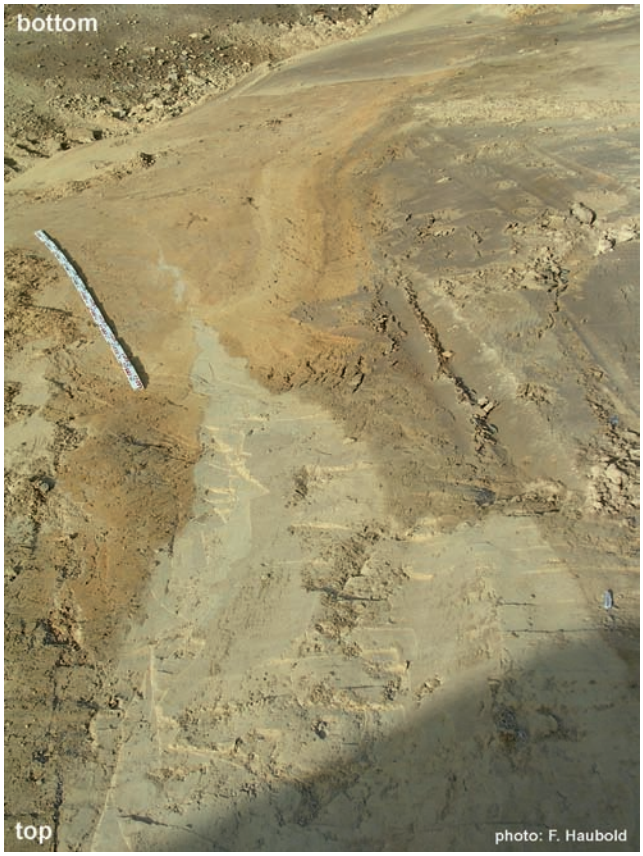

Fig. 3: Big ice wedges at the section Leippen (photo is upside down).

Abb. 3: Mächtige Eiskeilpseudomorphose im Profil Leippen (Foto steht auf dem Kopf).

3 Results

3.1 Section Leippen (Tab. 1; Fig. 2)

Due to roadcuts close to the village of Leippen (GK R 459345 H 566726) this section was open in summer 2005. A detailed description is given in Tab. 1. In general the section could be subdivided into four units, beginning at the top with a darkish decalcified part in which the Holocene soil is developed. The decalcification boundary at about 2 m is the lowermost limit of this unit. The underlying calcareous loess is characterized by a light yellowish colour and a typical porous fabric. This unit is composed of pure loess and resorted loess derivates wherein some darkish or reddish parts could be detected and are seen as interstadial soil features. During the deposition of this unit huge ice wedges were formed reaching even into the subjacent unit (Fig. 3).

The unit beneath is dominated by solifluction processes which generated different smaller layers. The whole unit shows markedly stronger colouring. The base is composed of material which seems to have undergone strong soil redeposition. The lowest unit is subdivided into two parts. The upper part shows a strong lamination with platy fabric including sandy bands indicating abluation processes; the lower part is less laminated and has a weaker structure. We assume that the lowest unit is already composed of Saalian deposits. A sample from the lower part of layer 18 shows an IRSL-age of 139 +/- 14 ka. Combining this IRSL-age with the increase of clay and sand in layer 16 and 17 and the increase of Fe-ratio we suspect a significant hiatus in this section. This hiatus is result of an erosion phase which hits the Eemian soil and the Early Weichelian deposits.

The geochemical analyses (Fig. 2) support the division into these units.

3.2 Section Seilitz (Tab. 2; Fig. 4)

The section is located close to the village of Seilitz (GK R 5388260, H 5673750) in a kaolin pit 1.5 km southwest of the recent course of the river Elbe. A detailed description is given in Tab. 2. The loess record covers a thick kaolin horizon derived from strong alteration processes of the monzodiorite. In between, a small sandy gravel layer is developed which is interpreted as remnants of moraine material of Saalian age. This stratigraphical situation makes a Weichselian loess deposition most likely. Following the different features within the whole loess section we propose to subdivide the Weichselian loess deposits into three units. According to the Leippen section the uppermost unit, a decalcified loess, correlates to the late Weichselian with the recent soil at the top. The following unit is about 5 m thick and contains several interstadial soils with the upper soil showing strong hydromorphic features (Fig. 4; layer 5 and 6). A dark grey horizon (layer 10) is seen as the strongest palaeosol-(sediment) in this section. The lower brownish palaeosol forms layer 12. The lower unit III is characterized by layers indicating strong solifluction, which are also recognizable at the section of Leippen (Fig. 5). Geochemical analyses such as the increased content of sand and clay (Fig. 4) show congruent results. For example the dark grey horizon (layer 10) shows enrichment of carbonate and of SOM. The pH-value marks the carbonate free parts of the Holocene soil development and fits well with the analyses of the carbonate content.

3.3 Section Zehren (Tab. 3; Fig. 6)

The Zehren section (GK R 4597625 H 5675325) is situated about 1.5 km to the north of Seilitz section. Tab. 3 contains a summarized description. At the top of the section a weak humic calcareous horizon is developed which indicates strong erosion processes in former times. We assume that at least 2 m of soil and loess material is lacking. Therefore the described unit from the top of section Seilitz and Leippen is not preserved in section Zehren. At about 3 m depth we detected a notable humic horizon with remarkable dark grayish colouring (layer 9) which has not been described in former studies. The main features of this horizon are the strong colour and the distinct lower and upper boundary. The base of this unit (layer 20) marks the boundary between loess and loess sediment (Fig. 6). From a depth of 7 m (layer 21) the section is composed of strongly reworked loess derivates up to a depth of 11 m. Considering the fact that at the top of this section 2 m of loess are missing we believe that this sections represents the thickest loess accumulation of the study area.

3.4 Section Ostrau (Tab. 4; Fig. 7)

This section is situated close to the town of Ostrau (GK R 4582462 H 5675008) in a limestone pit of the Ostrauer

E&G / Vol. 60 / No. 1 / 2011 / 47–65 / DOI 10.3285/eg.60.1.03

Kalkwerke GmbH and contains the most complete Weichselian loess sequence including the last interglacial palaeosol (Eemian). Tab. 4 shows a detailed description of section Ostrau. According to the sections of Leippen and Seilitz we are able to subdivide the sequence from section Ostrau into three upper units as well. As the section reaches into the last interglacial palaeosol, we added a fourth unit at the bottom of this section. From the top we observe the typical sequence starting with decalcified loess which includes the first three layers (Fig. 7). Unit II starts with layer 4 and ends at about 5 m depth with layer 8. In layer 5, a slightly reworked but strong soil is developed which we correlate with the strong soil at section Zehren (Fig. 6, layer 9). This soil formed after a stronger phase of reorganization of the surface as evidenced by deep gullies which are filled up (layer 5). A detailed draft (Fig. 8) of the upper part of the section shows the incision into layer 6.

The lowermost unit begins with layer 9 in which big ice wedges could be observed. Stratigraphically they belong to layer 8 (unit II). The lowermost unit III is composed of several derived loess layers and soil sediments indicating several environmental changes during this time. The grey solifluction layer (11) and the reddish loam (layer 12) mark the boundary between unit III and unit IV.

Tab. 1: Description of section Leippen.

Tab. 1: Profilbeschreibung Leippen.

Layer	Label	Description
1	Ap	humic dark horizon with a clear lower boundary
2	Bt	reddish brown clay enriched compact loam, weak pinprick structure and sporadically hydromorphic features (rust stains)
3	Bt+Cv	less clay than layer 2, oval bleached patches (diameter 5mm), pinpricks
4	LFZ	lamellar line-like structure between brownish clay-enriched (10Y5/6) and yellowish coarse silt (10Y6/4)
5	Bv	homogeneous light brownish grey, non calcareous silt, typical loosely packed loess structure with sporadic fine Manganese concretions, old backfilled earthworm burrows
6	NB	bedded light greyish calcareous loess with iron hydroxide lines, undulated lower boundary, old backfilled earthworm burrows (current term in work: bio-traces)
7	fAh	pale slightly dark loess
8	fAh/fBv	brown greyish homogeneous loess with pseudomycelia and sporadic big Mn-stains,
9		slight lamellar structure, light brown, big Mn-stains
10	fAh/fBv	brown greyish homogeneous loess with pseudomycelia, undulating lower limit
		laminated loess with big Manganese stains
11	fAh/fBv?	pale dark homogeneous loamy loess
12	NB	grey brownish loam with a typical iron-oxide grid
13		loamy, brown greyish loess derivate, numerous Mn-concretions (solifluction layer)
14		loam, grey, brown with some little stones
15	fBv	(soil sediment) stony (pebbles) layer, dark grey brown, numerous Mn-concretions, dense layering
16	fG	bleached grey layer with rosty tubes, hydromorphic features
17	fBv	reddish sandy material with cryoturbation features, parts with microstructure
18		clearly laminated material with sandy, loamy and silty layers (10YR5/6, 5/4, 6/8, 5/6), platy microstructure
19	fG	grey-(light purple)-bleached loam
20	NB/fG	grey-(light purple)-bleached loam, iron-oxides
21		Manganese enriched loam
22		thin layer of sand
23	fG	grey-(light purple)-bleached loam
24	fBv	(soil sediment) clay enriched, reddish brown soil sediment
25		yellowish loess
26	fG	grey-(light purple)-bleached loam
27	fBv	(soil sediment) stained silt, grey brown yellowish

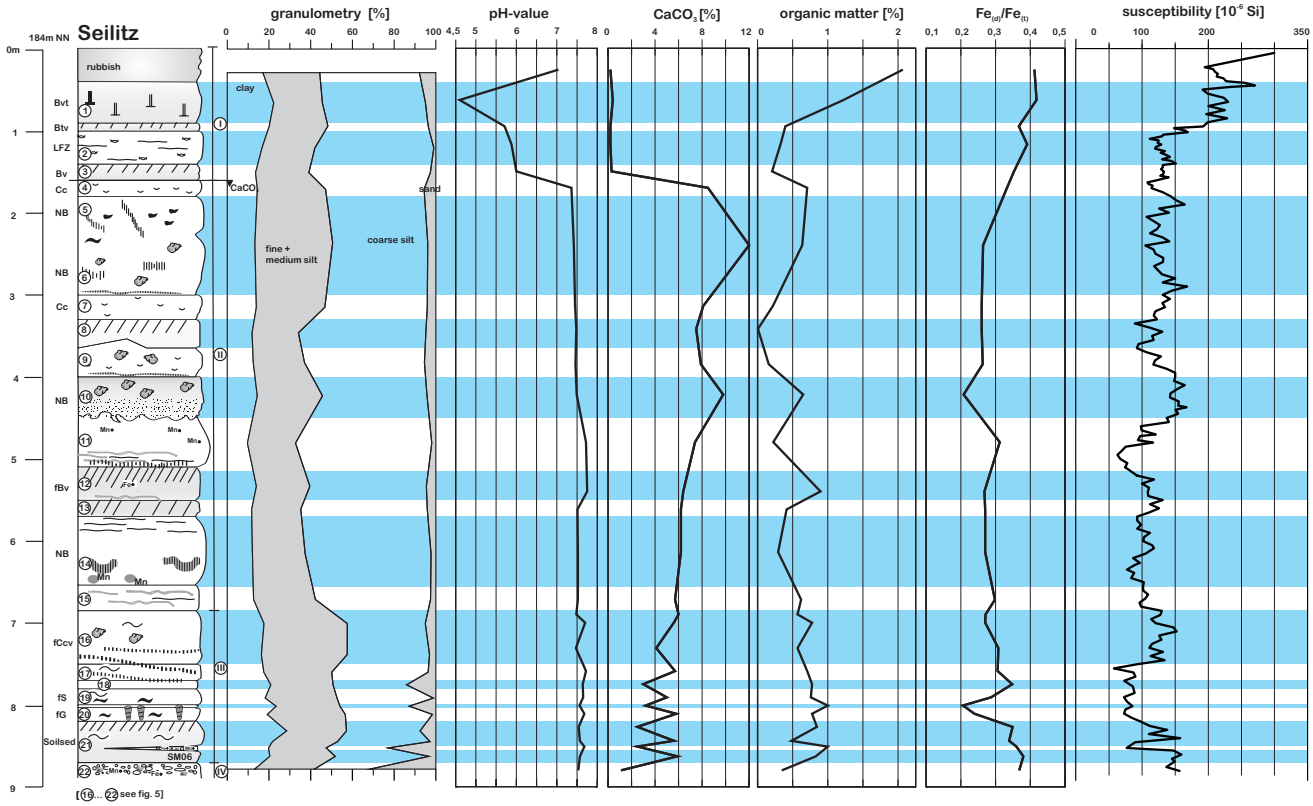

Fig. 4: Profile Seilitz with geochemical results.

Abb. 4: Profil Seilitz mit den dazugehörigen geochemichen Analyseergebnissen.

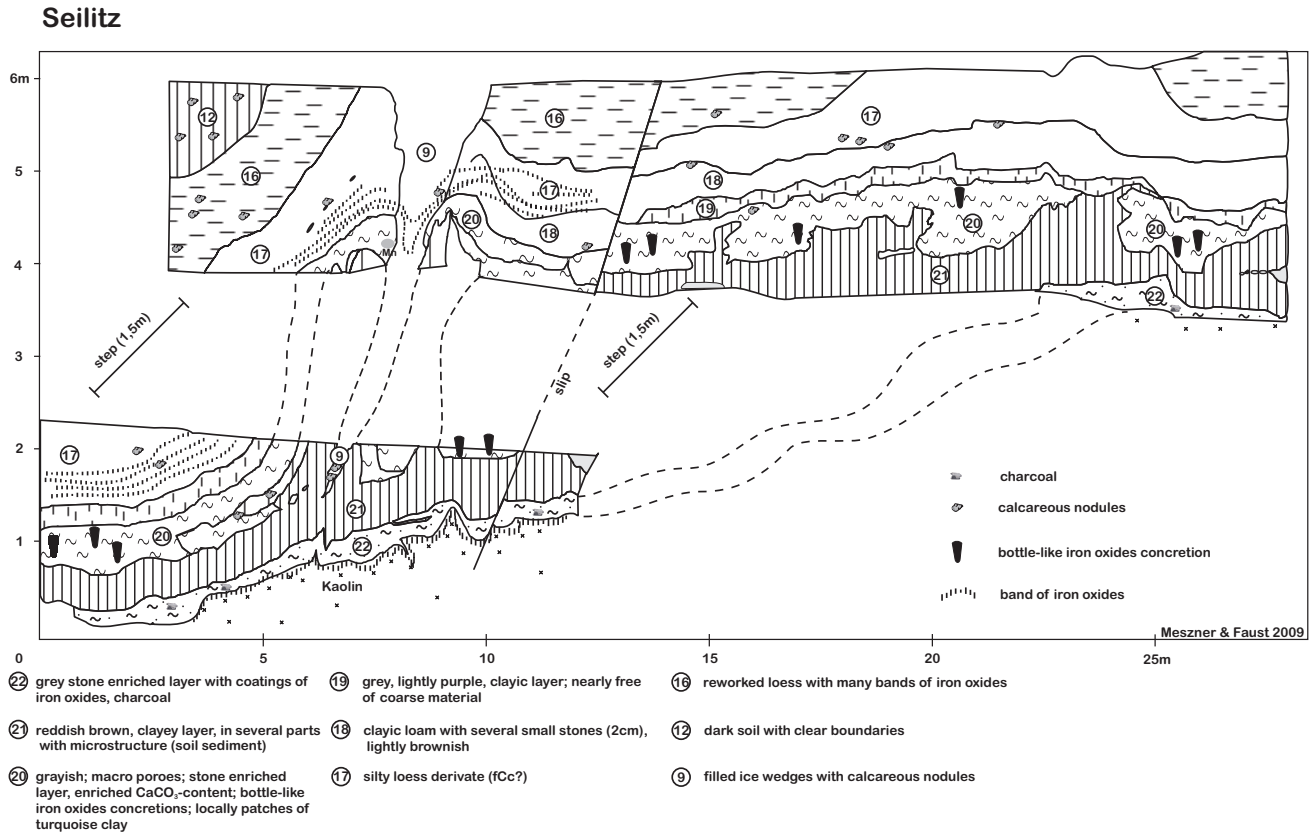

Fig. 5: Lower part of the section Seilitz (Nr.9: filled ice wedge).

Abb. 5: Der untere Wandabschnitt im Profil Seilitz (Nr. 9: Eiskeilpseudomorphose).

E&G / Vol. 60 / No. 1 / 2011 / 47–65 / DOI 10.3285/eg.60.1.03

Tab. 2: Description of section Seilitz.

Tab. 2: Profilbeschreibung Seilitz. NB = Naßboden

Layer	Label	Description
1	Bvt	brown illuvial horizon with weak hydromorphic features, in the lower part prismatic structure
2	LFZ	a very typical expression of lenticular horizon!; lamellar line-like structure between brownish clay-enriched and yellowish coarse silt, pores increasing with depth
3	Bv	light brown homogeneous horizon, decalcified, some fine pores
4	Cc	light yellow calcareous loess; bio-traces, small Mn-concretions,
5	NB	Concentric iron oxide rings around root channels, pseudomycelia, bleached grey stains, scattered fine pores
6	NB	light brown loess, diffuse iron oxide patches, pseudomycelia, small Mn-concretions, stained,
7		loess
8		reddish loess (fine dispersed iron oxides)
9		weak linear iron oxides on a pale matrix, calcareous nodules, lower limit marked by a strong line of iron oxides
10	NB	calcareous nodules, dark grey, many fine pores, loamy, 10% calcium carbonate, molluscs, soil structure, iron oxide stains, clearly limited, undulating lower boundary
11		bedded loess derivate with calcareous nodules and small Mn-concretions
12	fBv	no stratified loess, homogenous material, small globules of iron oxides, greyish brown colour, many pseudomycelia, undulating lower boundary
13		stratified material, hydromorphic features
14	NB	iron oxides diagonally ruled, big Mn-stains in the lower part
15		stratified loess derivates, strong reworked material
16	fCcv	some calcareous nodules, sporadically little stones
17		massive slight pale yellow calcareous loess with fine iron oxide bands
18		loess derivate with many Mn- and iron oxide concretions
19		grey brownish loam, bands of iron oxides and small calcareous concretions
20	fG	grey, bleached material, locally patches of turquoise clay, bottle-like iron oxide concretions (often formed like a sugar loaf)
21	(fBv)	(soil sediment) reddish brown loam, compact bedding, sometimes with weak platy microstructure
22		very massive layer, many stones, grey matrix with interfacial skins of iron oxides

Tab. 3: Description of section Zehren.

Tab. 3: Profilbeschreibung Zehren.

Layer	Label	Description
1	Ap	calcareous humic dark grey plough horizon
2		calcareous light yellow loess
3	NB	carbonate enrichment, some light grey bleached stains, patches and bands of iron oxides, biotraces
4		loess with calcareous nodules
5	fBvc	light brown yellowish loess, the upper boundary is marked by clearly visible and shredded layer of yellow material,
6		band of iron oxides on a grey yellowish bleached matrix
7		light brown yellowish loess, lower boundary is also marked by a shredded layer, pseudomycelia
8		loess with a fine layer of bleached patches, some pseudomycelia and iron oxides stains in the lower part
9	NB	dark grey loamy material, clear lower and upper boundary, some iron oxides and a very fine angular structure,
10		stains of iron oxide, bleached root channels

11		laminated loess with biotraces, in the lower part Mn-concretions
12	fBvc	light brown greyish material (not laminated!), small nodules of iron oxides
13		laminated loess with microcryoturbation
14	fBvc	brown greyish homogeneous material, iron and Mn-concretions, pseudomycelia, biotraces, clear iron oxide bands on the lower boundary
15		loess
16	NB	lightly grey bleached loess with iron oxide stains, clearly band of iron oxide
17		material showing weak lamination
18		light brown colouring
19		weakly laminated loess derivates
20		loess with distinct lamination and some iron oxides stains in the lower part, cryoturbation features
21	fS/Bv	brownish grey loam with iron oxide grid, big Mn-patches,

Tab. 4: Description of section Ostrau.

Tab. 4: Profilbeschreibung Ostrau.

Layer	Label	Description
1	Bt	lower part of truncated Bt-horizon of the Holocene Luvisol, spare hydromorphic features (iron oxide stains)
2	LFZ	short brown bands of loamy clayish material alternating with pale yellow loessic stains (lenticular horizon)
3	Bv	homogeneous pale brown material, some diffuse cloud-like Mn-stains
4	NB (Nassboden [germ] ~ Gelic Gleysol)	typical microstructure of loess, slightly brown colour, some parts show pale dark discolouration when the surface is drying; these discolourated parts look like filled earthworm burrows (current work determination: bio-traps), sporadic Mn-concretions
5	NB	dark grey bleached loamy material with rust stains and a clear microstructure (rough section surface after preparation), $CaCO_3$-concretions make crunching noise when cleaning the section, calcareous nodules horizontally bedded
6		laminated loess derivate, sparely iron oxides stains
7	fBv	light dark, pale brown (slightly purplish) colour; calcareous nodules, very distinct lower and upper boundary (undulating), rust stains, pseudomycelia, Mn-concretions; cryoturbation features
8		laminated loess derivate, in the lower part big Mn-stains
		stronger reworked material - clear changes in texture
9	fS/Bv	thick layer; brown, slightly reddish (10YR6/4); in the upper part stains of iron oxides (leopard skin-like), in the lower part increase of bleaching and iron oxides, fissures are lined with iron oxides skins, sporadically pseudomycelia; loamy, mixed with coarse fragments
10		bright yellow silt, without any features of pedogenesis, filled ice wedge
11		clear boundary, grey matrix (10YR5/4) with fragments of reddish brown clayic material, relative high content of coarse material and calcareous concretions, solifluction features
12	reworked Bt	dark yellowish (reddish) brown (10YR4/4) loam, sporadically angular structure, in the lower part strong hydromorphic features (grey bleached)
13	HZ	dark pale grey brown silt (mottles), least compacted
14	fS(e)w	conspicuous bright grey material; loose structure; charcoal; big fibril Mn-concretions
15	fSw/Bt	mottled yellow reddish orange horizon, bleached grey root channels subangular structure, in-situ Bt-horizon of a Luvisol with hydromorphic features
		buried stone layer
17		sand with clay coatings and a prismatic structure, intense reddish colour

HZ – Humuszone (humic horizon)

E&G / Vol. 60 / No. 1 / 2011 / 47–65 / DOI 10.3285/eg.60.1.03 / © Authors / Creative Commons Attribution License

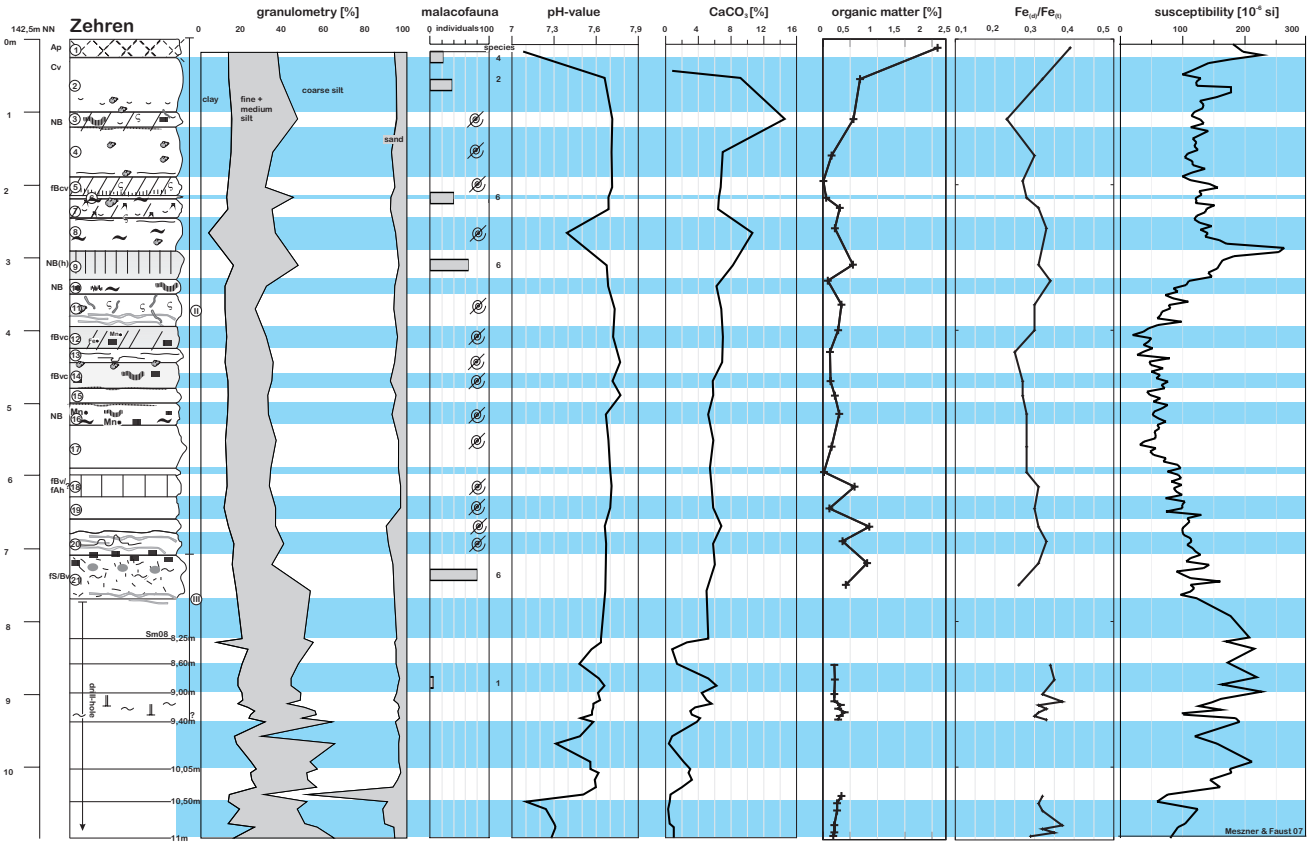

Fig. 6: Profile Zehren with geochemical results.

Abb. 6: Profil Zehren mit den dazugehörigen geochemichen Analyseergebnissen.

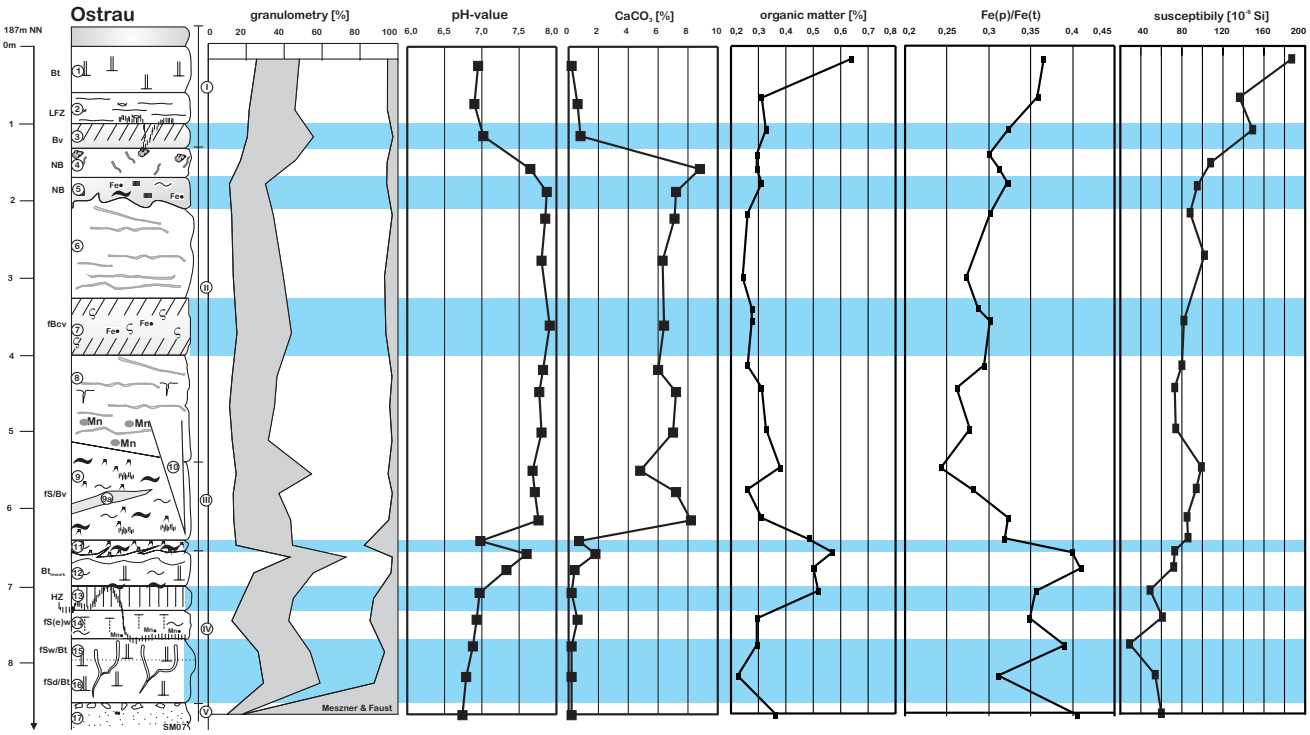

Fig. 7: Profile Ostrau with geochemical results.

Abb. 7: Profil Ostrau mit den dazugehörigen geochemichen Analyseergebnissen.

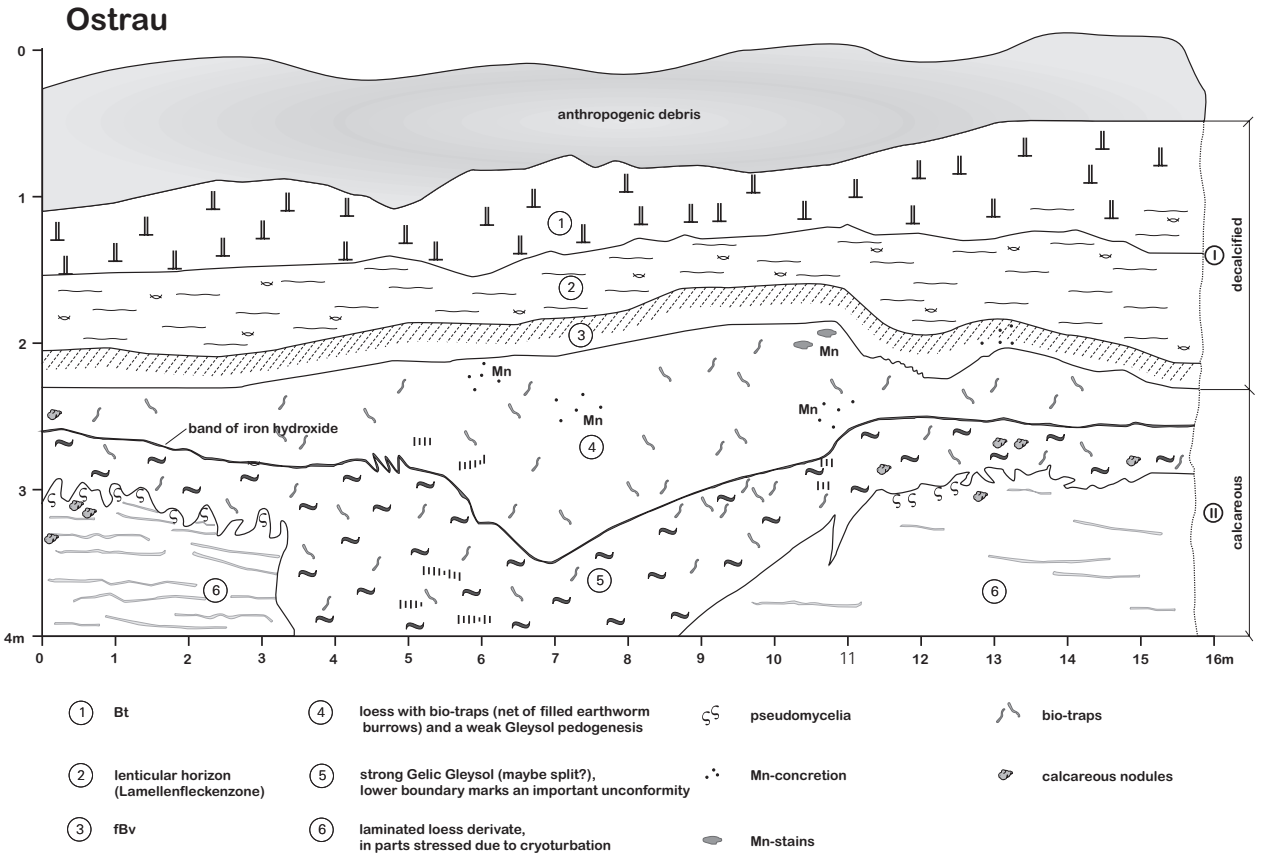

Fig. 8: Detailed draft of the upper part of section Ostrau.

Abb. 8: Detailzeichung des oberen Teils der Abbauwand im Profil Ostrau.

Tab. 5: Description of section Zschaitz.

Tab. 5: Profilbeschreibung Zschaitz.

Layer	Label	Description
1	Bt	reddish brown clay enriched compact loam, weak pinprick structure and sporadically hydromorphic features (rust stains)
2	LFZ	lamellar lined structure between brownish clay-enriched and yellowish coarse silt; in the upper part large and in the lower part narrow bedding, lenticular horizon
3	Bv	homogeneous light brownish grey, non calcareous silt, loose loess structure; several dark greyish curved structures (banana-like) crossing the boundary into the calcareous loess; boundary between non-calcareous and calcareous loess
4	NB	grey material, hydromorphic features, undulated lower limit
5		laminated material with small frost cracks
6	fBv	platy structure, Mn-concretions, pale grey-brown
7		loess
8	fBv	Mn-concretions, pale grey-brown
8a		slightly reworked loess, laminated
9	NB fBv/fG?	homogeneous greyish material; increase content of fine to medium silt and clay; deoxidation in the lowest part of this layer
10	fBv	brown loessic material with fine dispersed iron-oxides
11		light yellow greenish layer with fibered Mn- (2-5mm) and iron-oxide concretions
12	fG	grey, bleached material, locally patches of turquoise clay, bottle-like iron oxide concretions
13	Bt reworked	reddish layer with high content of clay; constant thickness; microstructure; the lower limit is marked by a crusted band of iron oxide; nearly no Mn-concretions; thin horizontal patches of bleached material
14	fBt-Sd	brown reddish, slightly purple material; well developed microstructure; bleached root channel, ice wedges are filled with fBt-Sd-material

E&G / Vol. 60 / No. 1 / 2011 / 47–65 / DOI 10.3285/eg.60.1.03 / © Authors / Creative Commons Attribution License

15	IIfBtSd	variocoloured horizon, orange reddish and grey parts, many stones, grey bleached channels
16		very coarse material, many stones
17		gravel from a palaeochannel of the Freiberger Mulde river

Tab.6: Description of section Klipphausen.

Tab. 6: Profilbeschreibung Klipphausen.

Layer	Label	Description
1	Bt/Sd	checkered loam with clay filled root channels; bleached clay
2		yellowish loam with numerous Mn-concretions
3		deoxidized greyish loam with bottle-like iron-oxide structures
4		reddish, grey-brown clayish loam
5		loessic laminated silty loam, platy microstructure
6		homogeneous brown clayish loam, compacted
7		light grey loam; in the upper part some patches of iron-oxide; the lower limit is marked by crusted band of iron oxides
8		silty loam, yellow matrix with rusty coatings
9		sandy loam with grey bleached patches in a reddisch oxidized matrix
10		bedded sand, upper limit is marked by a distinctive Mn-band

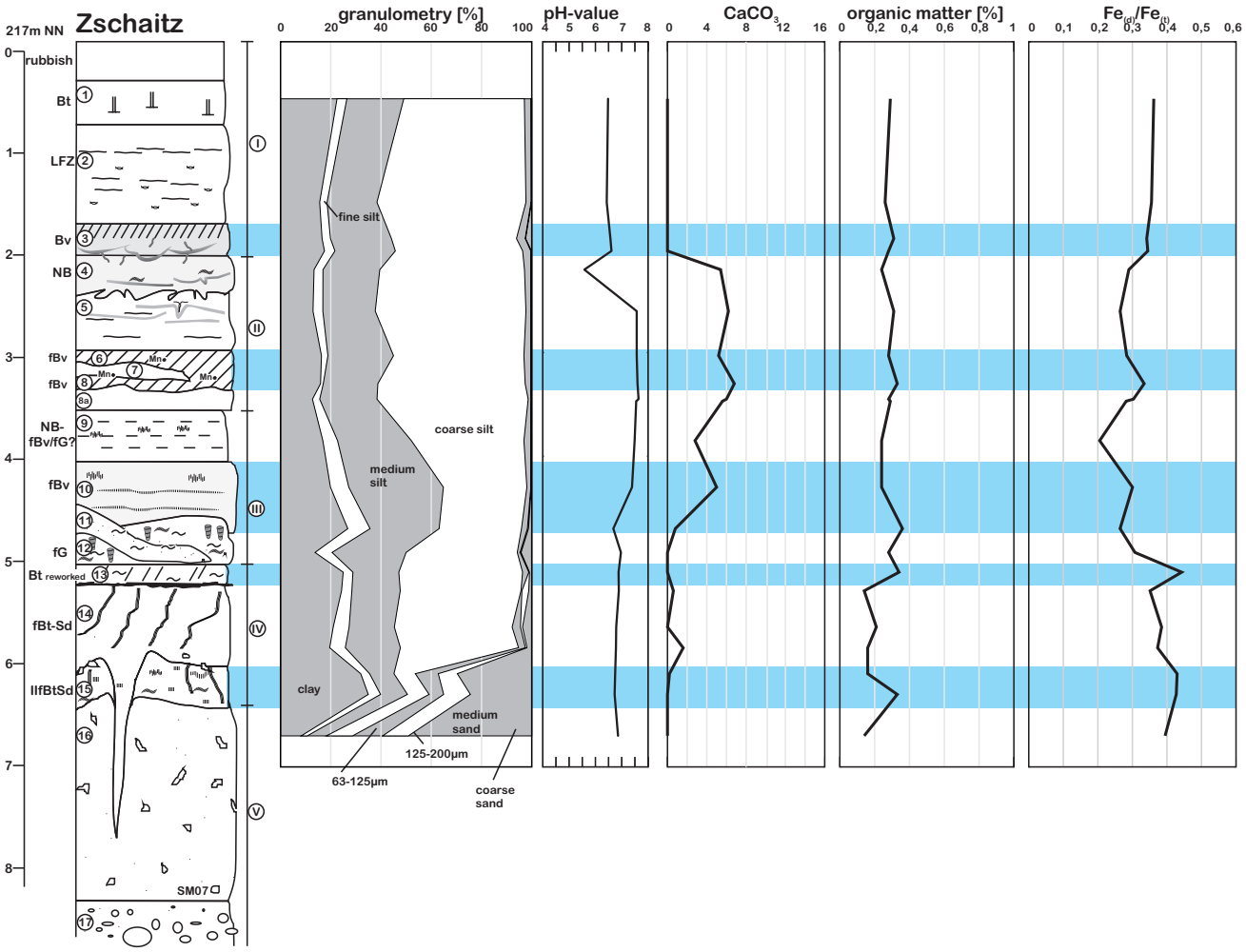

Fig. 9: Profile Zschaitz with geochemical results.

Abb. 9: Profil Zschaitz mit den dazugehörigen geochemichen Analyseergebnissen.

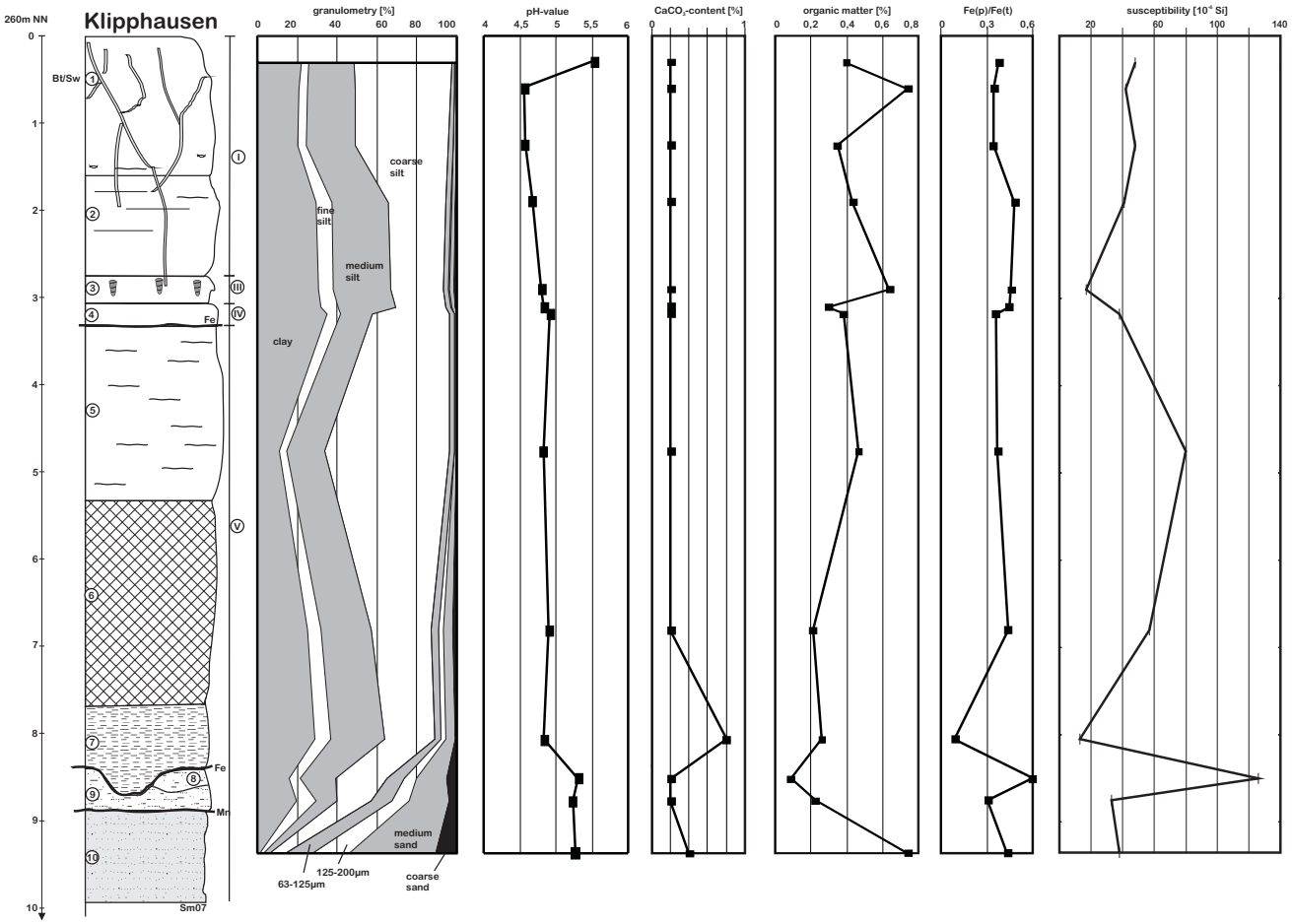

Fig. 10: Section Klipphausen (contrary hachures to fig. 16 in layer 6–10!: 6 - clayic loam; 7 - light grey loam; 8 - silty loam; 9 - sandy loam; 10 - bedded sand).

Abb. 10: Profil Klipphausen (von der Legende (Abb. 16) abweichende Schraffuren in Schicht 6–10!: 6 - toniger Lehm; 7 - hellgrauer Lehm; 8 - schluffiger Lehm; 9 - sandiger Lehm; 10 - geschichteter Sand).

Tab. 7: Description of section Gleina.

Tab. 7: Profilbeschreibung Gleina.

Layer	Label	Description
1	Bt	lower part of the truncated Bt-horizon
2	LFZ	lenticular horizon
3	Bv	homogeneous pale brown decalcified horizon
4		bleached stains (root channels), biotraps, at the lower part slightly brown with Mn-stains
5	NB	high porosity, many bleached stains, bright orange iron oxide rings around filled root channels
		loess with many iron hydroxide stains
6	NB	many small calcic nodules (Loesskindl); bleached, the lower part shows many Mn-dots
		loess, scattered small Mn-concretions, scarcely iron hydroxide stains
7	NB	calcareous nodules, strong bleaching; scattered rust stains, platy structure, clear boundaries
8		laminated loess derivate, loose density
9	NB	weak bleaching; homogeneous (not laminated), iron hydroxide stains, pseudomycelia
10		laminated material with small frost cracks, loess derivates
11	fBv	homogeneuos, diffuse distributed iron hydroxide stains, pseudomycelia; loamy, weak structure, many pores
12		weak laminated material with features of cryoturbation stress
13	fBv	pseudomycelia; no lamination, gathering of Mn-stains, small iron hydroxide concretions
14		upper boundary is marked by some slightly yellow undulating and thin layers of loess material, distort layers, big Mn-stains, small frost cracks

E&G / Vol. 60 / No. 1 / 2011 / 47–65 / DOI 10.3285/eg.60.1.03 / © Authors / Creative Commons Attribution License

15		transition zone between weakly modified and strongly reworked loess, above: many oval Mn-stains beneath: bigger Mn-stains, compact structure, loamy, typical iron oxide grid (leopard skin-like)
		increasing of medium and fine silt with depth, big Mn-stains with diffuse boundaries
16		Mn-stains and calcareous nodules, location of big (15cm) horizontal bedded calcareous nodules
17		increasing clay content with depth, scattered iron hydroxide stains, in the depth of 10.30 m gradual increase of carbonate, small admixture of coarse fragments; the lowest part is represented by a brown greyish clayish layer
18	fG	non calcareous, intense bleached, grey horizon (10BG 6/1); the lower boundary is marked by intense lines of iron hydroxides
19	fBv	reddish brown horizon, platy structure, bands of iron hydroxide that end abruptly at the upper boundary
20		gradually decrease of carbonate, bedded structure with embedded sandy lenses
21	HZ	dark pale grey brown silt, least compacted
22	fS(e)w reworked	bright grey bleached material, weak coherence, big Mn-concretions (0.5-1 cm) often with fibril structure; charcoal!
23	IIfS(e)w	intense mottles of reddish brown iron hydroxides, most parts are bleached, subangular structure;
24	fBtSd	intense bleached root channels, clearly subangular structure, decrease of colouring, in the lower part more reddish, more darkish at the top
25	$IIfBt_{(Sand)}$ $IIIfG_{(silt)}$	mixed layer with reddish clay and light gray silt
26		light ochre sand

Of particular interest is the humic horizon in layer 13 and the bleached lower part rich in charcoal remnants (layer 14). In Ostrau this stratigraphically lowest unit is composed of Saalian deposits in which two in situ horizons were formed (Eemian soil; layer 15/16).

3.5 Section Zschaitz (Tab. 5; Fig. 9)

At the Zschaitz section deposits of an ancient river branch of the Mulde river (Eissmann, 1964) are exposed in a gravel pit (GK R 4580416 H 5669191). These fluvial deposits are covered by loess sediments of two glacials. Four units could be identified in this section. Details are given in Tab. 5. Unit I is composed of decalcified sediment layers which could be correlated with almost all the other sections described in the present study. The lower boundary of this unit is marked by the boundary of the decalcified layer into the calcareous loess. Unit II is not as distinct as in the other sections and composed of the layers 4 to 8a. Unit III contains several soil sediments and solifluction layers. Its boundary to unit IV is distinct and clear. Unit IV has on its top remnants of the last interglacial soil. The deeper part shows big ice wedges and strongly reworked loess derivates with little gravel content. Within this deepest layer (16) close to the contact to the gravel deposits (layer 17) some artifacts (small bifaces) were found but have not been investigated yet.

3.6 Section Klipphausen (Tab. 6; Fig. 10)

This section is situated close to the village of Klipphausen (GK R 4605947 H 5660667). It is not accessible anymore because it existed only for a short period of time during house construction. The section Klipphausen is characterized by an additional pattern, not identified in the above described sections. The material of the upper three meters is loamy (20%–60% clay; fine and medium silt) and show a low pH-value. This is due to the fact that this section is located in the southern part of the study area close to the connecting slope into the southern mountain range (Erzgebirge). It is a typical position for the transition zone from the loess plateau with eolian dominated processes into the mountain landscape which was dominated by solifluction processes. The section is composed of different layers including loess derivates and solifluction layers. We only see similarities according to the other sections in the upper part of this sequence. There, gleyic features are found in a loess derivate (layer 3) which we correlate with layer 16 of the Leippen section (Fig. 2) and layer 20 of the Seilitz section (Fig. 4).

3.7. Section Gleina (Tab. 7; Fig. 11)

The Gleina section is located at the northern loess boundary (Lössrandstufe) at the western edge of the village Gleina (GK R 4586889 H 5678057). This former brickyard is the type locality for the so called "Gleinaer Bodenkomplex" which is an interstadial soil complex (Lieberoth & Haase, 1964).

The Gleina section was reopened by us in 2009. Fig. 11 shows the main stratigraphical units. The thick loess sequence of Gleina has comparable units which correlate well with the previously described profiles. The four important units already described are present in this section. The section also shows the "Gleinaer Bodenkomplex", which is easy to identify because of its intense colour changes from gray to reddish. In addition, this soil complex is characterized by its decalcified horizon between the top of the complex and the following interglacial soil below. However, in all the other sections, there is no clear evidence of this complex.

According to Neumeister (1966) who reported the thickest

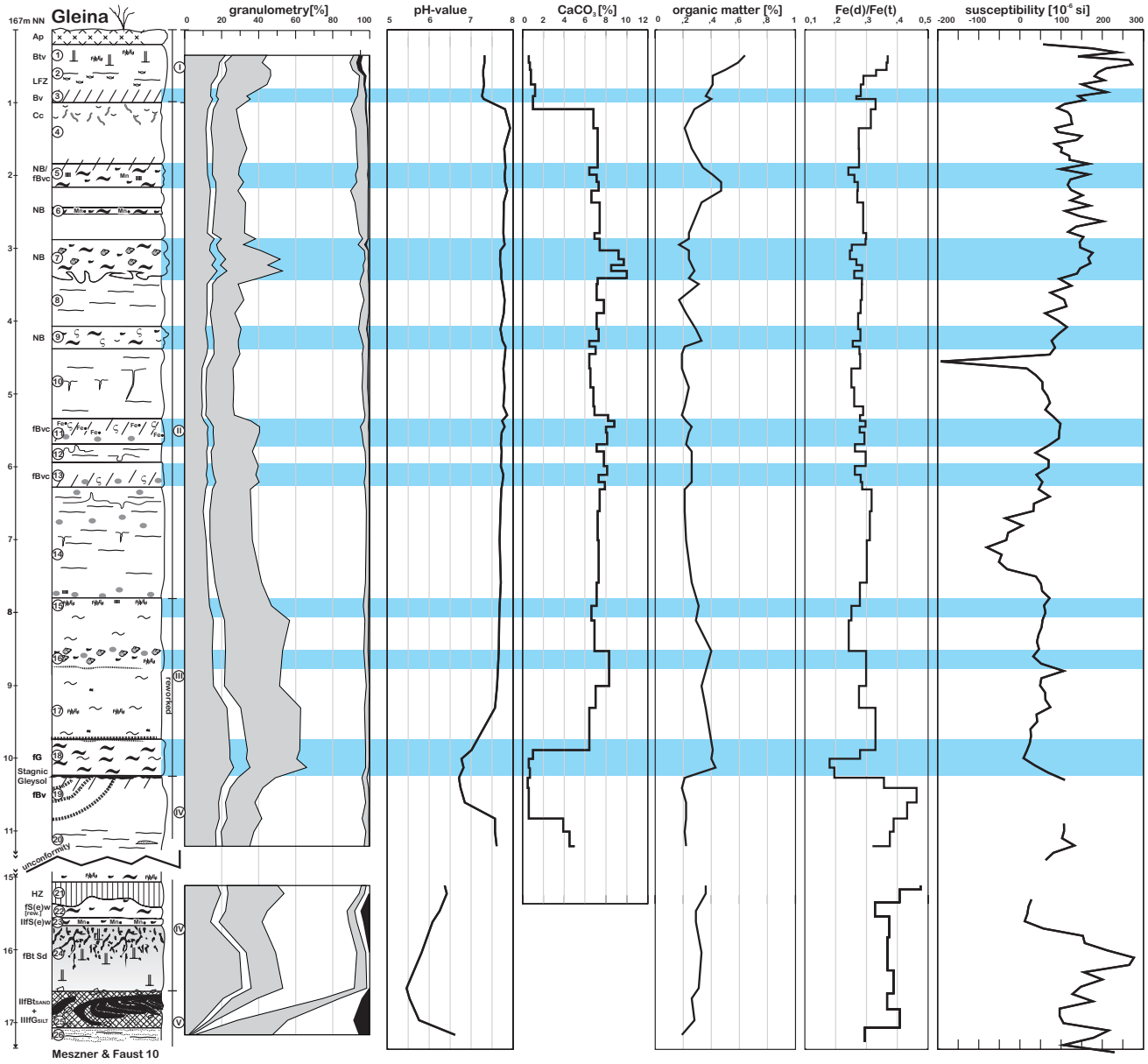

Fig. 11: Profile Gleina with geochemical results.

Abb. 11: Profil Gleina mit den dazugehörigen geochemichen Analyseergebnissen.

Weichselian loess layers in the northern boundary (Lössrandstufe) our findings show a similar pattern. The northernmost sections (Gleina and Zehren) show the thickest, and in the case of Gleina most complete Weichselian loess deposits. In contrast, the section Klipphausen, situated at the southern boundary of the loess plateau, shows only Weichselian loess deposits of 3 m thickness.

4 Interpretation and discussion

The main lithological and pedogenical features of all studied sections are used to establish a standard loess-palaeosol profile for the Saxonian loess region. In five sections (Leippen, Seilitz, Ostrau, Zschaitz, Gleina) the uppermost 2 m look almost similar. The material is decalcified and in the uppermost part a luvisol was formed during the Holocene. Below a well-developed Btv-horizon a lenticular horizon ("Lamellenfleckenzone" after Lieberoth, 1959) can be observed in all sequences. In some cases ice wedges just below the recent surface were formed and whose infilling show lenticular structure even if they reach into the underlying horizon. We assume that this widespread lenticular horizon was formed after a strong cooling which generated these ice wedges. The features of lenticular structure point to a pedogenesis which can be explained by alternations between frozen and unfrozen conditions, resulting in clear band shaped structures of different grain sizes. The underlying horizon is not affected by this process and shows no banded features (Fig. 12). We suggest a taiga like environment to form such features. Below the lenticular horizon of the former permafrost horizon a brownish palaeosol is preserved. At the lower boundary of the brownish palaeosol there is a change from decalcified to calcified loess. This distinct change in the carbonate content represents a clear horizontal boundary, which is hard to identify in the sections. All these findings belong to **unit I** (Fig. 14) and are in consistency with former studies (Haase et al. 1970; Lieberoth 1959, 1962a, 1962b, 1963).

E&G / Vol. 60 / No. 1 / 2011 / 47–65 / DOI 10.3285/eg.60.1.03 / © Authors / Creative Commons Attribution License

Unit II is a loess layer up to 7 m thick. Except for some palaeosols within this unit, the loess shows only minor evidences of reworking. Unit II contains at least four palaeosols, including two weak soils showing gelic Gleysol features.

Fig. 12: Close up view of the lenticular (2) and underlying Bv-horizon (3) from Seilitz section (Photo: S. Meszner).

Abb. 12: Detailaufnahme des unteren Teils der Lamellenfleckenzone (2) und des Bv-Horizontes (3) oberhalb der holozänen Entkalkungsgrenze aus dem Profil Seilitz.

Fig. 13: Bottle-like iron oxide concretion in the section Seilitz.

Abb. 13: Flaschenähnliche Eisenkonkretionen im Profil Seilitz.

One of the strong soils can be characterized as a Cambisol, the other ones are reworked greyish gelic Gleysols with elevated humic content (Fig. 4 and 6). At the Zehren section mollusk analyses were conducted showing a high number of individuals of several species in the reworked humic gelic Gleysol. In contrast to the pedological features showing gleyic conditions the mollusk analyses point to a steppic palaeoenvironment. The occurrence of *Cecilioides acicula* indicates drier climatic conditions during the formation of this horizon (Hamann, 2010 unpub.). This horizon is most likely of polygenetic origin, assuming humid conditions, which led to the formation of a gelic Gleysol. Later this gelic Gleysol was reworked, also documented in the Ostrau section with features of deep gullying. Schirmer (2000) described a similar situation from the lower Rhine loess region and termed this layer "Eben-Zone". It is possible that erosion and redistribution of sediments were widespread during this period. A IRSL-sample from the top of this gelic Gleysol in Leippen section is dated to an age of 21.6 +/-2,5 ka (Fig. 2).

In a next stage subsequent soil formation under drier conditions took place. A humic horizon was formed within the material of the reworked gelic Gleysol in which the mollusk assemblage developed. Antoine et al. (2009) describe comparable processes. The humic soil formation correlates to a short interstadial with slightly drier climatic conditions. At section Zehren and Seilitz these soil horizons have higher magnetic susceptibility values. These two strong palaeosols can be identified in five out of seven profiles and interpreted as characteristic marker soils. The more weakly developed palaeosols can be observed in three sections (Seilitz, Zehren, Gleina). In contrast, former studies by Haase et al. (1970) and Lieberoth (1959, 1962a, 1963) describe only one weak soil within this unit II instead of two strong and one weak palaeosol which we could identify for Unit II of the composite Saxonian loess sequence. Numerical dating at the basis of Unit II in the Leippen section shows an IRSL-age 26.4 +/- 3 ka (Fig. 2).

The structure of **unit III** is complex but differs significantly from the overlying unit because of a shift in terms of granulometric composition from silt dominated material in the overlying unit II to more loamy material in unit III. This unit shows clear evidences of reworking processes. Coarse silt decreases whereas clay, fine silt, and medium silt as well as the sand fraction increase. Some parts of unit III are also characterized by a certain content of small pebbles of 1 cm in diameter as seen in the sections of Leippen, Seilitz, Zehren and Ostrau (Fig. 2, 4, 6 & 7). In the upper part of the transition zone large dark manganese spots (lowest part of unit II) could be observed. Iron oxide patterns are abundant in the lower part (uppermost part of unit III). In terms of climatic conditions it is assumed that the transition shows a climatic change from more arid conditions (unit II) to more humid conditions (upper part of unit III). Unit III shows in the part beneath very clear features of solifluction with incorporated small pebbles in an unsorted material. According to Haase et al. (1970) and Koch & Neumeister (2005) the material shows properties of loess derivates that is varicoloured.

Beneath the varicoloured loess derivate we observe a grey hydromorphic solifluction layer that shows clear features of cryoturbation with bottle shaped struc-

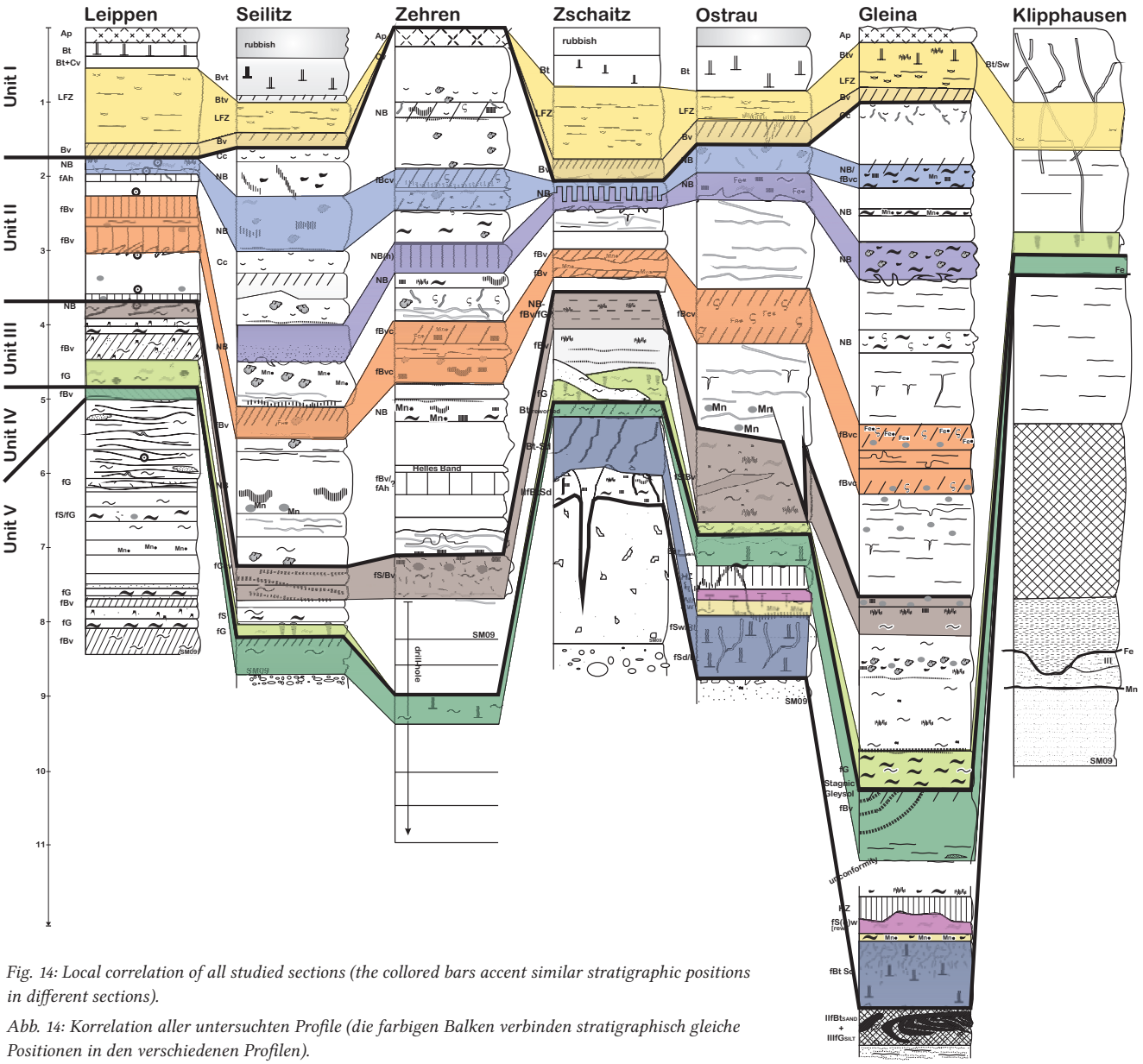

Fig. 14: Local correlation of all studied sections (the collored bars accent similar stratigraphic positions in different sections).

Abb. 14: Korrelation aller untersuchten Profile (die farbigen Balken verbinden stratigraphisch gleiche Positionen in den verschiedenen Profilen).

ture (Fig. 13). These features named "Roströhrengley" by Lieberoth (1963) can be seen in every section. The formation of this "Roströhrengley" is supposed to have been taken place during a cold and moist climate. This soil-like material (Roströhrengley) is integrated in the "Gleina Soil Complex" (Lieberoth, 1963). The Gleina Soil Complex contains furthermore an arctic brown soil below the gley soil that indicates slightly better climatic conditions. This complex is easy to identify by studying the graph of the iron-oxides ratio. The gley soil is mark by a profil-wide minimum of the Fe(d)/Fe(t)- ratio as can be seen in the sections Seilitz, Gleina, and Leippen. In contrast the underlying arctic brown soil is characterized by an increase of this ratio (Seilitz 21, Zschaitz 13, Ostrau 12, Gleina 19, Leippen 17). In the sections Gleina and Ostrau the values of iron-oxide ratios exceed in the reddish brown soil (arctic brown soil) the values of the Holocene and Eemian interglacial soils. Comparing these data we suppose a high activity of iron oxides caused by high oxidation-reduction potential during the formation of this interstadial complex.

In all sections, the arctic brown soil shows a reworked structure, whereas at the Gleina section this brown arctic soil was formed "in situ" however superimposing a reworked brown arctic soil sediment. This is proved by the fact that a distinct platy soil structure is developed.

Lieberoth (1962a) assumed that the "Gleina Soil Complex" was formed at the same time as the "Lohne Soil" (Semmel, 1968) respectively the "Paudorf Soil" (Fink, 1964). We do not support this interpretation because our findings point to a much older formation of the lower part of the "Gleina Soil Complex". This is supported by the observation that the lower part of unit III and the upper part of unit IV shows changes in terms of granulometric composition even between the "Roströhrengley" and the reworked arctic brown soil. Unconformities between unit III and IV in some sections indicate that prior to the formation of the "Roströhrengley" erosion and sedimentation took place. Finally it suggests a correlation of this soil complex ("Roströhrengley" and reworked arctic brown soil beneath) with the "Niedereschbacher Zone" described by Semmel (1968). It seems that processes of landscape disturbances and redistribution of soil material are typical for the Middle Weichselian in Saxony.

E&G / Vol. 60 / No. 1 / 2011 / 47–65 / DOI 10.3285/eg.60.1.03 / © Authors / Creative Commons Attribution License

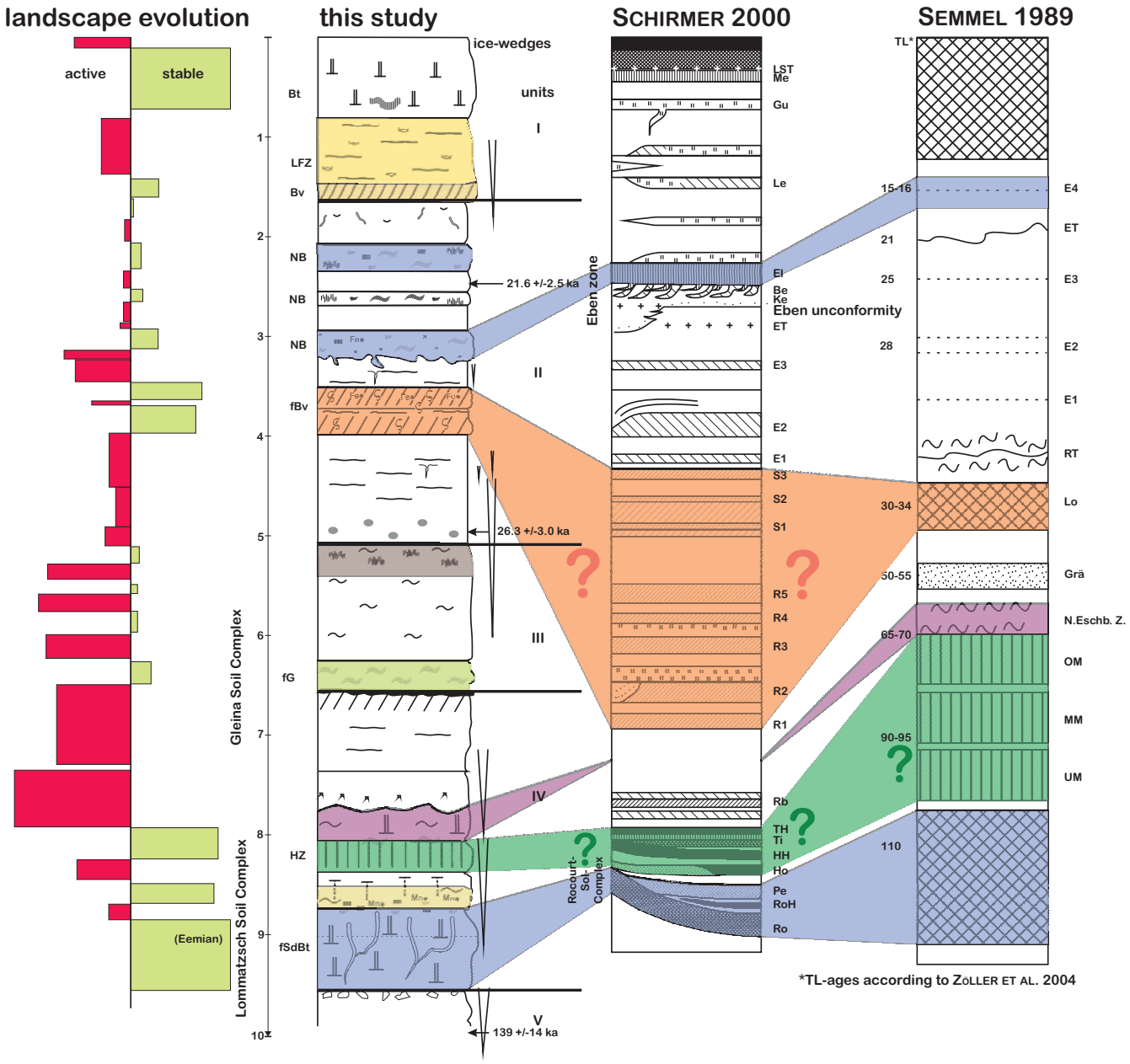

Fig. 15: Composite profile of Saxony and regional correlation with other loess areas in central Europe.

Abb. 15: Standardprofil der mittelsächsischen Lösse und mögliche Korrelation mit anderen Lössgebieten Mitteleuropas.

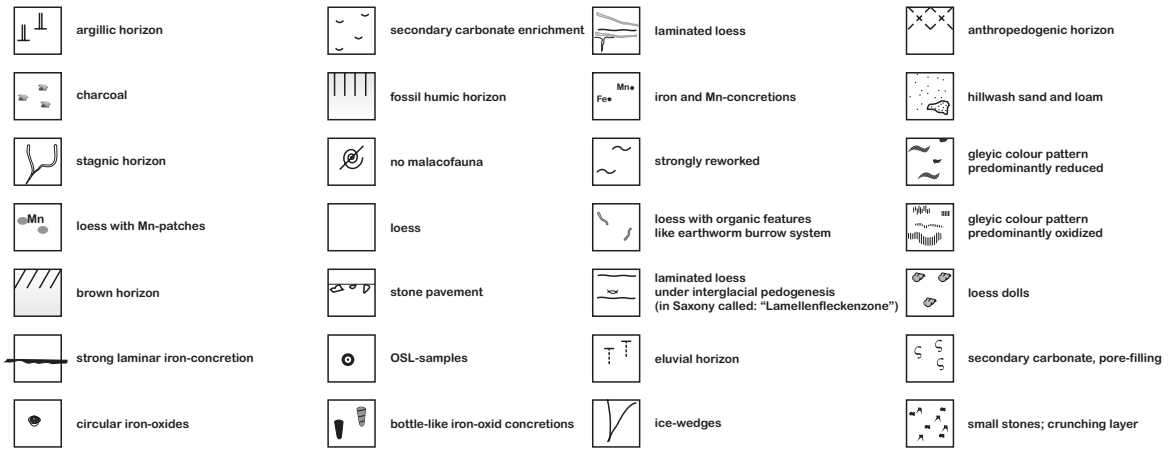

Fig. 16: Legend for all profile drawings presented in this study.

Abb. 16: Legende, für alle in dieser Arbeit verwendeten Profilskizzen.

Unit IV is only exposed at the sections of Ostrau, Gleina and with some modifications at the setting of Zschaitz. Compared to the unit above we observe only in the upper part reworking of soils in this unit. The reworked arctic brown soil is the result of a period of soil formation, followed by a period of solifluction. The increase of clay content and pedogenetic iron content (Fe_d/Fe_t) denote this soil formation. Obviously the arctic brown soil formed within material most probably eroded from the Eemian soil (OIS-5e). In section Gleina (Fig. 11) we observe a gradually increase of colour to the top of the arctic brown soil (layer 19) and a clear unconformity to the overlaying redeposited "Roströhrengley".
Most of the soils of unit IV are formed in situ. However, some soil-(sediments) show weak features of a short relocation. After deposition this material underwent soil formation. At the Ostrau section, the upper part of unit IV contains a humic soil that is preserved as well as at the section of Zschaitz, however slightly reworked. Lieberoth (1963) did not mention humic soils in this stratigraphic position although he described many profiles in Saxony. The occurance of such humic soils was reported from drier regions (e.g. Thuringian Basin and Harz foreland) by Ruske et al. (1962), Ruske & Wünsche (1964a, 1964b), Semmel (1968), and Schönhals et al. (1964). In accordance to these findings we postulate drier conditions during the formation of this humic soil in our study area.

Below the humic soil a pale soil sediment is present which can be observed in all sections, even if there has no humic horizon been found. This layer is supposed to be the earliest Weichselian deposit. The most obvious feature of this layer is the abundance of large manganese concretions. At sections Seilitz, Ostrau and Gleina this lowest part of unit IV is intermingled by these concretions and charcoal pieces. Macro remnant analyses of 25 pieces indicate, that only *Larix decidua* Mill. was found. It seems that at the end of the Eemian Interglacial and during the transition time towards the Early Weichselian a larch forest covered the landscape.

In the study area an Eemian soil (Pseudogley) is preserved below the Weichselian loess deposit at the sections of Ostrau, Zschaitz and Gleina. At all other profiles the lower boundary of the Weichselian loess can be hardly defined. The differences between an early Weichselian rebedding or a late Saalian rebedding is almost impossible because both layers show similar colouring and grain size distribution. Especially the grain size distribution varies in these layers in short interval (e.g. profile Leippen).

5 Conclusions

In order to develop a reliable stratigraphy, seven loess-palaeosol profiles were studied in detail and further profiles were discussed for comparison. Based on these investigations a high-resolution composite profile was compiled.

5.1 Local correlation

Fig. 14 shows an overview of all studied sections. The colour-bars represent correlations between the individual sections, based on lithological and palaeopedological analyses. Three IRSL-ages are provided for a first chronostratigraphic interpretation. Most of the sections to the north of the studied Saxonian loess plateau (Gleina, Zehren, Seilitz) are characterized by thick accumulations of loess with intercalated palaeosols. The sections Leippen and Zschaitz situated in the south of the Saxonian loess plateau show much less accumulations of loess, representing the general north-south trend of loess thickness.

5.2 Composite profile (Fig. 15)

According to our results a detailed composite profile (Fig. 15) for the Saxonian Loess Area is proposed. Main contributions to the findings of Haase et al. (1970) and Lieberoth (1963) are two strong soils and two weak soils formed within unit II. We consider the Gleina Soil Complex not to be correlated with the Lohne Soil Complex as proposed by Lieberoth (1962a, 1963) and Ricken (1983).

Another important feature that was not described in former studies is the humic horizon just above the Eemian soil complex. We correlate this humic horizon with one of the "Mosbacher Humuszonen" as described by Semmel (1997a, 1997b) and with the humic parts of the Rocourt-Sol-Complex by Schirmer (2000), respectively.

Ice wedges point to strong cold events without thick snow cover. Some of the ice wedges are even incised into lower units. In unit II the big ice wedges show a marginal bulge that indicate a longer phase of very cold winters. To form a marginal bulge of the ice wedge frequent changes of melting and strong freezing are necessary. The sequence is characterized by changes of soil formation, loess deposition and solifluction. These features are interpreted (left graph of Fig. 15) in terms of geomorphic conditions and landscape evolution. Stable conditions coincide with periods of soil formation, whereas geomorphic activity can be attributed to loess deposition or solifluction. The latter takes place in transition phases in terms of climatic conditions. Ice wedges indicate strong dry cooling events.

Two composite profiles of the western part of Germany (Semmel 1989; Zöller et al. 2004; Schirmer 2000, 2004) are added to the Saxonian composite profile in order to correlate similar findings into a chronostratigraphic approach. The very detailed analyses of the Nussloch section (Bibus et al. 2007; Antoine et al. 2001) are considered as well, however because of its high resolution it does not serve for overview comparison.

Acknowledgements

We would like to thank the Deutsche Forschungsgemeinschaft (DFG) for supporting this project (FA 239/13-1). Thanks to Carolin Hamann for mollusk analyses and to Andrea Seim for macro remnant analyses on charcoal pieces. For helpful comments, we are most thankful to Ludwig Zöller and Arno Semmel. The authors wish to thank their colleague Fritz Haubold for effective discussions in the field and the proofreading of the manuscript. Also thanks to Sieglinde Gerstenhauer and Beate Winkler for lab work. Special thanks to "Seilitzer Kaolin- und Tonwerk GmbH", to "Zschaitzer Sand- und Kiesgruben GmbH" and to "Ostrauer Kalkwerk GmbH" for giving always access to the studied sections. Mr. Dürasch from "Ostrauer Kalkwerk GmbH" supported all our activities in his pit and was always interested in our progress.
Finally, the authors want to thank all anonymous reviewers

for the helpful comments. Special thanks to Manfred Frechen who gave us fruitful advices and was always interested in the improvement of this paper.

References

Adamiec, G. & Aitken, M. (1998): Dose-rate conversion factors: update. – Ancient TL, 16: 37–50.

Aitken, M. & Xie, J. (1992): Optical dating: Recuperation after bleaching. – Quaternary Science Reviews, 11: 147–152.

Altermann, M., Haase, G., Lieberoth, I. & Ruske, R. (1978): Lithologie, Genese und Verbreitung der Löß- und Schuttsedimente im Vorland der skandinavischen Vereisungen. – Schriftenreihe der Geologischen Wissenschaften, 9: 231–255.

Antoine, P., Rousseau, D.D., Zöller, L., Lang, A., Munaut, A.V., Hatte, C. & Fontugne, M. (2001): High-resolution record of the last Interglacial-glacial cycle in the Nussloch loess-palaeosol sequences, Upper Rhine Area, Germany. – Quaternary International, 76/77: 211–229.

Antoine, P., Rousseau, D.D., Moine, O., Kunesch, S., Hatté, C., Lang, A., Tissoux, H. & Zöller, L. (2009): Rapid and cyclic aeolian deposition during the Last Glacial in European loess: a high-resolution record from Nussloch, Germany. – Quaternary Science Reviews, 28 (25-26): 1–19.

Bibus, E., Frechen, M., Kösel, M. & Rähle, W. (2007): Das jungpleistozäne Lößprofil von Nußloch (SW-Wand) im Aufschluss der Heidelberger Zement AG. – Eiszeitalter und Gegenwart, 56(4): 227–255.

Biering, K. & Frühauf, M. (1999): Untersuchung zu den natürlichen Schwermetallgehalten von Lößen im mitteldeutschen Raum. – Hallesches Jahrbuch für Geowissenschaften, Reihe A, 21: 83–96.

Dearing, J. (1999): Enviromental Magnetic Susceptibility. Using the Bartington MS2 System. – Bartington Instruments, 2. ed., 54 S.; Oxford.

Eissmann, L. (1964): Ausbildung und Gliederung des Pleistozäns in Mittelsachsen (Raum Döbeln-Riesa). – Geologie, 13: 942–969.

Eissmann, L. (1994): Grundzüge der Quartärgeologie Mitteldeutschlands (Sachsen, Sachsen-Anhalt, Südbrandenburg, Thüringen). – In: L. Eissmann & T. Litt (Hg.) Das Quartär Mitteldeutschlands – Ein Leitfaden und Exkursionsführer mit einer Übersicht über das Präquartär des Saale-Elbe-Gebietes, Altenburger Naturwissenschaftliche Forschungen, Bd. 7: 55-136, Mauritianum, Altenburg.

Fink, J. (1964): Die Subkommision für Lößstratigraphie der Internationalen Quartärvereinigung. – Eiszeitalter und Gegenwart, 15: 229–235.

Gallwitz, H. (1937): Fließerde und Frostspalten als Zeitmarken im Löß bei Dresden. – Geologische Rundschau, 28: 612–623.

Gellert, J.F. (Hg.) (1965): Die Weichselvereisung auf dem Territorium der Deutschen Demokratischen Republik. – 261 S.; Berlin (Akademie-Verlag).

Grahmann, R. (1925): Diluvium und Pliozän in Nordwestsachsen: – Abhandlungen der Mathematisch-Physischen Klasse der Sächsischen Akademie der Wissenschaften, Bd. 39, 82 S.; Leipzig (Hirzel).

Grahmann, R. (1932): Der Löss in Europa. – Mitteilungen der Gesellschaft für Erkunde 51: 5–24, Leipzig.

Haase, G. (1963): Stand und Probleme der Lößforschung in Europa. – Geographische Berichte, 8(2): 97–129.

Haase, G. (1968): Die Lössrandstufe in Nordsachsen. In: Periglazial-Löß-Paläolithikum: – Exkursionsführer der VII. Hauptversammlung der Geographischen Gesellschaft der DDR, Leipzig.

Haase, G., Lieberoth, I. & Ruske, R. (1970): Sedimente und Paläoböden im Lößgebiet. – In: H. Richter, G. Haase, I. Lieberoth & R. Ruske (Hg.) Periglazial-Löß-Paläolithikum im Jungpleistozän der Deutschen Demokratischen Republik. – Ergänzungsheft zu Pertermanns Geographischen Mitteilungen, Bd. 274: 99–212, Quartärkomitee der DDR bei der Deutschen Akademie der Wissenschaften zu Berlin, Gotha, Leipzig.

Hamann, C. (2010): Quartäre Molluskenfunde im mittelsächsischen Lösshügelland. – Biostratigraphische Untersuchungen der Profile Zehren, Ostrau und Gleina. – Diplomarbeit, Technische Universität Dresden, Lehrstuhl der Physische Geographie, unpublished.

Koch, R. & Neumeister, H. (2005): Zur Klassifikation von Lößsedimenten nach genetischen Kriterien. – Zeitschrift für Geomorphologie, 49(2): 183–203.

Lieberoth, I. (1959): Beobachtungen im nordsächsischen Lößgebiet. – Zeitschrift für Pflanzenernährung Düngung Bodenkunde, 86 (131)(2): 141–155.

Lieberoth, I. (1962a): Die jungpleistozänen Lösse Sachsens im Vergleich zu denen anderer Gebiete. Ein Beitrag zur Würmchronologie. – Petermanns Geographischen Mitteilungen, 106(2): 188–198.

Lieberoth, I. (1962b): Die mittel- und jungpleistozänen Lösse Nordsachsens. – In: G. Vient (Hg.) Das Pleistozän im sächsisch-thüringischen Raum – Exkursionsführer, 51–61, Geologische Gesellschaft in der Deutschen Demokratischen Republik, Leipzig.

Lieberoth, I. (1963): Lößsedimentation und Bodenbildung während des Pleistozäns in Sachsen. – Geologie, 12(2): 149–187.

Lieberoth, I. (1964a): Einige Bemerkungen zu paläopedologischen Problemen bei der Gliederung der Löße. – Berichte der Geologischen Gesellschaft der DDR, 9(Sonderheft 2): 689–695.

Lieberoth, I. (1964b): Bodenbildung aus Löß während des Pleistozäns und Holozäns in Sachsen. – Habilitation, 289 S.; Universität Leipzig.

Lieberoth, I. & Haase, G. (1964): Lößexkursion Nordsachsen. – In: G. Haase & R. Ruske (Hg.) 3. Arbeitstagung der Subkommission für Lößstratigraphie der INQUA-Exkursionsführer, 27–37, Leipzig.

Ložek, V. (1964): Quartärmollusken der Tschechoslowakei. Rozpravy Ústredního ústavu geologického, 31, 375 S.; Praha (Verlag der Tschechoslowakischen Akademie der Wissenschaften).

Meng, S. (2003): Kartierung des Quartärs und der Trias in der Umgebung von Freyburg/ U. – Diplomarbeit, Universität Halle, unveröffentlicht.

Neumeister, H. (1966): Die Bedeutung äolischer Sedimente und anderer Periglazialerscheinungen für die Bodenentwicklung in der Umgebung von Leipzig. – Dissertation, Math.-Nat. Reihe **15**, 244 (+160) S.; Math.-Nat. Fak. Karl-Marx-Universität Leipzig.

Oexle, J. (Hg.) (2000): Sachsen: archäologisch – 12000 v. Chr. – 2000 n. Chr. Katalog zur Ausstellung „Die Sächsische Nacht". – *Landesamt für Archäologie mit Landesmuseum für Vorgeschichte Dresden,* 88 S.; Dresden.

Pietzsch, K. (1922): Erläuterungen zur geologischen Spezialkarte von Sachsen. Blätter Wilsdruff und Tanneberg-Deutschenbora. Leipzig, 2. Aufl.

Richter, H., Haase, G., Lieberoth, I. & Ruske, R. (Hg.) (1970): Periglazial-Löß-Paläolithikum im Jungpleistozän der Deutschen Demokratischen Republik, Petermanns Geogrophischen Mitteilungen, Bd. Ergänzungsheft 274, 422 S.; Berlin (VEB Hermann Haack).

Ricken, W. (1983): Mittel- und jungpleistozäne Lößdecken im südwestlichen Harzvorland. – In: H.R. Bork & W. Ricken (Hg.) Bodenerosion, Holozäne und Pleistozäne Bodenentwicklung, Catena Supplement, 3: 95–138.

Ruske, R., Schulz, W. & Wünsche, M. (1962): Pleistozäne Ablagerungen im Gebiet südlich von Leipzig und der unteren Unstrut unter besonderer Berücksichtigung der Lösse und fossilen Böden. – In: G. Vient (Hg.) Das Pleistozän im sächsisch-thüringischen Raum – Exkursionsführer, 99–112, Geologische Gesellschaft in der Deutschen Demokratischen Republik, Leipzig.

Ruske, R. & Wünsche, M. (1964a): Lößexkursion Unteres Unstruttal. – In: G. Haase & R. Ruske (Hg.) 3. Arbeitstagung der Subkommission für Lößstratigraphie der INQUA-Exkursionsführer: 17–26, Leipzig.

Ruske, R. & Wünsche, M. (1964b): Zur Gliederung des Pleistozäns im Raum der unteren Unstrut. – Geologie, 13: 211–222.

Schirmer, W. (2000): Eine Klimakurve des Oberpleistozäns aus dem rheinischen Löss. – Eiszeitalter und Gegenwart, 50: 25–49.

Schirmer, W. (2004): Terrestrischer Klimagang des MIS 3. – In: DEUQUA Meeting Abstract Volume, 74, DEUQUA, Amsterdam.

Schlichting, E., Blume, H.P. & Stahr, K. (1995): Bodenkundliches Praktikum. Eine Einführung in pedologisches Arbeiten für Ökologen, insbesondere Land- und Forstwirte und für Geowissenschaftler. – Pareys Studientexte, Bd. 81. 2., neubearbeitete Aufl., 259 S.; Berlin (Blackwell Wissenschafts-Verlag).

Schönhals, E., Rohdenburg, H. & Semmel, A. (1964): Ergebnisse neuerer Untersuchungen zur Würmlöß-Gliederung in Hessen. – Eiszeitalter und Gegenwart, 15: 199–206.

Semmel, A. (1968): Studien über den Verlauf jungpleistozäner Formung in Hessen. – Frankfurter Geographische Hefte 45. Verlag Waldemar Kramer, Frankfurt am Main.

Semmel, A. (1997a): Referenzprofile des Würmlösses im Rhein-Main-Gebiet. – Jahresberichte der Wetterauischen Gesellschaft für die Gesamte Naturkunde zu Hanau, 148: 37–47.

Semmel, A. (1997b): Stop 3: Loess section of Mainz Weisenau. – In: Excursion Guide, Internat. Working Meeting Palaeopedology of ISSS and INQUA: 60–72.

Semmel, A. (1989): The importance of loess in the interpretation of geomorphological processes and for dating in the Federal Republic of Germany. – Catena Supplement, 15: 179–188.

Zöller, L., Rousseau, D.D., Jäger, K.D. & Kukla, G. (2004): Last interglacial, Lower and Middle Weichselian – a comparative study from the Upper Rhine and Thuringian loess areas. – Zeitschrift für Geomorphologie, 48(1): 1–24.

E&G Quaternary Science Journal
Volume 60 / Number 1 / 2011 / 66–77 / DOI 10.3285/eg.60.1.04
www.quaternary-science.net

GEOZON SCIENCE MEDIA
ISSN 0424-7116

The 'Palaeolithic Prospection in the Inde Valley' Project

Alfred F. Pawlik, Jürgen Thissen

Abstract:

The excavation of 20 deep test trenches of Pleistocene layers in the quarry Inden between Jülich-Kirchberg and Lamersdorf in 2005 and 2006 was part of the 'Palaeolithic Prospection in the Inde Valley' Project of the Foundation "Stiftung Archäologie im Rheinischen Braunkohlenrevier". They were aimed at finding and unearthing ancient landscape surfaces and potential Palaeolithic settlement structures. In December 2005, a Middle Palaeolithic archaeological layer correlating to the Eemian interglacial was discovered. This layer was investigated and excavated until September 2006 within an area of 3000sqm. About 700 lithic artefacts and pebble manuports were found together with evident features of pits and hearths. Three fallen-tree structures were situated in the center of the major concentration of artefacts and were probably part of the habitation.
The discovered artefacts showed no signs of re-deposition or secondary transport and still maintained their original surface structure and sharp edge with no or minor patination. They were very suitable for the successive microscopic use-wear analysis which delivered a variety of remarkable and outstanding results. Various microwear traces and residues were found on a total of 120 stone tools out of 136 artefacts selected for analysis. The residues were identified through SEM and EDX as birch pitch. 82 tools were either used as hafted impliments and fixed with birch pitch onto shafts or were being used for successive hafting-and-retooling activities. Birch pitch is the oldest synthetically produced material and is commonly associated with modern humans in the Upper Palaeolithic. The birch pitch residues found on the Micoquien tools of Inden suggest that hafting technologies, use of adhesives and multicomponent tool making already existed in the Middle Palaeolithic. The complex actions involved in composite-tool making indicate clearly modern human behaviour.

(Prospektion Paläolithikum im Indetal)

Kurzfassung:

Im Rahmen des Projektes „Prospektion Paläolithikum im Indetal" der Stiftung Archäologie im Rheinischen Braunkohlenrevier wurden in den Jahren 2005 und 2006 im Tagebau Inden zwischen Jülich-Kirchberg und Lamersdorf die pleistozänen Deckschichten mittels 20 Baggertiefschnitten sondiert. Ziel war es, fossile Landoberflächen und mögliche paläolithische Siedlungsplätze zu finden und freizulegen. Im Dezember 2005 konnte in der Ortslage Inden-Altdorf eine mittelpaläolithische Fundschicht aus dem Eem-Interglazial entdeckt werden, die bis September 2006 auf einer Fläche von 3000 m² archäologisch untersucht werden konnte. Es fanden sich 700 Steinartefakte und herbeigebrachte Gerölle, aber auch evidente Grubenbefunde und Feuerstellen. Drei Baumwürfe lagen mitten in der Hauptartefaktkonzentration und waren wohl in das Siedlungsgeschehen eingebunden. Die Artefaktoberflächen waren kantenscharf und nicht patiniert, so dass die durchgeführten Gebrauchsspurenanalysen außergewöhnlich erfolgreich waren. Auf 120 der insgesamt 136 für die Gebrauchsspurenanalyse ausgewählten Artefakte fanden sich Mikrospuren verschiedenartiger Tätigkeiten sowie Residuen. Diese konnten mittels Rasterelektronenmikroskopie und energiedispersiver Röntgenmikroanalyse als Reste von Birkenrindenpech identifiziert werden. 82 Geräte mit Residuen erwiesen sich entweder als geschäftete Einsätze, die mit diesem Pech an den Schäften befestigt wurden oder als Werkzeuge für die Reparatur von gebrauchten und mit Pech verklebten Schäftungen, und dem Auswechseln verbrauchter Feuersteineinsätze dienten. Birkenrindenpech kann als ältester synthetisch hergestellter Werkstoff angesehen werden und wird in der Regel mit dem Jungpaläolithikum und modernen Menschen assoziiert. Die auf den Micoquien Artefakten aus Inden vorgefundenen Birkenpechreste zeigen, daß sowohl Schäftungstechnologien, Gebrauch und Herstellung von Klebstoff als auch die Anfertigung von komplexen, aus mehreren Komponenten bestehenden Geräten im Mittelpaläolithikum durchaus üblich waren. Deren Vorhandensein, noch dazu in einer vergleichsweise hohen Anzahl, kann als deutlicher Hinweis auf moderne menschliche Verhaltensweisen gewertet werden.

Keywords: *Micoquian, Eemian, habitation features, microwear analysis, hafting, birch pitch residues, behavioural modernity*

Addresses of authors: **A. F. Pawlik**, University of the Philippines, Archaeological Studies Program, Lithic Studies Laboratory, Palma Hall, Diliman, Quezon City 1101, Philippines. E-Mail: afpawlik@gmail.com; **J. Thissen**, Amt für Bodendenkmalpflege im Rheinland (ABR), Aussenstelle Titz, Ehrenstr. 14–16, 52445 Titz-Höllen and Universität Bonn, Institut für Vor- und Frühgeschichtliche Archäologie, Regina-Pacis-Weg 7, 53113 Bonn (Germany)

1 Introduction

A sharp-edged, blue-and-white patinated middle palaeolithic handaxe found at the open-cast lignite mine Inden (in the area of Geuenich) urged one of the authors (JTh) in July 2004 to inspect this locality (Päffgen & Thissen 2005). The handaxe derived from a loess horizon correlating to the Weichselian period under which a fossil soil layer most likely correlating to the Eemian period (OIS 5e 128.000–115.000 BP) was localized. An early Pleistocene Maas terrace is cropping out between the Inde and Wurm valley, carrying large quantities of flint pebbles from the Dutch-Belgian "Kreideflint" region. Where the Maas terrace was exposed on the surface during the Pleistocene, Palaeolithic flint-knapper had an attractive and unlimited supply of raw material.

Several hand-axes and half-finished products were found, mainly by F. Schmidt (Aldenhoven), who is field-walking in this area since the mid 1970s. This open site, closely located to the Maas terrace, was identified as a workshop ("Atelier") of the Micoquien period (Thissen 2006). This promis-

E&G / Vol. 60 / No. 1 / 2011 / 66–77 / DOI 10.3285/eg.60.1.04

Fig. 1: Map of Germany with the location of the site Inden-Altdorf.

Abb. 1: Deutschlandkarte mit der Lage des Fundplatzes Inden-Altdorf.

ing topographical situation, which archaeologically seems to indicate a favoured area, led to the proposal of a survey project to the **Foundation "zur Förderung der Archäologie im Rheinischen Braunkohlenrevier"** that was granted in March 2005. The grant included the comprehensive lithic analysis of the archaeological finds. Additional to the morphological and technological assessment of the lithic materials, microscopic use-wear and residue analysis was conducted. In a pioneering study for the Middle Palaeolithic of the region, all modified tools and selected unmodified pieces underwent optical high and low power analysis as well as residue analysis using scanning electron microscopy and energy-dispersive X-ray microprobing.

2 Palaeolithic Prospection in the Inde Valley

2.1 Test excavations at Inden and Altdorf 2005

Several previous surveys of the embankment of the mining areas of Garzweiler and Inden were conducted to locate Middle or Upper Palaeolithic settlements but remained rather unsuccessful. In 1987 the Mesolithic site Bedburg-Königshoven was found at the Garzweiler mine (Thissen 1997), after a skull and antler of deer were discovered in the wall of the open cast pit. The archaeological layer was close to the surface below a turf layer in a silted-up meander of the Erft river.

According to experience, sites in loess deposits or in fossil soils are only found by widespread investigations of the Pleistocene landscape. Hence, the Inde Valley Project (Fig. 1) was explicitely designed to reveal palaeosurfaces with heavy equipment, specifically where the characteristic "Eemian soil" indicated an actual fossil surface.

A mechanical excavator set up a series of deep test trenches, first around the area of Inden in 2005 on the west bank of the river (WW 2005/51) that was under threat by the ongoing and approaching mining activities. These trenches were app. 2.5 to 4.5 metres wide, up to 4–6 metres deep and up to 75 metres long. In August and November 2005 seven deep test trenches (DT) were opened there, revealing the Weichselian loess and possible Eemian layers.

In the trenches nos. 1 to 5, 14 and 15 (see Fig. 2a and Table 1) different stratified sequences were documented. Coincidentally, the Roman Inde valley road from the Augustian period was discovered in the extension of Trench 1. The Pleistocene sediments in the trenches nos. 1, 2, 4 and 5 are generally well preserved, but neither Palaeolithic artefacts nor archaeological features could be found. It was also not possible to locate the Eemian soil. In the flooded Go/Gr layers of the presumable Eemian period river valley brown patinated silices were found, but all unworked. Trench no. 3 revealed gravels from the main terrace of the Rhine together with Tertiary deposits. Trenches no. 14 and no. 15 were situated in an erosive channel underneath the Geuenich hand-axe site. No redeposited Middle Palaeolithic tools were found.

Four other deep trenches at Altdorf (WW 2005/52) excavated to a depth of 8.4 m turned out to be more promising. An eroded brownish red soil, most likely Eemian sediments, and the first redeposited artefacts of Upper Palaeolithic as well as Middle Palaeolithic age were discovered.

2.2 Discovery of the Eemian artefact layer

Following the discovery of Eemian soils and nearby old, brown patinated lithic artefacts at Altdorf, a (last) test excavation (WW 2005/91) for this survey project was carried out.

In October 2005, the first Eemian soil in situ was observed in Trench no. 11. In Trench no. 12, opened at the former corner of Altdorf's Gartenstrasse and Chlodwigstrasse, an Eemian Bt horizon and the Maas terrace sediments were finally located in direct contact. This was the sought-after, potentially ideal position for a settlement of Palaeolithic groups during the Eemian-Interglacial. There, the Maas gravels were exposed by erosion forming a channel in north-eastern direction ("Altdorfer Tälchen") into the Inde valley. Trench no. 13, excavated in December 2005 delivered the first archaeological evidence: in a slightly re-deposited Al-horizon three non-patinated Middle Palaeolithic artefacts made of Maas flint were uncovered underneath a loess deposit of three metres thickness (Fig. 3). Based on this promising result, the Inde Valley Project could be extended for one more year to thoroughly study the new site.

2.3 Excavation of the Middle Palaeolithic open site Altdorf (WW 124)

In 2006 the research activities focussed on WW 2005/91 and WW 2006/74. Systematic probing of the area around the Middle Palaeolithic finds at Altdorf started in the beginning of January 2006. Initially, the excavation was done conven-

Tab.1: Palaeolithic Prospection in the Inde Valley, deep trenches 1–20.

Tab.1: Prospektion Paläolithikum im Indetal, Baggertiefschnitte 1–20.

Deep trench (Feature)	m ASL	Ah/Ap	Bt	Sediments (1)	Sediments (2)	Sediments (3)	Sediments (4)
Inden							
1 (2 u. 6)	107.73	x		Roman disturbance until 1.6 m	Weichselian loess until 4 m	Go/Gr (Eemian) until 4.5 m	Saalian gravel until 4.6 m – B
2 (8)	107.76	x	x		Weichselian loess until 4 m	Go/Gr (Eemian) until 4.5 m	Saalian gravel until 4.6 m – B
3 (9)	107.09	x				Rhein-HT until 1.5 m	Tertiär until 4.5 m – B
4 (10)	107.15	x	x		Weichselian loess until 3.8 m	Go/Gr (Eemian) until 4.5 m	Saalian gravel until 4.6 m – B
5 (11)	108.25	x	x		Weichselian loess until 3.8 m	Go/Gr (Eemian) until 4.5 m	Saalian gravel until 4.6 m – B
14 (12)	104.17			Colluvium	Alluvial loess until 3 m – B		
15 (24)	104.56			Colluvium	Alluvial loess until 3 m – B		
Altdorf							
6 (14)	109.53			Holocene disturbance until 0.8 m	Weichselian loess until 1.6 m	Weichselian loess, sand and dislocated (?) Eemian Bt until 5.9 m	Sand and gravel until 6.1 m – B
7 (15)	110.27	x		Colluvium	Weichselian loess and sand until 5.3 m	Dislocated (?) Eemian-Bt until 6.0 m	Saalian loess until 6.4 m – B
8 (16)				Colluvium until 2.5 m – B			
9 (17)	115.22	x	x		Weichselian loess, gravel and sand until 2.7 m	Dislocated (?) Eemian-Bt until 3.5 m	Saalian gravel until 3.75 m – B
10 (19)	107.13			Colluvium, roman Street, atlantic soil until 2.8 m	Alluvial loess until 3 m – B		
11 (21)	110.78				Weichselian loess until 0.9 m	Eemian-Bt in situ until 1.8 m	Saalian loess until 5.0 m – B
12 (22)	113.50	x		Colluvium	Weichselian loess until 1.8 m	Eemian-Bt in situ until 3.4 m	Maas terrace until 3.6 m – B
13 (23)	113.29	x			Weichselian loess until 3 m	Dislocated Al-horizon (Eem)	Eemian-horizon in situ until 4.0 m – B
16 (50)	111.32	x	x		Weichselian loess until 5.60 m	Eemian-Interglacial-Complex, OIS 5a - 5e until7.20 m	Saalian loess until 8.4 m – B
17 (3)	105.60	x		Colluvium until 1.3 m	Weichselian loess until 3.3 m	Weichselian loess and eroded Eemian soil until 5.4 m	Saalian loess until 5.6 m – B
18 (4)				3–4 mundocumented, surface profil section 102.05 m	Weichselian loess until 0.6 m	Eroded Al- and Bt-horizon until 1.5 m	Go/Gr (Eemian?) until 3.15 m – B
19 (6)				2-3 m un documented, surface profile section at the river bank 99.30 m	Weichselian loess until 0.15 m	Eroded Al- and Bt-horizon, underneath Eemian gley until 1,05 m	Saalian gravel until 1.25 m – B
20 (2)	102.05				Weichselian loess until 3.4 m	Gley until 3.6 m	Saalian gravel until 4.0 m – B

(– B: Trench bottom)

EGG / Vol. 60 / No. 1 / 2011 / 66–77 / DOI 10.3285/eg.60.1.04 / © Authors / Creative Commons Attribution License

Fig. 2: The position of the trial trenches, sondages and profile sections in a) Inden, b) Altdorf.

Abb. 2: Lage der Baggertiefschnitte, Sondagen und Profilabschnitte in a) Inden, b) Altdorf.

tionally in 1x1m units using spades and trowels. All artefacts recovered in situ were 3-D measured and documented. The excavated sediments were then sieved. However, only 12 small and unmodified artefacts were found in the investigated area of 50 square metres (Fig. 4, Feature 23) by a team of 2 to 3 excavators over a period of 12 weeks. This was far off the aim of the project to localise the Middle Palaeolithic sites. Therefore, it became necessary to adopt methods that could handle excessive amounts of sediments. The Eemian horizon could be carefully machine-excavated using a backhoe. The eastern slope seemed to be suitable for a settlement place, due to a wider view over the valley and the proximity of the river.

Fig. 3: Three flakes from the excavation WW 2005/91.

Abb. 3: Drei Abschläge von der Ausgrabung WW 20095/91.

In March 2006, the excavation of Trench no. 16 started to investigate the eastern slope (Fig. 4, Feature 50). Geology and stratigraphy of this area were documented in the stepped profile of Feature 70 (Fig. 5). Further soil samples and a lacquer profile section were taken from the southern edge of the slope (Fig. 4 and 6; Feature 125, see Kels et al. 2009).

Only few lithic artefacts were found within Feature 50, therefore the trench was extended to the south. Here, the archaeological layer was underneath about 6 metres of loess. There a first fireplace was discovered (Fig. 4, Feature 65) whereas the Al-horizon was sitting directly upon a Bt horizon, both correlating with the Eemian. The character of this feature was not fully understood, then, also because the Al-horizion of the upper slope showed large sections of charcoal specks. The possibility of forest fires causing the presence of charcoal rather than anthropogenic activities had to be considered. However, at the end of April a second fire place was uncovered (see Feature 90), and a significant concentration of artefacts came up within a long excavation trench in southern direction by the end of July (see Feature 180).

At the same time, the first evidence of pits being features was investigated (eg. Fig. 4, Feature 200). They appeared as lighter fillings in the reddish-brown Bt-horizon. The spoilheaps were rapidly getting bigger hampering the excavations. The prolongation of the excavation's duration permitted the enlargement of the excavated area and the transfer of the spoil to reach the new areas of interest (Fig. 6).

Furthermore, a larger artefact concentration was found inside the last extension of the diggings to the east (west of Jülicherstrasse), which at last turned out to be the Middle Palaeolithic camp we were seeking for.

From August 10 to 31, 2006, three large round features were found beside each other (Feature 240, 300 and 330, Fig. 4), clearly distinguishable from the surrounding reddish-brown soil by their light-colored sediment filling (Al-horizon), along with more fireplaces and pits. It became evident, that these were hollow fallen-tree structures (see

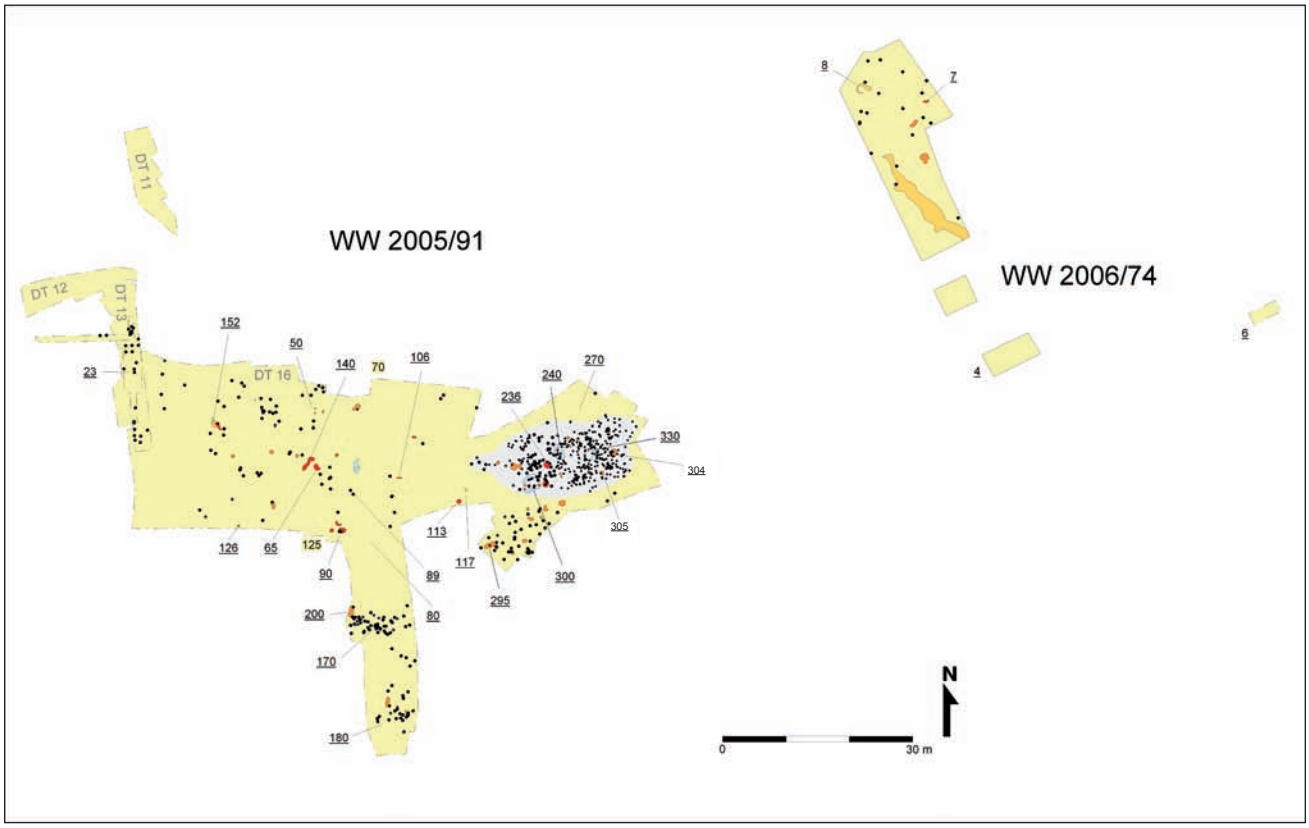

Fig. 4: General plan of the excavation WW 124 (Altdorf) with the activities WW 2005/91 and WW 2006/74 and the most important finds & features. Key: Excavation area (beige), Artefacts & stones (black dots), Pits (brown), fireplaces (red), concentration of artefacts in the camp (light grey) and Huts/Shelters (light blue).

Abb. 4: Gesamtplan der Ausgrabung WW 124 (Altdorf) mit den Aktivitäten WW 2005/91 und WW 2006/74, und die wichtigsten Funde und Befunde. Legende: Grabungsbereiche (beige), Artefakte und Gerölle (schwarze Punkte), Gruben (braun), Brand- u. Feuerstellen (rot), Artefaktkonzentration im Camp (hellgrau) und Hütten/Shelter (hellblau).

E&G / Vol. 60 / No. 1 / 2011 / 66–77 / DOI 10.3285/eg.60.1.04 / © Authors / Creative Commons Attribution License

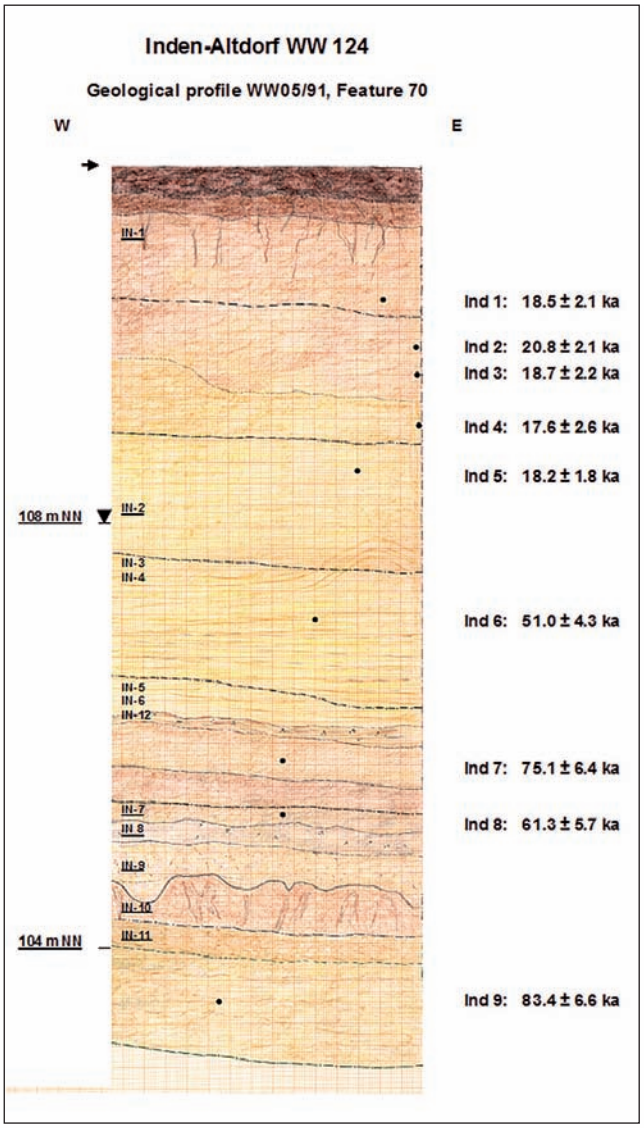

Probe	Beschreibung
IN 1	Lösslehm, MBt, rezent verlagert
IN 2	Brabant-Löss, in situ
IN 3	Gebleichter Löss, Eben-Zone (?)
IN 4	Gebleichter Löss, Eben-Zone (?)
IN 5	Weichsellöss, umgelagert, Keldach-Löss
IN 6	Weichsellöss, umgelagert, Keldach-Löss
IN 12	Kaiskorb Nassboden
IN 7	Humuszone OIS 5a, in situ
IN 8	Bleichzone (SwAl), umgelagert
IN 9	Bleichzone (SwAl+Bt), umgelagert
IN 10	Eem-Bt (SdBt), umgelagert
IN 11	Eem-Bt (SdBt2), in situ

Sample	Description
IN 1	Loess loam, MBt, modern soil
IN 2	Brabant-loess, in situ
IN 3	leached loess, Eben zone (?)
IN 4	leached loess, Eben zone (?)
IN 5	Weichselian loess, reworkt, Keldach-Loess
IN 6	Weichselian loess, reworkt, Keldach-Loess
IN 12	Loess, tundra gley paleosoil, Kaiskorb soil (?)
IN 7	Loess loam, A horizon, in situ, OIS 5a
IN 8	Loess loam, reworked, OIS 5
IN 9	Loess loam, reworked (Bt/Eg horizon)
IN 10	Loess loam, dense Btg horizon, reworked, Eemian soil (OIS 5e)
IN 11	Eemian Bt (OIS 5e), in situ

Fig. 5: Geological Stepped Profile Feature Nr. 70; soil samples IN 1–12: M. Kehl; IRSL samples Ind 1–9: Preliminary IRSL ages M. Frechen (drawing by M.Goerke, LVR-ABR).

Abb. 5: Geologisches Stufenprofil Stelle 70, Bodenproben IN 1–12: M. Kehl; IRSL-Proben Ind 1–9: Vorläufige IRSL-Alter M. Frechen (Profilzeichnung M. Goerke, LVR-ABR).

Kooi 1974), which originated from uprooted Eemian spruce trees. These shallow rooting trees have been determined for this period along with pine trees (see U. Tegtmeier in Kels et al. 2009). Pine trees, however, have deep roots and cannot be responsible to create such shallow pits.

The chronology as well as the character of the fallen-tree pits were additionally confirmed by microscopic analysis (see Kehl, Frechen & Thissen, in preparation). The fallen-tree structures appear to be favorable for habitation. The remaining root platform can be used as a construction element by the settlers to build a „fallen-tree shelter". This seems even more probable, since an oval concentration of lithic artefacts with clear boundaries appeared nearby to the central features (Fig. 4, grey area). It seems reasonable, that the people of the camp specifically sought out fallen tree groups near to the Maas terrace to build simple dwellings with little effort.

The excavation campaign WW124 (WW2005/91 and WW2006/74) ended by September 2006 and the excavation area was dug away by the mining operation. The archaeologically investigated area of the Palaeolithic site in Altdorf was about 3000 m².

The lithic assemblage, about 700 unmodified artefacts, retouched tools and cores includes typical Micoquien forms like unifacial knives, Kostenki- and Pradnik-knives, Levallois flakes and cores, and also Upper Palaeolithic elements like burins, scrapers, blades and blade-cores. This inventory can be favourably compared and correlated with the nearby Eemian site Moenchengladbach-Rheindahlen, layer B1 (c. 125 ka BP; Thissen 2006). Their well-preserved state and already macroscopically visible use traces made the Altdorf artefacts very suitable for microwear study.

3 Microscopic use-wear and residue analysis

In this study, all modified artefacts and selected non-retouched pieces from Inden-Altdorf were subjected to high and low power microscopic use-wear analysis (Pawlik & Thissen 2008). By March 2009, 120 artefacts out of presently 136 analysed were identified as used (Table 2). 144 activities were recognised including scraping, cutting, engraving, chiselling and combinations of these tasks. Five tools were used as perforators and 15 projectile implements were identified. A sandstone pebble was used as a grinder, perhaps for smoothing a wooden shaft. The assemblage contains three more grinding stones as well as two potential "querns" made of sandstone.

Table 2: Use-wear analysis: Reconstructed function and assumed contact material (136 analysed artefacts).

Tabelle 2: Gebrauchsspurenanalyse: Rekonstruierte Funktion und angenommenes Kontaktmaterial (136 untersuchte Artefakte).

Activity	Assumed contact material / Function												
	Meat/Skin processing, butchering	Hide/ Leather working	Wood / Bone / Antler	Ivory	Plants	Mineral	Birch tar production	"Hafting and Retooling"*	Multiple materials	Hunting	Undeterm.	No traces	Total
Projectile implement										15**			15
Scraping, Planing		1	17	1	3	1		7			1		31
Cutting	3	10	3		3				1				20
Scraping&Cutting		4	2	1	5				3				15
Other combinations		1							15				16
Drilling, perforating		4									1		5
Gouge, engraving			6			3		1	1				11
Chisel			6					3			2		11
Grinding								1					1
"Pitch catcher"							2						2
Undeterminable		1			2			5			9		17
No use traces												16	16
Total	3	21	34	2	13	4	2	17	20	15	13	16	160

* *"Hafting-and-Retooling (after Keeley 1982): Replacing worn and damaged implements; maintenance and reworking of shafts and fittings*

** *3 projectile implements were also used for cutting activities*

An important role for the reconstruction of Palaeohistoric activities and technologies at Altdorf played the determination of residues. Besides edge damage and micropolish, residues on stone tool surfaces are wear traces whose identification can give clues to their former use. Residues from the worked materials remain sometimes -although not frequently- on the functional parts of the tools. Approaches to the identification of blood or starch were extensively discussed by a number of authors (Loy 1983, 1991; Fullagar 1998; Torrence & Barton 2006).

Residues not only originate from the contact or working material but can be the remains from the tool's hafting and handling. Experimentally created birch pitch and archaeological birch pitch samples from several European Upper Palaeolithic, Mesolithic and Neolithic sites helped to identify these residues in a comparative multi-level analysis

E&G / Vol. 60 / No. 1 / 2011 / 66–77 / DOI 10.3285/eg.60.1.04 / © Authors / Creative Commons Attribution License

Fig. 6: The excavation in Altdorf during July 2006. To the right of the profile the colleagues M. Frechen, M. Kehl and M. Goerke, and by the mechanical excavator W. Schürmann.

Abb. 6: Die Ausgrabung in Altdorf im Juli 2006. Rechts am Profil die Kollegen M. Frechen, M. Kehl und M. Goerke, und am Hydraulikbagger W. Schürmann.

Fig. 7: a) unifacial point no. 279-4, b) triangular pointed flake no. 470-1, c) pointed flake no. 467-1, d) unilaterally hafted blade 455-1, e) scraper no. 291-1, f) sandstone pebble covered with pitch no. 261-3. Presumed hafted areas are shaded; areas where microphotographs were taken are circled.

Abb. 7: a) Unifaziale Spitze Nr. 279-4, b) dreieckiger, spitz zulaufender Abschlag Nr. 470-1, c) spitz zulaufender Abschlag Nr. 467-1, d) unilateral geschäftete Klinge Nr. 455-1, e) Schaber Nr. 291-1, f) mit Birkenpech bedecktes Sandsteingeröll Nr. 261-3. Mutmaßliche Schäftungsbereiche sind schattiert; photographierte Bereiche sind umrandet.

(Pawlik 1995, 1997, 2004; Baales 2002). It combined optical microscopy, SEM and energy-dispersive analysis of X-rays (EDX). The results lead to the identification of these residues as the remains of birch pitch used as hafting mastic (Rottländer 1991). More so, since archaeological evidence -at least for Europe- exists only for adhesives deriving from birch (Weiner 2005: 20).

Birch pitch is produced in a process called dry distillation (Sandermann 1965; Funke 1969; Rottländer 1991). It usually requires the use of air-tight containers known as retorts. The retort is filled with birch bark rolls and set into a charcoal fire. During the heating process, the hot oxygen-free atmosphere inside the retort causes the bark to completely transform into a liquid tar. While this retort distillation is known to have been practiced since the 10th century AD (Weiner 1988) the use of such containers can hardly be considered for prehistoric pitch production. Even for the Neolithic, there is a remarkable absence of retorts or any fragments of retorts in the archaeological record (Weiner 1992).

The comparative analysis of archaeological pitch and experimental replication suggested that prehistoric birch pitch could have been made by turning a narrow pit with stone cover into a "retort" (Pawlik 1995, 2004; Palmer 2007). A cigar-shaped roll of birch bark, similar to findings from the Mesolithic (Kind 1997), is lighted at one end and placed with the burning end ahead into the pit. The smouldering bark takes away the oxygen inside the pit and will cause the bark to "sweat out" pitch drops. A stone placed at the pit's bottom is helpful to catch the pitch. This pitch is a sticky liquid while hot and can be applied immediately.

Such residues were observed on 82 artefacts, on projectile points as well as working tools. They appear as blackish drops and streaks of resin-type material on the basal area, e.g. on a unifacial point (Fig. 7a) or in some cases completely cover the former hafted area like on a laterally hafted blade (no. 455-1;

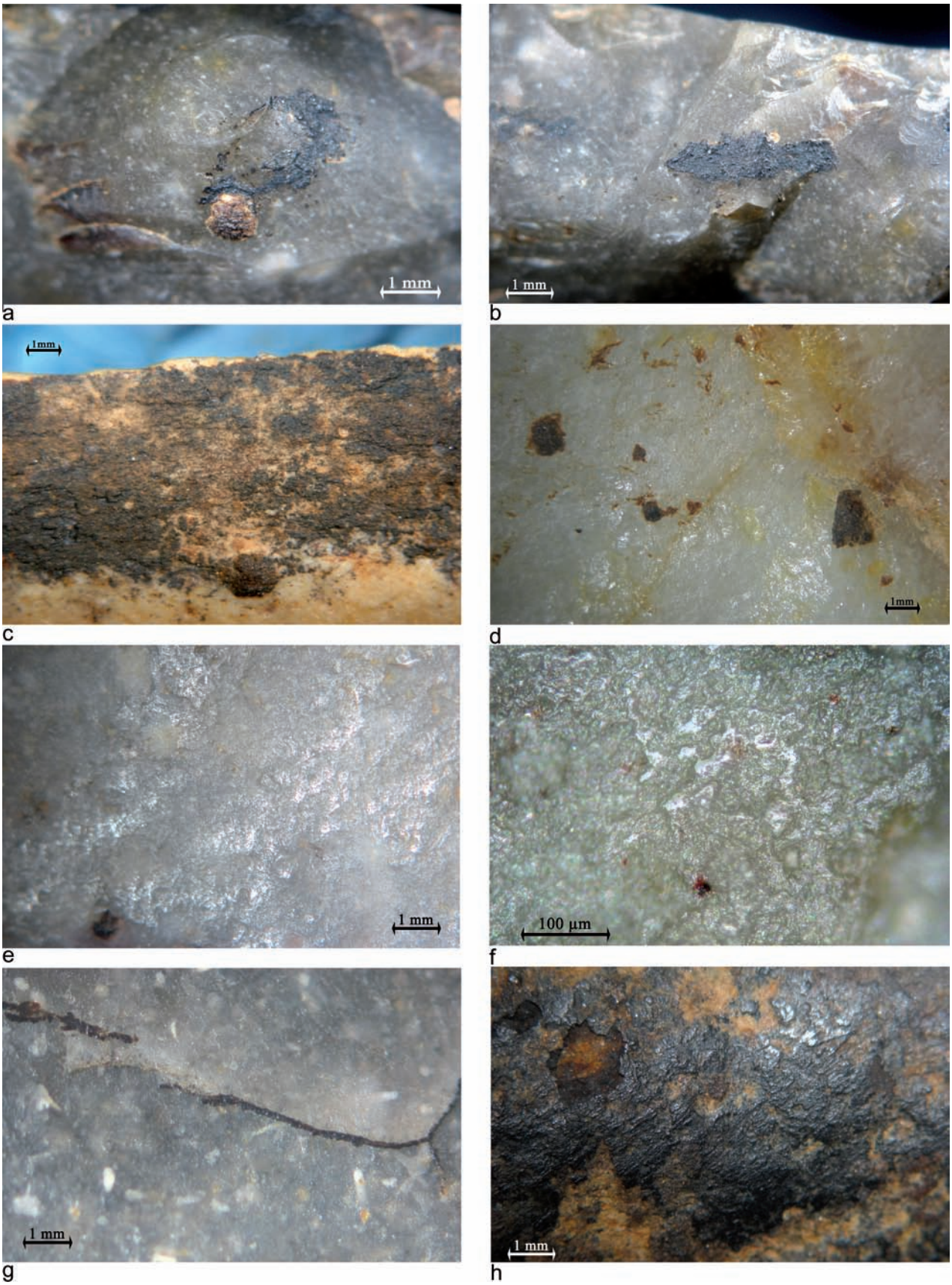

Fig. 8: a) Birch pitch residues on the bulb of no. 467-1, b) residues on the striking platform of no. 467-1, c) Birch pitch covering the lateral edge of no. 455-1, d) pitch residues associated with hafting wear on no. 470-1, e) residues associated with hafting micropolish on a unifacial point no. 279-4, f) residues and hafting micropolish on a Kostenki-knife fragment no 202-1, g) birch pitch filled hairline fissures on the surface of scraper no. 291-1, h) birch pitch cover on a flat sandstone pebble no. 261-3.

Abb. 8: a) Birkenpechresiduen auf dem Bulbus von Nr. 467-1, b) Residuen auf dem Schlagflächenrest von Nr. 467-1, c) mit Birkenpech bedeckte Lateralkante von Nr. 455-1, d) Gemeinsam mit Schäftungsgebrauchspuren auftretende Pechresiduen an Nr. 470-1, e) Residuen und Schäftungspolituren auf der unifaziellen Spitze Nr. 279-4, f) Residuen und Schäftungspolituren auf dem Fragment eines Kostenkimessers Nr. 202-1, g) In Haarrisse eingeflossenes Birkenpech auf der Oberfläche des Schabers Nr. 291-1, h) Mit Birkenpech bedecktes flaches Sandsteingeröll Nr. 261-3.

E&G / Vol. 60 / No. 1 / 2011 / 66–77 / DOI 10.3285/eg.60.1.04

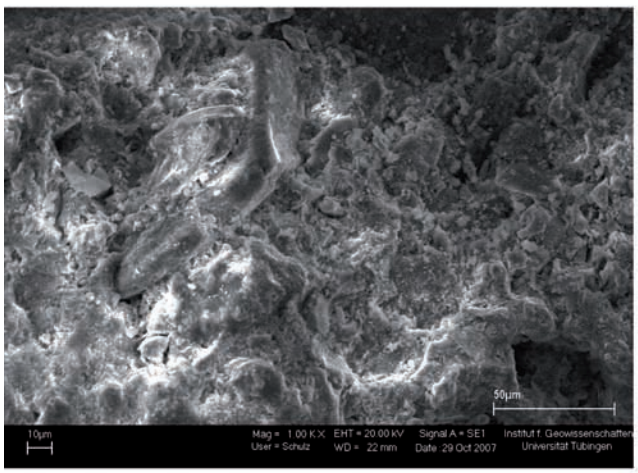

a

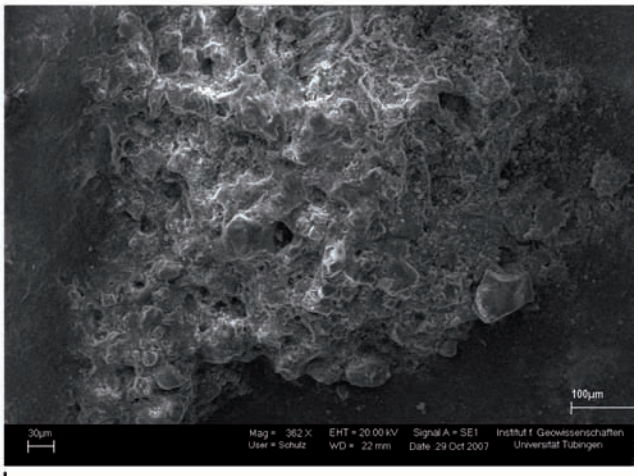

b

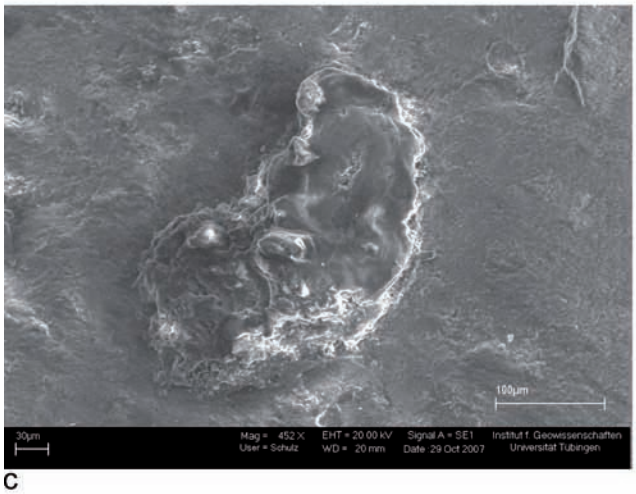

c

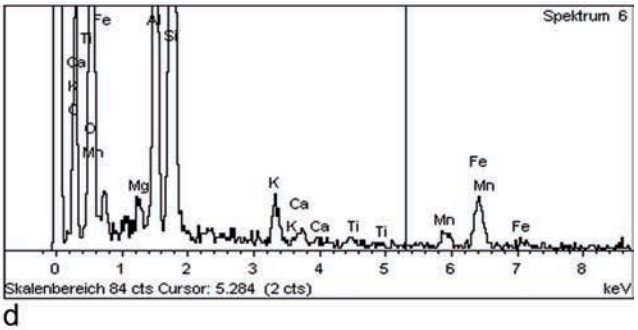

d

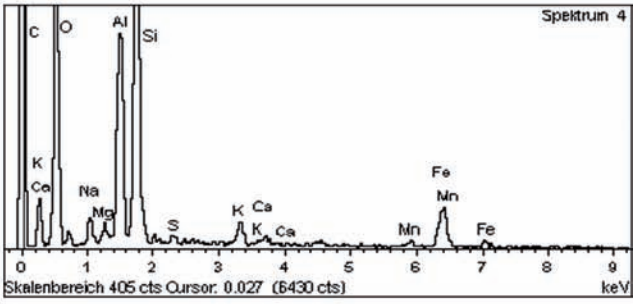

e

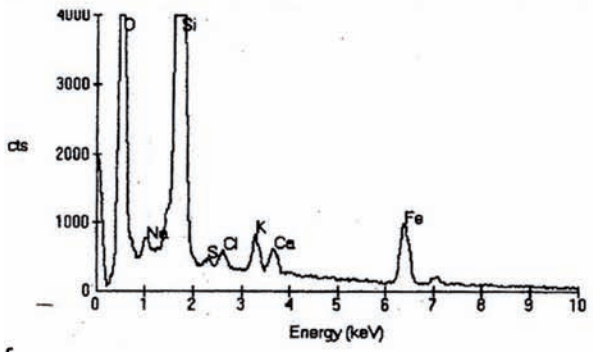

f

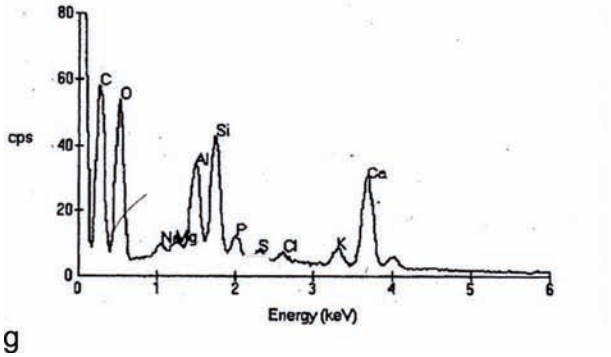

g

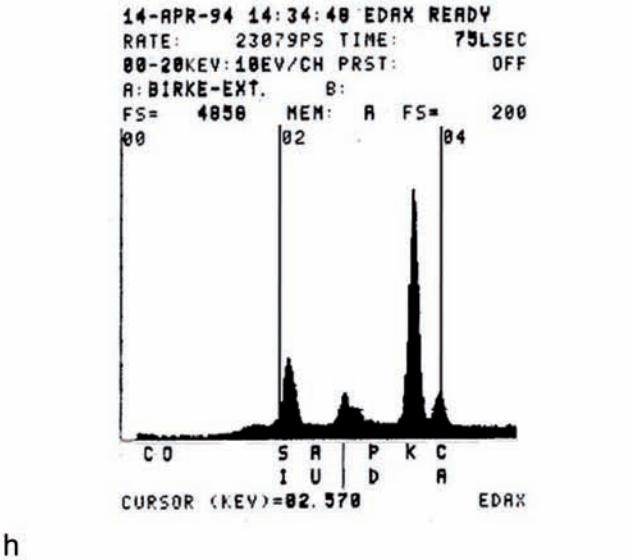

h

Fig. 9: a, b) SEM image of residues with molten plant tissue frazzles and fibres embedded in an amorphous matrix of solidified pitch on no. 470-1, c) sediment particles in a small clot of solidified pitch on no. 467-1, d and e) EDX analysis of residues from no. 470-1, f) EDX histogram of birch pitch residues from Burgäschisee-Süd, g) EDX histogram of birch pitch residues from Henauhof-Nord II, h) EDX histogram of experimental birch pitch.

Abb. 9: a, b) Rasterelktronmikroskopische Aufnahme der Residuen mit in eine amorphe Matrix aus Pech eingebetteten, angeschmolzenen Pflanzenfasern und -geweberesten auf Nr. 470-1, c) an einem erstarrten Pechklümpchen anhaftende Sedimentpartikel an Nr. 467-1, d , e) EDX-Analyse der Residuen auf Nr. 470-1, f) EDX-Histogramm von Birkenpechresten aus Burgäschisee-Süd, g) EDX-Histogramm von Birkenpechresiduen aus Henauhof-Nord II, h) EDX-Histogramm von experimentell hergestelltem Birkenrindenpech.

Fig. 7d). On artefacts identified as projectile implements, e.g. a pointed and triangular shaped flake (no. 470-1, Fig. 7b), and a blade with transverse termination (no. 467-1, Fig. 7c), residues occur mainly on their proximal parts including the platform remnant. They appear under the stereo-microscope as a dried brownish black viscous liquid (Fig. 8a-c). The residues are often associated with hafting micropolishes (Pawlik 2004) caused by minor movements of the shaft (Fig. 8d–f). The liquid state of the pitch during its application is substantiated by an observation on a scraper (no. 291-1, Fig. 7e): Here, the material filled hairline fissures in the flint surface before it solidified (Fig. 8g). A flat sandstone pebble (261-3, Fig. 7f) is almost completely covered with residues (Fig. 8h) to a maximum thickness of approximately 100 µm suggesting a potential use to catch the hot liquid pitch inside the pit (Palmer 2007).

The residues then underwent closer inspection under a scanning electron microscope LEO 1450-VP, Everhart-Thornley SE-Detector and 4-Quadrant BSE-Detector in connection with an EDX-system OXFORD INCA Energy 200 Premium Si (Li) SATW-Detector. The SEM showed layers of molten plant tissue frazzles and fibres in an amorphous matrix of solidified pitch, thus indicating the origin of the residues (Fig. 9a, b), and embedded sediment particles in the sticky pitch (Fig. 9c). The presence of unaltered primary plant matter within the amorphous matrix was as well a typical feature of experimental pitch and the aforementioned samples from Mesolithic and Neolithic contexts (Pawlik 1995: 209–211).

Following the SEM analysis, Energy-dispersive X-ray analysis was undertaken to detect the elementary composition of the residues. The spectrum of elements acquired from several residue samples shows a significant peak for carbon, verifying the organic nature of the samples (Fig. 9d, e). Various subsequent elements were detected: Potassium (K), Calcium (Ca), Sulphur (S) as well as Iron (Fe), Manganese (Mn), Aluminium (Al), Sodium (Na) and Magnesium (Mg). The latter elements very likely originate from the sediment. More significant is the presence of Ca, K and S. Their traces are shown in considerable quantities as well in the EDX-histograms of Mesolithic and Neolithic birch pitch (Fig. 9f, g). Also experimentally created pitch indicated the presence of Ca and K (Fig. 9h), presumably originating from the exposure to fire and ash during processing and use (Pawlik 1995: 197).

4 Discussion and Conclusion

Modern behavioural patterns and evidence for mastering complex technologies have been recognized at a c.120 ka old site in western Germany. In a multi-level micro-wear analysis, residues on stone tools from Inden-Altdorf have been identified as a pitch produced by the distillation of birch bark. Birch pitch is the oldest known synthetic material and was used in Prehistoric Europe as an adhesive to fix stone tools on wooden shafts (Weiner 2005). This kind of composite or multicomponent tool making requires planning and the execution of complex sequences of action and is regarded as indicator for modern human behaviour (Ambrose 2010). It was until now commonly associated with modern *Homo sapiens* of the last glacial period and the Holocene. The pitch residues found on the Micoquien tools from Inden-Altdorf predate this by far. The use of birch pitch in the Middle Palaeolithic is furthermore supported from another Micoquien site at Königsaue (Mania & Toepfer 1973; Koller et al. 2001; Grünberg 2002). However, only at Altdorf appeared formerly hafted tools in higher numbers and asscociated with settlements structures within a stratigraphical secured context.

This analysis delivered direct evidence that Micoquien lithic technology featured the use of stone tools as hafted implements fixed onto wooden shafts. The hafting traces appeared not only on projectile points but on working tools as well. The resemblance of their visual appearance and elementary spectrum with much younger Neolithic, Mesolithic and Upper Palaeolithic birch pitch is striking. It illustrates that at Inden-Altdorf a very similar, if not the same, material and method of pitch production was already in use during OIS 5e. A natural formation of the residues can be excluded due to their distribution on the tools, the absence of *Betula* charcoal at Altdorf and the production method itself.

Evidence for the production of synthetic pitch and the use of an innovative composite tool technology is still uncommon in the Palaeolithic record. The discovery by Böeda et al. (1996, 2008) of processed natural bitumen on two artefacts from the penultimate Moustérien layer at Umm el Tlel demonstrated the existence of composite technology to at least 40 ka to 70 ka BP. However, their proximity to overlying Transitional and Aurignacien levels at Umm el Tlel leaves open the question of which species of human was producing these pieces. The Königsaue evidence pushes the ability to create hafting mastic back to more than 45 ky to app. 80 ky as well; the Inden-Altdorf evidence pushes it back even further, to the last interglacial. Despite this much greater antiquity, distinguishing the likely fabricator as *Homo neanderthalensis* or *Homo sapiens* seems problematic.

Initial occupation of the Levant by *Homo sapiens* is currently dated to 130–100 ka BP (Grün et al. 2005). It has tended to be portrayed as an aborted settlement, with groups either becoming extinct or being forced to retreat into Africa because of worsening climatic conditions c.75 ka BP. Modern humans do not re-appear in the Levant until c.45 ka BP (Shea 2007) when they then move into the European peninsula. On current evidence, we also consider the second model and that the hominids connected with the Inden-Altdorf site were possibly early *Homo sapiens* (Thissen 2006: 141–171); an interpretation also suggested by Koller et al. (2001) for the Königsaue A find. These data are in support of the possibility that modern humans may have penetrated deeper into the European peninsula than previously thought during their first migration from Africa.

Acknowledgements

We thank the Foundation "zur Förderung der Archäologie im Rheinischen Braunkohlenrevier" who financed this research. Thankfully, we received significant support from the Director of the Titz-Höllen branch office of the Archaeological Services in Rheinland (LVR-ABR), Dr. Udo Geilenbrügge, who provided the project with more staff and mechanical aid. We thank Wilhelm Schürmann, the site supervisor and Dr. Hartmut Schulz, SEM Laboratory, Institute of Geology and Palaeontology, University of Tübingen for technical ad-

vice and support, and Alan Brown B.A. (LVR – ABR) for a (first) translation of chapters 1 & 2. Many thanks to Dr. Philip Piper (University of the Philippines), Dr. Ryan Rabett (University of Cambridge) and Dr. John Shea (Stony Brook University, NY) for commenting on early drafts of this paper.

Author contributions

J.Th. directed the excavations at Altdorf, prepared the excavation report and undertook the morphological analysis of the lithic materials. A.P. undertook the High Power and Low Power use-wear and residue analysis, SEM analysis and EDX analysis.

5 References

Ambrose, S.H. (2010): Coevolution of Composite-Tool Technology, Constructive Memory, and Language. Implications for the Evolution of Modern Human Behavior. Current Anthropology Vol. 51, Supplement 1: 135–147: Chicago.

Baales, M. (2002): Der spätpaläolithische Fundplatz Kettig. RGZM 51: Mainz.

Böeda, E., Connan, J., Dessort, D., Muhesen, S., Mercier, N., Valladas, H. & Tisnérat, N. (1996): Bitumen as a hafting material on Middle Palaeolithic artefacts. Nature 380, 336338: London.

Boëda, E., Bonilauri, S., Connan, J., Jarvie, D., Mercier, N., Tobey, M., Valladas, H., al Sakhel, H. & Muhesen, S. (2008): Middle Palaeolithic bitumen use at Umm el Tlel around 70,000 BP. Antiquity 82(318): 853–861: York.

Fullagar, R. (ed.) (1998): A Closer Look. Recent Australian Studies of Stone Tools. Sydney University Archaeological Methods Series 6: Sydney.

Funke, H. (1969): Chemisch-analytische Untersuchungen verschiedener archäologischer Funde. Doctoral thesis, University of Hamburg: Hamburg.

Grün, R., Stringer, C. McDermott, F. Nathan, R., Porat, N., Robertson, S., Taylor, L., Mortimer, G., Eggins, S. & McCulloch, M. (2005): U-series and ESR analyses of bones and teeth relating to the human burials from Skhul. Journal of Human Evolution 49, 316334: Elsevier, Amsterdam.

Grünberg, J.M. (2002): Middle Palaeolithic birch-bark pitch. Antiquity 76, 1516: Newbury.

Kels, H., Kehl, M., Lehmkuhl, F., Tegtmeier, U. & Thissen, J. (2009): Naturwissenschaftliche Untersuchungen zum mittelpaläolithischen Camp von Inden-Altdorf. In: Kunow, J. (Hrsg.) Archäologie im Rheinland 2008, 36–39: Stuttgart.

Keeley, L.H. (1980): Experimental Determination of Stone Tool Uses. University of Chicago Press: Chicago.

Kind, C.-J. (1997): Die letzten Wildbeuter. Henauhof Nord II und das Endmesolithikum in Baden-Württemberg. Materialhefte zur Archäologie in Baden-Württemberg, 39: Stuttgart.

Koller, J., Baumer, U. & Mania, D. (2001): High-Tech in the Middle Palaeolithic: Neanderthal-Manufactured Pitch Identified. European Journal of Archaeology 4, 3, 385397: Oxford.

Kooi, P. B. (1974): De orkaan van 13 November 1972 en het ontstan van 'hoefeijservormige' grondsporen. Helinium 14, 57: Wetteren.

Loy, T. H. (1983): Prehistoric blood residues: detection on tool surfaces and the identification of species of origin. Science 220, 126971: Washington.

Loy, T. H. (1991): Prehistoric organic residues: recent advances in identification, dating and their antiquity. In: W. Wagner & E. Pernicka (eds.), Archaeometry '90: Proceedings of the 27th International Symposium on Archaeometry, Heidelberg, 645656: Birkhäuser, Berlin.

Mania, D. & Toepfer, V. (1973): Königsaue. Gliederung, Ökologie und mittelpaläolithische Funde der letzten Eiszeit. Veröffentlichungen des Landesmuseums für Vorgeschichte Halle 26: Berlin.

McDougal, I., Brown, F. & Fleagle, J.F. (2005): Stratigraphic placement and age of modern humans from Kibish, Ethiopia. Nature 433, 733–736: London.

Odell, G.H. & Odell-Vereecken, F. (1980): Verifying the Reliability of Lithic Use Wear Assessments by "Blind Tests": The Low Power Approach. Journal of Field Archaeology 7, 87—120: Boston.

Palmer, F. (2007): Die Entstehung von Birkenpech in einer Feuerstelle unter paläolithischen Bedingungen. Mitteilungen der Gesellschaft für Urgeschichte, 16, 75—83: Tübingen.

Pawlik, A. (1995): Die mikroskopische Analyse von Steingeräten. Experimente – Auswertungsmethoden – Artefaktanalyse. Urgeschichtliche Materialhefte 10. Archaeologica Venatoria, 245: Tübingen.

Pawlik, A. (1997): Funktionsanalyse an Artefakten aus Henauhof Nord II. In: C.-J. Kind, Die letzten Wildbeuter. Henauhof Nord II und das Endmesolithikum in Baden-Württemberg. Materialhefte zur Archäologie in Baden-Württemberg, 39, 150178: Tübingen.

Pawlik, A. (2004): Identification of Hafting Traces and Residues by Scanning Electron Microscopes and Energy-dispersive Analysis of X-rays. In: E.A. Walker, F. Wenban-Smith & F. Healy (eds.), Lithics in Action: papers from the conference Lithic Studies in the Year 2000, Oxbow Books, 172183: Oxford.

Päffgen, B. & Thissen, J. (2005): Der Faustkeil von Geuenich. In: Kunow, J. (Hrsg.) Archäologie im Rheinland 2004, 3738: Stuttgart.

Pawlik, A. & Thissen, J. (2008): Birkenpechgewinnung und Rentierjagd im Indetal. In: Kunow, J. (Hrsg.) Archäologie im Rheinland 2007, 4144: Stuttgart.

Rottländer, R.C.A. (1991): Untersuchungen an der Kittmasse von geschäfteten Feuersteinklingen. In: H.T. Waterbolk & W. van Zeist (eds.), Niederwil, eine Siedlung der Pfyner Kultur. IV Holzartefakte und Textilien. Academica Helvetica I/IV, 249250 , Bern.

Sandermann, W. (1965): Untersuchungen vorgeschichtlicher „Gräberharze" und Kitte. Technische Beiträge zur Archäologie 2, 5873: Mainz.

Shea, J.J. 2007: Behavioral differences between Middle and Upper Palaeolithic *Homo sapiens* in the east Mediterranean Levant. Journal of Anthropological Research 63(4), 449488: New Mexico.

Thissen J. (1997): Jäger und Sammler. Paläolithikum und Mesolithikum im Gebiet des Linken Niederrhein. Doctoral thesis, University of Cologne: Köln.

Thissen J. (2006): Die paläolithischen Freilandstationen von Rheindahlen im Löss zwischen Maas und Niederrhein. In: Kunow, J. (Hrsg.) Rheinische Ausgrabungen 59. Philipp von Zabern, Mainz.

Thissen J. (2007): Ein Camp des Micoquien im Indetal bei Altdorf. In: Kunow, J. (Hrsg.) Archäologie im Rheinland 2006, 4245: Stuttgart.

Torrence, R. & Barton, H. (eds.), (2006): Ancient Starch Research. Left Coast Press Inc., California: Walnut Creek.

Weiner, J. (1988): Praktische Versuche zur Herstellung von Birkenpech. Archäologisches Korrespondenzblatt 18, 329–334: Mainz.

Weiner, J. (1992): Wo sind die Retorten? Überlegungen zur Herstellung von Birkenpech im Neolithikum. Acta praehistorica et archaeologica 23, 1519: Berlin.

Weiner, J. (2005): Another Word on Pitch. Some comments on a "Sticky Issue" from Old Europe. Bulletin of Primitive Technology 29, 2027: Berlin.

E&G Quaternary Science Journal
Volume 60 / Number 1 / 2011 / 78–89 / DOI 10.3285/eg.60.1.05
www.quaternary-science.net

GEOZON SCIENCE MEDIA
ISSN 0424-7116

Luminescence Chronology of the Schwalbenberg II Loess in the Middle Rhine Valley

Manfred Frechen, Wolfgang Schirmer

Abstract: The multiple aliquot protocol based Infrared Stimulated Luminescence (IRSL) and thermoluminescence (TL) data and those of the single aliquot regenerative protocol based post-IR IRSL at 225°C and fading-corrected IRSL at 50°C show that anomalous fading is only a minor problem for the loess and loess derivatives at the Schwalbenberg II loess section. Therefore, it is very likely that multiple aliquot based protocols, which were applied commonly in the 1990s for loess from the Middle Rhine Valley, yielded reliable IRSL and TL age estimates up to an age of about 70–80 ka. The loess/palaeosol sequence of the Schwalbenberg II loess section shows a remarkable detailed Weichselian Middle Pleniglacial (MIS 3) record. A detailed and more reliable chronological framework was set up by luminescence dating methods for the loess record resulting in four major accumulation periods for this last glacial record. The chronological results give further evidence for the litho-pedological correlation of the Hesbaye Formation and the Ahrgau Formation to MIS 2 and MIS 3, respectively. The Keldach Formation is designated to correlate to MIS 4 by means of litho-pedostratigraphy but gives deposition ages between 55 and 45 ka, which does suggest a correlation to MIS 3.

[Lumineszenz-Chronologie des Schwalbenberg II-Lösses im Mittelrheintal]

Kurzfassung: Der Vergleich von „multiple aliquot" Protokoll basierten IRSL- und TL-Altern mit denen von „single aliquot regenerative" Protokollen mittels des post-IR IRSL (225°C) und fading-korrigierten IR (50°C) zeigt, dass Signalverlust durch anomales Ausheilen für Lösse und Lössderivate des Schwalbenberg II Profils ein geringes Problem darstellt. Aus diesem Grund ist es sehr wahrscheinlich, dass auf „multiple aliquot" Messprotokollen beruhende Lumineszenz-Datierungen, die in den 1990er Jahren im allgemeinen für Lösse aus dem Mittelrheingebiet angewendet wurden, bis zu einem Alter von 70–80 ka innerhalb der 1-sigma Fehlerabweichung verlässliche IRSL und TL-Alter ergeben haben. Die Löss-/Paläobodensedimente des Schwalbenberg II Lössprofils zeigen einen bemerkenswert detaillierte weichselzeitliche mittelpleniglaziale Abfolge, die mit dem marinen Sauerstoffisotopenstadium 3 korreliert wird. Ein verlässlicher chronologischer Rahmen wurde durch Lumineszenz-Datierungsmethoden bestimmt. Vier Löss-Hauptakkumulationsphasen konnten für die letztglaziale Abfolge vom Schwalbenberg nachgewiesen werden. Die chronologischen Ergebnisse unterstützen die litho-pedologische Korrelation der Hesbaye Formation mit MIS 2 und der Ahrgau Formation mit MIS 3. Aufgrund von litho-pedologischen Befunden wird die Keldach Formation mit MIS 4 korreliert. Die Lumineszenz-Alter von 55 bis 45 ka legen jedoch eine Korrelation mit MIS 3 nahe.

Keywords: *loess, luminescence dating, Pleistocene, Germany, climate change*

Addresses of authors: **M. Frechen**, Leibniz Institute for Applied Geophysics (LIAG), Geochronology and Isotope Hydrology, Stilleweg 2, 30655 Hannover, Germany. E-Mail: Manfred.Frechen@liag-hannover.de; **W. Schirmer**, Dept. of Geology, Heinrich Heine University Düsseldorf. Postal address: 91320 Wolkenstein 24, Germany. E-Mail: schirmer@uni-duesseldorf.de

Introduction

In Central Europe, loess/palaeosol sequences provide excellent high-resolution terrestrial archives of climate and environment change for the past 130,000 years, the time span of the Upper Pleistocene. Thermoluminescence (TL) and Infrared Stimulated Luminescence (IRSL) dating me-thods have been successfully applied for numerous Upper Pleistocene loess records in Central Europe (e.g. Frechen, 1994; Frechen et al,. 2003; Schmidt et al. 2011; Zöller et al. 1994). During the 1990s mainly multiple aliquot additive dose (MAAD) protocols and multiple aliquot regeneration dose (MARD) protocols were applied to determine the equivalent dose (D_e) values for IRSL and TL dating. The latter studies provided apparently reliable numerical age estimates up to about 100 ka. In the past 15 years, luminescence dating of sediments has been significantly improved by establishing single aliquot regenerative (SAR) protocols for determining the equivalent dose. Schmidt et al. (2011) re-investigated the loess and its derivatives from the Tönchesberg section in the Middle Rhine area and found their single aliquot regenerative (SAR) protocol results in excellent agreement with those determined earlier by the MAAD and MARD protocols up to about 70–80 ka, and thus confirmed previously published results from Frechen (1992, 1994) and Zöller et al. (1991) for the Tönchesberg section. The results of Schmidt et al. (2011) show that reliable age estimates up to about 70 ka can be obtained by quartz Optically Stimulated Luminescence (OSL) and up to about 200 ka by feldspar pulsed post-IR IRSL for the last glacial and penultimate glacial loess in the Middle Rhine area, respectively. Therefore, we continue to study the application of multiple aliquot IRSL and TL with those of SAR post-IR IRSL on polymineral fine-grain material from the Schwalbenberg loess.

At the Schwalbenberg section, which is located in the Middle Rhine valley, a very detailed Middle Weichselian loess record is exposed (Schirmer 1990, 1991, 2000a, b, 2011). Altogether 44 samples were investigated, resulting in more

E&G / Vol. 60 / No. 1 / 2011 / 78–89 / DOI 10.3285/eg.60.1.05

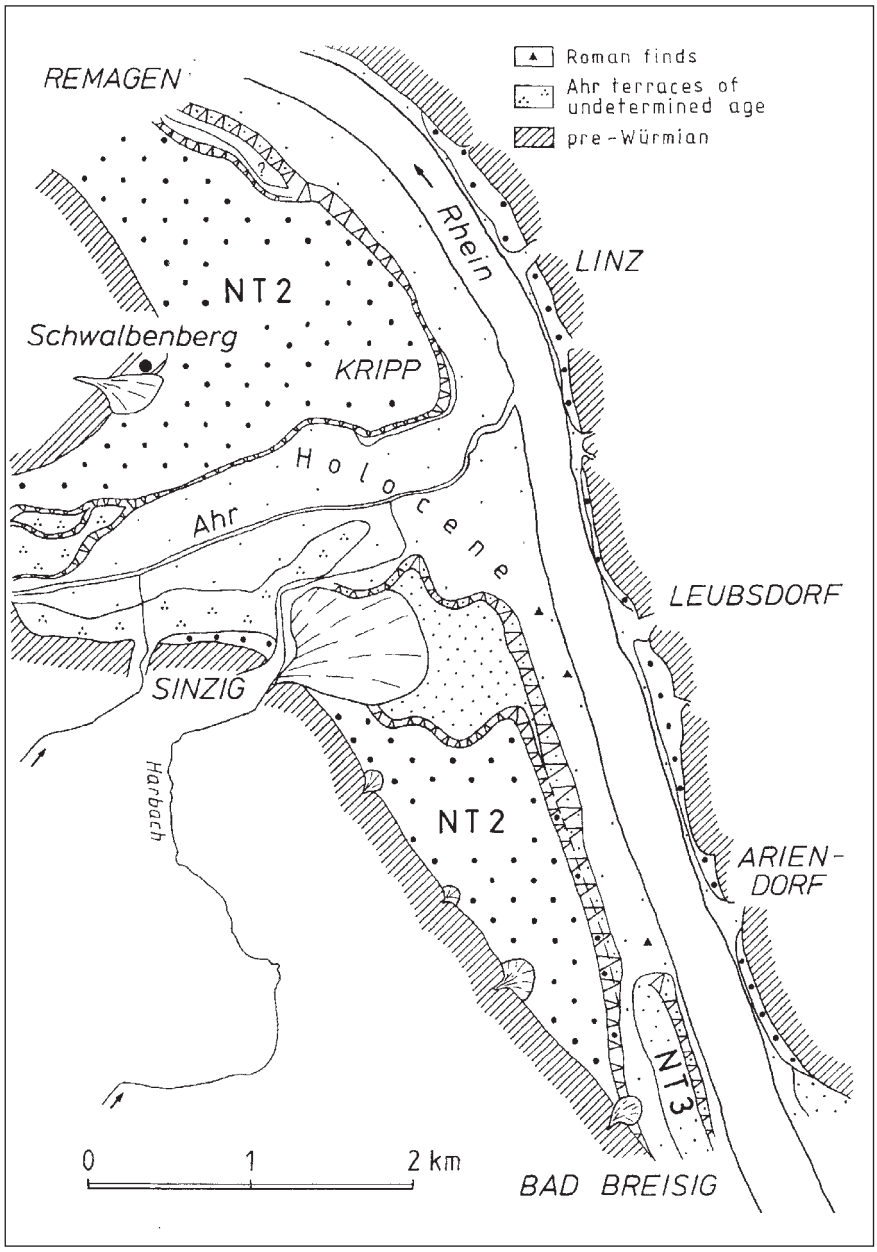

Fig. 1: Map showing the location of the Schwalbenberg section in the Middle Rhine Valley (from Schirmer 1995: 530, modified).

Abb. 1: Lage des Aufschlusses Schwalbenberg im Mittelrheintal (aus Schirmer 1995: 530, verändert).

than 140 IRSL and TL age estimates applying multiple aliquot additive dose and multiple aliquot regeneration dose protocols. Four samples were also investigated by single aliquot regenerative (SAR) protocols including IRSL at 50°C and post-IR IRSL at 225°C. Fading correction was applied for the IRSL 50°C signal.

The aim of this study is to set up a more reliable chronological framework for the loess/palaeosol record from the Schwalbenberg section. A further aim is to test whether the multiple aliquot IRSL and TL results from the 1990s are still suitable for geochronological interpretations. Based on the chronological framework of this paper and further high-resolution proxy data the loess/palaeosol record is correlated with the Greenland ice core records in a further paper (Schirmer, 2000a,b, 2011).

Geological Setting

The Schwalbenberg section is an artificial cliff close to the town of Remagen in the Middle Rhine valley (Fig. 1). An older outcrop (Schirmer 1990, 1991) was later named Schwalbenberg I, whereas Schwalbenberg II is an extended wall few meters behind the wall of Schwalbenberg I. Both sections exhibit 13.5 m loess deposits over a gravel of the Lower Middle Terrace that ends with a truncated interglacial luvisol. The loess record from the section at Schwalbenberg is exceptional owing to its excellent preservation of the Middle Weichselian record, designated to represent most parts of MIS 4 and 3. The section hosts most parts of the Keldach Formation (MIS 4) represented by the lower loess of the section, moreover an unusually complete Ahrgau Formation (MIS 3), represented by the tight loess-soil sequence of the section, and above parts of the Hesbaye and perhaps the Brabant Formations (MIS 2), represented by the upper loess of the section (Schirmer 1995, 2000a,b, 2002, 2010, 2011) (Fig. 4).

The high amount of intercalated interstadial soils is remarkable. The Ahrgau-Formation correlates with its soils excellently to the Greenland Ice Core record, especially the Greenland Interstadials 17 to 6, as supported by its ac-

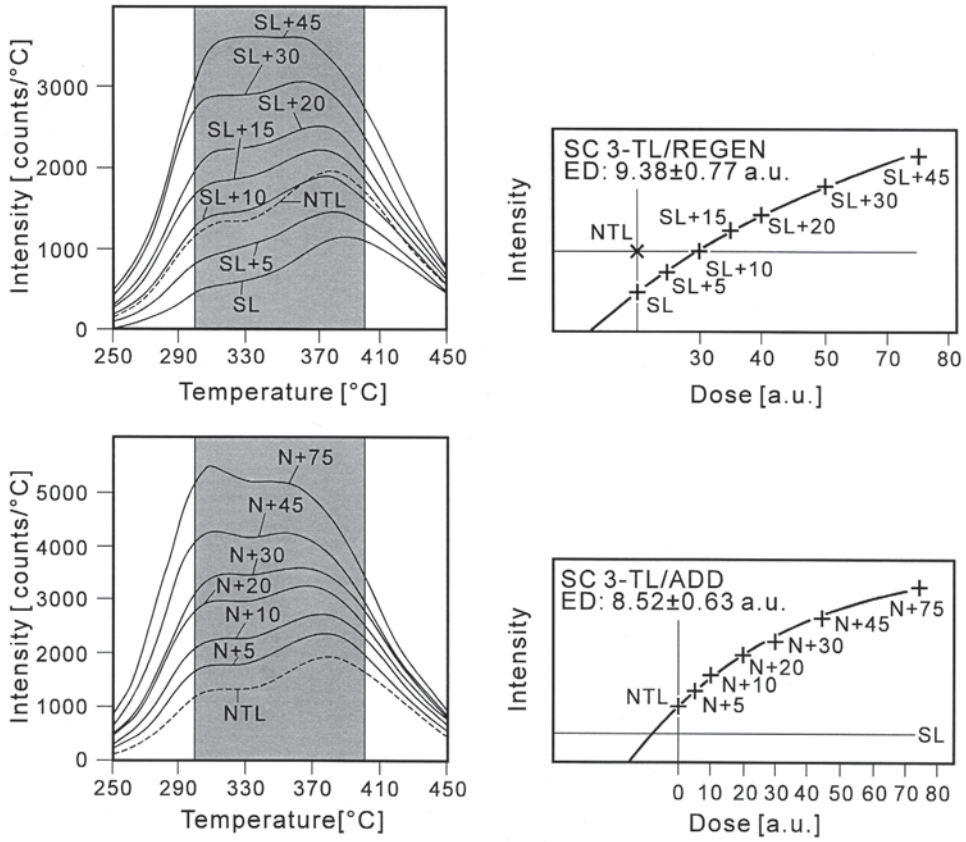

Fig. 2 (a): TL glow curves of sample Sc 3 and resulting growth curves, as determined by multiple aliquot protocols (regeneration and additive dose).

Abb. 2 (a): TL-Glühkurven von Probe Sc 3 sowie die resultierenden Aufbaukurven (Regenerierung und Additive Dosis).

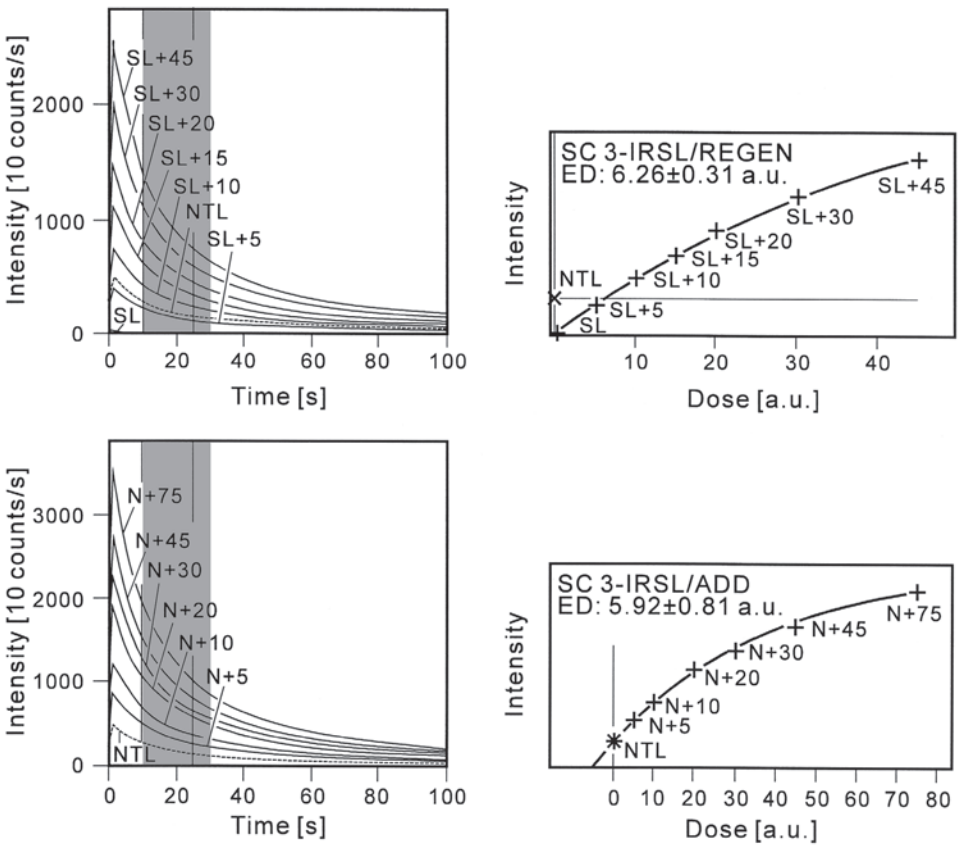

Fig. 2 (b): IRSL decay curves of sample Sc 3 and resulting growth curves, as determined by multiple aliquot protocols (regeneration and additive dose).

Abb. 2 (b): IRSL-Ausleuchtkurven von Probe Sc 3 sowie die resultierenden Aufbaukurven (Regenerierung und Additive Dosis).

count of soils, vertical distance of the soils, their rhythmic arrangement and their intensity indicated by the soil property curves. Thus, the Ahrgau Formation of the Schwalbenberg provides a good equivalent of the Greenland ice curves during MIS 3 (Schirmer 2000a, b, 2011). The Keldach Formation, represented by the lower loess, is from a lithostratigraphical point of view older than GIS 17, thus correlates to MIS 4. A detailed sedimentological/pedological description is given in Schirmer (2011).

Luminescence dating

Luminescence (including TL, OSL and IRSL) refers to the light emitted from crystals such as quartz, feldspar or zircon, when they are stimulated with heat or light after receiving a natural or artificial dose of radiation. As a result of natural radiation in sediments, the number of electrons migrating to traps that result from impurities and crystal defects, increases with time and dose. The equivalent dose (D_e) is a measure of the past radiation absorbed and, in combination with the dose rate, yields the time passed since the last exposure to sunlight. Natural radiation results from the radioactive decay of isotopes in the decay chains of ^{235}U, ^{238}U, ^{232}Th, and the decay of ^{40}K, some minor isotopes including ^{87}Rb, and cosmic rays. The luminescence age equals equivalent dose divided by dose rate. Further information about the methodological background is given by Preusser et al. (2008).

An important assumption for luminescence dating techniques is that the luminescence signals of the mineral grains have been bleached and reset to near zero by daylight prior to deposition. This assumption might be normally fulfilled for aeolian transport from the dust source, mainly floodplain of the Rhine Valley near the confluence of rivers Rhine and Ahr, and the area of deposition at the Schwalbenberg but might not necessarily be fulfilled for reworked loess, e.g. solifluction or slope wash. Unfortunately, thorough tests about the level of resetting of the signal and the application of statistical methods to determine the most likely deposition age have not yet been applied owing to the lack of appropriate methods in the application of polymineral fine-grain material.

Previous studies have shown that luminescence signals from feldspar can suffer from anomalous fading (Spooner 1994; Wintle 1973), an unwanted loss of signal, which can result in age underestimation. Anomalous fading causes a decrease of the luminescence signal with time, faster than expected from thermal stability measurements. Fading corrections involve inherent assumptions including that the fading rate observed on a laboratory timescale is relevant to geological time (Huntley & Lamothe, 2001), thus it is ideal to find a luminescence signal which shows negligible fading. Buylaert et al. (2009) applied an elevated temperature post-IR IRSL protocol proposed by Thomsen et al. (2008) and could reduce the fading rate by a factor of two using the post-IR IRSL at 225°C compared to the IRSL signal at 50°C. Their fading-corrected ages agreed well with ages derived from independent age control.

The reduced fading rate using post-IR IRSL signal was confirmed in several chronological studies about European loess (Thiel et al. 2011a, b).

Experimental details

Multiple aliquot additive dose and regeneration dose protocol

In this study all measurements were carried out on the 4–11 μm polymineral fine grain fraction, using the preparation technique described in Frechen (1994) and Frechen et al. (1997). The artificial irradiation for multiple aliquot protocols was performed using a Co-60 gamma source in Louvain-la-Neuve, Belgium, at the Institut Nucléaire et Chimie Inorganique. Bleaching was done using an UV lamp (Osram Ultra Vitalux 300W) for 16 hours to reset luminescence signals. The samples were stored at room temperature for at least four weeks between artificial irradiation and measurement. Furthermore, the samples were stored for at least 48 hours after preheating at 150°C for 16 hours on a heating plate in order to eliminate the unstable part of IRSL and TL signals and then measured. The signal emission, mainly from feldspar, was detected for all samples through a filter combination of Schott BG-39 and Chance Pilkington HA-3. After 25 seconds of IR stimulation at room temperature, the same discs were immediately heated to obtain their TL. The aliquots were measured with a heating rate of 5°C/s up to 450°C. D_e values were obtained by integrating the 10–25s regions of the IR decay curves and the 300–400°C regions of the TL glow curves. An exponential growth curve was fitted for the different dose steps and compared with the natural luminescence signals to estimate the equivalent dose. Examples for IR decay curves and TL glow curves and the growth curves are shown for sample SC 3 in Figure 2.

Single aliquot regenerative-dose protocol (SAR)

The development of SAR protocols was an important milestone improving accuracy and precision in luminescence dating of quartz, feldspar and polymineral fine-grains (Murray & Wintle 2000; Wallinga et al. 2000). The SAR protocol allows the determination of equivalent dose by interpolation with an about 5% precision. Sensitivity changes are monitored and corrected. Although anomalous fading has not been described as a significant problem for dating last glacial loess from the Rhineland, it can cause age underestimation. So far only samples from the Tönchesberg section situated in the Middle Rhine area have been investigated and cross-checked with both multiple aliquot (additive dose and regeneration) and SAR protocols for D_e determination including fading correction (Schmidt et al. 2011). However, fading correction is problematic and a reliable procedure is still under discussion (Huntley & Lamothe 2001). Based on the studies of Thomsen et al. (2008), Buylaert et al. (2009) proposed a modified SAR IRSL protocol which involves elevated temperature stimulation with IR for 100 s at 225°C following stimulation with IR at 50°C for 100 s, so-called post-IR IRSL measurement sequence. This protocol was successfully applied to penultimate and last glacial loess from the Middle Rhine area, Austria and Serbia (Schmidt et al. 2010, 2011; Thiel et al. 2011a, b). The latter studies have shown that the observed fading rates for the post-IR IRSL signal are significantly lower than those determined for the conventional IRSL at 50°C. Furthermore, it was demonstrated that

Tab. 1: Dosimetric results. Uranium, thorium and potassium content were determined by gammaspectrometry in the laboratory.

Tab. 1: Dosimetrische Ergebnisse. Uran-, Thorium- und Kaliumgehalt wurden im Labor mittels Gammaspektrometrie bestimmt.

Sample	Uranium [ppm]	Thorium [ppm]	Potassium [%]	a value IRSL	IR dose rate [Gy/ka]	a value TL	TL dose rate [Gy/ka]
SC1	2.90±0.20	10.36±0.73	1.59±0.11	0.070	3.74±0.30	0.090	3.99±0.33
SC2	2.72±0.19	10.06±0.70	1.47±0.10	0.075	3.60±0.29	0.101	3.91±0.32
SC3	2.72±0.19	9.55±0.67	1.40±0.10	0.070	3.18±0.26	0.090	3.39±0.29
SC4	2.67±0.19	9.93±0.70	1.47±0.10	0.065	3.44±0.27	0.079	3.69±0.30
SC5	2.88±0.20	10.42±0.73	1.58±0.11	0.065	3.67±0.29	0.086	3.93±0.32
SC6	2.72±0.19	10.46±0.73	1.59±0.11	0.072	3.71±0.29	0.085	3.87±0.31
SC7	2.65±0.19	10.00±0.70	1.57±0.11	0.077	3.67±0.30	0.095	3.89±0.32
SC8	2.76±0.19	9.68±0.68	1.56±0.11	0.080	3.71±0.30	0.103	3.98±0.33
SC9	2.82±0.20	9.81±0.69	1.52±0.11	0.068	3.56±0.29	0.080	3.71±0.30
SC10	2.83±0.20	10.52±0.74	1.59±0.11	0.077	3.82±0.31	0.098	4.08±0.34
SC11	2.80±0.20	10.13±0.71	1.55±0.11	0.080	3.77±0.31	0.098	3.99±0.33
SC12	2.27±0.16	7.70±0.54	1.09±0.06	0.087	2.95±0.23	0.118	3.24±0.27
SC13	2.56±0.18	8.76±0.61	1.26±0.06	0.073	3.18±0.24	0.096	3.44±0.27
SC14	2.67±0.19	8.81±0.62	1.26±0.06	0.085	3.37±0.26	0.095	3.48±0.28
SC15	2.55±0.15	8.72±0.61	1.16±0.06	0.074	3.10±0.24	0.098	3.36±0.27
SC16	2.64±0.18	9.20±0.64	1.25±0.06	0.066	3.18±0.24	0.076	3.29±0.25
SC17	2.64±0.18	8.97±0.63	1.26±0.06	0.078	3.29±0.25	0.089	3.42±0.27
SC18	2.46±0.17	9.14±0.64	1.21±0.06	0.064	3.05±0.23	0.068	3.09±0.24
SC19	2.73±0.19	9.45±0.66	1.19±0.06	0.065	3.17±0.24	0.080	3.35±0.26
SC20	2.64±0.18	8.78±0.61	1.16±0.06	0.065	3.04±0.23	0.099	3.42±0.27
SC21	2.37±0.17	7.87±0.55	1.09±0.06	0.066	2.80±0.21	0.121	3.35±0.28
SC22	2.47±0.17	8.34±0.58	1.11±0.06	0.087	3.12±0.25	0.098	3.24±0.26
SC23	2.54±0.18	8.54±0.60	1.17±0.06	0.093	3.29±0.26	0.119	3.57±0.30
SC24	2.43±0.17	7.81±0.55	1.03±0.05	0.073	2.83±0.22	0.106	3.16±0.26
SC25	2.47±0.17	8.36±0.59	1.14±0.06	0.061	2.88±0.22	0.076	3.03±0.23
SC26	2.10±0.15	7.41±0.52	0.95±0.05	0.073	2.59±0.20	0.099	2.83±0.23
SC27	2.36±0.16	7.86±0.55	1.08±0.06	0.064	2.76±0.21	0.103	3.15±0.25
SC28	2.31±0.16	7.44±0.52	0.99±0.05	0.065	2.63±0.20	0.099	2.96±0.24
SC29	2.63±0.18	8.75±0.61	1.23±0.06	0.065	3.10±0.23	0.082	3.28±0.26
SC30	2.52±0.18	9.69±0.68	1.33±0.07	0.091	3.54±0.28	0.105	3.70±0.30
SC31	2.89±0.20	9.95±0.70	1.51±0.08	0.063	3.61±0.29	0.084	3.79±0.31
SC32	2.88±0.20	10.46±0.73	1.55±0.08	0.069	3.70±0.30	0.075	3.77±0.31
SC33	2.85±0.20	10.50±0.74	1.59±0.08	0.071	3.75±0.30	0.055	3.55±0.28
SC34	2.90±0.20	10.91±0.76	1.62±0.08	0.051	3.58±0.28	0.055	3.63±0.29
SC35	2.82±0.17	10.43±0.63	1.61±0.08	0.050	3.48±0.26	0.058	3.58±0.27
SC36	2.96±0.21	10.60±0.74	1.59±0.08	0.048	3.50±0.27	0.058	3.63±0.29
SC37	2.95±0.21	10.06±0.70	1.51±0.08	0.055	3.47±0.28	0.066	3.61±0.29
SC38	2.67±0.19	9.52±0.67	1.38±0.07	0.057	3.23±0.26	0.072	3.40±0.27
SC39	2.74±0.19	9.29±0.65	1.39±0.07	0.072	3.41±0.27	0.092	3.65±0.30
SC40	3.12±0.22	10.66±0.75	1.39±0.07	0.078	3.79±0.31	0.092	3.97±0.33
SC41	3.11±0.18	10.21±0.61	1.34±0.07	0.079	3.70±0.29	0.095	3.91±0.32
SC42	3.33±0.23	10.96±0.77	1.39±0.07	0.081	3.94±0.32	0.098	4.18±0.35
SC43	3.12±0.22	10.31±0.72	1.33±0.07	0.091	3.87±0.32	0.119	4.23±0.36
SC44	2.85±0.20	9.42±0.66	1.37±0.10	0.085	3.61±0.30	0.105	3.85±0.32

E&G / Vol. 60 / No. 1 / 2011 / 78–89 / DOI 10.3285/eg.60.1.05 / © Authors / Creative Commons Attribution License

the post-IR IRSL at 225°C is bleachable by natural daylight/sunlight (Buylaert et al., 2009). Therefore, this approach was further tested in this study for loess and loess derivatives from the Schwalbenberg section. Optically stimulated luminescence (OSL) of fine-grain (4–11 µm) quartz has also been widely used to estimate the deposition age of sediments (Schmidt et al. 2011 and references therein) and is usually regarded as an accurate and precise dating method. However, the fast component of the quartz OSL, which is usually used for dating, saturates at doses between 200 and 400 Gy. Reliable quartz OSL age estimates were obtained for loess from the Middle Rhine area up to about 70 ka (Schmidt et al. 2011) and were in excellent agreement with post-IR IRSL results.

Polymineral fine-grain material was taken from four samples for applying SAR protocols to determine the D_e values and the g-values to calculate the fading-corrected IRSL age estimates. D_e measurements for all SAR protocols were performed with an automated Risö reader TL/OSL-DA-15 equipped with a $^{90}Sr/^{90}Y$ beta source at the Leibniz Institute for Applied Geophysics (LIAG) in Hannover. A Schott BG 39 and a Corning 7-59 filter combination passing the blue wavelength spectra between 320 and 460 nm were intercalated between samples and photomultiplier for measurements including IRSL at 50°C and post-IR IRSL at 225°C. The polymineral fine-grains were bleached after preheat at 250°C for 60 s with IR diodes at 50°C for 100s and subsequently luminescence-measured at 225°C for 100s. Within the applied post-IR IRSL protocol the standard IRSL signal at 50°C was also recorded. Thus it is possible to compare both the D_e values and the fading rates for IR at 50°C and post-IR IRSL at 225°C. Performance tests were adopted to test the reliability of SAR protocols, e.g. dose recovery test and the determination of residuals, as shown in Table 3.

Aliquots three each were bleached from four samples for four hours by a dr hönle SOL2 solar simulator and then the apparent dose was measured in the usual manner. The residual dose values range from 1.79±0.13 Gy to 1.84±0.13 Gy and from 4.75±0.33 to 6.40±0.39 Gy for IRSL at 50°C and for post-IR IRSL at 225°C, respectively. The SAR D_e results are shown in Table 3.

Dose recovery ratios were measured for four samples using the IRSL at 50°C and the post-IR IRSL at 225°C. Aliquots were first bleached in a dr hönle SOL 2 solar simulator for four hours and then a dose of 100 Gy was given, which is approximately equal to their natural dose. The dose recovery tests are between 0.89 and 0.99 and between 0.91 and 0.98, respectively. Dose recovery tests after subtracting residuals yield values ranging from 0.88 to 0.97 and from 0.85 to 0.93 for IRSL at 50°C and for post-IR IRSL at 225°C, respectively. Table 4 shows the individual dose recovery ratios for all aliquots. All dose response curves, for both IRSL at 50°C and post-IR IRSL at 225°C, were fitted using an exponential function.

Laboratory fading

No fading rates are available for the multiple aliquot approach. To minimize fading, the samples were stored for at least four weeks between irradiation and measurements. Furthermore, the 10–25s integral of the IR decay curves was taken for IRSL D_e determination; this part of the decay curve was found to show less fading than the initial part, e.g. the integral 0–1s. The laboratory fading rates were measured as an IRSL signal decrease over time on artificially irradiated aliquots. The same aliquots used for D_e measurements were used for fading measurements, six per sample; the aliquots were bleached and a dose of 100 Gy was given. The preheat was applied immediately after irradiation and before storage. After storage ranging from repeated prompt measurements to delays up to 65 hours, the aliquots were measured. Fading rates for the IRSL signal at 50°C range from 1.6 to 2.5%/decade, whereas for the post-IR IRSL signal at 225°C the fading rates are reduced ranging from 0.3 to 0.8%/decade. The less fading of the post-IR IRSL signal indicates that the post-IR IRSL signal at 225°C is more stable than the standard IRSL signal at 50°C. Following the suggestions of Thomsen et al. (2008) fading correction was not applied for g-values smaller than 1%/decade.

Dosimetry

Dose-rates for all samples were obtained from potassium, uranium and thorium content, as measured by gamma spectrometry in the laboratory (Geological Institute, University of Cologne), assuming a radioactive equilibrium for the sediments (Table 1). The measured *in situ* water content for section Schwalbenberg II was below 5% owing to decades of exposure. Therefore a water content of 15±5% was estimated for all samples. Alpha irradiation was carried out at the same institute with a ^{241}Am source for all samples to determine alpha efficiency (a value) (Table 1).

Results

The uranium, thorium and potassium content and total dose rates are shown in Table 1. The mean dose rate is 3.37 Gy/ka and 3.58 Gy/ka for IRSL and TL, respectively, ranging from 2.59 Gy/ka to 4.23 Gy/ka for all dose rates.

D_e values, as determined by MA regeneration and additive dose protocols, range from 61.8 to 196.4 Gray (Gy) and from 82.2 to 252.3 Gy for IRSL and TL, respectively. The mean IRSL/TL $D_e$ratio is 0.74 and 0.77 for the MA regeneration and additive dose protocol, respectively, indicating a significant average IRSL underestimation or TL overestimation very likely owing to insufficient bleaching prior to deposition (Fig. 3).

Four main IRSL age cluster can be distinguished for the loess/palaeosol sequence at the Schwalbenberg II section.

a. Lower Pleniglacial / early Middle Weichselian: IRSL age estimates between 55 and 45 ka
b. Early Middle Pleniglacial / middle Middle Weichselian: IRSL age estimates around 40 ka
c. Late Middle Pleniglacial/ late Middle Weichselian: IRSL age estimates between 35 and 25 ka
d. Upper Weichselian: between 25 and 18 ka

Samples SC 1–15 were taken from the lowermost 4 m of the profile, below the discontinuity at 4.0 m (Fig. 4 and 5). IRSL age estimates, as determined by the MA regeneration and additive dose protocol, range from 50.9±4.3 ka to 38.4±3.5 ka and from 50.3±4.3 ka to 37.7±4.2 ka, respectively. TL age

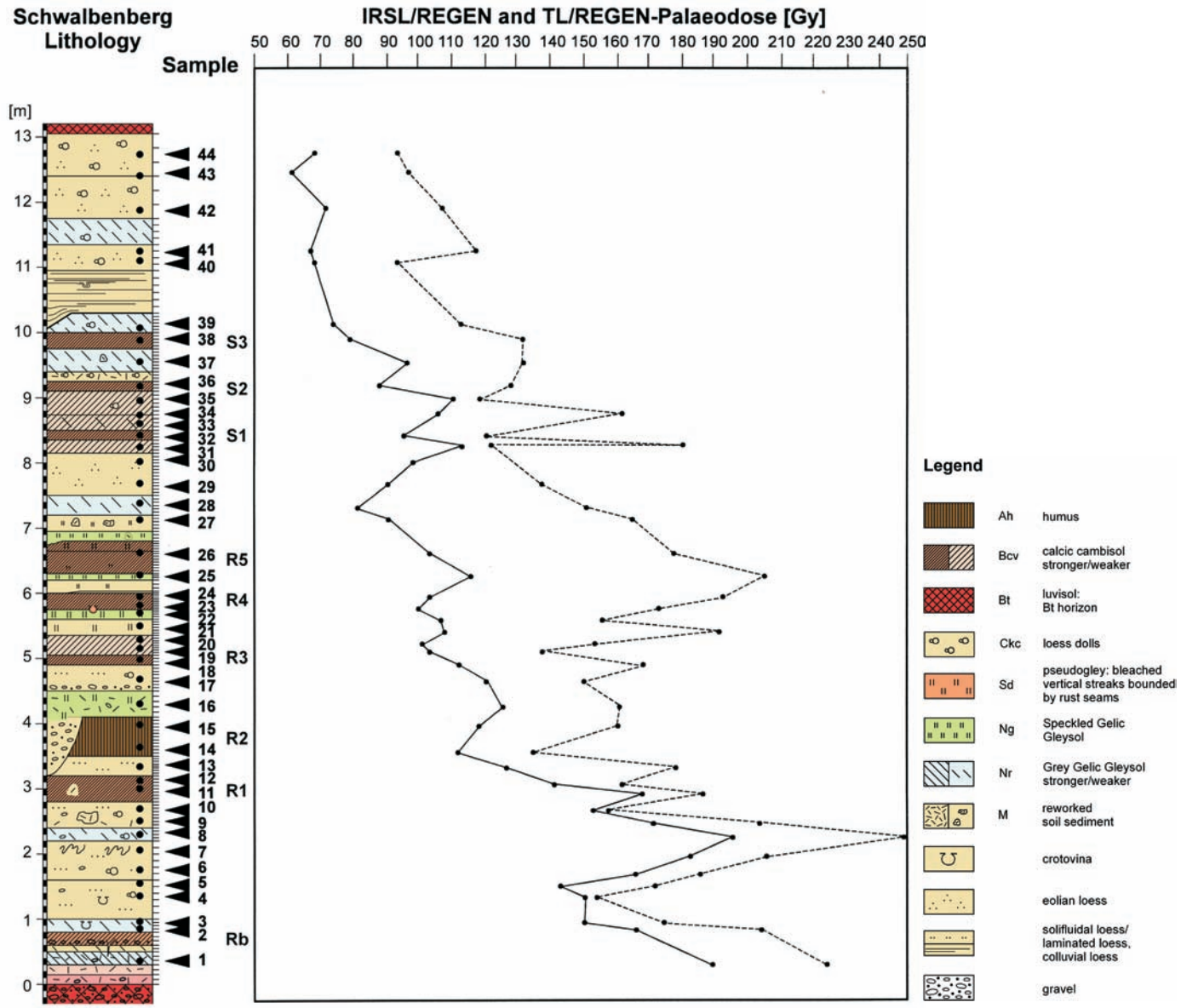

Fig. 3: Comparison of D_e values, as determined by IRSL and TL applying the multiple aliquot approach. Rb = Reisberg Soil, R1–5 = Remagen Soils 1–5, S 1–3 = Sinzig Soils 1-3.

Abb. 3: Vergleich von D_e-Werten mittels IRSL und TL im Multiple Aliquot Protokoll bestimmt. Rb = Reisberg-Boden, R1–5 = Remagen-Böden 1–5, S1–3 = Sinzig-Böden 1–3.

estimates have a slightly higher mean age but are in agreement within the 1-sigma standard deviation with the IRSL age estimates for most of the samples (Table 2). The TL results show a larger sample to sample scatter of $D_e$values, very likely owing to incomplete bleaching, as TL needs more daylight exposure time for complete resetting than IRSL.

Fading-corrected IRSL or TL age estimates are not available for the subsamples measured by multiple aliquot protocols. In order to minimize fading for aliquots measured by MA, samples were stored for at least four weeks after irradiation and prior to the measurement. Furthermore, the middle part of the IR decay curves was integrated, which is known to be the part of the IRSL decay curve showing less fading than the initial part of the curve. In order to test the reliability of the applied MA protocols, which were commonly applied in the 1990s (e.g. Frechen 1994; Frechen et al.1995; Zöller et al.1991) for samples from the Middle Rhine area, single aliquot regenerative protocols were applied using post-IR IRSL at 225°C and IRSL at 50°C including fading correction. Sample Sc 11 was chosen for comparison. The IRSL age estimates for IRSL at 50°C and post-IR IRSL at 225°C are 53.9±4.8 ka and 57.0±4.7 ka, respectively. The latter mean IRSL age estimates are about 20% higher than those determined by MA protocols but are in agreement within the 1-sigma standard deviation and hence do not alter the chronostratigraphic interpretation significantly.

Samples Sc 16–26 were taken between 4.00 m and 7.20 m. IRSL age estimates range from 39.7±3.6 ka and 40.4±4.4 ka (MA regeneration) and from 37.5±5.4 ka to 41.3±3.7 ka (MA additive dose) whereas TL age estimates are between 48.3±4.6 ka and 63.5±7.3 ka (MA regeneration) and between 46.8±4.3 ka and 35.0±3.9 ka (MA additive dose). TL results show a larger D_e and age scatter most likely caused by incomplete bleaching. Neither IRSL age estimates nor TL age estimates show age increase for this part of the sequence Samples Sc 27–39 were taken between 7.20 m and 9.80 m. IRSL age es-

E&G / Vol. 60 / No. 1 / 2011 / 78–89 / DOI 10.3285/eg.60.1.05 / © Authors / Creative Commons Attribution License

Table 2: D_e values, as determined by multiple aliquot protocols (additive dose and regeneration) and IRSL and TL age estimates. A delay between irradiation and measurement of at least four weeks and the late decay curve integral (10-25s) was taken for IRSL D_e determination to minimize fading. However, fading-correction was not applied for these samples.

Tabelle 2: D_e-Werte mittels Multiple Aliquot Protokoll (additive Methode und Regenerierungsmethode) sowie IRSL- und TL-Alter. Zwischen Bestrahlung und Messung der Proben wurde mindestens vier Wochen gewartet und der hintere Teil der IR-Zerfallskurve wurde für die D_e-Bestimmung integriert, um so eventuell vorkommendes Fading zu minimieren. Eine Fading-Korrektur wurde nicht durchgeführt.

Sample	IRSL/REGEN	IRSL/ADD	TL/REGEN	TL/ADD	IRSL/REGEN	IRSL/ADD	TL/REGEN	TL/ADD
	Equivalent dose in Gray [Gy]				Age in 1000 years [ka]			
SC1	190.2±5.4	188.1±6.1	224.6±20.2	189.6±2.3	50.9±4.3	50.3±4.3	56.3±6.8	47.5±3.9
SC2	167.2±8.5	158.1±44.9	205.2±14.1	190.1±16.8	46.5±4.4	44.0±13.0	52.5±5.7	48.6±5.9
SC3	151.1±9.4	134.6±5.9	175.7±12.3	164.1±2.9	47.6±4.9	42.4±4.0	51.8±5.7	48.4±4.2
SC4	151.5±8.8	182.7±10.3	155.0±8.8	199.7±11.9	44.0±4.3	53.1±5.2	42.0±4.2	54.1±5.5
SC5	144.1±10.4	151.8±10.9	173.5±9.4	184.3±9.3	39.3±4.2	41.4±4.4	44.1±4.3	46.9±4.5
SC6	166.6±8.6	176.5±16.4	186.3±8.7	190.8±9.2	44.9±4.2	47.6±5.8	48.2±4.5	49.3±4.6
SC7	183.7±9.1	181.2±22.6	207.2±8.0	208.3±17.5	50.0±4.7	49.3±7.3	53.3±4.8	53.6±6.3
SC8	196.4±13.1	165.8±26.1	252.3±12.4	179.1±20.7	53.0±5.6	44.7±7.9	63.4±6.1	45.0±6.4
SC9	171.9±16.2	181.1±18.3	204.9±20.9	204.1±10.1	48.2±6.0	50.8±6.6	55.2±7.2	55.0±5.2
SC10	154.0±11.3	156.3±3.1	158.3±16.3	160.2±5.7	40.3±4.4	40.9±3.4	38.8±5.1	39.2±3.5
SC11	168.9±2.2	172.7±25.8	187.8±19.1	173.9±3.6	44.9±3.7	45.9±7.8	47.1±6.2	43.6±3.7
SC12	141.9±9.7	149.5±19.6	163.3±10.3	220.6±9.5	48.2±5.0	50.8±7.7	50.3±5.2	68.0±6.3
SC13	127.3±11.0	122.8±11.7	178.9±20.3	167.2±6.3	40.0±4.6	38.6±4.7	52.1±7.2	48.7±4.3
SC14	112.8±10.2	99.5±13.0	136.2±13.0	128.2±7.6	33.5±4.0	29.6±4.5	39.2±4.9	36.9±3.7
SC15	119.1±6.2	116.9±9.3	162.3±8.4	157.4±7.2	38.4±3.5	37.7±4.2	48.3±4.6	46.8±4.3
SC16	125.9±6.1	118.9±14.4	161.9±8.8	180.7±3.9	39.7±3.6	37.5±5.4	49.2±4.6	54.9±4.4
SC17	121.9±7.9	127.3±10.5	150.5±11.2	163.3±5.2	37.0±3.7	38.6±4.4	44.0±4.8	47.8±4.1
SC18	113.1±8.5			169.5±12.0		37.1±4.0		54.9±5.7
SC19	104.0±8.0	90.6±11.2	138.4±12.0	120.6±6.7	32.8±3.6	28.6±4.2	41.4±4.8	36.0±3.5
SC20	101.9±14.3			154.5±21.6		33.5±5.3		45.2±7.3
SC21	108.1±5.5	115.4±5.8	191.0±20.0	201.0±10.5	38.7±3.5	41.3±3.7	57.1±7.6	60.1±5.9
SC22	107.8±12.3	104.9±10.0	156.4±25.7	147.4±10.7	34.5±4.8	33.6±4.2	48.3±8.8	45.6±4.9
SC23	100.0±5.4	80.9±7.2	174.0±20.0	124.8±9.3	30.4±2.9	24.6±2.9	48.7±6.9	35.0±3.9
SC24	103.5±10.8			192.8±23.5		36.6±4.7		61.0±8.9
SC25	116.1±6.1			205.8±9.1		40.4±3.7		67.9±6.0
SC26	104.7±8.2			179.7±14.9		40.4±4.4		63.5±7.3
SC27	91.3±6.4	81.3±7.4	165.5±28.1	136.5±13.1	33.0±3.4	29.4±3.5	52.5±9.9	43.3±5.4
SC28	81.8±7.5	72.1±13.6	151.8±12.1	116.9±9.2	31.1±3.7	27.4±5.6	51.3±5.8	39.5±4.4
SC29	90.8±5.5	92.6±11.5	137.3±13.1	148.7±10.0	29.3+2.8	29.9±4.4	41.8±5.1	45.3±4.7
SC30	98.5±4.8	102.5±6.9	113.4±8.8	117.6±6.6	27.8±2.6	29.0±3.0	30.7±3.4	31.8±3.1
SC31	122.5±11.7	115.5±27.7	180.4±15.1	192.1±15.7	33.9±4.2	32.0±8.1	47.5±5.6	50.6±5.9
SC32	95.8±4.4	100.4±6.0	120.7±6.0	128.9±2.9	25.9±2.4	27.2±2.7	32.0±3.0	34.2±2.9
SC33	67.1±3.6	67.7±3.2	43.9±5.7					
SC34	106.6±9.9	90.9±3.0	161.5±13.4	144.2±7.2	29.8±3.6	25.4±2.2	44.5±5.1	39.7±3.7
SC35	111.8±4.1	98.1±5.7	119.6±11.0	112.5±3.8	32.1±2.7	28.2±2.7	33.4±4.0	31.4±2.6
SC36	87.7±5.8	90.9±21.5	128.1±10.2	127.8±7.8	25.0±2.6	26.0±6.5	35.3±4.0	35.2±3.5
SC37	96.4±4.4	93.8±11.7	132.4±13.3	112.2±2.3	27.8±2.5	27.1±4.0	36.7±4.7	31.1±2.6
SC38	79.5±3.6	77.6±6.8	132.2±6.3	116.4±3.9	24.6±2.2	24.0±2.8	38.9±3.6	34.2±3.0
SC39	74.2±1.7			113.2±10.6		21.7±1.8		31.1±3.9
SC40	68.5±5.4	68.3±5.9	93.3±19.9	87.9±4.1	18.1±2.1	18.0±2.1	23.5±5.4	22.1±2.1
SC41	67.6±4.7	64.5±13.8	118.9±14.8	114.4±10.8	18.3±1.9	17.4±4.0	30.4±4.5	29.3±3.6
SC42	71.9±3.6	68.0±9.3	107.8±8.8	97.9±7.2	18.2±1.8	17.2±2.8	25.8±3.0	23.4±2.6
SC43	61.8±12.7			97.2±17.9		16.0±3.5		23.0±4.7
SC44	68.7±3.5	68.2±5.5	94.1±7.3	82.2±2.3	19.0±1.8	18.9±2.2	24.5±2.8	21.4±1.9

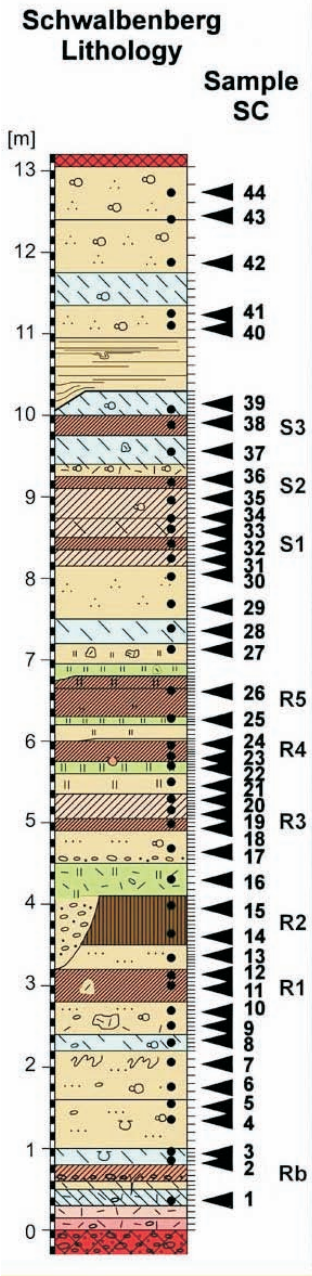

LITHO-PEDO STRATIGRAPHY		IRSL ages in [ka]		TL ages in [ka]	
		REGEN	ADD	REGEN	ADD
?Brabant Formation		19.0 ± 1.8 16.0 ± 3.5	18.9 ± 2.2	24.5 ± 2.8 23.0 ± 4.7	21.4 ± 1.9
		18.2 ± 1.8	17.2 ± 2.8	25.8 ± 3.0	23.4 ± 2.6
Hesbaye Formation		18.3 ± 1.9 18.1 ± 2.1	17.4 ± 4.0 18.0 ± 2.1	30.4 ± 4.5 23.5 ± 5.4	29.3 ± 3.6 22.1 ± 2.1
Ahrgau Formation	Sinzig Sub-formation	21.7 ± 1.8		31.1 ± 3.9	
		27.8 ± 2.5	27.1 ± 4.0	36.7 ± 4.7	31.1 ± 2.6
		32.1 ± 2.7	28.2 ± 2.7	33.4 ± 4.0	31.4 ± 2.6
		33.9 ± 4.2	32.0 ± 8.1	47.5 ± 5.6	50.6 ± 5.9
	Kripp Sub-formation	29.3 ± 2.8	29.9 ± 4.4	41.8 ± 5.1	45.3 ± 4.7
		33.0 ± 3.4	29.4 ± 3.5	52.5 ± 9.9	43.3 ± 5.4
	Upper Remagen Sub-formation	40.4 ± 3.7		67.9 ± 6.0	
		30.4 ± 2.9	24.6 ± 2.9	48.7 ± 6.9	35.0 ± 3.9
		38.7 ± 3.5	41.3 ± 3.7	57.1 ± 7.6	60.1 ± 5.9
		32.8 ± 3.6	28.6 ± 4.2	41.4 ± 4.8	36.0 ± 3.5
		37.0 ± 3.7	38.6 ± 4.4	44.0 ± 4.8	47.8 ± 4.1
	Lower Remagen Subform.	38.4 ± 3.5	37.7 ± 4.2	48.3 ± 4.6	46.8 ± 4.3
		40.0 ± 4.6	38.6 ± 4.7	52.1 ± 7.2	48.7 ± 4.3
Keldach Formation		44.9 ± 3.7	45.9 ± 7.8	47.1 ± 6.2	43.6 ± 3.7
		48.2 ± 6.0	50.8 ± 6.6	55.2 ± 7.2	55.0 ± 5.2
		50.0 ± 4.7	49.3 ± 7.3	53.3 ± 4.8	53.6 ± 6.3
		39.3 ± 4.2	41.4 ± 4.4	44.1 ± 4.3	46.9 ± 4.5
		47.6 ± 4.9	42.4 ± 4.0	51.8 ± 5.7	48.4 ± 4.2
		50.9 ± 4.3	50.3 ± 4.3	56.3 ± 6.8	47.5 ± 3.9
Rhine Lower Middle Terrace					

Fig. 4: IRSL and TL age estimates applying the multiple aliquot additive dose and regeneration protocol. Rb = Reisberg Soil, R1–5 = Remagen Soils 1–5, S 1–3 = Sinzig Soils 1-3. Legend see Fig. 3.

Abb. 4: IRSL und TL-Alter mit dem Multiple Aliquot Protokoll für die additive Methode und Regenerierungsmethode bestimmt. Rb = Reisberg-Boden, R1–5 = Remagen-Böden 1–5, S1–3 = Sinzig-Böden 1–3. Legende siehe Abb. 3.

timates range from 33.0±3.4 ka and 21.7±1.8 ka and from 29.4±3.5 ka and 24.0±2.8 ka, as determined by MA regeneration and additive dose protocols, respectively. TL age estimates are between 52.5±9.9 ka and 31.1±3.9 ka (MA regeneration) and between 43.3±5.4 ka and 34.2±3.0 ka (MA additive dose). The mean IRSL and TL values show a slight age increase with depth, whereas most of the single IRSL and TL age estimates are in agreement within the 1-sigma standard deviation.

Samples Sc 29 and Sc 35 were chosen for further investigation. Sample Sc 29 yielded IRSL age estimates for IRSL at 50°C and post-IR IRSL at 225°C of 30.3±2.7 ka and 30.6±2.6 ka, respectively. MA protocols and fading-corrected ages, as determined by SAR protocols for IRSL at 50°C and post-IR IRSL at 225°C, are in agreement within the 1-sigma standard deviation. A significant age underestimation for the MA IRSL and MA TL age estimates was not found for this sample. Sample Sc 35 yielded age estimates for IRSL at 50°C and post-IR IRSL at 225°C of 26.7±2.5 ka and 29.8±2.7 ka, respectively. MA protocols and fading-corrected SAR protocols for IRSL at 50°C and post-IR IRSL at 225°C are also in agreement within the 1-sigma standard deviation. An age underestimation of 5.4 % was calculated for the MA IRSL but TL age overestimation of 5.6% was calculated for this sample, if compared with the fading-corrected IRSL age estimates.

Samples Sc 40–44 were taken from the uppermost part of the profile between 9.80 m and 13.20 m. IRSL age estimates range from 18.1±2.1 ka to 19.0±1.8 ka (MA regeneration) and from 18.0±2.1 ka to 18.9±2.2 ka (MA additive dose) whereas TL age estimates are between 23.5±5.4 ka and 24.5±2.8 ka (MA regeneration) and between 22.1±2.1 ka and 21.4±1.9 ka (additive dose). Neither IRSL nor TL data indicates age increase with depth. Sample Sc 42 was further studied. IR at 50°C and post-IR IRSL at 225°C yielded IRSL age estimates of 23.6±2.7 ka and 25.8±2.2 ka, respectively. IRSL and TL show a significant age underestimation for sample Sc 42, if compared with the fading-corrected IRSL at 50°C and post-IR IRSL at 225°C age estimates. IRSL age underestimation exceeds the 1-sigma standard deviation but is in agreement within the

E&G / Vol. 60 / No. 1 / 2011 / 78–89 / DOI 10.3285/eg.60.1.05 / © Authors / Creative Commons Attribution License

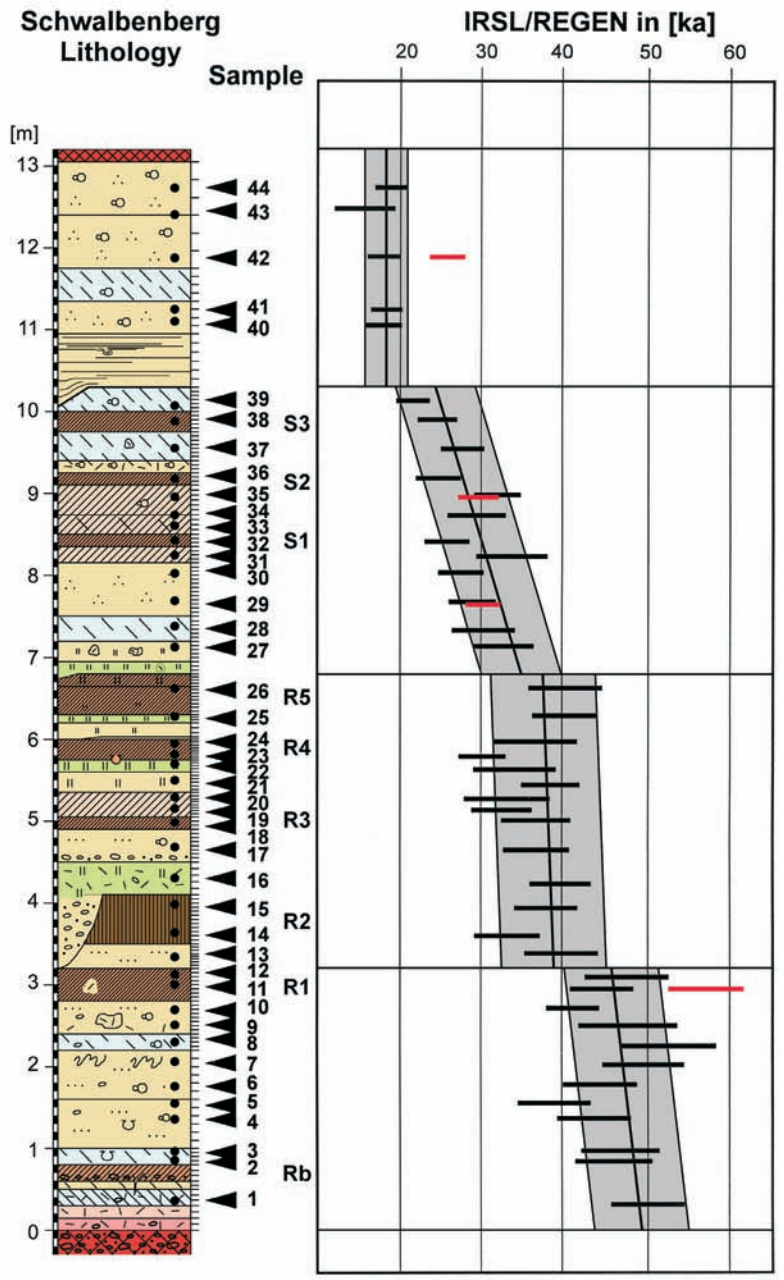

Fig. 5: MA IRSL age estimates (black) and fading corrected post-IR at 225°C age estimates (red). Rb = Reisberg Soil, R1–5 = Remagen Soils 1–5, S 1–3 = Sinzig Soils 1-3. Legend see Fig. 3.

Abb. 5: Multiple Aliquot IRSL-Alter (schwarzer Balken) und fading-korrigierte post-IR IRSL (225°C)-Alter (roter Balken). Rb = Reisberg-Boden, R1–5 = Remagen-Böden 1–5, S1–3 = Sinzig-Böden 1–3. Legende siehe Abb. 3.

2-sigma standard deviation. The MA TL age estimates are in agreement with the fading-corrected age estimates.

Discussion

The upper part of the penultimate glacial fluvial deposits (below m 0) is truncated, resulting in a hiatus (Keldach Discordance), which includes at least parts of the last interglacial (MIS 5e) and early last glacial record (MIS 5d-a).

The lower part (0.00 to 3.20m) of the loess/palaeosol sequence correlates to the Keldach Formation. The oldest loess-like sediments yielded IRSL and TL age estimates ranging from about 55 to 50 ka at its base. The fading-corrected IRSL age (SAR IR at 50°C) gave 53.9±4.7 ka and the post-IR IRSL (225°C) yielded 55.5±4.5 ka. These ages are rather young for early MIS 4 deposits, that start with 74–79 ka after ice core ages. Moreover, the luminescence ages of this lower loess may contain tendencies being even younger owing to the solifluidal facies of this lower loess, which very likely results in insufficient bleaching prior to deposition (which does result in age overestimation). Thus, this physical data rise the cautious question whether this lower loess could be an additional part of the Ahrgau Formation (MIS 3).

From litho-pedological aspect this lower loess unit is assigned by Schirmer (1990: 107, 1991, 2000a, 2000b, 2002, 2010 and 2011) to the Weichselian Lower Pleniglacial (MIS 4) for the following reasons:

- The widely distributed early loess between the Rocourt Solcomplex (MIS 5) and the soil complex of the Ahrgau Formation (MIS 3) is extraordinary thick here.
- Schirmer (2000a, b, 2011) suggested, that the Ahrgau-Formation with its soils matches excellently to the range of the Greenland Interstadials 17 to 6 by its account of soils, vertical distance of the soils, their rhythmic arrangement and their intensity indicated by the soil property curves. Thus, following Schirmer (2011), the lower loess must be older than GIS 17, and hence at least of MIS 4 age.
- Moreover, the loess facies of this lower loess is throughout solifluidal loess, which is typical for the Keldach Formation (MIS 4) in whole central Europe.

Tab. 3: D_e values and age estimates, as determined by the SAR protocol for IR at 50°C and post-IR IRSL at 225°C including fading-corrected age estimates.

Tab. 3: D_e-Werte und Alter mittels SAR-Protokolle für IR (50°C) und post-IR IRSL (225°C) bestimmt sowie die fading-korrigierten IRSL-Alter.

Sample ID	Post-IR IRSL at 225°C			IR at 50°C			
	Mean De [Gy]	g-value	Uncorrected pIRIR Age [ka]	Mean De [Gy]	g-value	Uncorrected IR50 Age [ka]	Fading-corrected IR50 Age [ka]
Sc42	76.5±1.8	0.8±0.1	24.1±2.1	60.6±0.5	2.4±0.1	19.1±2.2	23.6±2.7
Sc35	108.0±4.2	0.6±0.1	28.3±2.6	88.6±4.9	1.6±0.3	23.2±2.1	26.7±2.5
Sc29	112.5±2.5	0.6±0.1	29.1±2.5	93.7±4.8	2.5±0.1	24.2±2.2	30.3±2.7
Sc11	159.8±3.9	0.3±0.1	55.5±4.5	129.2±7.1	2.0±0.2	44.9±3.8	53.9±4.7

Tab. 4: Results of performance tests including dose recovery tests and the determination of the residuals.

Tab. 4: Ergebnisse der methodischen Voruntersuchungen inklusive dose recovery tests und das Bestimmen des unbleichbaren Rests („residuals").

Sample ID	Post-IR IRSL at 225°C			IR at 50°C		
	Mean dose recovery ratio	Dose recovery after residual subtraction	Mean residual dose [Gy]	Mean dose recovery ratio	Dose recovery after residual subtraction	Mean residual dose [Gy]
Sc11	0.94±0.04	0.87±0.06	6.40±0.39	0.93±0.02	0.91±0.07	1.79±0.13
Sc29	0.91±0.01	0.85±0.15	6.32±1.15	0.99±0.02	0.97±0.04	1.69±0.06
Sc35	0.94±0.01	0.89±0.14	5.54±0.86	0.89±0.00	0.88±0.06	1.85±0.12
Sc42	0.98±0.02	0.93±0.07	4.75±0.33	0.95±0.06	0.93±0.09	1.84±0.13

- Also, the grain size curve with coarse silt prevalence and organic carbon curve with low values plead for this assignment (Schirmer 2011).
- In addition, the grain size curve shows enhancement of sand in the lower part of this loess unit, which is also a common feature in central Europe (Schirmer 2011), whereas sand accumulation from the base of the Middle Pleniglacial soil complex is not recorded.
- The weak Reisberg cambisol fits well to the Keldach Formation, which shows two weak soils in its lower part (Schirmer 2002: 19).
- Consequently, from litho-pedostratigraphical point of view a link of the lower loess to the Ahrgau Formation is unlikely.

From a chronological point of view the calculated luminescence age estimates and thus the deposition ages are younger than 60 ka, and hence correlate to MIS 3. Furthermore, it is even very likely that the sediments from solifluidal facies are even age overestimated, which would result in even younger deposition ages. As the location of the Schwalbenberg section is close to the river plain and the confluence of rivers Rhine and Ahr, it is very likely that a great part of the sediment is of local origin, hence has undergone a near-distance aeolian transport. This fact would again result in age overestimation of the sediments owing to insufficient bleaching, which was shown for TL age estimates. However, we believe that insufficient bleaching owing to short-distance transport very likely is a minor problem for the sediments under investigation.

The second unit (3.2–6.8 m), including the Lower and Upper Remagen-Subformation, R1–R5, gives deposition ages around 40 ka by means of litho-pedostratigrapy and chronology. This part of the sequence correlates to the Middle Weichselian Pleniglacial (MIS 3). An age increase with depth is not determined, indicating a relatively fast deposition for the exposed 3.60 m of sediments. The existence of five fossil brown cambisols (R1–R5) within this unit let us expect a more extended amount of time than the 1-sigma standard deviation of the dating method, which is about ±10% and thus equals about 8 ka for this unit. These ages of the Remagen Soils are in the range of the lower Middle Weichselian weak brown soil at section Toenchesberg (Boenigk & Frechen 1999).

The third unit including the three Sinzig Soils or Sinzig-Subformation (Schirmer 2011) between 6.80 and 10.30 m gives IRSL ages between about 35 and 25 ka. The fading-corrected post-IR IRSL age estimates are about 30 ka. An age increase with depth is within the 1-sigma standard deviation indicating a high dust accumulation rate. The Sinzig pedocomplex correlates with the late Middle Weichselian. Zöller et al. (1991) reported two TL age estimates from a profile located in the vicinity of the section under study. These two TL age estimates are in good agreement with radiocarbon ages and are within the error in agreement with the results of this study. Finds of Middle to Upper Palaeolithic artifacts, which are contemporaneous with the Aurignacien or Gravettien (App et al. 1987), were investigated from a palaeosol near the Schwalbenberg II section.

The stratigraphically youngermost unit between 10.30 and 13.20 m gives IRSL and TL age estimates between about 25 and 18 ka. The fading-corrected post-IR IRSL at 225°C gives deposition ages of about 25 ka making a correlation with the Upper Weichselian most likely. The dust accumulation was most likely very high as no age increase with depth was found for this uppermost unit. The mass ("dust")

accumulation rates gave high values (Frechen et al. 2003) for the area of interest, at least for the Upper Pleniglacial and Late Glacial period.

The Upper Weichselian record is not complete, most likely owing to the morphological position close to the steep cut of the river Rhine. A more complete record for the Upper Pleniglacial was previously described from the right site of the Rhine valley near to the village of Ockenfels (Preusser & Frechen 1999), where several tundra gleysols, a brown arctic meadow and the Eltville Tephra are intercalated in the Upper Weichselian loess.

Conclusion

The multiple aliquot protocol based IRSL and TL data and those of the single aliquot regenerative protocol based post-IR IRSL at 225°C and fading-corrected IR at 50°C show that the fading-rate is small for the loess and loess derivatives from the Schwalbenberg II section. The age difference is within the error, the 1-sigma standard deviation, for most of the samples. Our results are in agreement with those of Schmidt et al. (2011) for the Tönchesberg section situated in the East Eifel Volcanic Field. From a stratigraphical point of view, there is disagreement between the litho-pedostratographical and the chronological approach for the stratigraphically oldest unit. the latter one is designated to correlate to MIS 4 by means of litho-pedostratigraphy but gives deposition ages between 55 and 45 ka. For the three stratigraphically younger units Middle and Upper Weichselian deposition ages were determined, which is in agreement with the litho-pedostratigraphical approach.

Acknowledgement

MF appreciates the methodological support and input of Dr. Sumiko Tsukamoto (LIAG) and for providing and explaining the post-IR IRSL data, furthermore for constructive comments of a previous version of the manuscript. We thank an anomymous reviewer for the constructive comments of the manuscript done within 36 hours!

References

Boenigk, W. & Frechen, M. (2001): The loess record at sections Koblenz-Metternich and Tönchesberg in the Middle Rhine area. – Quaternary International, 76/77: 201–209.

Buylaert, J. P., Murray, A. S., Thomsen, K. J. & Jain, M., (2009): Testing the potential of an elevated temperature IRSL signal from K-feldspar. Radiation Measurements, 44, 560–565.

Frechen, M. (1992): Systematic thermoluminescence dating of two loess profiles from the Middle Rhine Area (F.R.G.). Quaternary Science Reviews, 11, 93–101.

Frechen, M. (1994): Thermolumineszenz-Datierungen an Lössen des Tönchesberges aus der Osteifel.- Eiszeitalter und Gegenwart, 44: 79–93; Hannover.

Frechen, M., Boenigk, W. & Weidenfeller, M. (1995): Chronostratigraphie des „Eiszeitlichen Lößprofils" in Koblenz-Metternich. – Mainzer Geowissenschaftliche Mitteilungen, 24: 155–180; Mainz.

Frechen, M., Oches, E.A. & Kohfeld, K.E. (2003): Loess in Europe – mass accumulation rates during the Last Glacial Period. Quaternary Science Reviews, 22, 1835–1857.

Frechen, M., Schweitzer, U. & Zander, A. (1996). Improvements in sample preparation for the fine grain technique. Ancient TL, 14, 15–17.

Huntley, D.J. & Lamothe, M. (2001). Ubiquity of anomalous fading in K-feldspars, and the measurement and correction for it in optical dating. Canadian Journal of Earth Sciences, 38, 1093–1106.

Murray, A. S. & Wintle, A. G. (2000): Luminescence dating of quartz using an improved single-aliquot regenerative-dose protocol. Radiation Measurements, 32, 57–73.

Preusser, F. & Frechen, M. (1999): Ockenfels. – In: Becker-Haumann, R. & Frechen, M. (eds.): Terrestrische Quartärgeologie – Festschrift Wolfgang Boenigk. Verlag Sven-von-Loga, Köln.

Preusser, F., Degering, D., Fuchs, M., Hilgers, A., Kadereit, A., Klasen, N., Krbetschek, M., Richter, D. & Spencer, J. (2008): Luminescence dating: basics methods and application. Quaternary Science Journal (EuG) 57, 95–149.

Schirmer, W. (1990): Schwalbenberg südlich Remagen. – In: Schirmer, W. (ed.): Rheingeschichte zwischen Mosel und Maas. Deuqua-Führer, 1: 105–108; Hannover.

Schirmer, W. (1991): Würmzeitliche Paläoböden am Mittelrhein. – 10. Tagung des Arbeitskreises „Paläoböden" der Deutschen Bodenkundlichen Gesellschaft vom 30.05.–1.6.1991 in Bonn, Programm und Exkursionsführer: 70–83; Münster.

Schirmer, W. (1995), with contrib. by H. Berendsen, R. Bersezio, A. Bini, F. Bittmann, G. Crosta, W. De Gans, T. de Groot, D. Ellwanger, H. Graf, A. Ikinger, O. Keller, U. Schirmer, M. W. van den Berg, G. Waldmann, L. Wick: Rhein Traverse. – In: Schirmer, W. [ed.]: Quaternary field trips in Central Europe, 1: 475–558; München (Pfeil).

Schirmer, W. (2000a): Rhein loess, ice cores and deep-sea cores during MIS 2–5. – Zeitschrift der Deutschen Geologischen Gesellschaft, 151 (3): 309–332; Stuttgart.

Schirmer, W. (2000b): Eine Klimakurve des Oberpleistozäns aus dem rheinischen Löss. – Eiszeitalter und Gegenwart, 50: 25–49; Hannover.

Schirmer, W. (2002): Compendium of the Rhein loess sequence. – In: Ikinger, A. & Schirmer, W. [eds.]: Loess units and solcomplexes in the Niederrhein and Maas area. – Terra Nostra, 2002 (1): 8–23, 102–104; Berlin.

Schirmer, W. (2010): Interglacial complex and solcomplex. – Central European Journal of Geosciences, 2 (1): 32–40. DOI: 10.2478/v10085-009-0038-z

Schirmer, W. (2011): Rhine loess at Schwalbenberg II – MIS 4 and 3. – Eiszeitalter und Gegenwart, 60 (1) (this volume).

Schmidt, E., Frechen, M., Murray, A.S., Tsukamoto, S. & Bittmann, F. (2011): Luminescence chronology of the loess from the Toenchesberg section – a comparison of using quartz and feldspar as dosimeter to extend the age range beyond the Eemian. – Quaternary International, 234 (1–2): 10–22.

Spooner, N.A., (1994): The anomalous fading of infrared-stimulated luminescence from feldspars. Radiation Measurements 23, 625–632.

Thiel, C., Buylaert, J.P., Murray, A., Terhorst, B., Hofer, I., Tsukamoto, S. & Frechen, M. (2011a): Luminescence dating of the Stratzing loess profile (Austria) – Testing the potential of an enhanced elevated temperature post-IR IRSL protocol. – Quaternary International, 234 (1–2): 23–31.

Thiel, C., Buylaert, J.-P., Murray, A.S., Terhorst, B., Tsukamoto, S. & Frechen, M., (2011b): Investigating the chronostratigraphy of prominent palaeosols in Lower Austria using post-IR IRSL dating. – Quaternary Science Journal, 60 (1).

Thomsen, K. J., Murray, A. S., Jain, M. & Bøtter-Jensen, L. (2008): Laboratory fading rates of various luminescence signals from feldspar-rich sediment extracts. Radiation measurements, 43, 1474–1486.

Wallinga, J., MurrayA.S. & Wintle, A.G. (2000): The single-aliquot regenerative-dose (SAR) protocol applied to coarse-grain feldspar. Radiation Measurements, 32: 529–533.

Wintle, A.G. (1973): Anomalous fading of thermoluminescence in mineral samples. Nature, 245, 143–144.

Zöller, L., Conard, N.J. & Hahn, J. (1991): Thermoluminescence dating of Middle Palaeolithic open air sites in the Middle Rhine Valley/Germany. – Naturwissenschaften, 78: 408–410.

E&G Quaternary Science Journal
Volume 60 / Number 1 / 2011 / 90–104 / DOI 10.3285/eg.60.1.06
www.quaternary-science.net

GEOZON SCIENCE MEDIA
ISSN 0424-7116

The potential for dust detection by means of µXRF scanning in Eifel maar lake sediments

Stephan Dietrich, Frank Sirocko

Abstract: Data for the annual variability of aeolian sediments is obtained from continuous and high resolution µXRF geochemistry within maar lake sediments from the last 60 kyrs. Two sediment cores from Eifel maar lakes and dry maars (Germany) were analyzed, which covering the glacial inception of MIS-3, LGM and MIS-2, transition I as well as the Holocene. The energy dispersive XRF scanning is obtained on resin impregnated blocks of the sediment, which are the basis for the production of petrographic thin section. Thus, the measurement results can directly be compared with micro facies analysis. Quantification of the Eagle III µXRF carried out on one sediment core, using the standard free fundamental parameter method, shows that this quantification method gives suitable results by comparison with WD-XRF analysis of discrete samples. Each single maar differs in lithological composition, which is reflected in the geochemistry, too. The major processes of element deposition in lakes are therefore described, i.e. the different sedimentation and weathering processes as well as the circulation of the water body of the lake. Following on from this, it is shown that it is possible to derive an aeolian sediment signal by using principle component analysis of standardized variables. Because further knowledge about the lithology and environmental background is available (from the petrographic thin sections) it can be demonstrated that this principle component analysis approach gives reliable results for all the time slices investigated. The most prominent element for describing dust in both investigated cores Ca, which reaches highest values (>5 wt.-%) during glacial conditions and which have major influence on the dust factor obtained by principal component analysis. In combination with grayscale values both the Ca content and the dust factor serve to, calculated by principal component analysis, the serves to record aeolian dust in laminated lake sediments. In both cores periods with major dust events could be detected by µXRF geochemistry: during MIS-3 the largest Heinrich event H4 and the onset of dust increase coupled to the glacial inception of the Pleni-Weichselian, further on the whole MIS-2 including LGM and YD as well as enhanced dust supply forced by human activities since the Subboreal.

(Möglichkeiten der Detektion äolischen Staubs mittels µXRF-Scannen von Maarseesedimenten aus der Eifel)

Kurzfassung: Mittels kontinuierlicher und hochauflösender µXRF-Geochemieanalysen wird die Variabilität äolischer Sedimente der letzten 60.000 Jahre rekonstruiert. Dazu werden zwei Sedimentbohrkerne jeweils aus einem Maarsee und einem Trockenenmaar (Eifel, Deutschland) untersucht. Beide Kerne umfassen das letzte Glazial, einschließlich des MIS-3, des LGM und MIS-2, Transition I als auch das Holozän. Die energiedispersive RFA-Messungen der Eagle III µXRF wird direkt an Harz imprägnierten Proben angewendet. Diese sogenannten Tränklinge bilden die Grundlage für die Herstellung von petrographischen Dünnschliffen und somit können die Messergebnisse direkt mit einer Mikrofaziesanalyse verglichen werden. Anhand eines Sedimentkerns wird gezeigt, dass eine Quantifizierung der µXRF-Ergebnisse mittels der Fundamentalparametermethode geeignete ist. Eine Überprüfung der Ergebnisse findet dabei mit wellenlängen-dispersiven RFA-Messungen an diskreten Proben statt. Die Ergebnisse zeigen, dass sich jedes einzelne Maar in der lithologischen Zusammensetzung und damit auch geochemisch unterscheidet. Deshalb wird auf die grundlegenden Prozesse der Elementdeposition in die Seen eingegangen, die mit der Ablagerung von Sedimenten, der Variabilität der chemischen Verwitterung oder der Wasserzirkulation in Zusammenhang stehen. Mittels Hauptkomponentenanalysen standardisierter Variablen ist darüber hinaus die objektive Ableitung eines äolischen Sedimentsignals möglich. Es wird gezeigt, dass dieser Ansatz verlässliche Ergebnisse für alle untersuchten Zeitabschnitte liefert, solange für die Interpretation weitere Kenntnisse über die Lithologie und Paläoökologie zur Verfügung stehen. Das auffälligste Element zur Charakterisierung von Staub ist in beiden untersuchten Kernen Kalzium. Die höchsten Werte (>5 Gew.-%) werden während vollglazialer Bedingungen erreicht. Kalzium hat einen wesentlichen Einfluss auf den Staubfaktor der Hauptkomponentenanalyse. Eine zusätzliche Kombination der Kalziumgehalte mit dem Staubfaktor der Hauptkomponentenanalyse sowie Grauwertmessungen verbessert den Nachweis äolischen Staubs in laminierten Seesedimenten zusätzlich. In beiden Kernen konnten Sedimente mit erhöhten Staubkonzentrationen geochemisch nachgewiesen werden: Während des MIS-3 sind das vor allem das größte Heinrich-Ereignis H4 sowie der Anstieg des atmosphärischen Staubgehalts während der Wiedervereisung der Inlandsgletscher. Weiterhin ist das gesamte MIS-2 einschließlich LGM und der Jüngeren Dryas von starker Staubdeposition charakterisiert. Eine erhöhte Staubkonzentration ist ebenfalls ab dem Subboreal nachgewiesen und wird als anthropogene Aktivität gedeutet.

Keywords: *µXFR, geochemistry, lacustrine sediment, aeolian sediment, last glacial cycle, PCA*

Addresses of authors: S. Dietrich, F. Sirocko, Institute for Geosciences, University of Mainz, Becherweg 21, D-55099 Mainz, Germany. Tel.: +49 (6131) 39-23834, +49(6131)-39 22714, Fax: +49 (6131) 39-24769, E-Mail: sdietrich@uni-mainz.de, E-Mail: sirocko@uni-mainz.de.

1 Introduction

The investigation of long continuous aeolian sediment records, such as loess profiles or dunes are widely used to reconstruct the environmental and climate variability. Long records cover several glacial cycles and are primarily known from the large loess plains in Asia or from the Carpathian basin. Profiles with the possibility to archive annual resolution are less common. The West-Eifel Volcanic Field (WEVF), Germany, provides such records in maar lakes. Without a fluvial inlet, these lakes are perfect sediment traps for aeolian deposits (Dietrich & Sirocko 2009, Pfahl et al. 2009).

E&G / Vol. 60 / No. 1 / 2011 / 90–104 / DOI 10.3285/eg.60.1.06

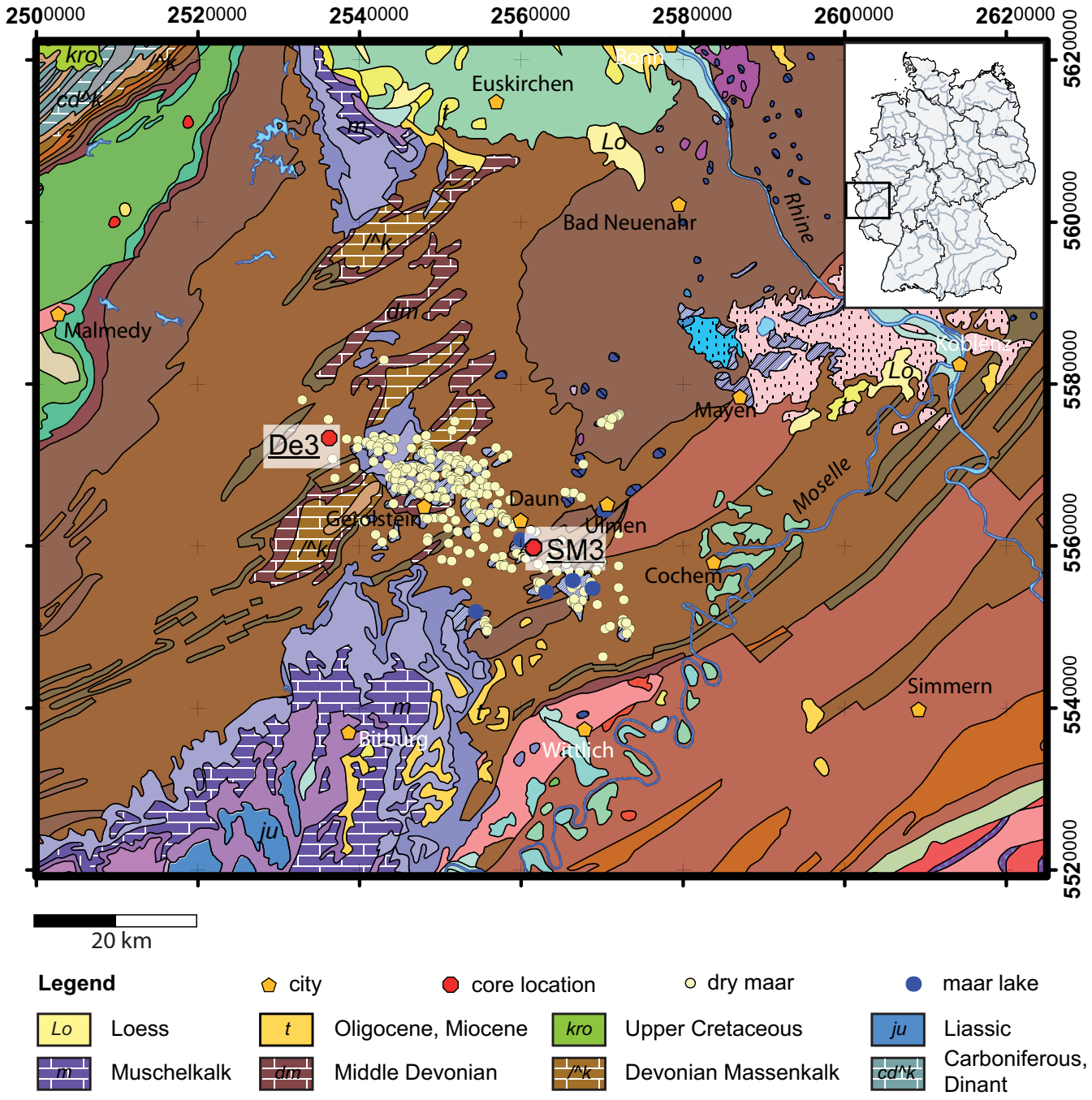

Fig. 1: Geological sketch map of the Eifel region and position of the cores SM3 (maar lake Schalkenmehren) and DE3 (Dehner dry maar). The map is based on the Geological Map of Germany (BGR, 1993), locations of dry maars after Büchel (1994).

Abb. 1: Geologische Übersichtskarte der Eifel mit den Positionen der beiden Bohrkerne SM3 (Schalkenmehrener Maar) und DE3 (Dehner Trockenmaar). Die Karte basiert auf der Geologischen Übersichtskarte von Deutschland (1:1 000 000; BGR, 1993), Lokationen der Trockenmaare nach Büchel (1994).

Furthermore, although the sediments do not show annual lamination, they are stratified by event layers due to anoxic conditions at the lake bottom (Zolitschka et al. 2000, Sirocko et al. 2005).

The detection of aeolian deposits in lake sediments is possible by using different approaches like micro facies analysis, measuring the minerogenous component of the bulk sediment (e.g. Zolitschka 1998), magnetic susceptibility (e.g. Yancheva et al. 2007) or grain size analysis (e.g. Seelos et al. 2009, Sun et al. 2002). However, in this study a geochemical scanning approach is applied to measure aeolian deposits. High resolution geochemical analysis of lacustrine sediments offers a reliable method for investigation of environmental changes in the past (Boyle 2001, Boyle 2000, Engstrom & Wright 1984, Melles et al. 2007). The potential of X-Ray fluorescence (XRF) core scanning is based on the rapid and non-destructive acquisition of high-resolution geochemical data from lacustrine sediment cores. This facilitates new approaches to many applications in paleolimnology, including pollution detection, varve counting, and estimation of past ecosystem productivity (Francus et al. 2009). The µXRF scanner acquires bulk-sediment chemical data with sufficient accuracy for major elements (Boyle 2000). Although elemental intensities are predominantly proportional to concentration, they are also influenced by the energy level of the

X-ray source, the count time, and the physical properties of the sediment, such as the poorly constrained measurement geometry attributable to inhomogeneity of the specimens (e.g. variable water content and grain-size distribution), and irregularities of the sample surface (Weltje & Tjallingii 2008, Rothwell et al. 2006). Nevertheless, the XRF methodology is a widely accepted, semi-quantitative core logging method that provides records of changing element intensities expressed in "total counts", reflecting the geochemical composition of the sediments. Quantitative analysis is made more difficult by matrix effects especially for light elements such as Al and Si (Böning et al. 2007). Reasons include the pore volume of interstadial water or resin or the roughness of the sediment surface. However, a recent approach to calibration of XRF core scanners for quantitative geochemical logging is applied by Weltje & Tjallingii (2008) or Kido et al. (2006). Beside the direct measurement of the core surface via core loggers the analysis of resin impregnated samples (RIS) is demonstrated in a growing number of studies. The single 10 cm long RIS are taken continuously down core. The pore volume of the sediment is substituted by resin during the production of the RIS. These geochemical data can be directly assigned to micro-facies data because XRF scanning has been carried out on the same impregnated sediment blocks from which thin sections can be prepared. High resolution applications are shown by different studies for example by Sorrel et al. (2007) or Brauer et al. (2008). The latter authors have applied a geo-chemical major element micro-X-ray fluorescence scanner at 50 µm resolution providing geochemical information for individual seasonal layers (5–8 data points/varve for the Allerød; 20–30 data points/varve for Younger Dryas) to investigate the structure and seasonal composition of varves. The first successful implementation of XRF techniques for the provenance analysis of dust is shown by Neff et al. (2008).

The objective of the work is to separate of different lithofacies, especially the aeolian input into the lake environment, by means of µXRF geochemistry and to test if µXRF data are not only a general paleoclimate signal but can be used to quantify the aeolian fraction directly to achieve dust records with annual resolution. In this study, we demonstrate how aeolian sediment within maar lake sediments might be classified by certain elements and new factors, calculated by principal component analysis (PCA).

2 Material and Methods

2.1 Cores and drilling locations

The west Eifel volcanic field (Germany) is characterized by more than 70 maar lakes and dry maar lakes (Büchel 1994). Two sediment cores, namely SM3 (N50°10'11.6", E6°51'31"), from lake Schalkenmehren and DE3 (N50°17'35.5", E6°30'22.7", 88 m depth) from the Dehner dry maar (Dehner Trockenmaar) were drilled in a maar lake and a dry maar, respectively (Fig.1). On the Eastern side of lake Schalkenmehrener Maar an older dry maar is located which is connected to the lake by a marsh. Earlier fluvial input into the maar lake from this extended catchment could be proved until the Medieval Times (Straka 1975). The rim of the Dehner dry maar exhibits a pronounced roundness and shows no ancient fluvial inflow but does have an outflow to the Northwest. The core SM3 from lake Schalkenmehrener Maar was drilled using a swimming platform and a piston corer (UWITEC, Austria), DE3 was drilled with the 'Seilkernverfahren'. These two cores from the ELSA repository (Eifel Laminated Sediment Archive) cover together the main periods with major climate changes of the last 60 kyrs, including the marine isotope stages MIS-3 and MIS-2 (DE3), and transition I as well as (anthropogenic) dust events during the Holocene (SM3). In total 82 meters of sediment cores with an average sedimentation rate of 1.5±0.5 mm/yr are analyzed. The sediments consist of detrital bearing sediment that documents weather extremes (flash floods and aeolian dust) or gyttja, containing a high amount of organic matter that documents past water conditions (temperature, nutrient content, pH), which are recorded in the remains of plants and animals that lived in the lake.

2.2 Chronology and lithology

The stratigraphy for both cores is published in Sirocko (Ed. 2009). The core SM3 spans the Holocene and the core DE3 from the Dehner dry maar covers the time span from MIS 4 to the eruption of Lake Laach (Laacher See). In DE3 a piece of spruce could be dated by radiocarbon to 45.8 +1.2 -1.04 kyrs BP at 55.56 m depth. Between these time marks are four stadial-interstadial sequences shown by high organic matter and therefore dark brownish color (Fig. 2). The tephra of the eruption of lake Laach (the Lacher See Tephra, LST, at 12.9 kyrs BP, van den Bogaard 1995, Wörner & Schmincke 1984) is identified geochemically (Veres, pers. comm.) in the core, SM3 at 6.5 m and in DE3 at 3.4 m depth. Thus, the LST is used as a tie point to merge both cores to a stack, which covers the last 60 kyrs.

Core DE3 (Fig. 2) shows significant changes in environmental and climatic conditions in its sediments and oscillates between warm and organic-rich and dust-rich glacial conditions. Starting at the bottom sequence of the core, dark brown gyttja is dominant and implicates an interstadial character between 70 and 50 m. At 43 to 41 m depth single but rather strong dust events had been deposited and the sediment has a brighter color until 40.50–38.90 m where dark, organic-rich matter recurs. Volcanic ashes from Eifel volcanism, mostly with unknown certain origin, cumulates between 80–78 m, and between 51–37 m. In the core meter 36 a slide is recorded as a decimeter large fold. The following ten meters are dominated by light brown gyttja with increasing dust influence. The content of aeolian sediment reaches the highest level at 26 m and keeps stable until 10 m depth. The next eight meters dust is decreasing and at 8 m the first grass pollen appears (Sirocko ed. 2009). Between 7 and 2.8 m the content on organic matter is increasing, whereas the uppermost core sequence is characterized by debris flow/solifluction debris. The core SM3 (Fig. 3) is fine laminated in the uppermost 6 meters with an high amount of organic gyttja between 3–5 m. From 6.5 m down core, the sediment changes significantly to loess gyttja with a bright grey color, showing a strong influence of aeolian sediments during this period.

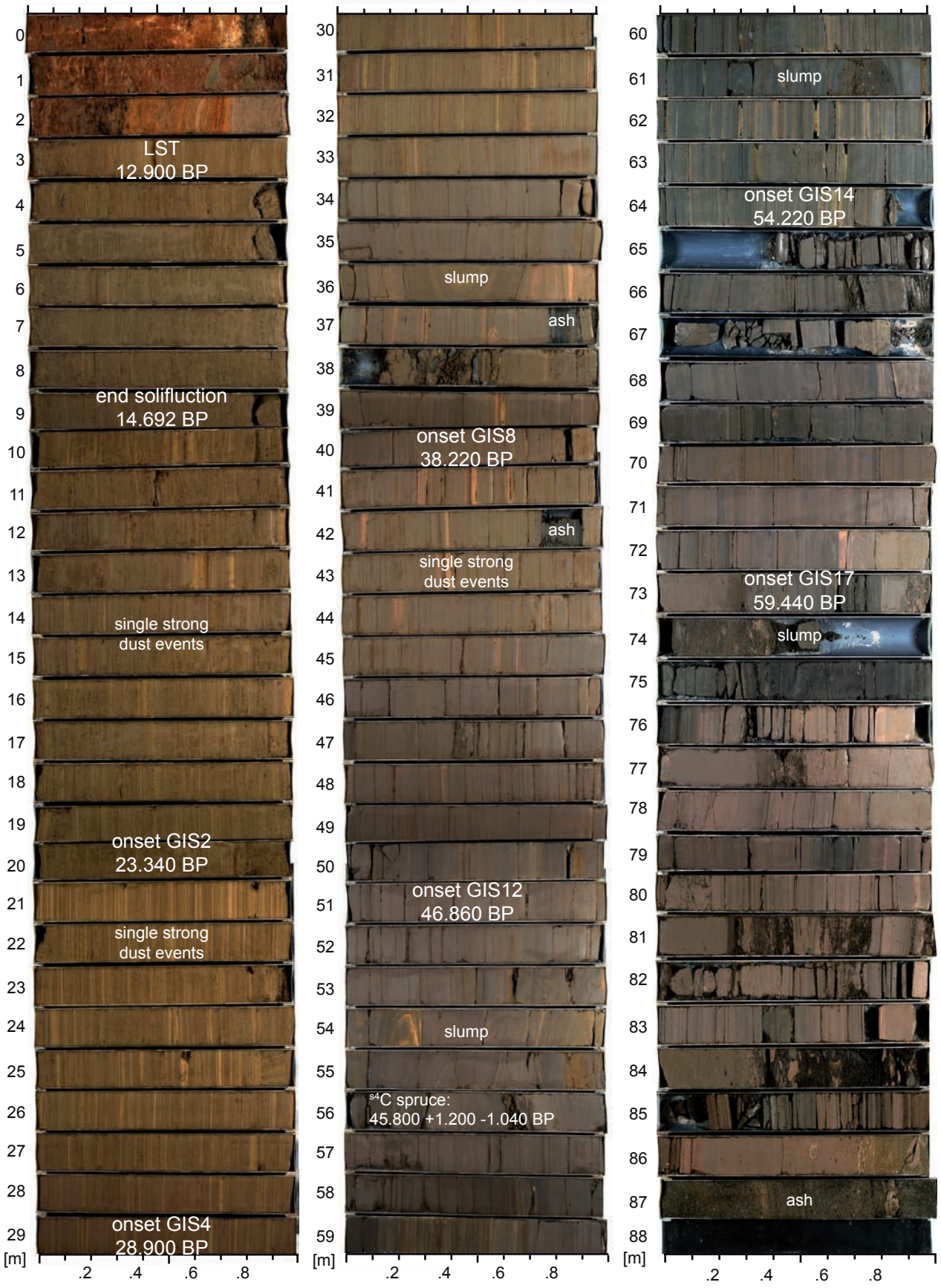

Fig. 2: Core photography and time marks (tuned to the Greenland ice core GICC05 stratigraphy (Svensson et al. 2008) of the core DE3. The ash of the LST is clearly visible at 3.5 m depth. The core sections between 35 and 10 m is dominated by single strong dust events (Seelos et al. 2009; Dietrich & Seelos 2010) and represent the time of the Middle Weichselian. Modified after Sirocko (Ed. 2009).

Abb. 2: Kernfotografie und Altersmarken des Sedimentkerns DE3. Das Altersmodell basiert auf 14C-Datierungen, Tephrochronologie und ist mit der GICC05-Stratigrafie der Grönländischen Eiskerne abgestimmt (Svensson et al. 2008). Die Laacher-See-Tephra (LST) ist in 3,5 m Tiefe deutlich erkennbar. Die Kernsequenz zwischen 35 und 10 m wird durch äolischen Staub dominiert (Seelos et al. 2009; Dietrich & Seelos 2010) und repräsentiert den Zeitraum der Weichsel-Vereisung. Überarbeitet nach Sirocko (Ed. 2009).

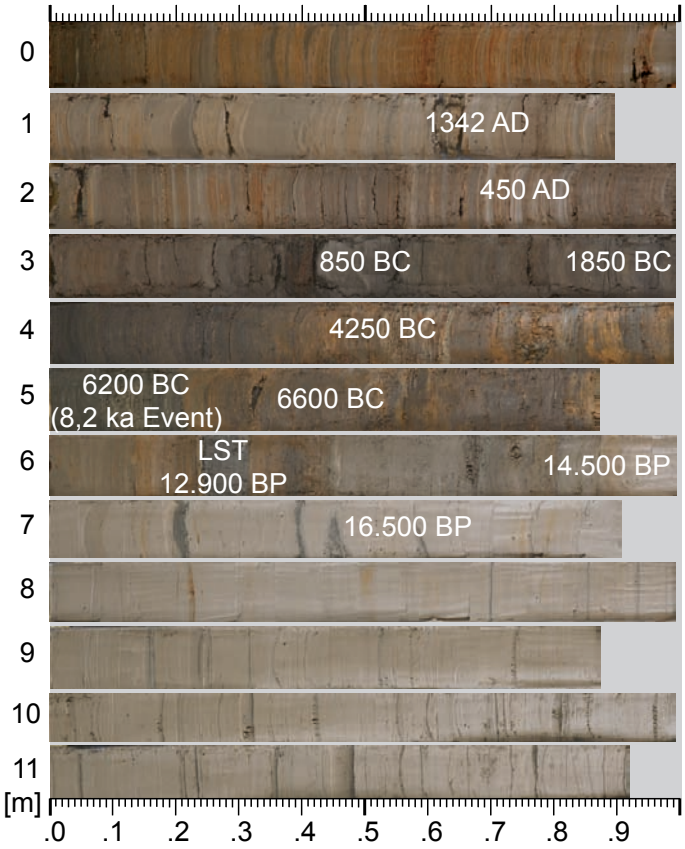

Fig. 3: Core photography and time marks of the core SM3. The ash of the LST is clearly visible (6.3 m depth). The deeper core sequence is dominated by bright colored aeolian sediment of the late Weichselian.

Abb. 3: Kernfotografie und Altersmarken des Sedimentkerns SM3. Die LST ist in 6,3 m Tiefe deutlich zu sehen. Die untere Kernsequenz ist durch die hellen äolischen Sedimente der späten Weichselkaltzeit gekennzeichnet.

2.3 Evaluation of chemical data

The three core sections were scanned for selected elements at 1 mm resolution using the energy dispersive X-ray fluorescence scanner Eagle III (Röntgenanalytik Meßtechnik GmbH, Germany) of the University of Mainz (Germany). The µXRF was used to measure major elements (e.g., Mg, Al, Si, P, S, K, Ca, Ti, Mn, and Fe) as well as trace elements (Sr, Zr, Cr, Ni, Cu, and Zn) on 10 cm long resin impregnated samples. Na is too light for detection via the Eagle III and is therefore not included in this study. The Araldite(R) impregnated blocks are a spin-off from to the production of thin sections (Dietrich & Sirocko 2009). Thus, the geochemical results can be directly interpreted in context with micro facies analysis. The µXRF scanner acquires bulk-sediment chemical data from these samples. Scans of pure Araldite indicate zero counts of the investigated element and thus do not bias the results. Although elemental intensities are dominantly proportional to concentration, they are also influenced by the energy level of the X-ray source, the count time, and the physical properties of the sediment (Röhl & Abrams 2000). The data were collected every 1 mm down-core with a 300 µm spot size of the X-ray beam. The generator setting was of 30 kV and 500 µA with a sampling time of 16 seconds and a mean death time of 30 µs. The sample chamber is evacuated during measurement, thus light elements like Si and Al are also stimulated. The emitted fluorescence radiation is detected by an energy dispersive Si(Li)-detector with an area of 30 mm^2 and an energy resolution of 135 eV at maximum.

Discrete reference samples are taken from core DE3 and glass beads with a five times dilution are measured by a Philips MagiXPRO via WD-XRF method (Rh-anode, 3.2 KW). The quantification is based on international standards (Govindaraju 1989). This study also examines whether a quantification of the Eagle III µXRF using the standard free fundamental parameter method is suitable. The alternative is using the intensities as relative results in combination with quantified but independent measurements by WD-XRF methodology.

2.4 Statistical processing of the data

Core sequences with reworked material were removed from the original data set. High amounts of resin (e.g. cracks caused by sample preparation) were detected by a locally low sum of measured intensities and are subsequently removed. Therefore a threshold of 500 cps was evaluated empirically.

A principal component analysis (PCA) was performed to detect different lithological facies, such as dust, by using inorganic geochemical data. The PCA was used to objectively describe the differences and similarities between the elements and to reduce the number of variables by showing the main variance of the data set by only a few factors. The factor loadings give the correlation between the newly found factor and the respective element. The higher the influence of an element for the factor, the higher is the factor loading. For all cores the following steps were performed before applying the PCA: (a) Using all measured values at 1 mm resolution results in a total sample amount of several thousands. Hence, data are resampled after smoothing using a Gaussian kernel filter with a 20 point window size to give a sample amount less than 1000. (b) Most of the parameters exhibited a pronounced skewness. PCA as well as Pearson correlation give unbiased results only for Gaussian distribution, which would be especially crucial for small data sets. However, the data were log transformed and z-normalized to zero mean and unit standard derivation for each parameter separately in order to weight equally the different parameters in the multivariate analysis. (c) Subsequently, outliers were removed by deleting values greater/less than mean plus/minus three time standard derivation of each measured element (includes 99.7% of all normal distributed values). The amount of significant and nontrivial new variables is measured using the scree test. Sulfur is not considered in the PCA since it correlates less well to the reference values and did not change the major findings of the PCA. However, S is known to be precipitated as pyrite and is thus a proxy for anoxic conditions of the bottom water. The concentration of an element in the lake sediment depends on the amount of influx and the degree of preservation of this element (Engstrom & Wright 1984). Thus, the new calculated variables (principal component factors) are controlled by the same mechanisms of influx and preservation. For all numerical analysis MATLAB (TheMathworks, version 2009b) were used.

E&G / Vol. 60 / No. 1 / 2011 / 90–104 / DOI 10.3285/eg.60.1.06

3 Results

3.1 Calibration of µXRF results

The results of the µXRF scanning are presented as intensities (counts per second, cps). Since core DE3 is one of the most important cores of ELSA, discrete (and destructive) sample analysis using the WD-XRF is obtained to evaluate the intensity values given by the ED-XRF scanner with certain element concentrations (Tab. 1). For most elements (Al, Ti, Fe, Mn, Mg, Ca, Zr) good correlation ($R2 > 0.75$) can be observed between the intensities counted by the Eagle III µXRF and the corresponding measured concentrations (Tab. 2). The correlation was also checked for the standard-free quantification (fundamental parameter method) for weight percentages and atomic percentages. While the main elements fit quite well, Zr is the only trace element which shows an acceptable correlation between the measurements by WD-XRF and the intensities but does not have a significant correlation with the quantified results. However, Si matches better with the calculated weight percentages than with the intensity. The elements Cr, Ni, Cu, and Zn which show only weak correlation with the WD-XRF results are not further considered in this study. In the following the intensities are represented for the core SM3 and for DE3 weight% are shown because of good correlation between the ED- and WD-XRF results.

3.2 The elemental stratification

The comparison of the geochemical stratification (Fig. 4, 5) with the lithology of each single core leads to the suggestion, that Ca, Si and, K are the most prominent elements for the classification of aeolian sediments.

Core DE3 covers a time period from MIS3–MIS2, including the glacial inception of the late Weichselian ice sheets. However, single but severe dust events can be found between 43–41 m depth, which corresponds to the marine H4 event (Hemming 2004), and beginning at 36 m the content of aeolian sediment is increasing, culminating in the last glacial maximum (LGM). Best correspondence with the lithological stratification can be found with the Si, Ca, and Zr. The stratification of the elements Si, Al, and Ti differ in the core DE3 (Fig. 4a, b). Si shows an overall increasing trend over the whole core section (from bottom to top), starting from around 60 wt.-% up to 70 wt.-%. The core section from 5–25 m has the highest content of Si with a slight increase between 15–25 m, while content in the core sections from 36–38 m and 58–60 m are decreases in relation to the overall trend and corresponding to an increase of organic matter in the sediment. In the core DE3 Ca is obviously enriched (CaO content around 5 wt.-%) in the upper section, with a depression between 10 and 20 m depth. Lower down core the content is around 1 wt.-% and reaches only higher values at 39 m, between 41–45 m, and in places between 59–68 m. The strong shift at 33 m depth from low to high amounts of Ca and Zr coincides with the last glacial ice advance of the late Weichselian, when the climate became colder and dryer and thus deflation processes became more frequent. Al and Ti are anti-correlated relating to Si and Mg and K are anti-correlated to Ca, showing a strong decrease between 33 and 25 m. Thus, these elements do not reflect a signal of allogenic aeolian input. Higher amounts of Al (around 15 wt.-%) correspond with the increase of gyttja and thus with an increase of chemical weathering due to more precipitation.

In the Holocene core SM3, the elements Si, Ti, Al, K and Ca are the most prominent ones to characterize loess gyttja and dust bearing sediment. Si, Al and Ti show corresponding stratigraphic patterns over the whole core (Fig. 5). Highest intensities of these elements are significant for the uppermost core meter and the core section 6.3–12.0 m. The latter is characterized by quite stable intensities of these geogenic elements, corresponding with loess gyttja. SM3 is characterized by a highly correlated stratification of Mg and K, corresponding to the signal of Ti and Al. Ca shows significant peaks. In core SM3 certain amounts of Ca are in the layer 5–5.5 m and 6.3–7 m depth. The sections 1–2 m and 7.5–10 m are also enriched in Ca. Al, Ti and Mg reaches the highest level in the uppermost meters. Si, K and Ca are enriched in the deepest part of the core and coincide with the highest dust occurrence of the core. In the core SM3 Zr shows a correlating trend to Si, Al and Ti, with maximum values around 2 m depth and from 6.5 m on down core. Sr peaks correspond to the major Ca peaks at 5 m and at 6.3 m. The latter peak represents the volcanic ash of the LST and shows strongly elevated values of the major geogenic elements, too.

In both cores the elements Fe, Mn, S and P match to core sections with higher amounts of organic matter and reflect environmental conditions with changing oxygenation of the bottom water or changes of the redox potential at the lake bottom. Over wide parts Fe and P correspond to the Al signal. S is mostly anticorrelated to these elements. This accords with vivianite concretions which are found in the core DE3 between 40 and 70 m depth. The mineral vivianite, $(Fe)_3(PO_4)_2{}^*8H_2O$, might be precipitated in absence of sulphur which would produce pyrite. In DE3 Fe, Mn and P have decreasing trends from the bottom to the top. Fe and Mn have corresponding trends, too. The Fe_2O_3(total) content increases from 10–5 wt.-% with an extraordinarily high value of nearly 20 wt.-% at 60 m depth. The MnO content is low and reaches a maximum of 1 wt.-% in 60 m, too. The highest values of S can be found at the same core sequence from 59 to 64 m depth. In this section the lost of ignition (LOI) is doubled from around 8 wt.-% to nearly 18 wt.-% (Tab. 1a). This section corresponds to the Greenland interstadial GIS-14, which is suggested to be the warmest interstadial of the last glacial cycle. The lowest levels of Fe and Mn are between 32 m depth until the top. A dip in their content is found between 40–46 m. Simultaneously Ca, Zr and S are enriched. In SM3 the elements Fe, Mn, P and S stratify the core from bottom to top into four parts and especially S is anti-correlated to the geogenic elements: (1) the deepest section (up to 7 m depth) is quite stable and shows only low counts of these elements. (2) Strong increase of S with decreasing Fe values and stable counts of Mn and P follows from 6.5–5.2 m. (3) In the sequence from 5.2 to 2.2 m all these elements correlate with each other and S shows its maximum values. Indeed, this is the section with the highest amount of organics in the core SM3. (4) In the uppermost section Fe, Mn and P correlate, and S is nearly anticorrelated to the other elements.

Tab. 1: WD-XRF results from the core DE3 from the Dehner dry maar, including main elements (upper panel) and trace elements (lower panel).
Tab. 1: WD-XRF-Ergebnisse des Kerns DE3 aus dem Dehner Trockenmaar inklusive Hauptelemente (obere Tafel) und Spurenelemente (untere Tafel).

Tiefe [m]	LOI [wt%]	SiO_2 [wt%]	TiO_2 [wt%]	Al_2O_3 [wt%]	Fe_2O_3(t) [wt%]	MnO [wt%]	MgO [wt%]	CaO [wt%]	Na_2O [wt%]	K_2O [wt%]	P_2O_5 [wt%]	SO_3 [wt%]	Sum [%]
4.50	7.05	74.28	0.95	10.59	4.41	0.09	1.54	4.26	0.68	2.39	0.12	0.404	99.7
6.49	7.68	73.93	0.96	10.87	4.45	0.07	1.56	4.96	0.66	2.43	0.11	0.472	100.5
8.70	7.45	73.58	1.02	11.39	4.81	0.07	1.64	4.52	0.67	2.49	0.13	0.452	100.8
10.60	6.14	78.70	1.08	8.05	3.40	0.06	1.33	4.72	0.74	1.98	0.11	0.422	100.6
14.50	6.56	75.87	0.98	10.60	4.32	0.07	1.54	3.67	0.73	2.37	0.12	0.322	100.6
20.10	6.68	75.68	1.05	10.80	4.21	0.06	1.49	3.58	0.73	2.31	0.11	0.225	100.3
21.78	6.33	79.17	0.91	8.05	2.93	0.06	1.33	4.73	0.85	1.93	0.09	0.225	100.3
23.45	6.73	77.60	0.96	8.85	3.39	0.06	1.48	4.97	0.8	2.03	0.11	0.207	100.5
29.50	7.84	71.78	0.99	12.55	4.71	0.09	2.01	4.70	0.78	2.64	0.16	0.175	100.6
33.50	6.30	69.05	1.15	16.16	6.23	0.11	2.11	1.51	0.72	3.19	0.18	0.062	100.5
39.55	6.41	67.84	1.25	17.00	6.8	0.09	2.00	1.25	0.68	3.27	0.20	0.022	100.4
41.31	9.61	55.75	1.01	26.20	8.53	0.09	2.2	1.04	0.36	4.96	0.20	0.035	100.4
41.45	6.73	69.14	1.16	15.18	5.99	0.11	2.05	2.41	0.75	3.00	0.19	0.117	100.1
43.81	7.07	69.16	1.17	15.33	6.14	0.09	2.09	2.55	0.76	2.98	0.20	0.119	100.6
49.50	7.31	66.31	1.39	17.90	7.44	0.09	2.09	1.16	0.64	3.20	0.27	0.022	100.5
52.50	7.20	66.00	1.55	16.31	8.08	0.15	2.73	1.93	0.51	2.70	0.30	0.023	100.3
57.51	8.09	63.86	1.77	18.05	9.30	0.16	2.16	1.39	0.46	2.86	0.35	0.011	100.4
59.57	16.98	59.15	1.22	12.72	19.42	0.93	1.52	1.52	0.23	1.96	2.04	0.025	100.7
63.26	16.50	66.05	1.47	14.57	10.33	0.45	1.91	1.69	0.27	2.26	1.46	0.086	100.6
68.47	9.05	60.60	1.48	20.83	9.11	0.18	2.53	1.08	0.47	3.70	0.30	0.03	100.3
68.63	10.05	56.71	1.37	19.81	12.35	0.21	2.42	0.97	0.43	3.58	2.38	0.018	100.3
71.70	8.69	61.19	1.44	20.59	8.66	0.11	2.43	1.04	0.48	3.74	0.36	0.03	100.1
77.88	6.75	62.61	1.35	19.59	8.12	0.08	2.82	1.40	0.47	3.70	0.22	0.023	100.4
80.70	7.04	61.02	1.19	19.84	8.12	0.15	2.54	2.03	0.48	3.79	0.92	0.01	100.1
83.31	10.19	61.64	1.44	20.10	8.07	0.08	2.84	1.83	0.45	3.57	0.26	0.043	100.3

Tiefe [m]	V (ppm)	Cr (ppm)	Co (ppm)	Ni (ppm)	Cu (ppm)	Zn (ppm)	Rb (ppm)	Sr (ppm)	Y (ppm)	Zr (ppm)	Nb (ppm)	Ba (ppm)	Pb (ppm)	La (ppm)	Ce (ppm)
4.50	79	97	13	33	18	54	90	132	36	545	19	379	21	42	85
6.49	80	98	13	31	22	62	94	142	37	541	20	391	21	46	79
8.70	80	103	15	37	34	61	96	137	39	551	19	401	19	41	84
10.60	60	110	8	24	13	46	69	134	45	956	22	344	20	48	84
14.50	78	105	13	34	15	57	91	128	38	615	20	367	18	47	90
20.10	77	104	11	30	16	58	90	131	41	649	20	387	19	50	87
21.78	48	91	4	20	10	41	70	141	38	721	19	347	16	51	79
23.45	59	99	8	29	14	48	73	143	39	681	19	337	16	42	82
29.50	88	105	14	40	23	64	105	154	37	469	20	407	21	43	83
33.50	122	120	20	53	34	81	135	160	38	368	23	535	23	60	99
39.55	137	121	24	60	39	85	140	142	37	341	28	505	25	46	107
41.31	195	149	17	71	58	99	224	153	29	183	31	497	33	59	119
41.45	117	113	21	52	40	76	126	150	37	380	26	486	21	49	102
43.81	121	109	17	54	39	78	125	164	38	379	28	532	21	50	104
49.50	160	133	23	62	54	91	149	184	36	313	37	623	24	62	115
52.50	179	161	26	87	105	91	127	189	35	303	42	667	24	57	117
57.51	201	156	26	80	71	92	136	180	38	345	51	705	25	63	118
59.57	220	106	22	76	74	91	99	134	24	166	42	568	22	49	99
63.26	260	109	30	82	93	107	115	158	26	187	53	735	23	66	114
68.47	215	146	36	88	87	120	170	151	34	222	40	625	35	65	140
68.63	199	132	33	79	67	112	158	148	34	205	39	612	30	56	118
71.70	205	151	32	82	75	113	168	149	34	228	37	567	33	70	131
77.88	176	142	30	79	74	104	156	233	35	238	33	669	30	69	123
80.70	164	139	27	76	62	96	164	225	34	226	29	573	33	56	117
83.31	284	135	29	75	102	110	154	174	33	216	45	573	32	76	134

E&G / Vol. 60 / No. 1 / 2011 / 90–104 / DOI 10.3285/eg.60.1.06 / © Authors / Creative Commons Attribution License

Tab. 2: Correlation of DE3 µXRF results (Intensity, Wt%, At%) with WD-XRF analysis. In general, the main elements show the highest correlations, at least in comparison with the measured intensity values with the WD-XRF results. Italic printed values are not significant at the 0.05 level. Highest values of correlation are highlighted with bold letters.

Tab. 2: Korrelationsergebnisse (DE3) der µXRF-Resultate (Intensität, Gew.-%, Atom.-%) mit den WD-XRF-Analysen an diskreten Proben. Höchste Korrelationen sind hervorgehoben. Kursiv gedruckte Werte sind auf dem Niveau von 0,05 nicht signifikant. Höchste Korrelationen sind fett hervorgehoben.

	SiO_2 (Wt%) WD	Si - Int.	Si - Wt%	Si - At%
SiO_2 (%) WD	1.00			
Si - Int.	*0.41*	1.00		
Si - Wt%	**0.69**	0.81	1.00	
Si - At%	0.53	0.74	0.97	1.00

	Na_2O (Wt %) WD	Na - Int.	Na - Wt%	Na - At%
Na_2O (%) WD	1.00			
Na - Int.	***0.41***	1.00		
Na - Wt%	*0.20*	*0.11*	1.00	
Na - At%	*0.17*	*0.10*	1.00	1.00

	TiO_2 (Wt%) WD	Ti - Int.	Ti - Wt%	Ti - At%
TiO_2 (%) WD	1.00			
Ti - Int.	**0.84**	1.00		
Ti - Wt%	0.70	0.86	1.00	
Ti - At%	0.71	0.82	0.98	1.00

	Cr (ppm) WD	Cr - Int.	Cr - Wt%	Cr - At%
Cr (ppm) WD	1.00			
Cr - Int.	***-0.32***	1.00		
Cr - Wt%	*-0.31*	*0.28*	1.00	
Cr - At%	***-0.32***	*0.33*	0.98	1.00

	Al_2O_3 (Wt%) WD	Al - Int.	Al - Wt%	Al - At%
Al_2O_3 (%) WD	1.00			
Al - Int.	0.66	1.00		
Al - Wt%	0.74	0.95	1.00	
Al - At%	**0.82**	0.91	0.98	1.00

	Ni (ppm) WD	Ni - Int.	Ni - Wt%	Ni - At%
Ni (ppm) WD	1.00			
Ni - Int.	***-0.21***	1.00		
Ni - Wt%	*-0.03*	*0.38*	1.00	
Ni - At%	*0.10*	*0.37*	0.94	1.00

	Fe_2O_3(t) (Wt%) WD	Fe - Int.	Fe - Wt%	Fe - At%
Fe_2O_3(t) (%) WD	1.00			
Fe - Int.	0.95	1.00		
Fe - Wt%	0.95	0.85	1.00	
Fe - At%	0.93	0.82	1.00	1.00

	Cu (ppm) WD	Cu - Int.	Cu - Wt%	Cu - At%
Cu (ppm) WD	1.00			
Cu - Int.	***-0.24***	1.00		
Cu - Wt%	*-0.18*	*0.05*	1.00	
Cu - At%	*-0.05*	*-0.15*	0.95	1.00

	MnO (Wt%) WD	Mn - Int.	Mn - Wt%	Mn - At%
MnO (%) WD	1.00			
Mn - Int.	**0.99**	1.00		
Mn - Wt%	0.98	0.98	1.00	
Mn - At%	0.98	0.97	1.00	1.00

	Zn (ppm) WD	Zn - Int.	Zn - Wt%	Zn - At%
Zn (ppm) WD	1.00			
Zn - Int.	***-0.35***	1.00		
Zn - Wt%	*-0.10*	0.60	1.00	
Zn - At%	*-0.01*	*0.46*	0.94	1.00

	MgO (Wt%) WD	Mg - Int.	Mg - Wt%	Mg - At%
MgO (%) WD	1.00			
Mg - Int.	**0.82**	1.00		
Mg - Wt%	0.72	0.77	1.00	
Mg - At%	0.79	0.81	0.99	1.00

	Sr (ppm) WD	Sr - Int.	Sr - Wt%	Sr - At%
Sr (ppm) WD	1.00			
Sr - Int.	*0.17*	1.00		
Sr - Wt%	*-0.34*	*0.28*	1.00	
Sr - At%	***-0.37***	*0.18*	0.98	1.00

	CaO (Wt%) WD	Ca - Int.	Ca - Wt%	Ca - At%
CaO (%) WD	1.00			
Ca - Int.	**0.98**	1.00		
Ca - Wt%	0.96	0.98	1.00	
Ca - At%	0.96	0.98	1.00	1.00

	Zr (ppm) WD	Zr - Int.	Zr - Wt%	Zr - At%
Zr (ppm) WD	1.00			
Zr - Int.	**0.78**	1.00		
Zr - Wt%	*0.39*	*0.02*	1.00	
Zr - At%	*0.24*	*-0.10*	0.96	1.00

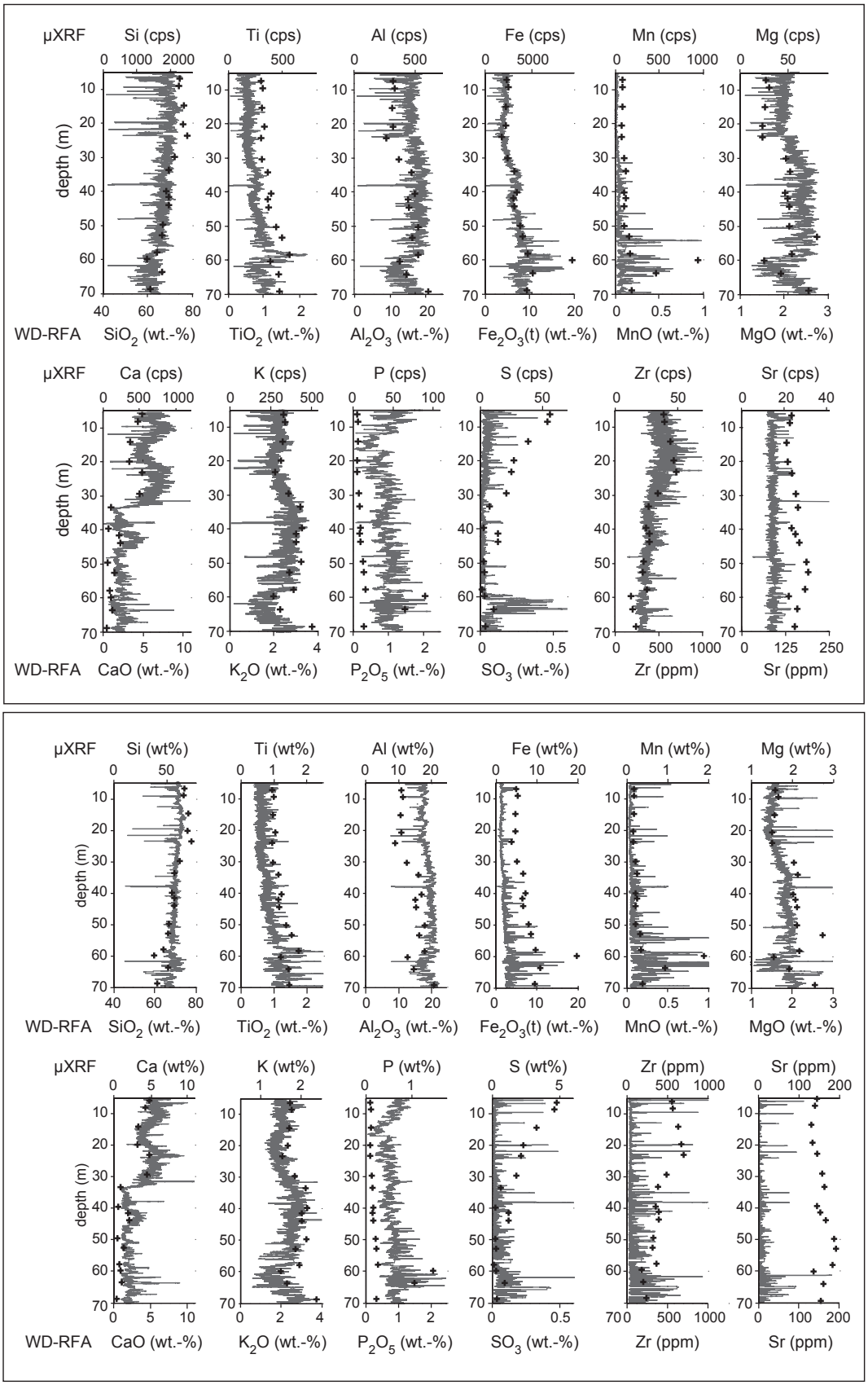

Fig. 4: Continuous measured element concentrations of the core DE3 in (upper panel) cps and (lower panel) quantified (expressed as wt.-% and ppm) using fundamental parameter method (smoothed by a 50-point running mean filter) and measured with the Eagle III µXRF. Black crosses are corresponding results from WD-XRF, measured on discrete samples. Apart from Al all energy dispersive measured elements are underrepresented but show clearly covarying trends. The Ca values represent a dust signal (Dietrich & Sirocko 2009).

Abb. 4: Mit der µRFA kontinuierlich gemessene Elementkonzentrationen des Sedimentkerns DE3, angegeben in (upper panel) counts per second (cps) und (lower panel) quantifiziert mittels der Fundamentalparametermethode in Gew.-% (ppm). Die Werte wurden durch einen gleitenden Mittelwert (Fensterbreite 50-Punkt) geglättet. Die schwarzen Kreuze entsprechen den Vergleichsmessungen an diskreten Proben, die mit einer WD-RFA bestimmt wurden. Mit Ausnahme von Aluminium, zeigen die energie-dispersiv gemessenen Werte niedrigere Konzentrationen an. Insgesamt zeigt die Elementverteilung mit beiden Methoden aber eine deutliche Kovarianz. Hohe Kalziumwerte weisen auf eine verstärkte Staubaktivität hin (Dietrich & Sirocko 2009).

E&G / Vol. 60 / No. 1 / 2011 / 90–104 / DOI 10.3285/eg.60.1.06 / © Authors / Creative Commons Attribution License

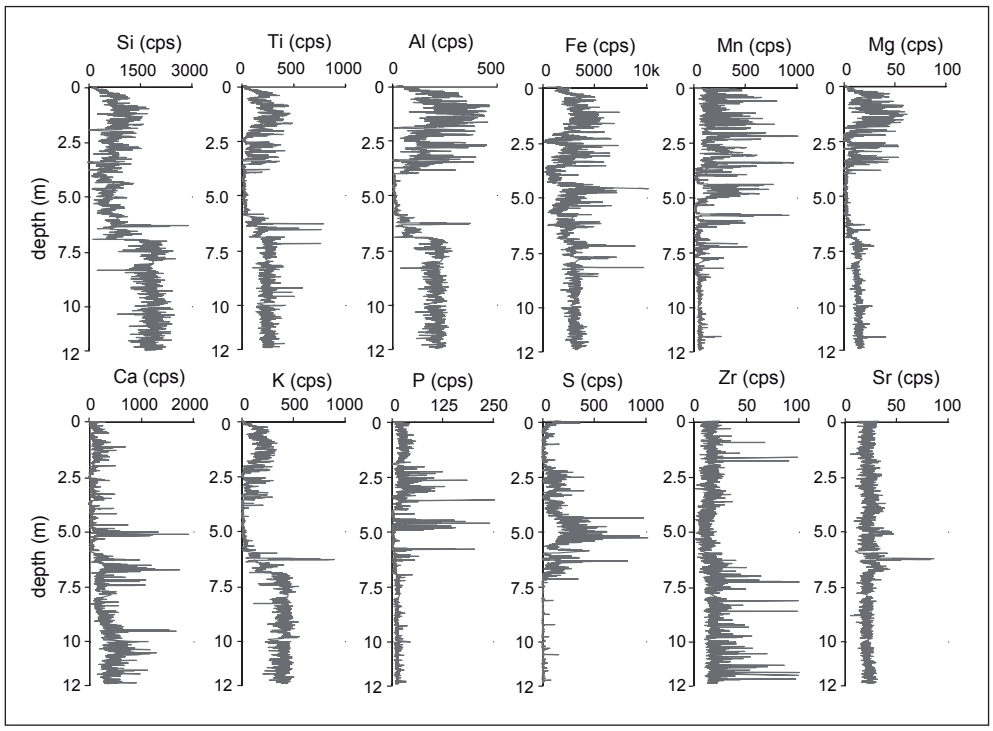

Fig. 5: Continuous measured element concentrations of the core SM3 measured in cps (smoothed by a 5-point running mean filter). The distinctive split in a glacial (>7 m depth) and an interglacial part is clearly visible in the element concentrations of minerogenous elements. The LST at 6.3 m depth is characterized by certain peaks of Si, Ti, Al, and K.

Abb. 5: Kontinuierlich gemessene Elementkonzentrationen des Sedimentkerns SM3 (in cps) und geglättet durch einen gleitenden Mittelwert (Fensterbreite 5-Punkt). Deutliche Unterschiede in der geochemischen Zusammensetzung sind vor allem beim Vergleich kaltzeitlicher Sedimente (> 7 m Tiefe) mit warmzeitlicher und organikreicher Sedimente zu sehen. Erstere sind durch deutlich höhere Konzentration minerogener Elemente gekennzeichnet. Die LST in 6,3 m Tiefe zeigt deutliche Spitzenwerte von Si, Ti, Al und K.

Tab. 3: Upper panel: Correlation matrix of main elements (core DE3 measured intensities by µXRF). Italic printed values are not significant at the 0.05 level. Lower panel: Factor loadings after PCA calculation of main elements (core DE3 measured intensities by µXRF), including Eigenwert (Eigen.), the described variance (dVar.) and the cumulative sum of dVar (% Cumul). Bold printed values (≥|0.4|) have a major influence on the single principle components.

Tab. 3: Obere Tafel: Korrelationsmatrix (DE3) der Hauptelemente auf Basis der mittels µXRF gemessenen Intensitäten. Kursiv gedruckte Werte sind auf dem Niveau von 0,05 nicht signifikant. Untere Tafel: Faktorladungen der Hauptkomponentenanalyse, inklusive der Eigenwerte (Eigen.) und der jeweiligen beschriebenen Varianz (dVar.). Fett gedruckte Werte (≥|0.4|) haben einen hohen Einfluß auf die einzelnen Hauptkomponenten.

	Mg	**Al**	**Si**	**P**	**K**	**Ca**	**Ti**	**Mn**	**Fe**
Mg	1	0.88	0.10	0.43	0.77	-0.48	0.56	0.29	0.58
Al	0.88	1	0.52	0.38	0.80	-0.24	0.28	0.05	0.29
Si	*0.10*	0.52	1	-0.15	0.40	0.40	-0.40	-0.45	-0.42
P	0.43	0.38	-0.15	1	0.11	-0.21	0.25	0.40	0.35
K	0.77	0.80	0.40	*0.11*	1	-0.27	0.20	0.00	0.28
Ca	-0.48	-0.24	0.40	-0.21	-0.27	1	-0.72	-0.54	-0.82
Ti	0.56	0.28	-0.40	0.25	0.20	-0.72	1	0.59	0.88
Mn	0.29	*0.05*	-0.45	0.40	*0.00*	-0.54	0.59	1	0.79
Fe	0.58	0.29	-0.42	0.35	0.28	-0.82	0.88	0.79	1

	PC 1	**PC 2**	**PC 3**	**PC 4**	**PC 5**	**PC 6**	**PC 7**	**PC 8**	**PC 9**
Eigen	4.27	2.55	0.93	0.45	0.33	0.29	0.12	0.04	0.01
dVar.	53.3%	22.4%	9.2%	5.2%	4.6%	3.8%	1.0%	0.6%	0.1%
% Cumul.	53.3%	75.7%	84.9%	90.1%	94.7%	98.4%	99.4%	99.9%	100.0%
Mg	0.21	0.34	-0.10	0.11	-0.15	0.20	**-0.60**	-0.25	**0.59**
Al	0.10	0.39	-0.13	0.01	-0.09	-0.09	**-0.44**	-0.10	**-0.77**
Si	-0.22	**0.54**	0.00	**-0.48**	0.08	**-0.59**	0.14	0.01	0.22
P	0.17	0.06	**-0.81**	0.38	-0.13	-0.24	0.28	0.09	0.06
K	0.14	**0.63**	0.12	0.14	0.21	**0.53**	0.39	0.27	-0.02
Ca	**-0.48**	0.00	-0.38	**-0.44**	**-0.40**	**0.49**	0.10	-0.17	-0.05
Ti	**0.49**	-0.02	0.18	-0.26	**-0.70**	-0.06	0.08	**0.40**	0.01
Mn	0.36	-0.19	-0.35	**-0.53**	**0.50**	0.16	-0.22	0.32	0.01
Fe	**0.50**	-0.02	0.02	-0.21	0.05	0.02	0.36	**-0.75**	-0.07

3.3 From geochemical stratification towards a dust signal

PCA is applied to reduce the amount of variables and to achieve an integrated signal which corresponds better to the lithology of the sediment than the single element stratications. In both cores the first principle component factor (PC 1) illustrated the change from facies containing glacial and aeolian sediment to those which are characterized by containing organic gyttja (Fig. 6). The discrimination into these two lithological groups gives reliable results for SM3 and DE3, which is also indicated by the described variances of the PC 1. This factor accounts for 53.3% in DE3 and for 56.9% in SM3, respectively (Tab. 3, 4). However, both cores show different factor loadings for the first variable. In core SM3 the main geogenic elements Si, Ti, and K represent those samples which are derived from aeolian sediment. In SM3 Calcium is an additional element characteristic of loess gyttja, and is also the most prominent element in the core DE3. The interpretation of the second PCA variable (PC 2) is more difficult, because of even larger differences between the single cores. In SM3 the PC 2 includes variables with high factor loadings on typical limnogenic and redox-sensitive elements like Mn, Fe, and P. High values of P are provided by oxic decay of organic matter. Fe and Mn can be used to indicate the redox conditions of the lake water (Engstrom & Wright 1984). When the lake is under anoxic conditions, Fe and Mn are present in soluble form and are easily released from the sediment. In DE3 the geogenic elements are the major contributors on PC 2. These elements are common constituents of primary minerals. Thus PC 2, with high factor loadings on geogenic elements, reflects the intensity of chemical weathering and leaching in the watershed and shows positive values from 35 m depth down core in DE3.

Summarizing these results one can find that analyses of the first principal component separates glacial and aeolian dominated sediment from interglacial/interstadial organic-rich matter. However, in each core the elements with highest loadings differ in the respective factor. In SM3 the geogenic elements are those which characterize the first PC. In the core DE3 the geogenic elements describe the second PC, whereas Ca and Si are the most important elements for classification of the glacial sediment in PC 1. On the other hand redox-sensitive elements like Mn and P have high loadings in PC 2 for core SM3 and are an indicator for

Tab. 4: Upper panel: Correlation matrix of main elements (core SM3 measured intensities by µXRF). Italic printed values are not significant at the 0.05 level. Lower panel: Factor loadings after PCA calculation of main elements (core SM3 measured intensities by µXRF), including Eigenwert (Eigen.), the described variance (dVar.) and the cumulative sum of dVar (% Cumul). Bold printed values (≥|0.4|) have a major influence on the single principle components.

Tab. 4: Obere Tafel: Korrelationsmatrix (SM3) der Hauptelemente auf Basis der mittels µXRF gemessenen Intensitäten. Kursiv gedruckte Werte sind auf dem Niveau von 0,05 nicht signifikant. Untere Tafel: Faktorladungen der Hauptkomponentenanalyse, inklusive der Eigenwerte (Eigen.) und der jeweiligen beschriebenen Varianz (dVar.). Fett gedruckte Werte (≥|0.4|) haben einen hohen Einfluß auf die einzelnen Hauptkomponenten.

	Mg	**Al**	**Si**	**P**	**K**	**Ca**	**Ti**	**Mn**	**Fe**
Mg	1	0.88	0.59	0.47	0.75	0.42	0.85	0.08	0.54
Al	0.88	1	0.67	0.52	0.81	0.40	0.89	0.02	0.48
Si	0.59	0.67	1	0.07	0.85	0.66	0.74	-0.35	0.50
P	0.47	0.52	*0.07*	1	0.12	-0.16	0.30	0.60	0.38
K	0.75	0.81	0.85	*0.12*	1	0.69	0.94	-0.31	0.56
Ca	0.42	0.40	0.66	-0.16	0.69	1	0.61	-0.32	0.41
Ti	0.85	0.89	0.74	0.30	0.94	0.61	1	-0.14	0.57
Mn	*0.08*	*0.02*	-0.35	0.60	-0.31	-0.32	-0.14	1	0.25
Fe	0.54	0.48	0.50	0.38	0.56	0.41	0.57	0.25	1

	PC 1	**PC 2**	**PC 3**	**PC 4**	**PC 5**	**PC 6**	**PC 7**	**PC 8**	**PC 9**
Eigen	5.144	2.0437	0.7322	0.3646	0.2889	0.2024	0.1461	0.0553	0.0227
dVar.	56.9%	23.8%	7.5%	3.8%	3.2%	2.2%	1.7%	0.6%	0.3%
% Cumul.	56.9%	80.8%	88.2%	92.0%	95.2%	97.5%	99.1%	99.7%	100.0%
Mg	0.39	-0.18	-0.19	-0.31	-0.33	0.13	0.72	-0.20	0.08
Al	**0.42**	-0.16	-0.34	-0.10	0.01	-0.18	-0.15	0.78	0.05
Si	0.36	0.20	0.06	**0.45**	0.33	**-0.60**	0.30	-0.13	-0.21
P	0.16	**-0.60**	-0.15	0.18	**0.62**	0.36	-0.03	-0.19	0.06
K	**0.42**	0.15	-0.03	0.08	-0.13	-0.08	-0.39	-0.34	0.71
Ca	0.30	0.32	**0.56**	**-0.50**	**0.44**	0.19	0.05	0.13	0.02
Ti	**0.43**	0.01	-0.11	-0.14	-0.20	0.11	**-0.45**	-0.31	**-0.66**
Mn	-0.06	**-0.63**	**0.44**	-0.29	-0.12	**-0.53**	-0.12	-0.09	0.02
Fe	0.25	-0.16	**0.55**	**0.55**	-0.36	0.34	0.05	0.25	-0.03

E&G / Vol. 60 / No. 1 / 2011 / 90–104 / DOI 10.3285/eg.60.1.06

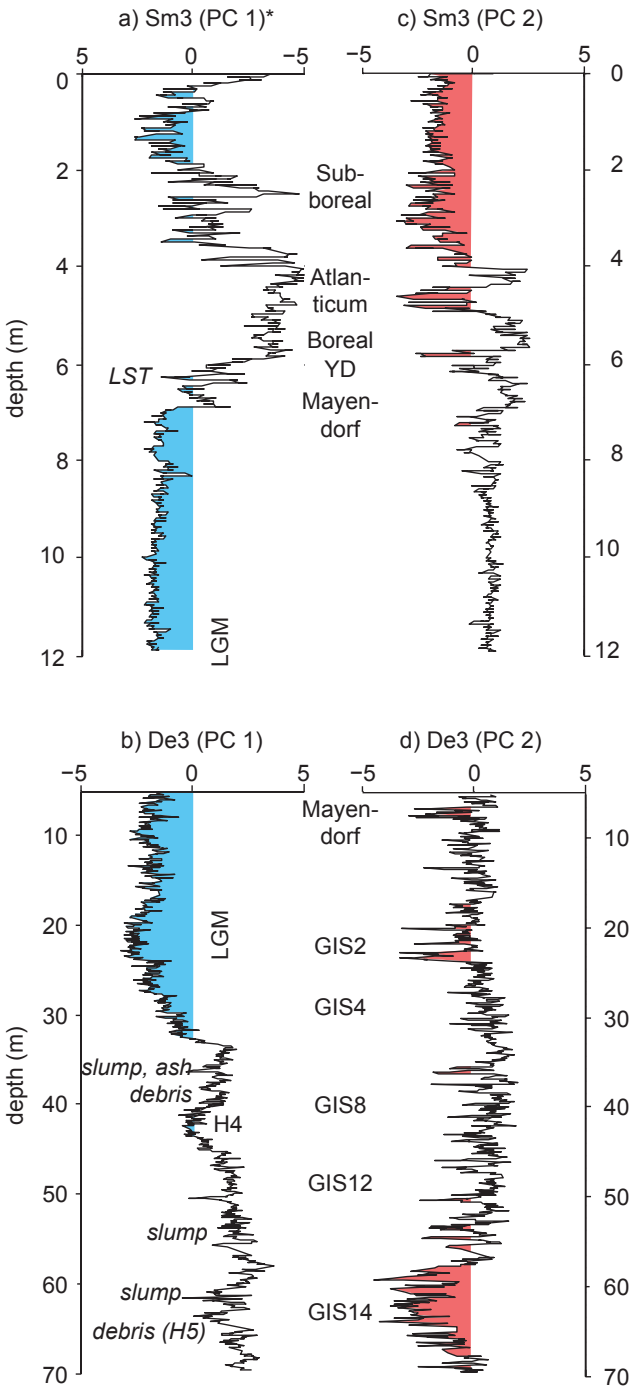

*Fig. 6: The first two principal components PC1 and PC2 of each core are shown versus the depth (see tables 3b, 4b for associated factor loadings). (a, b) PC1 isolates a signal of glacial/aeolian transported sediment (shaded in blue). Aeolian sediments have negative values in the core DE3 and positive ones in the core SM3, respectively (*For a better visualization the x-axis of (b) is inverted). (c ,d) PC2 in both cores has in common that they have negative values during warm/humid climate conditions (red color). However, in core SM3 PC2 is characterized by highly redox-sensitive elements (see text). PC2 of core DE3 depends strongly on elements which indicate enhanced chemical weathering.*

Abb. 6: Darstellung der beiden ersten Hauptkomponenten (PC1, PC2) gegen die Tiefe des jeweiligen Sedimentkerns (s. Tab. 3b, 4b für dazugehörige Faktorladungen). (a, b) Äolischer Staub (blaue Füllung) ist im Kern DE3 durch negative PC1-Werte gekennzeichnet, im Kern SM3 durch positive Werte. Zur Verdeutlichung des staubhaltigen Sediments ist die x-Achse der PC1 des Kerns SM3 invers dargestellt. (c, d) PC 2 ist in beiden Kernen unterschiedlich zu interpretieren deutet aber auf klimatisch warm/humiden Einfluss hin (rote Färbung). Im Kern SM3 ist PC2 durch redox-sensitive Elemente charakterisiert (s. Text). Im Kern DE3 hängt PC2 stark vom Vorkommen von Elementen ab, die auf erhöhte chemische Verwitterung hindeuten.

the redox conditions at the lake bottom with contemporaneous high amount of organic matter. The other factors do not influence aeolian sediment input into the maar lake and account only for a lower percentage of the total variation. In addition, the result of the scree test suggests using the first two factors, only. Consequently, they are of minor interpretative use for this study and not further considered.

4 Discussion

For the derivation of paleoclimate or economic conditions from geochemical data two assumptions must hold true (Boyle, 2001): (1) At any one time the sediment concentration must be proportional to the external element loading and (2) the element concentrations in the sediment must not change after burial. The latter is in discussion especially as regards the role of Mn and Fe reduction in potential remobilization of trace elements. Boyle (2001) has shown that post depositional alteration and migration is likely, but that this is only significant at extremely low sediment mass accumulation rates and is not likely for high glacial sediment yields. Thus we suggest that the elicitation of a dust signal within maar lake sediments is possible by application of inorganic geochemistry. However, a wider knowledge about the lake's regional setting (location, morphology, presence of inflows, etc) is necessary. Thus, additional information from other proxies is required. This is shown in this study, since all cores show different inorganic geochemical reactions to environmental changes dependent on the regional setting. An example is the stratification of the geogenic elements in the core SM3: All of these elements have a major influence on PC 1, but only the typical "loess-elements" Si, Ca, and K have their highest values during glacial conditions.

The results show that there are three different groups of main elements which characterize the sediment. (i) Typical geogenic elements are magnesium (low differentiated volcanic products), potassium (low differentiated volcanic products), titanium and aluminum (lithics, feldspars). In oligotrophic lakes silica, aluminum as well as titanium and potassium represent the clastic input. This is clearly shown for all the cores. The alkali metal K and the alkaline earth metals Ca and Mg are major bedrock constituents. High amounts of these elements represent reduced soil stability and increased erosion. But Ca and Mg might have also significant concentrations in authigenic carbonate and skeletal carbonates from invertebrates. The supply of conservative cations K (and also Na) increases with periods of rapid chemical erosion, similar to Ti. These elements are thus enriched during the Holocene and MIS-3 and only minor during MIS-2, when climate was more arid. (ii) Sulphur and phosphorous belong are limnogenic and redox-sensitive elements and thus the precipitation and release processes are complex. The deposition and conservation of the elements Fe, Mn, S, and P is strongly controlled by pH and redox conditions at the lake bottom (Engstrom & Wright 1984). Since maar lakes usually have anoxic bottom water reduced Fe(II) precipitates in combination with S, forming the mineral pyrite (FeS_2). Blue colored vivianite crystals, a ferrous phosphate, occur with increased burial of undecomposed organics. High rates of organic matter deposition

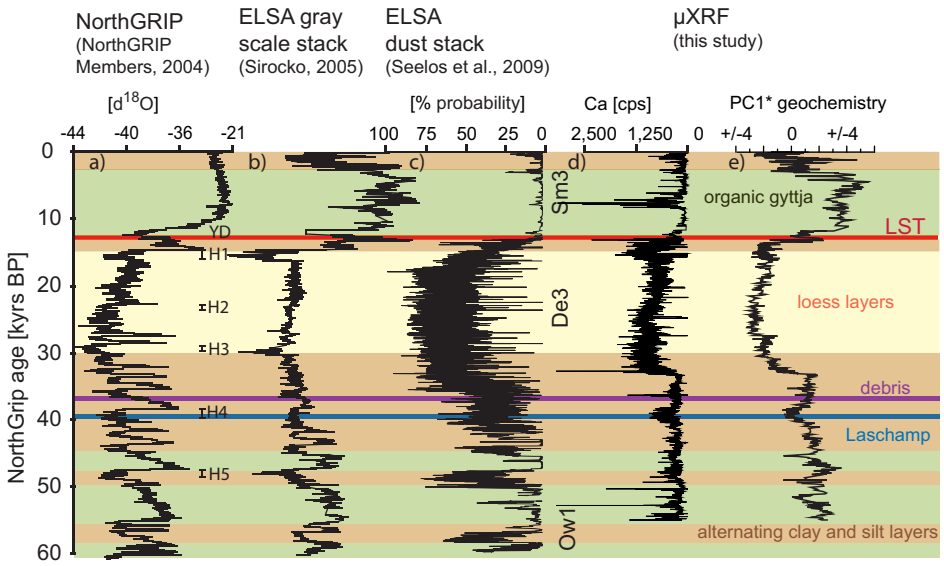

Fig. 7: µXRF geochemistry stacks versus the time, (a) NorthGRIP d18O record, (b) the ELSA grayscale stack, (c) the ELSA dust stack, and major litho zones of the last 60 kyrs. Ca (d) as well as the PCA stack (e) clearly shows the influence of aeolian sediment (The SM3 part of the PC 1-stack is inverse; see Fig. 6). Heinrich events after Hemming (2004).*

*Abb. 7: µXRF-Geochemie-Stacks gegen das Alter: (a) NorthGRIP d18O-Rekord, (b) der ELSA Graustufen-Stack, (c) der ELSA Staub-Stack und die wichtigsten Lithozonen der Bohrkerne. Die Ca-Werte (d) sowie der PC1-Stack (e) zeigen deutlich den Einfluss des äolischen Sediments (*der SM3-Abschnitt des PC1-Stacks ist invers aufgetragen; siehe Abb. 6). Marine Heinrich-Ereignisse nach Hemming (2004).*

occur only during interstadials and interglacials. A second prerequisite for the formation of vivianite is the presence of orthophosphates which are provided by oxic decay. Thus, the occurrence of vivianite in organic rich sediment sections is not a proxy for paleoproductivity (Fagel et al., 2005). It is an indicator of at least temporary deep circulation at high organic production (Voigt et al., 2008) and clearly precedes the formation of sulphides in the course of eutrophication (Gächter & Müller, 2003). The presence of Pyrite shows on the other hand the level of aeration of the maar deep water and the occurrence of a monimolimnion, with anoxic water conditions for at least a period of several mixing cycles. Vivianite is found in the cores with a high content of Phosphorous in the DE3 47.7–50 m and at 70.7–72.7 m depth, in particular. (iii) The DE3 at third class is a mixed type: Silicon represents minerogenous SiO_2 in the clastic fraction as well as amorphous and autogenic SiO_2 production, mainly by the silicon shell of diatoms. Calcium is a major constituent of aeolian dust sediments (with provenance of the Devonian or Triassic limestone). Further reasons for high contents of Ca are the precipitation of $CaCO_3$ caused by detraction of CO_2 in the lake water, and biogenic calcium precipitation e.g. in the lime shell of ostracods. Authigenic carbonates were not observed during glacial periods in the core DE3 (Dietrich & Seelos 2010) and we suggest this for the other glacial sequences, too. During times of dominant physical weathering $CaCO_3$ grains will be transported to the lake and most of them should quickly reach the lake bottom without significant in-lake chemical reaction (Koinig et al. 2003). Thus, we suggest that the content of calcium has not changed during settlement at glacial conditions and can be interpreted as a major contributor to the measured dust signal. However, a stack of the elemental stratification of different cores does not seem to be appropriate. The influence of the catchment, different biogeochemical processes in the lake water and bottom makes each maar lake unique, which is reflected in the distribution of the elements.

The focus of this study is on the detection of aeolian sediments by µXRF scanning and PCA. It is shown that the methodology gives reliable results within acceptable error margins but still needs additional information, at least from facies and micro-facies analysis. However, in this study time slices including major climate changes of the last glacial were used to evaluate this approach and are already discussed in early ELSA publications: e.g. the late Weichselian glacial inception and Heinrich events during MIS-3 and 2 (Dietrich & Seelos 2010), transition I, the Younger Dryas and internal variability of the Holocene (Seelos et al. 2009). A major finding of this study is that the previously used approach demonstrates weaknesses in comparison to high resolution grain size analysis which was used in the mentioned publications by applying the RADIUS technique (Seelos & Sirocko 2005). For example, the variability of MIS-2 dust sources could only be shown by a combination of mineralogical/geochemical analysis and grain size sorting parameters (Dietrich & Seelos 2010). However, the transition into the glacial climate state is shown within an abrupt trend towards negative values of PC 1 in the core DE3. This signal is highly correlated to the dust detection for the same core published as ELSA dust stack (Fig. 8). The timing of increased dust transport towards the Eifel maar lakes correspond with the global decrease of sea-level 35 kyrs ago (Clark et al. 2009). An increased east wind frequency for Western Europe was suggested by Dietrich & Seelos (2010) for the time slice between 33 and 24 kyrs BP. These layers are enriched in aeolian transported carbonate grains in the same sediment core DE3. Since, Ca has a major influence of DE3's PC1, these layers are also reflected in PC 1 (Fig. 7d, e). In addition a severe cold phase which corresponds to the strong Heinrich event H4 (Hemming 2004) is detected by the PCA approach. Another major dust event correlates with H5 (Seelos et al. 2009) which is reworked by debris in the core DE3 at 65 m depth, and thus could not be shown by the applied approach.

The younger sediment sequence shows in core SM3 the major climate change from the last glacial to interglacial conditions of the Holocene. Fast environmental changes from the last glacial to the interglacial including the YD are also documented in this core. However, the tephra of the lake Laach eruption shows negative factor scores, too, and is wrongly classified as glacial and aeolian sediment. PC 1 shows a high variability during the Holocene, which is also shown in the lithology and in the grayscale values of the core (Fig. 7). The strong shifts in the aeolian sedi-

E&G / Vol. 60 / No. 1 / 2011 / 90–104 / DOI 10.3285/eg.60.1.06

ment proxy in the Holocene (especially the Atlanticum) might also be influenced by changing lake levels during the Holocene. Correlations between the North Atlantic IRD events defined by Bond et al. (1993) and lake level changes in mid-European lakes have been pointed out (Magny 2004, 1999; Friedrich et al. 1999), supporting the hypothesis that changes in solar activity have been an important forcing factor of Holocene climate (Renssen & Isarin 2001). A pronounced Ca peak corresponds to the strong cold spell of the 8.2-ka-event. This event is only minor correlated with an enhanced dust input in the Eifel area (Seelos et al. 2009). Here, we suggest that a strong ventilation of the bottom water has led to the precipitation of carbonate minerals. However, Prasad et al. (2009) suggested temperature to be the primary control on calcite formation. These authors focused on seasonal carbonate precipitates in the sublayers of single warves and found distinct minima of calcite during the 8.2-ka-event which were used as an proxy for cold summer temperatures. In deed, the calcium maximum in SM3 is not continuously on a high level when looking at high resolution µXRF scans, but also shows several phases with minimum values (not shown). The major impact of the 160 year 8.2-ka-event on the environment of Central Europe is also shown in many other records e.g. in reduced tree-ring widths from Central German oaks (Friedrich et al. 1999). However, in the Holocene the deposition of aeolian dust plays only a minor role. The elements Al, K, Ti have the highest factor loadings in PC 1 of SM3 and reflect soil destabilization which goes along with erosion and enhanced dust transport. Until the Boreal the environment is characterized by more open landscapes and high physical weathering. These conditions change within the Atlanticum when conditions changed to a warmer and more humid climate. Hence, the soils became more stabilized and the slopes were covered by dense forests. Human activities in the catchment are traced back to ca. 15.5 kyrs BP, long before late glacial warming ca. 14.7 kyrs BP (Street et al. 2006), but became most pronounced around 3,700 BP (Sirocko, ed. 2009). Deforestation, grazing, and agriculture caused an increase in erosion, physical weathering and thus enhanced deflation of dust. Since then the dust signal in the lake Schalkenmehrener Maar is mainly anthropogenically altered.

5 Conclusion

This study investigates whether the detection of aeolian sediment by µXRF scanning of resin impregnated sediment samples with a subsequent PCA approach give reliable results. Changes of aeolian supply over time are suggested in the inorganic geochemistry data, especially in Ca, Si, and the first new calculated PCA factor (PC 1) which is mainly influenced by Ca, Si, and Ti. It is demonstrated that this approach works well since for the interpretation further knowledge about the lithology and environmental background is available. The signal of geochemical aeolian proxies might be influenced by autochthonous and allochthounous accumulation changes and without further knowledge and necessary inter proxy comparison the results might be inconsistent or difficult to interpret. Thus, the detection of dust using high resolution grain size analysis is advantageous, because this approach recognizes different transport mechanisms of the sediment and is so far the only method which is able to quantify the content of aeolian dust in sediment. A µXRF is a fast and inexpensive scanning method of the elemental stratification within sediment cores. In addition, the quantification of the main elements via standard less fundamental parameter method gives significant results in comparison to the reference samples, which are measured by WD-XRF. Thus, a calibration of the µXRF results is reliable, if this evaluation is based on at least a reference sample for each litho zone.

Cores SM3 and DE3 show both fully glacial sediment and warm and wet climate conditions and the major dust deposition events and phases could be detected by µXRF geochemistry. These include the largest Heinrich event H4 during MIS-3, the onset of dust increase coupled to the growing of the Scandinavian Ice sheet, later on the whole MIS-2 including LGM, the YD as well as enhanced dust supply generated by human activities since the Subboreal. In the applied PCA approach PC 1 discriminates in both lake sediment cores aeolian from non aeolian material. Volcanic ash and tephra is mostly classified as aeolian sediment because of the major influence of geogenic elements (Si, Al, Ti, K and mostly Ca) to PC 1. Ca has a major influence on the dust signal in both cores and a combination of Ca with the grayscale values gives the best signal of aeolian sediment. The occurrence of vivianite coincides with enriched amounts of P and Fe in organic rich gyttja and is thus suggested as a proxy for low sedimentation rates during interstadial climate conditions. In summary, µXRF scanning of bulk geochemistry has shown to be a sensitive indicator of both changes in the lake and in its (aeolian) catchment, if it is used together with other proxy data such as micro facies or grain size analysis.

Acknowledgements

The authors thank Erzsébet Horváth for her constructive comments and Manfred Frechen for his comments and great support as an editor. We would like to thank Klaus Schwibus and Günther Ritschel for sample preparation and Saskia Rudert for her great assistance at sample measuring. This work is part of the Stephan Dietrich's Phd thesis and funded by the German Science Foundation (DFG, Si594/21-2).

6 References

BGR. 1993. Geological Map of Germany. (ger: Geologische Karte der Bundesrepublik Deutschland). scale 1:1,000,000, Hannover.

Bond, G., W. Broecker, S. Johnsen, J. McManus, L. Labeyrie, J. Jouzel & G. Bonani. 1993. Correlations between climate records from North Atlantic sediments and Greenland ice. Nature 365: 143–147.

Böning, P., E. Bard & J. Rose. 2007. Toward direct, micron-scale XRF elemental maps and quantitative profiles of wet marine sediments. Geochemistry, Geophysics, Geosystems. 8: Q05004.

Boyle, J. F. 2000. Rapid elemental analysis of sediment samples by isotope source XRF. Journal of Paleolimnology 23: 213–221.

Boyle, J. F. 2001. Inorganic geochemical methods in palaeolimnology. In: W. M. Last, J. P. Smol & H. J. B. Birks (Eds.). Tracking Environmental Change Using Lake Sediments: Physical and Geochemical Methods. Vol. 2, pp. 83–141. Springer.

Brauer, A., G. H. Haug, P. Dulski, D. M. Sigman & J. F.W. Negendank. 2008. An abrupt wind shift in western Europe at the onset of the Younger Dryas cold period. Nature Geoscience 1: 520–523.

Büchel, G. 1994. Vulkanologische Karte West- und Hocheifel. Landesvermessungsamt Rheinland-Pfalz.

Clark, P. U., A. S. Dyke, J. D. Shakun, A. E. Carlson, J. Clark, B. Wohlfarth, J. X. Mitrovica, S. W. Hostetler & A. M. McCabe. 2009. The Last Glacial Maximum. Science 325: 710–714.

Dietrich, S. & K. Seelos. 2010. The reconstruction of easterly wind directions for the Eifel region (Central Europe) during the period 40.3–12.9 ka BP. Climate of the Past 6: 145–154.

Dietrich, S. & F. Sirocko. 2009. Korngrößenanalyse und Sedimentgeochemie als Grundlage der Klima- und Wetterrekonstruktion. In F. Sirocko (Ed.). Wetter, Klima, Menschheitsentwicklung. Von der Eis-zeit bis ins 21. Jahrhundert, pp. 26–32. Wissenschaftliche Buchgesellschaft, Darmstadt.

Engstrom, D. R. & H. E. Wright Jr. 1984. Chemical stratigraphy of lake sediments as a record of environmental change. In E. Y. Haworth & J. W. G. Lund (Eds.). Lake sediments and environmental history. Leicester University Press.

Fagel, N., L. Y. Alleman, L. Granina, F. Hatert, E. Thamo-Bozso, R. Cloots & L. Andre. 2005. Vivianite formation and distribution in Lake Baikal sediments. Progress towards reconstructing past climate in Central Eurasia, with special emphasis on Lake Baikal. Global and Planetary Change 46: 315–336.

Francus, P., H. Lamb, T. Nakakawa, M. Marshall, E. T. Brown & Suigetsu 2006 Project Members. 2009. The potential of high-resolution X-ray fluorescence core scanning: Applications in paleolimnology. A new generation of XRF core scanners allows rapid, non-destructive acquisition of high-resolution geochemical and X-radiographic data from lacustrine sediment cores, facilitating new approaches to many applications in paleolimnology, including pollution detection, varve counting& estimation of past ecosystem productivity. PAGES news 17: 93–95.

Friedrich, M., B. Kromer, M. Spurk, J. Hofmann & K. Felix Kaiser. 1999. Paleo-environment and radiocarbon calibration as derived from Lateglacial/Early Holocene tree-ring chronologies. Quaternary International 61: 27–39.

Gächter, R. & B. Müller. 2003. Why the Phosphorus Retention of Lakes Does Not Necessarily Depend on the Oxygen Supply to Their Sediment Surface. Limnology and Oceanography, 48(2), 929–933, http://www.jstor.org/stable/3096591.

Govindaraju, K. 1989. 1989 compilation of working values and sample description for 272 geostandards. Geostandards and Geoanalytical Research 13: 1–113.

Hemming, S. R. 2004. Heinrich events: Massive late Pleistocene detritus layers of the North Atlantic and their global climate imprint. Reviews of Geophysics, 42(RG1005), 1--43, http://dx.doi.org/10.1029/2003RG000128.

Kido, Y., T. Koshikawa & R. Tada. 2006. Rapid and quantitative major element analysis method for wet fine-grained sediments using an XRF microscanner. Marine Geology 229: 209–225.

Koinig, K. A., W. Shotyk, A. F. Lotter, C. Ohlendorf & M. Sturm. 2003. 9000 years of geochemical evolution of lithogenic major and trace elements in the sediment of an alpine lake – the role of climate, vegetation & land-use history. Journal of Paleolimnology 30: 307–320.

Magny, M. 1999. Lake-level fluctuations in the Jura and french subalpine ranges associated with ice-rafting events in the north atlantic and variations in the polar atmospheric circulation. Quaternaire 10: 61–64.

Magny, M. 2004. Holocene climate variability as reflected by mid-European lake-level fluctuations and its probable impact on prehistoric human settlements. The record of Human /Climate interaction in Lake Sediments. Quaternary International 113: 65–79.

Melles, M., J. Brigham-Grette, O. Glushkova, P. Minyuk, N. Nowaczyk & H.-W. Hubberten. 2007. Sedimentary geochemistry of core PG1351 from Lake El'gygytgyn – a sensitive record of climate variability in the East Siberian Arctic during the past three glacial–interglacial cycles. Journal of Paleolimnology 37: 89–104.

Neff, J. C., A. P. Ballantyne, G. L. Farmer, N. M. Mahowald, J. L. Conroy, C. C. Landry, J. T. Overpeck, T. H. Painter, C. R. Lawrence & R. L. Reynolds. 2008. Increasing aeolian dust deposition in the western United States linked to human activity. Nature Geosciences 1: 189–195.

Pfahl, S., F. Sirocko, K. Seelos, S. Dietrich, A. Walter & H. Wernli. 2009. A new windstorm proxy from lake sediments – a comparison of geological and meteorological data from western Germany for the period 1965–2001. Journal of Geophysical Research, 114(D18106), 1–13, doi:10.1029/2008JD011643.

Prasad, S., A. Witt, U. Kienel, P. Dulski, E. Bauer & G. Yancheva (2009). The 8.2 ka event: Evidence for seasonal differences and the rate of climate change in western Europe. Global and Planetary Change 67 (3–4), 218–226.]

Renssen, H. & R. F.B. Isarin. 2001. The two major warming phases of the last deglaciation at ~14.7 and ~11.5 ka cal BP in Europe: climate reconstructions and AGCM experiments. Global and Planetary Change 30: 117–153.

Röhl, U. & L. J. Abrams. 2000. High-resolution, downhole and non-destructive core measurements from sites 999 and 1001 in the Caribbean Sea: application to the late Paleocene thermal maximum. In R. M. Leckie, H. Sigurdsson, G. D. Acton and G. Draper (Eds.). Proceedings of the. Ocean Drilling Program. Vol. 165, pp. 191–203, College Station, TX.

Rothwell, R. G. (Ed.). 2006. New Techniques in Sediments Core Analysis - New techniques in sediment core analysis. Vol. 267. Geological Society, London.

Seelos, K. & F. Sirocko. 2005. RADIUS – rapid particle analysis of digital images by ultra-high-resolution scanning of thin sections. Sedimentology: Vol. 52, No. 3 (2005),669–681.

Seelos, K., F. Sirocko& S. Dietrich. 2009. A continuous high resolution dust record for the reconstruction of wind systems in Central Europe (Eifel, Western Germany) over the last 133 ka. Geophysical Research Letters, 36(L20712), 1–6, doi:10.1029/2009GL039716.

Sirocko, F., K. Seelos, K. Schaber, B. Rein, F. Dreher, M. Diehl, R. Lehne, K. Jager, M. Krbetschek & D. Degering. 2005. A late Eemian aridity pulse in central Europe during the last glacial inception. Nature 436: 833–836.

Sirocko, F. (Ed.). 2009. Wetter, Klima, Menschheitsentwicklung. Von der Eiszeit bis ins 21. Jahrhundert. Wissenschaftliche Buchgesellschaft, Darmstadt.

Sorrel, P., H. OberhÄnsli, N. Boroffka, D. Nourgaliev, P. Dulski & U. Rohl. 2007. Control of wind strength and frequency in the Aral Sea basin during the late Holocene. Reconstructing past environments from remnants of human occupation and sedimentary archives in western Eurasia. Quaternary Research 67: 371–382.

Straka, H. (1975). Die spätquartäre Vegetationsgeschichte der Vulkaneifel. Beiträge zur Landespflege in Rheinlandand-Pfalz 3, 1–163.

Street, M., F. Gelnhausen, S. Grimm, F. Moseler, L. Niven, E. Turner, S. Wenzel & O. Jöris. 2006. L'occupation du basin de Neuwied (Rhénanie centrale, Allemagne) par les Magdaléniens et les groupes à Federmesser (aziliens). Bulletin de la Société préhistorique française 103: 753–780.

Sun, D., J. Bloemendal, D. K. Rea, J. Vandenberghe, F. Jiang, Z. An & R. Su. 2002. Grain-size distribution function of polymodal sediments in hydraulic and aaeolian environments & numerical partitioning of the sedimentary components. Sedimentary Geology 152: 263–277.

Svensson, A., K. K. Andersen, M. Bigler, H. B. Clausen, D. Dahl-Jensen, S. M. Davies, S. J. Johnsen, R. Muscheler, F. Parrenin, S. O. Rasmussen & others. 2008. A 60 000 year Greenland stratigraphic ice core chronology. Climate of the Past 4: 47–57.

van den Bogaard, P. 1995. 40Ar/39Ar ages of sanidine phenocrysts from Laacher See Tephra (12,900 yr BP): Chronostratigraphic and petrological significance. Earth and Planetary Science Letters 133: 163–174.

Voigt, R., E. Grüger, J. Baier, & D. Meischner. 2008., Seasonal variability of Holocene climate: a palaeolimnological study on varved sediments in Lake Jues (Harz Mountains, Germany), Journal of Paleolimnology, 40(4), 1021–1052, http://dx.doi.org/10.1007/s10933-008-9213-7.

Weltje, G. J. & R. Tjallingii. 2008. Calibration of XRF core scanners for quantitative geochemical logging of sediment cores: Theory and application. Earth and Planetary Science Letters 274: 423–438.

Wörner, G. & H. U. Schmincke. 1984. Petrogenesis of the Zoned Laacher See Tephra. Journal of Petrology 25: 836–851.

Yancheva, G., N. R. Nowaczyk, J. Mingram, P. Dulski, G. Schettler, J. F.W. Negendank, J. Liu, D. M. Sigman, L. C. Peterson & G. H. Haug. 2007. Influence of the intertropical convergence zone on the East Asian monsoon. Nature 445: 74–77.

Zolitschka, B. 1998. A 14,000 year sediment yield record from western Germany based on annually laminated lake sediments. Geomorphology 22: 1–17.

Zolitschka, B., A. Brauer, J. F.W. Negendank, H. Stockhausen & A. Lang. 2000. Annually dated late Weichselian continental paleoclimate record from the Eifel, Germany. Geology 28: 783–786.

E&G Quaternary Science Journal
Volume 60 / Number 1 / 2011 / 105–115 / DOI 10.3285/eg.60.1.07
www.quaternary-science.net

GEOZON SCIENCE MEDIA
ISSN 0424-7116

IRSL Signals from Maar Lake Sediments Stimulated at Various Temperatures

Esther Dorothe Schmidt, Andrew S. Murray, Frank Sirocko, Sumiko Tsukamoto, Manfred Frechen

Abstract: Optically stimulated luminescence (OSL) and infrared stimulated luminescence (IRSL) have been measured from seven fine-grained samples from core JW3 from the dry maar of Jungfernweiher (West Eifel /Germany). Two different elevated temperature post-IR IRSL protocols in the blue detection were applied to polymineral fine grains (4–11 µm). These protocols involve stimulation with IR for up to 200s at 50°C prior to elevated temperature stimulation with IR for 100s at 225°C or 200s at 290°C. Quartz OSL saturates at doses of 260–300 Gy, and the D_e values obtained using IRSL at 50°C (IR_{50}) do not increase with depth indicating that this signal is also in field saturation at ~500 Gy. However, the post-IR IRSL signals at 225°C ($pIRIR_{225}$) and 290°C ($pIRIR_{290}$) increase with depth from ~800 Gy to ~1400 Gy, suggesting a minimum (fading uncorrected) age of ~200 ka for the youngest sediments. Mean laboratory fading rates are 4.09 ± 0.02%/decade for IR_{50} and 2.55 ± 0.14%/decade for polymineral $pIRIR_{225}$. For sample JWS1 a g-value of 0.52 ± 1.12%/decade for the $pIRIR_{290}$ was obtained. Both fading corrected $pIRIR_{225}$ and uncorrected $pIRIR_{290}$ D_e values from the youngest sample (~16 m below modern surface) indicate an age estimate of ~250 ka for the uppermost sample increasing up to ~400 ka for the oldest samples taken ~94 m below modern surface.

[IRSL Signale von Maarseesedimenten stimuliert mit verschiedenen Temperaturen]

Kurzfassung: Optisch stimulierte Lumineszenz (OSL) und infrarot stimulierte Lumineszenz (IRSL) wurden an sieben Feinkorn Proben von Kern JW3 aus dem Trockenmaar Jungfernweiher gemessen. Zwei verschiedene post-IR IRSL Messprotokolle (blaue Detektion) wurden an den polymineralischen Feinkörnern (4–11 µm) angewandt. Diese Protokolle beinhalten eine Stimulation mit IR bei 50°C für bis zu 200 s vor einer weiteren IR Stimulation bei erhöhten Temperaturen bei 225°C für 100 s oder 290°C für 200 s. Die OSL von Quarz sättigt bei Dosen von 260–300 Gy und die De-Werte, die mit IRSL bei 50°C (IR_{50}) erhalten werden, nehmen mit der Tiefe nicht zu. Dies weist darauf hin, dass auch dieses Signal bei ~500 Gy in Sättigung geht. De-Werte des post-IR IRSL Signals bei 225°C ($pIRIR_{225}$) und 290°C ($pIRIR_{290}$) nehmen jedoch mit der Tiefe von ~800 Gy bis ~1400 Gy zu, und zeigen ein korrigiertes Minimalalter von ~200 ka für die jüngsten Sedimente an. Die durchschnittlichen im Labor gemessene Fadingraten liegen für IR50 bei 4.09 ± 0.02%/decade und für $pIRIR_{225}$ bei 2.55 ± 0.14%/decade. Für Probe JWS1 wurde für $pIRIR_{290}$ ein g-value von 0.52 ± 1.12%/decade gemessen. Sowohl fading korrigierte $pIRIR_{225}$ als auch unkorrigierte $pIRIR_{290}$ D_e-Werte der jüngsten Probe (~16 m unterhalb der heutigen Erdoberfläche) weisen auf ein Alter von ~250 ka für die oberste Probe hin. Für die ältesten Proben, die in ~94 m unterhalb der heutigen Erdoberfläche genommen wurden, wurden Alter von bis zu ~400 ka gemessen.

Keywords: *luminescence dating, IRSL, OSL, fading, fine grain, maar lake, Jungfernweiher, ELSA*

Addresses of authors: **E. D. Schmidt***, **S. Tsukamoto**, **M. Frechen**, Leibniz Institute for Applied Geophysics (LIAG), Section 3: Geochronology and Isotope Hydrology, Stilleweg 2, 30655 Hannover, Germany. E-Mail: Esther.Schmidt@liag-hannover.de, EstherDorothe.Schmidt@googlemail.com; **E. D. Schmidt**, **A.S. Murray**, Nordic Laboratory for Luminescence Dating, Department of Earth Sciences, Aarhus University, Risø DTU, DK-4000 Roskilde, Denmark; **F. Sirocko**, University of Mainz/Germany, Institute for Geoscience. **corresponding author*

1 Introduction

Maars are volcanic craters caused by phreatomagmatic eruptions. Volcanic depressions and craters such as those of maar lakes form excellent sediment traps, and so can record past climatic and environmental changes. Sediments accumulating in maar lakes are often thought to have undergone continuous deposition since the eruption of the maar volcanoes, and hence may contain unique continuous local records of climate change. Aeolian dust (loess) can make up a large part of the sediment inventory, because the catchment surrounding the lake often only extends to the rim of the crater. Because of its more or less continuous supply during cold periods, loess is one of the most detailed and wide-spread terrestrial archives of climate and environment change. As a result it often provides information on local and regional environmental processes and conditions for the Middle and Late Pleistocene. The West Eifel volcanic field (Fig.1) contains dry maars, maar lakes, scoria cones and small stratovolcanoes. The Jungfernweiher is one of about 60 dry maars; with a diameter of 1500 m it is the biggest maar in the Eifel area. Nowadays there is a pond in the dry maar lake (Schaber & Sirocko, 2005). Sediment cores have been drilled within the framework of the ELSA project (Eifel Laminated Sediment Archive) in Eifel dry maar lakes (Sirocko et al. 2005), and samples for luminescence dating were taken from core JW3 and JW2 from the Jungfernweiher.

Luminescence dating is used to date the time that has passed since the last exposure of minerals (quartz or feldspar) to daylight (Aitken, 1998). Such minerals are able to store energy (as trapped electrons) within their crystal structure; this energy originates from ionising radiation (alpha, beta and gamma) from environmental radioactivity,

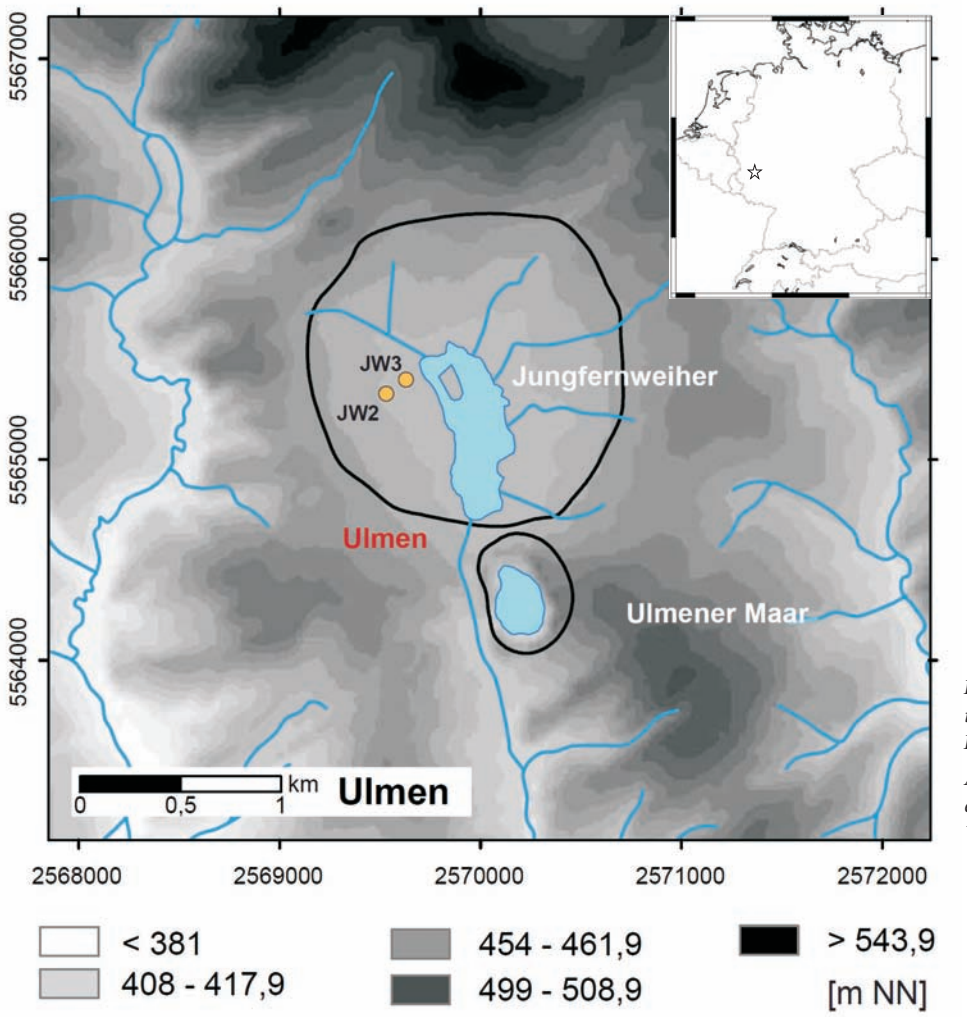

Fig. 1: Map showing coring locations of the dry maar of Jungfernweiher, West Eifel Volcanic Field.

Abb. 1: Lage der Bohrpunkte des Trockenmaars Jungfernweiher, Vulkanfeld der Westeifel.

and from cosmic rays. The trapped electrons can be stored for long periods at lattice defects in the crystal lattice. In the laboratory the grains are stimulated with light and the trapped electrons are released. During recombination they release their stored energy as light (luminescence). A measurement of this luminescence allows an estimation of the radiation dose (palaeodose or equivalent dose, D_e) that the crystal has absorbed since the last exposure to daylight. The most important requirement is that the sediments are well bleached or zeroed at the time of deposition due to a sufficient exposure to daylight. For loess it is expected that any residual trapped charge has been completely removed during the long aeolian transport. The optically stimulated luminescence (OSL) of quartz has been widely used to estimate the deposition age of sediments and is usually regarded as an accurate and precise dating method (e.g. Murray & Olley, 2002). However, the fast component of the quartz OSL signal (the component normally used for dating) saturates at doses of 200–400 Gy (Wintle & Murray, 2006). This implies a quartz upper age limit of ~50–70 ka for loess deposits for a typical dose rate of between 3 and 4 Gy/ka (e.g. Frechen, 1992, Roberts, 2008, Schmidt et al., 2011).

In contrast, the infrared stimulated luminescence (IRSL) signals from feldspars grow to much higher doses than those from quartz, and this offers the possibility of significantly extending the age range. Several studies report the application of luminescence to limnic sediments (e.g. Degering & Krbetschek, 2007b), but infrared stimulated luminescence (IRSL) on maar sediments has only been used in a few studies (e.g. Lang & Zolitschka, 2001, Degering & Krbetschek, 2007a). Lang & Zolitschka (2001) obtained reliable IRSL ages only for clastic-rich horizons; IRSL ages of sediments with high concentrations of biogenic material were inaccurate. Degering & Krbetschek (2007a) provided two IRSL ages (multiple aliquot additive dose protocol, MAAD) from the Jungfernweiher.

Luminescence dating of feldspars tends to underestimate the age, because of anomalous fading (Wintle, 1973) caused by quantum-mechanical tunnelling (Visocekas, 1985). Feldpar dating is normally carried out using a 50° C IR stimulation with detection in the blue (-violet) spectrum. Many studies have shown that the IRSL ages without fading correction consistently underestimate quartz OSL ages (e.g. Schmidt et al., 2010) due to anomalous fading. Hence the fading rate (g-value; Aitken, 1985) has to be determined in the laboratory and the ages corrected for this effect. Several methods of age corrections have been proposed (e.g. Huntley & Lamothe, 2001; Lamothe et al., 2003) and many studies give corrected IRSL ages which are in good agreement with quartz OSL ages. However, there is no ge-neral consensus as to which correction method should be used and the most commonly adopted method is only valid for the 'linear part' of the dose response curve (Huntley & Lamothe, 2001). Clearly, if the fading rate could be reduced, feldspar dating would be more

E&G / Vol. 60 / No. 1 / 2011 / 105–115 / DOI 10.3285/eg.60.1.07 / © Authors / Creative Commons Attribution License

reliable. Thomsen et al. (2008) found out that stimulation at elevated temperatures significantly reduces the fading rate. Based on this study Buylaert et al. (2009) tested a SAR protocol with detection in the blue (320–460 nm); this involves a stimulation with IR for 100s at 50°C prior to an elevated temperature stimulation with IR for 100s at 225°C, a so called post-IR IRSL measurement sequence. They have shown that the observed fading rates for the post-IR IRSL signal are significantly lower than those from the conventional IRSL at 50°C and that the signal is bleachable in nature. Thiel et al. (2011) extended this investigation following the observation of Murray et al. (2009) that the IR dosimetry trap lies above 320°C, and hence preheat temperatures up to this temperature can be used. In their study they chose a preheat of 320°C (60s) and a stimulation temperature of 290°C (200s) for the post-IR IRSL signal. They found natural signals from a sample below the Brunhes/Matuyama boundary in saturation on a laboratory growth curve and they concluded that they were unable to detect fading in this field sample.

The aim of this study is to investigate the applicability of luminescence dating using maar sediments, and ultimately to determine the accumulation rate of sediments within the archive and temporal succession of dust storms. The different IRSL signals are compared and discussed in regard to their performance in SAR; the equivalent doses (D_e) and the fading rates are then determined and ages calculated. The IRSL signal measured at 50°C and the subsequent post-IR IRSL signals measured at 225°C and 290°C are hereafter referred to as IR_{50}, $pIRIR_{225}$ and $pIRIR_{290}$ respectively. The results are discussed in terms of continuity of sedimentation and sedimentation rates.

2 Geological setting

The West Eifel volcanic field/Germany with an aerial extension of 600 km^2 is aligned NW-SE from Ormont to Bad Bertrich in Rhineland Palatinate, i.e. west of the river Rhine. Volcanism in the West Eifel Area started ca. 700 ka ago producing 250 eruptive centers with more than 50 maars, of which 8 are still filled with water (Büchel, 1984, Negendank & Zolitschka, 1993).

Sediment cores have been drilled by the ELSA project (Eifel Laminated Sediment Archive) in Eifel dry maar lakes to reconstruct the palaeoclimatic and palaeoenvironmental conditions as well as the history of the volcanism in the Eifel/Central Europe during the last glacial cycles. Two drillings (JW2 and JW3) have been carried out at the Jungfernweiher. JW3 was drilled close to center of the maar and exhibits a more undisturbed sedimentation and a better core quality than core JW2 which is located closer to the edge of the maar (Schaber & Sirocko, 2005). Seven samples for luminescence dating were taken from core JW3. According to Schaber & Sirocko (2005) coversand and loess layers were accumulated during high-glacial conditions and during cold phases rhythmic stratification of clay and silt was dominating. All samples were taken from a glacial cycle with mainly silt lamination. Additionally, one sample was taken from the drill core JW2. The sampled material consists of loessic gyttja with intercalated small bands of coarser silty to sandy material, which is supposed to originate from dust storms. Some independent age control is provided by 16 radiocarbon age estimates. However, the uncalibrated ages range from 35 ± 2 ka to 56 ± 4 ka and do not increase with depth. A study carried out by Lenaz et al. (2010) presents mineralogical data from core JW3 suggesting that the tephra layer at a depth of 107.39 m could be correlated with the Rocourt Tephra which has an age range between 90.3 and 74 ka (Pouclet et al., 2008). Luminescence dating was carried out by Degering & Krbetschek (2007a) on two samples with a depth of 104.5 m and 122.5 m from core JW2. They applied a multiple aliquot additive dose (MAAD) protocol on the polymineral fine-grain fraction and could not detect anomalous fading for their samples. They obtained equivalent doses (D_e) of 441 ± 49 Gy and 517 ± 62 Gy and calculated ages of 98 ± 15 ka and 117 ± 18 ka.

3 Experimental details

Samples were extracted under subdued red light and pretreated with 10% hydrochloric acid to remove carbonates, sodium oxalate to dissolve aggregates and 30% hydrogen peroxide to remove organic matter. The 4–11 µm silt fraction was separated and divided into two parts: (i) an untreated fraction used for polymineral infrared stimulated luminescence (IRSL) measurements, and (ii) a fraction from which quartz grains were extracted. The latter polymineral fraction was treated with 34% fluorosilicic acid (H_2SiF_6) for 6 days, preferentially dissolving feldspar grains, and leaving behind a quartz-rich extract. Finally, samples were prepared for measurement by settling either the polymineral or the quartz grains (4–11 µm) from acetone onto aluminium discs. The purity of the quartz extract was checked using the IR depletion ratio (Duller, 2003). All OSL/IRSL measurements were performed using an automated Risø TL/OSL-DA20 equipped with a $^{90}Sr/^{90}Y$ beta source. Quartz blue-stimulated OSL was measured for 40 s at 125°C and the signals were detected through 7.5 mm of Hoya U-340 filter (passing from 260 to 390 nm, i.e. UV). Feldspar IRSL was detected through Schott BG-39 and Corning 7-59 filters (passing from 320 to 460 nm; i.e. blue). For measurement of the equivalent dose (D_e) of quartz fine-grains a conventional SAR protocol (Murray & Wintle, 2000) was applied. The signal was integrated over the initial 1 s of stimulation, and a background based on the last 5 s of simulation subtracted. D_e estimates from polymineral fine-grains were determined using a post-IRSL elevated-temperature IR SAR protocol.

Radionuclide concentrations for all samples were obtained using high-resolution gamma spectrometry of sediment collected from the immediate surrounding of the samples. A water content of 20 ± 5 % was estimated for all samples. To derive the effective alpha dose rate, mean a-values of 0.04 ± 0.02 for quartz OSL and of 0.08 ± 0.02 for polymineral IRSL were assumed (Rees-Jones, 1995). The uranium, thorium, potassium contents and the dose rate of the samples are summarised in Table 1. The concentrations of uranium, thorium and potassium were converted into infinite-matrix dose rates using the conversion factors of Adamiec & Aitken (1998) and water-content attenuation factors (Aitken, 1985). Estimation of the cosmic-ray dose rate was calculated according to Prescott & Stephan (1982) and Prescott & Hutton (1994) from a knowledge of burial depth, altitude, matrix density, latitude and longitude for

Tab. 1: Dose rate data from potassium, uranium and thorium content, as measured by gamma spectrometry.

Tab. 1: Dosimetrische Ergebnisse basierend auf Kalium, Uran und Thorium Gehalt (gemessen mit Gammaspektrometrie).

Sample	Uranium (ppm)	Thorium (ppm)	Potassium (%)	IRSL dose rate (Gy/ka)	OSL dose rate (Gy/ka)
JWS1	2.78 ± 0.04	13.33 ± 0.10	2.49 ± 0.02	4.25 ± 0.21	3.85 ± 0.21
JWT3	2.90 ± 0.04	14.22 ± 0.12	2.59 ± 0.03	4.44 ± 0.21	4.02 ± 0.22
JWT9	2.85 ± 0.04	14.56 ± 0.04	2.76 ± 0.03	4.60 ± 0.23	4.18 ± 0.23
JWT5	3.03 ± 0.04	11.85 ± 0.09	1.91 ± 0.02	3.70 ± 0.19	3.31 ± 0.19
JWT7	2.67 ± 0.04	11.59 ± 0.10	1.81 ± 0.02	3.96 ± 0.20	3.65 ± 0.20
JWS8	3.43 ± 0.05	11.81 ± 0.12	1.55 ± 0.03	3.51 ± 0.18	3.09 ± 0.18
JWT8	3.21 ± 0.04	11.55 ± 0.10	1.74 ± 0.02	3.58 ± 0.18	3.18 ± 0.18
JWT9	3.17 ± 0.05	13.27 ± 0.08	2.22 ± 0.02	4.04 ± 0.21	3.67 ± 0.21

each sample. The uranium, thorium, potassium content and total dose rates are shown in Table 1. The mean dose rate is 3.61 ± 0.15 Gy/ka for quartz and 4.01 ± 0.15 Gy/ka for polymineral samples.

4 Luminescence dating

4.1 OSL dating of quartz

To test the suitability of the SAR protocol to the samples from the Jungfernweiher, and to confirm the most appropriate preheat temperature, the dose recovery ratio (Murray & Wintle, 2003) was determined for preheat temperatures between 200 and 260°C for 10 s following all natural and regeneration doses, and 200°C for 1 s following all test doses, using sample JWS 1. The aliquots were first bleached twice with 1000 s blue stimulation at room temperature separated by a 5000 s pause to allow the decay of any charge transferred to the 110°C TL trap, before giving a dose approximately equal to the natural dose. This dose was then measured in the same manner as if measuring the equivalent dose to provide confirmation that the protocol is able to recover a known dose successfully. If the SAR protocol is appropriate for our samples, the measured to given dose ratio should be close to unity. The measured dose/given dose ratio is close to unity for preheat temperatures of 220°C and 240°C (0.99 ± 0.01). We chose a preheat temperature of 240°C for our measurements. Fig. 2 shows the dose response curve for sample JWS1. This curve is representative for all measured samples. Fine-grain equivalent doses (D_e) were measured for samples JWS1, JWT3 and JWT7 and range from 440 ± 30 Gy to 580 ± 40 Gy (Table 3); the D_0-values for all samples are about ~130-150 Gy, when the dose response curve is fitted to a single saturating exponential plus linear function,

$$I = I_{max} (1-\exp(-D/D_0)) + kD,$$

(1) where I is the sensitivity corrected OSL intensity, I_{max} is saturation intensity of OSL, D is dose, and D_0 is the characteristic saturation dose.

Wintle & Murray (2006) suggested equivalent dose (D_e) values should only be reported up to ~$2D_0$. In our case it should therefore be possible to measure doses up to about ~260–300 Gy using our material, although the laboratory-generated dose response curves continue to grow up to ~ 1000 Gy, because of a more slowly saturating component which is expressed by the linear term in equation 1. Buylaert et al. (2007), Timar et al. (2010) and Lowick et al. (2010a,b) made similar observation for their fine-grain quartz samples and concluded that equivalent doses larger than $2D_0$ (~120-140 Gy) were not very reliable. At doses higher than this value they observed an increasing age underestimation towards the Eemian. The samples described by Lowick et al. (2010b) passed all standard performance criteria and still show an increasing dose response curve at 500 Gy. Taking all these observations into account, we consider our quartz fine-grain equivalent doses to be in or close to saturation, and conclude that they provide a minimum dose estimate of ~450 Gy for the youngest sample.

4.2 IRSL dating of polymineral fine-grains

Post-IR IRSL measurement sequence

Based on the work of Thomsen et al. (2008), Buylaert et al. (2009) proposed a new SAR protocol, with detection in the blue (320–460 nm). This protocol involved elevated temperature stimulation with IR for 100 s at 225°C ($pIRIR_{225}$), following stimulation with IR for 100 s at 50°C, a so-called post-IR IRSL measurement sequence (Table 2), and these authors chose a preheat of 250°C to make their results comparable to other studies. Recently Thiel et al. (2011) used a preheat of 320°C for 60 s for their post-IR IRSL protocol and used a stimulation at 290°C for 200 s after bleaching the aliquots with IR diodes at 50°C for 200 s to date polymineral fine-grains. Buylaert et al. (2009) showed that the observed fading rates for their post-IR IRSL signal (stimulated at 225°C) were significantly lower than from the conventional IR_{50} and that the signal is bleachable in nature. Thiel et al. (2011) reported

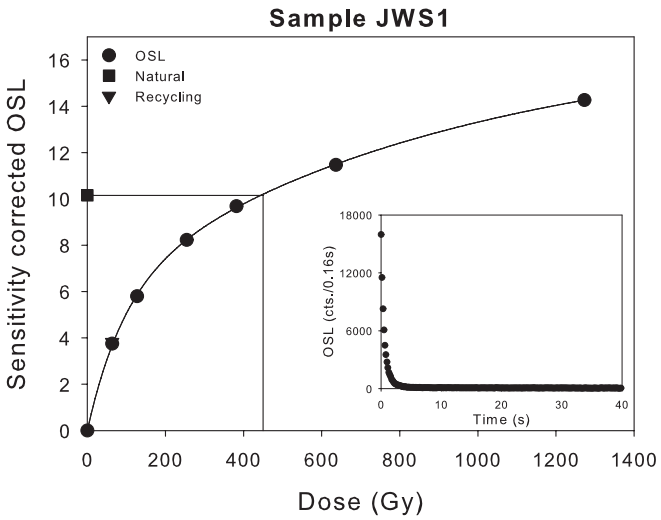

Fig. 2: Dose response and decay curve for sample JWS1 showing the OSL from fine grain quartz.

Abb. 2: Aufbaukurve und Zerfallskurve für Probe JWS1 für OSL von Feinkorn Quarz.

Tab. 2: Elevated temperature post-IR IRSL measurement sequence.

Tab. 2: Post-IR IRSL Messprotokoll.

Step	Treatment	Observed
1	Dose	
2	Preheat, 60s at 250°C / 60s at 320°C	
3	IR stimulation, 100s at 50°C / 200s at 50°C	Lx
4	IR stimulation, 100s at 225°C / 200s at 290°C	Lx
5	Test dose	
6	Preheat, 60s at 250°C / 60s at 320°C	
7	IR stimulation, 100s at 50°C / 200s at 50°C	Tx
8	IR stimulation, 100s at 225°C / 200s at 290°C	Tx
9	IR stimulation, 40s at 290°C / 40s at 325°C	
10	Return to step 1	

natural signals in saturation on the laboratory growth curve and concluded that fading is negligible for their samples.

In this study, the $pIRIR_{225}$ protocol is applied to polymineral fine-grains from the Jungfernweiher, and in addition the $pIRIR_{290}$ is measured for two samples. The initial 2 s of the post-IR IR signal are used for calculating the D_e values, with a background based on the signal observed in the last 10 s of the decay curve. To test for anomalous fading and to compare the fading rates of the IR_{50}, the $pIRIR_{225}$ and the $pIRIR_{290}$, those aliquots which had been used for D_e measurement were then used to test for fading, by dosing and preheating the aliquots and then storing for various delays after irradiation and before measurement. This sequence was repeated several times on each aliquot. The fading rates are expressed in terms of the percentage decrease of intensity per decade of time (g-value; Aitken, 1985; Auclair et al., 2003). G-values were calculated according to Huntley & Lamothe (2001) using the signal integration limits as for the D_e calculation. Fading corrections use the methods proposed in Huntley & Lamothe (2001); it is recognised that this method is strictly applicable only for natural doses in the linear region of the growth curve, although Buylaert et al. (2008; 2009; in press) have shown that the correction can give accurate ages outside of this range.

Luminescence characteristics and performance in SAR

The dose response curves and the decay curves for IR_{50} and $pIRIR_{225}$ for the uppermost sample JWS1 (~17 m) and for the lowermost sample JWT8 (~94 m) is shown in Fig. 3a,b. The curves are representative for all the other samples measured using the $pIRIR_{225}$. The natural IRSL signal clearly lies below the natural post-IR IRSL signal, by about 15–20% on average. The shapes of the growth curves are similar but the growth curve for IR_{50} tends to lie somewhat above the curve for $pIRIR_{225}$ for all our samples. Fig.4 a, b shows corresponding dose response and decay curves for IR_{50} and $pIRIR_{290}$ for the uppermost sample JWS1 (~17 m) and for one of the lowermost samples JWS8 (~94 m). As for $pIRIR_{225}$, the natural $pIRIR_{290}$ lies clearly above the natural IRSL signal, and the growth curves for IR50 lie somewhat above the curves for $pIRIR_{290}$ for all samples. Fig. 5 a, b show dose response curves and decay curves for IR_{50}, the $pIRIR_{225}$ and $pIRIR_{290}$ for sample JWT9. This is in contrast to the study of Buylaert et al. (2009) who observed that the shape of the growth curves for IR50 and $pIRIR_{225}$ are indistinguishable. Thiel et al. (2011) also investigated IR_{50} and $pIRIR_{290}$ growth curves and observed very similar shapes. In our study, the $pIRIR_{225}$ from all the samples is brighter (~12-20%) than for the IR_{50}. The $pIRIR_{290}$ is ~3 times brighter than for the IR_{50}. Buylaert et al. (2009) and Thiel et al. (this issue) made similar observations. Recycling ratios for our samples range from 0.96 ± 0.01 to 1.02 ± 0.02 for the IR_{50} and from 0.95 ± 0.02 to 0.98 ± 0.01 for $pIRIR_{225}$. Recuperation for all the IRSL, $pIRIR_{225}$ and $pIRIR_{290}$ signals is below 5% of the natural signal. To test the applicability of the post-IR IRSL protocol using a stimulation temperature of 225°C, the dose recovery ratio was measured for all samples (Murray & Wintle, 2003). The aliquots were bleached for 4 hours in a Hönle SOL2 solar simulator before giving a dose approximately equal to the natural dose. Fig. 6a shows the results of the dose recovery test for all samples for IR_{50} and $pIRIR_{225}$. The mean ratio of the measured to given dose is 1.060 ± 0.011, n = 21 for IR_{50} and 0.98 ± 0.006, n = 21 for $pIRIR_{225}$ confirming the suitability of our post-IR IRSL protocol. To confirm that IRSL and post-IR IRSL signals are bleachable by natural daylight we exposed three aliquots per sample for four hours to a Hönle SOL2 solar simulator and then measured the apparent dose in the usual manner. The results are shown in Fig. 6 b. The residual doses range from 2.21 ± 0.13 Gy to 2.84 ± 0.01 Gy, with a mean of 2.37 ± 0.15 Gy (n = 18) for IR_{50} and from 3.92 ± 0.51 Gy to 5.54 ± 0.91 Gy, with a mean of 4.88 ± 0.19 Gy (n = 19) for $pIRIR_{225}$. The residual doses were subtracted from the measured equivalent doses (D_e) for age calculation.

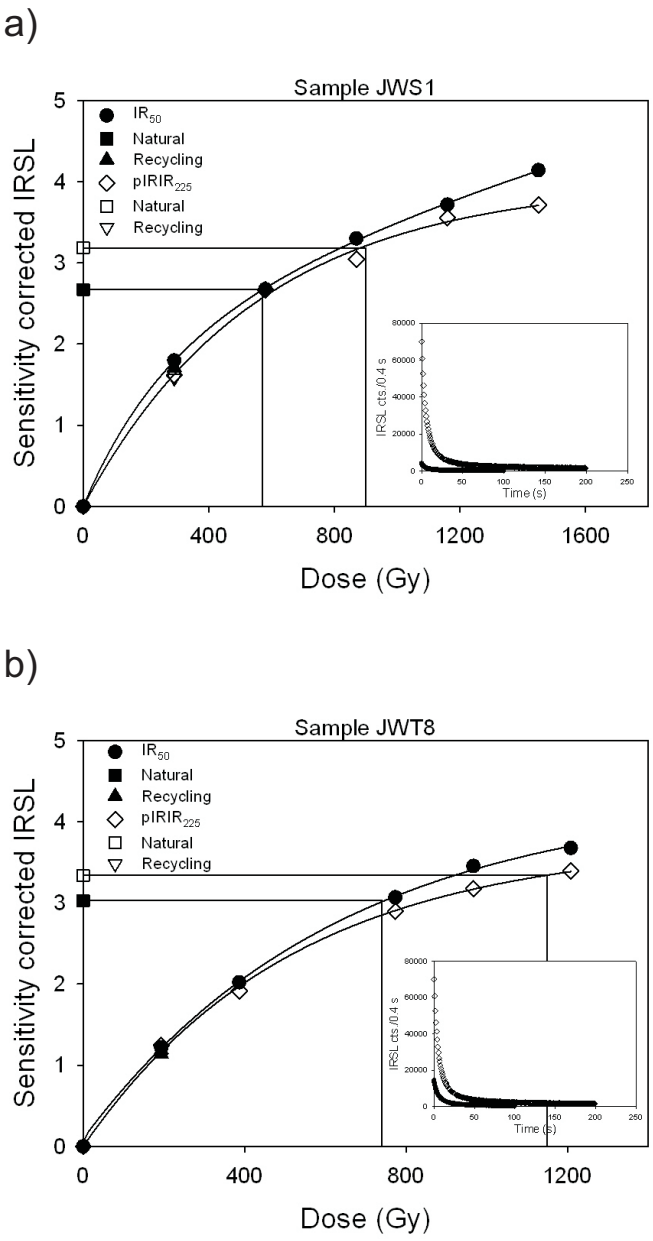

Fig. 3: Dose response and decay curves for sample a) JWS1 and b) JWS8 showing the IR_{50} (filled symbols) and the $pIRIR_{225}$ (open symbols).

Abb. 3: Aufbaukurve und Zerfallskurve für Proben a) JWS1 (gefüllte Symbole) und b) JWS8 (offene Symbole) für das IR_{50} und das $pIRIR_{225}$ Signal.

Equivalent Dose (D_e), fading rates and age estimates

Equivalent doses (D_e) have been measured using IR_{50} and $pIRIR_{225}$ for all samples, and $pIRIR_{290}$ for three samples. Table 3 summarises the equivalent doses, saturation of the signal, recycling ratio, dose recovery results, residual doses, g-values and the resulting luminescence ages for all samples. The equivalent doses (D_e) obtained using the IR_{50} are in the range of ~500–700 Gy for core JW3 except for sample JWT8 which gives a significantly higher dose of 871 ± 63 Gy. These De estimates give minimum (uncorrected for fading) age estimates between 113 ± 9 ka and 240 ± 20 ka. De values obtained for IR_{50} do not increase systematically with depth, and indicate that this signal is in field saturation (equilibrium between the accumulation of new charge and the loss by anomalous fading) at ~500 Gy. Similar results were obtained by Degering & Krbetschek (2007a) on two samples with a depth of 104.5 m and 122.5 m from core JW2 from Jungfernweiher. They applied a multiple aliquot additive dose (MAAD) protocol to the polymineral fine-grain fraction and obtained equivalent doses (De) of 441 ± 49 Gy and 517 ± 62 Gy. The D_0-values of all IRSL and post-IR IRSL signals are about ~500–600 Gy suggesting that doses up to about ~1000-1200 Gy can be measured. The equivalent doses obtained using $pIRIR_{225}$ from feldspar range from 846 ± 52 Gy to 1174 ± 64 Gy for core JW3, which is ~25–50% higher than those obtained using IR_{50}. The De values of $pIRIR_{225}$ increase with depth, but the values for the lowermost two samples are already in the range of $2D_0$. This suggests a minimum uncorrected age of ~200 ka for the youngest sample. De values for $pIRIR_{290}$ signal are only available for sample JWS 1 (1137 ± 17 Gy) and for sample JWS 8 (1373 ± 53 Gy); these values are ~15–25% higher than the equivalent doses (D_e) obtained using the $pIRIR_{225}$ and give minimum age estimates of ~260 ka for the youngest sample and ~390 ka for one of the two oldest samples of JW3. The ages increase with depth but the De values are in the range of or exceed $2D_0$. The uncorrected $pIRIR_{225}$ ages underestimate the uncorrected $pIRIR_{290}$ age estimates by about 25–30 % on average, presumably because the $pIRIR_{225}$ signals have to be corrected for fading. The ratio of the sensitivity-corrected natural signal to the laboratory saturation level was calculated for IR_{50}, $pIRIR_{225}$ and for $pIRIR_{290}$ signals, and average values of 0.58 ± 0.04, 0.79 ± 0.03 and 0.79 ± 0.01 for IR_{50}, $pIRIR_{225}$ and $pIRIR_{290}$ were obtained, respectively. Schmidt et al. (submitted) tested the $pIRIR_{290}$ protocol on polymineral fine grains from Serbian loess investigating the behavior of both IR_{50} and $pIRIR_{290}$ in material close to or in saturation with a focus on the relationship between field and laboratory saturation. They could demonstrate that field saturation is equal to laboratory saturation for $pIRIR_{290}$, i.e., the ratio of the natural signal to the laboratory saturation level is close to 1. These findings show that the measured samples are not yet in field saturation for $pIRIR_{290}$ signal. Sample JWT9 (Fig.5 a,b), which was taken from core JW2 was measured using IR_{50}, $pIRIR_{225}$ and $pIRIR_{290}$. The equivalent doses (D_e) obtained using IR50 are around 600 Gy, which is in the range of the field saturated results for JW3 using this signal. For pIRIR225 an equivalent dose (D_e) of 1041 ± 30 Gy was measured, which is in the range of $2D_0$. For $pIRIR_{290}$ an equivalent dose (D_e) could not be calculated as the natural signal lies very close to the saturation level; the ratio of the sensitivity-corrected natural signal to the laboratory saturation level is 0.99 ± 0.01 (n=3) indicating that this sample is in saturation. Therefore, only a minimum dose estimate of ~270 ka based on the $2D_0$ value (86% of saturation) can be derived (~1100 Gy).

The measured fading rates for IR_{50}, $pIRIR_{225}$ and $pIRIR_{290}$ are shown in Fig. 7. For IR_{50}, the g-values range from 3.64 ± 0.12%/decade to 4.79 ± 0.11%/decade, with an average of 4.09 ± 0.02%/decade, n = 21, and for the $pIRIR_{225}$ signal, from 2.1 ± 0.2%/decade to 3.3 ± 1.0%/decade, with an average of 2.55 ± 0.14%/decade, n = 21 (Fig. 8). These data suggest that $pIRIR_{225}$ fades by ~40% less than IR_{50}. For sample JWS1 a g-value of 0.5 ± 1.1%/decade for $pIRIR_{290}$ was obtained. Similar fading rates for the $pIRIR_{225}$ and $pIRIR_{290}$ are reported by Thiel et al. (this issue) for their polymineral fine-grain samples, although they measured lower fading rates for IR_{50}. The fading corrected age estimates for IR_{50} and $pIRIR_{225}$ are

E&G / Vol. 60 / No. 1 / 2011 / 105–115 / DOI 10.3285/eg.60.1.07

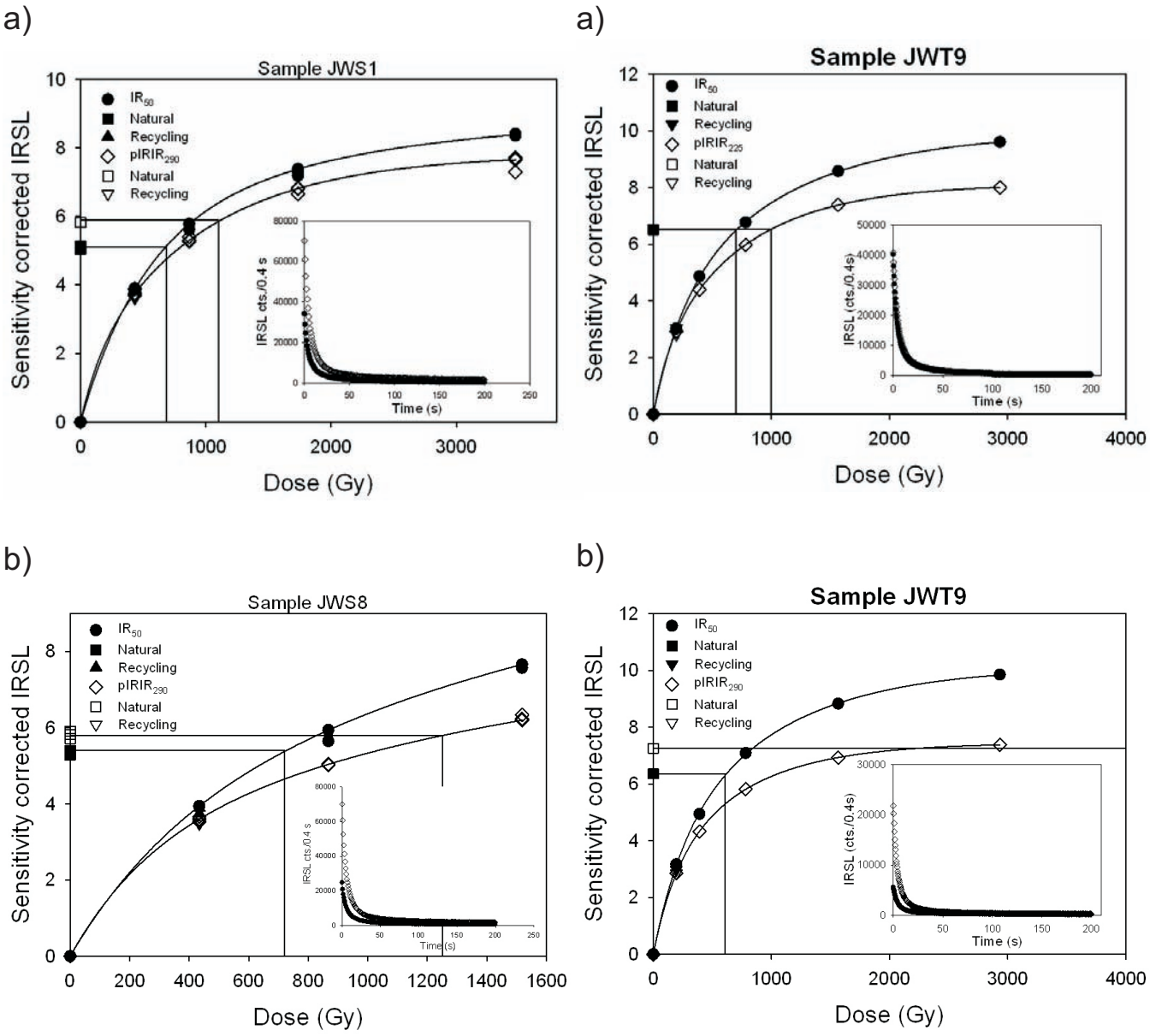

Fig. 4: Dose response and decay curves for sample a) JWS1 and b) JWT8 showing the IR_{50} (filled symbols) and the $pIRIR_{290}$ (open symbols).

Abb. 4: Aufbaukurve und Zerfallskurve für Proben a) JWS1 (gefüllte Symbole) und b) JWS8 (offene Symbole) für das IR_{50} und das $pIRIR_{290}$ Signal.

Fig. 5 a, b: Dose response and decay curves for sample JWT9 showing the IR_{50}, $pIRIR_{225}$ and the $pIRIR_{290}$.

Abb. 5 a, b: Aufbaukurve und Zerfallskurve für Probe JWT9 für das IR_{50}, das $pIRIR_{225}$ und das $pIRIR_{290}$ Signal.

listed in Table 3. The IR_{50} age estimates range from 188 ± 19 ka to 400 ± 80 ka. The age estimates for $pIRIR_{225}$ range from 270 ± 40 ka to >450 ka. The age estimates for $pIRIR_{290}$ are not fading corrected; Thiel et al. (2011) argue that fading rates below 1%/decade may not be significant, based on their finding of natural signals in saturation on a laboratory growth curve. The age estimates obtained for IR_{50} are consistently lower than those from $pIRIR_{225}$, except for sample JWT 3 and JWT 8. In contrast, our fading corrected $pIRIR_{225}$ age estimates are consistent with those from the uncorrected $pIRIR_{290}$. The underestimates from IR_{50} are consistent with the observation that this signal is in field saturation.

5 Discussion

Both $pIRIR_{225}$ and $pIRIR_{290}$ D_e values from the youngest sample (~16 m below modern surface) indicate a minimum (uncorrected for fading) age of ~200 ka for the deposits from Jungfernweiher. Fading corrected $pIRIR_{225}$ and uncorrected $pIRIR_{290}$ age estimates increase with depth from ~250 ka for the uppermost sample up to ~400 ka for the oldest samples taken ~94 m below modern surface indicating an accumulation of ~100 m over at least 150 ka. Thus according to post-IR IRSL ages, Jungfernweiher was effectively filled up with sediments ~250 ka ago, and there either has been very little deposition since then, or younger sediments have been eroded. However, there are uncalibrated radiocarbon age estimates ranging from 34.5 ± 2.1 ka BP to 56 ± 4 ka BP (no systematic increase with depth) which might indicate that these deposits are of late Weichselian age. Lenaz et al. (2010) also regard it as possible that the tephra layer at a depth of 107.39 m could be correlated with the Rocourt Tephra which has an age range between 90.3 and 74 ka. One possible explanation for our high D_e-values can be based on

Tab. 3: Summary of equivalent dose (D_e), saturation level, recycling ratio, dose recovery, residual doses, fading and luminescence ages. Six aliquots were measured per sample for dose determination. For the fading tests three aliquots/sample were measured.

Tab. 3: Äquivalenzdosen (D_e), Sättigungsniveau, Recycling Ratio, Dose Recovery, residuale Dosen, Fading und Lumineszenzalter. Sechs Aliquots wurden pro Probe für die Aquivalenzdosis-Bestimmung gemessen. Für die Fadingmessungen wurden drei Aliquots/Probe verwendet.

Sample	Depth	Measurement	De [Gy]	Saturation	Recycling	Measured/ given dose	Residuals [Gy]	g-value [%]	uncorrected Age [ka]	corrected Age [ka]
JWS1	16.60–16.62 m	IR50	527 ± 29	0.47 ± 0.02	0.96 ± 0.01	1.02 ± 0.003	2.49 ± 0.22	3.64 ± 0.12	124 ± 9	188 ± 19
		pIRIR225	846 ± 52	0.72 ± 0.04	0.98 ± 0.01	0.94 ± 0.05	3.92 ± 0.51	2.63 ± 0.34	199 ± 16	271 ± 35
		pIRIR290	1137 ± 17	0.79 ± 0.004	0.97 ± 0.01			0.52 ± 1.12	>270	
		OSL	441 ± 28		0.99 ± 0.02	0.97 ± 0.01			>100	
JWT3	18.54–18.56 m	IR50	686 ± 66	0.58 ± 0.03	0.99 ± 0.01	1.02 ± 0.13	2.21 ± 0.13	4.79 ± 0.11	154 ± 16	270 ± 31
		pIRIR225	921 ± 63	0.79 ± 0.03	0.97 ± 0.01	0.98 ± 0.03	5.54 ± 0.91	2.31 ± 0.48	207 ± 17	271 ± 44
		pIRIR290								
		OSL	523 ± 17		0.97 ± 0.01				>100	
JWT9	21.58–21.70 m	IR50	524 ± 30	0.41 ± 0.02	0.97 ± 0.02	1.04 ± 0.007		4.52 ± 0.23	113 ± 9	191 ± 28
		pIRIR225	936 ± 46	0.69 ± 0.03	0.97 ± 0.03	0.97 ± 0.04		3.33 ± 1.02	203 ± 14	297 ± 99
		pIRIR290								
		OSL								
JWT5	44.64–44.72 m	IR50	602 ± 26	0.6 ± 0.002	1.01 ± 0.07	1.10 ± 0.11	2.53 ± 0.04	4.35 ± 0.50	162 ± 12	271 ± 42
		pIRIR225	928 ± 38	0.79 ± 0.04	0.98 ± 0.01	0.99 ± 0.015	5.14 ± 0.63	2.45 ± 0.19	250 ± 18	336 ± 39
		pIRIR290								
		OSL								
JWT7	65.29–65.40 m	IR50	641 ± 37	0.65 ± 0.02	1.02 ± 0.02	1.12 ± 0.001	2.59 ± 0.02	3.98 ± 0.37	161 ± 12	258 ± 44
		pIRIR225	927 ± 61	0.87 ± 0.02	0.97 ± 0.01	1.00 ± 0.01	5.65 ± 0.28	2.51 ± 0.24	234 ± 20	316 ± 39
		pIRIR290								
		OSL	581 ± 54		0.98 ± 0.02				>100	
JWS8	93.12–93.15 m	IR50	598 ± 32	0.57 ± 0.03	0.96 ± 0.02	1.08 ± 0.002	2.84 ± 0.01	4.21 ± 0.43	170 ± 13	279 ± 41
		pIRIR225	1174 ± 64	0.86 ± 0.02	0.98 ± 0.02	0.96 ± 0.03	4.83 ± 0.03	2.48 ± 0.38	334 ± 25	>450
		pIRIR290	1373 ± 53	0.78 ± 0.03	0.98 ± 0.01				>390	
		OSL								
JWT8	93.73–93.83 m	IR50	871 ± 63	0.75 ± 0.05	0.98 ± 0.02	1.04 ± 0.01	2.52 ± 0.26	4.15 ± 0.61	243 ± 22	397 ± 79
		pIRIR225	1143 ± 49	0.86 ± 0.01	0.95 ± 0.01	1.02 ± 0.02	4.97 ± 0.23	2.11 ± 0.21	319 ± 21	>410
		pIRIR290								
		OSL								
JWT9 (core JW2)	104.5–104.6 m	IR50	600 ± 24	0.65 ± 0.01	0.99 ± 0.02				149 ± 10	
		pIRIR225	1041 ± 30	0.87 ± 0.01	0.98 ± 0.01				259 ± 15	
		pIRIR290 OSL	> 930*	0.99 ± 0.01	0.97 ± 0.01				>270	

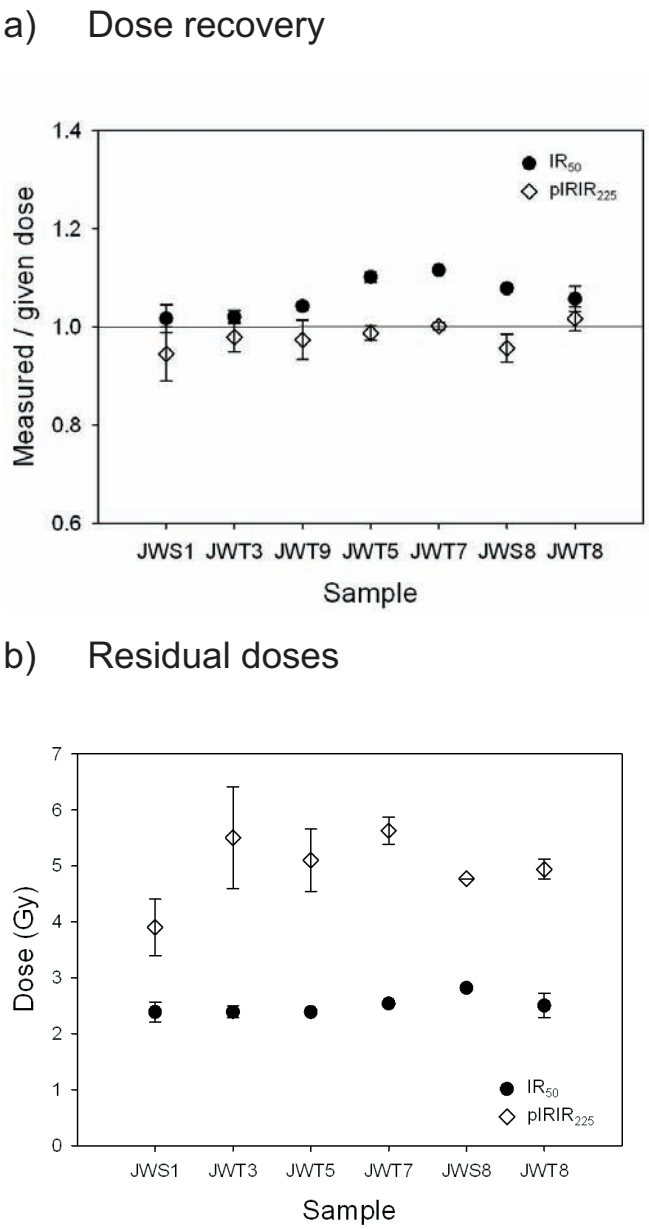

Fig. 6: Dose recovery test (a) and the residual doses (b) for the IR_{50} and the $pIRIR_{225}$ signal for all samples. Three aliquots were measured per sample. Error bars represent 1-sigma standard error.

Abb. 6: Dose recovery test (a) und residuale Dosen (b) für das IR_{50} und das $pIRIR_{225}$ Signal für alle Proben. Drei Aliquots wurden pro Probe gemessen. Die Fehlerbalken stellen den 1-sigma Standardfehler dar.

mixing of well-bleached aeolian dust with locally eroded old (field saturated) crater-wall sediment – then the sediment would have been deposited with an average finite residual dose, perhaps close to saturation. However, a simple mixing model indicates that for such a mixture to have been deposited at, say, ~20 ka, one would require >75% of the total lake sediment to be locally-derived old material in order to give a dose indistinguishable from field saturation today. Such a large catchment input to a maar lake seems very unlikely. Overestimated D_e-values could, of course, also arise because of incomplete bleaching. However, it seems most likely that the laminated coarser dust-storm and loess layers were deposited during high-glacial times; if such aeolian dust is making up a very large part of the sediment inventory it is difficult to accept that the IRSL is not well-bleached. There is considerable evidence in the literature that the IR_{50} from loess and from sediments originating from dust storms is well bleached (Roberts, 2008). It is also known that the fast component of quartz can be depleted in only a few minutes exposure to daylight (Godfrey-Smith et al., 1988) and yet we still obtain an equivalent dose for the fine-grain quartz of 441 ± 28 Gy giving a minimum age estimate of ~100 ka based on the $2D_0$ value of ~260–300 Gy for the youngest sample. Finally, a study from a nearby East Eifel crater fill (Schmidt et al, 2011) showed that the pulsed $pIRIR_{150}$ from loess deposits in this area is in fact well bleached. Their luminescence age estimates are in good agreement with stratigraphic evidence and with independent age control provided by $^{40}Ar/^{39}Ar$ dating of intercalated air-fall tephra and scoria. Thus we appear to have a discrepancy between the established stratigraphy and all IRSL data. Most of the radiocarbon ages are in the range of ~43–55 ka (except for one of ~35 ka) which is at or close to the upper age limit of the method. Luminescence age estimates are provided by Degering & Krbetschek (2007a) on two samples with a depth of 104.5 m and 122.5 m from core JW2 yielding equi-valent doses (D_e) of 441 ± 49 Gy and 517 ± 62 Gy. Age estimates of 98 ± 15 ka and 117 ± 18 ka were calculated for these samples. To enable comparison of our results for samples from the drill core JW3 and the published age estimates of Degering & Krbetschek (2007a) we additionally measured one sample (JWT9) from drill core JW2 taken from a depth of 104.5 m. The results show that this sample is in saturation for all the different signals, IR_{50}, $pIRIR_{225}$ and for $pIRIR_{290}$ suggesting a minimum age estimate of ~270 ka for $pIRIR_{290}$ signal for this sample. The calculated age estimates of Degering & Krbetschek (2007a) are underestimating our results significantly. One possible reason might be field saturation of their signal, i.e. the trap filling and anomalous fading had reached to the equilibrium state. In addition, the association of the tephra at 107 m with the Rocourt Tephra is not secure. In our view the post-IR IRSL ages represent the most secure ages for this deposit. It has to be mentioned, that one co-author (F.Sirocko) does not agree with this interpretation and proposes an alternative stratigraphy for core JW3 and neighbouring core JW2 (see appendix).

6 Conclusion

We have investigated the application of luminescence dating to maar lake sediments from the dry maar Jungfernweiher in the West Eifel volcanic field by using quartz OSL and two different protocols for feldspar IRSL. Using OSL, we obtained D_e values ranging from 440 ± 30 Gy to 580 ± 40 Gy for the fine-grain quartz extracts.All these results exceed the 2D0 value of ~260–300 Gy corresponding to minimum ages of ~80–100 ka (although the laboratory growth curve does not fully saturate before ~1000 Gy). For polymineral fine-grains, the D_e values obtained for IR_{50} do not increase with depth, and indicate that this signal is in field saturation at ~500 Gy. The D_e values for $pIRIR_{225}$ and $pIRIR_{290}$ are increasing with depth from ~800 Gy to ~1400 Gy, suggesting a minimum age of ~200 ka for the youngest material, although the obtained equivalent doses (D_e) are already in the range or exceeding $2D_0$ for two bottom samples for JW3 and the sample from JW2. Mean laboratory fading rates are 4.09 ± 0.02%/decade for IR_{50} and 2.55 ± 0.14%/decade for $pIRIR_{225}$.

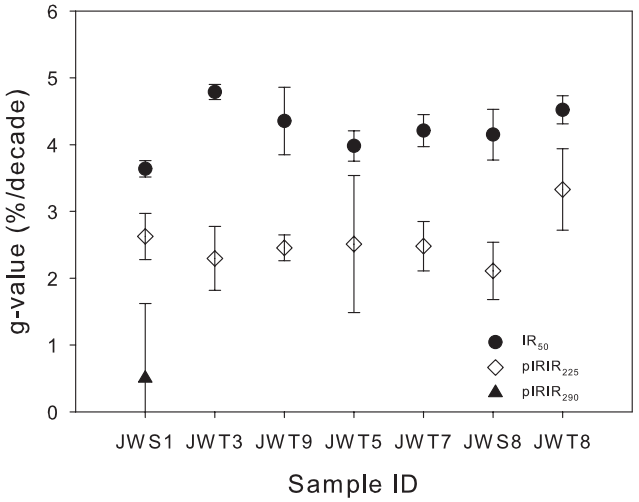

Fig. 7: Fading rates for the post the IR_{50} and $pIRIR_{225}$ signals for all samples. Three aliquots were measured per sample. Error bars represent 1-sigma standard error.

Abb. 7: Fadingraten für das IR_{50} und das $pIRIR_{225}$ Signal für alle Proben. Drei Aliquots wurden pro Probe gemessen. Die Fehlerbalken stellen den 1-sigma Standardfehler dar.

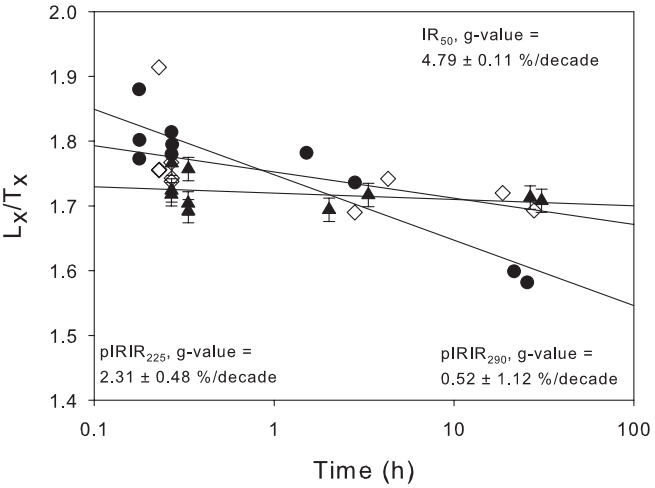

Fig. 8: Anomalous fading of $IRSL_{50}$, $pIRIR_{225}$ and $pIRIR_{290}$ signals.

Abb. 8: Anomalous fading für $IRSL_{50}$, das $pIRIR_{225}$ und das $pIRIR_{290}$ Signal.

Although we observed a g-value of 0.52 ± 1.12%/de-cade for $pIRIR_{290}$ from sample JWS1, we have chosen not to correct the age estimates for $pIRIR_{290}$ for fading. Corrected age estimates for $pIRIR_{225}$ range from 270 ± 40 ka to >450 ka. These ages are consistent with uncorrected $pIRIR_{290}$ age estimates. Not surprisingly, fading corrected age estimates obtained for IR_{50} underestimate the fading corrected age estimates for $pIRIR_{225}$. However radiocarbon age estimates and a possible tephra association suggest that these dated deposits should be of late Weichselian age. Based on the results from a simple sediment mixing model and on the results from analyses of well-bleached aeolian material from the nearby East Eifel, it is not likely that the high D_e-values observed within this study could originate from mixing or incomplete bleaching. Therefore we regard the results from the luminescence measurements conducted within this study to represent the most reliable age estimates for the sediments from the Jungfernweiher. The discrepancy between the established stratigraphy and the IRSL data from this study remains to be explained.

Acknowledgements

This research is part of the PhD study of EDS in the framework of the "Leibniz Pakt für Forschung und Innovation" at the LIAG-Institute in Hannover. EDS wishes to thank all members of the Sedimentology group of the Institute of Geosciences at the Johannes Gutenberg University in Mainz for their timely help, especially Stephan Dietrich, Klaus Schwibus and Frank Dreher. Christopher Lüthgens and an anonymous reviewer are thanked for the useful comments on the manuscript.

References

Adamiec, M. & Aitken, M.J. (1998): Dose-rate conversion factors: update. – Ancient TL 16: 37–50.

Aitken, M.J. (1985): *Thermoluminescence* Dating, London.

Aitken, M.J. (1998): An Introduction to Optical Dating, Oxford.

Auclair, M., Lamothe, M. & Huot, S. (2003): Measurement of anomalous fading for feldspar IRSL using SAR. – Radiation Measurements 37: 487–492.

Büchel, G. (1984): Die Maare im Vulkanfeld der Westeifel, ihr geophysikalischer Nachweis, ihr Alter und ihre Beziehung zur Tektonik der Erdkruste. – PhD-Thesis, Univ. Mainz, 385 pp.

Buylaert, J.P., Murray A.S. & Huot S. (2008): Optical dating of an Eemian site in Northern Russia using K-feldspar. Radiation Measurements 43: 715–720.

Buylaert, J.P., Murray, A.S., Thomson, K.J. & Jain, M. (2009): Testing the potential of an elevated temperature IRSL signal from K-feldspar. – Radiation Measurements 44: 560–565.

Buylaert, J.P., Huot, S., Murray, A.S. & Van den haute, P., in press. Infrared stimulated luminescence dating of an Eemian (MIS 5e) site in Denmark using K-feldspar. – Boreas, 10.1111/j.1502-3885.2010.00156.x.

Buylaert, J.P., Vandenberghe, D., Murray, A.S., Huot, S., De Corte, F. & Van den haute, P. (2007): Luminescence dating of old (>70 ka) Chinese loess: a comparison of single-aliquot OSL and IRSL techniques. – Quaternary Geochronology 2: 9–14.

Degering, D. & Krbetschek, M. R. (2007a): Dating of Interglacial Deposits by Luminescence Methods. – In: Sirocko et al. (Eds.): The Climate of Past Interglacials, Elsevier: 157–172.

Degering, D. & Krbetschek, M. R. (2007b): Lumineszenzdatierungen an limnischen Sedimenten von Klinge/Kreis Forst. – Natur und Landschaft: 120–128.

Duller, G.A.T. (2003): Distinguishing quartz and feldspar in single grain luminescence measurements. – Radiation Measurement 37: 161–165.

Duller, G.A.T. (2004): Luminescence dating of quaternary sediments: recent advances. – Journal of Quaternary Science 19(2): 183–192.

Frechen, M. (1991): Systematic thermoluminescence dating of two loess profiles from the middle Rhine area (F.R.G.). – Quaternary Science Reviews 11: 93–101.

Godfrey-Smith, D.I., Huntley, D.J. & Chen, W.-H. (1988): Optical dating of quartz and feldspar extracts. – Quaternary Science Reviews 7: 373–380.

Huntley, D.J. & Lamothe, M. (2001): Ubiquity of anomalous fading in K-feldspars and the measurement and correction for it in optical dating. – Canadian *Journal* of *Earth* Sciences 38: 1093–1106.

Lamothe M., Auclair M., Hamzaoui C. & Huot S. (2003): Towards a prediction of long-term anomalous fading of feldspar IRSL. – Radiation Measurements 37: 493–498.

Lang, A. & Zolitschka, B. (2001): Optical dating of annually laminated lake sediments A test case from Holzmaar/Germany. – Quaternary Science Reviews 20: 737–742.

Lenaz, D., Marciano, R., Veres, D., Dietrich, S. & Sirocko, F. (2010): Mineralogy of the Dehner and Jungfernweiher maar tephras (Eifel, Germany). – N.Jb.Geol.Palaont.Abh. Fast track DOI 10.1127/0077-7749/2010/0062.

Lowick, S., Preusser, F., Wintle, A. (2010a): Investigating quartz optically stimulated luminescence dose-response curves at high doses. –Radiation Measurements 45: 975–984.

Lowick, S.E., Preusser, F., Pini, R. & Ravazzi, C. (2010b): Underestimation of fine grain quartz OSL dating towards the Eemian: comparison with palynostratigraphy from Azzano Decimo, northeastern Italy. –Quaternary Geochronology 5: 583–590.

Murray, A.S., Buylaert J.P., Thomsen, K.J. & Jain M. (2009): The effect of preheating on the IRSL signal from feldspar. – Radiation Measurements 44: 554–559.

Murray, A.S. & Wintle, A.G. (2003): The single regenerative dose protocol: potential for improvements in reliability. – Radiation Measurements 37: 377–381.

Murray, A.S. & Olley, J.M. (2002): Precision and accuracy in the optically stimulated luminescence dating of sedimentary quartz: a status review. – Geochronometria 21: 1–16.

Negendank, J.F.W. & Zolitschka, B. (1993): Maars and maar lakes of the Westeifel volcanic field. In: J.F.W. Negendank and B. Zolitschka (Editors), Paleolimnology of European Maarlakes. – Lecture Notes in Earth Sciences. Springer-Verlag: 61–80.

Pouclet, A., Juvigné, E. & Pirson, S. (2008): The Rocourt Tephra, a widespread 90-74 ka stratigraphic marker in Belgium. – Quaternary Research 70: 105–120.

Prescott, J.R. & Hutton, J.T. (1994): Cosmic ray contribution to dose rates for luminescence and ESR dating: large depths and long-term time variations. – Radiation Measurements 23: 497–500.

Prescott, J.R. & Stephan, L.G. (1982): The contribution of cosmic radiation to the environmental dose for thermoluminescence dating. – PACT 6: 17–25.

Rees-Jones, J. (1995): Optical dating of young sediments using fine-grain quartz. – Ancient TL 13: 9–14.

Roberts, H.M. (2008): The development and application of luminescence dating to loess deposits: a perspective on the past, present and future. – Boreas 37: 483–507.

Schaber, K. & Sirocko, F. (2005): Lithologie und Stratigraphie der spätpleistozänen Trockenmaare der Eifel. – Mainzer geowiss. Mitt. 33: 295–340.

Sirocko, F., Seelos, K., Schaber K., Rein, B., Dreher, F., Diehl, M., Lehné, R., Jäger, K., Krbetschek, M. & Degering, D. (2005): A Late Eemian Aridity Pulse in central Europe during the last glacial inception. – Nature 436: 833–836.

Schmidt, E.D., Murray, A.S., Stevens, T., Buylaert, J.P., Marković, S.B., Tsukamoto, S. & Frechen, M., submitted. Elevated temperature IRSL dating of the lower part of the Stari Slankamen loess sequence (Vojvodina, Serbia) – investigating the saturation behaviour of the pIR-IR290 signal. – Quaternary Geochronology.

Schmidt, E.D., Frechen, M., Murray, A.S., Tsukamoto, S. & Bittmann, F. (2011): Luminescence chronology of the loess record from the Tönchesberg section – a comparison of using quartz and feldspar as dosimeter to extend the age range beyond the Eemian. – Quaternary International 234: 10–22.

Schmidt, E.D., Machalett, B., Marković, S. B., Tsukamoto, S. & Frechen, M. (2010): Luminescence chronology of the upper part of the Stari Slankamen loess sequence (Vojvodina, Serbia). – Quaternary Geochronology 5: 137–142.

Thiel, C., Buylaert, J.P., Murray, A.S., Terhorst, B., Hofer, I., Tsukamoto, S. & Frechen, M. (2011): Luminescence dating of the Stratzing loess profile (Austria) – Testing the potential of an elevated temperature post-IR IRSL protocol. – Quaternary International 234: 23–31.

Thiel, C., Buylaert, J.P., Murray, A.S., Terhorst, B., Tsukamoto, S. & Frechen, M. this issue. The chronostratigraphy of prominent palaeosols in Lower Austria: testing the performance of two post-IR IRSL dating protocols. – Eiszeitalter und Gegenwart.

Timar, A., Vandenberghe, D., Panaiotu, E.C., Panaiotu, C.G., Necula, C., Cosma, C. & Van den haute, P. (2010): Optical dating of Romanian loess using fine-grained quartz. – Quaternary Geochronology 5: 143–148.

Thomsen, K.J., Murray, A.S., Jain, M. & Bøtter-Jensen, L. (2008): Laboratory fading rates of various luminescence signals from feldspar-rich sediment extracts. – Radiation Measurements 43: 1474–1486.

Visocekas, R. (1985): Tunnelling radiative recombination in labradorite: Its association with anomalous fading of thermoluminescence. – Nuclear Tracks and Radiation Measurements 10 (4–6): 521–529.

Wintle, A. G. & Murray, A. S. (2006): A review of quartz optically stimulated luminescence characteristics and their relevance in single-aliquot regeneration dating protocols. – Radiation Measurements 41: 369–391.

Wintle, A.G. (1973): Anomalous fading of thermoluminescence in mineral samples. – Nature 245, 143–144.

Appendix

One of the co-authors (Frank Sirocko) has a different chronostratigraphical interpretation, which he describes in detail in a paper under submission. F. Sirocko interprets the luminescence dates from this study as result of a mixture of an eolian fraction with grains from the wave-generated erosion of soil material, which is again a mixture from the Devonian bedrock and loess of MIS6 or older.

According to Sirocko et al. (unpublished) the stratigraphical framework for JW2 and JW3 is as follows:

Scoria from the Laacher See eruption is apparent in the soil at 1 m depth, correlating to an eruption age of about 12.9 ka. Sediments from 1–22 m are free of clay and are regarded as a mixture from eolian deposition and wave generated suspensions. These sediments are free of pollen and correlate to the last glacial maximum (LGM). The relative paleointensity variation of sediment magnetisation places the Mono Lake Event at 24 m indicating an age of 30 ka according to the GLOPIS paleomagnetic stack, which is based on a GISP2 derived age model. A tuning of the greyscale variations between 25 and 41 m reproduces almost perfectly the succession of the Greenland Interstadials GI3–17. The second minimum of the relative paleointensity is at 32.5 m and correlates most likely to the Laschamps Event. The MIS3 sections of JW2 and JW3 have been studied by several ^{14}C dates giving ages around 50 ka representing the upper dating limit of the ^{14}C method. This would imply that all organic particles in JW3 are derived from soils of GI14, which was the warmest period of MIS3.

The markers of MIS5 start with a prominent step in the paleomagnetic inclination record at 81 m representing a principle change that was dated in the Monticchio record to 75 ka. The end of this inclination maximum is at 99 m, representing 86 ka. A tephra consisting of the same geochemical composition as the Roucourt tephra in France is visible in JW3 at 107.4 m, which would place this depth at around 90 ka. The sediments below yield two IRSL ages of 93 ka and 100 ka (Degering & Krbetschek, 2007a). The greyscale record between 75 m and 130 m can be perfectly tuned to the Greenland ice core stadial/interstadial succession and also the North Atlantic C-events. A tephra with an identical zonation to the Dümpelmaar tephra is visible at 139 m; this tephra was dated at the Herchenberg section to 116±10 ka. The succession of the markers of core JW3 ends with the occurrence of interglacial pollen at depth below 145 m most likely representing the Eemian.

E&G Quaternary Science Journal
Volume 60 / Number 1 / 2011 / 116–125 / DOI 10.3285/eg.60.1.08
www.quaternary-science.net

GEOZON SCIENCE MEDIA
ISSN 0424-7116

Luminescence dating of the loess/palaeosol sequence at the gravel quarry Gaul/Weilbach, Southern Hesse (Germany)

Esther Dorothe Schmidt, Arno Semmel, Manfred Frechen

Abstract: A thick Middle and Late Pleistocene loess/palaeosol sequence is exposed at the gravel quarry Gaul located east of Weilbach in the southern foreland of the Taunus Mountains. The loess/palaeosol sequence correlates to the last three glacial cycles. Seven samples were dated by luminescence methods using an elevated temperature IRSL (post-IR IRSL) protocol for polymineral fine-grains to determine the deposition age of the sediment and to set up a more reliable chronological framework for these deposits. The fading corrected IR_{50} and the $pIRIR_{225}$ age estimates show a good agreement for almost all samples. The fading corrected IRSL ages range from 23.7 ± 1.6 ka to >350 ka indicating that the oldest loess was deposited during marine isotope stage (MIS) 10 or earlier and that the humic-rich horizon (Weilbacher Humuszone) was developed during the late phase of MIS 7. Loess taken above the fCc horizon most likely accumulated during MIS 6 indicating that the remains of the palaeosol are not belonging to the last interglacial soil. The two uppermost samples indicate that the youngest loess accumulated during MIS 2 (Upper Würmian). Age estimates for the loess-palaeosol sequence of the gravel quarry Gaul/Weilbach could be obtained up to ~350 ka using the $pIRIR_{225}$ from feldspar.

[Lumineszenz-Datierung der Löss-Paläoboden-Sequenz in der Kiesgrube Gaul/Weilbach, Südhessen]

Kurzfassung: Eine mächtige Löss-Paläoboden-Sequenz des Mittel- und Spätpleistozäns ist in der Kiesgrube Gaul östlich von Weilbach im südlichen Taunusvorland aufgeschlossen. Lösse der letzten drei Glazialzyklen, mit zwischengeschalteten Paläoböden, sind aufgeschlossen. Sieben Proben wurden mit der Lumineszenz-Datierungsmethode, basierend auf einem post-IR IRSL Messprotokoll, untersucht, um einen verlässlicheren chronologischen Rahmen für diese Sedimente zu etablieren. Die „fading" korrigierten IR50 und die $pIRIR_{225}$ Alter sind für fast alle Proben in guter Übereinstimmung. Die IRSL Alter reichen von 23.7 ± 1.6 ka bis >350 ka und deuten an, dass der älteste Löss während des marinen Isotopenstadiums (MIS) 10 oder früher abgelagert wurde, und dass die Weilbacher Humuszonen sehr wahrscheinlich während einer späten Phase des MIS 7 gebildet wurden. Lösse über dem fCc Horizont wurden sehr wahrscheinlich während des MIS 6 abgelagert, was darauf hindeutet, dass die Reste des Paläobodens nicht mit dem letzten Interglazial korrelieren. Die beiden obersten Proben deuten darauf hin, dass der jüngste Löss während dem letzten Pleniglazial (Oberwürm, MIS 2) abgelagert wurde. Mit dem $pIRIR_{225}$ Signal konnten Alter bis ~350 ka für die Proben der Löss-Paläoboden-Sequenz in der Kiesgrube Gaul gemessen werden.

Keywords: *loess, luminescence dating, IRSL, fading, Weilbach, chronostratigraphy*

Addresses of authors: **M. Frechen**, **E.D. Schmidt***, **A. Semmel**†, Leibniz Institute for Applied Geophysics (LIAG), Section 3: Geochronology and Isotope Hydrology, Stilleweg 2, 30655 Hannover, Germany. E-Mail: Esther.Schmidt@liag-hannover.de, Estherdorothe.Schmidt@google-mail.com; **corresponding author*

† *Einen Tag nach Erhalt eines Briefes mit Korrekturen an unserem gemeinsamen Manuskript, erreichte uns völlig überraschend die traurige Nachricht vom Tode Arno Semmels. Wir werden ihn als Mensch, Kollegen und Wissenschaftler vermissen.*

Introduction

Loess records are sensitive archives of climate change and provide important information on local and regional environmental processes and conditions for the Middle and Late Pleistocene period in Europe. The southern foreland of the Taunus mountains (Fig.1), which are part of the Rhenish Massif in Germany, consists mainly of Pleistocene terraces of the river Main covered by thick loess/palaeosol sequences.

For these deposits it was suggested that each palaeosol or fossil Bt horizon (= fossil argillic B horizon) correlates to an interglacial *sensu stricto* (Fink, 1973). Semmel (1967, 2005) questioned this suggestion because there are loess sequences in Western Europe which contain much more fossil Bt horizons than evidenced by palynological studies. The Upper Pleistocene Lower terraces of the river Main (t6 and t7 sensu Semmel, 1969) are not covered by such argillic horizons. The stratigraphically older terraces t5 and t4 are covered by loess and intercalated by a fossil Bt horizon and by two Bt horizons, respectively.

In contrast to the studies of Semmel (1969), only one burried Bt horizon, intercalating the loess covering terrace t4, was found at the gravel quarry Gaul located east of Weilbach during the excavation of the past years (Semmel, 2005). The latter Bt horizon is covered by two humic horizons ("Humuszonen"). A significant hiatus truncates the uppermost humic horizon followed by the typical Late Würmian loess succession including Lohne Soil, tundra gleys ("Naßböden") E2 and E3, and the Eltville Tephra (Semmel, 1967; stratigraphy after Schönhals et al., 1964; local description after Semmel, 2005a). This loess/palaeosol sequence was studied along an about 1 km long exposed wall at the gravel quarry Gaul. However, below a weak palaeosol designated to correlate to the Middle Würmian Lohne Soil, a continuous fCc horizon including large, mainly vertical exposed carbonate concre-

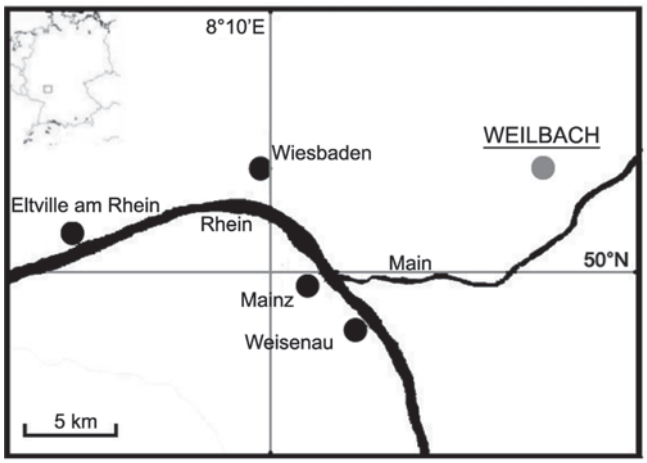

Fig. 1: Map showing the location of the loess/palaeosol sequence exposed at the gravel quarry Gaul/Weilbach.

Abb. 1: Lage der Löss-Paläoboden Sequenz in der Kiesgrube Gaul/Weilbach.

tions ("loess dolls") of about 20 cm length, sometimes with remains of brown clayey loam, was exposed. It is likely that these remains belong to a fossil Bt horizon (Semmel, 2005). Independent stratigraphical age control is provided by the occurrence of the Eltville Tephra, a widespread marker horizon in this region which most likely resulted from an eruption of the Eifel volcanic field (Semmel, 2007). The Eltville Tephra has been investigated by several dating studies at different sections. The mean luminescence age values are between 19.2 ka and 20.6 ka for this tephra horizon (Wintle & Brunnacker, 1982; Zöller, 1989; Frechen & Preusser, 1996; Antoine et al., 2009). Zöller & Semmel (2001) provided mean TL age estimates of 21 ka for loess above the Eltville Tephra and 25 ka below. So far numerical age estimates are still lacking for the loess deposits from the Weilbach section making it difficult to interpret the terrestrial climate archives as well as to correlate the loess/palaeosol sequences with other loess records. The nearby loess record from Mainz-Weisenau was described in detail by Semmel (1995). Thermoluminescence (TL) age estimates for the deposits of the Mainz-Weisenau section were presented by Buschbeck (1993) and Zöller (1995). Frechen & Preusser (1996) provided thermoluminescence (TL) and infrared stimulated luminescence (IRSL) age estimates. These previous studies provided TL and IRSL ages up to about 100 ka, which was thought to be the upper dating limit that time (Frechen, 1999).

This study presents the first optically stimulated luminescence (OSL) dating results from the loess/palaeosol sequence at the gravel quarry Gaul located east of Weilbach based on a post-IR IRSL measurement sequence. The IRSL signal measured at 50°C and the subsequent post-IR IRSL signal measured at 225°C using the latter sequence are hereafter referred to as IR_{50} and $pIRIR_{225}$, respectively. Our study aims to set up a more reliable chronological framework for this loess/palaeosol sequence. Furthermore, we want to answer the question whether the oldest Bt horizon correlates to the Middle Pleistocene (antepenultimate or penultimate interglacial) or to the Upper Pleistocene.

Loess/palaeosol sequence at the gravel quarry Gaul/Weilbach

The loess/palaeosol sequence with indicated sample positions for luminescence dating is shown in Fig. 2. The coordinates of the section under study are 55°46'28,7'' N and 8°44'35,5'' E. The location of the profile under study within the terrace sequence of river Main is shown in Fig. 3. The gravel of terrace t4 is covered by carbonate-free flood loam, which changes to the top into calcareous loess (1 in Fig. 2). Sample Wei 7 was taken from this loess unit. This layer is covered by a 30 cm thick fCc horizon including large carbonate concretions, which form the bottom of a reddish brown fBt horizon (2 in Fig. 2). The truncated palaeosol is pale coloured owing to secondary carbonate infiltration. In the profile under study the fBt horizon is about 90 cm thick but varies strongly in thickness along the quarry wall owing to erosion postdating the soil forming processes. The truncated palaeosol is covered by carbonate-rich, greyish brown loess loam (about 30 cm thick) below a brown spotted dark humic-rich horizon ("Weilbacher Humuszone") (4 in Fig. 2, about 70 cm thick). Sample Wei6 was taken from this horizon. The humic-rich horizon is covered by a solifluction layer of reworked humic-rich material including loess loam and calcareous loess, which is about 60 cm thick. Sample Wei5 was taken from this unit (5 in Fig. 2). This layer is covered by light brown about 50 cm thick loess with carbonate pseudomicelium including a truncated fCc horizon with up to 20 cm large carbonate concretions (6 in Fig. 2). Sample Wei4 was taken from this reworked loess. Along the quarry wall, reddish brown remains of loam are found around these carbonate concretions (Fig. 2a). Close to the profile from Fig.2 a truncated Bt horizon about 60 cm thick is exposed along the quarry wall above the fCc horizon in a dell filled with loess (Fig. 2b). The uppermost part of the loess/palaeosol sequence includes weak palaeosols correlating to the Middle Würmian Lohne Soil (7 in Fig. 2) and to the Upper Würmian sequence including tundra gley E2 (8 in Fig. 2), tundra gley E3 and the Eltville Tephra (9 in Fig. 2). Sample Wei3 was taken below the Lohne Soil, sample Wei2 below the tundra gley E2 and sample Wei1 below the tundra gley E3.

The stratigraphic interpretation of the profile is based on the local stratigraphical loess scheme (Semmel, 1968; 2005) suggesting that the oldest exposed fBt horizon (2 in Fig. 2) correlates to the antepenultimate or penultimate interglacial designated to be older than ~200 ka. The humic-rich horizon correlates most likely to the "Weilbacher Humuszone", which correlates to an interstadial period during the early penultimate glacial period (Semmel, 1968) and the fCc horizon (6 in Fig. 2) most likely correlates to the last interglacial. The loess sequence covering the fCc horizon correlates most likely to the Middle and Upper Würmian, as indicated by the exposed typical marker horizons.

Experimental details

The samples were taken in light-tight plastic cylinders and the sediment was extracted under subdued red light and pretreated with 10% hydrochloric acid to remove carbonates, sodium oxalate to dissolve aggregates and 30% hydrogen peroxide to remove organic matter. The material was then re-

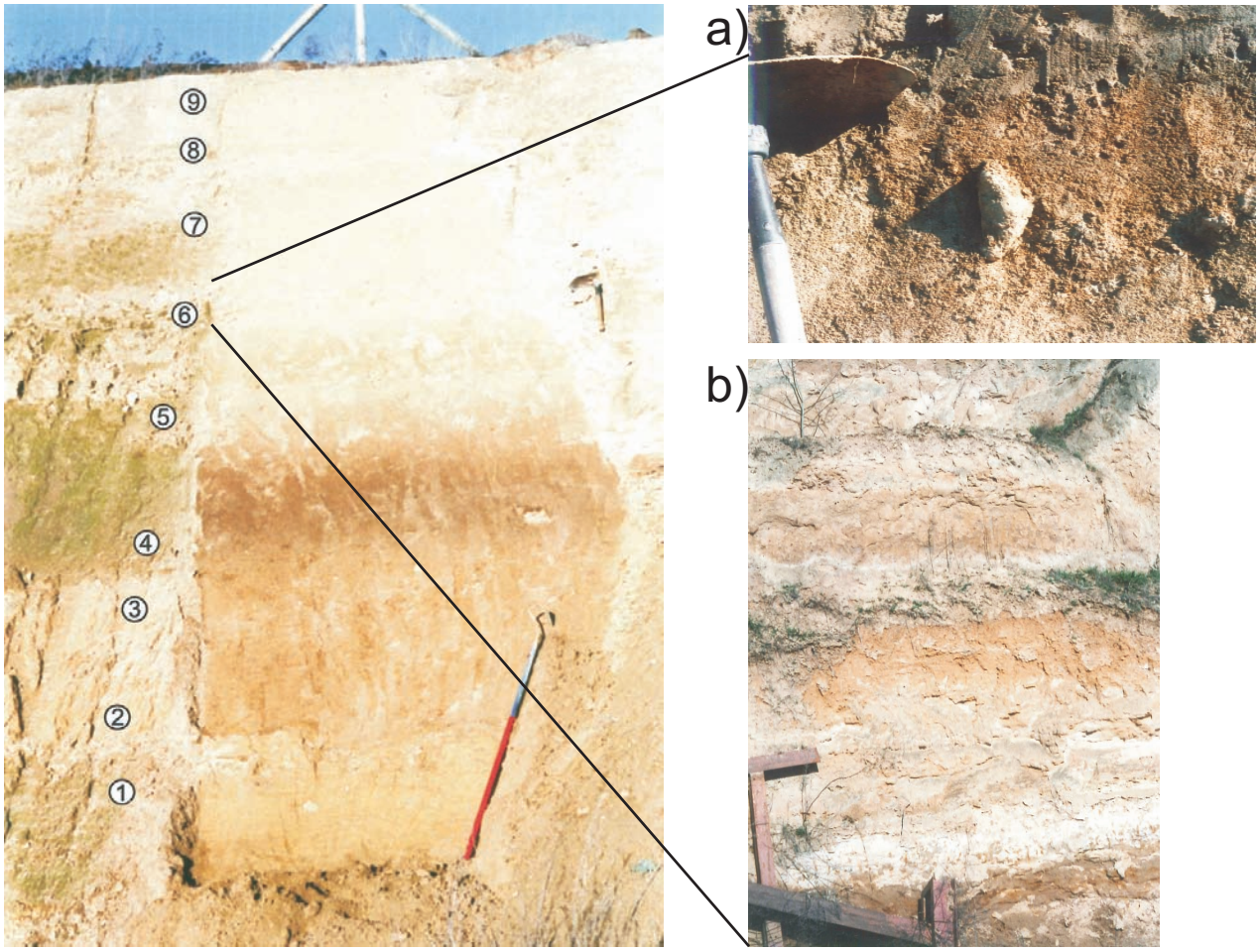

Fig. 2: Loess/palaeosol sequence at the gravel quarry Gaul/Weilbach with a) loess concretions of the fCc horizon with remains of brown Bt material and b) two fossil Bt-horizons near the profile of Fig. 2. 9 = E3 tundra gley, above the Eltville tephra (Wei1 was taken below), 8 = E2 tundra gley, greyish compact loess (Wei2 was taken below), 7 = Lohne soil (Wei3 was taken below), 6 = fCc-horizon with carbonate concretions (Wei4 was taken below), 5 = reworked humic-rich material (Wei5), 4 = humic-rich horizon ("Weilbacher Humuszone") (Wei6), 3 = reworked carbonate-rich loess loam, 2 = fBt-horizon, 1 = oldest loess (Wei7)

Abb. 2: Löss-Paläoboden Sequenz in der Kiesgrube Gaul/Weilbach mit a) Lösskindl im fCc-Horizont mit Resten braunen Bt-Lehms und b) zwei fossilen Bt-Horizonten nahe des Hauptprofils. 9 = E3-Nassboden mit hangendem dunkleren Bändchen des Eltviller Tuffs (darunter wurde Wei1 entnommen), 8 = E2-Nassboden, grauer dichter Löss (darunter wurde Wei2 entnommen), 7 = Lohner Boden (olivgrauer feinblattiger Löss mit $CaCO_3$-Pseudomycel) (darunter wurde Wei3 entnommen), 6 = fCc-Horizont mit Lößkindeln (darunter wurde Wei4 entnommen), 5 = umgelagerte Humuszone (Wei5), 4 = Weilbacher Humuszone (Wei6), 3 = umgelagerter kalkhaltiger Lößlehm, 2 = fBt-Horizont, 1 = ältester Löss (Wei7)

fined to a fine silt (4–11 µm) fraction. Finally, samples were prepared for measurement by settling the polymine-ral grains (4–11 µm) from acetone onto aluminium discs. All OSL/IRSL measurements were performed using an automated Risø TL/OSL-DA20 equipped with a $^{90}Sr/^{90}Y$ beta source. Feldspar IRSL signals were detected through Schott BG-39 and Corning 7–59 filters (passing 320 to 460 nm; i.e. blue).

Radionuclide concentrations for all samples were obtained using high resolution gamma spectrometry of sediment collected from the immediate surrounding of the samples. A water content of 20 ± 5% was estimated for all samples. It has to be mentioned that the estimation of water content since the loess was deposited is associated with a high degree of uncertainty. Mean a-values of 0.08 ± 0.02 for polymineral IRSL were used to derive the effective alpha dose rate (Rees-Jones, 1995). The concentrations of uranium, thorium and potassium were converted into infinite-matrix dose rates using the conversion factors of Adamiec & Aitken (1998) and water-content attenuation factors (Aitken, 1985). Estimation of the cosmic-ray dose rate was calculated according to Prescott & Stephan (1982) and Prescott & Hutton (1994) from knowledge of burial depth, altitude, matrix density, latitude and longitude for each sample. The uranium, thorium, potassium content and total dose rates are shown in Table 1.

Luminescence dating

Luminescence dating enables to determine the depositional age of various sediments such as loess over a range from a few decades to several hundred thousand years by dating the time that has passed since the last exposure of the minerals0 to daylight (Aitken, 1998). Quartz or feldspar grains (the most common minerals in sediments) are used as natural dosimeters. They are able to store energy within their crystal structure, which is coming mainly from an omnipresent ionising radiation (alpha, beta and gamma) as well as from cosmic radiation. The charge can be stored in imperfections in the crystal lattice for long periods. In the laboratory the grains are first heated, and then stimulated with IR or blue LEDs which release the electrons from their traps in the form of

E&G / Vol. 60 / No. 1 / 2011 / 116–125 / DOI 10.3285/eg.60.1.08

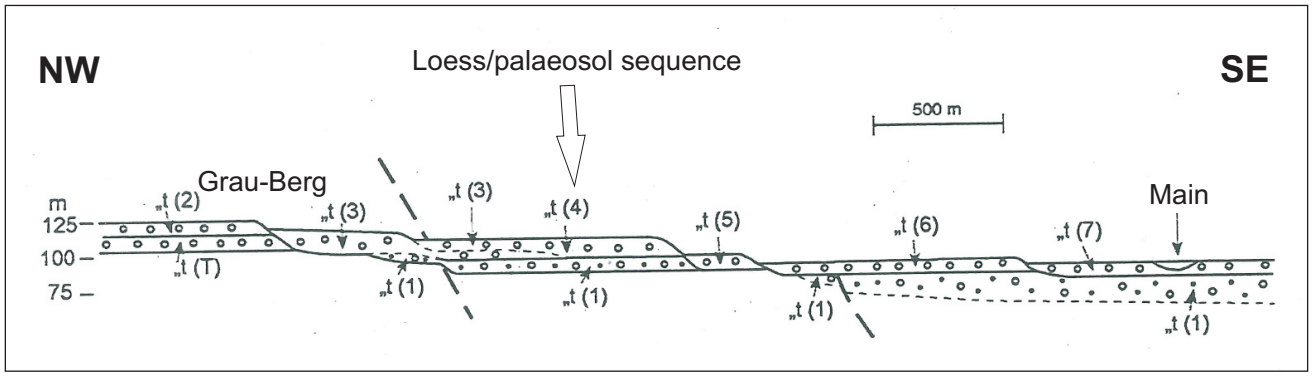

Fig. 3: Terrace sequence of the river Main in the southern foreland of the Taunus mountains. The Loess/palaeosol sequence is located close to the symbol "t4".

Abb. 3: Schnitt durch die Main-Terrassenfolge im südlichen Taunusvorland. Das beprobte Profil liegt nahe dem Symbol „t4".

visible light (luminescence). Such a measurement allows estimating the dose of radiation (palaeodose or equivalent dose, De) which the crystal has absorbed since the last exposure to daylight. The luminescence signals from feldspars grow to much higher doses than those from quartz, which offers the possibility of significantly extending back the age range. However, luminescence dating of feldspars has a tendency to underestimate the geological age, because of anomalous fading (Wintle, 1973) which is caused by quantum-mechanical tunnelling (Visocekas, 1985). Feldspar dating is normally carried out using a 50°C IR stimulation with detection in the blue (-violet) spectrum. IRSL ages underestimate often consistently the quartz OSL ages most likely due to anomalous fading. Several methods of age corrections have been proposed (e.g. Huntley & Lamothe, 2001; Lamothe et al., 2003) and many studies show corrected IRSL ages which are in good agreement with quartz OSL ages. But these corrections rely on different assumptions, including e.g. the fact that the logarithmic time dependence is relevant to geological time (Huntley & Lamothe, 2001) and there is no general consensus which correction method should be used. Furthermore, the correction method is strictly applicable only for natural doses in the linear region of the growth curve (Huntley & Lamothe, 2001), although Buylaert et al. (2009; in press) have shown that the correction can give accurate ages outside this range. However, if the fading rate can be reduced, feldspar dating will be more reliable.

Post-IR IRSL measurement sequence

Thomsen et al. (2008) found out, that stimulation at elevated temperatures significantly reduces the fading rate. Based on this work Buylaert et al. (2009) proposed a new single aliquot regenerative dose (SAR) protocol, with detection in the blue (320–460 nm). This protocol which includes elevated temperature stimulation with IR for 100 s at 225°C, following stimulation with IR for 100 s at 50°C, is called post-IR IRSL measurement sequence and is presented in Table 2. Buylaert et al. (2009) have shown that the observed fading rates for the post-IR IRSL signal are significantly lower than from the conventional IR_{50} and that the signal is bleachable in nature. Buylaert et al. (submitted) measured a mean residual dose value of 10 ± 2 Gy on polymineral fine-grains extracted from modern Chinese loess. This post-IR IRSL measurement protocol is applied to the polymineral fine-grains from the Weilbach section. The initial 2.0 s of the post-IR IR signal is used for calculating the De values, with a background subtraction based on the signal observed in the last 10 s of the decay curve. All dose response curves were fitted using an exponential saturating function. Tests were carried out on the same aliquots as for De measurement to check for anomalous fading and to compare the fading rates of the IR_{50} and the $pIRIR_{225}$. The aliquots were dosed, preheated and then stored for various delays after irradiation and before measurement. This sequence was repeated several times on each aliquot. The fading rates are expressed in terms of the percentage of the decrease of intensity per decade of time (g-value; Aitken, 1985; Auclair, Lamothe & Huot, 2003). The g-values were calculated according to Huntley & Lamothe (2001) using the same integration limits as for the De calculation. The g-values were used to correct the ages.

Tab. 1: Dose rate data from potassium, uranium and thorium content, as measured by gamma spectrometry.

Tab. 1: Dosimetrische Ergebnisse basierend auf Kalium, Uran und Thorium Gehalt (gemessen mit Gammaspektrometrie).

Sample	Uranium (ppm)	Thorium (ppm)	Potassium (%)	Cosmic dose rate (Gy/ka)	IRSL dose rate (Gy/ka)
Wei 1	3.03 ± 0.03	10.09 ± 0.06	1.23 ± 0.01	0.19 ± 0.02	3.00 ± 0.16
Wei 2	3.40 ± 0.03	11.24 ± 0.06	1.38 ± 0.01	0.18 ± 0.02	3.32 ± 0.18
Wei 3	3.24 ± 0.02	11.41 ± 0.06	1.30 ± 0.01	0.14 ± 0.01	3.18 ± 0.17
Wei 4	2.76 ± 0.02	9.38 ± 0.05	1.18 ± 0.01	0.13 ± 0.01	2.72 ± 0.15
Wei 5	2.80 ± 0.03	11.12 ± 0.06	1.31 ± 0.01	0.12 ± 0.01	3.01 ± 0.16
Wei 6	3.33 ± 0.03	13.55 ± 0.06	1.43 ± 0.01	0.09 ± 0.01	3.45 ± 0.18
Wei 7	2.92 ± 0.03	10.73 ± 0.06	1.30 ± 0.01	0.06 ± 0.01	2.94 ± 0.16

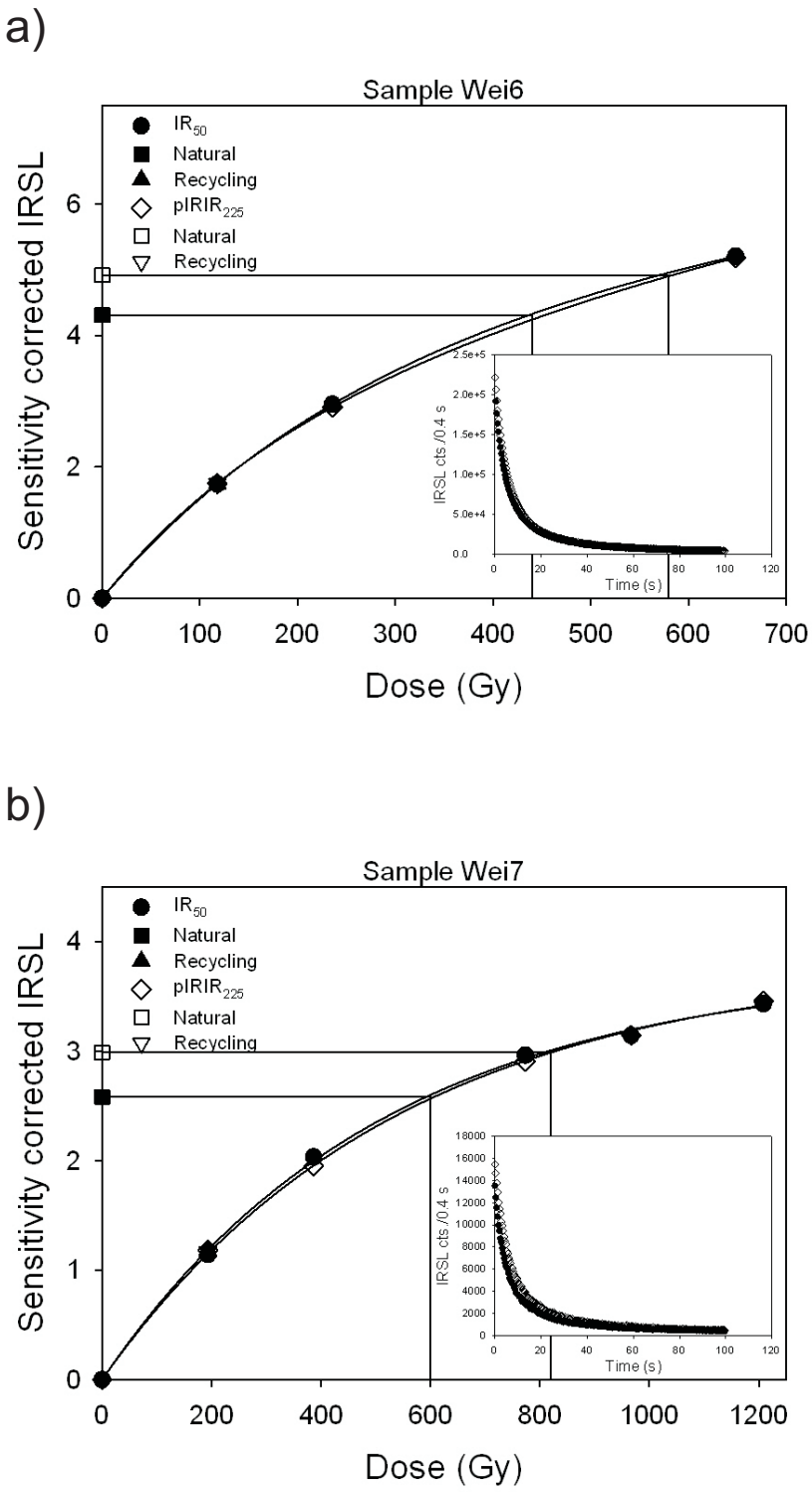

Fig. 4: Dose response and decay curves for samples a) Wei 6 and b) Wei 7 showing the IR_{50} (filled symbols) and the $pIRIR_{225}$ signal (open symbols).

Abb. 4: Aufbaukurve und Zerfallskurve für Proben a) Wei 6 (gefüllte Symbole) und b) Wei7 (offene Symbole) für das IR_{50} und das $pIRIR_{225}$ Signal.

Luminescence characteristics and performance tests

Figure 4 shows the dose response curves and the decay curves for the IR_{50} and the $pIRIR_{225}$ for the stratigraphically oldest samples Wei6 (Fig. 4a) and Wei7 (Fig. 4b). These curves are selected to be representative for all samples. The natural IR_{50} has about 10–15% lower signal intensity than the natural $pIRIR_{225}$. The growth curves for the $pIRIR_{225}$ lies above the curve for the IR_{50} for all samples. However, the shapes of the growth curves are indistinguishable. Buylaert et al. (2009) observed that the shape of the growth curves for the IR_{50} and the $pIRIR_{225}$ are indistinguishable for their samples. The $pIRIR_{225}$ of all the measured samples is much brighter (~10–15%) than for the IR_{50} (inlay of Fig. 4a and b) confirming the results of Buylaert et al. (2009). Recycling ratios for the samples range from 0.98 ± 0.03 to 1.01 ± 0.003 for the IR_{50} and from 0.91 ± 0.04 to 0.99 ± 0.003 for the $pIRIR_{225}$. Recuperation is below 5% of the natural signal. To test the applicability of the post-IR IRSL protocol using a stimulation temperature of 225°C, the dose recovery ratio was measured for all samples (Murray & Wintle, 2003). The aliquots were bleached for 4 hours in a Hönle SOL2 solar simulator before giving a dose approximately equal to the natural dose, except for sample Wei7, where a smaller dose was chosen. This dose was then measured in the same manner as the equivalent dose in or-

E&G / Vol. 60 / No. 1 / 2011 / 116–125 / DOI 10.3285/eg.60.1.08

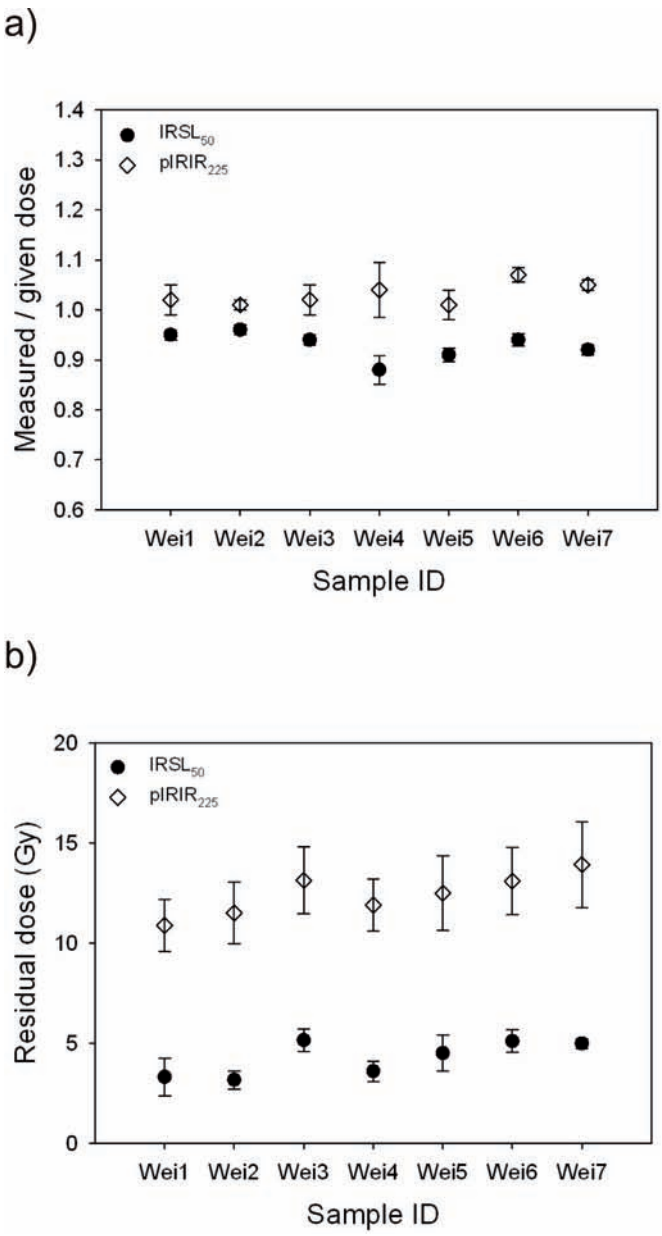

Fig.5: Dose recovery test (a) and the residual doses (b) for the IR_{50} and the $pIRIR_{225}$ signal for all samples. Three aliquots were measured per sample. Error bars represent 1-sigma standard error.

Abb. 5: Dose recovery test (a) und residuale Dosen (b) für das IR_{50} und das $pIRIR_{225}$ Signal für alle Proben. Drei Aliquots wurden pro Probe gemessen. Die Fehlerbalken stellen den 1-sigma Standardfehler dar.

der to confirm that the protocol is able to recover a known dose successfully. If the SAR protocol is suitable, the measured to given dose ratio should be close to 1. Fig. 5a shows the results of the dose recovery test for all samples for the IR_{50} and the $pIRIR_{225}$. The obtained ratios of the measured to given dose range from 0.88 ± 0.02 to 0.94 ± 0.01, with a mean of 0.93 ± 0.01 Gy (n = 21) for IR50 and from 1.01 ± 0.03 to 1.07 ± 0.01, with a mean of 1.03 ± 0.01 Gy (n = 21) for $pIRIR_{225}$. This data indicates the applicability of the post-IR IRSL protocol. To confirm that the IRSL and the post-IR IRSL are bleachable by natural daylight we exposed three aliquots per sample for four hours to a Hönle SOL2 solar simulator and then measured the apparent dose in the usual manner. The results are shown in Fig. 5b and Table 3. The residual doses range from 3.2 ± 0. 5 Gy to 5.6 ± 0.2 Gy, with a mean of 4.4 ± 0.9 Gy (n = 7) for IR_{50} and from 10. 9 ± 1.3 Gy to 14.9 ± 2.1 Gy, with a mean of 12.7 ± 0.5 Gy (n = 7) for $pIRIR_{225}$.

Equivalent Dose (D_e), fading rates and age estimates

In Table 3 the equivalent doses, dose recovery results, residual doses, g-values and the resulting luminescence ages, both uncorrected as well as fading corrected, are summarized for all samples. The D_e-s obtained using the IR_{50} from feldspar range from 52.9 ± 1.3 Gy to 423 ± 4 Gy. The obtained equivalent doses gave uncorrected age estimates between 17.6 ± 1.1 ka and 139 ± 8 ka. D_e values obtained for the IR_{50} increase clearly with depth from sample Wei1 to sample Wei5. The values obtained for sample Wei6 and Wei7 do not increase considerably with depth indicating that this signal is in field saturation at ~400 Gy. The D_e-s calculated using the $pIRIR_{225}$ from feldspar range from 64.9 ± 2.3 Gy to 921 ± 41 Gy. The D_e values are in average ~20% higher than those obtained using the IR_{50}. The $pIRIR_{225}$ does not show evidence of field saturation (equilibrium between the accumulation of new charge and the loss by anomalous fading), and increases with depth. The characteristic saturation doses (D_0) are about ~450 Gy for the IR_{50} and the $pIRIR_{225}$. According to Wintle & Murray (2006) it is only possible to obtain reliable equivalent doses (D_e) up to a dose value of $2D_0$ and therefore it is important to test if the equivalent dose values exceed $2D_0$. Following this suggestion it is possible to measure D_e values up to about ~900 Gy for our material. Fading tests were carried out for all samples using the post-IR IRSL measurement sequence. The g-values are shown in Fig. 6 for the IR_{50} and the $pIRIR_{225}$. The g-values range from 2.9 ± 0.3%/decade to 3.2 ± 0.2%/decade, with an average of 3.01 ± 0.04%/decade (n = 7) for the IR_{50} and from 1.6 ± 0.3%/decade to 2.0 ± 0.4%/decade, with an average of 1.8 ± 0.1%/decade (n = 7) for the $pIRIR_{225}$ indicating that the $pIRIR_{225}$ fades ~40% less than the IR_{50}. The fading corrected ages are listed in Table 3. Fading corrections use the methods proposed in Huntley & Lamothe (2001). The fading corrected age estimates for the IR_{50} range from 23.7 ± 1.6 ka to >190 ka and from 25.2 ± 1.6 ka to >350 ka for the $pIRIR_{225}$. The IR_{50} and the $pIRIR_{225}$ are in agreement for samples Wei1-Wei6. For sample Wei7 the IR_{50} underestimates the $pIRIR_{225}$. We assume that the fading corrected $pIRIR_{225}$ values yield more reliable age estimates. The IR_{50} is most likely in field saturation for sample Wei7. The $pIRIR_{225}$ age estimate for sample Wei7 (>350 ka) can be regarded as minimum age only, as the D_e value of 921 ± 41Gy is in the range of $2D_0$.

Discussion

Our study presents the first luminescence age estimates for the loess/palaeosol sequence of the gravel quarry Gaul located east of Weilbach based on an elevated temperature infrared stimulated luminescence (IRSL) signal which has been shown to fade at a very much lower rate than the conventional IRSL signal (Thomsen et al., 2008, Buylaert et al., 2009). The fading corrected IR_{50} and the $pIRIR_{225}$ show good agreement for samples Wei1–Wei6. For sample Wei7 the IR_{50} underestimates the $pIRIR_{225}$. Our interpretation is hence based on the fading corrected $pIRIR_{225}$ age estimates (Fig. 7). Sample Wei7, which was taken from the calcareous loess covering

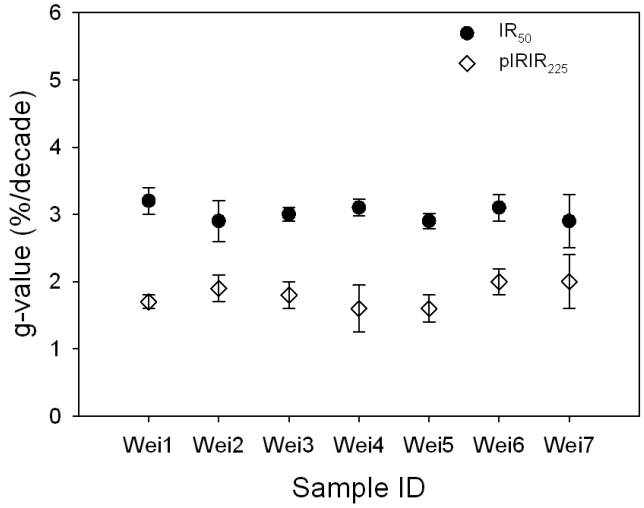

Fig. 6: Fading rates for the post the IR_{50} and $pIRIR_{225}$ signals for all samples. Three aliquots were measured per sample. Error bars represent 1-sigma standard error.

Abb. 6: Fadingraten für das IR_{50} und das $pIRIR_{225}$ Signal für alle Proben. Drei Aliquots wurden pro Probe gemessen. Die Fehlerbalken stellen den 1-sigma Standardfehler dar.

the gravel of terrace t4 (1 in Fig. 2) yielded an age estimate of >350 ka indicating loess deposition during marine Isotope Stage (MIS) 10 or earlier and suggesting that terrace t4 has a minimum deposition age of ~350 ka. The calcareous loess is covered by a fCc horizon which forms the bottom of a reddish brown fBt horizon (2 in Fig. 2). This truncated palaeosol is covered by about 30 cm thick loess loam and a brown dark humic-rich horizon (4 in Fig. 2).

Sample Wei6 was taken from this layer and yields an age estimate of 198 ± 12 ka indicating a formation of the "Weilbacher Humuszone" during the late phase of MIS 7. Thus the oldest reddish brown fBt horizon (2 in Fig. 2) is older than ~200 ka and was most likely developed during the antepenultimate or penultimate interglacial. The humic-rich horizon is covered by a solifluction layer of reworked humic-rich material including loess loam and calcareous loess (Sample Wei5 was taken from this horizon, 5 in Fig. 2). This layer yielded an age estimate of 202 ± 14 ka and is covered by about 50 cm thick reworked loess (Wei4) with macroscopically visible pseudomicelium, which gives an age estimate of 203 ± 22 ka. These layers can probably be correlated with a cold phase during MIS 7. It has to be mentioned that samples Wei5 and Wei4 were taken from reworked material. They could eventually be contaminated with older material, which would lead to an age overestimation. Therefore the ages have to be regarded more carefully. The reworked loess is covered by a fCc horizon with up to 20 cm large carbonate concretions (6 in Fig. 2). Reddish brown remains of loam are found around these carbonate concretions (Fig. 2a). Above the fCc horizon loess accumulated; sample Wei3 was taken from this horizon and yielded an age estimate of 146 ± 9 ka indicating accumulation during the penultimate glaciation (MIS 6). This result shows that the remains of the palaeosol very likely do not correlate to the last interglacial period but very likely correlate to a warm phase of MIS 7. The last interglacial soil (MIS 5) and the deposits of the lower Würmian are missing in this profile. Bibus, Rähle & Wedel (1996, 2002) provided a detailed description of the latter ones from the Mainz-Weisenau section and Frechen & Preusser (1996) provide TL and IRSL age estimates ranging from 68–113 ka for these deposits. The results of Bibus, Rähle & Wedel (1996, 2002) show that there is evidence for three warmer phases after the last interglacial, revealing the significant hiatus for our profile. Above the loess layer the Middle Würmian Lohne Soil (7 in Fig. 2) is developed followed by an Upper Würmian sequence including tundra gley E2 (8 in Fig. 2), tundra gley E3 and the Eltville Tephra (9 in Fig. 2). Sample Wei2 was taken below the tundra gley E2 giving an age estimate of 28.1 ± 2.3 ka and Sample Wei1 below the tundra gley E3 yielding an age estimate of 25.2 ± 1.6 ka indicating accumulation during the last Pleniglacial (Upper Würmian) correlating to MIS2. Frechen & Preusser (1996) obtained age estimates of ~20 ka for the Eltville tephra and Zöller & Semmel (2001) provided mean TL age estimates of 21 ka for loess above the Eltville Tephra and 25 ka below. According to Frechen (1999) an eruption age between 17–23 ka for the Eltville tephra is most likely, which is in good agreement with our results.

Our results are not in complete agreement with the loess stratigraphy proposed by Semmel (1968, 2005). However, they support the assumption that the oldest exposed fBt horizon (2 in Fig. 2) correlates to the antepenultimate or penultimate interglacial and that the humic-rich horizon most likely correlates to the "Weilbacher Humuszone", designated to be an interstadial period during the early penultimate glacial period (Semmel, 1968). But contrary to the suggestion that the fCc horizon (6 in Fig. 2) most likely correlates to the last interglacial, an age estimate of 146 ± 9 ka was obtained for the loess sediments accumulated above the fCc horizon and the carbonate concretions. This age estimate indicates that the soil formation correlates most likely to a warm phase of MIS 7. Sample Wei1 and Wei 2 are in good agreement with the stratigraphical loess scheme (Semmel, 1968; 2005) and support the assumption that this loess deposits correlates to the Upper Würmian, which is also indicated by the exposed typical marker horizons.

Conclusion

In our study we applied an elevated temperature IRSL (post-IR IRSL) protocol for polymineral fine-grains of the loess/palaeosol sequence at the gravel quarry Gaul/Weilbach (i) to set up a more reliable chronological framework for this loess/palaeosol sequence and (ii) to answer the question whether the oldest Bt horizon correlates to the Middle Pleistocene (antepenultimate or penultimate interglacial) or to the Upper Pleistocene (last interglacial). Performance tests such as dose recovery and residual checks were carried out to confirm the suitability of our SAR protocol. The IR_{50} and the $pIRIR_{225}$ signals are in good agreement for samples Wei1-Wei6. For sample Wei7 the IR_{50} underestimates the $pIRIR_{225}$. Fading corrected IR_{50} and $pIRIR_{225}$ ages range from 23.7 ± 1.6 to >350 ka. These age estimates indicate that the oldest loess was deposited during marine isotope stage (MIS) 10 or earlier suggesting that the terrasse t4 yield a minimum age of ~350 ka. According to our results the humic-rich horizon was developed during the late phase of MIS 7 and can hence be correlated to the "Weilbacher Humuszone". The oldest exposed fBt horizon most likely correlates to the antepenultimate or penultimate interglacial. Loess above the fCc horizon most

E&G / Vol. 60 / No. 1 / 2011 / 116–125 / DOI 10.3285/eg.60.1.08

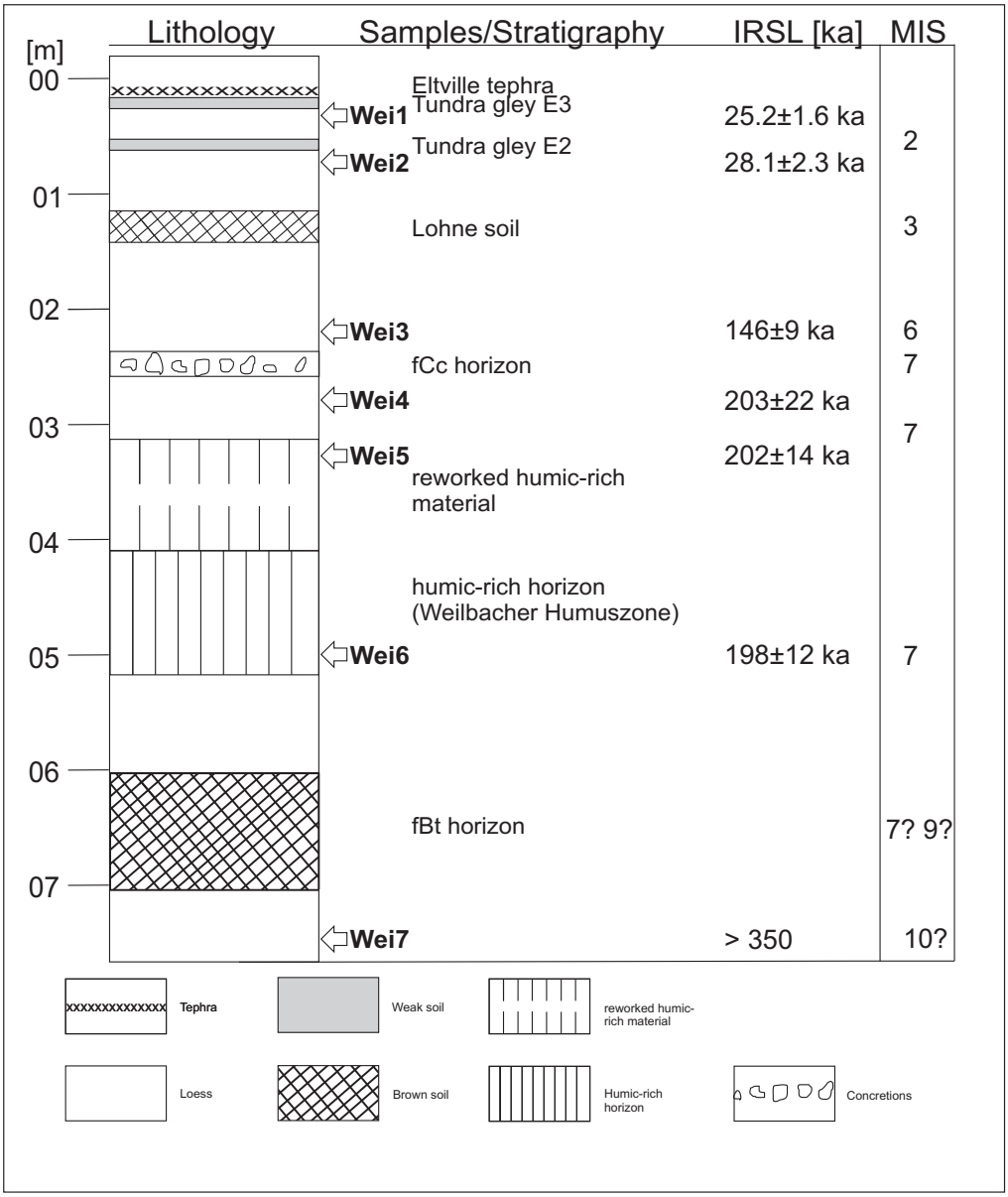

Fig. 7.: Lithology and luminescence ages of the loess/palaeosol sequence exposed at the gravel quarry Gaul/Weilbach. Fading corrected $pIRIR_{225}$ age estimates are presented.

Abb. 7: Lithologie und Lumineszenzalter für die Löss-Paläoboden Sequenz in der Kiesgrube Gaul/Weilbach basierend auf den fading korrigierten $pIRIR_{225}$ Altern.

Table 2: The elevated temperature post-IR IRSL measurement.

Tabelle 2: Post-IR IRSL Messprotokoll.

Step	Treatment	Observed
1	Dose	
2	Preheat, 60s at 250°C	
3	IR stimulation, 100s at 50°C	Lx
4	IR stimulation, 100s at 225°C	**Lx**
5	Test dose	
6	Preheat, 60s at 250°C	
7	IR stimulation, 100s at 50°C	Tx
8	IR stimulation, 100s at 225°C	**Tx**
9	IR stimulation, 40s at 290°C	
10	Return to step 1	

Table 3: Summary of equivalent dose (D_e), recycling ratio, dose recovery, residual doses, fading and luminescence ages. Six aliquots were measured per sample for De determination. For the fading tests three aliquots/sample were measured.

Tabelle 3: Äquivalenzdosen (D_e), Recycling Ratio, Dose Recovery, residuale Dosen, Fading und Lumineszenzalter. Sechs Aliquots wurden pro Probe für die Aquivalenzdosis-Bestimmung gemessen. Für die Fadingmessungen wurden drei Aliquots/Probe verwendet.

Sample	Depth (m)	Measurement	D_e (Gy)	Recycling	Measured/given dose	Residual doses (Gy)	g-value (%/decade)	Uncorrected age (ka)	Corrected age (ka)
Wei 1	0.33	IR_{50}	52.9 ± 1.3	0.99 ± 0.01	0.95 ± 0.01	3.3 ± 0.9	3.2 ± 0.2	17.6 ± 1.1	23.7 ± 1.6
		$pIRIR_{225}$	64.9 ± 2.3	1.02 ± 0.01	1.02 ± 0.03	10.9 ± 1.3	1.7 ± 0.1	21.6 ± 1.4	25.2 ± 1.6
Wei 2	0.75	IR_{50}	65.5 ± 0.9	0.99 ± 0.01	0.96 ± 0.01	3.7 ± 0.5	2.9 ± 0.3	19.8 ± 1.1	25.9 ± 1.9
		$pIRIR_{225}$	78.3 ± 3.5	1.01 ± 0.01	1.01 ± 0.01	11.5 ± 1.6	1.9 ± 0.2	23.5 ± 1.7	28.1 ± 2.3
Wei 3	2,15	IR_{50}	331 ± 4	1.01 ± 0.01	0.94 ± 0.01	5.2 ± 0.6	3.0 ± 0.1	104 ± 9	140 ± 8
		$pIRIR_{225}$	393 ± 3	0.98 ± 0.01	1.02 ± 0.03	13.1 ± 1.7	1.8 ± 0.2	123 ± 6	146 ± 9
Wei 4	2,75	IR_{50}	337 ± 2	1.01 ± 0.003	0.88 ± 0.02	3.6 ± 0.5	3.1 ± 0.1	123 ± 9	177 ± 14
		$pIRIR_{225}$	454 ± 10	0.98 ± 0.01	1.04 ± 0.06	11.9 ± 1.3	1.6 ± 0.3	167 ± 9	203 ± 22
Wei 5	3,25	IR_{50}	388 ± 3	1.00 ± 0.003	0.91 ± 0.01	4.6 ± 0.9	2.9 ± 0.1	129 ± 9	178 ± 12
		$pIRIR_{225}$	503 ± 10	0.99 ± 0.003	1.01 ± 0.03	12.5 ± 1.9	1.6 ± 0.2	167 ± 9	202 ± 14
Wei 6	5,00	IR_{50}	423 ± 4	1.00 ± 0.003	0.94 ± 0.01	5.6 ± 0.2	3.1 ± 0.2	122 ± 7	169 ± 10
		$pIRIR_{225}$	557 ± 7	0.99 ± 0.003	1.04 ± 0.06	14.9 ± 2.1	2.0 ± 0.1	162 ± 9	198 ± 12
Wei 7	7,48	IR_{50}	411 ± 18	0.98 ± 0.03	0.92 ± 0.01	5.00 ± 0.5	2.9 ± 0.4	139 ± 8	>190
		$pIRIR_{225}$	921 ± 41	0.91 ± 0.04	1.05 ± 0.01	13.9 ± 1.1	2.0 ± 0.4	313 ± 22	>350

likely accumulated during MIS 6 indicating that the remains of the palaeosol do not correlate to the last interglacial soil. The two uppermost samples indicate that the youngest loess was accumulated during MIS 2 (Upper Würmian). This is in good agreement with the results of other dating studies regarding the Eltville tephra.

Acknowledgements

This research is part of a PhD study in the frame of the "Leibniz Pakt für Forschung und Innovation" at the LIAG-Institute in Hanover. Ludwig Zöller and Lara Wacha are thanked for the useful comments on the manuscript.

References

Adamiec, M. & Aitken, M.J. (1998): Dose-rate conversion factors: update. – Ancient TL 16: 37–50.

Aitken, M.J. (1985): *Thermoluminescence* Dating, London, 359 pp.

Aitken, M.J. (1998): An Introduction to Optical Dating, Oxford, 267 pp.

Antoine, P., Rousseau, D.-D., Moine, O., Kunesch, S., Hatté, C., Lang, A., Tissoux, H. & Zöller, L. (2009): Rapid and cyclic eolian deposition during the Last Glacial in European loess: a high-resolution record from Nussloch, Germany. – Quaternary Science Reviews 28: 2955–2973.

Auclair, M., Lamothe, M. & Huot, S. (2003): Measurement of anomalous fading for feldspar IRSL using SAR. – Radiation Measurements 37: 487–492.

Bibus, E., Rähle & Wedel, J. (2002): Profilaufbau, Molluskenführung und Parallelisierungs-möglichkeiten des Altwürmabschnitts im Lößprofil Mainz-Weisenau. – Eiszeitalter und Gegenwart 51: 1–14.

Bibus, E., W. Bludau, W., C. Bross, C. & Rähle, W. (1996): Der Altwürm- und Rissabschnitt im Profil Mainz-Weisenau. Frankfurter geowissenschaftliche Arbeiten D20: 21–52.

Buschbeck, H.M. (1993): Thermolumineszenz und ihre Anwendung zu Altersbestimmungen in Geologie und Archäologie. – Diss. Univ. Frankfurt, p.155.

Buylaert J.-P., Thiel, C., Murray, A.S., Vandenberghe, D.A.G., Yi, S. & Lu, H., submitted. IRSL and post-IR IRSL residual doses recorded in modern dust samples from the Chinese Loess Plateau. Geochronometria.

Buylaert, J.P., Murray, A.S., Thomson, K.J. & Jain, M. (2009): Testing the potential of an elevated temperature IRSL signal from K-feldspar. –Radiation Measurements 44: 560–565.

Fink, J. (1973): Internationale Lößforschung, Bericht der INQUA-Lößkommission. – Eiszeitalter & Gegenwart 23/24: 415–426.

Frechen, M. (1999): Upper Pleistocene loess stratigraphy in Southern Germany. Quaternary Science Reviews 18: 243–269.

Frechen, M. & Preusser, F. (1996): Kombinierte Lumineszenz-Datierungen am Beispiel des Lößprofils Mainz-Weisenau. – Frankfurter geowissenschaftliche Arbeiten D 20: 53–66.

Huntley, D.J. & Lamothe, M. (2001): Ubiquity of anomalous fading in K-feldspars and the measurement and correction for it in optical dating. – Canadian *Journal* of *Earth* Sciences 38: 1093–1106.

Lamothe M., Auclair M., Hamzaoui C. & Huot S. (2003): Towards a prediction of long-term anomalous fading of feldspar IRSL. – Radiation Measurements 37: 493–498.

Murray, A.S. & Wintle, A.G. (2003): The single regenerative dose protocol: potential for improvements in reliability. – Radiation Measurements 37: 377–381.

Murray, A.S. & Olley, J.M. (2002): Precision and accuracy in the optically stimulated luminescence dating of sedimentary quartz: a status review. – Geochronometria 21: 1–16.

Prescott, J.R. & Hutton, J.T. (1994): Cosmic ray contribution to dose rates for luminescence and ESR dating: large depths and long-term time variations. – Radiation Measurements 23: 497–500.

Prescott, J.R. & Stephan, L.G. (1982): The contribution of cosmic radiation to the environmental dose for thermoluminescence dating. – PACT 6: 17–25.

Rees-Jones, J. (1995): Optical dating of young sediments using fine-grain quartz. – Ancient TL 13: 9–14.

Roberts, H.M. (2008): The development and application of luminescence dating to loess deposits: a perspective on the past, present and future. – Boreas 37: 483–507.

Schönhals, E., Rohdenburg, H. & Semmel, A. (1964): Ergebnisse neuerer Untersuchungen zur Würmlöß-Gliederung in Hessen. – Eiszeitalter & Gegenwart 15: 199–206.

Semmel, A. (1967): Neue Fundstellen von vulkanischem Material in hessischen Lössen. – Notizbl. hess. L.-Amt Bodenforschung 94: 104–108.

Semmel, A. (1968): Studien über den Verlauf jungpleistozäner Formung in Hessen. – Frankfurter geogr. Hefte 45: 133 S.

Semmel, A. (1969): Quartär.- Erl. geol. Kte. Hessen, Bl. 5916 Hochheim a.M.: 51–99, Wiesbaden.

Semmel, A. (1995): Quarry of the Portlandzementwerke Heidelberg at Mainz-Weisenau. – In: Schirmer, W. (ed.): Quaternary field trips in Central Europe, 1: 452–454, München.

Semmel, A. (2005): Probleme der Abgrenzung und Datierung pleistozäner Terrassen - erörtert an Beispielen aus dem Untermaingebiet. – Geologisches Jahrbuch Hessen 132: 113–129.

Semmel, A. (2005a): 7. Exkursionshalt IV Paläopedologische Probleme im Löß am Mainzer Dreieck S Hofheim a.Ts. – 51 S., Selbstverlag Hofheim/Ts.

Semmel, A. (2007): Löss als Indikator der Landschaftsentwicklung in der Wetterau und am Untermain. – Jahresberichte der Wetterauischen Gesellschaft für die gesamte Naturkunde 153–157: 7–35.

Thomsen, K.J., Murray, A.S., Jain, M. & Bøtter-Jensen, L. (2008): Laboratory fading rates of various luminescence signals from feldspar-rich sediment extracts. – Radiation Measurements 43: 1474–1486.

Visocekas, R. (1985): Tunnelling radiative recombination in labradorite: Its association with anomalous fading of thermoluminescence. – Nuclear Tracks and Radiation Measurements 10 (4–6): 521–529.

Wintle, A.G. (1973): Anomalous fading of thermoluminescence in mineral samples. – Nature 245: 143–144.

Wintle, A.G. & Brunnacker, K. (1982): Ages of volcanic tuff in Rheinhessen obtained by thermoluminescence dating of loess. – Naturwissenschaften 69: 181–183.

Wintle, A.G. & Murray, A.S. (2006): A review of quartz optically stimulated luminescence characteristics and their relevance in single-aliquot regeneration dating protocols. Radiation Measurements 41: 369–391.

Zöller, L. (1989): Geomorphologische und geologische Interpretation von Thermolumineszenz-Daten.- Bayreuther Geowissenschaftliche Arbeiten 14:103–112.

Zöller, L. (1995): Würm- und Rißlößstratigraphie und Thermolumineszenz-Datierung in Süddeutschland und angrenzenden Gebieten. – Habil.schrift Fak. f. Geowiss. Univ. Heidelberg, (unpublished).

Zöller, L. & Semmel, A. (2001): 175 years of loess research in Germany – long records and "uncon-formities". – Earth Science Reviews 54: 19–28

E&G Quaternary Science Journal
Volume 60 / Number 1 / 2011 / 126–136 / DOI 10.3285/eg.60.1.09
www.quaternary-science.net

GEOZON SCIENCE MEDIA
ISSN 0424-7116

Pleistocene loess deposits and mollusc assemblages in the Eastern Pre-Alps

Christa Frank, Birgit Terhorst, Bodo Damm, Christine Thiel, Manfred Frechen, Robert Peticzka

Abstract: In comparison to other areas in low mountain regions, the widespread occurrence and thickness of loess is impressive in the northern Vienna Forest. Due to differences in grain size, it is obvious that the loess deposits of the Hagenbach Valley deviate from those of other locations. In comparison to the results of Krems and Stillfried, the loess of the Hagenbach Valley has a pronounced maximum in the sand fraction reflecting an essential influence of the Flysch sandstone and a proximity to the source sarea. The loess of the Hagenbach Valley is specified as sediment with significant local impact due to a remarkable influence of short distance transport. Partly, the loess is of alluvial origin as it contains small pebbles and therefore it reflects cool and wet paleoenvironmental conditions. The malacological evidences coincide with the geomorphodynamic conditions. Redeposition processes cause a generally high degree of fragmentation. The malacological analyses proved 28 species of terrestrial gastropoda, with a total number of 3,283 specimens. The results indicate very humid and cool climate and a weakly expressed, slightly more favorable period is visible in one of the horizons.

[Pleistozäne Lösssedimente und Molluskengesellschaften in der östlichen Voralpenzone]

Kurzfassung: Die Lössablagerungen im nördlichen Wienerwald sind im Vergleich mit anderen Mittelgebirgsregionen aufgrund ihrer Mächtigkeit sehr eindrucksvoll. Charakterista in der Korngrößenverteilung zeigen deutlich, dass die Lösse im Hagenbachtal sich von denen anderer Lösssgebiete unterscheiden. Ein Vergleich mit Lössprofilen in Krems und Stillfried hat ergeben, dass der Löss im Hagenbachtal einen erhöhten Sandanteil aufweist und damit den Einfluss der Flysch-Sandsteine widerspiegelt. Das spricht für einen lokalen Sedimenteintrag und kurze äolische Transportstrecken. Zudem wurde der Löss unter kühl-humiden Paläoklimabedingungen zum Teil als Schwemmlöss abgelagert. Die malakologischen Ergebnisse stimmen mit den geomorphodynamischen Bedingungen überein. Die Umlagerungsprozesse haben zu einer intensiven Fragmentierung der Schalenreste geführt. Die malakologischen Untersuchungen belegen insgesamt 28 unterschiedliche Arten von terrestrischen Gastropoden mit 3283 Individuen. Die paläoökologische Auswertung spricht für sehr humide, kühle Klimabedingungen mit einer schwach ausgeprägten, klimatisch etwas günstigeren Phase.

Keywords: *Molluscs, dating, loess, low mountain area, Vienna Forest, Upper Pleistocene*

Addresses of authors: C. **Frank**, University of Vienna, Department of Anthropology, Althanstr. 14, A-1090 Vienna/Austria; **B. Terhorst**, University of Würzburg, Institute of Geography and Geology, Am Hubland, D-97074 Würzburg/Germany. E-Mail: birgit.terhorst@uni-wuerzburg.de; **B. Damm**, University of Vechta, ISPA, Universitätsstr. 5, D-49377 Vechta/Germany. E-Mail: bdamm@ispa.uni-vechta.de; **C. Thiel** and **M. Frechen**, Leibniz Institute for Applied Geophysics, S3: Geochronology and Isotope Hydrology, Stilleweg 2, D-30655 Hannover/Germany. E-Mail: Christine.thiel@liag-hannover.de; Manfred.frechen@liag-hannover.de.; **R. Peticzka**, University of Vienna, Institute of Geography and Regional Research, Althanstr. 14, A-1090 Vienna/Austria.

1 Introduction

In Lower Austria, eolian sediments are widespread (Fig. 1) and form thick and well developed loess sequences. These deposits of Lower Austria have been studied for several decades. Detailed descriptions and sedimentological data exist for many loess/paleosol sequences situated in the basins of Vienna and the Alpine foreland (Fink 1976; Kohl 1976; Haesaerts et al. 1996, Terhorst 2007, Peticzka et al. 2010). Geochronological framework for these deposits are most commonly based on radiocarbon (e.g. Haesearts et al. 1996) and luminescence dating (Wallner et al. 1990; Noll et al. 1994, Zöller et al. 1994; Thiel et al. 2011a, 2011b, c). Both dating methods are suitable, at least for the time range of up to 40 ka for radiocarbon (Hajdas 2008) and to 300 ka for luminescence (Thiel et al. 2011a), for the sediments under question and have been proven to be reliable approaches.

While detailed descriptions, sedimentological and chronological data exist for many loess/paleosol sequences in the Vienna basin and the Alpine foreland (e.g. Fink 1956, 1976, 1978; Kukla 1975, Döppes & Rabeder 1997, Terhorst 2007), loess sediments in the low mountain areas have not been studied up to present. The map of loess distribution for Lower Austria clearly shows that loess covers the northern margins of the Vienna Forest (Fig.1). There, loess deposits are frequent and occur in altitudes above 300 m a.s.l. and reach remarkable thicknesses of 4 m in steep slope positions (Damm & Terhorst 2010). Inside the Hagenbach Valley, loess sequences are exposed by landslide processes.

Conforming to several studies, the Vienna Forest offers excellent and suitable conditions for the development of rich malacocoenoses (Klemm 1974; Reischütz 1986, 1988; Frank 1988/89, 1992; Tröstl, 1996, 1997a, b, 1998a, b, 1999, 2000). The variable landscape and favorable climate, the diversity of plant assemblages and the Pleistocene periglacial paleoenvironment offer multifarious possibilities for molluscan life in different ecological niches (mixed deciduous woods, underwood, herbaceous vegetation, mild humus, litter and dead wood, rocky ground).

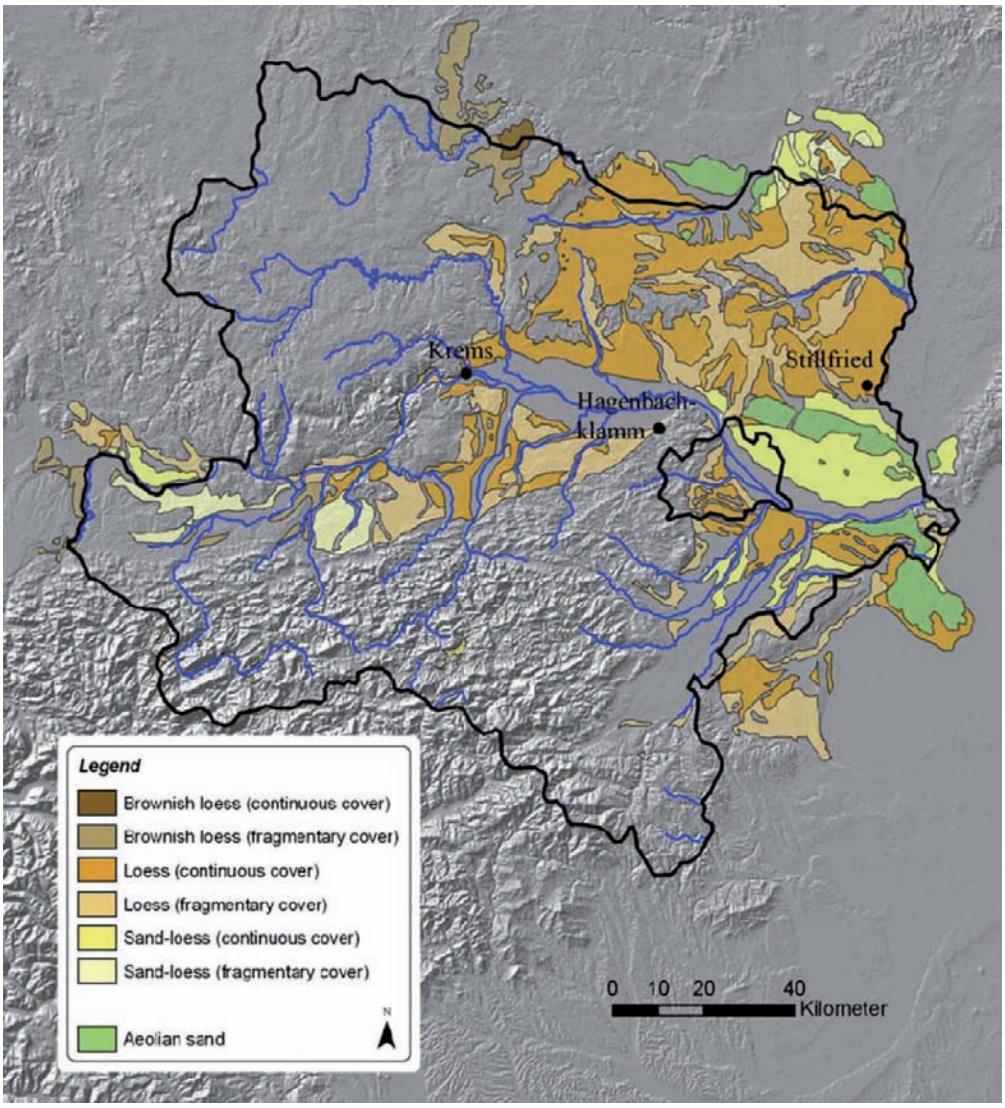

Fig. 1. Loess distribution map of Lower Austria with study sites (black points) (Terhorst et al. 2009).

Abb. 1. Lössverbreitungskarte von Niederösterreich mit Untersuchungsgebieten (Terhorst et al. 2009).

In general, the malacological analyses of a complete pedo-sedimentary sequence of the Hagenbach Valley are promising for insights into the faunal and paleoenvironmental development during the last Middle to Late Glacial period.

Two characteristic sequences and first dating results combining both radiocarbon and luminescence dating are presented with a focus on mollusc analyses in this study. The results are compared to characteristic loess sequences of Lower Austria.

Study area

The Hagenbach Valley (Hagenbachklamm) is situated approximately 16 km to the NW of the city of Vienna (Fig. 2). Climate data for the period between 1971 and 2000 show mean annual temperature of 9.2°C and mean annual precipitation of 741.5 mm (Zamg 2002). The valley is part of the northern margin of the Vienna Forest that represents a rolling landscape of the Central European low mountain regions. The flat-topped mountains of the Vienna Forest with altitudes between 300 and 500 m a.s.l. are deeply incised by valleys.

The study area belongs to the Rhenodanubian Flysch Zone, which is W-E oriented and consists of various layers of (calcareous) sandstones, marly shales, calcareous marls and clay schists. The formations inside the Hagenbach Valley belong to the Altlengbach and the Greifenstein beds. They are dominated by calcareous quartzitic sandstones, which are subdivided by stratified marls and clays (Wessely 2006).

The slopes of the Hagenbach Valley are characterized by various types of Quaternary sediments. The bedrock is covered by loess and Pleistocene periglacial cover beds.

First results concerning Quaternary slope deposits have been published by Damm & Terhorst (2010) and Terhorst et al. (2009). However, the chronology of loess deposits and periglacial layers is not known up to present in the Vienna Forest.

2 Methods

Field survey and sedimentological analyses

The description and determination of soil horizons were conducted according to the German Field Book for Soil Survey (AD-HOC-Arbeitsgruppe Boden 2005). The field description was adapted to the World Reference Base for soil resources (IUSS Working Group WRB, 2006). During the field survey information on texture, bedding, content of carbonate, and colour of soils and sediments was gathered. The differentiation of periglacial cover beds was based on

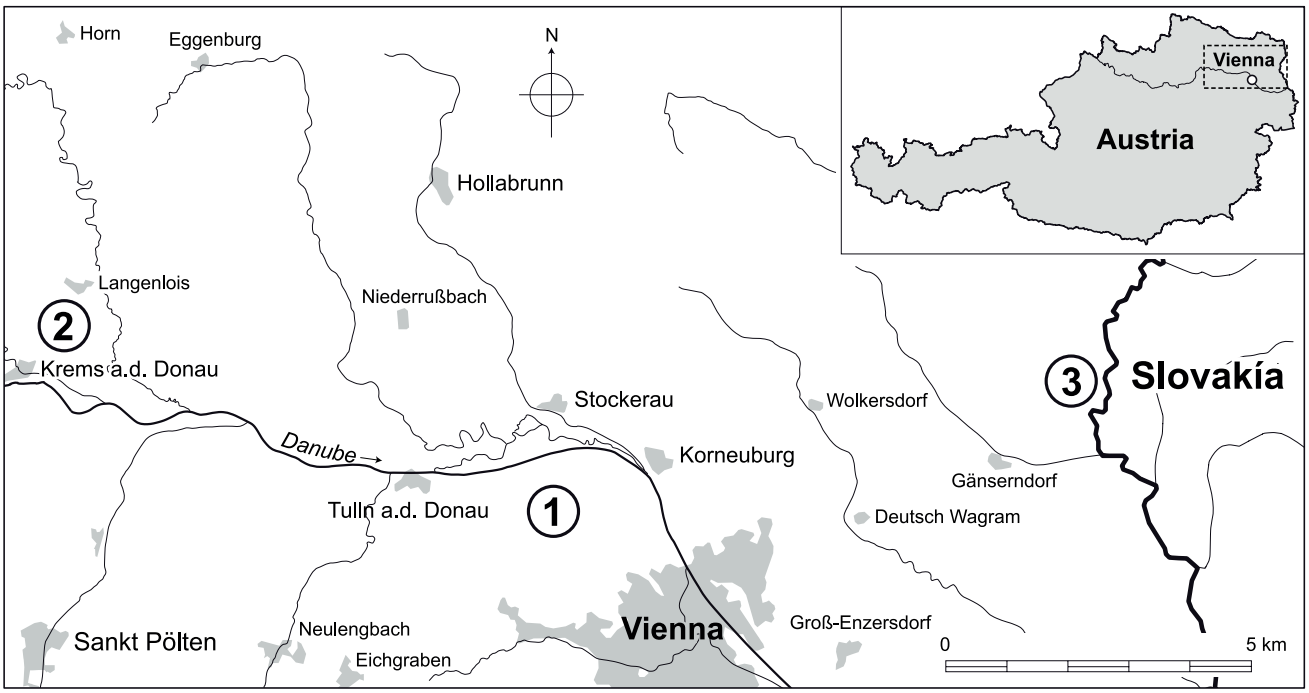

Fig. 2. Study areas in the Vienna Forest and in the loess regions of Lower Austria. 1 = Hagenbach Valley, 2 = Krems, 3 = Stillfried.

Abb. 2. Untersuchungsgebiete im Wienerwald und in den Lössregionen Nierderösterreichs. 1 = Hagenbachklamm, 2 = Krems, 3 = Stillfried.

the German Field Book for Soil Survey (AD-HOC-Arbeitsgruppe Boden 2005). The main criteria were given by sedimentological features such as the occurrence of specific silt contents and rock fragments, which are essential indicators for the differentiation of periglacial cover beds (Semmel & Terhorst 2010). Samples were taken by horizons. Two sequences (A and B) are presented in detail (Fig. 3).

Laboratory analyses included grain size determination according to the combined sieve- and pipette-analysis according to Köhn (Schlichting et al. 1995). The calcium carbonate contents ($CaCO_3$) were measured gasvolumetrically with the Scheibler instrument.

Radiocarbon and luminescence dating

For age determination both radiocarbon and luminescence dating have been applied. Whereas radiocarbon dating estimates the time elapsed since the death of an organism (e.g. Hajdas 2008), luminescence dating techniques determine the time passed since the last exposure of mineral grains to sunlight, and thus enable to constrain the time of deposition (Aitken 1998).

The radiocarbon age (Hv25871) was obtained from charcoal using gas proportional counters. The sample was taken in Sequence B at a depth of 3.9 m in loessic sediments. The calculation of the radiocarbon age is based on the radioactive half-life after Libby, i.e. 5568 years. The age was fitted to the international radiocarbon timescale by NBS oxalic acid standard; the data is $\delta^{13}C$ corrected. All uncertainties of the chemical and technical treatment of the sample are included in the expressed age error (2-sigma standard deviation).

Two luminescence samples were taken in the loess of Sequence A (Fig. 3) by hammering metal tubes into the freshly cleaned profile; sample 1217 was taken at a depth of 2.4 m and sample 1218 at 3.1 m, respectively. Luminescence measurements were made with an automated Risø TL/OSL readers (DA-15; Bøtter-Jensen et al. 2003) equipped with a calibrated $^{90}Sr/^{90}Y$ beta source. The feldspar signal of the polymineral samples was stimulated with infra-red (IR) light diodes emitting at 870 nm, and the luminescence was detected in the blue-violet region through a Schott BG39/Corning 7–59 filter combination.

For equivalent dose (D_e) determination, a single-aliquot regenerative (SAR; Murray & Wintle 2000) protocol with a preheat of 250°C (60 s) and IR stimulation at 50°C for 100 s was applied. An IR illumination at 280°C (100 s) was inserted at the end of each SAR cycle (Murray & Wintle 2003). The laboratory fading rate was measured as the IRSL signal decrease over time using artificially irradiated ali-quots (Lamothe et al. 2003); this is expressed in terms of the percentage decrease of signal intensity per decade (the *g*-value; Aitken 1985, Appendix F).

Material for dosimetry measurements (as part of the luminescence dating) were taken from immediately around the luminescence samples. After drying and homogenizing, 50 g of each sample were packed in N-type beakers, which were stored at least for one month to ensure equilibrium between radon and its daughter nuclides. The concentrations of U, Th and K were determined by high-resolution gamma-ray spectrometry. The dose rates were derived using the conversion factors of Adamiec & Aitken (1998). Calculation of the cosmic dose rate is based on Prescott & Hutton (1994). A water content of 20 ± 5% was estimated, allowing for changes in water content throughout time, and a mean a-value of 0.08 ± 0.01 was used.

Mollusc analyses

Soaked samples (1000g) were treated by wet sieving to 2 mm–630 µm and 200 µm mesh, dried and selected. The 200 µm fraction contained thousands of minute fragments, so only the significant ones (apices, apertures) were picked out for calculating the individual numbers (as proposed by Ložek 1964).

E&G / Vol. 60 / No. 1 / 2011 / 126–136 / DOI 10.3285/eg.60.1.09 / © Authors / Creative Commons Attribution License

Tab. 1: Grain size and calcium carbonate content of sequences A and B, modified after Terhorst et al. (2009).

Tab. 1: Ergebnisse der Korngrößen- und Kalziumkarbonatanalysen der Profile A und B, geändert nach Terhorst et al. (2009).

Sample	Horizon/layer	Clay %	Silt %				Sand %				$CaCO_3$
			fine	middle	coarse	total	fine	middle	coarse	total	
	µm	<2	2–6	6–20	20–63		63–200	200–630	630–2000		%
Sequence A											
6–1	Luvisol, E horizon	19.0	6.3	15.6	40.4	62.3	16.9	1.5	0.3	18.7	0
6–2	Luvisol, EBt horizon	25.4	5.4	12.5	38.6	56.5	16.6	1.3	0.2	18.1	0
6–3	Luvisol, Bt horizon	29.5	4.1	10.6	35.1	49.7	19.1	1.4	0.3	20.8	0
6–4	C1, loess, upper part	6.8	3.4	9.0	43.1	55.5	33.8	3.2	0.7	37.7	34.9
6–5	C1, loess, lower part	7.8	3.4	10.6	48.0	62.0	22.4	3.6	4.2	30.2	36.2
6–6	C2, loess	7.4	4.0	10.0	45.5	59.5	30.0	2.2	0.9	33.1	36.2
6–7	C3, basal periglacial cover bed	31.8	19.7	20.8	13.3	53.8	4.8	4.1	5.5	14.4	31.9
7	Flysch marls	23.3	6.4	16.1	35.6	58.1	16.1	2.3	0.2	18.6	not measured
8	Decomposed Flysch sandstone	7.1	4.7	9.4	17.6	31.7	35.0	20.6	5.6	61.2	6.0
10	Decomposed Flysch sandstone	3.0	1.8	5.3	10.3	17.4	36.0	42.3	1.4	79.7	2.8
11	Decomposed Flysch sandstone	4.0	2.6	6.3	11.1	19.9	31.6	39.9	4.6	76.1	41.7
Sequence B											
17–1	Luvisol, Bt horizon	33.8	5.9	12.8	33.9	52.5	11.8	1.6	0.3	13.7	3.7
17–3	C1, 1.5m, loess	6.7	3.4	15.1	50.7	69.2	19.3	2.4	2.4	24.1	33.9
17–4	C1, 2.0m, loess	9.6	4.3	8.2	55.4	67.9	20.2	1.1	1.1	22.5	23.0
17–5	C1, 2.3m, loess	11.3	5.0	14.4	54.2	73.5	13.0	1.2	1.0	15.2	22.3
17–6	C1 2.5m, loess	10.2	4.7	13.7	56.6	75.0	12.3	1.3	1.1	14.8	23.2
17–7	C2, 2.0m, loess	13.2	5.2	15.0	55.2	75.4	9.4	1.1	0.8	11.3	23.4
17–8	C2, 2.8m, loess	14.8	4.8	15.7	49.7	70.2	12.4	1.6	1.0	14.9	23.4
17–9	C2, 3.0m, loess	13.9	5.2	15.8	52.7	73.7	10.4	1.4	0.5	12.3	21.8
17–10	C2, 3.7m, loess	18.1	5.7	16.7	47.3	69.7	8.6	2.3	1.2	12.2	20.7
17–11	C2, 4.0m, loess	15.6	5.5	15.4	49.5	70.5	11.5	1.7	0.7	13.9	21.4
17–12	C3, basal periglacial cover bed	9.0	2.6	5.1	10.6	18.4	25.6	32.6	14.1	72.6	9.7

3 Results

Field survey and sedimentological analyses

Two sequences at a distance of 300 m were studied. The altitude of both profiles ranges between 260 m and 310 m a.s.l.. Sequence A is situated on the western slope of the Hagenbach Valley, sequence B on the eastern slope. Both loess deposits are situated on top of basal periglacial cover bed (Flysch debris) superimposed on Flysch. In general, a Luvisol is developed on top of the loess.

Sequence A

The sequence starts with a Luvisol consisting of a thin A horizon, an E horizon, partly followed by a transitional EBt horizon, Bt horizon and, as parent material, loess that forms the C horizon (Fig. 3). Soil horizons are free of calcium carbonate and show a loose structure interspersed with pores of different sizes.

Below the 1 m thick Luvisol, a loess deposit with a thickness of 1.4 m is recorded (Fig. 4). The loess shows a pale yellow colour, involves partly small rounded sandstone fragments as well as secondary carbonates. On average, the silt content in the loess deposits is higher than in related soil horizons. Inside the silt fraction, coarse silt constitutes with values from 43.1% to 48.0% makes up the most important fraction (Table 1: 6–4 to 6–6), whereas the fine and middle silt contents are comparatively small. The loess has low clay contents with a maximum value of 7.8%. The carbonate content of the unweathered loess deposits ranges from 34.9% to 36.2% (Table 1). The basal part of the loess (Fig. 3) is characterized by the occurrence of hydromorphic features such as thin brownish and grayish Fe-bands.

Below the eolian deposits, a periglacial cover bed is present, which consists of clays, marls, and debris (Fig. 3). The clay content amounts to 31.8%, the silt content to 53.8% and the sand fraction is lower than in the previously described layers. The carbonate content is 31.9%. The consistence and distribution inside the silt classes deviates from those of the loess. In

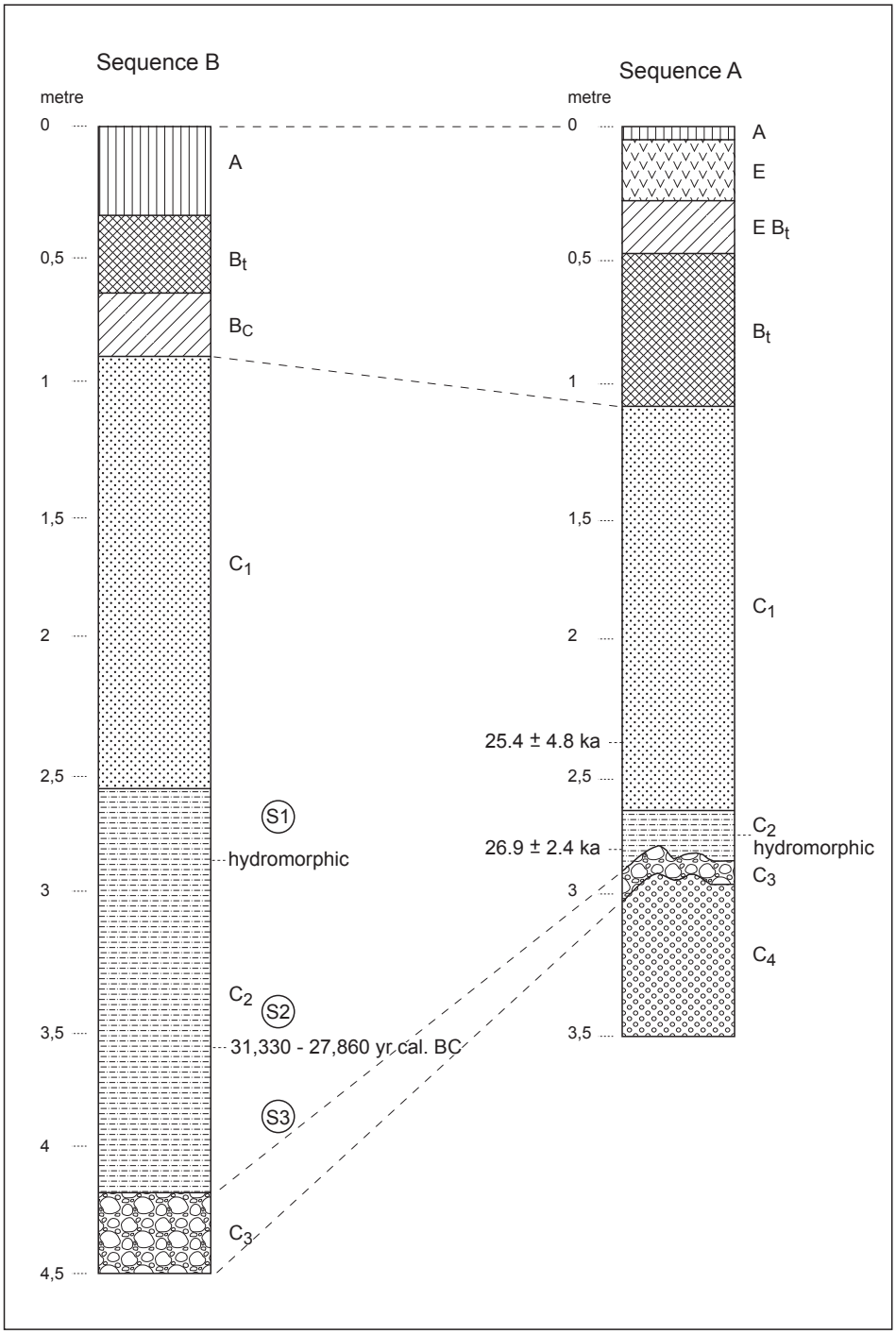

Fig. 3. Loess sequences A and B in the Hagenbach Valley. The profile illustrates the Flysch basement (C4), the basal periglacial cover beds with marls, and sandstone debris (C3), the loess deposits (C1, C2), the Bt horizons of the Luvisos (A/B) as well as the E/EBt horizon (A). The recent soil in sequence B corresponds to an eroded Luvisol.

Abb. 3. Lössprofil A und B in der Hagenbachklamm. Das Profil zeigt den basalen Flysch (C4), die Basislage mit Mergeln und Sandsteinschutt (C3), Lösssedimente (C1, C2), den Bt-Horizont der Parabraunerde (A/B) sowie den E/EBt-Horizont (A). Der rezente Boden in Profil B stellt eine erodierte Parabraunerde dar.

the case of the periglacial cover bed the contents of fine, middle, and coarse silt are more or less homogeneously distributed. The stratum is densely bedded, has an intensively undulated boundary and the debris is composed of Flysch bedrock. The latter meets the diagnostic pre-requisites for the classification as a Pleistocene basal periglacial cover bed.

Samples were taken in the surface formations of the Flysch sandstones to compare loess deposits with the local bedrock (Table 1: 8, 10, 11). Weathered bedrock varies in carbonate content between 2.8% and 6.0%, whereas the carbonate content of less weathered Flysch bedrock can reach values up to 41.7% and reflects the potential carbonate level of the bedrock (Table 1: 11).

Samples that originate from decomposed sandstone are certainly dominated by the sand fraction, which varies between 61.2% and 79.7% (Table 1: 8, 10, 11). It is two to three times higher than in the loess and marls. The maximum contents are in the middle and fine sand fraction, whereas the coarse fraction is of minor importance. Silt contents range between 17.4% and 31.7% with maxima in coarse silt.

Sequence B

The second example of a characteristic pedosedimentary sequence (Fig. 3, B) is situated on the E slope of the Hagenbach Valley, in about 300 m linear distance from sequence A. The upper part of the sequence is formed by a Bt horizon of an eroded Luvisol, disturbed by anthropogenic impact and redeposition of colluvial material. The eroded Luvisol has formed in loess, which has a remarkable thickness of 3.5 m. The upper part of the pale yellow loess shows low clay con-

E&G / Vol. 60 / No. 1 / 2011 / 126–136 / DOI 10.3285/eg.60.1.09 / © Authors / Creative Commons Attribution License

Fig. 4. Loess sequence A in the Hagenbach Valley. Loess deposit on top of Flysch sediments. The uppermost part corresponds to a Haplic Luvisol (see Fig. 3).

Abb. 4. Lössprofil A in der Hagenbachklamm. Lösssedimente auf Flyschgesteinen. Der oberste Profilabschnitt zeigt eine Parabraunerde (vgl. Abb. 3).

tents between 6.7% and 10.2% (Table 1: 17–3 to 17–6). The silt content dominates the grain size distribution and reaches values up to 75.0%. The sand content ranges from 14.8% to 24.1%. The $CaCO_3$ contents are on average about 23%, and only the parts of the sequence, which have secondary carbonates, contain more $CaCO_3$ (33.9%, Table 1: 17–3). In the basal parts of the loess hydromorphic features are present (Fig. 3). The horizon C2 is interspersed with small mottles and bands of rusty iron alternating with grayish mottles of reduced iron. The lowermost horizon, C3 (17–12) consists of sandstone debris and sand, which is exclusively made of Flysch sediments. This debris layer corresponds to the Pleistocene basal periglacial cover bed of sequence A. It consists of local bedrock fragments with stone fragments orientated related to the slope inclination.

Comparison of loess sites in Lower Austria

The characteristics of the loess deposits of the Hagenbach Valley differ significantly from other loess deposits in Lower Austria (Table 2). The loess sediments of the Vienna Forest show a higher percentage in the sand fraction and lower clay content. However, the silt fraction is comparable with those of the loess sequence in Stillfried (Table 2: 20–1 and 20–2). There is a significant analogy in the coarse silt fraction for all study sites. On the contrary, the loess of Krems contains, with values up to 83.5%, significantly more silt in total as well as in the coarse silt fraction (Table 2: 59.1% to 62.3%). In general, the portion of middle silt is higher in the loess regions and reduced in the Vienna Forest study sites.

Dating

The charcoal sampled in Sequence B was dated to 31,330–27,860 years cal. BC (Table 3; calibration after Reimer et al. 2009).

For the luminescence samples the dose recovery tests for all aliquots were within 10% of unity, showing the applicability of the protocol to our samples. Recycling ratios, which show the ability of a measurement protocol to reproducibly measure the response to a laboratory dose given after repeated heating of the sample, are close to unity (1.01 ± 0.01; n=30), and are hence very satisfactory. Furthermore, recuperation for all aliquots was measured to be <5%. The dose rates of 2.4 ± 0.2 Gy/ka and 2.7 ± 0.2 Gy/ka, respectively, are in the range known from Lower Austrian loess deposits (e.g. Thiel et al. 2011a, b, c; Zöller et al. 1994) (Table 3).

The fading uncorrected age for sample 1217 is 20.7 ± 3.7 ka, and sample 1218 was dated to 22.2 ± 1.2 ka. However, for both samples a fading rate of >2%/decade was measured, implying that these uncorrected ages are underestimating the depositional age. Fading correction had to be applied; this is based on Equation 4 of Huntley & Lamothe (2001). The fading corrected ages of 25.4 ± 4.8 ka (sample 1217) and 26.9 ± 2.4 ka (sample 1218) are considered more reliable.

Mollusc analyses / Coenological analysis

Mollusc samples (Table 4 and Table 5) originate from the lower part of the loess sequence B (Fig. 3). They have been taken in a vertical order from the sample position S1 (top) to S3 (base). In sample S2 there is a remarkable decrease in total number of individuals (S1: 1344, S2: 843). However, in sample S3 the number of species is declining (S2: 25, S3: 21), whereas the number of individuals increases noticeably (1106) (Fig. 5 and Fig. 6).

Singular shell fragments of highly demanding woodland species appear only in S1 and S2: *Ena montana* and *Ruthenica filograna* in both of them, cf. *Cochlodina laminata* only in S1, *Aegopinella cf. nitens* only in S2. *Semilimax kotulae* has been found all over the profile. This species occurs also in thanatocoenoses (=mollusc assemblages) pointing to moderate or cold climate. The first-mentioned species are allochthoneous in samples S1 and S2.

There is a range of features common to all three thanatocoenoses (from S1 to S3):

- Petrophile character due to the clausiliid species *Neostyriaca corynodes austroloessica* (rates: S1: 5.7%, S2: 9.8%, S3: 7.4%) and *Clausilia dubia* (S1: 2.4%, S2: 4.6%, S3: 4.3%).
- The presence of *Orcula dolium*.
- The percentage rates of all three species are 9.0% (S1), 15.4% (S2) and 13.1% (S3).
- The indication of humidity due to the predominance of *Trochulus hispidus* and *Trochulus suberectus* (together: S1: 61.7%, S2: 47.9%, S3: 55.0%).
- Elements inhabiting areas of medium humidity, with herbaceous vegetation, hedges or clumps of trees are more distinctly represented in S2 (12%) and S3 (12.2%) than in S1 (3.9%).
- The percentage rates of *Pupilla* species (mostly: *sterrii*, fur-

thermore *triplicata* and *bigranata*) are very low; S1: < 0.9%, S2: 3.6% and S3: < 2.8%.
- Loess elements occur only scarcely with the highest percentages in samples S1 (9.4%). The percentages of S2 and S3 are lower (5.5% and 6.7%, respectively).
- Cold-resistant species *Vertigo modesta arctica* (Wallenberg 1858) and *Vertigo parcedentata* (Braun 1847) occur nowhere in the profile.
- *Cochlicopa lubrica* and *Euconulus praticola*, which are species indicating humid to damp microhabitats appear only in negligible percentages (S1: 0.7%, S2: 0.5%, S3: 0.8%).
- The percentages of *Succinella oblonga*, a species frequently associated with *Trochulus hispidus*, in the Upper Pleistocene layers are rather insignificant (S1: 2.1%, S2: 3.9%, S3: 3.1%; in S1: single specimens of *f. elongata*).
- *Orcula dolium infima* (Zimmermann 1932), a subspecies

Tab. 2: Grain size and calcium carbonate content of sequences A and B in comparison to analyses of loess profiles of Krems and Stillfried in Lower Austria (Terhorst et al. 2009).

Tab. 2: Ergebnisse der Korngrößen- und Kalziumkarbonatanalysen der Profile A und B, im Vergleich mit den Analysen der Lössprofile in Krems und Stillfried in Niederösterreich (Terhorst et al. 2009).

Sample	Profile	Clay	Silt				Sand			
			fine	middle	coarse	total	fine	middle	coarse	total
		<2	2–6	6–20	20–63		63–200	200–630	630–2000	
6–4	Vienna Forest, Hagenbach, loess (E slope)	6.8	3.4	9.0	4,1	55.5	33.8	3.2	0.8	37.7
6–5	Vienna Forest, Hagenbach, loess (E slope)	7.8	3.4	10.6	48.0	62.0	22.4	3.6	4.2	30.2
6–6	Vienna Forest, Hagenbach, loess (E slope)	7.4	4.0	10.0	45.5	59.5	30.0	2.2	0.9	33.1
17–3	Vienna Forest, Hagenbach, Loess (W slope)	6.7	3.4	15.1	50.7	68.2	19.3	2.4	2.4	24.1
17–4	Vienna Forest, Hagenbach, loess (W slope)	9.6	4.3	8.2	55.4	67.9	20.2	1.1	1.1	22.5
17–5	Vienna Forest, Hagenbach, Loess (W slope)	11.3	5.0	14.4	54.2	73.5	13.0	1.2	1.0	15.2
18–1 (B16/9)	Loess region, Krems-Wachtberg	14.0	4.3	15.0	61.9	81.2	6.7	0.6	0.1	7.4
18–2 (B16/10)	Loess region, Krems-Wachtberg	13.5	3.4	17.3	59.1	79.8	6.9	0.4	0.1	7.4
19–1 (SW 1)	Loess region, Krems-Hundsteig	15.3	4.4	14.8	59.8	79.0	8.2	1.1	0.3	9.6
19–2 (SW 7)	Loess region, Krems-Hundsteig	12.4	3.6	17.6	62.3	83.5	7.4	0.6	0.1	8.1
20–1 (StillB10)	Loess region, Stillfried	17.7	5.0	12.8	47.9	65.7	10.5	2.5	0.1	13.1
20–2 (StillB14)	Loess region, Stillfried	18.6	5.9	15.8	40.8	62.5	10.6	2.1	0.1	12.8

Tab. 3: Radiocarbon age and IRSL ages (fading uncorrected and fading corrected) and its corresponding information (dose rates, equivalent doses, fading rates).

Tab. 3: Radiokarbon- und IRSL-Alter (nicht korrigiert und korrigiert für anomales Ausheilen und korrigiert) und die dazugehörigen Informationen (Dosisleistung, Äquivalenzdosis und Fadingrate).

Lab ID	Hv25871	LUM 1217	LUM 1218
Sequence	B	A	A
Depth [m]	3.6	2.35	2.90
Material	charcoal	sediment	sediment
Dating Method	^{14}C	IRSL	IRSL
$\delta^{13}C$ [‰]	-24,3	-	-
Conventional age [a BP]	26,950 ± 1,665	-	-
Calibrated age [a cal. BC]	31,330 – 27,860	-	-
Dose rate [Gy/ka]	-	2.7 ± 0.2	2.4 ± 0.2
D_e [Gy]	-	56.3 ± 3.6	54.1 ± 1.1
g-value [%/decade]	-	2.6 ± 0.3	2.4 ± 0.3
uncorrected age [ka]	-	20.7 ± 3.7	22.2 ± 1.2
corrected age [ka]	-	25.4 ± 4.8	26.9 ± 2.4

E&G / Vol. 60 / No. 1 / 2011 / 126–136 / DOI 10.3285/eg.60.1.09

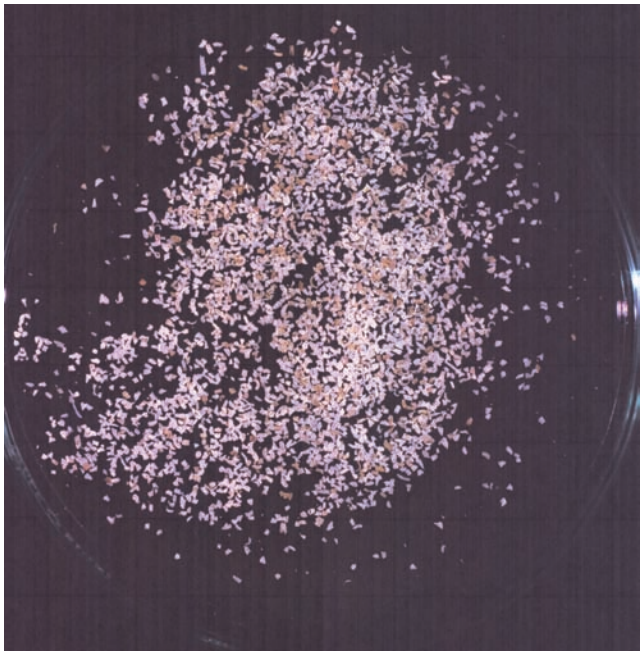

Fig. 5. Mollusc assemblage of sample S1 (see Table 4 and 5).

Abb. 5. Molluskengesellschaft in der Probe S1 (vgl. Tab. 4 und 5).

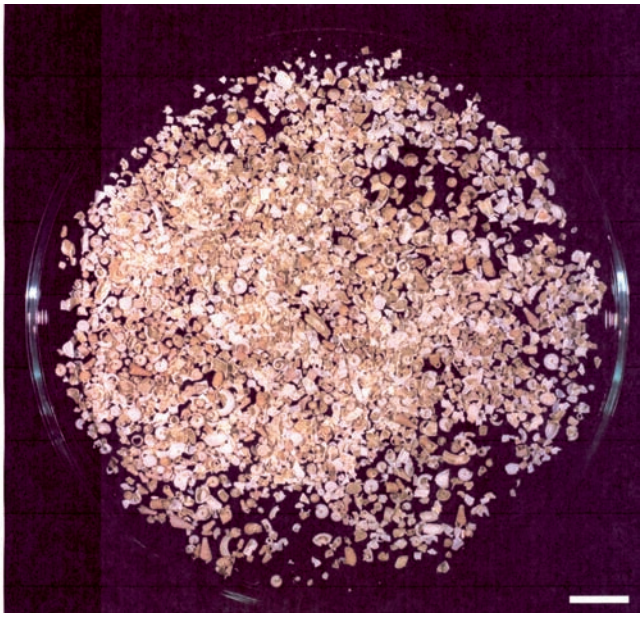

Fig. 6. Mollusc assemblage of sample S3 (see Table 4 and 5).

Abb. 6. Molluskengesellschaft in der Probe S3 (vgl. Tab. 4 und 5).

living in present day malacocoenoses in the neighbourhood of the excavation area, does not occur in the studied samples. This large form seems to be restricted to some regions of the Vienna Forest, at colline to low-mountain altitudes with favourable climate.

- Contaminations and redeposition of material is expressed in the thanatocoenoses of horizons S1 and S2, at a depth of 2.8–3.7m, where single minute, corroded shell fragments of highly demanding woodland species (*Ena montana, Cochlodina laminata, Ruthenica filograna, Aegopinella nitens*) appear. These species certainly occurred in the study area during the middle Holocene climatic optimum but also live there today.

4 Discussion

In comparison to central European low mountain regions, the widespread occurrence and thickness of loess is impressive in the northern Vienna Forest. It is clearly distinguishable from other sediments such as periglacial cover beds and decomposed Flysch bedrock. Furthermore, loess deposits of the characteristic loess regions of Lower Austria can be clearly distinguished. Due to differences in grain size, it is obvious that the loess deposit of the Hagenbach Valley deviates from those of the other locations. The loess profiles of Krems and Stillfried show the characteristic grain size distribution of periglacial eolian sediments with an enhanced input of grains originating from a far distance transport (Pécsi & Richter 1996). In comparison to the results of Krems and Stillfried, the loess of the Hagenbach Valley has a pronounced maximum in the sand fraction, thus reflecting an essential influence of the Flysch sandstone. However, short distance eolian transport is significantly higher in the area under study than in the main loess regions of Lower Austria. Therefore, the loess of the Hagenbach Valley might be specified as sediment with a considerable local impact. Partly, the loess has been redeposited as it contains small pebbles and therefore it reflects cool and wet paleoenvironmental conditions. The results of the datings might be interpreted in this way as well.

The malacological evidences coincide with geomorphodynamic processes like erosion and sedimentation as assumed by Damm & Terhorst (2007, 2010), Damm et al. (2008), and Terhorst et al. (2009). Furthermore, redeposition of loess is suggested by the generally high degree of fragmentation of molluscs shells, especially in sample S1. The periglacial origin of the sediments is reflected by the structure of the thanatocoenoses, which is distinctly contradictory to the rich and varied molluscan assemblage of today.

Malacological evidence points to comparatively least favorable paleoenvironmental factors during the deposition of the uppermost part of the basal loess (Fig. 3, S1). The conditions reflected in the lowermost sample S3 are equally infavorable, but of mitigated character, whereas the sedimentation period of S2 appears slightly moderated.

Following this, the sedimentation period is marked by very humid and cool climate, which does not coincide with the occurrence of very manifold vegetation:

- mainly open to semi-open, probably tundra-like areas
- predominantly herbaceous vegetation and undemanding trees or brushwood
- not very extensive damp habitats
- rocks overgrown with mosses and lichens, shady or exposed

Although the three thanatocoenoses reflect rather cold climate, extreme conditions are nowhere recognizable, indicated by the low percentage rates of the typical loess species *Pupilla*, *Vallonia tenuilabris* and *Columella columella*, the absence of cold-tolerant *Vertigo*'s, the obviously not very differentiated structure of the thanatocoenoses, the mass development of the *Trochulus* species, and the presence of the *Neostyriaca corynodes* subspecies *austroloessica*. According to Klemm (1969), the latter is associated with environmental conditions similar to those in the Eastern Alps from about

Tab. 4: Species list with absolute numbers.

Tab. 4: Liste der Spezies mit absoluten Zahlen.

Family	Genus	Species	S1	S2	S3	Total
Succineidae	Succinella J.Mabille 1871	S. oblonga (Draparnaud 1801)	28[1]	33	34	95
Cochlicopidae	Cochlicopa A.Férussac 1821	C. lubrica (O.F.Müller 1774)	4	3	3	10
Orculidae	Orcula Held 1838	O. dolium (Draparnaud 1801)	12	8	15	35
Valloniidae	Vallonia Risso 1826	V. costata (O.F.Müller 1774)	7	4	12	23
		V. tenuilabris (A.Braun 1843)	1	3	3	7
Pupillidae	Pupilla Fleming 1828	P. alpicola densegyrata Ložek 1954)	21	8	17	46
		P. muscorum (Linnaeus 1758)	15	7	8	30
		P. bigranata (Rossmaessler 1839)	1	-	3	4
		P. triplicata (S. Studer 1820)	3	3	5	11
		P. sterrii (Voith 1840)	8	27	23	58
		P. loessica (Lozek 1954)	6	2	1	9
		Apices	81[2]	26[3]	45[4]	152
Vertiginidae	Columella Westerlund 1878	C. columella (G.v.Martens 1830)	3	1	-	4
	Vertigo O.F. Müller 1773	V. substriata (Jeffreys 1833)	1	-	-	1
Enidae	Ena Turton 1831	E. montana (Draparnaud 1801)	2[5]	1[6]	-	3
Clausiliidae	Cochlodina A. Férussac 1821	C. laminata (Montagu 1803)	1[7]	-	-	1
	Ruthenica Lindholm 1924	R. filograna (Rossmaessler 1836)	1[8]	1[9]	-	2
	Clausilia Draparnaud 1805					
	Clausilia (Andraea) L. Pfeiffer 1848	C. (A.) dubia (Draparnaud 1805)	32	39	48	119
	Neostyriaca A.J.Wagner 1920	N. corynodes (Held 1836): austroloessica (Klemm 1969)	77	83	82	242
Punctidae	Punctum Morse 1864	P. pygmaeum (Draparnaud 1801)	39	34	19	92
Pristilomatidae	Vitrea Fitzinger 1833	V. crystallina (O.F.Müller 1774)	32	86	111	229
Euconulidae	Euconulus Reinhardt 1883	E. fulvus (O.F.Müller 1774)	5	3	1	9
		E. praticola (Reinhardt 1883)	5	1	6	12
Oxychilidae	Aegopinella Lindholm 1927	A. nitens (Michaud 1831)	-	3[10]	-	3
Vitrinidae	Semilimax Agassiz 1845					
	Semilimax (Hessemilimax) Schileyko 1986	S. (H.) kotulae (Westerlund 1883)	1	1	4	6
Hygromiidae	Euomphalia Westerlund 1889	E. strigella (Draparnaud 1801)	1	-	-	1
	Trochulus Chemnitz 1786	T. hispidus (Linnaeus 1758)	452	204	294	950
		T. suberectus (Clessin 1878)	377	200	314	891
		T. sp.: Embryonic whorls	112[11]	50[12]	48[13]	210
Helicidae	Arianta Turton 1831	A. arbustorum (Linnaeus 1758)	16	12	10	38
		Total number	1,344	843	1,106	3,293

1 single specimens: +/- var. elongata (Sandberger 1875), 2 most of them: muscorum, alpicola densegyrata, 3 most of them: alpicola densegyrata, loessica 4 muscorum, alpicola densegyrata, loessica, 5 fragments of body whorl, 6 atypical fragment, 7 cf. fragment of aperture, 8 cf. fragment of body whorl, 9 atypical fragment, 10 cf. two of them: fragments of body whorl, 11 hispidus + suberectus, 12 like in S1, 13 like in S1 and S2

Tab. 5: Minute, atypical fragments, estimated number (S3: ca. 3,700 fragments, S1: ca. 5,700 fragments).

Tab. 5: Winzige, unspezifische Windungsfragmente, geschätzte Anzahl (S3: ca. 3.700 Fragmente, S1: ca. 5.700 Fragmente).

	S1	S2	S3	Total
Number	**~5.750**	**~2.150**	**~3.700**	**~11.600**
Contents	Mostly Trochulus hispidus, Trochulus suberectus, Orcula dolium, Clausilia dubia, Neostyriaca corynodes.	Mostly both Trochulus sp., Neostyriaca corynodes, Clausilia dubia.	Mostly both Trochulus sp., Clausilia dubia, Neostyriaca corynodes, Pupilla sp., Vitrea crystallina, also Arianta arbustorum, Euconulus sp., Cochlicopa lubrica, Succinella oblonga.	

E&G / Vol. 60 / No. 1 / 2011 / 126–136 / DOI 10.3285/eg.60.1.09 / © Authors / Creative Commons Attribution License

1,400 m upwards to about 2,300 m asl. Klemm (1969) has listed the occurrence in different loess deposits in the Danube Valley of Upper and Lower Austria (c.f. Frank 2006).

Furthermore, the absence of large *Orcula dolium* specimens is worth mentioning in this context, since the study area is situated within the "infima zone" sensu Zimmermann (1932) and Klemm (1974). Local populations of such "fattened" forms would rather point to optimum living conditions. Therefore, one may conclude that this large subspecies that occur nowadays in the southern and eastern Vienna Forest have developed subsequently during the Postglacial warming.

In general, there is good agreement between malacological results and the obtained dating results. The slightly older age estimate for the charcoal compared to the luminescence age could be either due to problems in fading correction as observed by others (e.g. Wallinga et al. 2007), i.e. even after fading correction the luminescence ages are underestimates, or due to reworking and correspondingly later incorporation of the charcoal into the hydromorphic unit C2. However, within two standard deviations, there is good agreement of the obtained ages.

Both, ^{14}C- and IRSL-dating indicate deposition of loess and loess-like sediments prior to the Last Glacial Maximum. This is consistent with formerly presented luminescence ages of ~25–30 ka (Thiel et al., 2011a, b, c) for loess deposits in the Kremser Feld. From these studies it seems evident that the phase of loess deposition during the Last Glacial Maximum is not well documented in Lower Austria, whereas the period between ~25–30 ka can be found in several outcrops, for instance in Stillfried (cf. Frank 1997), in the archaeological sites Willendorf (Haesaerts et al. 1996), and Krems-Wachtberg (Neugebauer-Maresch 2008). Hence, the observations made for the Hagenbach Valley fit to results obtained from other loess sequences of Lower Austria. However, there is still a lack of high resolution dating in relevant profiles, also for the Hagenbach Valley. Moreover, investigations have focussed on the relevant archaeological horizons of a sequence (Haesaerts et al. 1996), and younger loess might not have been observed due to sampling and dating strategies. It is evident that loess/paleosol sequences of the LGM are ubiquitous in Upper Austria (Terhorst et al. 2002; Starnberger et al. 2009).

Acknowledgements

We would like to thank C. Hermann (University of Vienna, Institute of Geography and Regional Research) for laboratory assistance, G. Hillebrand (Zoological Garden of Vienna / Schönbrunn) for picking the numerous shell fragments and S. Pohl (University of Vienna, Facility for Cell Imaging and Ultrastructure Research) for taking the photographs. We are grateful to S. Riemenschneider (Leibniz Institute for Applied Geophysics) for preparation of the luminescence samples. Furthermore, we thank Gudrun Drewes and Petra Posimowski for preparation and measurement of the radiocarbon sample.

References

Adamiec, G. & Aitken, M. J. (1998): Dose-rate conversion factors: update. – Ancient TL, 16: 37–50.

AD-HOC-Arbeitsgruppe Boden (2005): Bodenkundliche Kartieranleitung. – 438 pp., 5th ed., Hannover.

Aitken, M. J. (1985): Thermoluminescence Dating. – 359 pp., Academic Press, London.

Aitken, M. J. (1998): An introduction to optical dating – The Dating of Quaternary Sediments by the Use of Photon-Stimulated Luminescence. – 267 p., Oxford University Press, Oxford.

Bøtter-Jensen, L., Andersen, C. E., Duller, G. A. T. & Murray, A. S. (2003): Developments in radiation, stimulation and observation facilities in luminescence measurements. - Radiation Measurements, 37: 535–541.

Damm, B. & Terhorst, B. (2007): Quaternary slope formation and landslide susceptibility in the Flysch Zone of the Vienna Forest (Austria). – Geomorphology for the Future, Innsbruck University Press, Innsbruck (Austria), pp. 89–96.

Damm, B. & Terhorst, B. (2010): A model of slope formation related to landslide activity in the Eastern Prealps, Austria. Geomorphology, 122/3–4: 338–350.

Damm, B., Terhorst, B., Köttritsch, E., Ottner, F. & Mayrhofer, M. (2008): Zum Einfluss bodenphysikalischer und bodenmechanischer Parameter in quartären Deckschichten auf Massenbewegungen im Wienerwald. – Abhandlungen der Geologischen Bundesanstalt, 62: 33–37.

Döppes, D. & Rabeder, G. (Eds.) (1997): Pliozäne und pleistozäne Faunen Österreichs. – pp. 123–130, Verlag der Österreichischen Akademie der Wissenschaften, Wien.

Fink, J. (1956): Zur Korrelation der Terrassen und Lösse in Österreich. – Eiszeitalter und Gegenwart, 7: 49–77.

Fink, J. (1976): Exkursion durch den österreichischen Teil des nördlichen Alpenvorlandes und den Donauraum zwischen Krems und Wiener Pforte. – Erweiterter Führer zur Exkursion aus Anlass der 2. Tagung der IGCP-Projektgruppe, Quaternary Glaciations in the Northern Hemisphere'. Mitteilungen der Kommission für Quartärforschung der Österreichischen Akademie der Wissenschaften, 1: 113 p.

Fink, J. (1978): Exkursion durch den österreichischen Teil des nördlichen Alpenvorlandes und den Donauraum zwischen Krems und Wiener Pforte. – Ergänzung zu Band 1. Mitteilungen der Kommission für Quartärforschung der Österreichischen Akademie der Wissenschaften, 2: 31 p.

Frank, C. (1988/89): Ein Beitrag zur Kenntnis der Molluskenfaunen Österreichs. Zusammenfassung der Sammeldaten aus Salzburg, Oberösterreich, Niederösterreich, Steiermark, Burgenland und Kärnten (1965–1987). – Jahrbuch für Landeskunde Niederösterreichs, pp. 85–144.

Frank, C. (1992): Malakologisches aus dem Ostalpenraum. – Linzer Biologische Beiträge, 24/2: 383–662.

Frank, C. (1997): Stillfried-Typusprofile. In: Döppes, D. & Rabeder, G. (Eds.): Pliozäne und pleistozäne Faunen Österreichs. – pp. 123–130, Verlag der Österreichischen Akademie der Wissenschaften, Wien.

Frank, C. (2006): Plio-pleistozäne und holozäne Mollusken Österreichs. Teil 1 und 2. – Mitteilungen der Prähistorischen Kommission der Österreichischen Akademie der Wissenschaften 62: 1–395; 397–860.

Haesaerts, P., Damblon, F., Bachner, M. & Trnka, G. (1996): Revised stratigraphy and chronology of the Willendorf II sequence, Lower Austria. – Archaeologia Austriaca, 80: 25–42.

Hajdas, I. (2008): Radiocarbon dating and its application in Quaternary studies. – Eiszeitalter und Gegenwart, 57: 2–24.

Huntley, D. J. & Lamothe, M. (2001): Ubiquity of anomalous fading in K-feldspars and the measurement and correction for it in optical dating. – Canadian Journal of Earth Science, 38: 1093–1106.

IUSS Working Group WRB, 2006. World Reference Base for Soil Resources. – World Soil Resources Reports 103, FAO, Rome.

Klemm, W. (1969): Das Subgenus *Neostyriaca* A.J. WAGNER 1920, besonders der Rassenkreis *Clausilia (Neostyriaca) corynodes* HELD 1836. – Archiv für Molluskenkunde, 99(5/6): 285–311, Frankfurt/Main.

Klemm, W. (1974): Die Verbreitung der rezenten Land-Gehäuse-Schnecken in Österreich. – Denkschrift Österreichische Akademie der Wissenschaften, 117: 503pp., Springer Verlag, Wien/New York.

Kohl, H. (1976): Lehmgrube der Ziegelei Würzburger in Aschet bei Wels. – Mitteilungen der Kommission für Quartärforschung der Österreichischen Akademie der Wissenschaften, 1: 37–41.

Kukla, G.J. (1975): Loess stratigraphy of central Europe. In: K.W. Butzer and L.I. Isaac, Editors, *After Australopithecenes*, Mouton Publishers, The Hague, pp. 99–187.

Lamothe, M., Auclair, M., Hamzaoui, C. & Huot, S. (2003): Towards a prediction of long-term anomalous fading of feldspar IRSL. – Radiation Measurements, 37: 493–498.

Ložek, V. (1964): Quartärmollusken der Tschechoslowakei. – Rozpravy ústředního ústavu geoglogichékho, 31: 374 p., Prag.

Murray, A. S. & Wintle, A. G. (2000): Luminescence dating of quartz using an improved single-aliquot regenerative-dose protocol. – Radiation Measurements, 32: 57–73.

Murray, A. S. & Wintle, A. G. (2003): The single aliquot regenerative dose protocol: potential for improvements in reliability. – Radiation Measurements, 37: 377–381.

Neugebauer-Maresch, C. (2008): Krems-Hundssteig – Mammutjägerlager der Eiszeit. – 347 p., Verlag der Österreichischen Akademie der Wissenschaften, Wien.

Noll, M., Leitner-Wild, E., Hille, P. (1994): Thermoluminescence dating of loess deposits at Paudorf, Austria. Quaternary Geochronology (Quaternary Science Reviews), 13: 473–476.

Pécsi, M. & Richter, G. (1996): Löss Herkunft – Gliederung – Landschaften. – Zeitschrift für Geomorphologie, N. F. Suppl., 98: 391 p.

Peticzka, R., Holawe, F., Riegler, D. (2010): Structural analyses on the modified paleosol-sequence of "Stillfried B" with high resolution measurements of selected laboratory parameters. – Quaternary International, 222: 168–177.

Prescott, J. R. & Hutton, J. T. (1994): Cosmic ray contributions to dose rates for luminescence and ESR dating: large depths and long-term variations. – Radiation Measurements, 23: 497–500.

Reimer, P.J., Baillie, M.G.L., Bard, E., Bayliss, A., Beck, J.W., Bertrand, C.J.H., Blackwell, P.G., Buck, C.E., Burr, G.S., Cutler, K.B., Damon, P.E., Edwards, R.L.,Fairbanks, R.G., Friedrich, M., Guilderson, T.P., Hogg, A.G., Hughen, K.A., Kromer, B., McCormac, F.G., Manning, S., Bronk Ramsey, C., Reimer, R.W., Remmele, S., Southon, J.R., Stuiver, M., Talamo, S., Taylor, F.W., van der Plicht, J. & Weyhenmeyer, C.E. (2004): IntCal04 terrestrial radiocarbon age calibration, 0–26 cal kyr BP. - Radiocarbon, 51: 1111–1150.

Reischütz, P. L. (1986): Die Verbreitung der Nacktschnecken Österreichs (Arionidae, Milacidae, Limacidae, Agriolimacidae, Boettgerillidae). – Sitzungsberichte der Österreichischen Akademie der Wissenschaften, Mathemathisch-naturwissenschaftliche Klasse, Abt. I, 195(1–5): 67–190, Springer Verlag, Wien/New York.

Reischütz, P. L. (1988): Contributions to the mollusc fauna of Lower Austria, VII. The distribution of the Hydrobioidae of Lower Austria, Vienna and Burgenland. – De Kreukel, 1963: 67–87.

Schlichting, E., Blume, H.-P. &Stahr, K. (1995): Bodenkundliches Praktikum. – 295 pp., Blackwell, Wien.

Semmel, A. & Terhorst, B. (2010): The concept of the Pleistocene periglacial cover beds in Central Europe – A review. Quaternary International 222/1–2: 120–128.

Starnberger, R., Terhorst, B., Rähle, W., Peticzka, R. & Haas, J.N. (2009): Paleoecology of periglacial environments during OIS-2 in the forefields of the Salzach Glacier (Upper Austria). – Quaternary International, 198: 51–61.

Terhorst, B., Frechen, M. & Reitner, J. (2002): Chronostratigraphische Ergebnisse aus Lößprofilen der Inn- und Traun-Hochterrassen in Oberösterreich. – Zeitschrift für Geomorphologie N.F., 127: 213–232.

Terhorst, B. (2007): Korrelation von mittelpleistozänen Löß-/Paläobodensequenzen in Oberösterreich mit einer marinen Sauerstoffisotopenkurve. E & G Quaternary Science Journal, 56/3: 172–185.

Terhorst, B. Damm, B., Peticzka, R. & Köttritsch, E. (2009): Reconstruction of Quaternary landscape formation as a tool to understand present geomorphological processes in the Eastern Prealps (Austria). – In: Costantini, E., Makeev, A. & Sauer, D. (eds.): Recent Developments and New Frontiers in Paleopedology. Quaternary International, 209: 66–78.

Terhorst, B., Frechen, M. & Reitner, J. (2002): Chronostratigraphische Ergebnisse aus Lößprofilen der Inn- und Traun-Hochterrassen in Oberösterreich. – Zeitschrift für Geomorphologie, N. F. Suppl., 127: 213–232.

Thiel, C., Buylaert, J.-P., Murray, A. S., Terhorst, B., Hofer, I., Tsukamoto, S. & Frechen, M. (2011a): Luminescence dating of the Stratzing loess profile (Austria) – Testing the potential of an elevated temperature post-IR IRSL protocol. – Quaternary International. 234/1–2: 23–31.

Thiel, C., Buylaert, J.-P., Murray, A. S., Terhorst, B., Tsukamoto, S. & Frechen, M. (2011b): Investigating the chronostratigraphy of prominent palaeosols in Lower Austria using post-IR IRSL dating. – E&G Quaternary Science Journal.

Thiel, C., Terhorst, B., Jaburová, I., Buylaert, J.-P., Murray, A. S., Fladerer, F. A., Damm, B., Frechen, M. & Ottner, F., (2011c): Quaternary landscape evolution in Lower Austria revealed in the brickyard of Langenlois. Geomorphology. doi:10.1016/j.geomorph.2011.02.011.

Tröstl, R. A. (1996): Faunistisch-ökologische Untersuchungen der Molluskenfauna verschiedener Mischwaldtypen des Wienerwaldes (Ost-Österreich). – 226 p., phD thesis University of Vienna.

Tröstl, R. A. (1997a): Faunistisch-ökologische Betrachtungen der Schneckengemeinschaften des Wienerwaldes. 1. Gipfel-Eschenwald (Aceri-Carpinetum subass. aegopodietosum KLIKA 1941 em. HUSOVÁ 1982) des Hermannskogels und Linden-Kalkschutthalden-Wald (Aceri carpinetum KLIKA 1941 s.l.) des Leopoldsberges. – Verhandlungen der Zoologisch-Botanischen Gesellschaft Österreich, 134: 7–91, Wien.

Tröstl, R. A. (1997b): Faunistisch-ökologische Betrachtungen der Schneckengemeinschaften des Wienerwaldes. 2. Eichen-Hainbuchenwälder (Verband Carpinion betuli ISSLER 1931) des Leopolds-, Latis- und Gränberges; 3. Wärmeliebende Eichenmischwälder (Ordnung Quercetalia pubescentis KLIKA 1933) des Leopoldsberges. – Verhandlungen der Zoologisch-Botanischen Gesellschaft Österreich, 134: 93–117, Wien.

Tröstl, R. A. (1998a): Faunistisch-ökologische Betrachtungen der Schneckengemeinschaften des Wienerwaldes. 4. Waldmeister-Buchenwald (Asperulo odoratae-Fagetum SOUGNEZ & THILL 1959) des Kahlenberges, Hinterhainbachs (Umgebung), des Hermannskogels und Gränberges; 5. Wimperseggen-Buchenwald (Carici pilosae-Fagetum OBERDORFER 1957) des Sauberges. – Verhandlungen der Zoologisch-Botanischen Gesellschaft Österreich, 135: 231–258.

Tröstl, R. A. (1998b): Faunistisch-ökologische Betrachtungen der Schnecken-gemeinschaften des Wienerwaldes. 6. Grenzwaldkomplex des Kalenderberges (Mödlinger Klause). – Verhandlungen der Zoologisch-Botanischen Gesellschaft Österreich, 135: 259–270.

Tröstl, R. A. (1999): Faunistisch-ökologische Betrachtungen der Schneckengemeinschaften des Wienerwaldes. 7. Synoptische Schlußbetrachtung. – Verhandlungen der Zoologisch-Botanischen Gesellschaft Österreich, 136: 127–147.

Tröstl, R. A. (2000): Über das Vorkommen von *Orcula dolium* (DRAPARNAUD, 1801) im nordöstlichsten Teil des Flysch-Wienerwaldes. – Verhandlungen der Zoologisch-Botanischen Gesellschaft Österreich, 137: 147–152.

Wallinga, J., Bos, A. J. J., Dorenbos, P., Murray, A. S. & Schokker, J., (2007): A test case for anomalous fading correction in IRSL. Quaternary Geochronology, 2: 216–221.

Wallner, G., Wild, E., Aref-Azar, H., Hille, P. & Schmidt, W.F.O. (1990): Dating of Austrian loess deposits. Radiation Protection Dosimetry, 34: 69–72.

Wessely, G. (2006): Geologie der Österreichischen Bundesländer – Niederösterreich. – Geologische Bundesanstalt Wien, pp. 416.

Zamg (2002): Klimadaten von Österreich 1971–2000. Klimadaten von über 200 Stationen in ganz Österreich. – Daten-CD.

Zimmermann, S. (1932): Über die Verbreitung und die Formen des Genus *Orcula* Held in den Ostalpen. – Archiv für Naturgeschichte, N.F., 1: 1–56.

Zöller, L., Oches, E. A. & McCoy, W. D. (1994): Towards a revised chronostratigraphy of loess in Austria with respect to key sections in the Czech Republic and in Hungary. – Quaternary Geochronology (Quaternary Science Reviews) 13: 465–472.

E&G Quaternary Science Journal
Volume 60 / Number 1 / 2011 / 137–152 / DOI 10.3285/eg.60.1.10
www.quaternary-science.net

GEOZON SCIENCE MEDIA
ISSN 0424-7116

Investigating the chronostratigraphy of prominent palaeosols in Lower Austria using post-IR IRSL dating

Christine Thiel, Jan-Pieter Buylaert, Andrew S. Murray , Birgit Terhorst, Sumiko Tsukamoto, Manfred Frechen, Tobias Sprafke

Abstract: The age of most Lower Austria loess deposits is unknown; this is especially true for Middle Pleistocene loess because there is no generally applicable dating method available. Recently it has been shown that infrared stimulated luminescence (IRSL) signals measured at elevated temperatures after an infrared (IR) stimulation are more stable than the standard IRSL signal measured at 50°C. These signals offer new opportunities to extend the datable age range by minimising or circumventing the undesirable anomalous fading correction. In this study we apply, for the first time, two post-IR IRSL single-aliquot regenerative (SAR) dating protocols to polymineral fine-grain samples from three loess/palaeosol sequences in Lower Austria. The luminescence characteristics and ages derived from these protocols are compared with the IRSL results obtained at 50°C. Recycling ratios, recuperation and dose recovery tests show that these protocols are applicable to the loess under investigation. Fading rates for the post-IR IRSL signals are significantly smaller than for the IRSL at 50°C; the differences in fading rates between post-IR IRSL at 225°C and post-IR IRSL at 290°C are less obvious. Significant fading corrections are needed for the ages derived from the IRSL signal at 50°C. From our study we conclude that the fading corrected post-IR IRSL at 225°C and the fading uncorrected post-IR IRSL at 290°C provide the best age estimates; we prefer the latter because no fading correction is apparently needed. Our data strongly suggest that the pedocomplex 'Paudorfer Bodenbildung' developed during marine isotope stage (MIS) 5, whereas the pedocomplex 'Göttweiger Verlehmungszone' is significantly older (≥ 350 ka) than has been suggested in former studies.

(Untersuchungen zur Chronostratographie von bekannten Paläoböden in Niederösterreich mittels post-IR IRSL-Datierung)

Kurzfassung: Das Alter der meisten Lössablagerungen in Niederösterreich ist nicht bekannt. Das gilt insbesondere für mittelpleistozänen Löss, weil es keine allgemein anwendbare und akzeptierte Datierungsmethode für diesen Zeitraum gibt. Vor kurzem wurde gezeigt, dass infrarot-stimulierte Lumineszenz-(IRSL)-Signale, die bei erhöhten Temperaturen nach einer IR-Stimulation gemessen werden, wesentlich stabiler sind als standardmäßig bei 50°C gemessene IRSL-Signale. Diese Signale eröffnen die Möglichkeit, die datierbare Altersgrenze zu erweitern, indem der anomale Signalverlust (Fading) minimiert oder gar komplett umgangen wird. In dieser Arbeit wenden wir erstmalig zwei post-IR IRSL Single-Aliquot (SAR)-Datierungsprotokolle für polymineralische Feinkornextrakte von drei unterschiedlichen Löss-Paläoboden-Sequenzen aus Niederösterreich an. Die Lumineszenzcharakteristika und Alter der unterschiedlichen Protokolle werden mit denen von Messungen bei 50°C verglichen. Standardisierte Tests (recycling ratios, recuperation und dose recovery) zeigen, dass die Protokolle auf den untersuchten Löss anwendbar sind. Die Fading-Raten für die post-IR IRSL-Signale sind wesentlich geringer als für IRSL bei 50°C, während die Unterschiede in gemessenen Fading-Raten für post-IR IRSL bei 225°C und post-IR IRSL bei 290°C weniger offensichtlich sind. Signifikante Fading-Korrekturen für IRSL bei 50°C sind notwendig. Basierend auf unseren Daten schlussfolgern wir, dass die fading-korrigierten post-IR IRSL Alter bei 225°C und die nicht-korrigierten post-IR IRSL Alter bei 290°C die besten Altersabschätzungen für die untersuchten Sedimente liefern. Wir bevorzugen die letztgenannten Alter, weil keine Abhängigkeit zu Fading-Korrekturen besteht. Unsere Daten weisen darauf hin, dass die Paudorfer Bodenbildung sich während MIS 5 entwickelte, während die Göttweiger Verlehmungszone wesentlich älter ist (≥ 350 ka) als in den meisten vorangegangen Studien angenommen wurde.

Keywords: *post-IR IRSL; fading; loess; Middle Pleistocene; Lower Austria*

Addresses of authors: **C. Thiel***, **S. Tsukamoto**, **M. Frechen**, Section S3: Geochronology and Isotope Hydrology, Leibniz Institute for Applied Geophysics, Stilleweg 2, 30655 Hannover, Germany. E-Mail: christine.thiel@liag-hannover.de; sumiko.tsukamto@liag-hannover.de; manfred.frechen@liag-hannover.de; **C. Thiel**, **J.-P. Buylaert**, **A. S. Murray**, Nordic Laboratory for Luminescence Dating, Department of Earth Sciences, Aarhus University, Risø DTU, 4000 Roskilde, Denmark. E-Mail: jabu@risoe.dtu.dk; anmu@risoe.dtu.dk; **J.-P. Buylaert**, Radiation Research Division, National Laboratory for Sustainable Energy, Risø DTU, 4000 Roskilde, Denmark; **B. Terhorst**, **T. Sprafke**, Institute of Geography, Department for Physical Geography, University of Würzburg, Am Hubland, 97074 Würzburg, Germany. E-Mail: birgit.terhorst@uni-wuerzburg.de; t.sprafke@gmx.de. **corresponding author*

1 Introduction

Loess/palaeosol sequences contain detailed archives of terrestrial palaeoenvironmental changes and landscape evolution. Unfortunately, most loess sequences lack a reliable absolute chronology and hence these changes are difficult to constrain in time. Especially for Middle Pleistocene loess deposits, geochronological information is scarce because there is, as yet, no generally applicable and reliable instrumental dating method which can be used for this age range. Luminescence dating has proved to be a useful tool to date loess deposits (Roberts, 2008), not only because of the wide age range covered by this technique (from a few years to, theoretically, several hundred thousand years; Aitken, 1998) but also because of the long sub-aerial transport of the particles which make up loess; this is confidently expected to have bleached any luminescence signal prior to deposition. Loess is also made up almost entirely of quartz and feldspar, both of which are suitable dosimeters for luminescence dating. The main drawback in the optically

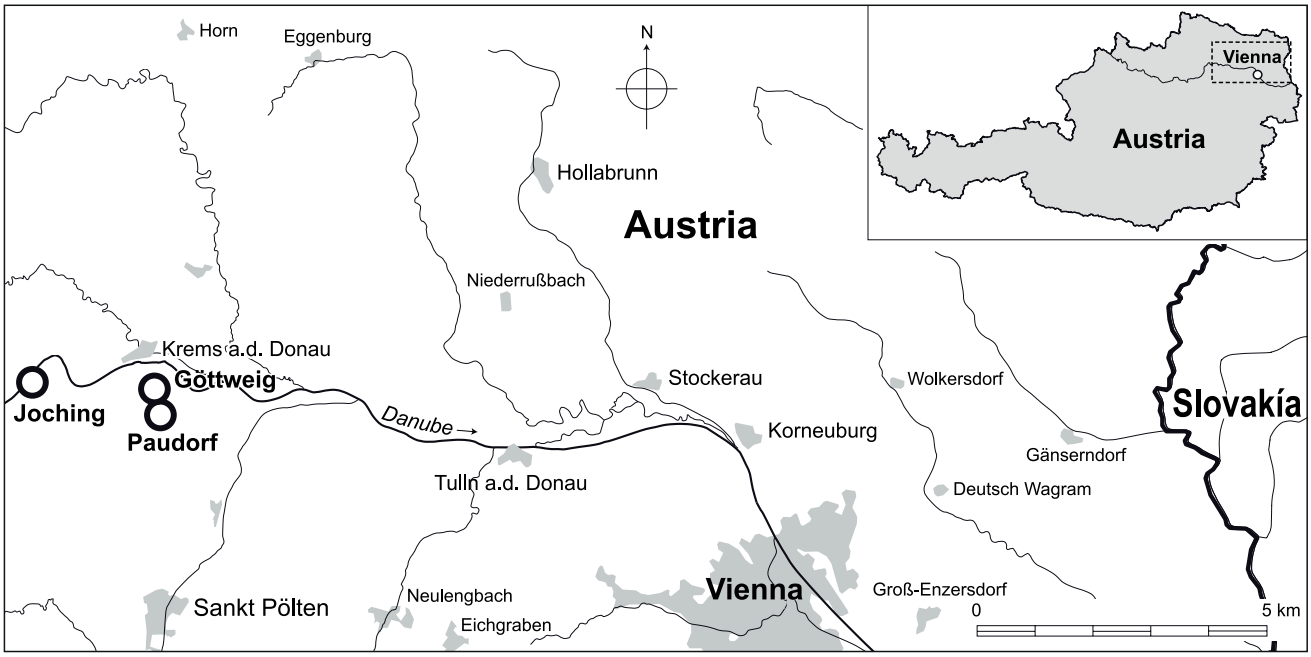

Fig. 1: Map of the study area, showing the locations of Göttweig (Furth and Aigen), Paudorf, and Joching.

Abb. 1: Karte des Untersuchungsgebietes mit den Lokalitäten Göttweig (Furth und Aigen), Paudorf und Joching.

stimulated luminescence (OSL) dating of quartz extracted from loess is the low saturation level of ~200 Gy; this is equivalent to ~50–70 ka assuming a dose rate of between 3 and 4 Gy/ka (typical for loess, e.g. Frechen et al., 1997; Novothny et al., 2002, 2009; Wang et al., 2006; Buylaert et al., 2007; Lai et al., 2010; Thiel et al., 2011a, b). In contrast, feldspar infrared stimulated luminescence (IRSL) signals have a much higher saturation dose (~1500–2000 Gy; equivalent to ~500–700 ka) but, on the other hand, most feldspars suffer from athermal signal loss, referred to as anomalous fading (Wintle, 1973; Spooner, 1994). Because of this phenomenon, IRSL ages tend to significantly underestimate the depositional age. Huntley & Lamothe (2001) have presented a model that can be used to correct the age underestimation, but these corrections are theoretically only applicable to the linear part of the growth curve, i.e. to young samples. Approaches which allow for correction beyond the linear region have been proposed by Lamothe et al. (2003) and Kars et al. (2008); in principle these models can be used for older material (in case of loess >50 ka), but there is little or no testing of these models available in the literature. Although fading corrections can give apparently accurate ages (Huntley & Lamothe, 2001; Buylaert et al., 2011) it seems more advisable to make use of IRSL signals that show less or no fading (Thiel et al., 2011a, submitted) because all correction models involve untestable assumptions, including that the fading rate observed on a laboratory timescale is relevant to geological time. In addition, there are examples where feldspar IRSL ages underestimate when compared with independent age control, even after fading correction (e.g. Wallinga et al., 2007).

Recent developments in luminescence dating offer the potential to circumvent the problem of anomalous fading, and thus to extend the reliable dating range to the Middle Pleistocene (126 to 781 ka; Head et al., 2008). The post-IR IRSL signal (IR stimulation at 50°C and subsequent IRSL measurement at 225°C, blue detection; Thomsen et al., 2008) seems to have great potential; in the laboratory, this signal fades more slowly than conventional IRSL measured at 50°C. Buylaert et al. (2009) tested the applicability of this post-IR IRSL signal to dating sand-sized potassium feldspar grains; the fading rate of the post-IR IRSL signal was two times smaller than the one of the IRSL signal measured at 50°C. Thiel et al. (2011a) used a preheat of 320°C (60 s), IR stimulation at 50°C (200 s) and subsequent post-IR IR stimulation at 290°C (200 s) for polymineral fine grains (4–11 µm). They measured the natural signal and dose response curve of a sample from below the Brunhes/Matuyama boundary (~780 ka, expected natural dose >2700 Gy), and found the natural signal in saturation on the laboratory regenerated growth curve; from that they concluded that for their samples they were unable to detect any evidence for anomalous fading in the field using post-IR IRSL at 290°C.

Even though post-IR IRSL dating in its different forms has now been applied in several studies (Buylaert et al., 2009; Thiel et al., 2010, 2011a, accepted; Reimann et al., 2011) no study has compared the performance of the two different post-IR IRSL dating protocols now in use. In this paper we compare the ages derived from the IR signal at 50°C and two post-IR IRSL signals (post-IR IR stimulation at 225°C, Buylaert et al., 2009; post-IR IR stimulation at 290°C, Thiel et al., 2011a) for three loess/palaeosol sequences in Lower Austria: i) Joching, ii) Paudorf, and iii) Göttweig. These sites have a long scientific history, starting with the investigations of Bayer (1927) and Götzinger (1936). Nevertheless the ages of the pedocomplexes 'Paudorfer Bodenbildung' and 'Göttweiger Verlehmungszone' are still controversial (Fink, 1976; Noll et al., 1994; Zöller et al., 1994; Smolíková et al., 1994) due to discontinuities as the result of intensive erosional phases (cf. Havlíček et al., 1998), and illustrate the need for a more reliable numerical dating method. We first demonstrate that our measurement pro-

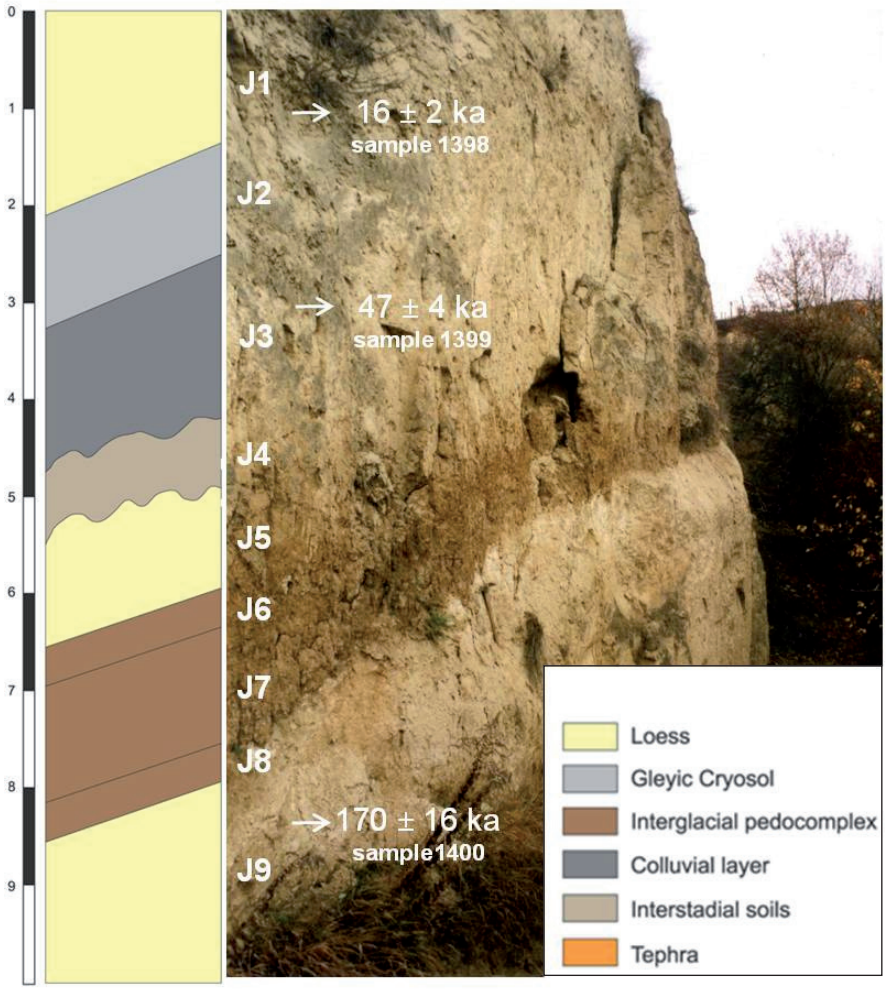

Fig. 2: Photograph and simplified sketch of the loess/palaeosol sequences at Joching. The luminescence ages presented are uncorrected post-IR IRSL ages at 290°C. For details on the material composition, sampling depths and dating see text. (Photo: Reinhard Roetzel)

Abb. 2: Fotographie und vereinfachte Profilzeichnung der Löss-Paläoboden-Sequenz in Joching. Die präsentierten Lumineszenzalter sind nicht-korrigierte post-IR IRSL Alter bei 290°C. Siehe Text für detaillierte Informationen zu Material, Probentiefe und Datierung. (Foto: Reinhard Roetzel)

tocols are applicable to these samples, by examining recuperation, recycling ratios and the ability of these protocols to measure a known dose given in the laboratory. Subsequently the luminescence characteristics, the equivalent doses and laboratory fading rates for the various signals are compared and the derived ages (corrected and uncorrected) are discussed in terms of their reliability. Finally, the most reliable set of IRSL ages is used to unravel the chronostratigraphy of the prominent palaeosols in Lower Austria.

2 Site descriptions and sampling

The loess/palaeosol sequences investigated in this study are located in the Kremser Feld in Lower Austria (Fig. 1); this region is covered by up to 30 m of loess deposits. Three sites exhibiting the prominent palaeosols 'Paudorfer Bodenbildung' and 'Göttweiger Verlehmungszone' were investigated; samples for luminescence dating were taken by hammering metal tubes into the freshly cleaned profile. Samples for dosimetry measurements (~1000 g) were taken from immediately around the luminescence samples.

2.1 Joching

The village of Joching is located on the left bank of the Danube (Fig. 1) and is the furthest upstream of our sites. The loess/palaeosol sequence has a total thickness of about 10 m, with at least two distinct palaeosols (Fig. 2). Below silty yellowish-brown loess (unit J1) a zone of Cryosol horizons (unit J2) is underlain by stratified loamy pellet sands ('Bröckelsande'; unit J3) of up to 4 m thickness. These sands cover a palaeosol horizon with interstadial intensity (J4). About 1.0 m of silty yellowish-brown loess rich in secondary carbonates and with few mollusc fragments (unit J5) is exposed below this soil. The loess is underlain by a pedocomplex (units J6–8) which intensity implies interglacial conditions. Loess (unit J9) is exposed below this pedocomplex.

At this site three luminescence samples were taken (Fig. 2). Sample 1398 was taken from the loess unit J1 1.3 m below top ground surface. The 'Bröckelsand' (unit J3) was sampled (sample 1399) 0.2 m below the Cryosol complex (unit J2), and sample 1400 was taken in the loess unit J9 0.7 m below the pedocomplex, i.e. ~8.3 m below top ground surface.

2.2 Paudorf

The village of Paudorf is located on a right bank tributary of the Danube. The loess/palaeosol sequence is exposed in a former brickyard and is the type locality of the 'Paudorfer Bodenbildung' *sensu* Götzinger (1936). The outcrop, last described by Fink (1976) and thermoluminescence (TL) dated by Zöller et al. (1994) and Noll et al. (1994), is about 9.5 m thick (Fig. 3). At least two well-developed pedocomplexes are preserved at this site; the uppermost soil complex is the prominent 'Paudorfer Bodenbildung' (Fig. 3).

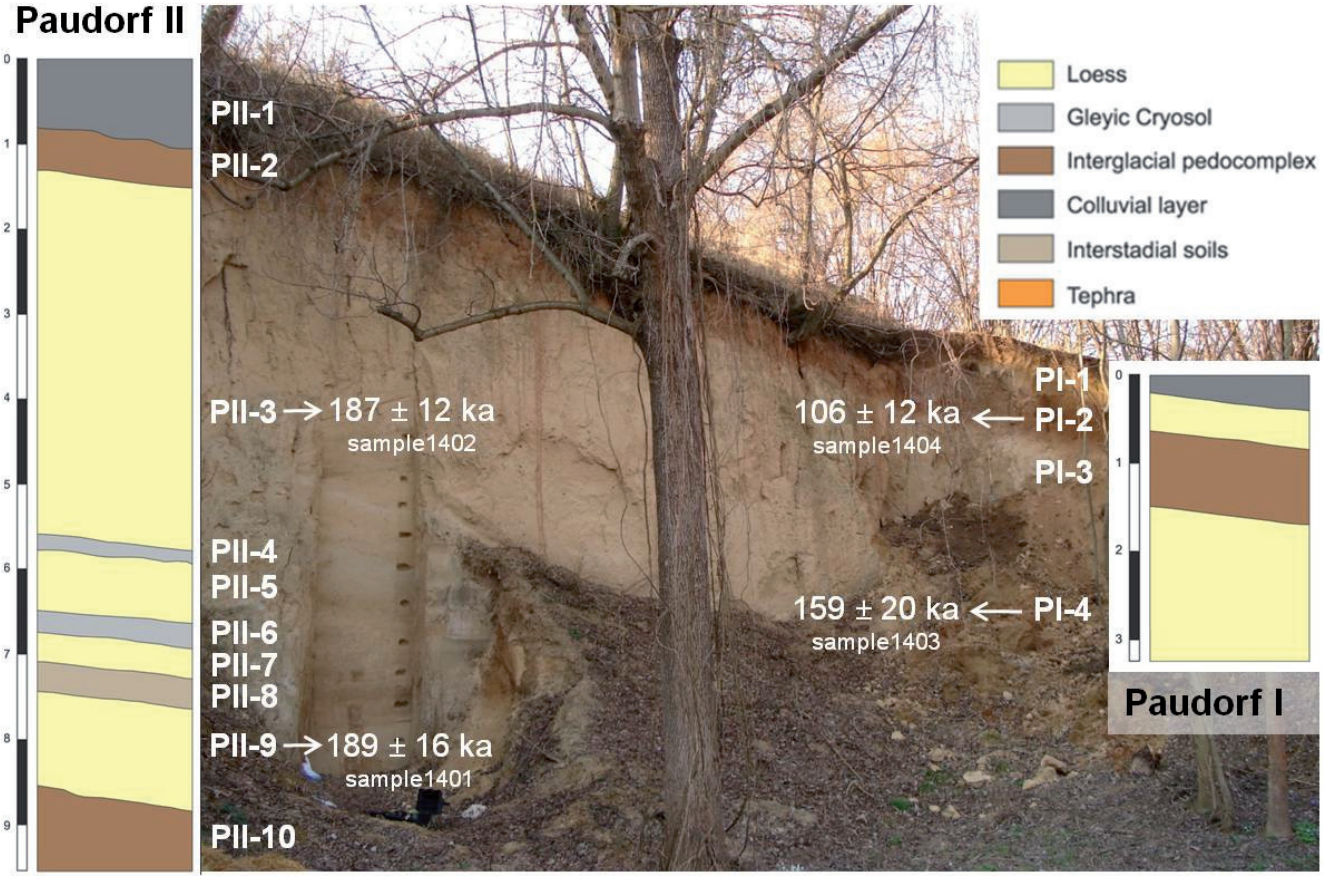

Fig. 3: Photograph and simplified sketches of the loess/palaeosol sequence at Paudorf. The presented ages are based on post-IR IRSL dating at 290°C (except sample 1403, for which corrected post-IR IRSL at 225°C was used). For details on the material composition, sampling depths and dating see text.

Abb. 3: Fotographie und vereinfachte Profilzeichnungen der Löss-Paläoboden-Sequenz in Paudorf. Die präsentierten Lumineszenzalter sind nicht-korrigierte post-IR IRSL Alter bei 290°C (bis auf Probe 1403, für die das korrigierte post-IR IRSL Alter bei 225°C genommen werden musste). Siehe Text für detaillierte Informationen zu Material, Probentiefe und Datierung.

The luminescence sampling points are shown in Figure 3; two adjacent profiles were sampled (Paudorf I and II). The uppermost sample 1404 was taken in loess (unit PI-2) 0.3 m above the 'Paudorfer Bodenbildung' (unit PI-3), which is here developed as a reddish-brown, clay-rich palaeosol with crotovina. The loess unit PI-4 below the 'Paudorfer Bodenbildung', was sampled 2.9 m below top ground surface (sample 1403).

In profile Paudorf II, the 4 m thick loess (PII-3) was sampled below the 'Paudorfer Bodenbildung' at a depth of 4.2 m (sample 1402); because of induration, this sample had to be taken as a block. The loess deposit is underlain by alternating Cryosol and loess horizons (PII-4 to PII-7). In its lower parts a weak brownish palaeosol is exposed (PII-8). A loess layer (PII-9) bracketing the weak palaeosol and the basal pedocomplex (PII-10), originally correlated with the 'Göttweiger Verlehmungszone' (Götzinger, 1936), was sampled at a depth of 7.8 m (sample 1401).

2.3 Göttweig

Two different sections were investigated near the monastery of Göttweig, just north of the loess sequence at Paudorf (Fig. 4). Section I (Fig. 4a) is the classical site of the 'Göttweiger Verlehmungszone' *sensu* Bayer (1927) and Götzinger (1936), located near the town of Furth in a sunken path. The pedocomplex 'Göttweiger Verlehmungszone' (unit GI-4) and the overlying up to 6 m thick loess is exposed horizontally over several hundred meter and lies on a Danube terrace; the correlation with other terraces is unclear. A continuous thin layer (unit GI-2) can be identified in the loess package; preliminary magnetic analysis suggest that this layer is a tephra (pers. comm. U. Hambach), whose origin and age is unfortunately unclear.

The luminescence sampling points at Section I are shown in Figure 4a. Sample 1406 comes from silty loess (unit GI-1) 0.6 m above the tephra (unit GI-2), and sample 1405 was taken in sandy-silty yellowish-brown loess (unit GI-3) 0.3 m below the tephra. Another sample (1407; not shown in Fig. 4) was taken 300 m upslope 30 cm below reworked loess which includes pebbles and sandy layers; the position of this sample with respect to the other samples is not unambiguously established but the sampling point definitely lies above the tephra layer.

Section II is located in the hollow way near the village of Aigen (between Göttweig and Paudorf), where a pedocomplex correlated with the 'Paudorfer Bodenbildung' is exposed (Fink, 1976; Fig. 4b). However the pedocomplex (unit GII-3) is eroded at this site, deduced from the lack of an A horizon and a package of 30 cm thick reworked soil sediment (unit GII-2) covering the soil. The fine-silty yellowish-brown loess (unit GII-1) was sampled 0.7 m below top ground surface and 0.6 m above the 'Paudorfer Bodenbildung' (sample 1408); due to induration the sample had

E&G / Vol. 60 / No. 1 / 2011 / 137–152 / DOI 10.3285/eg.60.1.10

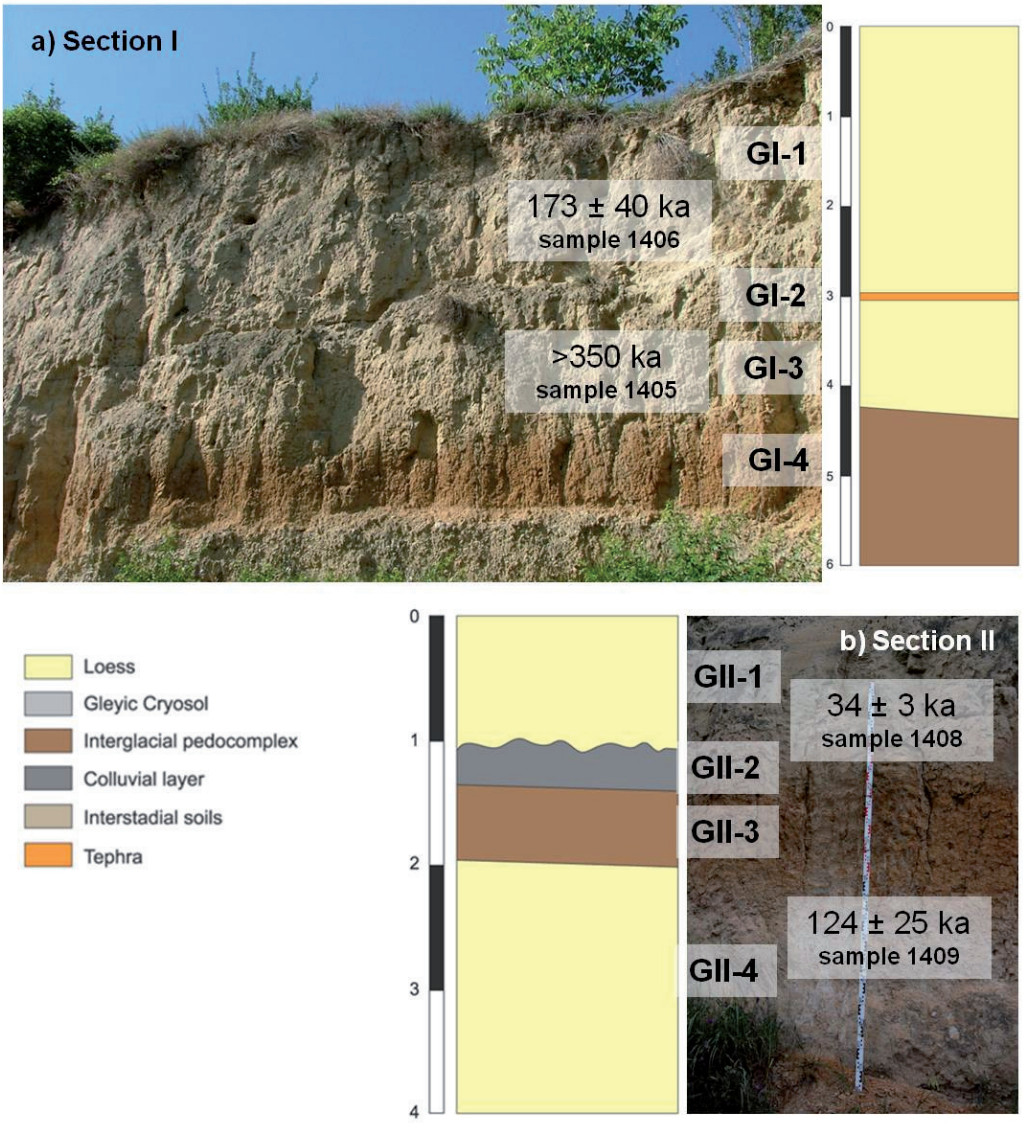

Fig. 4: Photographs and simplified sketches of the loess/palaeosol sequences at Göttweig. a) Section I: type locality of the 'Göttweiger Verlehmungszone' (Göttweig-Furth), b) Section II (Göttweig-Aigen), with 'Paudorfer Bodenbildung' (Fink, 1976). Sample 1407 was taken 300 m upslope from Section I and is not shown in the figure. All ages are derived by post-IR IRSL dating at 290°C. For details on the material composition, sampling depths and dating see text.

Abb. 4: Fotographie und vereinfachte Profilzeichnungen der Löss-Paläoboden-Sequenzen in der Nähe von Göttweig. a) Aufschluss I: Typlokalität der Göttweiger Verlehmungszone (Göttweig-Furth); b) Aufschluss II (Göttweig-Aigen) mit der Paudorfer Bodenbildung (Fink, 1976). Probe 1407 wurde 300 m hangaufwärts in Göttweig-Furth genommen und ist in der Abbildung nicht zu sehen. Alle Alter wurden mittels post-IR IRSL bei 290°C bestimmt. Siehe Text für detaillierte Informationen zu Material, Probentiefe und Datierung.

to be taken as a block. Sample 1409 was taken in carbonate rich silty loess (unit GII-4) 0.6 m below the 'Paudorfer Bodenbildung' (i.e. 2.5 m below top ground surface).

3 Sample preparation and analytical facilities

In the laboratory, all samples for equivalent dose (D_e) determination were treated under subdued red light. The outer ends (~1 cm) of the samples might have been exposed to daylight during sampling; these were discarded and the remaining sample treated with hydrochloric acid, sodium oxalate, and hydrogen peroxide. Between each treatment step the sediment was washed with distilled water. Special attention was paid to samples 1402 and 1408 (taken as blocks); all surfaces were scraped off to a depth of >1 cm before chemical treatment. The fine-silt fraction (4–11 µm) of the samples was extracted by repeated settling and washing (Frechen et al., 1996). The polymineral fine-grains were then deposited on aluminium discs (diameter 9.7 mm) from a suspension in acetone (2 mg/ml). Luminescence measurements were made with automated Risø TL/OSL readers (DA-15 and DA-20, respectively; Bøtter-Jensen et al., 2003; Thomsen et al., 2006) fitted with calibrated $^{90}Sr/^{90}Y$ beta sources calibrated using fine-grained quartz on aluminium discs. The feldspar signal of the polymineral samples was stimulated with infrared light diodes emitting at 870 nm, and the luminescence was detected in the blue-violet region (325–450 nm) through a Schott BG39/Corning 7–59 filter combination.

4 Dosimetry

The concentrations of U, Th and K were determined by high-resolution gamma-ray spectrometry equipped with a high-purity germanium detector. 700 g of each sample of

Tab. 1: Summary of dosimetry data. A water content of 15 ± 5% was estimated for all samples.

Tab.1: Zusammenfassung der Dosimetriedaten. Ein Wassergehalt von 15 ± 5% wurde für alle Proben angenommen.

Sample	K [%]	U [ppm]	Th [ppm]	Cosmic dose rate [Gy/ka]	Total dose rate [Gy/ka]
1398	1.2 ± 0.1	3.0 ± 0.1	10.6 ± 0.3	0.18 ± 0.02	3.1 ± 0.1
1399	1.7 ± 0.1	3.2 ± 0.1	11.5 ± 0.4	0.14 ± 0.02	3.5 ± 0.2
1400	0.8 ± 0.1	2.3 ± 0.1	7.3 ± 0.3	0.08 ± 0.01	2.1 ± 0.1
1401	2.2 ± 0.1	2.8 ± 0.2	11.4 ± 0.4	0.13 ± 0.01	3.8 ± 0.2
1402	1.4 ± 0.1	2.5 ± 0.1	9.4 ± 0.3	0.15 ± 0.02	2.9 ± 0.1
1403	1.5 ± 0.1	2.5 ± 0.1	9.9 ± 0.3	0.17 ± 0.02	3.0 ± 0.1
1404	1.6 ± 0.1	2.8 ± 0.1	10.9 ± 0.4	0.20 ± 0.02	3.3 ± 0.1
1405	1.6 ± 0.1	2.9 ± 0.1	11.0 ± 0.4	0.09 ± 0.01	3.2 ± 0.2
1406	1.4 ± 0.1	2.8 ± 0.1	9.8 ± 0.3	0.10 ± 0.01	2.9 ± 0.1
1407	1.5 ± 0.1	2.9 ± 0.1	12.9 ± 0.3	0.11 ± 0.01	3.4 ± 0.2
1408	1.3 ± 0.1	2.9 ± 0.1	10.1 ± 0.3	0.20 ± 0.02	3.0 ± 0.3
1409	0.9 ± 0.2	2.2 ± 0.1	6.9 ± 0.2	0.16 ± 0.02	2.1 ± 0.1

dried material was homogenised and packed in Marinelli beakers, sealed and stored for at least one month to ensure equilibrium between radon and its daughter nuclides before counting. Details about the procedures for dosimetry measurements at the Leibniz Institute for Applied Geophysics (LIAG) laboratory in Hannover are given by Kunz et al. (2010).

The dose rates were derived using the conversion factors of Adamiec & Aitken (1998). For all samples a water content of 15 ± 5% was used (Frechen et al., 1997) to allow for possible changes in water content throughout time, and a mean a-value of 0.08 ± 0.02 was assumed (Rees-Jones, 1995). Calculation of the cosmic dose rate is based on Prescott & Hutton (1994)

The dosimetry data are summarised in Table 1. The total dose rates range from 2.1 ± 0.1 Gy/ka to 3.8 ± 0.2 Gy/ka. The rather low dose rate of 2.1 ± 0.1 Gy/ka for samples 1400 and 1409 originate in the relatively low Th (~7 ppm) and K (<1%) contents. Nevertheless, all dose rates are within the range expected for European loess (Zöller et al., 1994; Frechen et al., 1997; Novothny et al., 2002, 2009; Thiel et al., 2011a, 2011b).

5 Post-IR IRSL dating

Since Thomsen et al. (2008) first identified reduced laboratory fading rates from various feldspar signals, several studies have tested or made use of elevated temperature post-IR IRSL signals (e.g. Buylaert et al., 2009; Thiel et al., 2010, 2011a, b; Reimann et al., 2011).

Buylaert et al. (2009) used a preheat of 250°C for 60 s (used in many studies in the past), and their post-IR IR stimulation temperature was chosen to be 225°C. Because Murray et al. (2009) showed for sand-sized grains of potassium feldspar that there is no systematic increase in equivalent dose measured at 50°C for preheat temperatures ranging from 80°C up to 320°C (60 s duration), Thiel et al. (2011a) adopted a more stringent preheat of 320°C for 60 s to date their polymineral fine-grains with a post-IR IRSL protocol. This allowed them to use post-IR IR stimulation at significantly higher temperatures. They chose to investigate the use of stimulation at 290°C and observed the natural signal of a polymineral fine grain extract from below the Brunhes/Matuyama boundary (~780 ka, i.e. ~2700 Gy) in saturation on a laboratory growth curve. Based on these observations, they concluded that there is no detectable anomalous fading in nature of the post-IR IRSL signal at 290°C, even though they were able to measure a finite laboratory fading rate of ~1-1.5%/decade. Thiel et al. (submitted) have since compared ages obtained using the same post-IR IRSL at 290°C protocol with independent age control based on both fission track and radiocarbon dating as well as quartz OSL at two loess sites in Japan (Watanuki et al., 2005) and obtained very consistent results back to ~600 ka. Again they observed a low fading rate in the laboratory (1.1 ± 0.2%/decade; n=15) but argued that no fading correction was necessary.

In the following sections we compare the results obtained using the post-IR IRSL protocol described by Buylaert et al. (2009) (post-IR IRSL at 225°C) with those of Thiel et al. (2011a) (post-IR IRSL at 290°C) (Table 2). For comparison the results of the IRSL signal at 50°C (measured as part of the post-IR IRSL at 225°C protocol) are also discussed.

5.1 Post-IR IRSL measurements at 225°C

For these post-IR IRSL measurements we used the same temperature and stimulation conditions as Buylaert et al. (2009). After a preheat of 250°C for 60 s, we bleached the polymineral fine-grains (six aliquots per sample) with IR diodes at 50°C for 100 s to recombine the near-neighbour trap/centre pairs which fade most rapidly (discussed in e.g. Poolton et al., 2002; Thomsen et., 2008, 2011), and then held the aliquot at 225°C while measuring the IRSL for 100 s. The response to a test dose (~70 Gy) was measured in the same manner (Table 2), and an IR illumination at 290°C for 40 s was inserted at the end of each SAR measurement cycle to reduce the effect of any recuperation (based on Murray & Wintle, 2003). The initial 2.4 s of the decay curve were used for D_e determination after subtracting a background from the last 60 s.

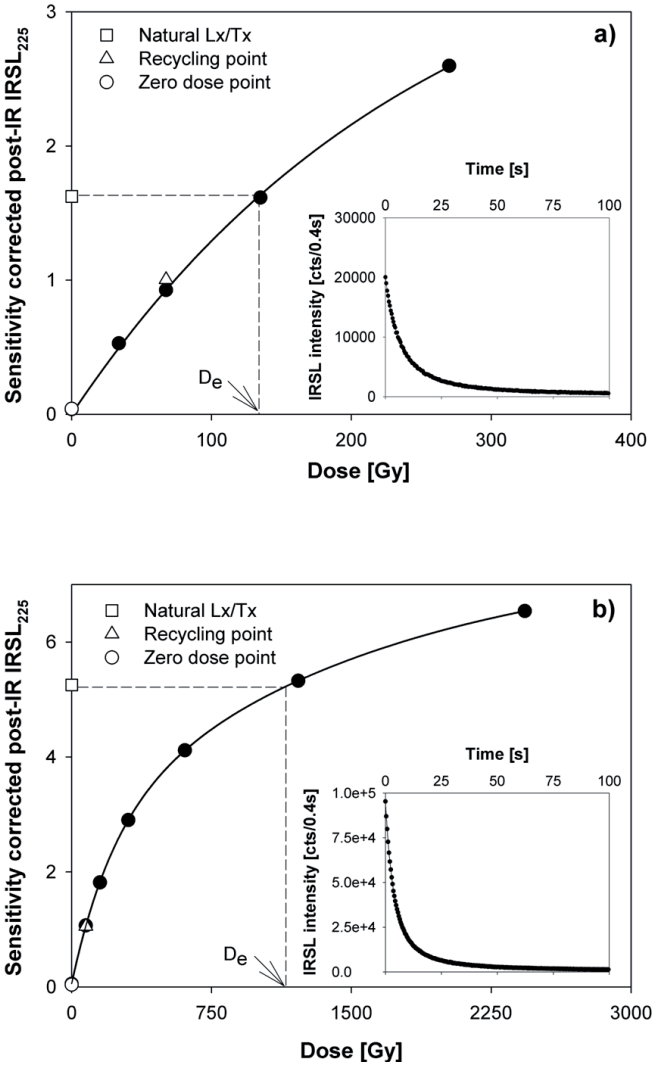

Fig. 5: Dose response and natural decay curves for the post-IR IRSL measurements at 225°C. a) Dose response curve for sample 1399, representative of younger samples. The inset shows the post-IR IRSL intensity against time (100 s). b) Dose response curve for sample 1407, representative of older samples. The natural sensitivity corrected post-IR IRSL signal (Lx/Tx) is beyond the linear part of the curve. The inset shows the post-IR IRSL intensity against time (100 s).

Abb. 5: Wachstumskurven und natürliche Ausleuchtkurven für die post-IR IRSL-Messungen bei 225°C. a) Wachstumskurve für Probe 1399 (repräsentiert junges Material). Die eingesetzte Abbildung zeigt die post-IR IRSL-Intensität gegen die Zeit (100 s). b) Wachstumskurve für Probe 1407 (repräsentiert altes Material). Das natürliche, sensitivitätskorrigierte post-IR IRSL-Signal (Lx/Tx) ist jenseits des linearen Bereiches. Die eingesetzte Abbildung zeigt die post-IR IRSL-Intensität gegen die Zeit (100 s).

The laboratory fading rate was measured on three aliquots per sample as the IRSL signal decreased over time using artificially irradiated aliquots; this is expressed in terms of the percentage decrease of signal intensity per decade of time (the *g*-value; Aitken, 1985, Appendix F). After a final IR illumination at 290°C for 40 s, the same aliquots as for equivalent dose measurements were given doses of ~50 Gy ('young samples') and ~200 Gy ('old samples'), respectively, to monitor anomalous fading using the SAR protocol outlined in Table 2. The storage times after irradiation and preheating (Auclair et al., 2003) varied from as brief as experimentally possible ('prompt') to delays of up to ~10 hours. The *g*-values, calculated using Equation 4 of Huntley & Lamothe (2001), were normalised to a measurement time delay of 2 days after irradiation.

The dose response curves and the post-IR IRSL decay curves of samples 1399 (a 'young' sample) and 1407 (an 'old' sample) are shown in Figure 5; they are representative of all the other samples presented in this study. The sensitivity-corrected natural of the post-IR IRSL signal of sample 1399 lies on the relatively linear part of the dose response curve, whereas the natural post-IR IRSL signal of sample 1407 (Fig. 5b) clearly lies beyond the linear region, which thus reduces the accuracy of the Huntley & Lamothe (2001) fading correction.

The ability of a measurement protocol to reproducibly measure the response to a laboratory dose given after repeated heating of the sample is represented by the recycling ratio, which ought to yield values indistinguishable from unity. The recycling ratios for the samples vary between 0.99 ± 0.01 (n=6; sample 1407) and 1.05 ± 0.02 (n=5; sample 1399) (Table 3 and Fig. 6a). Recuperation is well below 5% of the natural signal for all except the uppermost sample of the Joching profile (sample 1398), which shows a recuperation of 8.8 ± 0.5% (n=6) (Fig. 6b).

Satisfactory recycling ratios do not necessarily mean that doses given before any heating can also be measured accurately (which is the closest we can come to reproducing natural conditions). We therefore carried out a dose recovery test. Three natural aliquots of samples 1399 (Joching), 1401 (Paudorf) and 1405 (Göttweig) were bleached for 4 hours in a Hönle SOL2 simulator (sample to lamp distance ~1.2 m to avoid heating of the aliquots). The aliquots were then given a beta dose similar to the measured D_e for each sample and the given dose was measured in the usual manner. The results of the dose recovery test are shown in Fig. 7a. For all samples, measured/given doses are within 10% of unity. Because of the residual signals (and hence doses) observed for the post-IR IRSL signal at 225°C in other studies (Thomsen et al. 2008; Buylaert et al., 2009) we measured the residual signal after bleaching on separate aliquots of the same samples (three per sample). These residual signals were equivalent to a dose of 4.7 ± 0.5 Gy (n=9). After subtraction of these residual doses the measured/given dose ratios vary between 0.97 ± 0.01 (n=3; sample 1404) and 1.02 ± 0.04 (n=3; sample 1399). Both the measured to given ratios before and after residual subtraction are very close to unity (Fig. 7), demonstrating the accuracy of the measurement protocol when measuring an artificial beta dose given prior to any heating.

5.2 Post-IR IRSL measurements at 290°C

Following Thiel et al. (2011a), after preheating the samples (six aliquots per sample) at 320°C for 60 s we bleached the polymineral fine-grains with IR diodes at 50°C for 200 s and subsequently measured the IRSL at 290°C for 200 s. The response to a test dose was measured in the same manner, and an IR illumination at 325°C for 100 s was inserted at the end of each SAR measurement (Table 2). The light sum of the initial 2.4 s of the post-IR IRSL signal was used for D_e determination, less a background derived from the last 100 s. The fading rates on three aliquots per sample were measured in exactly the same way as for the IR at 225°C signal but using the preheating and stimulation conditions of the post-IR IRSL at 290°C protocol.

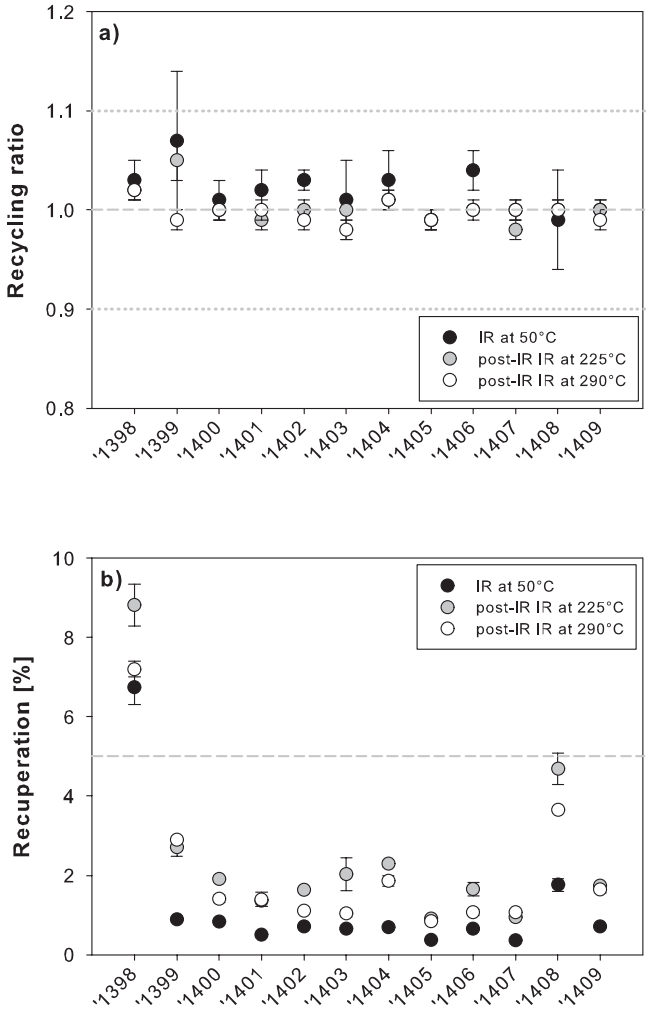

Fig. 6: Recycling ratios and recuperation. a) For all signals and samples the recycling ratios are within 10% of unity. b) Recuperation [% of natural signal] for all signals and samples. Sample 1398 shows recuperation >5% for all (post-IR) IRSL signals, whereas for all other samples it is well below 5%; for IRSL at 50°C it is below 2%.

Abb. 6: Recycling Ratios und Recuperation. a) Die Recycling Ratios sind für alle Signale und Proben im Rahmen der zulässigen 10%-Abweichung. b) Recuperation [% des natürlichen Signals] für alle Signale und Proben. Probe 1398 zeigt einen Wert >5% für alle (post-IR)-IRSL-Signale, während für alle anderen Proben der Wert <5% ist. Für IRSL bei 50°C liegen die Werte unter 2%.

The dose response curves and the post-IR IRSL signals at 290°C of two samples (1399 and 1407) are shown in Figure 8. Whereas the natural post-IR IRSL signal of sample 1399 lies in the linear region of the dose response curve, the natural post-IR IRSL signal of sample 1407 is well above and is approaching saturation. Recycling ratios are very close to unity for all samples (Table 3 and Fig. 6a), and recuperation varies between 0.91 ± 0.06% (n=6; sample 1405) and 7.2 ± 0.2% (n=6; sample 1398) (Fig. 8b); except for sample 1398 recuperation is well below 5% of the natural (the acceptance threshold for quartz OSL suggested by Murray & Wintle, 2003).
Bleaching for dose recovery tests and residual determination was conducted in the same manner as for the post-IR IRSL measurements at 225°C. After giving a beta dose close to the natural the dose was measured using the settings described above. Without subtraction of the residual signals (13 ± 2 Gy; n=9), measured to given dose ratios vary between 1.04 ± 0.02 (n=3; sample 1404) and 1.08 ± 0.02 (n=3; sample 1399; Fig. 7a); after subtraction of the residual signals the ratios are 0.99 ± 0.02 (n=3; sample 1404) and 1.00 ± 0.01 (n=3; sample 1407; Fig. 7b).

5.3 IRSL measurements at 50°C

The luminescence characteristics and SAR performance for IRSL at 50°C presented here are part of the post-IR IRSL measurements at 225°C. Thus, the data originate from the same aliquots measured in the post-IR IRSL protocol but the decay curves of the IRSL at 50°C stimulations are used for all calculations (Table 2). For D_e determination the initial 2.4 s of the decay curve were used after subtracting a background from the last 60 s.

The dose response curves for samples 1399 and 1407 are shown in Figure 9. Recycling ratios for all samples are all within 10% of unity (Table 3 and Fig. 6a), and recuperation varies between 0.4 ± 0.02% (n=6; sample 1407) and 6.7 ± 0.4% (n=6; sample 1398). The high recuperated signal of sample 1398 is unusual compared to the other values, which are all below 2% (Fig. 6b).

The residual signals are equivalent to 1.5 ± 0.2 Gy (n=9). Without subtraction of the residual signals the measured to given dose ratios vary between 1.09 ± 0.02 (n=3; sample 1399) and 1.11 ± 0.04 (n=3; sample 1409; Fig. 7a), whereas after subtraction the ratios lie between 1.08 ± 0.02 (n=3; sample 1399) and 1.10 ± 0.04 (n=3; sample 1409; Fig. 7b). Although the results are within 10% of unity there does seem to be a systematic tendency to overestimate the given dose. Nevertheless, we consider these results acceptable, because they are within the 10% range.

6 Comparison of the fading rates and ages derived from the different signals

The laboratory fading rates for all samples and signals are listed in Table 3 and plotted in Fig. 10. The mean fading rate for IRSL at 50°C is 3.3 ± 0.4%/decade (excluding the two outliers 1398 and 1400), 2.1 ± 0.3%/decade for post-IR IRSL at 225°C, and 1.0 ± 0.4%/decade for post-IR IRSL at 290°C, confirming that post-IR IR stimulation at higher temperatures reduces fading (Thomsen et al., 2008).
The fading rates for the IRSL measurements at 50°C vary between 1.0 ± 0.7%/decade (sample 1401) and 9.9 ± 0.5%/decade (sample 1400) and are much higher than for the post-IR IRSL measurements, with the exception of sample 1401; the latter has a fading rate comparable to those of the post-IR IRSL signals (Fig. 10). If this sample indeed does not fade significantly, then the various (uncorrected) D_e values should be similar, and ages should be indistinguishable. This, however, is not observed; the D_e values for the post-IR IRSL signals are significantly higher than for the IRSL measurement at 50°C and as a result the ages do not agree (Table 3 and Fig. 11). Unexpectedly, for sample 1405 the laboratory fading rate of the IRSL signal at 50°C is slightly lower (3.4 ± 0.3%/decade) than that of the post-IR IRSL signal at 225°C (4.3 ± 0.5%/decade); the post-IR IRSL at 290°C fading rate is much lower (0.8 ± 0.4%/decade) than for both the other signals. Given the fact that our aliquots are made up of many hundreds of thousands of grains, which ought to result in homogeneous luminescence behaviour, the variability observed in the fad-

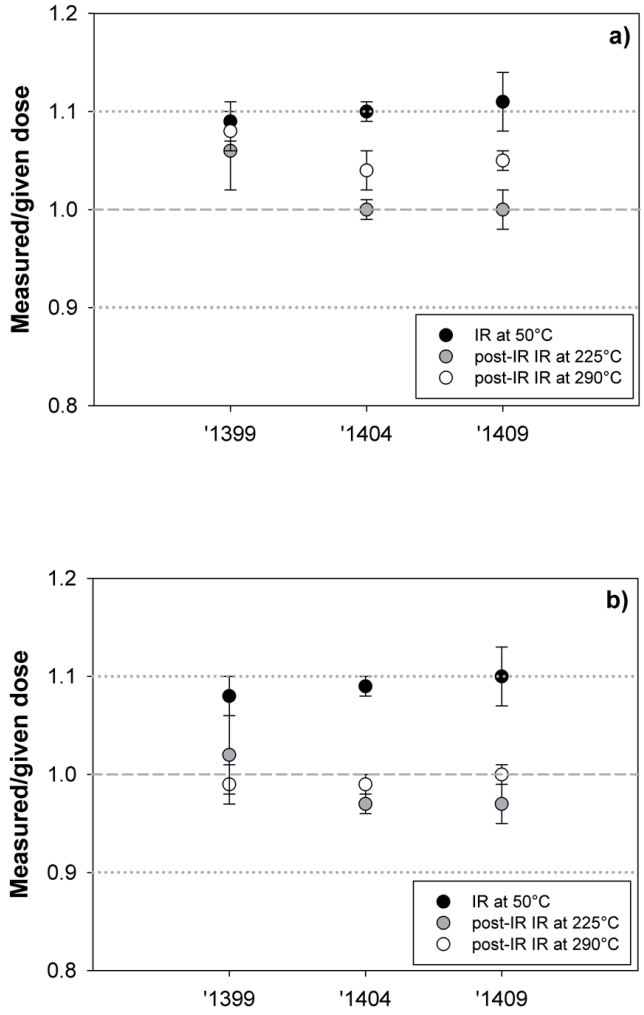

Fig. 7: Results of dose recovery tests a) without residual subtraction, b) with residual subtraction. The residual signal is 1.5 ± 0.2 Gy (n=9) for the IRSL measurements at 50°C, 4.7 ± 0.5 Gy (n=9) for the post-IR IRSL measurements at 225°C, and 13 ± 2 Gy (n=9) for the post-IR IRSL measurements at 290°C. For details about the bleaching conditions and residual measurements see text.

Abb. 7: Ergebnisse der Dose Recovery Tests a) ohne das Restsignal abzuziehen, b) mit Subtraktion des Restsignals. Das Restsignal ist 1.5 ± 0.2 Gy (n=9) für die IRSL-Messungen bei 50°C, 4.7 ± 0.5 Gy (n=9) für die post-IR IRSL-Messungen bei 225°C, und 13 ± 2 Gy (n=9) für die post-IR IRSL-Messungen bei 290°C. Siehe Text für Details zu den Belichtungsexperimenten und Messungen.

ing rates, especially for the IR at 50°C signal, is surprising and difficult to explain; although it could originate from e.g. a change in source area, it seems more likely that it reflects some unknown laboratory source of variability.

Thiel et al. (2011a) measured fading rates of 1–1.5%/decade using the post-IR IRSL signal measured at 290°C for their polymineral fine-grain samples; they argued that because the natural signals from these samples were in saturation on a laboratory growth curve, it was unlikely that the natural signal had faded significantly. In addition, they also measured a fading rate of ~1%/decade for fine-grained quartz dominated by a fast OSL component; it seems clear that at the very least their post-IR IRSL signal did not fade any more than the blue-stimulated OSL signals from quartz. It may be that fading rates below 1%/decade are not meaningful, and in fact reflect systematic errors in laboratory fading measurements.

We have confirmed that for the higher temperature signals smaller fading rates are obtained and as a consequence it is expected that the fading uncorrected ages of the IRSL signal at 50°C ought to be younger than for any post-IR IRSL measurement. If fading measurements and fading corrections are applicable (Huntley & Lamothe, 2001), and if post-IR IRSL at 290°C does not show significant anomalous fading as suggested by Thiel et al. (2011a, accepted), fading corrected IRSL ages at 50°C and fading corrected post-IR IRSL ages at 225°C should be indistinguishable from fading uncorrected ages for the post-IR IRSL at 290°C, at least over the dose range for which the Huntley & Lamothe (2001) correction may be applicable in practice (~200 Gy; Buylaert et al., 2011). The fading uncorrected and fading corrected ages are listed in Table 3 and shown in Figure 11. We assume that the post-IR IRSL at 290°C gives the most accurate age estimates because there is evidence that these signals do not fade in nature (Thiel et al., 2011a, accepted); this can also be concluded from sample 1405, which is in or close to saturation, since laboratory saturation in feldspar is only possible when fading is negligible.

As expected, the fading uncorrected ages of the IRSL signal at 50°C (showing the largest fading rates) underestimates compared to the post-IRSL at 290°C (Fig. 11a); the age underestimation is most evident for the older samples. On the other hand, uncorrected post-IR IRSL at 225°C ages only slightly underestimate compared to post-IR IRSL at 290°C (Fig. 11b). The measured post-IR IRSL at 225°C laboratory fading rates (0.6 to 4.3%/decade; Table 3), at least when >1%/decade, are probably significant, and it seems clear that the post-IR IRSL at 225°C needs fading correction. A similar observation was made by Buylaert et al. (2009) for their Eemian samples (see supplementary table in Buylaert et al., 2009). The fading corrected ages for post-IR IRSL at 225°C are plotted against corrected ages for post-IR IRSL at 290°C in Figure 11c, and against uncorrected ages for post-IR IRSL at 290°C in Figure 11d. It is recognised that the correction model is theoretically not applicable at higher doses, but such qualifications become of second order importance when the correction is so small. The fading correction for post-IR IRSL at 290°C is, on average, < 10% of the age and so Figures 11c and 11d are very similar. In both figures the agreement between the ages derived from the two signals is satisfactory with one exception (sample 1403), for which either post-IR IRSL at 225°C underestimates, or post-IR IRSL at 290°C overestimates.

The agreement between the fading corrected ages for IRSL at 50°C with the fading uncorrected (or corrected) ages for post-IR IRSL at 290°C is slightly poorer, especially for the older samples (> 100 ka; Fig. 11e). Sample 1400, which has a fading rate of 9.9 ± 0.5%/decade resulted in a significantly overestimated age after correction of 679 ± 74 ka (Table 3). This sample is well outside the applicable range of the Huntley & Lamothe (2001) correction model, but this should result in an underestimation, not overestimation; however, it is most likely that the fading rate for this sample is overestimated. A depositional age of >600 ka for this sample is unlikely not only from a stratigraphical point of view but also when compared with the post-IR IRSL age estimates. The overestimation is consistent with the observations of Reimann et al. (2011) using Holocene coastal sediments (to which the correction model is defi-

Tab. 2: Flowcharts of the post-IR IRSL SAR protocols (Buylaert et al., 2009; Thiel et al., 2011a). For IRSL at 50°C steps 3 and 7 of protocol a) were used for equivalent dose determination.

Tab. 2: Ablaufschema für die post-IR IRSL SAR-Protokolle (Buylaert et al., 2009; Thiel et al., 2011a). Für IRSL bei 50°C wurden Schritt 3 und 7 von Protokoll a) für die Äquivalenzdosis-Bestimmung verwendet.

a]			b]		
Step	**Treatment**	**Observed**	**Step**	**Treatment**	**Observed**
1	Give dose, D_i		1	Give dose, D_i	
2	Preheat, 250°C, 60 s		2	Preheat, 320°C, 60 s	
3	IR stimulation, 100 s at 50°C		3	IR stimulation, 200 s at 50°C	
4	IR stimulation, 100 s at 225°C	L_x	4	IR stimulation, 200 s at 290°C	L_x
5	Give test dose, D_T		5	Give test dose, D_T	
6	Preheat, 250°C, 60 s		6	Preheat, 320°C, 60 s	
7	IR stimulation, 100 s at 50°C		7	IR stimulation, 200 s at 50°C	
8	IR stimulation, 100 s at 225°C	T_x	8	IR stimulation, 200 s at 290°C	T_x
9	IR stimulation, 40 s at 290°C		9	IR stimulation, 100 s at 325°C	
10	Return to 1		10	Return to 1	

nitely applicable); they show that fading correction of the IRSL signal at 50°C for *g*-values >6 %/decade overestimates their depositional ages for which independent age control is available.

In most post-IR IRSL dating studies (e.g. Buylaert et al., 2009; Thiel et al., 2011a, b; Reimann et al., 2011) it has been observed that a significant residual post-IR IRSL signal is present after daylight or solar simulator bleaching in the laboratory. Thomsen et al. (2008) showed in a bleaching experiment that there is no obvious difference in signal resetting between the IRSL at 50°C signal and the post-IR IRSL signal at 225°C. Nevertheless, using the same post-IR IRSL signal, Buylaert et al. (2009) found apparent residuals of up to 2 Gy for modern samples while residuals measured using IR at 50°C were ~0.5 Gy; either the two signals bleach to different degrees, or there are differences in thermal transfer. In contrast, Thiel et al. (2011a) measured laboratory residuals equivalent to 15–20 Gy for the post-IR IRSL signal at 290°C. For their samples it was difficult to decide on the relevance of these residual measurements to naturally bleached samples because there were no modern analogues available at their site. Again, some or all of the residual doses may have arisen through thermal transfer following the higher preheat temperature of 320°C. Thus it remains unclear to what degree the post-IR IRSL signals bleach more slowly than the IR at 50°C for these samples, or whether the differences are a result of the different preheat temperatures used (i.e. thermal transfer).

None of the ages presented here have had a residual dose subtracted. From laboratory bleaching experiments, apparent residuals can vary between 1.5 ± 0.2 Gy (n=9) for IRSL at 50°C and 13 ± 2 Gy (n=9) for post-IR IRSL at 290°C. In nature bleaching is likely to be episodic and take place over much longer times than is typical for laboratory bleaching experiments. One can test the size of any residual by determining the luminescence age on material of independently known young age, or by examining the dose in recently transported modern material (modern analogues). Unfortunately, there are no modern analogues available at our sites. To test the bleachability of the different IRSL signals the ages of the younger (<70 ka) samples are compared (Fig. 11f). The IRSL at 50°C ages are taken as reference because there is good evidence in the literature that the signal can be bleached to very low levels (e.g. Huntley & Clague, 1996) and in this age range the fading correction is generally expected to yield accurate results (Huntley & Lamothe, 2001; Buylaert et al., 2011). For the youngest sample (sample 1398; IRSL at 50°C D_e: 15 ± 2 Gy), which might be expected to be significantly affected by residual doses, the post-IR IRSL ages are slightly older than the corrected IRSL age at 50°C. However, for this sample the corrected IRSL age at 50°C of 10 ± 1 ka seems, from a geological point of view too young, since there was no loess deposition in Lower Austria during the Holocene. The post-IR IRSL ages are thus closer to the expected age. This gives confidence that the post-IR IRSL signals are bleachable in nature, and as a result we do not subtract any residual from any of our ages. Nevertheless this assumption needs further testing using modern analogues and/or very young samples.

In summary, for young samples, for which the fading correction of the 225°C signal is likely to be accurate, both the fading corrected ages for post-IR IRSL at 225°C and the fading uncorrected ages for post-IR IRSL at 290°C seem to yield comparable results. For older samples any fading correction is likely to be increasingly inaccurate, and we favour the age estimates from the post-IR IRSL at 290°C, which apparently do not require significant fading correction (Thiel et al., 2011a, accepted). The following discussion on the chronological framework of the palaeosols is hence based on this IRSL signal unless otherwise stated.

7 Chronostratigraphy of the palaeosols

In Joching the loess unit J1 above the Cryosol complex (sample 1398) was dated to 16 ± 2 ka, whereas the 'Bröckelsand' (sample 1399) was dated to 47 ± 3 ka. This allows for formation of the Cryosol complex sometime between ~45 ka and ~20 ka. Cryosols in Lower Austria were described at Stratzing and luminescence dated to ~27–33 ka (Thiel et al., 2011a). This is in agreement with Haesearts et al. (1996), who have

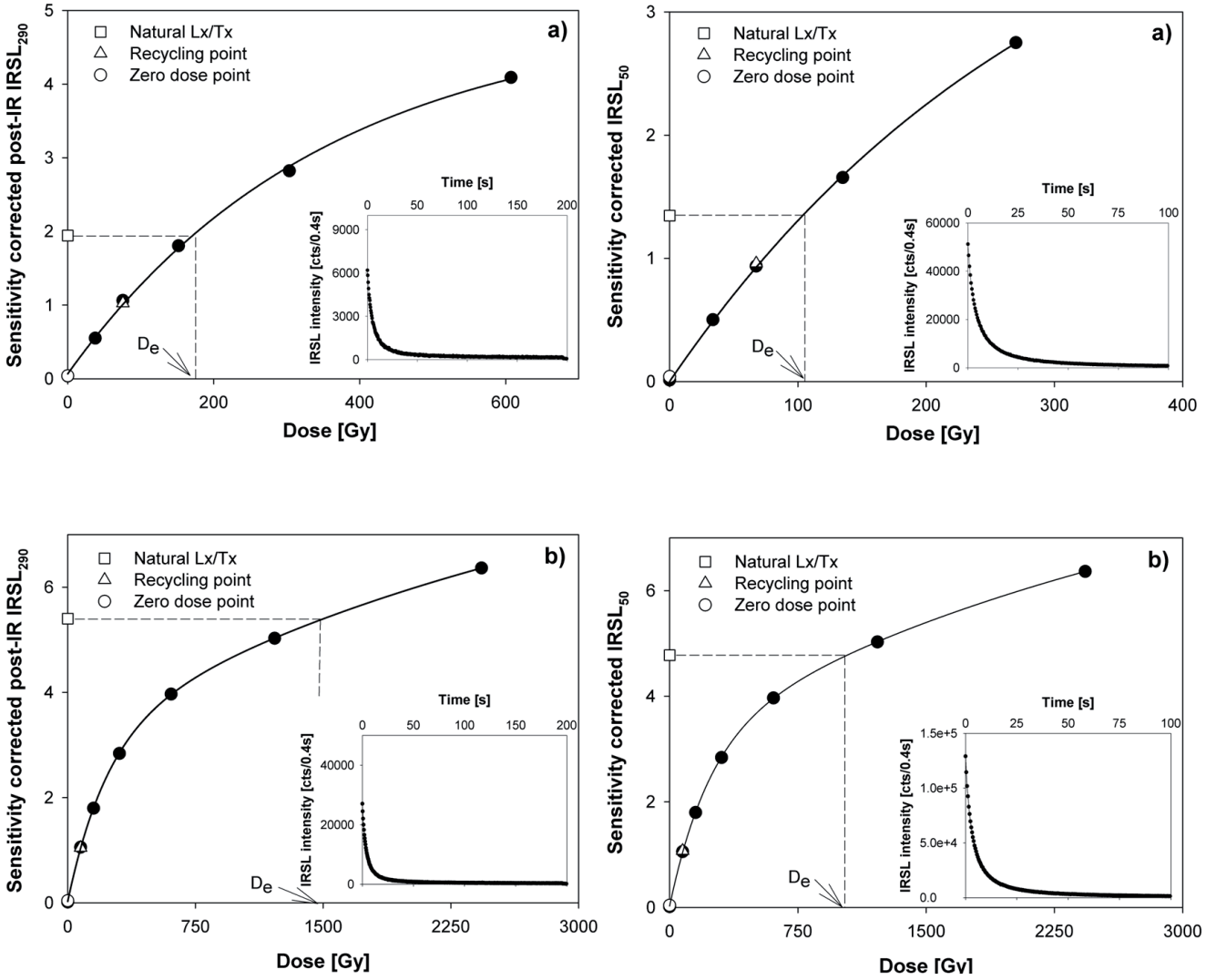

Fig. 8: Dose response and natural decay curves for the post-IR IRSL measurements at 290°C. a) Dose response curve for sample 1399, representative of younger samples. The natural Lx/Tx lies in the linear part of the curve. b) Dose response curve for sample 1407, representative of older samples. The natural Lx/Tx approaches saturation. The insets show the IRSL intensity against time (200 s).

Abb. 8: Wachstumskurven und natürliche Ausleuchtkurven für die post-IR IRSL-Messungen bei 290°C. a) Wachstumskurve für Probe 1399 (repräsentiert junges Material). Das natürliche Signal (Lx/Tx) liegt im linearen Bereich der Kurve. b) Wachstumskurve für Probe 1407 (repräsentiert altes Material). Das natürliche, sensitivitätskorrigierte post-IR IRSL-Signal (Lx/Tx) liegt nahe der Sättigungsgrenze. Die eingesetzten Abbildungen zeigen die post-IR IRSL-Intensität gegen die Zeit (200 s).

Fig. 9: Dose response and natural decay curves for the IRSL measurements at 50°C as part of the post-IR IRSL measurements at 225°C, i.e. the same aliquots are used. a) Dose response curve for sample 1399, representative of younger samples. The natural Lx/Tx lies in the linear part of the curve. b) Dose response curve for sample 1407, representative of older samples. The natural Lx/Tx is beyond the linear part of the curve, nevertheless nowhere near saturation. The insets show the IRSL intensity against time (100 s).

Abb. 9: Wachstumskurven und natürliche Ausleuchtkurven für die IRSL-Messungen bei 50°C (als Teil der post-IR IRSL-Messungen bei 225°C, d.h. dieselben Aliquoten wurden verwendet). a) Wachstumskurve für Probe 1399 (repräsentiert junges Material). Das natürliche Signal (Lx/Tx) liegt im linearen Bereich der Kurve. b) Wachstumskurve für Probe 1407 (repräsentiert altes Material). Das natürliche, sensitivitätskorrigierte post-IR IRSL-Signal (Lx/Tx) liegt oberhalb des linearen Bereiches, jedoch nicht annähernd in Sättigung. Die eingesetzten Abbildungen zeigen die post-IR IRSL-Intensität gegen die Zeit (100 s).

presented several radiocarbon ages (charcoal) from various sites in Lower Austria pointing to formation of the Cryosols between 27 and 39 ka. The loess unit J9 underlying the pedocomplex (sample 1400) was dated to 170 ± 16 ka (MIS 6); it is therefore likely that the pedocomplex (unit J6–J8) developed during MIS 5; however, an unequivocal attribution to a sub-stage is not possible. Because the pedocomplex is composed of three horizons, it is possible that it comprises the entire MIS 5 with its sub-stages. The pedocomplex in Joching might thus be correlated with the 'Paudorfer Bodenbildung' (unit PI-3; Fig. 3), which at its type locality in Paudorf developed during MIS 5. This is shown by the age of the loess unit PI-2 above the 'Paudorfer Bodenbildung' of 106 ± 12 ka (sample 1404), whereas the loess below (unit PI-4) gives an age of 159 ± 20 ka (post-IR IRSL at 225°C; sample 1403). Here, it has to be noted that the age of 299 ± 33 ka derived from post-IR IRSL at 290°C seems to be an overestimate; this is likely because the ratio of D_e's obtained (post-IR IRSL at 290°C/post-IR IRSL at 225°C) is for all samples <1.5, whereas for sample 1403 it is 2.1. Hence, for sample 1403, the fading corrected post-IR IRSL at 225°C age of 159 ± 20 (Table 3) seems the most reliable result and is, within errors, in agree-

*Tab. 3: Recycling ratios, equivalent doses (D_e), fading rates, and fading uncorrected and fading corrected ages for the three (post-IR) IRSL signals. For all samples six aliquots were measured for D_e determination. The fading uncorrected ages for the post-IR IRSL signal at 290°C **(in bold)** are considered the most reliable (apart from sample 1403 for which the corrected age of post-IR IRSL at 225°C is considered the most reliable estimate). For details see text.*

*Tab. 3: Recycling Ratios, Äquivalenzdosen (D_e), Fading-Raten und nicht-korrigierte sowie korrigierte Alter für die drei (post-IR) IRSL-Signale. Für alle Proben wurden sechs Aliquoten für die Bestimmung der Äquivalenzdosis verwendet. Die nicht-korrigierten Alter des post-IR IRSL-Signals bei 290°C **(in fett)** sind die zuverlässigsten (bis auf Probe 1403, für die das korrigierte Alter des post-IR IRSL-Signals bei 225°C am zuverlässigsten angesehen wird). Siehe Text für Details.*

Location	Sample	Signal	Recycling ratio	D_e [Gy]	Fading rate [%/decade]	Fading uncorrected age [ka]	Fading corrected age [ka]
Joching	1398	IRSL at 50°C*	1.03 ± 0.02	15 ± 2	8.0 ± 0.5	5 ± 1	10 ± 1
		pIR IRSL at 225°C	1.02 ± 0.01	33 ± 3	2.8 ± 0.2	11 ± 1	13 ± 1
		pIR IRSL at 290°C	1.02 ± 0.01	50 ± 5	1.3 ± 0.5	**16 ± 2**	18 ± 2
	1399	IRSL at 50°C*	1.07 ± 0.07	140 ± 15	4.3 ± 0.5	40 ± 4	58 ± 8
		pIR IRSL at 225°C	1.05 ± 0.02	148 ± 11	1.8 ± 0.1	42 ± 2	49 ± 4
		pIR IRSL at 290°C	0.99 ± 0.01	163 ± 10	0.9 ± 0.5	**47 ± 4**	50 ± 5
	1400	IRSL at 50°C*	1.01 ± 0.02	329 ± 34	9.9 ± 0.5	157 ± 17	679 ± 74
		pIR IRSL at 225°C	1.00 ± 0.01	337 ± 32	2.7 ± 0.2	160 ± 17	201 ± 19
		pIR IRSL at 290°C	1.00 ± 0.01	356 ± 32	1.0 ± 0.3	**170 ± 16**	183 ± 19
Paudorf	1401	IRSL at 50°C*	1.02 ± 0.02	474 ± 37	1.0 ± 0.7	125 ± 10	135 ± 12
		pIR IRSL at 225°C	0.99 ± 0.01	596 ± 20	1.2 ± 0.2	157 ± 10	172 ± 15
		pIR IRSL at 290°C	1.00 ± 0.01	714 ± 58	1.1 ± 0.2	**189 ± 16**	204 ± 20
	1402	IRSL at 50°C*	1.03 ± 0.01	344 ± 15	2.2 ± 0.6	119 ± 6	141 ± 13
		pIR IRSL at 225°C	1.00 ± 0.01	427 ± 44	0.6 ± 0.6	147 ± 16	154 ± 20
		pIR IRSL at 290°C	0.99 ± 0.01	538 ± 34	0.7 ± 0.5	**187 ± 12**	195 ± 20
	1403	IRSL at 50°C*	1.01 ± 0.04	353 ± 19	4.3 ± 0.6	118 ± 7	172 ± 19
		pIR IRSL at 225°C	1.00 ± 0.01	414 ± 44	1.8 ± 0.1	138 ± 15	**159 ± 20**
		pIR IRSL at 290°C	0.98 ± 0.01	897 ± 97	0.7 ± 0.3	299 ± 33	315 ± 41
	1404	IRSL at 50°C*	1.03 ± 0.03	234 ± 20	3.7 ± 0.6	71 ± 6	97 ± 12
		pIR IRSL at 225°C	1.01 ± 0.01	225 ± 19	1.5 ± 0.2	68 ± 6	77 ± 9
		pIR IRSL at 290°C	1.01 ± 0.01	351 ± 40	1.5 ± 0.4	**106 ± 12**	120 ± 16
Göttweig	1405	IRSL at 50°C*	0.99 ± 0.01	728 ± 51	3.4 ± 0.3	228 ± 17	304 ± 30
		pIR IRSL at 225°C	0.99 ± 0.01	1295 ± 83	4.3 ± 0.5	>300	>300
		pIR IRSL at 290°C	0.99 ± 0.01	1845 ± 483	0.8 ± 0.4	**>350**	>350
	1406	IRSL at 50°C*	1.04 ± 0.02	440 ± 47	4.6 ± 0.6	152 ± 16	230 ± 34
		pIR IRSL at 225°C	1.00 ± 0.00	537 ± 30	2.3 ± 0.3	185 ± 12	233 ± 19
		pIR IRSL at 290°C	1.00 ± 0.01	503 ± 115	1.2 ± 0.3	**173 ± 40**	190 ± 46
	1407	IRSL at 50°C*	1.00 ± 0.01	847 ± 125	3.2 ± 0.3	249 ± 38	327 ± 53
		pIR IRSL at 225°C	0.98 ± 0.01	1149 ± 96	2.9 ± 0.5	>280	>280
		pIR IRSL at 290°C	1.00 ± 0.01	1265 ± 78	0.9 ± 0.3	**>300**	>300
	1408	IRSL at 50°C*	0.99 ± 0.05	75 ± 6	3.3 ± 0.4	25 ± 2	33 ± 4
		pIR IRSL at 225°C	1.00 ± 0.01	83 ± 6	2.0 ± 0.5	28 ± 3	32 ± 4
		pIR IRSL at 290°C	1.00 ± 0.01	101 ± 8	0.9 ± 0.4	**34 ± 3**	36 ± 4
	1409	IRSL at 50°C*	1.00 ± 0.01	244 ± 16	3.1 ± 0.3	116 ± 8	151 ± 13
		pIR IRSL at 225°C	1.00 ± 0.01	294 ± 23	1.3 ± 0.4	140 ± 13	155 ± 15
		pIR IRSL at 290°C	0.99 ± 0.01	263 ± 53	0.7 ± 0.3	**124 ± 25**	132 ± 30

** The equivalent doses of the IRSL signal at 50°C are derived from the same measurement cycle as the post-IR IRSL (225°C) results, i.e. preheat of 250°C. The same applies to the measured fading rates.*

E&G / Vol. 60 / No. 1 / 2011 / 137–152 / DOI 10.3285/eg.60.1.10

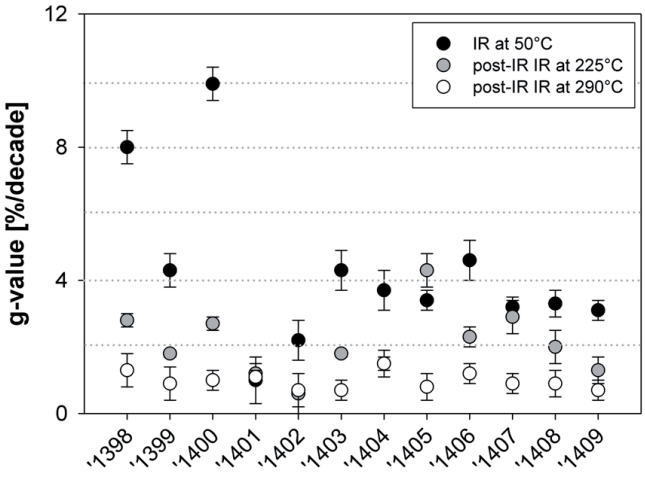

Fig. 10: Comparison of laboratory fading rates [%/decade] for all samples using the different (post-IR) IRSL signals. Lowest fading rates are observed for the post-IR IRSL measurements at 290°C. For details about laboratory fading measurements see text.

Abb.10: Vergleich der experimentell ermittelten Fading-Raten [%/Dekade] für alle Proben bei Anwendung der verschiedenen (post-IR) IRSL-Signale. Die geringsten Fading-Raten wurden für das post-IR IRSL-Signal bei 290°C gemessen.

ment with the age of sample 1402 (unit PII-3), which also originates from below the 'Paudorfer Bodenbildung' (Fig. 3) and was dated to 187 ± 12 ka. The individual soils of the 'Paudorfer Bodenbildung' might thus have formed during sub-stages of MIS 5. Originally the formation of the soil was attributed to a Würmian interstadial by Götzinger (1936); at that time it was not recognised as being a pedocomplex. Ložek (1976) revised the attribution of Götzinger (1936), because an interglacial mollusc fauna was found in the lowermost part of the 'Paudorfer Bodenbildung', i.e. the lower part of this pedocomplex developed most likely during MIS 5e. This is in agreement with our dating results and with the TL results of Zöller et al. (1994), who state that their age of 103 ± 11 ka below the 'Paudorfer Bodenbildung' at its type locality should be regarded as a minimum age. The attribution of the 'Paudorfer Bodenbildung' to MIS 3 as suggested by Noll et al. (1994) can clearly be dismissed. At profile Paudorf II, the BC horizon, i.e. the weakly developed palaeosol (unit PII-8, Fig. 3) is younger than 189 ± 16 ka (sample 1401); a correlation with other soils in this area remains unclear and needs further investigations. For the underlying pedocomplex (unit PII-10), which has been correlated with the 'Göttweiger Verlehmungszone', it can only be concluded that it has to be older than 189 ± 16 ka. Hence further investigations are needed to address the question whether this soil is equivalent to the 'Göttweiger Verlehmungszone', which is dated to >350 ka (sample 1405; minimum age based on $2*D_0$ for post-IR IRSL at 290°C; Wintle & Murray, 2006) at its type locality in Göttweig/Furth (Fig. 4a). Originally the 'Göttweiger Verlehmungszone' (unit GI-4) was attributed to MIS 5e (Götzinger, 1936), but Zöller et al. (1994) observed natural TL signals from above and below the 'Göttweiger Verlehmungszone' close to saturation and concluded that their ages of ~200 ka have to be interpreted as minimum ages. Furthermore, the alle/Ile ratio of *Pupilla* shells taken from loess immediately above the 'Göttweiger Verlehmungszone' soil is too high to be from penultimate glacial loess (Zöller et al., 1994). Smolíková (1994) suggest that this pedocomplex is perhaps of Holsteinian age, which at present is correlated with MIS 11 or MIS 9. Our minimum age is consistent with these findings. This age model is also supported by the dating of the loess sample 1407 above the tephra, 300 m upslope of Section I, which yielded ≥300 ka; the loess sample 1406 above the tephra was dated to 173 ± 40 ka, clearly showing a hiatus in the sequence. It has to be noted that the tephra, if found in other sequences, might be a useful Middle Pleistocene marker, dated to ≥300 ka.

At Section II (Göttweig/Aigen; Fig. 3b) the loess unit GII-1 above the reworked loess (unit GII-2) and the pedocomplex (unit GII-3) is dated to 34 ± 3 ka (sample 1408) , and is thus in good agreement with Zöller et al.'s (1994) TL results of 28 ± 3 ka. They dated the loess below the pedocomplex to 107 ± 10 ka (regenerative dose method) and 119 ± 13 ka (additive dose method) and concluded that the soil formation lasted about 90 ka. Even though we have obtained a very similar age of 124 ± 25 ka for the loess from below the soil (sample 1409), we argue that there is certainly some break in the sedimentary record, rather than a long pedogenetic phase, because the pedocomplex is clearly eroded (indicated by the lack of an A horizon and a covering of soil sediment). Nevertheless, the age suggests that the pedocomplex exposed in Göttweig/Aigen corresponds with the 'Paudorfer Bodenbildung' at its type locality (Götzinger, 1936).

8 Conclusions

We have used two recently suggested post-IR IRSL dating protocols (Buylaert et al., 2009; Thiel et al., 2011a) to compare ages and so unravel the chronostratigraphy of prominent palaeosols in Lower Austria. In addition, we have compared the fading rates and ages derived from post-IR IRSL dating with IRSL at 50°C (measured as part of the post-IR IRSL measurements at 225°C).

The samples behave satisfactorily in the two post-IR IRSL SAR protocols, i.e. recycling ratios and dose recoveries are close to unity and recuperation is well below 5% for most of the samples. The lowest laboratory fading rates are observed using the post-IR IRSL signal at 290°C, followed by post-IR IRSL at 225°C, and fading rates for IR at 50°C tend to be the highest. The fading rates of the post-IR IRSL at 290°C are in most cases below 1%/decade, and based on the observations of Thiel et al. (2011a) we conclude that fading for this signal is probably negligible over geological time and so we do not attempt any fading correction of this signal. Good agreement between the ages derived from the post-IR IRSL signals and those from IRSL at 50°C on young samples shows that the post-IR IRSL signals are bleachable. Nevertheless it remains unclear whether the residual dose observed following laboratory bleaching, or some part of it, needs to be subtracted from the D_e. The fading corrected ages for post-IR IRSL at 225°C are in generally good agreement with the uncorrected ages for post-IR IRSL at 290°C. Both post-IR IRSL signals could be used for dating; we prefer the post-IR IRSL at 290°C because no fading correction seems to be needed, and so there are no dose/age limitations imposed by the use of a correction model. However, one 290°C age appeared significantly overestimated in the stratigraphical context, which has to be a matter of future investigations.

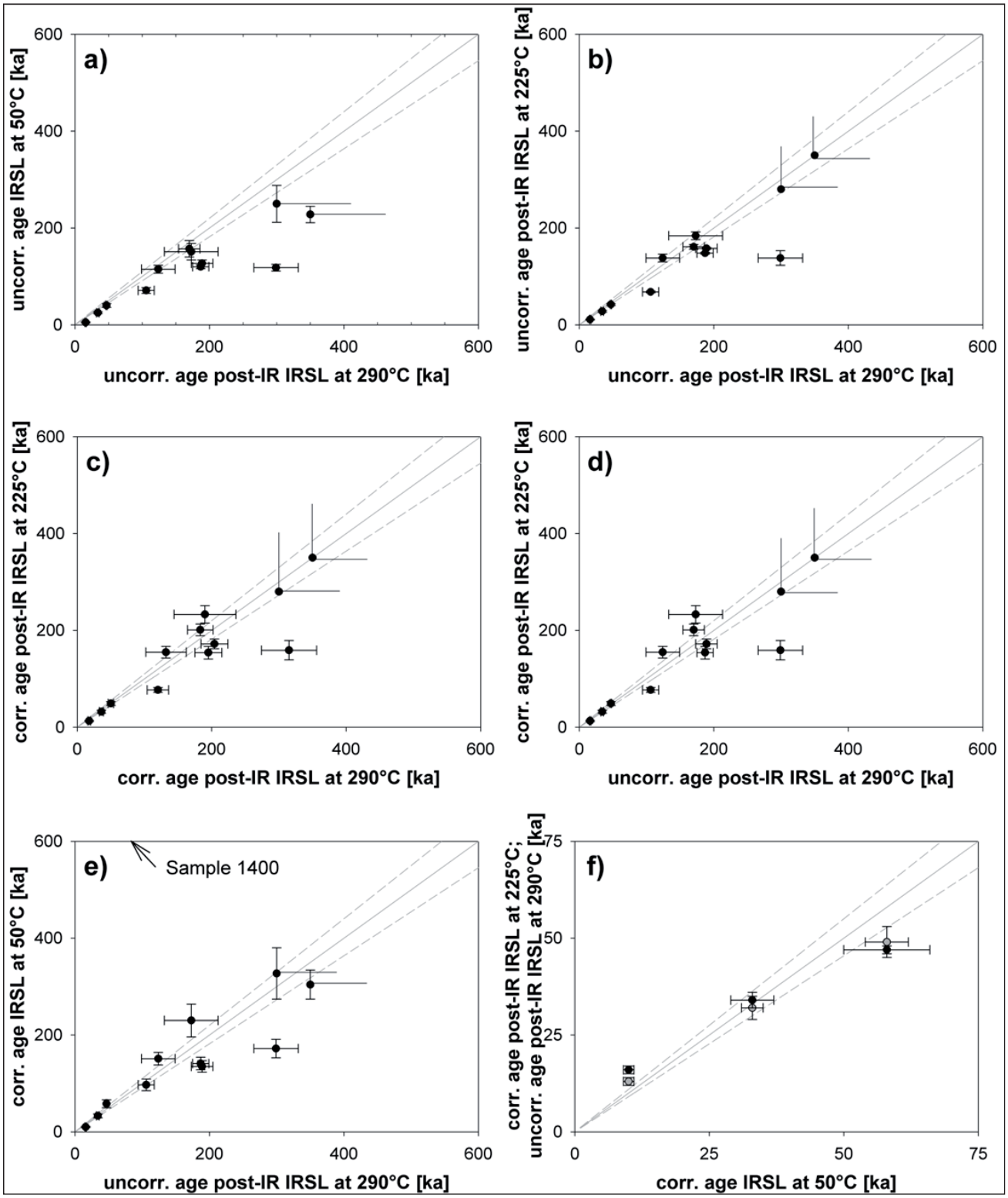

Fig. 11: Comparison of ages for all samples using the different (post-IR) IRSL signals. The ages shown are without subtraction of the residuals. a) Fading uncorrected ages for IRSL at 50°C against fading uncorrected ages for post-IR IRSL at 290°C, b) fading uncorrected ages for post-IR IRSL at 225°C against fading uncorrected ages for post-IR IRSL at 290°C, c) fading corrected ages for post-IR IRSL at 225°C against fading corrected ages for post-IR IRSL at 290°C, d) fading corrected ages for post-IR IRSL at 225°C against fading uncorrected ages for post-IR IRSL at 290°C, e) fading corrected ages for IRSL at 50°C against fading uncorrected ages for post-IR IRSL at 290°C, and f) young (<70 ka) fading corrected ages for post-IR IRSL at 225°C (grey circles) and fading uncorrected ages for post-IR IRSL at 290°C (black circles) against corrected ages for IRSL at 50°C, to show the relative bleachability of the post-IR IRSL signals. Minimum ages are shown with open error bars. Solid line is a 1:1 line, and dashed lines represent ±10%.

Abb. 11: Vergleich der Alter für alle Proben unter Verwendung der verschiedenen (post-IR) IRSL-Signale. Die angeführten Alter sind ohne Subtraktion des Restsignals. a) Nicht-korrigierte Alter für IRSL bei 50°C gegen nicht-korrigierte post-IR IRSL-Alter bei 290°C, b) nicht-korrigierte post-IR IRSL-Alter bei 225°C gegen nicht-korrigierte post-IR IRSL-Alter bei 290°C, c) korrigierte post-IR IRSL-Alter bei 225°C gegen korrigierte post-IR IRSL-Alter bei 290°C, d) korrigierte post-IR IRSL-Alter bei 225°C gegen nicht-korrigierte post-IR IRSL-Alter bei 290°C, e) korrigierte Alter für IRSL bei 50°C gegen nicht-korrigierte post-IR IRSL-Alter bei 290°C, und f) junge (<70 ka) korrigierte Alter für post-IR IRSL bei 225°C (graue Punkte) und nicht-korrigierte Alter für post-IR IRSL bei 290°C (schwarze Punkte) gegen korrigierte IRLS-Alter bei 50°C, um die relative Zurücksetzung der post-IR IRSL-Signale zu zeigen. Minimale Alter sind mit offenen Fehlerbalken gezeigt. Die durchgezogene Linie zeigt die 1:1-Linie, und die gestrichelten Linien repräsentieren ±10%.

We assign the 'Paudorfer Bodenbildung' at its type locality in Paudorf to MIS 5. It is furthermore very likely that the pedocomplex in Göttweig/Aigen developed during the same time and can hence be correlated with the 'Paudorfer Bodenbildung'. The same is true for the pedocomplex exposed in Joching. The absolute age of the 'Göttweiger Verlehmungszone' remains unclear due to saturation of the sample above this soil; the saturation implies an age >350 ka for the 'Göttweiger Verlehmungszone'. The discontinuities in sedimentation observed at these sites are hence significant. It has to be noted that sampling at higher resolution is needed to draw final conclusions on the extent of the discontinuities. The correlation of Lower Austrian loess deposits and their interleaved palaeosols thus remains problematic. Advances in absolute dating techniques such as post-IR IRSL dating are of importance to address the many remaining open questions on loess stratigraphy in the future.

Acknowledgements

This study was supported by the Leibniz Pakt Project for Research and Innovation 2008–2010. We are indebted to Bodo Damm for assistance during field work and to Sonja Riemenschneider for support in the laboratory. We thank Kristina Thomsen and Mayank Jain for fruitful discussions on post-IR IRSL dating. Sébastien Huot is thanked for the Excel macros which were used to calculate fading rates in a fast and elegant manner.

References

Adamiec, G. & Aitken, M.J. (1998): Dose-rate conversion factors: update. – Ancient TL, 16: 37–50.

Aitken, M.J. (1985): Thermoluminescence Dating. London (Academic Press).

Aitken, M.J. (1998): An Introduction to Optical Dating. The Dating of Quaternary Sediments by the Use of Photon-stimulated Luminescence. Oxford (Oxford University Press).

Auclair, M., Lamothe, M. & Huot, S. (2003): Measurement of anomalous fading for feldspar IRSL using SAR. – Radiation Measurement, 37: 487–492.

Bayer, J. (1927): Der Mensch im Eiszeitalter; I. und II. Teil. Wien (Deutike).

Bøtter-Jensen, L., Andersen, C.E., Duller, G.A.T. & Murray, A. S. (2003): Developments in radiation, stimulation and observation facilities in luminescence measurements. – Radiation Measurements, 37: 535–541.

Buylaert, J.P., Vandenberghe, D., Murray, A.S., Huot, S., De Corte, F. & Van den haute, P. (2007): Luminescence dating of old (>70 ka) Chinese loess: A comparison of single aliquot OSL and IRSL ages. –Quaternary Geochronology, 2: 9–14.

Buylaert, J.P., Murray, A.S., Thomsen, K.J. & Jain, M. (2009): Testing the potential of an elevated temperature IRSL signal from K-feldspar. – Radiation Measurements, 44: 560–565.

Buylaert, J.P., Huot, S., Murray, A.S. & Van den haute, P. (2011). Infrared stimulated luminescence dating of an Eemian (MIS 5e) site in Denmark using K-feldspar. – Boreas, 40: 46–56.

Duller, G.A.T. & Wintle, A.G. (1991): On infrared stimulated luminescence at elevated temperatures. – Nuclear Tracks and Radiation Measurements, 18: 379–384.

Fink, J. (1976): Exkursion durch den österreichischen Teil des nördlichen Alpenvorlandes und den Donauraum zwischen Krems und Wiener Pforte. Erweiterter Führer zur Exkursion aus Anlass der 2. Tagung der IGCP-Projektgruppe „Quaternary Glaciations in the Northern Hemisphere. – Mitteilungen der Kommission für Quartärforschung der Österreichischen Akademie der Wissenschaften,1: 113 pp.

Frechen, M., Horváth, E. & Gábris, G. (1997): Geochronology of Middle to Upper Pleistocene Loess Sections in Hungary. – Quaternary Research, 48: 291–312.

Frechen, M., Schweitzer, U. & Zander, A. (1996): Improvements in sample preparation for the fine grain technique. – Ancient TL, 14: 15–17.

Götzinger, G. (1936): Das Lößgebiet um Göttweig und Krems an der Donau. Führer für die Quartär-Exkursionen in Österreich 1, pp. 1–11.

Haesaerts, P., Damblon, F., Bachner, M. & Trnka, G. (1996): Revised stratigraphy and chronology of the Willendorf II sequence, Lower Austria. – Archaeologia Austriaca, 80: 25–42.

Havlíček, P., Holásek, O., Smolíková, L. & Roetzel, R. (1998): Zur Entwicklung der Quartärsedimente am Südostrand der Böhmischen Masse in Niederösterreich. – Jahrbuch der Geologischen Bundesanstalt, 141: 51–72.

Head, M.J., Gibbard, P.L. & Salvador, A. (2008): The Quaternary: its character and definition. – Episodes, 31: 234–238.

Huntley, D.J. & Clague, J.J. (1996): Optical dating of tsunami-laid sands. – Quaternary Research, 46: 127–140.

Huntley, D.J. & Lamothe, M. (2001): Ubiquity of anomalous fading in K-feldspars and the measurement and correction for it in optical dating. – Canadian Journal of Earth Science, 38: 1093–1106.

Kars, R.H., Wallinga, J. & Cohen, K.M. (2008): A new approach towards anomalous fading correction for feldspar IRSL dating – tests on samples in field saturation. – Radiation Measurements, 43: 786–790.

Kunz, A., Frechen, M., Ramesh, R. & Urban, B. (2010): Revealing the coastal event-history of the Andaman Islands (Bay of Bengal) during the Holocene using radiocarbon and OSL dating. – International Journal of Earth Science (Geologische Rundschau), 8: 1741–1761.

Lai, Z.P., Zhang, W.G., Chen, X., Jia, Y. L., Liu, X.J., Fan, Q.S. & Long, H. (2010): OSL chronology of loess deposits in East China and its implications for East Asian monsoon history. – Quaternary Geochronology, 5: 154–158.

Lamothe, M. & Auclair, M. (1999): A solution to anomalous fading and age shortfalls in optical dating of feldspar minerals. – Earth and Planetary Science Letters, 171: 319–323.

Lamothe, M., Auclair, M., Hamzaoui, C. & Huot, S. (2003): Towards a prediction of long-term anomalous fading of feldspar IRSL. – Radiation Measurements, 37: 493–498.

Ložek, V. (1976): Stop 8a/3: Hohlweg Aigen, Malakologie. In: Fink, J. (ed.): Exkursion durch den österreichischen Teil des nördlichen Alpenvorlandes und den Donauraum zwischen Krems und Wiener Pforte. Erweiterter Führer zur Exkursion aus Anlass der 2. Tagung der IGCP-Projektgruppe „Quaternary Glaciations in the Northern Hemisphere. – Mitteilungen der Kommission für Quartärforschung der Österreichischen Akademie der Wissenschaften, 1: 72–75.

Murray, A.S. & Wintle, A.G. (2000): Luminescence dating of quartz using an improved single-aliquot regenerative-dose protocol. – Radiation Measurements, 32: 57–73.

Murray, A.S. & Wintle, A.G. (2003): The single aliquot regenerative dose protocol: potential for improvements in reliability. - Radiation Measurements, 37: 377–381.

Murray, A.S., Buylaert, J.P., Thomsen, K.J. & Jain, M. (2009): The Effect of Preheating on the IRSL Signal from Feldspar. – Radiation Measurements, 44: 554–559.

Noll, M., Leitner-Wild, E. & Hille, P. (1994): Thermoluminescence dating of loess deposits at Paudorf, Austria. – Quaternary Geochronology (Quaternary Science Reviews), 13: 473–476.

Novothny, Á., Horváth, E. & Frechen, M. (2002): The loess profile of Albertirsa, Hungary – Improvements in loess stratigraphy by luminescence dating. – Quaternary International, 95–96: 155–163.

Novothny, Á., Frechen, M., Horváth, E., Bradák, B., Oches, E. A., McCoy, W. D. & Stevens, T. (2009): Luminescence and amino acid racemisation chronology of the loess-paleosol sequence at Süttő, Hungary. – Quaternary International, 198: 62–76.

Novothny, Á., Frechen, M., Horváth, E., Krbetschek, M. & Tsukamoto, S. (2010): Infrared stimulated luminescence and radiofluorescence dating of aeolian sediments from Hungary. – Quaternary Geochronology, 5: 114–119.

Poolton, N.R.J., Ozanyan, K.B., Wallinga, J., Murray, A.S. & Bøtter-Jensen, L. (2002): Electrons in feldspar II: a consideration of the influence of conduction band-tail states on luminescence processes. – Physics and Chemistry in Minerals, 29: 217–225.

Prescott, J.R. & Hutton, J.T. (1994): Cosmic ray contributions to dose rates for luminescence and ESR dating: large depths and long-term variations. – Radiation Measurements, 23: 497–500.

Rees-Jones, J. (1995): Optical dating of young sediments using fine-grain quartz. – Ancient TL, 13: 9–14.

Reimann, T., Tsukamoto, S., Naumann, M. & Frechen, M., (2011). The potential of using K-rich feldspars for optical dating of young coastal

sediments – A test case from Darss-Zingst peninsula (southern Baltic Sea coast). – Quaternary Geochronology, 6: 207–222.

Roberts, H.M. (2008): The development and application of luminescence dating to loess deposits: a perspective on the past, present and future. – Boreas, 37: 483–507.

Smolíková, L. (1994): Paleopedologický výzkum významných lokalit Paudorf, Göttweig, Krems a Stranzendorf. Zpr. Geol. Výzk. v Roce, 80.

Spooner, N.A (1994): The anomalous fading of infra-red stimulated luminescence from feldspars. – Radiation Measurements, 23: 625–632.

Thiel, C., Coltorti, M., Tsukamoto, S. & Frechen, M. (2010): Geochronology for some key sites along the coast of Sardinia (Italy). – Quaternary International, 222: 36–47.

Thiel, C., Buylaert, J.-P., Murray, A.S., Terhorst, B., Hofer, I., Tsukamoto, S. & Frechen, M. (2011a): Luminescence dating of the Stratzing loess profile (Austria) – Testing the potential of an elevated temperature post-IR IRSL protocol. – Quaternary International, 234: 23–31.

Thiel, C., Terhorst, B., Jaburová, I., Buylaert, J.-P., Murray, A.S., Fladerer, F.A., Damm, B., Frechen, M. & Ottner, F. (2011b): Sedimentation and erosion processes in Middle to Late Pleistocene sequences exposed in the brickyard of Langenlois/Lower Austria. – Geomorphology, in press (doi: 10.1016/j.geomorph.2011.02.011).

Thiel, C., Buylaert, J.-P., Murray, A.S. & Tsukamoto, S. (accepted): On the applicability of post-IR IRSL dating to Japanese loess. Geochronometria.

Thomsen, K.J., Bøtter-Jensen, L., Denby, P.M., Moska, P. & Murray, A.S. (2006): Developments in luminescence measurement techniques. – Radiation Measurements, 41: 768–773.

Thomsen, K.J., Murray, A.S., Jain, M. & Bøtter-Jensen, L. (2008): Laboratory fading rates of various luminescence signals from feldspar-rich sediment extracts. – Radiation Measurements, 43: 1474–1486.

Thomsen, K.J., Murray, A.S. & Jain, M. (2011): Stability of IRSL signals from sedimentary K-feldspar samples. – Geochronometria, 38: 1–13.

Wallinga, J., Bos, A.J.J., Dorenbos, P., Murray, A.S. & Schokker, J. (2007): A test for anomalous fading correction in IRSL dating. – Quaternary Geochronology, 2: 216–221.

Wang, X.L., Lu, Y.C. & Wintle, A. G. (2006): Recuperated OSL dating of fine-grained quartz in Chinese loess. – Quaternary Geochronology, 1: 89–100.

Watanuki, T., Murray, A.S. & Tsukamoto, S. (2005): Quartz and polymineral luminescence dating of Japanese loess over the last 0.6 Ma: Comparison with an independent chronology. – Earth and Planetary Science Letters, 240: 774–789.

Wintle, A.G. (1973): Anomalous Fading of Thermo-luminescence in Mineral Samples. – Nature, 245: 143–144.

Wintle, A.G. & Murray, A.S. (2006): A review of quartz optically stimulated luminescence characteristics and their relevance in single-aliquot regeneration dating protocols. -Radiation Measurements, 41: 369–391.

Zöller, L., Oches, E.A. & McCoy, W.D. (1994): Towards a revised chronostratigraphy of loess in Austria with respect to key sections in the Czech Republic and in Hungary. – Quaternary Geochronology (Quaternary Science Reviews), 13: 465–472.

E&G Quaternary Science Journal
Volume 60 / Number 1 / 2011 / 153-169 / DOI 10.3285/eg.60.1.11
www.quaternary-science.net

GEOZON SCIENCE MEDIA
ISSN 0424-7116

The Loess Chronology of the Island of Susak, Croatia

Lara Wacha, Snježana Mikulčić Pavlaković, Manfred Frechen, Marta Crnjaković

Abstract: A high-resolution infrared stimulated luminescence (IRSL) and radiocarbon dating study was performed on the loess-paleosol sequence from the island of Susak, situated in the North Adriatic Sea in Croatia. The dating results show that a detailed Late Pleistocene record is preserved on Susak, correlating to the marine Oxygen Isotope Stages (OIS) 5 to 2, with a very thick Middle Pleniglacial record predominating. Due to its extraordinary thickness (which is recorded to be up to 90 metres), the loess on Susak is unique in this area. The numerous paleosols intercalated in the loess give evidence for climate variations which were warmer than in other loess regions (e.g. the Carpathian Basin). The great thickness of the OIS3 deposits correlates to the general increased dust accumulation in Europe during that time. Based on numerical ages a correlation of the loess on Susak with the loess in North Italy and the Carpathian basin, a more detailed time-based reconstruction of climate and environment changes in the study area was achieved.

[Löss-Chronologie der Insel Susak in Kroatien]

Kurzfassung: Zahlreiche infrarot optisch stimulierte Lumineszenz (IRSL)- und Radiokohlenstoff (14C)-Datierungen wurden an mächtigen Löss-/Paläobodenabfolgen der Insel Susak in der nördlichen Adria von Kroatien durchgeführt. Die Datierungsergebnisse zeigen, dass eine sehr detaillierte spätpleistozäne Sedimentabfolge auf Susak erhalten geblieben ist, die mit den marinen Sauerstoffisotopenstadien (OIS) 5 bis 2 korreliert. Hervorzuheben ist ein besonders mächtiges und gut gegliedertes Mittelpleniglazial. Aufgrund der großen Mächtigkeit von bis zu 90 m bildet der Löss auf Susak ein einzigartiges außerordentlich hoch aufgelöstes Klimaarchiv in dieser Region. Die zahlreichen im Löss zwischen geschalteten Paläoböden weisen auf Klimavariationen, die auf Susak wärmer gewesen sind als beispielsweise im benachbarten Karpatenbecken. Die große Mächtigkeit der Abfolge korreliert mit den während des OIS 3 allgemein höheren Staubakkumulationen in Europa. Basierend auf den nummerischen Altern kann die Löss-/Paläobodenabfolge aus Susak mit denen aus Norditalien und dem Karpatenbecken verglichen werden und ermöglichen eine detailliertere zeit-basierte Rekonstruktion der Klima- und Umweltveränderungen im Arbeitsgebiet.

Keywords: *Susak, Croatia, loess-paleosol sequence, geochronology, IRSL dating, radiocarbon dating*

Addresses of authors: **L. Wacha**, dipl. ing. geol., Leibniz Institute for Applied Geophysics, S3 Geochronology and Isotope Hydrology, Stilleweg 2, D-30655 Hannover, Germany; Croatian Geological Survey, Department of Geology, Sachsova 2, HR-10000 Zagreb, Croatia. E-Mail: Lara.Wacha@liag-hannover.de, lwacha@hgi-cgs.hr; **Mr. Sci. S. Mikulčić Pavlaković & Dr. M. Crnjaković**, Croatian Natural History Museum, Department of Mineralogy and Petrography, Demetrova 1, HR-10000 Zagreb, Croatia. E-Mail: Snjezana.Mikulcic@hpm.hr, Marta.Crnjakovic@hpm.hr; **Prof. Dr. M. Frechen**, Leibniz Institute for Applied Geophysics, S3 Geochronology and Isotope Hydrology, Stilleweg 2, D-30655 Hannover, Germany. E-Mail: Manfred.Frechen@liag-hannover.de

1 Introduction

Evidence of Pleistocene climatic changes can be found in more or less continuous terrestrial sediment records like loess-paleosol sequences. Great efforts are made into the high resolution sampling and investigation of loess records using different disciplines and methods with the purpose of identifying climate oscillations and environmental changes (Buylaert et al., 2008; Stevens et al., 2008; Bokhorst & Vandenberghe, 2009). The correlation with oxygen isotope stages (OIS) and the GRIP data (GRIP Members, 1993) is a common practice. However, a robust and detailed chronology is mandatory to make a reliable correlation possible.

Loess and loess-like deposits in the North Adriatic region are found along the fringes of mountain chains like the Alps and the Apennines in Italy and along the coast and islands of Croatia. During the last Glacial period, the sea le-vel of the Mediterranean was about 100 metres lower than today (Van Straaten, 1970; Cremaschi, 1987; Amorosi, et al., 1999). Therefore, the North Adriatic was an extended and closed basin exposed to a strong input of fluvial Alpine material carried by the river Po and other tributaries. The thickness of the loess and loess-like deposits in the North Adriatic area is relatively small, only up to a few meters (Ferraro, 2009), but the deposits are widely distributed. In Italy, loess and loess derivatives can be found on fluvial terraces (Cremaschi et al., 1990), on moraines and fluvio-glacial deposits e.g. Val Sorda (Ferraro, 2009; Ferraro et al., 2004), or on the carbonate platform (Coudé-Gaussen, 1990) where they cover the carbonate basement and fill caves and shelters (Cremaschi, 1987; Peresani et al., 2008). Along the Croatian coast and on the islands loess and loess derivatives are common. In Istria loess can be found in the south, in Premantura and Mrlera, and in the north-west, in Savudrija (Durn, Ottner & Slovenec, 1999; Durn, et al., 2007) as well as on the islands of Unije, Velike and Male Srakane, Krk and Lošinj in the Kvarner region and on the islands Hvar and Mljet in South Dalmatia, with reported thickness ranging from a few meters up to about 20 m (Bognar, 1979). In Savudrija loess is up to 4 m thick and covers terra rossa (Durn, Ottner & Slovenec, 1999; Durn et al., 2003, 2007). The influence of loess was recognised by Durn, Ottner & Slovenec

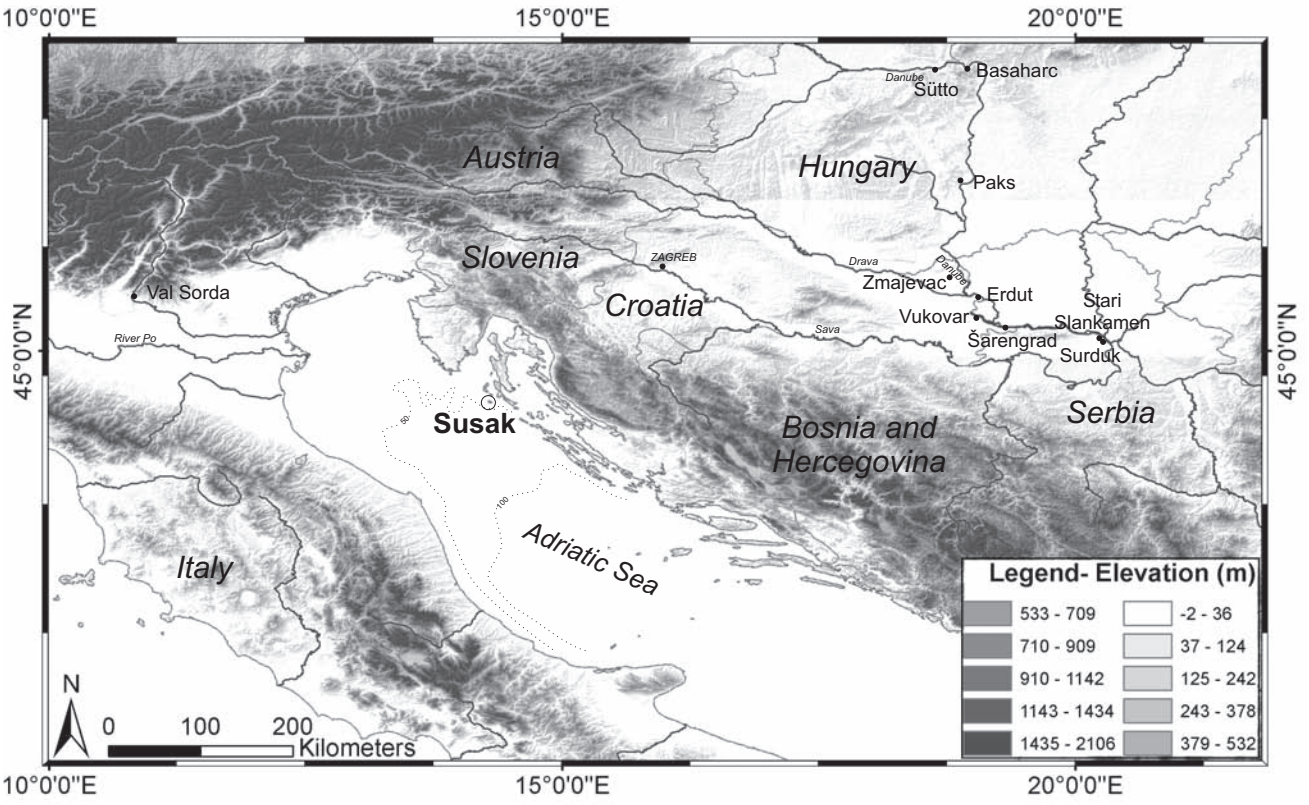

Fig. 1: Geographical setting of the Island of Susak in Croatia and its relation to the river Po in North Italy and to the Danube loess region with indicated locations of loess-paleosol sections used for correlation. Elevation map for the area is prepared using the DEM image obtained from ASTER GDEM (product of METI and NASA).

Abb. 1: Geographische Lage der Insel Susak in Kroatien sowie die Lage der für die Korrelation wichtigen Löss-/Paläoboden-Aufschlüsse in der Po-Region in Norditalien und entlang der Donau. Die Höhenlinien beziehen sich auf ein digitales Höhenmodell basierend auf ASTER GDEM-Daten (METI und NASA).

(1999) and Durn et al. (2007) in the upper parts of terra rossa profiles in Istria. The most extraordinary loess-paleosol record of this area is the one found on the island of Susak in Croatia (Fig. 1). The genesis and the composition of the deposits on the island have been a matter of interest and discussion for a long time, since the two past centuries (Fortis, 1771; Marchesetti, 1882; Kišpatić, 1910; Šandor, 1914; Mutić, 1967; Wein, 1977; Bognar, 1979; Bognar et al., 1983; Cremaschi, 1987; 1990; Bognar & Zámbó, 1992; Bognar, Schweitzer & Kis, 2002; Bognar, Schweitzer & Szöőr, 2003; Lužar-Oberiter et al., 2008; Mikulčić Pavlaković et al., 2011; Wacha et al., 2011). Based on the mineralogical investigations of the deposits from Susak, most of the researchers concluded that the provenance of the material is the river Po plain, situated in the northern part of Italy. Cremaschi (1990) stated that the deposition of loess on Susak is related to the 100 metres drop of the sea level in the Mediterranean during the last glacial period. Recently, the loess-paleosol record on Susak has been successfully dated using infrared stimulated luminescence (Wacha et al., 2011). These first results showed that most of the loess-paleosol record correlates to Oxygen Isotope Stage (OIS) 3, but the deposition age of the stratigraphically older and younger part of the sequence has not yet been determined.

In Croatia, loess and loess-like deposits are well known from the north of the country, on the Bilogora Mountain, around Đakovo, and the eastern part of the country along the river Danube, in Baranja, Srijem and on the Fruška gora

Fig. 2: Photo of Kalučica bay on the easternmost cape of the island, with the characteristic dissected morphology of the Susak loess sequence.

Abb. 2: Foto der Kalučica Bucht am östlichsten Kap der Insel mit der charakteristischen morphologischen Ausprägung der Lösse auf Susak.

(gora = mountain). Loess deposits in this region were investigated by Šandor (1912), Gorjanović-Kramberger (1912, 1915, 1922), Bronger (1976, 2003), Bognar (1979), Galović & Mutić (1984), Poje (1985, 1986), Mutić (1990) and others. The first age estimates of these deposits were presented by Singhvi et al. (1989), using the thermoluminescence (TL) dating method, and by Galović et al. (2009) using the infrared stimulated luminescence (IRSL).

E&G / Vol. 60 / No. 1 / 2011 / 153–169 / DOI 10.3285/eg.60.1.11

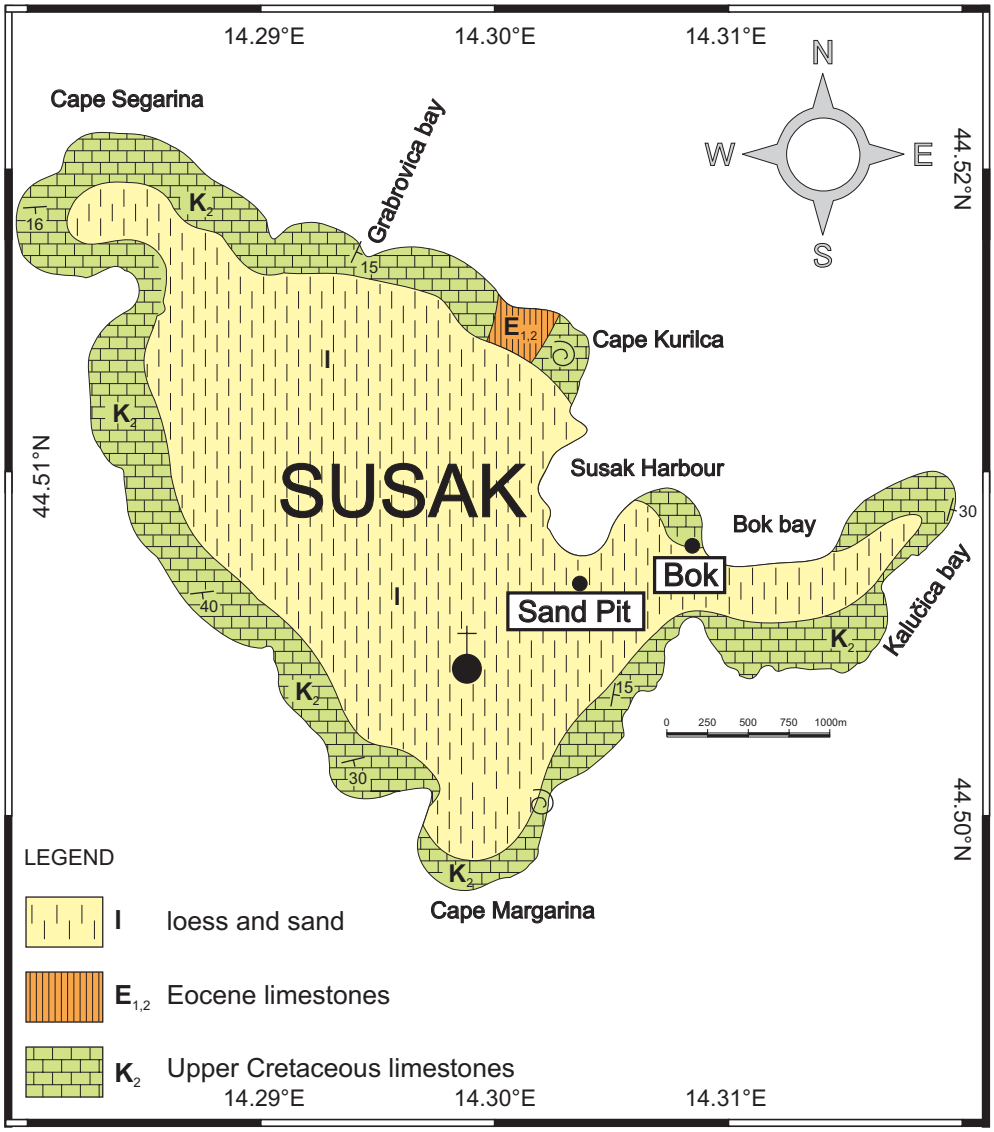

Fig. 3: Geological map of the Island of Susak (simplified after Mamužić, 1965).

Abb. 3: Geologische Karte der Insel Susak (vereinfacht nach Mamužić, 1965).

Fig. 4: Carbonate basement covered with the red paleosol which represents the beginning of the Quaternary loess-paleosol sequence on Susak. (Photo by E. Schmidt.)

Abb. 4: Karbonatisches Basement mit überlagerndem roten Paläoboden, der den Beginn der quartären Löss-/Paläoboden-Sequenz repräsentiert (Foto: E. Schmidt).

In this study the geochronological framework of the loess record from the island of Susak presented in Wacha et al. (2011) is significantly improved by new infrared stimulated luminescence (IRSL) and radiocarbon data. Furthermore, the detailed loess-paleosol sequence is compared with the contemporaneous loess deposits from the North Adriatic Basin and the Pannonian (Carpathian) Basin and an attempt of a chronostratigraphical correlation is given. The loess provinces mentioned above differ in many ways. The loess in the Adriatic region is often neglected when major correlations of loess in Europe are made. In this study the differences and similarities of these two genetically different loess provinces are summarized and they are correlated based on their chronology.

The aim of this study is to establish a more detailed geochronological framework for the unique loess record on the Island of Susak in the North Adriatic Sea as a basis for further high-resolution proxy studies including grain-size and palaeomagnetic approaches (Wacha et al., in preparation) and to settle the Quaternary sediment succession of the Island in a wider context, that of the North Mediterranean and Pannonian (Carpathian) area.

Fig. 5: Three macroscopically visible tephra layers were detected intercalating the Susak loess-paleosol sequence, described in more detail by Mikulčić Pavlaković et al. (2011). a) TF1 – a thin yellow layer of the lowermost, oldest tephra; b) the thin brown paleosol with patches of orange-yellow middle tephra (TF2); c) TF3 – the uppermost and stratigraphically youngest most tephra intercalating loess on Susak is found as a thin olive green layer.

Abb. 5: Drei makroskopisch sichtbare Tephralagen sind den Löss-/Paläobodenabfolgen auf Susak zwischen geschaltet. A) TF1 – dünne gelbe Lage der untersten und stratigraphisch ältesten Tephra; b) TF2 - dünner brauner Paläoboden mit taschenartigen Anreicherungen einer orange-gelben Tephra; c) TF3 – oberste und stratigraphisch jüngste Tephra als olivgrüne Lage im Löss zwischen geschaltet.

2 Geological setting and the sediment succession

The island of Susak is situated in the western part of the Kvarner Archipelago in the North Adriatic Sea in Croatia (Fig. 1). It is the outermost and quite isolated island with an area of 3.8 km^2. The highest peak is at 96 m above sea level (asl). Susak is located between 44.50° and 44.52°N and 14.28° and 14.32°E. The geomorphology of the island has all characteristics of a loess plateau (Bognar, Schweitzer & Szöőr, 2003) dissected by numerous gorges, steep bluffs and gullies (Fig. 2). Human activity during historical times had and still has a major influence on the morphology and erosion of the island because the island is a wine yard area since Roman times resulting in numerous artificial plateaus.

Geotectonically, Susak belongs to the West Istrian autochton of the Northern Adriatic Carbonate Platform (Mamužić, 1973). The basement of the island is made of Upper Cretaceous limestones (Fig. 3 & 4). On the northern coast, Eocene limestones can be found (Mamužić, 1973). The bedrock is covered by up to 90 metres of Quaternary sediments, recently described by Cremaschi (1990), Bognar, Schweitzer & Szöőr (2003), Mikulčić Pavlaković et al. (2011) and Wacha et al. (2011). Pliocene and Pleistocene sediments are usually transgressive on the Jurassic and Cretaceous carbonates of the Istrian platform, and on Neogene or Paleogene deposits in the Po basin as seen in cores from the North Adriatic Sea (Kalac, et al., 1995). The Quaternary deposits on Susak are made of loess, loess derivatives and sand, and are intercalated by numerous paleosols and at least three tephra layers (Fig. 5).

Wacha et al. (2011) and Mikulčić Pavlaković et al. (2011) described altogether four smaller sections from the Eastern part of the island in more detail (Fig. 3). In the bay of Bok (Fig. 3) a red paleosol, overlain by a second red paleo-sol, covers the carbonate basement (Fig. 4). The thickness of these red paleosols is up to 100 cm but changes laterally. On some locations on the island only one red paleosol is exposed. The paleosols are separated with septarian carbonate concretions, up to 20 cm in diameter. Sandy loess covers the red paleosols and is in its lower part lithified forming a sandstone bench. In the upper part of the sandy loess horizon vertical carbonate concretions up to 10 cm long are found. Secondary carbonates are described in more detail by Bognar & Zámbó (1992) and Mikulčić Pavlaković et al. (2011) and indicate strong water percolation from the upper part of the section. The lower part of

E&G / Vol. 60 / No. 1 / 2011 / 153–169 / DOI 10.3285/eg.60.1.11

the loess-paleosol sequence on Susak is dominated by three about 1 metre thick paleosols, two of them brown and one orange-brown in colour. In the upper part of the loess sequence numerous thin brown paleosols are exposed, some of them containing dispersed charcoal and charcoal pieces (Fig. 6). The charcoal pieces found in two horizons were investigated by Bognar, Schweitzer & Szöőr (2003). They concluded that these remains are the results of forest fires, caused by self-inflammation or human activity and determined the Pinus sylvestris group of tree species from the charcoal. In the middle part of the loess-paleosol record homogenous and laminated sand can be found, in a form of a few centimetres thick layers and dune sand. The sand indicates stronger wind activity, a near-distance transport and a very likely local source of the material. The transition from sand into loess is mostly gradual. The general trend of loess coarsening upwards was observed by Mikulčić Pavlaković et al. (2011) and is supported by the results of grain-size analysis from an ongoing study (Wacha et al., in preparation). Three tephras were detected intercalating the loess of Susak; two in a form of continuous layers (TF1 and TF3) and one as accumulations (pockets) in a thin brown paleosol (TF2) (Fig. 5). The sedimentological, geochemical and mineralogical properties of loess, sand, paleosols and the tephras are presented in more detail by Mikulčić Pavlaković et al. (2011). In Fig. 7 all the investigated and sampled sections are presented along with the indicated sample positions and IRSL and radiocarbon ages.

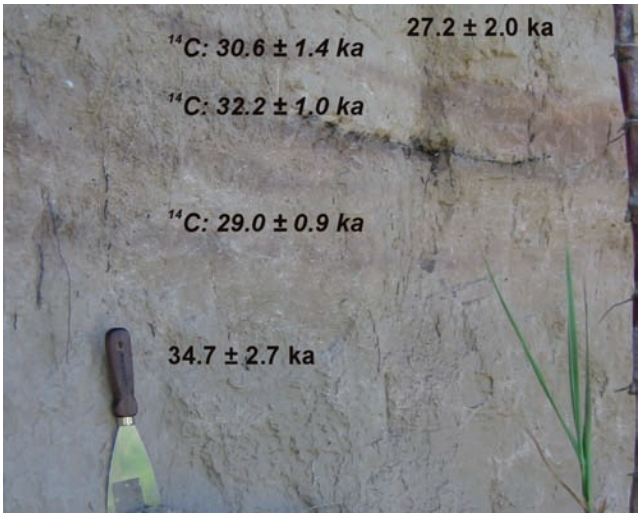

Fig. 6: A detail from the upper part of the Sand Pit section showing the weakly developed brown paleosols with dispersed charcoal remains and the IRSL and radiocarbon dating results.

Abb. 6: Detailansicht der schwach entwickelten braunen Paläoböden (OIS 3) mit zahlreichen Holzkohleresten aus dem Sand Pit-Aufschluss sowie den IRSL- und ^{14}C-Datierungsergebnissen.

3 Dating methods

3.1 Luminescence Dating

Loess has proved to be excellent material for luminescence dating (Frechen, Horváth & Gábris, 1997; Lu, Wang & Wintle, 2007; Roberts et al., 2003; Roberts, 2008; Novothny, Horváth & Frechen, 2002; Novothny et al., 2009, 2010; Schmidt et al., 2010) because it fulfils the basic dating assumption which is the complete bleaching of the latent luminescence signal in the mineral grains (quartz and feldspar) prior to deposition. Aeolian transportation of dust is a good mechanism for the fulfilment of such an assumption because during transport the particles are exposed to sunlight which releases most of the trapped charges in the crystal lattice of the minerals and resets the dosimeter to zero. After the deposition and after the material had been buried, the minerals are again exposed to the natural radioactivity of the surrounding sediment. This ionizing radiation moves the charges from their original position into charge traps caused by impurities or crystal lattice defects, from where they can only be released by additional energy. Releasing these electrons from the traps and their recombination with the positive charges in the crystal lattice results in the emission of light (luminescence), and can be measured by a photomultiplier in the laboratory. With time the amount of such dislocated charge grows, meaning that the luminescence signal is proportional to the depositional age of the sediment. The intensity of the luminescence signal increases with the deposition age of the sediment. The equivalent dose (D_e) is a measure of the past radiation and, if divided by the dose rate, gives the time elapsed since the last exposure of the sediment to sunlight, i. e. the deposition. The principles of luminescence dating are given in detail by Aitken (1985, 1998), Wintle (1997), Bøtter-Jensen, McKeever & Wintle (2003) and Preusser et al. (2008, 2009) and a more recent review about luminescence dating of loess is presented by Roberts (2008).

Twenty-one samples were collected in 2008 using light-proof plastic tubes, by pushing or hammering into a previously cleaned loess wall. Additional material was taken for dose rate determination by gamma spectrometry. In this study we applied the same sample preparation procedure for the extraction of the polymineral fine-grained material, as described in Wacha et al. (2011).

The same protocols and measurement procedures were used as presented in Wacha et al. (2011), because they have proved to be satisfactory. All measurements were performed using two automated Risø TL/OSL-DA15 readers at the Leibniz Institute for Applied Geophysics equipped with a ^{90}Sr/^{90}Y β-source, with dose rates of 0.101 Gy/s and 0.096 Gy/s, respectively, for fine grains mounted on aluminium discs.

Fading tests were performed on the same aliquots which were previously used for D_e measurements for all samples using the suggestion of Huntley & Lamothe (2001) and Auclair, Lamothe & Huot (2003). The same measuring conditions were used as for the D_e evaluation. The mean of the six aliquots was used for fading corrections and their standard errors. The fading rates (g-values) were calculated according to Huntley & Lamothe (2001) using the same integration limits as for the D_e calculation. The g-values were used for age corrections.

The dose rates of the sediment were measured by gamma spectrometry with a HPGe (High-Purity Germanium) N-type coaxial detector in the laboratory at the Leibniz Institute for Applied Geophysics. 700 g of dried and homogenized material was used for the measurements. Each sample was placed into a Marinelli-beaker and cap sealed to avoid the loss of ^{222}Rn in the ^{238}U decay chain and stored for a minimum of four weeks in order to re-establish the radioactive

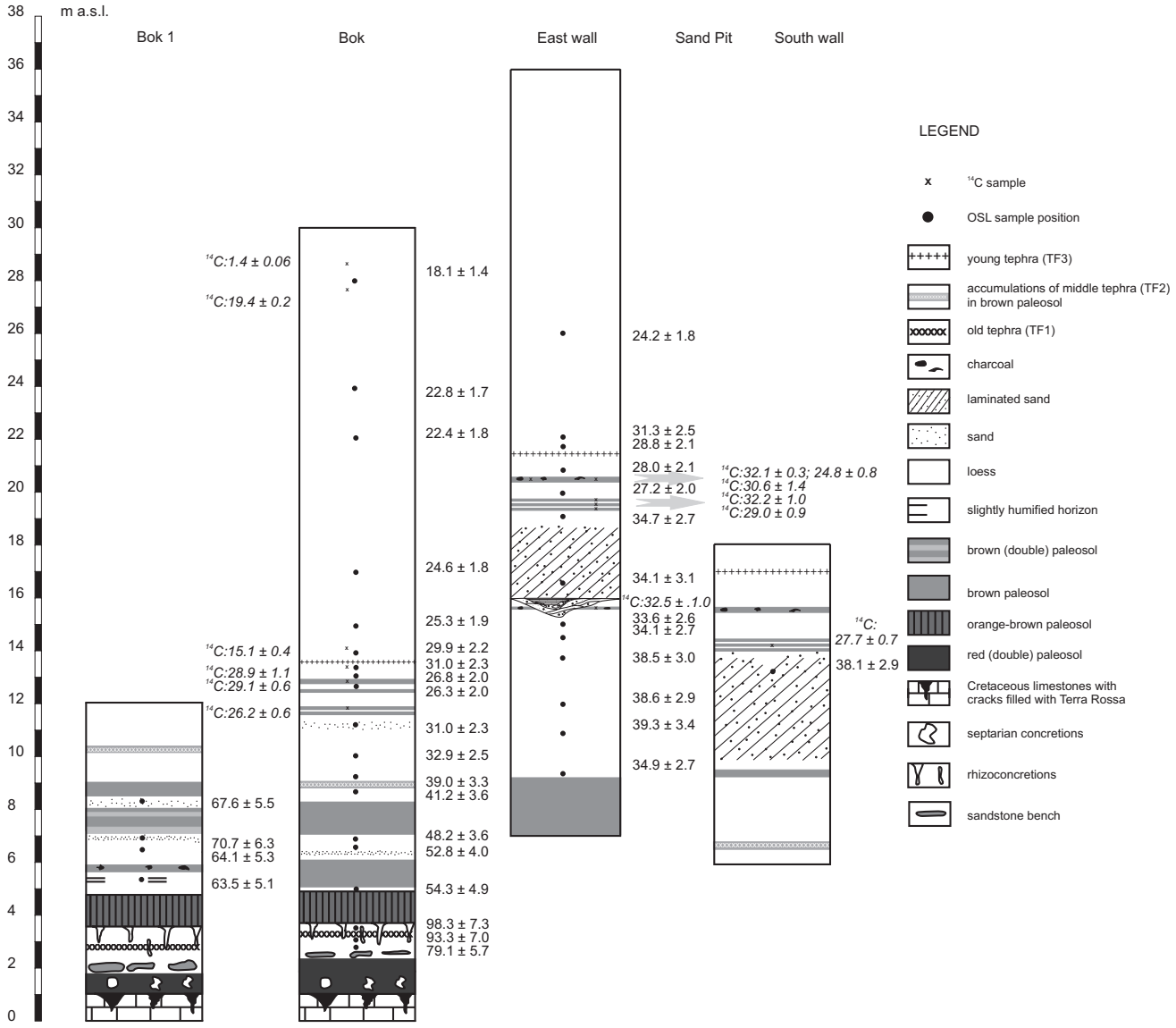

Fig. 7: The investigated loess-paleosol sections on Susak, with indicated IRSL and radiocarbon sampling positions and age estimates, and their correlation.

Abb. 7: Die untersuchten Löss-/Paläobodenaufschlüsse auf Susak mit IRSL- und ^{14}C-Probenpositionen und Altersergebnissen sowie die Korrelation der Horizonte.

equilibrium. The measuring time was one day. The measured activities of ^{40}K; and ^{210}Pb, ^{234}Th, ^{214}Bi and ^{214}Pb radionuclides from the ^{238}U; and ^{228}Ac, ^{208}Tl and ^{212}Pb radionuclides from the ^{232}Th decay chains were used for the calculation of potassium, uranium and thorium contents, respectively. The radioactive equilibrium was assumed for the decay chain, which is normally the case for loess; no radioactive disequilibrium was detected by gamma spectrometry. Cosmic dose rates were corrected for the altitude and sediment thickness (Prescott & Hutton, 1994). The alpha efficiency was estimated to a mean value of 0.08 ± 0.02 for polymineral IRSL (Rees-Jones, 1995). The water content was assumed to be from 15 ± 5% to 20 ± 5%, depending on the depth (Pécsi, 1990). For the calculation of the total dose rate the conversion factors published by Adamiec & Aitken (1998) were used. A systematic error of 2% is included for the gamma spectrometry. An error of 10% is estimated for the cosmic dose. The uranium, thorium and potassium contents, as well as the total dose rates, the cosmic dose rates, the g-values, the uncorrected and corrected ages are given in Table 1.

3.2 Radiocarbon dating

In this study seven new radiocarbon ages are presented, six from the Bok section and one from the Sand Pit section. Among them four samples were molluscs (Hv 25895–25898) and three were charcoal remains (Hv 25899–25901). The specific activity of ^{14}C was measured radiometrically by proportional counters (Geyh, 1990, 2005) at the Leibniz Institute for Applied Geophysics (LIAG). The radiocarbon ages were converted into calibrated calendar ages using the radiocarbon calibration curve based on coral samples and program after Fairbanks et al. (2005). The sample positions are shown in Fig. 7 and the calibrated and uncalibrated ages are given in Table 2. The radiocarbon ages presented in Wacha et al. (2011) are shown as well.

4 Dating results

Altogether 37 luminescence and 13 radiocarbon samples were measured from the loess sequence on Susak to set up

E&G / Vol. 60 / No. 1 / 2011 / 153–169 / DOI 10.3285/eg.60.1.11 / © Authors / Creative Commons Attribution License

a chronological framework for the very detailed sediment archive. Results from the dosimetry, the equivalent doses, g-values, the uncorrected and corrected age estimates are given in Table 1 and the dating results are given in Fig. 7. The uncalibrated and calibrated radiocarbon ages are given in Table 2.

The uranium, thorium and potassium contents range from 2.17 to 4.74 ppm, 7.63 to 15.67 ppm and 1.14 to 1.91%, respectively. The dose rates of the sediment for the fine-grained material range from 2.46 to 4.40 mGy/a, with a mean value of 3.53 ± 0.20 mGy/a which is typical for European loess (see Frechen, Horváth & Gábris, 1997; Galović et al, 2009; Novothny et al. 2009; Schmidt et al., 2010).

The D_e values from fine-grain feldspar are between 49.1 ± 2.5 Gy to 276.9 ± 14.0 Gy. For the samples collected at the Bok section, the D_e values show a systematic increase with depth, with a few exceptions and inversions. None of the dose response curves indicated luminescence signal saturation. The calculated age estimates are in good stratigraphic order. For the Sand Pit section the D_e values and the calculated ages are quite uniform with a slight increase of age with depth. Fading corrections were performed for all samples indicating only low anomalous fading rates. The calculated g-values range from 1.3 to 2.7%/decade which is very low compared to other locations (e.g. Serbian loess (Schmidt et al., 2010) or Hungarian loess (Novothny et al., 2010)). Fading corrections were done, and the uncorrected and corrected ages, as well as the g-values, are presented in Table 1.

At the Bok section an almost continuous increase of age with depth can be seen (Fig. 8). The lowermost loess with the abundant carbonate accumulations and intercalated by the oldest tephra (TF1; Fig 5a & 7) yielded age estimates ranging from 98.3 ± 7.3 ka to 79.1 ± 5.7 ka. According to the IRSL dating results from the loess underlying and covering the oldest tephra (TF1), the age of the tephra is between 98.3 ± 7.3 ka and 93.3 ± 7.0 ka. The sample collected from the same loess horizon, but a few metres away from the investigated section gave an age of 79.1 ± 5.7 ka. This horizon is covered by an orange-brown paleosol. The latter soil formation took place prior to 54.3 ± 4.9 ka, which is the IRSL age of the loess covering the orange-brown paleosol. The next 4 metres of the sequence are made of three brown paleosols, one of them containing the middle tephra (TF2; Fig. 5b & 7). In the middle part of this interval a sand layer is present, giving an IRSL age of 52.8 ± 4.0 ka. The age of the thin brown paleosol with the tephra patches (TF2) is between 41.2 ± 3.6 ka and 39.0 ± 3.3 ka (Fig 5b). Above this paleosol about 20 metres of loess is exposed. The IRSL ages from the loess range from 39.0 ± 3.3 ka to 18.1 ± 1.4 ka, for the loess immediately covering the paleosol with the tephra (TF2), and the stratigraphically youngest loess collected at this section, respectively. In this interval, four thin brown paleosols, some of them with charcoal remains, and another tephra layer (TF3) (Fig. 5c) are intercalated in the loess. IRSL age estimates from the loess below and above this thin tephra are between 31.0 ± 2.3 ka and 29.9 ± 2.2 ka. The radiocarbon ages of charcoal remains collected from the thin brown paleosols gave calibrated ages of 26.2 ± 0.6 ka and 29.1 ± 0.6 ka and are in excellent agreement with the IRSL ages. The radiocarbon age of molluscs collected from below TF3 is in agreement with IRSL ages and calibrated radiocarbon ages from charcoal, whereas the mollusc sample taken from the top of TF3 shows an age of 15.1 ± 0.4 ka, which is very likely underestimated for this part of the sequence, probably due to contamination with younger mollusc species. Two mollusc samples were collected in the uppermost part of the section, from the youngermost exposed loess. The radiocarbon age of 19.4 ± 0.2 ka is in excellent agreement with the uppermost collected IRSL sample. The radiocarbon age of 1.4 ± 0.06 ka from molluscs collected on top of the section correlates to modern species which were very probably washed out from the modern soil.

Mikulčić Pavlaković et al. (2011) described a second section in the bay of Bok. At the Bok1 section, four luminescence samples were collected from the loess covering the orange brown paleosol (Fig 7). The IRSL age estimates range from 70.7 ± 6.3 ka to 63.5 ± 5.1 ka. This interval of the section – loess intercalated with brown paleosol – gave a slightly higher ages than the stratigraphical equivalent at the Bok section. These horizons fill the time gap between the orange-brown paleosol and the brown paleosol at the Bok section and can hence be correlated with each other and interpolated. The differences between these two nearby sections could be a result of a different paleorelief evolution and possible erosion.

The Sand Pit section starts with a thick brown paleosol which is covered by about 8 metres of loess. This loess gave age estimates ranging from 39.3 ± 3.4 ka to 33.6 ± 2.6 ka. The thin brown soil on the top of this loess horizon containing charcoal yielded a calibrated radiocarbon age of 32.5 ± 1.0 ka and is in excellent agreement with the IRSL ages. Loess is covered by a few meters thick laminated sand horizon which gave an IRSL age estimate of 34.1 ± 3.1 ka. Within error limits, the age is in agreement with the calibrated radiocarbon age. Another sample from this laminated sand horizon was taken from the South wall of the investigated section and yielded an age of 38.1 ± 2.9 ka. The charcoal collected from the thin brown paleosols, yielded radiocarbon ages ranging from 32.2 ± 1.0 ka to 24.8 ± 0.8 ka (Fig. 6 & 7). A deposition of the laminated sand during a very short time period is very likely. The cross-laminated sand is of aeolian origin (Mikulčić Pavlaković et al., 2011) and probably represents a dune (Cremaschi, 1990). The upper part of the Sand Pit section consists of loess which is in its lower part intercalated by the youngest tephra (TF3; Fig. 5c & 7). IRSL age estimates of the loess from below and above the tephra gave 28.0 ± 2.1 ka and 28.8 ± 2.1 ka, respectively, and within error limits correlate to the IRSL ages from samples taken from the stratigraphically same position at the Bok section. The uppermost sample collected from the Sand Pit section gave an IRSL age of 24.2 ± 1.8 ka. About ten metres of loess is still covering the investigated section, but unfortunately this part of the section was not reachable for sampling during our fieldwork. In Fig. 7, the IRSL and the radiocarbon dating results are presented. They show an excellent correlation for both sections.

5 Discussion

Wacha et al. (2011) presented the first infrared stimulated luminescence (IRSL) dating results for the loess from Susak including thirteen samples. In their study a part of the loess-paleosol sequence was investigated only from the easternmost part of the island. The present study gives an improved,

Tab. 1: Sample list with depth below surface, results from the dosimetry, the SAR IRSL measurements, g-values, the uncorrected and corrected ages for fine-grained feldspar. The dose rate is the sum of the dose rates of the alpha, beta, gamma and cosmic radiation.

Tab. 1: Probenliste mit Tiefe unter Geländeoberkante, Dosimetrie-Daten, SAR-IRSL-Messungen, g-values, unkorrigierten und korrigierten Altern für die Feinkornextrakte. Die Dosisleistung ist die Summe aus Alpha-, Beta- und Gamma- sowie kosmischer Strahlung.

	Sample name	Sample ID	Depth (m)	Uranium (ppm)			Thorium (ppm)			Potassium (%)			Cosmic dose (mGy/a)			Dose rate (mGy/a)			De (Gy)			g-value (%/decade)			Uncorrected age (ka)			Corrected age (ka) [1*]		
Bok Section	Sus08-16	1753	2.00	3.30	±	0.01	9.87	±	0.03	1.23	±	0.01	0.150	±	0.015	3.16	±	0.19	49.1	±	2.5	1.7	±	0.2	15.5	±	1.2	18.1	±	1.4
	Sus13	1438	8.00	3.84	±	0.05	11.90	±	0.13	1.28	±	0.02	0.062	±	0.006	3.48	±	0.20	65.4	±	3.3	2.1	±	0.1	18.8	±	1.5	22.8	±	1.7
	Sus08-15	1752	8.50	4.10	±	0.02	13.89	±	0.04	1.61	±	0.01	0.062	±	0.006	4.03	±	0.22	74.5	±	3.7	2.1	±	0.3	18.5	±	1.4	22.4	±	1.8
	Sus08-14	1751	13.00	3.84	±	0.02	12.02	±	0.06	1.51	±	0.01	0.036	±	0.004	3.66	±	0.21	77.0	±	3.9	1.7	±	0.03	21.0	±	1.6	24.6	±	1.8
	Sus08-13	1750	15.00	3.50	±	0.01	9.72	±	0.03	1.31	±	0.01	0.030	±	0.003	3.16	±	0.19	67.8	±	3.4	1.8	±	0.1	21.4	±	1.7	25.3	±	1.9
	Sus12	1437	15.80	4.52	±	0.05	14.48	±	0.12	1.70	±	0.02	0.028	±	0.003	4.26	±	0.24	106.1	±	5.4	2.0	±	0.1	24.9	±	1.9	29.9	±	2.2
	Sus11	1436	16.30	4.15	±	0.05	13.26	±	0.13	1.68	±	0.03	0.027	±	0.003	4.01	±	0.22	104.6	±	5.3	1.9	±	0.1	26.1	±	2.0	31.0	±	2.3
	Sus08-12	1749	17.00	3.99	±	0.02	12.69	±	0.04	1.67	±	0.01	0.026	±	0.003	3.90	±	0.22	88.6	±	4.4	1.8	±	0.03	22.7	±	1.7	26.8	±	2.0
	Sus08-11	1748	17.60	3.81	±	0.03	12.12	±	0.06	1.62	±	0.01	0.025	±	0.002	3.74	±	0.21	84.2	±	4.2	1.7	±	0.1	22.5	±	1.7	26.3	±	2.0
	Sus08-10	1747	18.80	2.94	±	0.02	10.57	±	0.06	1.31	±	0.01	0.023	±	0.002	3.06	±	0.17	79.6	±	4.0	1.9	±	0.1	26.0	±	2.0	31.0	±	2.3
	Sus08-9	1746	19.80	4.11	±	0.02	13.27	±	0.04	1.60	±	0.01	0.022	±	0.002	3.92	±	0.22	110.3	±	5.6	1.7	±	0.1	28.1	±	2.1	32.9	±	2.5
	Sus10	1435	20.80	4.19	±	0.08	13.33	±	0.14	1.76	±	0.03	0.021	±	0.002	4.09	±	0.23	128.8	±	6.5	2.3	±	0.4	31.5	±	2.4	39.0	±	3.3
	Sus9	1434	21.30	3.50	±	0.05	10.04	±	0.12	1.40	±	0.02	0.021	±	0.002	3.26	±	0.19	108.4	±	5.5	2.3	±	0.4	33.2	±	2.6	41.2	±	3.6
	Sus08-8	1745	23.00	3.48	±	0.01	11.06	±	0.03	1.43	±	0.01	0.019	±	0.002	3.20	±	0.18	130.6	±	6.6	1.8	±	0.1	40.8	±	3.1	48.2	±	3.6
	Sus08-7	1744	23.60	2.71	±	0.01	9.24	±	0.03	1.38	±	0.01	0.019	±	0.002	2.77	±	0.16	124.8	±	6.4	1.7	±	0.1	45.0	±	3.5	52.8	±	4.0
	Sus08-6	1743	25.00	2.58	±	0.02	8.38	±	0.05	1.14	±	0.01	0.018	±	0.002	2.46	±	0.15	112.8	±	5.7	1.8	±	0.02	45.9	±	3.6	54.3	±	4.9
	Sus08-18	1755	26.70	3.27	±	0.01	11.28	±	0.03	1.46	±	0.01	0.018	±	0.002	3.18	±	0.18	261.2	±	13.1	1.9	±	0.1	82.1	±	6.2	98.3	±	7.3
	Sus08-17	1754	27.00	3.38	±	0.02	11.33	±	0.06	1.44	±	0.01	0.018	±	0.002	3.20	±	0.18	249.7	±	12.6	1.9	±	0.1	77.9	±	5.9	93.3	±	7.0
	Sus08-5	1742	28.00	4.09	±	0.03	15.67	±	0.08	1.91	±	0.01	0.018	±	0.002	4.18	±	0.22	276.9	±	14.0	1.9	±	0.02	66.2	±	4.8	79.1	±	5.7
Bok1	Sus08-4	1741	21.90	2.17	±	0.01	7.63	±	0.04	1.36	±	0.01	0.020	±	0.002	2.58	±	0.15	140.2	±	7.8	2.3	±	0.2	54.3	±	4.4	67.6	±	5.5
	Sus08-3	1740	23.00	3.48	±	0.03	12.02	±	0.06	1.44	±	0.01	0.019	±	0.002	3.47	±	0.19	193.7	±	11.1	2.5	±	0.4	55.8	±	4.5	70.7	±	6.3
	Sus08-2	1739	23.50	3.55	±	0.03	11.92	±	0.06	1.43	±	0.01	0.019	±	0.002	3.47	±	0.20	177.3	±	10.0	2.4	±	0.2	51.0	±	4.1	64.1	±	5.3
	Sus08-1	1738	24.70	3.83	±	0.02	12.80	±	0.06	1.50	±	0.01	0.019	±	0.002	3.70	±	0.21	181.8	±	10.1	2.7	±	0.2	49.1	±	3.9	63.5	±	5.1

Sand Pit section	Sus8	1433	10.00	4.16 ± 0.05	13.32 ± 0.14	1.60 ± 0.03	0.050 ± 0.005	3.97 ± 0.22	80.0 ± 4.0	2.0 ± 0.1	20.1 ± 1.5	24.2 ± 1.8
	Sus08-24	1761	14.00	3.57 ± 0.02	11.17 ± 0.04	1.55 ± 0.01	0.033 ± 0.003	3.53 ± 0.20	106.2 ± 7.7	2.0 ± 0.2	26.1 ± 2.0	31.3 ± 2.5
	Sus5	1430	14.50	4.74 ± 0.05	14.99 ± 0.14	1.73 ± 0.03	0.032 ± 0.003	4.40 ± 0.24	105.7 ± 5.3	2.0 ± 0.1	24.0 ± 1.8	28.8 ± 2.1
	Sus4	1429	15.30	4.40 ± 0.05	13.44 ± 0.10	1.71 ± 0.02	0.030 ± 0.003	4.14 ± 0.23	101.1 ± 5.1	1.5 ± 0.2	24.5 ± 1.8	28.0 ± 2.1
	Sus3	1428	16.20	4.30 ± 0.05	12.81 ± 0.12	1.68 ± 0.03	0.028 ± 0.003	4.02 ± 0.23	94.8 ± 4.8	1.6 ± 0.1	23.6 ± 1.8	27.2 ± 2.0
	Sus2	1427	17.00	2.32 ± 0.04	7.77 ± 0.11	1.31 ± 0.02	0.027 ± 0.003	2.61 ± 0.16	75.9 ± 3.8	1.9 ± 0.1	29.1 ± 2.3	34.7 ± 2.7
	Sus1	1426	18.00	2.31 ± 0.04	8.12 ± 0.09	1.15 ± 0.02	0.024 ± 0.002	2.50 ± 0.15	79.0 ± 4.0	2.0 ± 0.1	31.7 ± 2.5	38.1 ± 2.9
	Sus7	1432	19.50	3.57 ± 0.04	11.03 ± 0.11	1.37 ± 0.02	0.023 ± 0.002	3.35 ± 0.19	91.4 ± 4.6	2.4 ± 0.5	27.3 ± 2.1	34.1 ± 3.1
	Sus6	1431	20.70	3.71 ± 0.05	11.09 ± 0.12	1.40 ± 0.03	0.022 ± 0.002	3.42 ± 0.20	96.6 ± 4.9	1.9 ± 0.1	28.2 ± 2.2	33.6 ± 2.6
	Sus08-23	1760	20.80	3.50 ± 0.02	10.85 ± 0.04	1.50 ± 0.01	0.021 ± 0.002	3.42 ± 0.20	93.2 ± 4.9	2.4 ± 0.2	27.2 ± 2.1	34.1 ± 2.7
	Sus08-22	1759	22.20	3.56 ± 0.02	11.86 ± 0.04	1.51 ± 0.01	0.020 ± 0.002	3.54 ± 0.20	105.7 ± 5.6	2.7 ± 0.2	29.8 ± 2.3	38.5 ± 3.0
	Sus08-21	1758	23.80	4.18 ± 0.02	13.86 ± 0.04	1.64 ± 0.01	0.019 ± 0.002	4.03 ± 0.22	126.9 ± 6.7	2.2 ± 0.1	31.5 ± 2.4	38.6 ± 2.9
	Sus08-20	1757	25.40	4.11 ± 0.05	13.27 ± 0.12	1.57 ± 0.03	0.018 ± 0.002	3.90 ± 0.22	122.6 ± 7.4	2.4 ± 0.3	31.5 ± 2.6	39.3 ± 3.4
	Sus08-19	1756	26.80	3.83 ± 0.01	12.05 ± 0.03	1.74 ± 0.01	0.018 ± 0.002	3.65 ± 0.20	113.2 ± 5.7	1.3 ± 0.3	31.0 ± 2.3	34.9 ± 2.7

**After calibration of the Risø Reader for fine-grained material mounted on Al discs, the data from samples presented in Wacha et al. (2011) were recalculated because the new dose rates of the reader were lower than previously used. In the table the complete Susak data set is presented.*

precise and very detailed geochronological framework of the investigated loess-paleosol sequence which resulted from denser sampling.

Wacha et al. (2011) used the single aliquot regenerative-dose (SAR) protocol on polymineral fine-grained material separated from loess for the determination of the equivalent doses (D_e). Furthermore, fading tests and fading corrections were carried out and a few samples were additionally measured using the older multiple aliquot additive-dose (MAAD) protocol for an easier correlation with previously published data, like recently published in Galović et al. (2009). The results showed that the loess-paleosol record on Susak correlates to the Oxygen Isotope Stage (OIS) 3 with the fading corrected data ranging from 50.3 ± 3.5 ka to 27.5 ± 3.5 ka. The ages calculated after the MAAD protocols are between 38.0 ± 2.2 ka and 15.1 ± 1.1 ka and hence underestimating the results of the SAR measurements and the true deposition age of the deposits. Underestimation of these ages is expected due to the anomalous fading of feldspar infrared stimulated (IRSL) signals (Wintle, 1973; Spooner, 1994). Nevertheless, both protocols gave data which led to the same conclusion, that the loess-paleosol record on Susak is an amazing and very detailed OIS3 record. Mikulčić Pavlaković et al. (2011) presented four more IRSL ages from a further nearby section in the bay of Bok on Susak. This IRSL dating study used the same methodological approach as discussed in Wacha et al. (2011) which was proved to be successful. The IRSL ages range from 90.0 ± 6.8 ka to 80.8 ± 5.0 ka. The results presented in these previous publications do not cover the complete loess sequence but concentrate only on the middle part. Therefore, additional samples were collected with the aim to fill previous sampling gaps and to extend the numerical framework to the oldest and youngest deposits and so get a very detailed geochronological record of the last interglacial/glacial cycle.

The stratigraphically oldest soil found on the island is the fossil terra rossa, named that way by Bognar, Schweitzer & Szöőr (2003) (FTR according to Mikulčić Pavlaković et al., 2011), seen in the cracks of the limestone basement. Bognar, Schweitzer & Szöőr (2003) assumed the age of the fossil terra rossa to be 3 to 4 million years BP, but no evidence was provided for such statement. It is still not known, i.e. there are still no exact data about the age of the thick red paleosols which cover the carbonate basement of the island. Bognar, Schweitzer & Szöőr (2003) suggested that the red paleosol presents the lower or the lowermost Pleistocene. Paleomagnetic measurements carried out by Bognar, Schweitzer & Szöőr (2003) showed negative inclination in the red paleosol, so they correlated the apparent polarity change to the Brunhes-Matuyama boundary (0.78 Ma; Spell & McDougall, 1992; OIS19). They also correlated the red paleosol with the Paks Double (PD) type paleosol from the Hungarian loess stratigraphy. The PD type paleosol belongs to the Hungarian "old loess series",

*Tab. 2: Uncalibrated and calibrated radiocarbon dating results. The results were calibrated using the Fairbanks et al (2005) calibration curve spanning from 0 to 50,000 years BP and transferred in ka B. P. in order to make the radiocarbon results better comparable with luminescence ages. *radiocarbon dating results presented in Wacha et al. (2011). +Radiocarbon ages are by definition "Age before 1950".*

*Tab. 2: Unkalibrierte und kalibrierte Radiokarbon-Datierungsergebnisse. Die Daten wurden mittels der Kalibrationskurve nach Fairbanks et al. (2005), welche von 0 bis 50.000 Jahre reicht, kalibriert und in ka B.P. umgerechnet, um eine bessere Vergleichbarkeit der Radiokarbonalter mit dem Lumineszenz-datierungen zu gewährleisten. +Radiokarbonalter sind per Definition „vor 1950". * Radiokarbonalter aus Wacha et al. (2011).*

Sample name	Radiocarbon age ka B.P.+			Calendar age cal. B.P.			Calendar age ka cal. B.P.			Material type
Hv 25696*	24215	±	750	29023	±	923	29.0	±	0.9	charcoal
Hv 25697*	26890	±	950	32176	±	1042	32.2	±	1.0	charcoal
Hv 25698*	26810	±	200	32103	±	261	32.1	±	0.3	charcoal
Hv 25699*	23040	±	600	27650	±	696	27.7	±	0.7	charcoal
Hv 25700*	27150	±	910	32458	±	986	32.5	±	1.0	charcoal
Hv 25701*	25515	±	1170	30602	±	1390	30.6	±	1.4	charcoal
Hv 25895	1510	±	60	1391	±	60	1.4	±	0.1	molluscs
Hv 25896	16240	±	200	19365	±	202	19.4	±	0.2	molluscs
Hv 25897	12950	±	290	15073	±	371	15.1	±	0.4	molluscs
Hv 25898	24095	±	900	28888	±	1092	28.9	±	1.1	molluscs
Hv 25899	24300	±	455	29097	±	571	29.1	±	0.6	charcoal
Hv 25900	21765	±	420	26156	±	546	26.2	±	0.6	charcoal
Hv 25901	20755	±	640	24814	±	836	24.8	±	0.8	charcoal

also called Paks series, corresponding to OIS 9–24 (Pécsi, 1993). In loess from below this PD paleosol in the type locality at the Paks section the Brunhes-Matuyama boundary was identified (Pécsi, 1993). There is no evidence for such pedostratigraphical correlation of paleosols from Susak with paleosols from Hungary key loess sections and hence this approach is questionable. Durn, Ottner & Slovenec (1999), Durn (2003) and Durn et al. (2007) investigated terra rossa and loess from Istria (Savudrija) and based on similarities with loess deposits on Susak described by Cremaschi (1990) tentatively proposed an Eemian age of the red paleosol below the loess complex in Savudrija, but without any dating results. They also showed the importance of Late Pleistocene loess as parent material of these paleosols in Istria. Mikulčić Pavlaković et al. (2011) concluded that the source material of the thick red paleosol which covers the carbonate and can be seen in the basement of the loess sequence in the bay of Bok on Susak is of a predominantly aeolian origin (loess) with a minor influence of material remained after limestone karstification and that they are similar to Istrian terra rossa. Loess covering the red paleosol on Susak showed age estimates ranging from 98.3 ± 7.3 ka to 79.1 ± 5.7 ka and so numerically correlates to OIS5c–a and 4, respectively. Based on these dating results, and the assumed aeolian origin of the red paleosols covering the carbonate basement on Susak and similar red paleosols below loess from Istria, we can conclude that soil formation on Susak took place during the last interglacial optimum or any older interglacial period and that the oldest loess from Susak deposited prior to OIS5e, probably in OIS6 or any other glaciation predating the Eemian. The OIS5 interglacial was marked by three distinct high sea level stands (Surić & Juračić, 2010). During OIS5e the sea level stand was the highest, up to a few meters higher than today (Lambeck & Chappell, 2001). The OIS5a is characterized by two sea level high stands, around 84 ka and 77 ka BP, with sea level above -14 m, and low sea-stand in between, at around 80 ka BP (Surić & Juračić, 2010). The sea level of the Adriatic Sea was about 100 metres lower than today (Cremaschi, 1990; Amorosi, et al. 1999; Lambeck et al., 2004) during a part of the Upper Pleistocene making the North Adriatic a vast basin exposed to various sedimentary processes as well as to aeolian activity during the glacials which resulted in loess deposition.

Red paleosols are often reported to underlie loess in the Pannonian basin in Hungary (Kovács, 2008) and in China (e.g. Bronger & Heinkele, 1989) and are found on different rock type basements, representing the beginning of loess deposition. The origin of such paleosols is still under discussion (e.g. Kovács, 2008) but the aeolian origin is probable (Yang & Ding, 2004). The age of these paleosols very likely belongs to the Pliocene (Bronger & Heinkele, 1989; Ding et al., 1999; Kovács, 2008). Such red paleosols are the result of specific climatic conditions and should be correlated only in that context. Correlating these paleosols based only on their physical properties, without any dating results, can lead to wrong geochronological conclusions.

The age of the tephra (TF1) found in loess covering the red paleosol is between 98.3 ± 7.3 ka and 93.3 ± 7.0 ka (Fig. 5a). Based on these ages, the mineral and geochemical characteristics (Mikulčić Pavlaković et al., 2011), the tephra could be related to the Middle and South Italian volcanic provinces.

The oldest loess is covered by an orange-brown paleosol up to 150 cm thick. The pedogenesis of this paleosol took place after 93.3 ± 7.0 ka (or 79.1 ± 5.7 ka, if the sample Sus08-5 is considered, which was not collected directly from the investigated outcrops but a few meters away) and before 54.3 ± 5.7 ka, which is the age estimate from the thin loess horizon covering the thick orange-brown paleosol in the Bok section. This orange-brown paleosol is widespread

E&G / Vol. 60 / No. 1 / 2011 / 153–169 / DOI 10.3285/eg.60.1.11

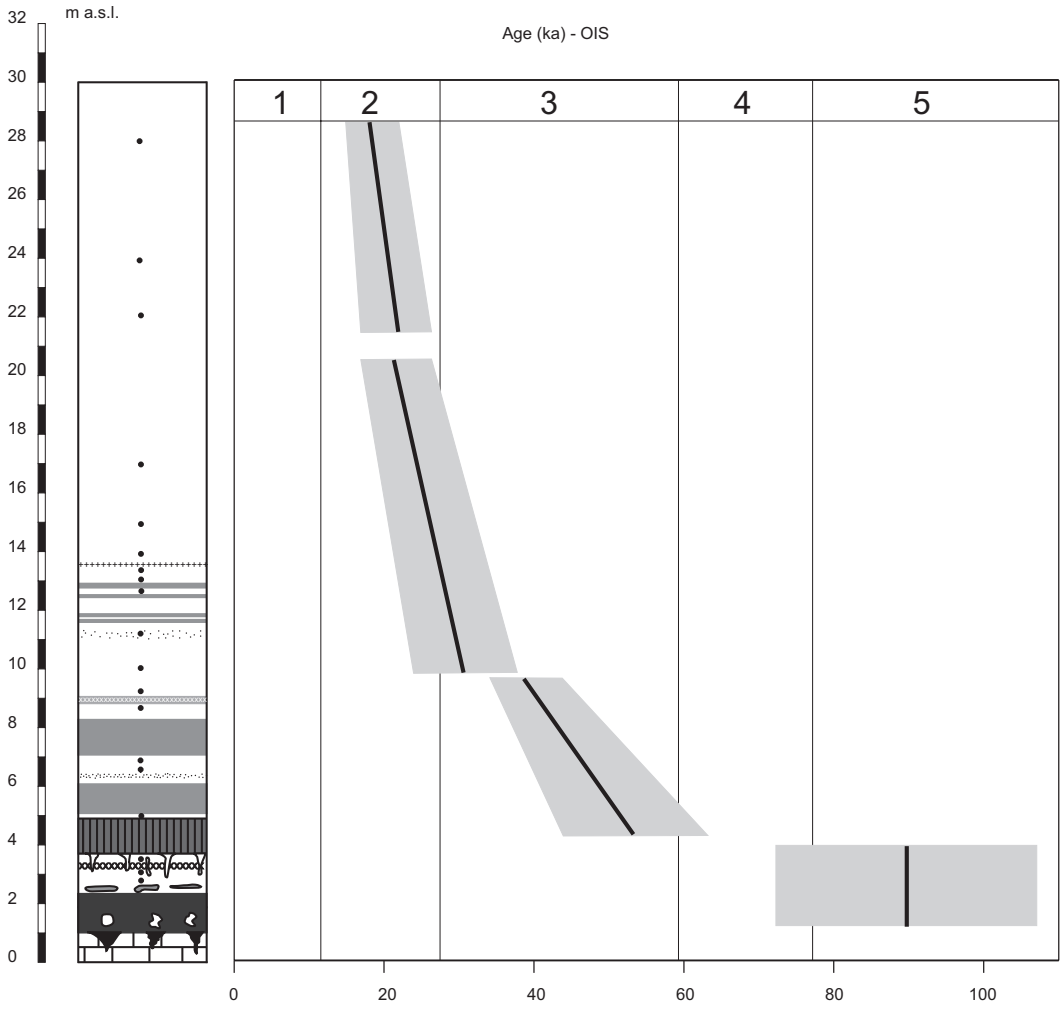

Fig. 8: The sketch of all IRSL dating results from the Bok section. A continuous increase with depth is evident, showing an increased accumulation of loess during the OIS3 and OIS2. Part of the OIS4 deposits are missing in this section but can be found at the Bok1 section (see legend in Fig. 7).

Abb. 8: IRSL-Datierungsergebnisse des Bok-Aufschlusses. Die IRSL-Alter sind stratigraphisch konsistent und nehmen mit der Tiefe zu. Die Ergebnisse zeigen eine verstärkte Staubakkumulation während des OIS3 und OIS2. Teile von OIS4 sind erodiert und fehlen in diesem Aufschluss, sind aber im Bok 1-Aufschluss vorhanden (Legende in Abb. 7).

over the island and with a more or less constant thickness. Bognar, Schweitzer & Szöőr (2003) correlated this orange-brown paleosol with the Mende Base (MB)-type paleosol from Hungarian stratigraphy. Wintle & Packman (1988) and Frechen, Horváth & Gábris (1997) proved that the age of the MB paleosol is significantly older than the last interglacial (OIS5e). At the Süttő section in Hungary, the OIS5 is represented by a MB-type paleosol (Novothny et al., 2009). The results from this study discarded such correlation completely. The orange-brown paleosol is covered by 4 to 5 metres thick loess. This loess is intercalated by brown paleosols and sand layers and a thin brown paleosol containing patches of the orange-yellow middle tephra (TF2). At the Bok section two, up to 100 cm thick, brown paleosols are developed while at the Bok 1 section the situation differs. There, alterations of loess and sand are intercalated by two brown paleosols, one of them containing charcoal pieces, and one double paleosol i.e. a brown paleosol directly overlain by another brown paleosol. This horizon gave IRSL age estimates ranging from 54.3 ± 4.9 ka, measured from loess collected between the orange-brown and the first brown paleosol at the Bok section, and 41.2 ± 3.6 ka, sample collected below the TF2 containing paleosol. At the Bok 1 section the IRSL age estimates showed slightly older ages ranging from 70.7 ± 6.3 ka to 63.5 ± 5.1 ka. Based on the IRSL results we can conclude that this sequence very likely correlates to OIS4. The differences between these two investigated sections are probably due to the differences in the paleorelief. It is very likely that a part of the record is missing at the Bok section. A layer of thin loess covering the orange-brown paleosol at the Bok section might be the evidence for the later statement.

The brown paleosol covering the thin loess horizon was correlated to the Basaharc Lower (BA)-type paleosol from the Hungarian loess stratigraphy by Bognar, Schweitzer & Szöőr (2003). When compared to the new IRSL dating results of this study and data presented by Frechen, Horváth & Gábris (1997), who showed that the BA paleosol formed during the antepenultimate interglacial, such a statement can be discarded.

Indent estimates of loess from below and above the paleosol containing the middle tephra (TF2) range from 41.2 ± 3.6 ka to 39.0 ± 3.3 ka (Fig 5b). This tephra layer was found on several locations on the island and hence is an excellent

marker horizon for better correlation. The tephra layer was investigated by Mikulčić Pavlaković et al. (2011) and could be correlated to the Campanian Ignimbrite eruption of the Phlegraean Fields, which was dated around 39 ka (De Vivo et al., 2001).

On top of the paleosol with TF2 patches about 20 metres of loess is exposed. In the lower part of this loess a sand layer and four thin brown paleosols are present. The IRSL ages are in stratigraphic order, as presented in Figs. 7 and 8, showing a continuous loess deposition during OIS3. Four radiocarbon samples were collected: two charcoal samples from the thin brown paleosols and two samples from loess molluscs. The radiocarbon ages are in agreement with the IRSL dating results. The youngest tephra (TF3) (Fig 5c), which is exposed in this part of the sequence, has IRSL age estimates ranging from 31.0 ± 2.3 ka to 29.9 ± 2.2 ka and could be related to the Middle and South Italian volcanic provinces based on the geochemical analysis, mineral composition and vitroclast morphology (Mikulčić Pavlaković et al., 2011). The youngest sample collected from the top of the section, at the highest accessible position, gave an IRSL age estimate of 18.1 ± 1.4 ka and represents the loess accumulated during a period of increased dust accumulation most likely during the last glacial maximum (OIS2). This IRSL age is in agreement with the radiocarbon dating results of molluscs collected from loess.

The steep loess wall of the Sand Pit sections shows similarities with the upper part of the Bok section. There, only loess and laminated sand are exposed correlating to OIS3. The contact with the carbonate basement is not exposed; the sequence starts with a thick brown paleosol which is older than 34.9 ± 2.7 ka and 39.3 ± 3.4 ka, which are IRSL age estimates of the loess covering the brown paleosol. This paleosol very likely correlates with the second brown paleosol (the upper one) from the Bok section. At the Sand Pit section the middle tephra (TF2) was previously found in the South Wall but was not exposed during our fieldwork. The main difference between the two investigated sections (Bok and Sand Pit) is the predominance of cross-laminated sand in the Sand Pit section which probably represents a dune. Such aeolian sands are often seen on the islands in the Adriatic Sea (Marković-Marjanović, 1976; Borović et al., 1977; Korolija et al., 1977; Bognar et al., 1992; Pavelić, Kovačić & Vlahović, 2006) but they have scarcely been investigated (Pavelić et al., submitted). The sand on Susak very likely came from a proximal source. An erosional channel which was seen in the Sand Pit section on the East Wall was a result of local, short and intensive water activity. Four brown paleosols containing charcoal remains, which can be seen in the lower part of the loess covering the dune sands, gave calibrated radiocarbon age estimates ranging from 32.2 ± 1.0 ka to 24.8 ± 0.8 ka and are in excellent agreement with IRSL dating results (Fig. 6); the loess below the first paleosol gave an IRSL age of 34.7 ± 2.7 ka and the loess above the fourth, the uppermost paleosol yielded an IRSL age of 28.0 ± 2.1 ka. The youngest tephra layer (TF3) is clearly visible above the uppermost paleosol. Its IRSL age estimates range from 28.8 ± 2.1 ka to 28.0 ± 2.1 ka and is in agreement with the IRSL ages from the samples collected at the Bok section. The uppermost collected loess gave an age estimate of 24.2 ± 1.8 ka and so correlates to OIS3. This sample location is covered by at least 10 metres of loess; this part of the sequence probably correlates to OIS2.

When comparing both major investigated sections, a strong similarity is evident. Minor differences are very likely due to the evolution and shape of the paleorelief. Such sediment succession is representative for the eastern part of the island and a similar situation was exposed on the southern part of the island. But still no outcrops are available on the northern and the western part, the part of the island which morphologically forms a plateau. It would be interesting to know the succession of the depo-sits in the thickest location and its relations to the carbo-nate basement. The question about the great thickness of the deposits and the sediment succession in the northern part of the island and its relation to the carbonate bedrock still remains open.

In northern Italy, the Val Sorda loess-paleosol sequence is located in the river Po basin. Along the Danube, the Zmajevac section in eastern Croatia, Stari Slankamen and Surduk sections in Serbia and the Süttő section in Hungary were chosen for correlation and comparison (Fig. 9). These sections were selected because of their detailed geochronological studies allowing a correlation with the last interglacial-glacial cycle. These two major loess areas differ in climatic conditions during periods of increased dust deposition in the Upper Pleistocene, hence providing different loessevolution. If we place Susak in a wider perspective and compare it with coeval loess-paleosol sequences from nearby regions, the most amazing thing is the great thickness of the deposits on such a small island in the Northern Adriatic Sea and the fact that such a sequence remained preserved. Loess has been found on other nearby islands in the area (Unije, Velike and Male Srakane, Lošinj), but only as a few metres thick local appearances. Durn, Ottner & Slovenec (1999) and Durn et al. (2003) recognised the influence of Upper Pleistocene loess in upper parts of terra rossa profiles from Istria. Further north, in the river Po plain region, loess can also be found, but there no such amazing thicknesses have been registered. The most representative loess-paleosol sequence in North Italy is the Val Sorda sequence (Ferraro et al., 2004, Ferraro, 2009; Fig. 9). This section is about 6 metres thick, starts with a rubefied clayey paleosol covering fluvioglacial deposits and consists of about 4 metres of loess intercalated by three chernosem paleosols (Ferraro et al., 2004; Ferraro, 2009). Ferraro et al. (2004) concluded that the periods of loess deposition alternated with three stable phases of interstadial pedogenesis under steppe climate. Loess has been dated by means of radiocarbon and IRSL methods and gave age estimates ranging from 63.3 ± 6.7 ka to 18.7 ± 2.1 ka. These data presented in Ferraro (2009) were measured using the multiple aliquot additive dose (MAAD) method and may require a correction for anomalous fading. The published IRSL ages can be compared and are in agreement with those from the study on Susak. Dating results of artefacts from the Fumane Cave in Northern Italy, also containing loess, were correlated with the Aurignacian cultural layer which represents the OIS3 (Peresani et al., 2008). At the Bagaggera loess sequence TL dating results of artefacts also showed an OIS4 to OIS2 age (Cremaschi et al., 1990), with soil formation during most of OIS3. The rubefied clayey paleosol at the bottom of the Val Sorda sequence can

very likely be correlated with the red paleosols covering the carbonate basement on Susak and the red paleosol described in Savudrija in Istria (Durn et al., 2003). The OIS 5 (5e – Last Interglacial paleosol) paleosols in the Carpathian basin are usually chernozem-type paleosols. At the Zmajevac section the second paleosol from the top is correlated to OIS5 (Galović et al., 2009). In the Serbian stratigraphy the OIS5 paleosol is termed S1 and is also of chernozem-type (Antoine et al., 2009; Marković et al., 2007, 2009). In the Hungarian loess sections, the OIS5 paleosol is a forest steppe-type paleosol (Frechen, Horváth & Gábris, 1997; Novothny, Horváth & Frechen, 2002). At the Süttő section (Novothny et al., 2011), based on a detailed geochronological investigation and grain-size analysis, the paleosols correlated to OIS5 were divided into interstadials and the reddish-brown paleosol, below the chernozem-like paleosol, was correlated to OIS5e (Fig. 9). The overlying chernozem-like paleosol was correlated to OIS5c, which was a warm and drier interstadial. The two thinner brown steppe-like paleosols intercalated by a thin loess layer, indicate a shorter and/or less warm and humid interstadial period, most likely correlating to the 5a substage. The subdivision of the red paleosols on Susak is still not possible; detailed investigations are required. These different paleosol types in different geographical regions are a clear evidence for different paleoclimatic conditions during coeval periods.

In the Carpathian (Pannonian) basin OIS4 is represented only by loess deposition (Fig. 9), while on Susak the Early Pleniglacial record is probably incomplete. A thin loess horizon intercalated with thin brown paleosols and occasionally with sand is exposed at the Bok section. The loess covering the orange-brown paleosol in the Bok 1 section (Fig. 7) can also be correlated to OIS4. Loess accumulation during OIS4 is also evidenced in the Val Sorda section in a small amount (Ferraro, 2009). Novothny et al. (2011) reported an increase in sand content for the Lower Pleniglacial (OIS4) loess due to a colder and drier climate and increased wind intensity in Süttő.

In the Pannonian (Carpathian) basin OIS3 is characterised by soil development during the interstadials alternating with loess accumulation during stadials. In Zmajevac (Fig. 9) in Eastern Croatia, one weakly developed paleosol correlates to OIS3 (Galović et al., 2009). In loess from Serbia the Middle Pleniglacial (OIS3) is represented by a weakly developed paleosol complex (called L1S1 in Serbian stratigraphy, Marković, Kostić & Oches, 2004; Marković et al., 2004, 2005, 2006, 2007, 2008, 2009). A single, weakly developed chernozem is described from the Ruma section (Marković et al., 2006), a weakly developed double paleosol at the Petrovaradin brickyard (Marković et al., 2005), the Batajnica (Marković et al., 2009) and Irig sections (Marković et al., 2007) and multiple paleosol at the Stari Slankamen (Schmidt et al., 2010) and Surduk (Antoine et al., 2009) sections (Fig. 9). In Hungary, Novothny et al. (2011) reported a brown paleosol in Süttő, previously termed MF1 in the Hungarian loess stratigraphy (Novothny, Horváth & Frechen, 2002; Frechen, Horváth & Gábris, 1997). On Susak, increased dust deposition interrupted by many soil forming periods is evidenced for the Middle Pleniglacial period. In the bay of Bok on Susak at least five thin brown paleosols are intercalated in the loess but it is even very likely that more of such weak paleosols are present. Beside these weakly developed paleosols, two thick brown paleosols are present as well, possibly correlating with the Hengelo or Denekamp Interstadials of the NW European stratigraphy, both correlating to OIS3. The great thickness of the OIS3 deposits on Susak is the result of the generally increased dust accumulation in Europe (Frechen, Oches & Kohfeld, 2003; Machalett et al., 2008) as well as a suitable geographical and morphological position in the North Adriatic basin, which was very likely a vast plateau with a large material input from the extended floodplain of the river Po and its tributaries. The numerous paleosols give evidence that the climate on Susak was milder than in the Carpathian basin. Three brown paleosols are described in the Val Sorda sequence in North Italy (Ferraro et al., 2004; Ferraro, 2009). Novothny et al. (2011) concluded that at Süttő the climate had an intermediate character, which was between the wetter climate in the Western European loess sequences and the drier loess successions in the southern Carpathian basin. A relatively "warmer" climate was proposed for the Irig section in Vojvodina by Marković et al. (2007). On Susak, loess deposition was continuous and intensive from OIS3 to 2, if compared with the Carpathian basin. Based on the numerous paleosols found intercalating aeolian deposits on Susak an even "warmer" climate is assumed for the North Adriatic area.

6 Conclusion

As a part of an ongoing multidisciplinary study, IRSL dating of loess-paleosol sequences from Susak was applied to provide a detailed geochronological framework. The results indicate that the deposits on Susak are a very detailed Last Glacial-Interglacial record. Within error limits, the results are in stratigraphic order, showing a quasi-continuous record spanning from OIS5 (and possibly OIS6 or older) to OIS2. The most impressive sequence is the Middle Pleniglacial (OIS3) record, including evidence for intensive dust accumulation, interrupted by numerous soil forming processes and two volcanic events. The IRSL dating results are in excellent agreement with the radiocarbon dating results. Although dating results are consistent for both dating methods, a more precise method should be used for estimating the volcanic activity. The grain size of the tephras on Susak does not allow the use of the Ar-Ar dating method. Nevertheless, mineralogical and geochemical investigations of the tephras (Mikulčić Pavlaković et al., 2011) showed that the volcanism involved could be related to the Italian volcanic provinces. The red paleosol covering the carbonate basement on Susak correlates at least to OIS5 but an older age can not be excluded. A more detailed investigation regarding the age of the oldest exposed paleosol is needed. Such red paleosols are typical for the whole North Adriatic area.

If the loess record on Susak is correlated with the Danube loess-paleosol sequences of the Carpathian basin, the differences are obvious. Loess deposition in the Carpathian basin was continuous, interrupted by interglacial or interstadial soil-forming processes as evidenced by in thick continuous paleosol layers. On Susak the deposition of aeolian

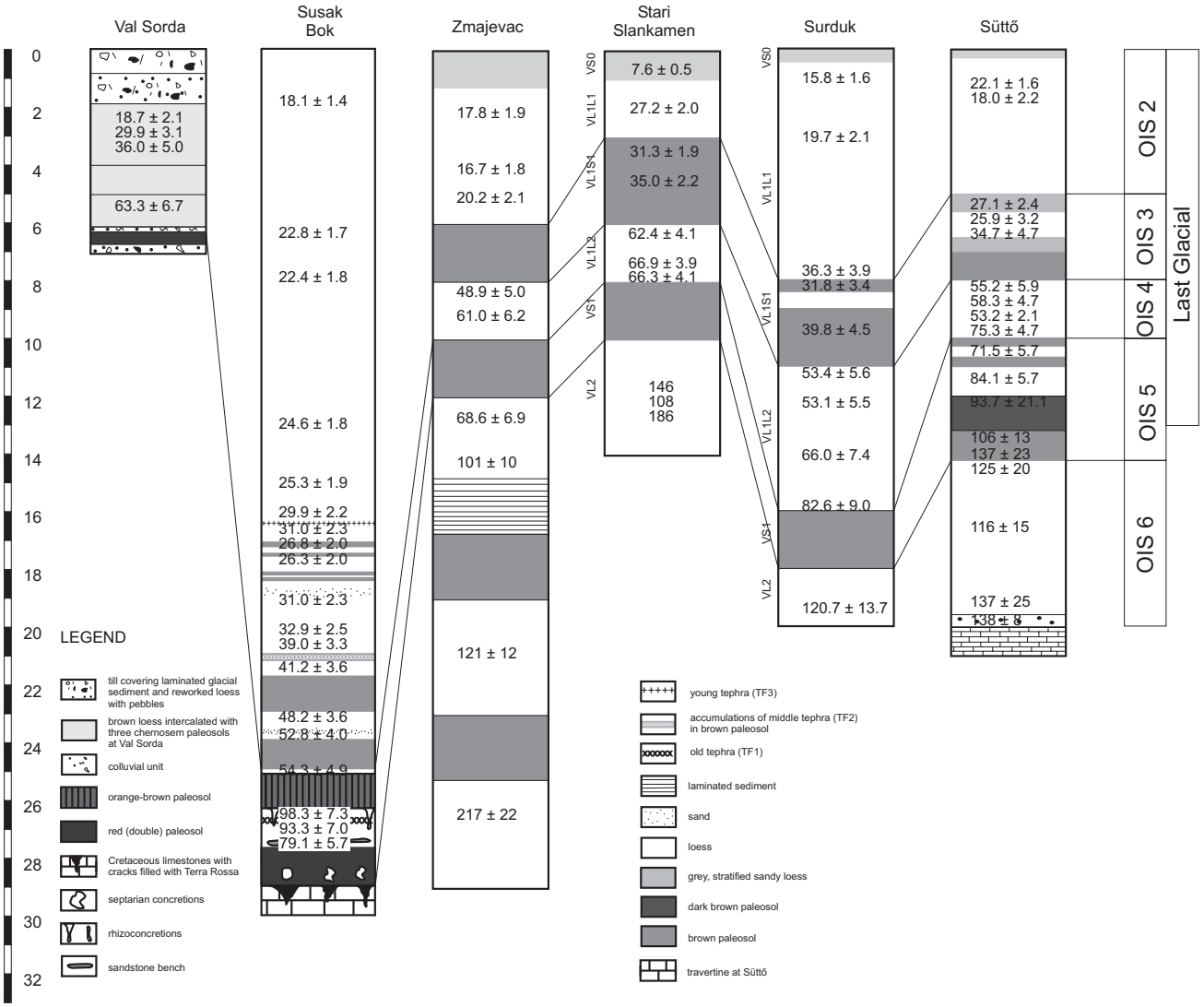

Fig. 9: Bok section, selected to be the most representative section on Susak, correlated with the Val Sorda section in North Italy (Ferraro, 2009), Zmajevac in East Croatia (Galović et al., 2009), Stari Slankamen (Schmidt et al., 2010) and Surduk (Antoine et al., 2009; Fuchs et al., 2008) in Serbia and Süttő in Hungary (Novothny et al., 2009; 2010).

Abb. 9: Der Aufschluss Bok mit der für Susak repräsentativsten Löss-/Paläobodenabfolge und die Korrelation mit den Aufschlüssen Val Sorda in Norditalien (Ferraro, 2009), Zmajevac in Ostkroatien (Galović et al. 2009), Stari Slankamen (Schmidt et al., 2010) und Surduk (Antoine et al., 2009; Fuchs et al., 2008) in Serbien und Süttö in Ungarn (Novothny et al., 2009, 2010).

sediment was more often interrupted by soil forming processes, as evidenced by the numerous paleosols, some of them are well developed, some probably representing only initial pedogenesis. The same major climatic shifts during the Last Glacial are responsible for the development of the deposits on Susak, as in the Carpathian and Pannonian basin. The main difference is the aridity of the climate involved. The climate on Susak was very likely more humid and milder than in other regions.

The detailed geochronological framework presented in this work is an excellent base for future high-resolution investigations of climate proxies. Such studies are in progress.

The loess-paleosol succession on Susak proves that the North Adriatic region is a separate and unique periglacial environment and should not be neglected when investigating the global Glacial-Interglacial evolution.

7 Acknowledgements

This research has been financed by the DAAD (German Academic Exchange Service); the Leibniz Institute for Applied Geophysics (LIAG), Hannover, Germany; the Croatian Ministry of Science, Education and Sports, Projects Nr. 0181001, 0183008 and 183-0000000-3201. This work could not be possible without the help of colleagues of S3 from LIAG, especially Linto Alappat and Alexander Kunz. The authors wish to thank Dr. Lidija Galović for many fruitful discussions and her support and to Ira Wacha-Biličić for correcting English. Help from Dr. Francesca Ferraro and Prof. Dr. Davor Pavelić, who supplied us with the needed literature, is appreciated. We are grateful to Prof. Dr. Goran Durn and Dr. Ágnes Novothny for their criticism and constructive comments of an earlier version of the manuscript.

8 References

Adamiec, G. & Aitken, M.J. (1998): Dose-rate conversion factors: update. – Ancient TL, 16: 37–50.

Aitken, M.J. (1985): Thermoluminescence Dating. – 351 S.; London, (Academic Press).

Aitken, M.J. (1998): An introduction to optical dating. – 280 S.; Oxford, (Oxford University Press).

Amorosi, A., Colalongo, M.L., Pasini, G. & Preti, D. (1999): Sedimentary response to Late Quaternary sea-level changes in the Romagna plain (northern Italy). – Sedimentology, 46: 99–121.

Antoine, P., Rousseau, D.D., Fuchs, M., Hatté, C., Gauthier, C., Marković, S.B., Jovanović, M., Gaudenyi, T., Moine, O. & Rossignol, J. (2009): High-resolution record of the last climatic cycle in the southern Carpathian Basin (Surduk, Vojvodina, Serbia). – Quaternary International, 198: 19–36.

Auclair, M., Lamothe, M. & Huot, S. (2003): Measurement of anomalous fading for feldspar IRSL using SAR. – Radiation Measurements, 37: 487–492.

Bognar, A. (1979): Distribution, properties and types of loess and loess-like sediments in Croatia. – Acta Geologica Academiae Scientiarium Hungaricae, 22: 267–286.

Bognar, A., Klein, V., Tončić-Gregl, R., Šercelj, A., Magdalenić, Z. & Culiberg, M. (1983): Kvartarne naslage otoka Suska i Baške na otoku Krku i njihovo geomorfološko značenje u tumačenju morfološke evolucije kvarnerskog prostora. – Geografski glasnik, 45: 7–32.

Bognar, A., Klein, V., Mesić, I., Culiberg, M., Bogunović, M., Sarkotić-Šlat, M. & Horvatinčić, N. (1992): Quaternary sands at the southeastern part of the Mljet Island. – In: Bognar, A. (ed.): Proceedings of the International Symposium "Geomorphology and Sea" and the Meeting of the Geomorphological Commission of the Carpatho-Balcan Countries: 99–110; Zagreb (University of Zagreb).

Bognar, A. & Zámbó, L. (1992): Some new data of the loess genesis on Susak island. – In: Bognar, A. (ed.): Proceedings of the International Symposium ''Geomorphology and Sea'' and the Meeting of the Geomorphological Commission of the Carpatho-Balcan Countries: 65–72; Zagreb (University of Zagreb).

Bognar, A., Schweitzer, F. & Kis, E. (2002): The Reconstruction of the Paleoenvironmental History of the Northern Adriatic Region Using of the Granulometric Properties of Loess Deposits on Susak Island, Croatia. – Special issue of the fifth International Conference on geomorphology Loess and eolian dust, 23/5: 795–810.

Bognar, A., Schweitzer, F. & Szöőr, G. (2003): Susak – environmental reconstruction of a loess island in the Adriatic. – 141 S; Budapest, (Geographical Research Institute, Hungarian Academy of Sciences).

Bokhorst, M. & Vandenberghe, J. (2009): Validation of wiggle matching using a multi-proxy approach and its palaeoclimatic significance. – Journal of Quaternary Science, 24/8: 937–947.

Borović, I., Marinčić, S., Majcen, Ž. & Magaš, N. (1977): Osnovna geološka karta SFRJ 1:100 000. Tumač za listove Vis K 33-33 Jelsa 33–34 Biševo 33-35. – 67 S; Beograd (Institut za geološka istraživanja, Zagreb 1968, Savezni geološki zavod Beograd).

Bøtter-Jensen, L., McKeever, S.W.S. & Wintle, A.G. (2003): Optically stimulated luminescence dosimetry. – 355 S.; Amsterdam (Elsevier).

Bronger, A. (1976): Zur quartaeren Klima- und Landschaftsentwicklung des Karpatenbeckens auf (palaeo)-pedologischer und bodengeographischer Grundlage. – 45 S.; Kiel (Kieler Geographische Schriften).

Bronger, A. (2003): Correlation of loess-paleosol sequences in East and Central Asia with SE Central Europe: towards a continental Quaternary pedostratigraphy and paleoclimatic history. – Quaternary International, 106/107: 11–31.

Bronger, A. & Heinkele, Th. (1989): Micromorphology and Genesis of Paleosols in the Luochuan Loess Section, China: Pedostratigraphic and Environmental Implications. – Geoderma, 45: 123–143.

Buylaert, J.P., Murray, A.S., Vandenberghe, D., Vriend, M., De Corte, F. & Van den haute, P. (2008): Optical dating of Chinese loess using sand-sized quartz: Establishing a time frame for Late Pleistocene climate changes in the western part of the Chinese Loess Plateau. – Quaternary Geochronology, 3/1–2: 99–113.

Coudé-Gaussen, G. (1990): The loess and loess-like deposits along the sides of the western Mediterranean Sea: genetic and palaeoclimatic significance. - Quaternary International, 5: 1–8.

Cremaschi, M. (1987): Loess deposits of the Po plain and the adjoining Adriatic basin (Northern Italy). – In: Pecsi, M. & French, H.D. (eds.): Loess and Periglacial Phenomena: 125–140, Budapest (Akademiai Kiado).

Cremaschi, M. (1990): Stratigraphy and palaeoenviromental significance of the loess deposits on Susak Island (Dalmatian archipelago). – Quaternary International, 5: 97–106.

Cremaschi, M., Fedoroff, N., Guerreschi, A., Huxtable, J., Colombi, N., Castelletti, L. & Maspero, A. (1990): Sedimentary and pedological processes in the Upper Pleistocene loess of North Italy. The Bagaggera sequence. – Quaternary International, 5: 23–38.

De Vivo, B., Rolandi, G., Gans, P.B., Calvert, A., Bohrson, W.A., Spera, F.J. & Belkin, H.E. (2001): New constraints on the pyroclastic eruptive history of the Campanian volcanic Plain (Italy). – Mineralogy and Petrology, 73: 47–65.

Ding, Z.L., Xiong, S.F., Sun, J.M., Yang, S.L., Gu, Z.Y. & Liu, T.S. (1999): Pedostratigraphy and paleomagnetism of a ~7.0 Ma eolian loess–red clay sequence at Lingtai, Loess Plateau, north-central China and the implications for paleomonsoon evolution. – Palaeogeography, Palaeoclimatology, Palaeoecology, 152: 49–66.

Durn, G., Ottner, F. & Slovenec, D. (1999): Mineralogical and geochemical indicators of the polygenetic nature of terra rossa in Istria, Croatia. – Geoderma, 91/1–2: 125–150.

Durn, G. (2003): Terra rossa in the Mediterranean region: Parent materials, composition and origin. – Geologia Croatica, 56/1: 83–100.

Durn, G., Ottner, F., Tišljar, J., Mindszenty, A. & Barudžija, U. (2003): Regional Subaerial Unconformities in Shallow-Marine Carbonate Sequences of Istria: Sedimentology, Mineralogy, Geochemistry and Micromorphology of Associated Bauxites, Palaeosols and Pedo-sedimentary Complexes. – In: Vlahović, I. & Tišljar, J. (eds): Evolution of depositional environments from the Palaeozoic to the Quaternary in the Karst Dinarides and the Pannonian Basin. – Field trip guidebook of the 22nd IAS Meeting of Sedimentology: 209–255; Zagreb (Institute of Geology).

Durn, G., Aljinović, D., Crnjaković, M. & Lugović, B. (2007): Heavy and light mineral fractions indicate polygenesis of extensive terra rossa soils in Istria, Croatia. – In: Mange, M. & Wright, D. (eds.): Heavy Minerals in Use, Developments in Sedimentology, 58: 701–737, Amsterdam (Elsevier).

Fairbanks, R.G., Mortlock, R.A., Chiu, T.-C., Cao, L., Kaplan, A., Guilderson, T.P., Fairbanks, T.W. & Bloom, A.L. (2005): Marine radiocarbon calibration curve spanning 0 to 50,000 years B.P. based on paired 230Th/234U/238U and 14C dates on pristine corals. – Quaternary Science Reviews, 24: 1781–1796.

Ferraro, F. (2009): Age, sedimentation and soil formation in the Val Sorda loess sequence, Northern Italy. – Quaternary International, 204: 54–64.

Ferraro, F., Terhorst, B., Ottner, F. & Cremaschi, M. (2004): Val Sorda: an upper Pleistocene loess–palaeosol sequence in northeastern Italy. – Revista Mexicana de Ciencias Geológicas, 24/1: 30–47.

Fortis, A. (1771): Saggio d´osservazioni sopra l´isola di Cherso ed Osero. – 167 S.; Venezia.

Frechen, M., Horváth, E. & Gábris, G. (1997): Geochronology of Middle and Upper Pleistocene loess sections in Hungary. – Quaternary Research, 48/3: 291–312.

Frechen, M., Oches, E.A. & Kohfeld, K.E. (2003): Loess in Europe - mass accumulation rates during the Last Glacial Period. – Quaternary Science Reviews, 22/18–19: 1835–1857.

Fuchs, M., Rousseau, D.-D., Antoine, P., Hatté, C., Gauthier, C., Marković, S. & Zoeller, L (2008): Chronology of the Last Climatic Cycle (Upper Pleistocene) of the Surduk loess sequence, Vojvodina, Serbia. – Boreas, 37: 66–73.

Galović, L., Frechen, M., Halamić, J., Durn, G. & Romić, M. (2009): Loess chronostratigraphy in Eastern Croatia – A first luminescence dating approach. - Quaternary International, 198/1–2: 85–97.

Galović, I. & Mutić, R. (1984): Gornjopleistocenski sedimenti istočne Slavonije (Hrvatska). – Rad JAZU, 411: 299–356; Zagreb.

Geyh, M.A. (1990): 14C dating of loess. - Quaternary International, 7/8: 115-118.

Geyh, M.A. (2005): 14C dating - still a challenge for users? – Zeitschrift für Geomorphologie, Neue Folge, Supplementband 139: 63–86.

Gorjanović-Kramberger, D. (1912): Iz prapornih predijela Slavonije. – Vijesti geološkog povjerenstva, 2: 28–30; Zagreb.

Gorjanović-Kramberger, D. (1915): Die Hydrographischen Verhältnisse der Lössplateaus Slavoniens. – Glasnik hrvatskoga prirodoslovnoga društva, 27: 70–75; Zagreb.

Gorjanović-Kramberger, D. (1922): Morfologijske i hidrografijske prilike prapornih predjela Srijema, te pograničnih česti županije virovitičke. – Glasnik hrvatskoga prirodoslovnoga društva, 34: 111–164; Zagreb.

Greenland Ice-Core Project (GRIP) Members (1993): Climate instability during the last interglacial period recorded in the GRIP ice core. – Nature, 364: 203–207.

Huntley, D. J. & Lamothe, M. (2001): Ubiquity of anomalous fading in K-feldspars, and the measurement and correction for it in optical dating. – Canadian Journal of Earth Sciences 38, 1093–1106.

Kalac, K., Bajraktarević, Z., Marković, Z., Barbić, Z & Gušić, I. (1995): Stratigrafija pliocensko-pleistocenskih sedimenata u bušotinama podmorja Jadrana. – In: Vlahović, I., Velić, I. & Šparica, M.: Proceedings of the First Croatian Geological Congress, 1: 281–284; Zagreb (Croatian Geological Institute).

Kišpatić, M. (1910): Der Sand von der Insel Sansego (Susak) bei Lussin und dessen Herkunft. – Verhandlungen geologischer Reichsanstalt, 13: 294–305; Wien.

Korolija, B., Borović, I., Marinčić, S., Jagačić, T., Magaš, N. & Milanović, M. (1977): Osnovna geološka karta SFRJ 1:100 000. – Tumač za list Lastovo K 33–46 Korčula K 33–47 Palagruža K 33–57. –53 S., Beograd (Institut za geološka istraživanja Zagreb 1968, Savezni geološki zavod Beograd).

Kovács, J. (2008): Grain-size analysis of the Neogene red clay formation in the Pannonian Basin. – International Journal of Earth Sciences, 97: 171–178.

Lambeck, K. & Chappell, J. (2001): Sea level change through the Last Glacial Cycle. – Science, 292: 679–686.

Lambeck, K., Antonioli, F., Purcell, A. & Silenzi, S. (2004): Sea-level change along the Italian coast for the past 10.000 yr. – Quaternary Science Reviews, 23: 1567–1598.

Lu, Y.C., Wang, X.L. & Wintle, A.G. (2007): A new OSL chronology for dust accumulation in the last 130,000 yr for the Chinese Loess Plateau. – Quaternary Research, 67: 152–160.

Lužar-Oberiter, B., Mikulčić Pavlaković, S., Crnjaković, M. & Babić, Lj. (2008): Variable sources of beach sands of north Adriatic islands: examples from Rab and Susak. – Geologia Croatica, 61/2–3: 379–384.

Machalett, B., Oches, E. A., Frechen, M., Zöller, L., Hambach, U., Mavlyanova, N. G., Marković, S. B. & Endlicher, W. (2008): Aeolian dust dynamics in central Asia during the Pleistocene: Driven by the long-term migration, seasonality, and permanency of the Asiatic polar front. – Geochemistry, Geophysics, Geosystems, 9, Q08Q09, doi:10.1029/2007GC001938.

Mamužić, P. (1965): Osnovna geološka karta SFRJ 1:100 000. List Lošinj L 33-155. Institut za geološka istraživanja, Zagreb, Savezni geološki zavod, Beograd.

Mamužić, P. (1973): Osnovna geološka karta SFRJ 1:100 000. Tumač za list Lošinj L 33–155. – 34 S; Beograd (Institut za geološka istraživanja, Zagreb, Savezni geološki zavod, Beograd).

Marchesetti, C. (1882): Cenni geologici sul'isola di Sansego. – Bollettino della Societa´ adriatica di Scienze Naturali, 7: 289–304; Trieste.

Marković, S.B., Kostić, N.S. & Oches, E.A. (2004): Palaeosols in the Ruma loess section (Vojvodina, Serbia). – Revista Mexicana de Ciencias Geológicas, 21: 79–87.

Marković, S.B., Oches, E.A., Gaudenyi, T., Jovanović, M., Hambach, U., Zöller, L. & Sümegi, P. (2004): Paleoclimate record in the late Pleistocene loess-palaeosol sequence at Miseluk (Vojvodina, Serbia). – Quaternaire, 15: 361–368.

Marković, S.B., McCoy, W.D., Oches, E.A., Savić, S., Gaudenyi, T., Jovanović, M., Stevens, T., Walther, R., Ivanisević, P. & Galić, Z. (2005): Paleoclimate record in the upper Pleistocene loess-palaeosol sequence at Petrovaradin brickyard (Vojvodina, Serbia). – Geologica Carpathica, 56: 545–552.

Marković, S.B., Oches, E., Sümegi, P., Jovanović, M. & Gaudenyi, T. (2006): An introduction to the middle and upper Pleistocene loess-palaeosol sequence at Ruma brickyard, Vojvodina, Serbia. – Quaternary International, 149: 80–86.

Marković, S.B., Oches, E.A., McCoy, W.D., Frechen, M. & Gaudenyi, T. (2007): Malacological and sedimentological evidence for ''warm'' glacial climate from the Irig loess sequence, Vojvodina, Serbia. – Geochemistry Geophysics Geosystems, 8, Q09008. doi:10.1029/2006GC001565.

Marković, S.B., Bokhorst, M.P., Vandenberghe, J., McCoy, W.D., Oches, E.A., Hambach, U., Gaudenyi, T., Jovanović, M., Stevens, T., Zöller, L. & Machalett, B. (2008): Late Pleistocene loess-palaeosol sequences in the Vojvodina region, North Serbia. – Journal of Quaternary Science, 23/1: 73–84.

Marković, S.B., Hambach, U., Catto, N., Jovanović, M., Buggle, B., Machalett, B., Zöller, L., Glaser, B. & Frechen, M. (2009): The middle and late Pleistocene loess palaeosol sequences at Batajanica, Vojvodina, Serbia. – Quaternary International, 198: 255–266.

Marković-Marjanović, J. (1976): Kvartarni sedimenti ostrva Hvara – Srednji Jadran. – Glasnik prirodnjačkog muzeja, A/31: 199–214; Beograd.

Mikulčić Pavlaković, S., Crnjaković, M., Tibljaš, D., Šoufek, M., Wacha, L., Frechen, M. & Lacković, D. (2011): Mineralogical and Geochemical Characteristics of Quaternary Sediments from the Island of Susak (Northern Adriatic, Croatia). – Quaternary International, 234/ 1–2: 32–49.

Mutić, R. (1967): Pijesak otoka Suska. – Geološki Vjesnik 20: 41–57.

Mutić, R. (1990): Korelacija kvartara istočne Slavonije na osnovi podataka mineraloško-petrografskih analiza (Istočna Hrvatska, Jugoslavija) – Dio II: Lesni ravnjak. – Acta Geologica 20/2: 29–80; Zagreb.

Novothny, Á., Horváth, E. & Frechen, M. (2002): The loess profile at Albertirsa, Hungary – improvements in loess stratigraphy by luminescence dating. – Quaternary International, 95–96: 155–163.

Novothny, Á., Frechen, M., Horváth, E., Bradák, B., Oches, E.A., McCoy, W.D. & Stevens, T. (2009): Luminescence and amino acid recemization chronology of the loess-palaeosol sequence at Süttő, Hungary. – Quaternary International, 198/1–2: 62–76.

Novothny, Á., Frechen, M., Horváth, E., Krbetschek, M. & Tsukamoto, S. (2010): Infrared stimulated luminescence and radiofluorescence dating of aeolian sediments from Hungary. – Quaternary Geochronology, 5: 114–119.

Novothny, A., Frechen, M., Horváth, E., Wacha, L. & Rolf, C., (2011): Investigating the penultimate and last glacial cycles of the Süttő loess section (Hungary) using luminescence dating, high-resolution grain size, and magnetic susceptibility data – Quaternary International, 234/1–2: 75–85.

Pavelić, D., Kovačić, M. & Vlahović, I. (2006): Periglacial aeolian-alluvial interaction: Pleistocene of the Island of Hvar (Eastern Adriatic, Croatia). - In: Hoyanagi, K., Takano, O. & Kano, K. (eds.): From the Highest to the Deepest. – Abstracts book of the 17th International Sedimentological Congress, Volume A, Fukuoka.

Pavelić, D., Kovačić, M., Vlahović, I. & Wacha, L.: Pleistocene aeolian–fluvial interaction in a steep relief karstic coastal belt (Island of Hvar, Eastern Adriatic, Croatia). – (submitted to Sedimentary Geology).

Pécsi, M. (1990): Loess is not just the accumulation of dust. – Quaternary International, 7/8: 1–21.

Pécsi, M. (1993): Quaternary and loess research. – In: Bassa, L., Keresztesi, Zs. & Lóczy, D. (eds.): Loess in Form, 2, 82 S; Budapest (Hungarian Academy of Science).

Peresani, M., Cremaschi, M., Ferraro, F., Falguères, C., Bahain, J.-J., Gruppioni, G., Sibilia, E., Quarta, G., Calcagnile, L. & Dolo, J.-M. (2008): Age of the final Middle Palaeolithic and Uluzzian levels at Fumane Cave, Northern Italy, using 14C, ESR, 234U/230Th and thermoluminescence methods. – Journal of Archaeological Science 35: 2986–2996.

Poje, M. (1985): Praporne naslage vukovarskog profila i njihova stratigrafska pripadnost. – Geološki Vjesnik, 38: 45–66.

Poje, M. (1986): Ekološke promjene na vukovarskom prapornom ravnjaku proteklih cca 500.000 godina. – Geološki Vjesnik, 39: 19–42.

Prescott, J.R. & Hutton, J.T. (1994): Cosmic ray contributions to dose rates for luminescence and ESR dating: large depths and long-term time variations. – Radiation Measurements, 23: 497–500.

Preusser, F., Degering, D., Fuchs, M., Hilgers, A., Kadereit, A., Klasen, N., Krbetschek, M., Richter, D. & Spencer, J.Q.G. (2008): Luminescence dating: basics, methods and applications. – Eiszeitalter und Gegenwart (Quaternary Science Journal), 57/1–2: 95–149.

Preusser, F., Chithambo, M.L., Götte, T., Martini, M., Ramseyer, K., Sendezera, E.J., Susino, G.J. & Wintle, A.G. (2009): Quartz as a natural luminescence dosimeter. – Earth-Science Reviews, 97: 184–214.

Rees-Jones, J. (1995): Optical dating of young sediments using fine-grain quartz. – Ancient TL, 13: 9–14.

Roberts, H.M. (2008): The development and application of luminescence dating to loess deposits: a perspective on the past, present and future. – Boreas, 37: 483–507.

Roberts, H.M., Muhs, D.R., Wintle, A.G., Duller, G.A.T. & Bettis III, E.A. (2003): Unprecedented last-glacial mass accumulation rates determined by luminescence dating of loess from western Nebraska. – Quaternary Research, 59: 411–419.

Schmidt, E., Machalett, B., Marković, S.B., Tsukamoto, S. & Frechen, M. (2010): Luminescence chronology of the upper part of the Stari Slankamen loess sequence (Vojvodina, Serbia). – Quaternary Geochronology, 5: 137–142.

Singhvi, A.K., Bronger, A., Sauer, W. & Pant, R.K. (1989): Thermoluminescence dating of loess-paleosol sequences in the Carpathian basin (East-Central Europe): a suggestion for a revised chronology. – Chemical Geology: Isotope Science Section, 73: 307–317.

Spell, T.L. & McDougall, I. (1992): Revisions to the age of the Brunhes – Matuyama Boundary and the Pleistocene geomagnetic polarity timescale. – Geophysical Research Letters, 19/12: 1181–1184.

Spooner, N.A. (1994): The anomalous fading of infrared-stimulated luminescence from feldspars. – Radiation Measurements, 23, 2/3: 625–632.

Stevens, T., Lu, H., Thomas, D.S.G. & Armitage, S.J. (2008): Optical dating of abrupt shifts in the late Pleistocene East Asian Monsoon. – Geology, 36/5: 415–418.

Surić, M. & Juračić, M. (2010): Late Pleistocene-Holocene environmental changes – records from submerged speleothems along the Eastern Adriatic coast (Croatia). – Gelogia Croatica, 63/2: 155–169.

Šandor, F. (1912): Istraživanja prapora iz Vukovara, Bilo gore i sa Rajne. – Vijesti geološkog povjerenstva, 2: 103–107, Zagreb.

Šandor, F. (1914): Praporasti nanos otoka Suska. – Vijesti geološkog povjerenstva Hrvatske i Slavonije, 3–4, Zagreb.

Van Straaten, L.M.J.U. (1970): Holocene and Late Pleistocene sedimentation in the Adriatic Sea. – Geologische Rundschau, 60: 106–131.

Wacha, L., Mikulčić Pavlaković, S., Novothny Á., Crnjaković, M. & Frechen, M. (2011): Luminescence Dating of Upper Pleistocene Loess from the Island of Susak in Croatia. – Quaternary International, 34/1–2: 50–61.

Wacha, L., Frechen, M., Rolf, Ch. & Hambach, U. (in preparation): The high-resolution grain-size and palaeomagnetic record of the OIS3 loess deposits from Susak, Croatia.

Wein N. (1977): Die Lössinsel Susak – eine naturgeographische Singularität in der jugoslawischen Inselwelt. – Petermanns geographische Mitteilungen, 2: 123–132; Gotha/Leipzig.

Wintle, A.G. (1973): Anomalous fading of thermoluminescence in mineral samples. – Nature, 245: 143–144.

Wintle, A.G. (1997): Luminescence dating: laboratory procedures and protocols. – Radiation Measurements, 27: 769–817.

Wintle, A.G. & Packman, S.C. (1988): Thermoluminescence ages for three sections in Hungary. – Quaternary Science Reviews, 7: 315–320.

Yang, S.L. & Ding, Z.L. (2004): Comparison of particle size characteristics of the Tertiary "red clay" and Pleistocene loess in the Chinese Loess Plateau: implications for origin and sources of the "red clay". – Sedimentology, 51: 77–93.

E&G Quaternary Science Journal
Volume 60 / Number 1 / 2011 / 170–187 / DOI 10.3285/eg.60.1.12
www.quaternary-science.net

GEOZON SCIENCE MEDIA
ISSN 0424-7116

Novel methodological approaches in loess research – interrogating biomarkers and compound-specific stable isotopes

Michael Zech, Roland Zech, Björn Buggle, Ludwig Zöller

Abstract: Loess-paleosol sequences are unique terrestrial archives for the reconstruction of Quaternary landscape and climate history. The development of novel, more quantitative paleoclimate proxies may initiate a new era of loess research over the next decade. This review paper presents the principles, analytical backgrounds, and first applications of some of these new proxies that are currently being developed. We discuss the potential of (i) n-alkanes as plant leaf wax-derived biomarkers for reconstructing vegetation history, (ii) amino acid racemization and glycerol dialkyl glycerol tetraether (GDGT) indices as proxies for reconstructing paleotemperature and (iii) compound-specific δD and $\delta^{18}O$ analyzes of plant-derived n-alkanes and monosaccharides, respectively, as proxies for reconstructing paleoclimate/-aridity. While we want to inspire the readership about the exciting methodological and analytical developments and their potential for loess research, the current limitations and shortcomings of each proxy should not be overlooked. Degradation effects and possible post-depositional 'contamination', for example, need to be considered when interpreting biomarker records, and the deconvolution of varying factors influencing the isotopic signals can be challenging.

[Neue methodische Ansätze in der Lössforschung – Biomarker- und substanzspezifische Stabilisotopen-Analytik]

Kurzfassung: Löss-Paläoboden Sequenzen sind wichtige terrestrische Archive für die Rekonstruktion der quartären Landschafts- und Klimageschichte. Die Entwicklung neuer, quantitativerer Paläoklima-Proxies könnte in den kommenden Jahren eine neue Ära in der Lössforschung einleiten. Dieser Review-Artikel stellt die Prinzipien, die zugrunde liegende Analytik, und erste Anwendungsbeispiele für einige dieser Proxies vor, welche derzeit entwickelt werden. Wir diskutieren das Potential von (i) pflanzenwachsbürtigen n-Alkanen als Biomarker für die Rekonstruktion der Vegetationsgeschichte, (ii) Aminosäure Razemisierung und Glycerin-Dialkyl-Glycerin-Tetraether (GDGT) Indizes als Proxies für die Rekonstruktion der Paläotemperatur und (iii) substanzspezifischen δD and $\delta^{18}O$ Analysen an pflanzenbürtigen n-Alkanen bzw. Zuckern für die Entwicklung von Proxies zur Rekonstruktion von Paläoklima/-aridität. Während wir versuchen, die Leserschaft für die methodischen und analytischen Neuentwicklungen und deren Potential für die Lössforschung zu begeistern, verweisen wir gleichzeitig auch auf die Limitierungen und Schwächen der jeweiligen Methoden. So müssen beispielsweise Degradationseffekte oder postsedimentäre ‚Kontamination' bei der Interpretation von Biomarker-Rekords berücksichtigt und weiter untersucht werden. Des Weiteren könnte sich die Quantifizierung der unterschiedlichen Einflussfaktoren auf Deuterium- und ^{18}O-Rekords als herausfordernd erweisen.

Keywords: *Loess, paleoenvironment, paleoclimate, biomarker, molecular fossil, n-alkane, glycerol dialkyl glycerol tetraether, amino acid racemization, sugar, stable isotope, δD, $\delta^{18}O$*

Addresses of authors: **M. Zech**[*,#], **L. Zöller**, Chair of Geomorphology, University of Bayreuth, Universitätsstr. 30, 95440 Bayreuth, Germany. E-Mail: michael_zech@gmx.de; **M. Zech, B. Buggle**, Department of Soil Physics, University of Bayreuth, Universitätsstr. 30, 95440 Bayreuth, Germany. **M. Zech, B. Buggle**, Department of Terrestrial Biogeochemistry, Martin-Luther University Halle-Wittenberg, Weidenplan 14, D-06120 Halle, Germany. **R. Zech**[#], Geological Institute, Brown University, 324 Brook Street, Providence RI 02912, USA. **R. Zech** now at: Geological Institute, ETH Zurich, Sonneggstr. 5, 8092 Zurich, Switzerland. *[#]these authors contributed equally to this manuscript. [*]corresponding author*

1 Introduction

Ocean sediments and polar ice cores have provided invaluable insights into the climate system, its natural variability, forcings and mechanisms over the last few decades. However, it is the terrestrial, non-polar regions that provide most of the ecosystem services that we depend on. In view of global warming and the anticipated negative effects for ecosystems and economies, increasing scientific efforts should focus on reconstructing past climate and environmental conditions on land. We need a profound understanding of climate change-induced geomorphological processes and ecological consequences.

Loess-paleosol sequences (LPS) are unique terrestrial archives for this purpose. Most famous from the Chinese Loess Plateau, LPS have also accumulated tens to hundreds of meters at places in Europe, Siberia, Alaska and South America (Markovic et al. 2009; Zöller & Faust 2009; Frechen 2011). The typical succession of loess and paleosols generally reflects glacial and interglacial periods, respectively, and thus the characteristic climate variability of the Quaternary, the last ~2.6 Ma. The international 'Loessfest 2009' (Markovic 2011) in Novi Sad, Serbia, recently provided a platform for presenting scientific results, for discussing new methodological developments, and strengthening the international cooperation in loess research. An overview over the progresses made during the last decade is provided in Zöller (2010). Emphasis therein was mainly put on the developments of the dating methods, as well as on high-resolution magnetic susceptibility and grain-size measurements, because these

allow detailed reconstructions of pedogenesis and wind strength.

The aim of this review is to elaborate further on the most recent proxy developments. Our motivation stems from the anticipation that sophisticated analytical equipment, including HPLC (high performance liquid chromatography) and GC-IRMS (gas chromatography – isotope ratio mass spectrometry), will become more widely available and boost loess research over the next decade. The new tools will provide valuable, complementary paleoclimate and paleoenvironmental proxies. In this review, we can only give an overview over the principles of the proxies that we are currently working on, so by no means it should be considered to cover the full range of interesting, promising, new methods. The potential, as well as the current limitations of the presented methods will be illustrated in selected case studies.

2 Biomarkers and compound-specific stable isotope analyzes (CSIA) – some basics

Biomarkers are organic molecules that are produced by certain organisms or groups of organisms and thus have more or less specific sources. In many cases, they serve essential biophysiological functions, for example as membrane lipids in soil-thriving bacteria, or as leaf waxes for plants. Provided that the biomarkers are sufficiently resis-tant to degradation and mineralization, they are preserved in soils and can be extracted and analyzed in paleosols to reconstruct past changes in vegetation or bacterial communities. Biomarkers can thus be considered as molecular fossils (Eganhouse 1997; Eglinton & Eglinton 2008).

The analytical determination of biomarkers generally starts with an (i) extraction or hydrolysis step. For example, lipid biomarkers are extracted from soil/sediment samples with organic solvents traditionally using Soxhlet apparatuses and biomarkers that form macromolecules such as aminoacids (in proteins) or sugars (in polysaccharides) are hydrolytically released using acids. (ii) Subsequently, there commonly follow various purification steps e.g. to remove interfering cations. (iii) Quantification of the individual molecules is in many cases carried out via gas chromatography (GC) coupled to flame ionisation detectors (FID) or to mass spectrometers (MS). Frequently, molecules have to be derivatised to be measurable via GC because they are low-volatile or not volatile at all. For instance, transformation of hydroxyl groups into trimethylsilyl-(TMS-)derivatives using e.g. N,O-Bis(trimethysilyl)fluoroacetamid (BSTFA) increases the volatileness of molecules by disabling hydrogen bonds. But as HPLC becomes more common and available, this step is not necessary any more for those biomarkers that can be measured via HPLC.

Concerning stable isotopes, $\delta^{13}C$ and $\delta^{15}N$ analyzes of bulk samples, for instance of soil or sediments samples, can be accomplished relatively easy via elemental analysis – isotope ratio mass spectrometry (EA-IRMS). Carbon and nitrogen of samples are thereby transformed into carbon dioxide (CO_2) and nitrogen (N_2), respectively, in the EA. Subsequently, the abundance of heavy versus light isotopes ($^{13}C/^{12}C$ and $^{15}N/^{14}N$, respectively) in these gases is directly determined online in the coupled IRMS. Hence, these analyzes are meanwhile well established in many different scientific communities and allow, for example, reconstructing C3–C4 vegetation changes (Boutton 1996; Liu et al. 2005; Zech et

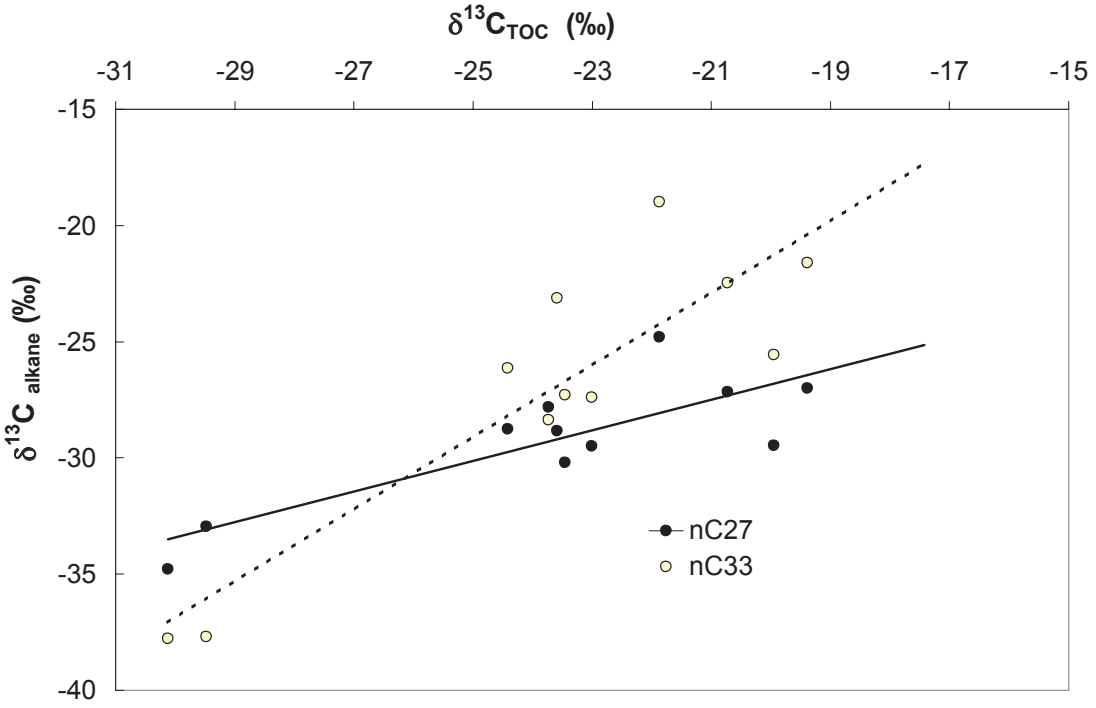

Fig. 1: Correlation of compound-specific $\delta^{13}C$ (shown here are nC_{27} and nC_{33}) with bulk $\delta^{13}C$ (on total organic carbon, TOC) in a sediment core from Argentina (Zech et al. 2009b). The higher amplitude for $\delta^{13}C$ of nC_{33} compared to $\delta^{13}C$ of nC_{27} reflects the dominant origin of nC_{33} from C3- or C4-grasses, whereas nC_{27} primarily derives from C3 trees and shrubs.

Abb. 1: Korrelation von substanz-spezifischen Alkan-$\delta^{13}C$-Werten (dargestellt für nC_{27} und nC_{33}) mit Gesamt-$\delta^{13}C$-Werten (Gesamt organischer Kohlenstoff, TOC) für einen Sediment-Bohrkern aus Argentinien (Zech et al. 2009b). Die größere Amplitude von $\delta^{13}C$ für nC_{33} verglichen mit $\delta^{13}C$ von nC_{27} kann damit erklärt werden, dass nC_{33} überwiegend von C3- oder C4-Gräsern stammt, wohingegen nC_{27} hauptsächlich von C3 Bäumen und Sträuchern stammt.

al. 2009b) and changes in the nitrogen (N-)cycle (Zech et al. 2007; Schatz et al. 2010).

A more sophisticated analytical approach is the combination of biomarker- and stable isotope analyzes. From a technical point of view, this is mostly accomplished by the coupling of a GC to an IRMS via an 'online' combustion unit (GC-C-IRMS). Thus, the isotopic composition of individual biomarkers eluting successively from the GC-column can be determined to provide more specific information than bulk isotope analyzes (Glaser 2005; Glaser & Zech 2005; Amelung et al. 2008). Zech et al. (2009b), for example, have shown for a sediment core from NE-Argentina that the $\delta^{13}C$ values of all individual plant leaf-wax derived n-alkanes nC_{27}, nC_{29}, nC_{31} and nC_{33} correlate significantly with bulk $\delta^{13}C$. However, the isotopic variations are most pronounced for nC_{31} and nC_{33} (Fig. 1), which corroborates the fact that the n-alkane biomarkers nC_{31} and nC_{33} derive primarily from grasses and are thus very sensitive for C3–C4 changes, whereas nC_{27} and nC_{29} derive primarily from trees and shrubs (C3 vegetation).

As the natural abundances of deuterium and ^{18}O in rainfall mainly depend on climatic factors, namely temperature (Fig. 2) and the amount of precipitation (Craig 1961; Dansgaard 1964; Gat 1996; Araguas-Araguas et al. 2000), δD and $\delta^{18}O$ records from LPS would be of great value, too. It is no surprise that various kinds of archives and chemical

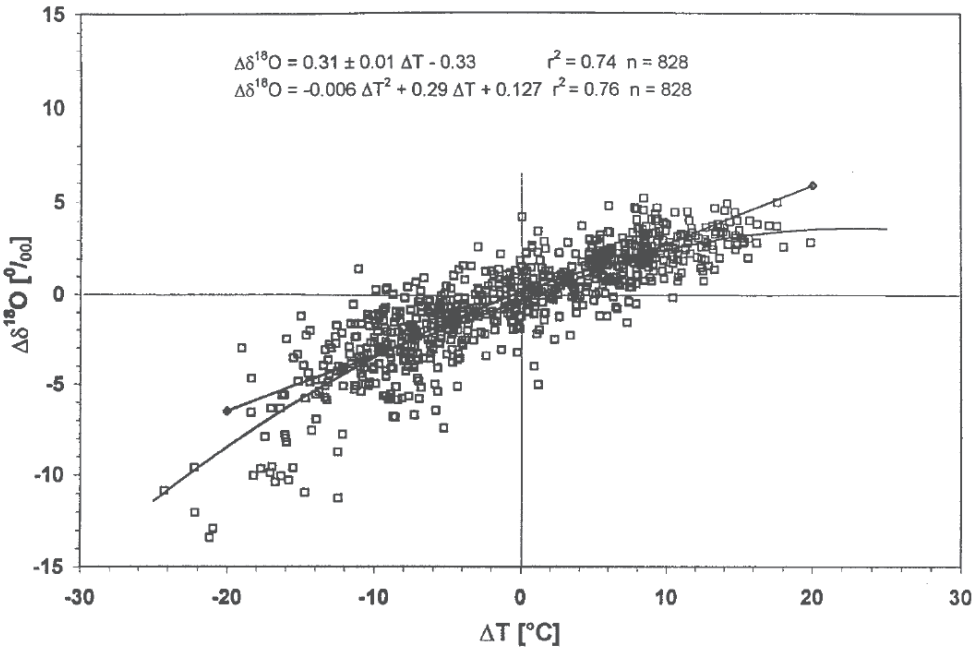

Fig. 2: Correlation between $\delta^{18}O$ of monthly precipitation and surface air temperature for the IAEA/WMO network stations situated between 40 °N and 60 °N (from Araguas-Araguas et al. 2000, Fig. 4a).

Abb. 2: Korrelation von $\delta^{18}O$ im monatlichen Niederschlag mit Lufttemperatur für IAEA/WMO Klimastationen zwischen 40 °N und 60 °N (aus Araguas-Araguas et al. 2000, Abb. 4a).

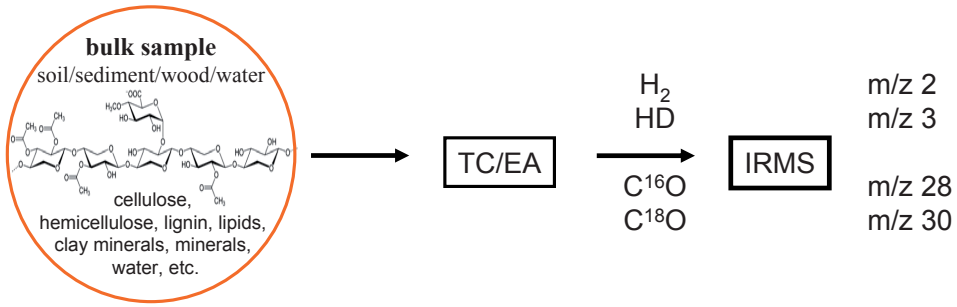

Fig. 3: Principle of bulk TC/EA-IRMS δD and $\delta^{18}O$ analyzes. All hydrogen/oxygen atoms of a sample are converted at high temperature into hydrogen (H_2) / carbon monoxide (CO), for which δD and $\delta^{18}O$ are determined 'online' via a coupled IRMS by detecting the masses m/z 2 and 3, and m/z 28 and 30, respectively.

Abb. 3: Prinzip von Gesamt TC/EA-IRMS δD und $\delta^{18}O$ Analysen. Alle Wasserstoff-/Sauerstoff-Atome einer Probe werden bei hoher Temperatur in Wasserstoff- (H_2) / Kohlenmonoxid- (CO) Gas umgewandelt. Mittels eines ‚online' gekoppelten IRMS werden für diese Gase die δD bzw. $\delta^{18}O$-Werte durch Detektion der Massen m/z 2 und 3 bzw. m/z 28 and 30 gemessen.

E&G / Vol. 60 / No. 1 / 2011 / 170–187 / DOI 10.3285/eg.60.1.12

compounds that record the deuterium and ^{18}O signatures of precipitation have been targeted extensively in paleoclimate studies, including ice cores, speleothems, lacustrine and pedogenetic carbonates, and plant cellulose (e.g. Sternberg 1988; Mayer & Schwark 1999; e.g. Danis et al. 2006; Wang et al. 2006; Gessler et al. 2009). However, these proxies are hardly applied to LPSs so far.

From an analytical point of view, δD and $\delta^{18}O$ analy-zes of bulk samples can be carried out via thermo conversion/elemental analysis (TC/EA-) IRMS 'online' coupling on pyrolytically produced hydrogen (H_2, HD) and carbon monoxide ($C^{16}O$, $C^{18}O$), respectively (Werner et al. 1996; Kornexl et al. 1999; Werner 2003) (Fig. 3). However, oxygen and hydrogen occur in many different organic and inorganic pools in soils and sediments (crystal water, aliphatic compounds, aromatic compounds, alcohols, plant-derived organic material, microbial-derived organic material, etc.). As these pools can have distinct isotopic signals, it is very difficult to disentangle a real paleoclimatic signal when changes in pool sizes cannot be excluded. Another metho-dological shortcoming is that many hydrogen and oxygen atoms are not strongly bound and that they are therefore prone to exchange reactions (Schimmelmann et al. 2006). Consider for example R-COOH (carboxyl-) groups, where the isotopes will equilibrate (post-depositionally) with the ambient soil water. We will discuss ways to overcome these problems further below.

3 Novel methodological approaches

3.1 Plant leaf-wax derived n-alkanes

n-Alkanes with 25 to 33 carbon atoms (nC_{25}–nC_{33}) and a strong odd-over-even predominance (OEP) are important constituents of cuticular plant leaf waxes (Eglington & Hamilton 1967; Kolattukudy 1976). With the litter-fall they are deposited and stored in soils and sediments, for example in aeolian sediments, where they are assumed to be relatively resistant against biogeochemical degradation (Cranwell 1981; Lichtfouse 1998; Lichtfouse et al. 1998). Since different vegetation types have distinct n-alkane patterns and hence a so-called "chemical fingerprint", n-alkanes have the potential to serve as biomarkers. For instance, they are used to differentiate between autochthonous (lacustrine) and allochthonous (terrestrial) organic matter in lake sediments (Bourbonniere et al. 1997; Ficken et al. 2000; Mügler et al. 2008; Zech et al. 2009b), or to reconstruct vegetation changes, predominantly in terms of the relative proportions of grasses and trees (Cranwell 1973; Schwark et al. 2002; Zech 2006). The latter is based on the finding that the n-alkanes nC_{27} and nC_{29} dominate in most modern trees and shrubs, whereas nC_{31} and nC_{33} dominate in grasses.

n-Alkanes can be easily extracted from dried and grin-ded plant (~0.5 g) or sediment samples (up to 150 g) with accelerated solvent extraction (ASE) or Soxhlet systems (e.g. Wiesenberg et al. 2004). In the method described for instance by Zech & Glaser (2008), an azeotropic methanol/toluene mixture (7/3) is used as solvent and deuterated n-tetracosane (d_{50}-n-C_{24}) as internal standard. The extracts are concentrated and co-eluted esters are saponified with 0.5M KOH in methanol. Purification of the n-alkane fraction is performed on aluminium oxide/silica gel columns (both 5% deactivated) with hexane/toluene (85:15) as eluent. After concentration of the hydrocarbon fraction using rotary evaporation, deuterated n-eicosane (d_{42}-n-C_{20}) is added as recovery standard and the n-alkanes are quantified by injection into an HP 6890 GC equipped with a flame ionization detector (FID). Fig. 4 illustrates exemplarily a GC-FID n-alkane chromatogram for a loess sample from the 'Crvenka' LPS, Serbia.

Although the n-alkane biomarker method itself is known already for many decades, it is applied to LPS only relatively recently (Liu & Huang 2005; Zhang et al. 2006; Bai et al. 2009). Zech et al. (2008a) pointed out that the n-alkane patterns change over time and that a correction procedure is necessary to account for this degradation effect and to avoid deceptive interpretations when reconstructing vege-tation changes from sedimentary n-alkanes. Two correction proce-

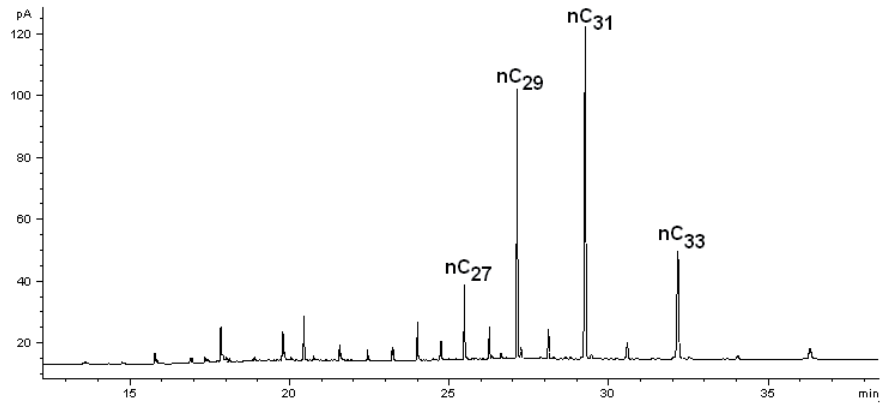

Fig. 4: GC-FID n-alkane chromatogram for a loess sample from Crvenka, Serbia. The highest abundance of nC_{31} indicates a former vegetation cover dominated by grasses; the relatively higher abundance of nC_{27}, nC_{29}, nC_{31} and nC_{33} compared to nC_{26}, nC_{28}, nC_{30} and nC_{32} is called odd-over-even predominance (OEP) and indicates little degradation.

Abb. 4: GC-FID n-Alkan-Chromatogramm für eine Lössprobe aus dem Profil Crvenka, Serbia. Die Dominanz des Alkans nC_{31} belegt, dass die frühere Vegetation überwiegend aus Gräsern bestand; das stärkere Auftreten von nC_{27}, nC_{29}, nC_{31} und nC_{33} verglichen mit nC_{26}, nC_{28}, nC_{30} und nC_{32} bezeichnet man als odd-over-even predominance (OEP) und ist charakteristisch für wenig stark degradiertest pflanzliches Ausgangsmaterial.

dures have meanwhile been suggested, both of which employ the odd over even predominance (OEP) as degradation index (Zech et al. 2009a; Buggle et al. 2010).

Case study: Vegetation reconstruction in the Carpathian Basin

Based on pollen findings it is widely assumed that tree-less tundra expanded vast areas of Europe during glacial periods. For the Carpathian Basin, this traditional paradigm of treeless full glacial (stadial) paleoenvironments has first been called into question by fossil charcoal and malacological evidence from Hungarian LPSs (Willis et al. 2000; Rudner & Sümegi 2001). The studies of Schatz et al. (2011) and Zech et al. (2009a) were initiated to contribute to the discussion about "trees or no trees?" (Willis & Andel 2004) from an n-alkane biomarker perspective. In order to estimate the percentage contribution of n-alkanes (trees versus grasses) to the Crvenka LPS in Northern Serbia, Zech et al. (2009a) proposed an end member modelling approach based on modern reference samples. This approach is illustrated exemplarily for the n-alkane ratio $(nC_{31}+nC_{33})/(nC_{27}+nC_{29})$ in Fig. 5A. The results, taking degradation effects into account, allowed the authors to infer that grasses always dominated during the whole last glacial cycle, but that a small contribution of trees is likely during the glacial periods and the Holocene. Note that the accuracy of the n-alkane biomarker method is limited by the scattering of the modern datasets for grasslands and forests (Fig. 5A). This large interspecie variability can be attributed for instance to leaf and needle aging (Prügel et al. 1994) or to environmental stress (Shepherd & Griffiths 2006). Fig. 5B illustrates that this can result in 'negative' tree cover percentages. Yet the modelling results for several relevant n-alkane ratios [$(nC_{31}+nC_{33})/(nC_{27}+nC_{29})$, nC_{31}/nC_{27}, nC_{33}/nC_{27}, and nC_{31}/nC_{29})] all reveal very similar and systematic shifts, which increases the confidence that degradation-corrected n-alkane patterns can be used to reconstruct past changes in vegetation. Accordingly, the n-alkane biomarker results of both Schatz et al. (2011) and Zech et al. (2009a) provide additional evidence challenging the paradigm of treeless full glacial paleoenvironments.

The reliability of n-alkanes as well as most other biomarkers as proxies in loess-paleosol sequences depends on the absence of strong post-sedimentary overprinting of the original organic matter signal. We highly acknowledge efforts aiming at quantifying such effects and point to studies published by Gocke et al. (2010) for rhizoliths in loess. The authors found that the n-alkane patterns of rhizolith organic matter are dominated by nC_{31} (Gocke et al. 2010, Fig. 6), Although this is not typical for above-ground lipids from most trees and shrubs but for grasses, the authors favor post-sedimentary incorporation of root-derived orga-nic matter in loess. Further studies should therefore firstly address n-alkane concentrations in roots as the latter are assumed to be very low compared to above-ground litter; secondly, datasets for modern reference n-alkane patterns from roots, lacking so far, should be established. And thirdly, we

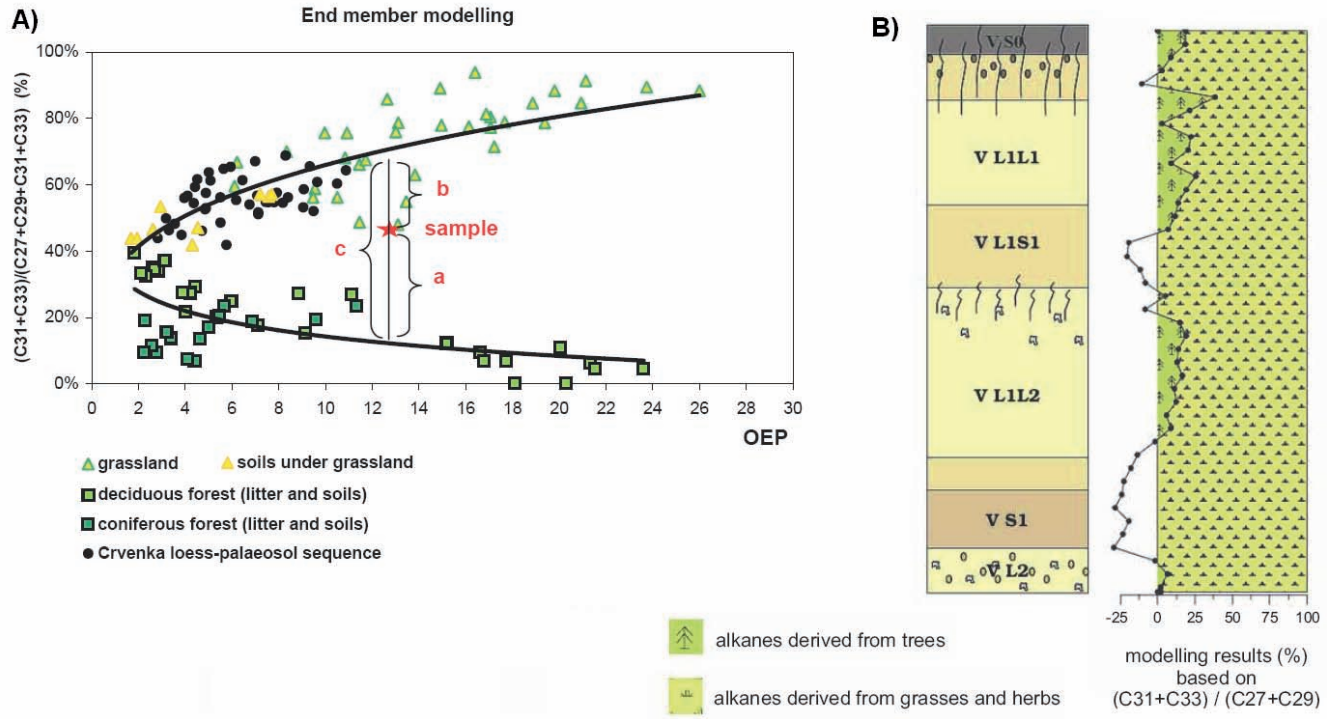

Fig. 5: A) End member modelling approach for the n-alkane ratio $(nC_{31}+nC_{33})/(nC_{27}+nC_{29})$. Based on modern plant and soil n-alkane ratios, degradation lines are calculated using the OEPs as degradation proxy. The percentage of trees and grasses contributing to a loess-paleosol sample is estimated by the quotients b/c and a/c, respectively. B) Pedostratigraphy of the Crvenka LPS in Northern Serbia and modelling results for the contribution of tress and grasses (adopted from Zech et al. 2009a).

Abb. 5: A) End Member Modell für das n-Alkanverhältnis $(nC_{31}+nC_{33})/(nC_{27}+nC_{29})$. Basierend auf n-Alkanverhältnissen von rezenten Pflanzen und Böden werden Degradationslinien ermittelt. Die OEP-Werte dienen dabei als Proxy für den Degradationsgrad. Die Anteile von Baum- bzw. Gras-n-Alkanen zu einer LPS-Probe lassen sich anhand der Quotienten b/c bzw. a/c abschätzen. B) Pedostratigraphie der LPS Crvenka in Nordserbien und Modellierungs-Ergebnisse für die Anteile von Bäumen im Vergleich zu Gräsern (aus Zech et al. 2009a).

highly encourage further investigations especially applying compound-specific ^{14}C-dating of different biomarkers in LPS for which independent and high resolution luminescence dating of the sedimentary history is available.

3.2 Amino acid racemization

Amino acids, mainly bound in proteins, constitute an important N-pool in soils (Amelung 2003). They are no bio-markers *sensu strictu*, because they do not originate from specific organisms. However, they may provide valuable insights in the aging of soil organic matter (SOM) and past temperatures. Amino acids contain a chiral C-atom, and they can therefore occur either in the left-handed form (L-enantiomer) or in the right-handed form (D-enantiomer). Living organisms primarily produce L-amino acids, but the D-enantiomers are then formed during racemization – an abiotic process that is mainly time-, temperature- and pH-dependent (Bada 1985) (Fig. 6). It has therefore been suggested that D/L-ratios of amino acids can be used for dating. Mahaney & Rutter (1989), for instance, found the D/L-ratio of aspartic acid to be a suitable geochronometer in buried soils. For the last 15 years, amino acid geochronology in loess research was mainly based on measuring the ratio alloisoleucine/isoleucine in fossil gastropod shells and was successfully used to distinguish between loess from different glacial cycles (Zöller et al. 1994; Oches & McCoy 2001; Novothny et al. 2009). Principally, of course, amino acid racemization could also be used to reconstruct paleotemperatures, but independent age control needs to be available, and such applications are very rare so far (Kaufman 2003).

Most geochronological studies have focussed on amino acids in fossil gastropod shells, based on the notion that these likely provide the best 'closed systems' available, i.e. that post-depositional amino-acid losses or contamination are minimal (Penkman et al. 2008). Amelung & Zhang (2001), however, also proposed a method for determining amino acid enantiomers in bulk soil samples. Sample preparation comprises pre-extraction of free and water-soluble amino acids, hydrolysis of protein-bound amino acids, purification over columns (Dowex W X8), and derivatization. Quantification is carried out using GC-MS. As racemization is known to be catalysed by low pH and high temperatures, conditions that are also applied during hydrolysis, Amelung & Brodowski (2002) quantified the hydrolysis-induced racemization using deuterium labelling. They show that less than 10% of D-Asp and D-Lys were formed during the analytical procedure in environmental samples older than 3000 years. Hence, Amelung (2003) suggested that aspartic acid (asp) and lysine (lys) are the most suitable amino acids for dating purposes in soils.

Case study: Temperature reconstruction in Siberia

Zech et al. (2008b) applied the method of Amelung & Zhang (2001) to 10 selected samples from a Siberian permafrost LPS ('Tumara'), which probably comprises the last two glacial cycles. For details concerning the (chrono-) stratigraphy, the geochemical, the isotopic and the biomarker characterization of this sequence the reader is referred to Zech et al. (2007; 2008b; 2010a). In brief, dark organic-rich paleosols alternate with brown and more intensively mineralised and weathered paleosols (Fig. 7). Based on numeric dating results and a multi-proxy approach, the dark units B, C2 and D are correlated with glacial periods, whereas the brown units A, C1, C2 and E are correlated with interglacial/-stadial periods. The D/L ratios obtained for aspartic acid (asp) and lysine (lys) are plotted versus depth in Fig. 7 and can be roughly described by exponential fits. In addition, the brown units are generally characterized by higher ratios than the dark grey units. Nevertheless, D/L ratios overall increase with depth and reveal that the apparent racemization rates are smaller for lysine than for aspartic acid (the latter having higher D/L ratios). This is in agreement with findings from Amelung (2003), who furthermore emphasised that lysine racemization rates are more or less constant in different soil types. Given that the soil pH reveals only minor variations ranging from 7 to 8 throughout the whole profile, temperature and time can be assumed to be the main factors controlling the

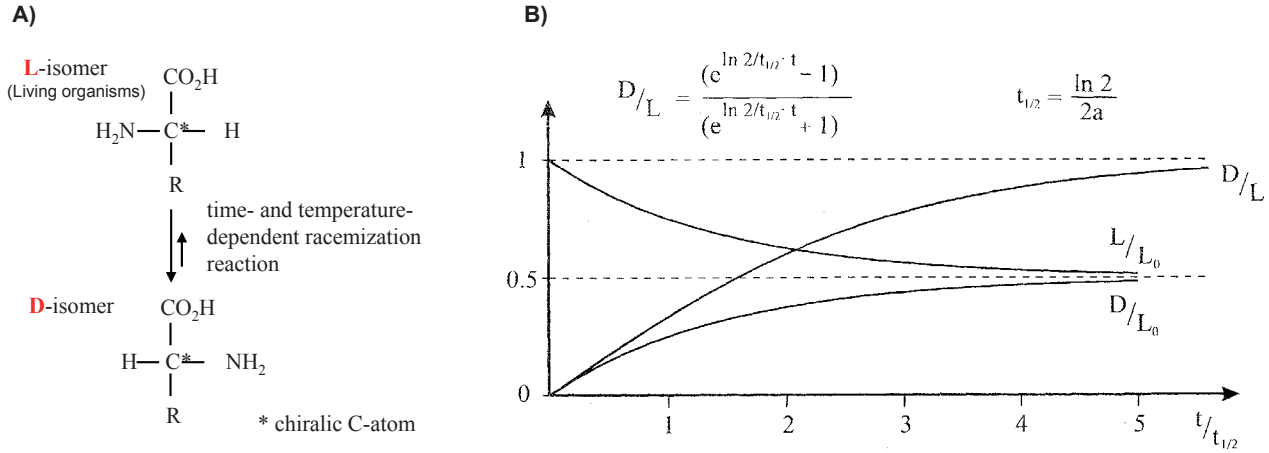

Fig. 6: Principle of amino acid geochronology: A) Time- and temperature-dependent racemization reaction. B) Exponential functions describing the time-dependency of racemization; t1/2 = half-life time, L0 = initial amount of L-enantiomers, D/L = ratio of D- to L-enantiomers (from Wagner 1998, p. 342, Fig. 142).

Abb. 6: Prinzip der Aminosäure-Geochronology: A) Die zeit- und temperaturabhängige Gleichgewichtsreaktion der Razemisierung. B) Exponentielle Funktionen die die Zeitabhängigkeit der Razemisierung beschreiben; t1/2 = Halbwertszeit, L0 = Anfangsgehalt des L-Enantiomers, D/L = Verhältnis von D- zu L-Enantiomeren (aus Wagner 1998, Seite 342, Abb. 142).

amino acid racemization. Consequently, Zech et al. (2008b) suggest that the higher D/L ratios that characterize the brown Units A, C1 and C3 are primarily the result of higher temperatures during formation of the respective paleosols.

Based on these results, we see high potential for the amino acid racemization method to provide a paleotemperature proxy in LPS. A high sampling resolution might also help depicting sedimentary hiatuses, which should yield abrupt increases of the D/L ratios with depth. Unfortunately, the described method is relatively laborious and will require some further optimisation, particularly for the application to organic-poor loess samples. An important step would probably be already made when using a HPLC instead of a GC system, because that will supersede the derivatization step.

3.3 GDGTs

Over the last few years, several new proxies have been proposed based on GDGTs (Fig. 8), membrane lipids of Archaea and Bacteria. The exact chemical composition of the GDGTs is thought to reflect adjustments of membrane permeability and fluidity to environmental conditions (e.g. pH and temperature). Thus the analyzes of GDGTs may offer interesting, new approaches to quantitatively reconstruct past climate and environmental variability from various geological archives. The TEX_{86}, for example, is a new paleotemperature proxy based on the cyclicity of isoprenoid GDGTs, which are mainly derived from Archaea living in oceans and lakes (Schouten et al. 2002; Kim et al. 2008; Powers et al. 2010). Although it has meanwhile been found that isoprenoid

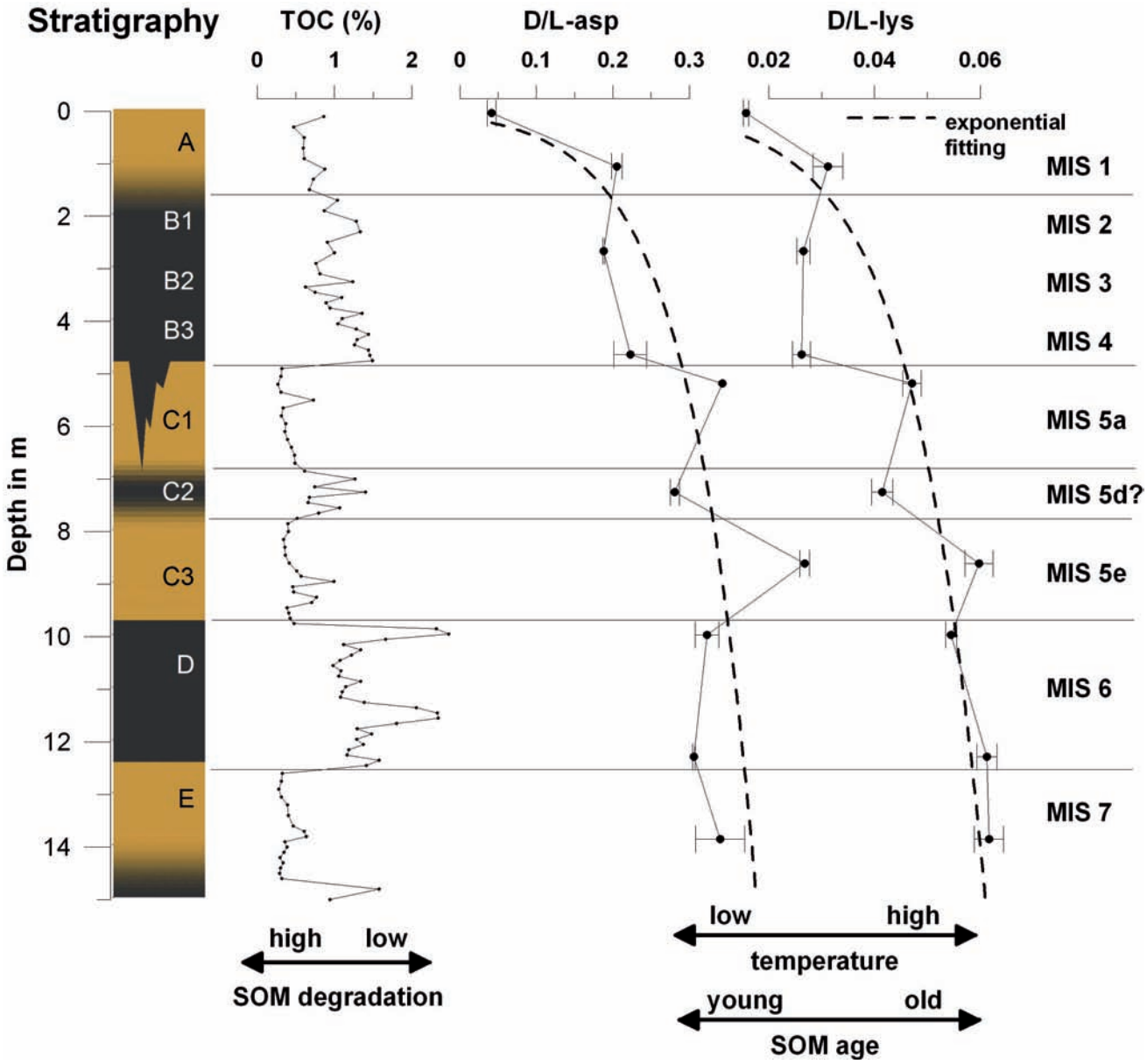

Fig. 7: Stratigraphy and tentative chronostratigraphy of the Tumara LPS, NE-Siberia. D/L-ratios for Asp and Lys increase with depth, reflecting the time dependency of the racemization. Higher ratios in the brown units compared to lower ratios in the dark units are suggested to reflect the temperature dependency of amino acid racemization (from Zech et al. 2008b).

Abb. 7: Stratigraphie und Chronostratigraphie der LPS Tumara, NO-Sibirien. D/L-Verhältnisse für Asp and Lys werden mit zunehmender Tiefe weiter. Dies spiegelt die Zeitabhängigkeit der Razemisierung wider. Weitere Verhältnisse in den braunen Paläoböden verglichen mit den dunklen Paläoböden lassen sich mit der Temperaturabhängigkeit der Razemisierung erklären (aus Zech et al. 2008b).

E&G / Vol. 60 / No. 1 / 2011 / 170–187 / DOI 10.3285/eg.60.1.12

GDGTs also occur in soils, another proxy, the BIT (branched versus isoprenoid GDGTs), has been suggested to allow the quantification of terrestrial versus autochthonous organic matter in lacustrine and marine sediments (Schouten et al. 2002). This index is further based on the original assumption that branched GDGTs are only derived from soil-thriving bacteria. Meanwhile, however, it has been found that branched GDGTs are also produced within the water column of oceans and lakes (Blaga et al. 2009; Peterse et al. 2009a; Bechtel et al. 2010; Tierney et al. 2010), which warrants caution when interpreting the BIT and TEX_{86} indices.

The branched GDGTs, which are presumably derived from yet unknown anaerobic, heterotrophic soil bacteria (Weijers et al. 2010), may be promising biomarkers for loess-paleosols research. An empirical study based on 134 soil samples from 90 globally distributed locations has shown that branched GDGTs vary in their degree of cyc-lisation and methylation (expressed as CBT and MBT, i.e. cyclisation and methylation index of branched tetraethers) depending on soil pH (R^2 = 0.70) and mean annual air temperature (MAAT, R^2 = 0.82) (Weijers et al. 2007). Local calibration studies along altitudinal transects at Mt. Kilimanjaro, Tanzania, and Mt. Gongga, China, have meanwhile corroborated the suggested pH and temperature dependency of the CBT/MBT indices (Schouten et al. 2002; Peterse et al. 2009b). The analysis of branched GDGTs in lake and ocean sediments might therefore provide a valuable, new proxy for catchment-wide pH and MAAT reconstructions, provided that they are derived from eroded soils only. As mentioned above, however, there is evidence that branched GDGTs are also produced autochthonously in lakes and oceans, which prevents robust interpretation of the CBT and MBT indices in respective studies thus far. Surpri-singly, to our knowledge, no studies have been published yet applying the CBT/MBT indices for paleoenvironmental reconstructions in loess-paleosols.

The analysis of GDGTs comprises (i) lipid extraction from typically freeze-dried soil or sediment samples (5–50 g depending on abundance), (ii) separation into the apolar and polar (containing the GDGTs) fraction over a Al_2O_3 column using e.g. hexane:dichloromethane (DCM) (9:1) and DCM:Methanol (1:1), and (iii) filtering, prior to quantification of the various GDGTs by HPLC/atmospheric pressure chemical ionization-mass spectrometry (APCI-MS). So-called selective ion monitoring allows detecting specific molecular masses, i.e. specific GDGT molecules (Fig. 8).

Case studies: Application of GDGT indices to the Tumara LPS, Siberia, and Crvenka LPS, Serbia

The first case study presents GDGT results from the Tumara LPS (Fig. 9). The BIT indices are generally high (>0.84), which is in agreement with the notion that branched GDGTs are mainly derived from soil-thriving

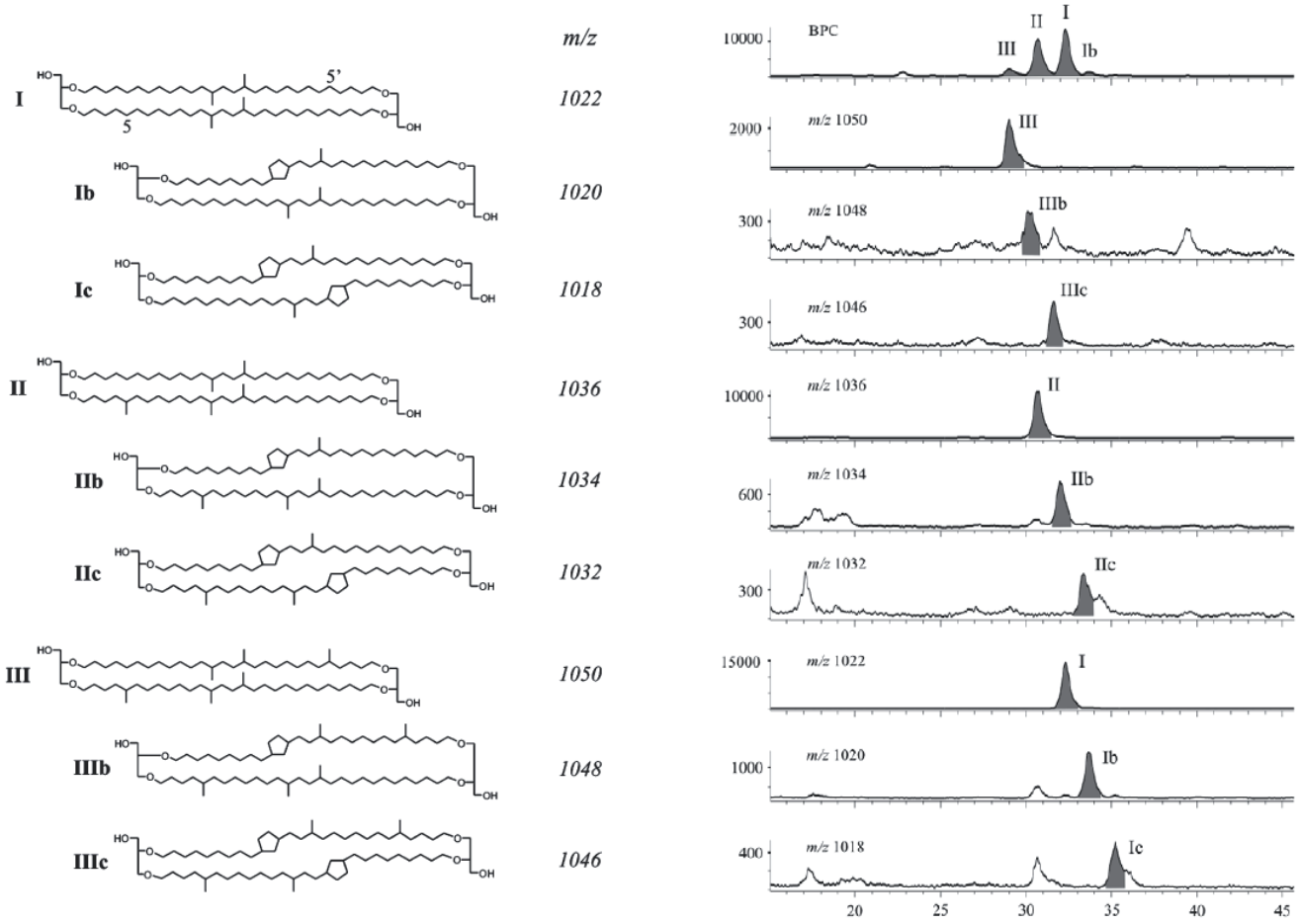

Fig. 8: Chemical structures of the branched GDGTs (left), and total and selective ion mass [M+H]+ chromatograms for a soil sample (modified after Weijers et al. 2007).

Abb. 8: Chemische Strukturen für verzweigte GDGTs (links), und Chromatogramme für die Gesamtmasse bzw. einzelner Massen [M+H]+ für eine Bodenprobe (abgeändert nach Weijers et al. 2007).

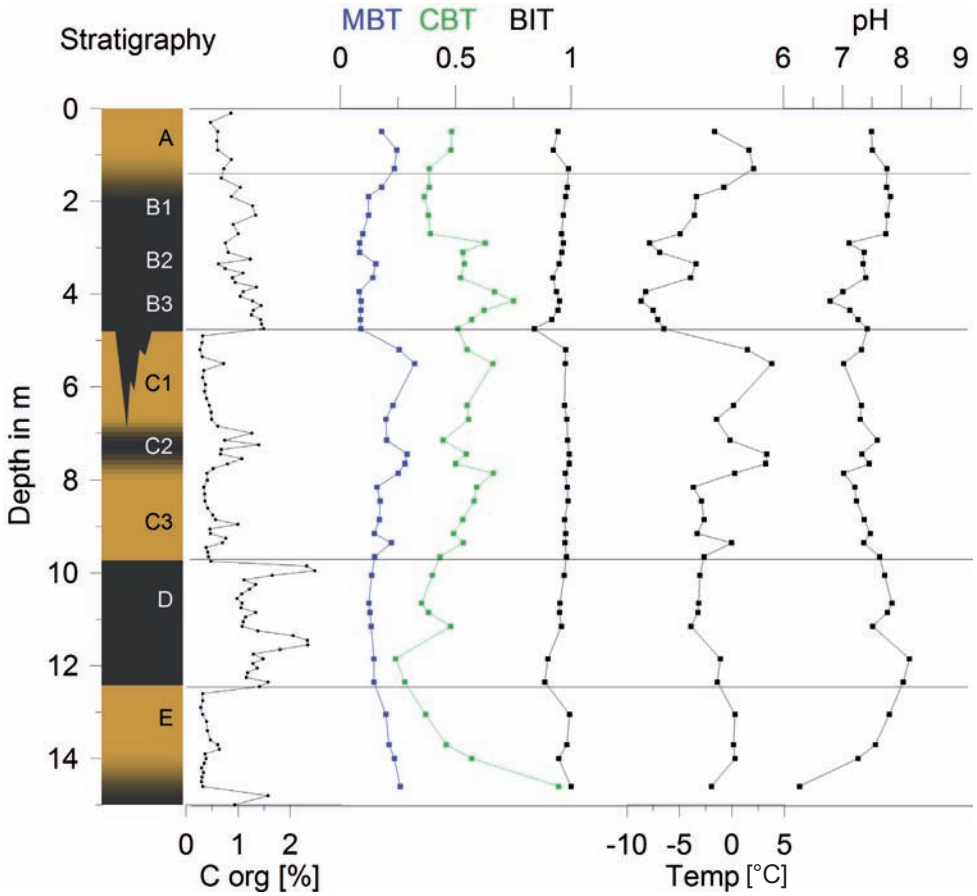

Fig. 9: Pedostratigraphy of the Tumara LPS, NE-Siberia, GDGT indices MBT, CBT and BIT, and reconstructed temperatures and soil pH. While the reconstructed relative interglacial-glacial temperature variability in the upper 7 m of the profile is in agreement with the expected temperature variability derived from the chronostratigraphy, reconstructed temperatures for the presumably penultimate glacial Unit D seem to be too high.

Abb. 9: Pedostratigraphie der LPS Tumara, NO-Sibirien, GDGT Kennzahlen MBT, CBT und BIT, sowie die rekonstruierten Temperaturen und Boden pH-Werte. Während die rekonstruierten relativen interglazial-glazial Temperaturschwankungen in den oberen 7 Metern des Profils der Chronostratigraphie übereinstimmen, scheinen die rekonstruierten Termperaturen im vorherigen, älteren Glazial zu hoch zu sein.

bacteria. The MBT indices range from 0.08 to 0.32, and the CBT ranges from 0.24 to 0.95. This translates into reconstructed MAAT between -8.7 and 3.8℃, and soil pH between 6.3 and 8.1.

Replicate measurements of a soil standard ("Yongsong's garden") throughout the course of the measurements indicate laboratory precision of 0.2℃ for MAAT, and 0.01 for pH. However, much higher uncertainties regarding the accuracy of the reconstructed parameters may arise for several reasons:

(i) The reconstructed temperatures for the Tumara LPS are partly well below 0℃ and thus beyond the lowest values in the global calibration data set. Although a recent study in Svalbard indicates that mean annual air temperatures below 0℃ may be successfully reconstructed using branched GDGTs (Peterse et al. 2009a), comparison of our uppermost sample (-1.7℃) with estimated MAAT of ~-15℃ suggests a significant positive bias. At this stage, we can only speculate that the observed discrepancy might be due to seasonal (summer) growth of the soil bacteria, differences between MAAT and soil temperatures, or other unknown methodological shortcomings.

(ii) Analytical challenges regarding the new proxies have become evident, because one of the target compounds (m/z 1050, III in Fig. 10a), which is generally characterized by a minor "contamination" shoulder on the right side, turned out to be dominated by that "contamination" (compound III, probably an isomer of III (Weijers et al. 2010)). When coupling two HPLC columns to achieve better peak separation, it is possible to quantify the two compounds individually (Fig. 10b, Y. Huang, pers. comm.). However, no calibration studies are available yet that take the separated compounds into account. Moreover, other target peaks also turned out to consist of multiple, yet unidentified compounds. Clearly, further research is necessary to improve compound separation and identification.

(iii) There are two other effects that might constrain the applicability of GDGT-based reconstructions in loess-paleosols, which we refer to here as "changing community effect" and "growth depth effect": The first one addresses the possibility that changes in the GDGT-producing bacterial communities could result in changes in the structural composition of the membrane lipids without necessarily reflecting changes in environmental conditions. In that sense, as long as the GDGT-producing organisms are not identified, cultured and tested individually, we have to rely on empirical calibration studies as they exist today even if they do not fully capture all possible factor affecting GDGD distributions.

The "growth depth effect" has to do with the fact that we

E&G / Vol. 60 / No. 1 / 2011 / 170–187 / DOI 10.3285/eg.60.1.12

still know very little about the soil bacteria's ecology, including for example the soil depth at which the bacteria thrive and produce GDGTs. A non-negligible subsurface production of GDGTs could thus result in an overprint of 'older' paleo-environmental signals at depth. The growth depth effect might limit the temporal resolution of reconstructions, mute the variability of the real signal, and render 'absolute' reconstructions very challenging from loess-paleosols LPS.

With these methodological limitations in mind, the interpretation of paleo-data should be very cautious. Our first case study from Siberia shows that Unit A and C, which were most likely deposited during the Holocene and the Eemian, respectively, are characterized by higher reconstructed temperatures than the glacial Unit B (Fig. 9). Although the absolute MAAT are likely overestimated systematically, the glacial-interglacial temperature difference of ~10°C is reasonable. One could also speculate that the last glacial pattern is real, with coldest conditions during Marine Isotope Stage (MIS) 2 and 4 and slightly warmer conditions during MIS3. Surprising features, however, are (i) relatively warm conditions during MIS2 compared to MIS4, (ii) Unit C not displaying a commonly expected temperature peak maximum for MIS5e (Unit C3, Fig. 9), and (iii) 'too warm' reconstructed temperatures for the penultimate glacial Unit D. Provided that the presented chronostratigraphy of the Tumara LPS is correct, our results suggest that the growth depth effect might have overprinted and muted the paleo-signals, i.e. warm conditions during the Holocene are now overprinting the cold MIS2 signal, and the very warm conditions during the Eemian have allowed GDGT-producing bacteria at depth to strongly affect the record below 5 m depth.

In our second case study for GDGTs, unpublished data from the Crvenka LPS (Fig. 11), pose similar challenges to a robust interpretation of GDGT indices. Here, the topsoil samples show reconstructed MAAT of ~15°C, which is in reasonable agreement with estimated MAAT of 11°C, although with a slight bias to too high temperatures. Subsurface samples reach 20°C reconstructed temperatures, which might indeed reflect warmer conditions during the mid-Holocene optimum. However, reconstructed temperatures remain very high in the underlying MIS2 loess (V L1L1). As above, we speculate that this might reflect that GDGTs were produced during the Holocene at depth and thus overprinted the cold, glacial signal. While reconstructed temperatures drop to values as low as ~4°C deeper in the profile, which would be reasonable in terms of expected glacial-interglacial temperature variability, reconstructed lowest temperatures also characterize the interglacial Eemian paleosol V S1, although the latter should be characterized by highest temperatures. Is this again due to the growth depth effect? Or does this indicate other methodological shortcomings that are not yet fully understood?

In summary, we advise caution when interpreting GDGT-derived proxies from LPS. GDGT analyzes are a promising new tool for paleoclimate reconstruction, but there are many yet unresolved questions that need to be addressed before robust conclusions can be inferred from respective proxies.

3.4 Compound-specific δD-analyzes of n-alkanes

As discussed earlier, both δD and $\delta^{18}O$ have a high potential for paleoclimatic reconstructions. Albeit with certain biosynthetic fractionation factors, plant photosynthetic products incorporate the isotopic climate signal of precipitation, because their δD values are related to the source water δD values (Sternberg 1988; Sessions et al. 1999; Sauer et al. 2001; Sachse et al. 2004). During soil organic matter formation, this climate signal is also inherited by soils. However, changing soil organic matter pool sizes (e.g. lipids, lignin, cellulose) and isotopic exchange reactions in soils and sediments have prevented the simple use of bulk analyzes (Balabane 1983).

One approach to overcome at least the latter problem is to equilibrate bulk samples in water with known isotopic composition, and then to correct for the exchange reactions after bulk measurements via TC/EA-IRMS (Ruppenthal et al. 2010). Yet technical improvements now also allow a more elegant and more specific approach, namely determining the isotopic composition of individual biomarkers by coupling

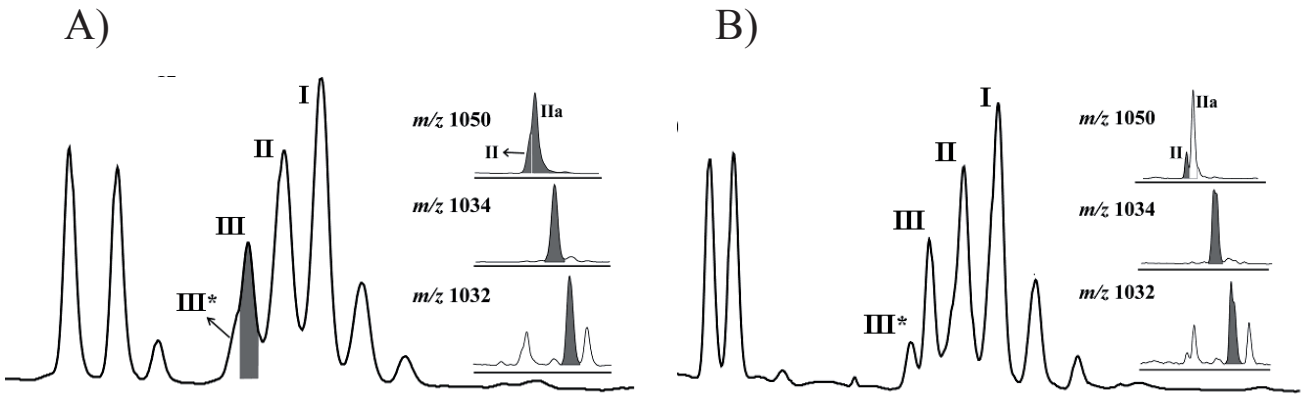

Fig. 10: Total ion chromatogram of one of the Siberian samples, illustrating the existence of two isomers III and III for m/z 1050. A) Standard chromatogram and B) chromatogram with improved peak separation.*

Abb. 10: Beispiel für ein HPLC Chromatogramm der siberischen Proben. Es zeigt das Vorhandensein von zwei Isomeren mit der Massenzahl m/z 1050 (III und III). A) Standardchromatogramm und B) Chromatogramm mit verbesserter Peak-Trennung.*

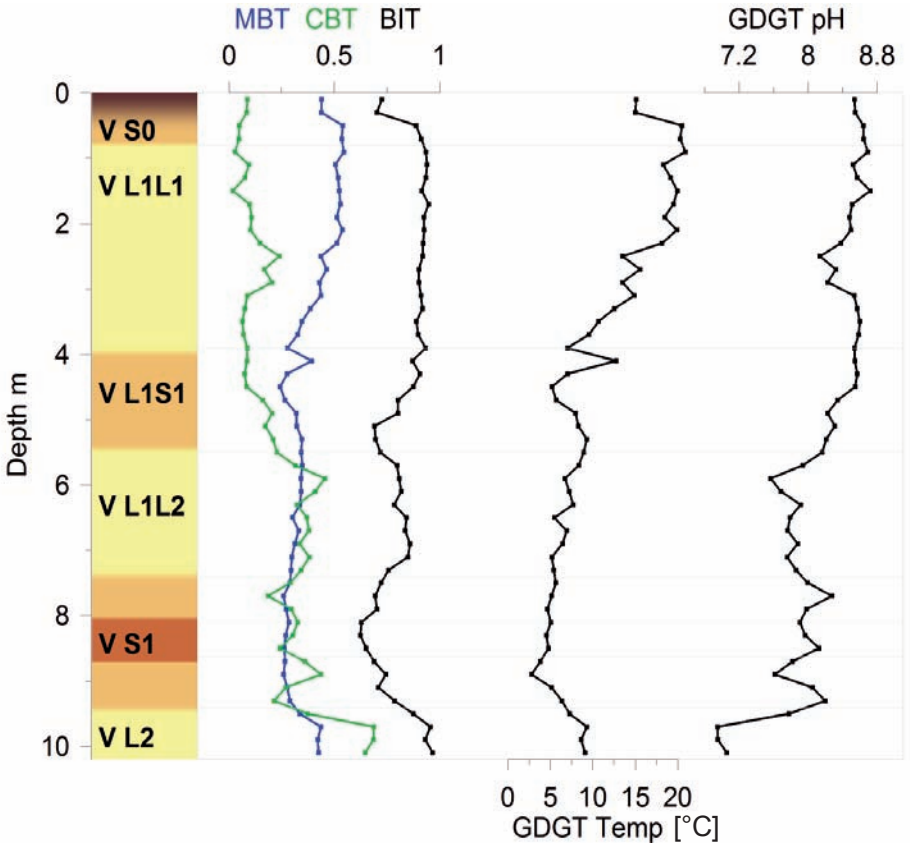

Fig. 11: Pedostratigraphy of the Crvenka LPS in Northern Serbia, GDGT indices MBT, CBT and BIT, and reconstructed temperatures and soil pH. Similar to the Tumara LPS, reconstructed GDGT temperatures are not always in agreement with what can be expected from the chronostratigraphy, e.g. lowest reconstructed temperatures coincide with the presumably last interglacial Eemian soil V S1. Possibly, the "growth depth effect" prevents a simple interpretation of GDGT proxies in LPSs.

Abb. 11: Pedostratigraphie der LPS Crvenka in Nordserbien, GDGT Kennzahlen MBT, CBT und BIT, und rekonstruierte Temperaturen und Boden pH-Werte. Ähnlich wie bei der LPS Tumara, stimmen die rekonstruierten GDGT-Temperaturen nicht immer mit der Chronostratigraphie überein. Insbesondere überraschen die für den vermutlich letzt-interglazialen Eemboden V S1 rekonstruierten niedrigen Temperaturen. Eine einfache Interpretation der neuen Proxies in LPS ist möglicherweise durch das Wachstum von GDGT-produzierenden Archaebakterien in tieferen Bodenschichten erschwert.

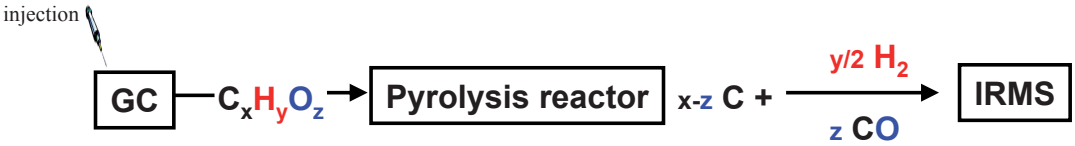

Fig. 12: Principle of compound-specific δD- and $\delta^{18}O$-analysis of biomarkers using GC-Py-IRMS. Biomarkers eluting successively from the GC-column are converted "online" in a pyrolysis reactor to hydrogen (H_2) and carbon monoxide (CO) and the isotopic composition of these gases are determined directly in a coupled IRMS.

Abb. 12: Prinzip der substanz-spezifischen δD- und $\delta^{18}O$-Analytik von Biomarkern mittels GC-Py-IRMS. Die nacheinander von der GC-Säule eluierenden Biomarker werden im 'online' Verfahren in einem Pyrolysreaktor in Wasserstoff- (H_2) und Kohlenmonoxid-Gas (CO) umgewandelt. Die Isotopenzusammensetzung dieser Gase wird in einem direkt gekoppelten IRMS gemessen.

of GC and IRMS via an 'online' pyrolysis reactor (Py) (Burgoyne & Hayes 1998; Hilkert et al. 1999) (Fig. 12)

With this new tool at hand, compound-specific δD became a popular paleoclimate proxy (Liu et al. 1999; Huang et al. 2004; Sachse et al. 2004; Xie et al. 2004; Pagani et al. 2006; Mügler et al. 2008). Plant-derived *n*-alkanes are probably the most useful biomarkers to target, because they are well-preserved in sediments and soils (Lichtfouse et al. 1998), and because their alkyl hydrogen atoms are less prone to exchange reactions compared to other biomarkers (Sessions et al. 2004; Pedentchouk et al. 2006; Dawson et al. 2007).

Of course, ultimately, one has to take into account that evaporative enrichment of soil and plant water, as well as biosynthetic fractionation are also important factors controlling the isotopic signature of the targeted biomarker (Schmidt et al. 2001; Liu et al. 2006; Smith & Freeman 2006; Barbour 2007; Hou et al. 2007; Feakins & Sessions 2010).

Two case studies: Paleoclimate reconstructions from Tumara and Crvenka

To our knowledge, the first and only application of compound-specific δD analyzes of n-alkanes to a LPS was carried out by Liu & Huang (2005) on the Chinese Loess Plateau. We will here present two case studies based on own data to illustrate the methodological potentials and limitations. The first case study aimed at more quantitative temperature reconstruction for the Tumara LPS in Northeast Siberia (Zech et al. 2010b). The δD records of all three n-alkanes that had sufficient concentration for the δD measurements (nC_{27}, $_{29}$ and $_{31}$) show very similar patterns along the ~240 ka profile (Fig. 13). The authors therefore concluded that vegetation changes, which have been reconstructed for Tumara employing n-alkane patterns and pollen analyzes (Zech et al. 2010a) did not play a dominant role for the isotopic signal. The mean δD record can thus be interpreted to reflect past changes in the isotopic composition of soil water, which in turn dominantly reflects temperature at high latitudes. More negative values (-280‰) characterize the organic-rich Units B, C2 and D, which confirms our earlier interpretation that those units were deposited during cold, glacial conditions. More positive values (>-250‰) characterize the Units A, C1, C3 and E, which is in agreement with deposition during warm, interglacial periods.

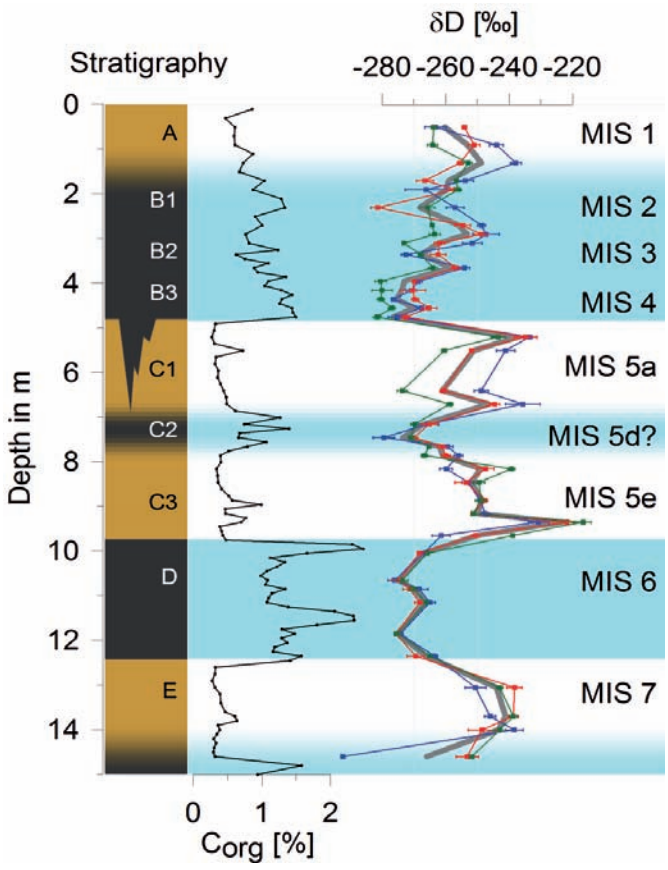

Fig. 13. Stratigraphy, organic carbon content (C_{org}) and δD measured on the n-alkanes nC_{27}, nC_{29} and nC_{31} (in blue, red and green; the mean value is displayed in grey) from the Tumara LPS. More negative δD-values are interpreted to reflect colder paleotemperatures. Correlation with marine isotope stages (MIS) is shown to the right (Zech et al. 2010b).

Abb. 13. Stratigraphie, organischer Kohlenstoffgehalt (C_{org}) und ermittelte δD-Werte für die n-Alkane nC_{27}, nC_{29} und nC_{31} (in blau, rot und grün; Mittelwerte in grau) der LPS Tumara. Stärker negative δD-Werte lassen sich mit kälteren Paläotemperaturen erklären. Die Korrelation mit den Marinen Isotopen Stadien (MIS) ist rechts dargestellt (aus Zech et al. 2010b).

Zech et al. (2010b) note that a correction could be applied for the fact that the glacial oceans and thus precipitation became more positive (~8‰, the global ice volume effect). This would increase the glacial-interglacial differences in the investigated record, but would require a more robust age control than the one being at hand. Another cautionary note is that changing evaporation might also have affected the presented record. Zech et al. (2010b) suggested that evaporation effects are probably only of second-order importance at this site because of the low temperatures. Assuming that evaporation had a measurable effect, it should have led to isotopic enrichment during the more arid glacial periods. This might in fact explain the slightly smaller glacial-interglacial range in δD (~30‰) compared to respective ranges in ice core records (up to 50‰).

Our second case study presents unpublished δD data for Crvenka. The n-alkanes C_{29} and $_{31}$ were most abundant in the samples and therefore targeted for the δD measurements. Overall, the two records mostly track each other reasonably well (Fig. 14), although the measurement precision of 3.1 and 2.9‰ for the external standards nC_{27} and C_{29}, respectively (run during the course of the whole measurement period), as well as mean standard deviations of 1.5 and 1.2‰ for the triplicate measurements of the samples indicate that some of the differences between δD C^{29} and C^{31} may be real. One may speculate that C^{29} and C^{31} derive proportionally from distinct plant species being to a greater or lesser extent sensitive to evaporative δD enrichment. However, for the purpose of this review, we will discuss primarily the broad, common patterns ('δD mean' in Fig. 14).

The first feature we would like to draw the attention to is the ~10‰ drop in δD from the Holocene (~-200‰) to the MIS2 loess V L1L1. As above, correction for the global ice volume effect would increase this difference, but still the difference is much less than what one would expect from a high to mid-latitude temperature signal alone. For compa-rison, the δD record from Vostok, Antarctica, is plotted in Fig. 14. One possible explanation might be that the soil water was isotopically enriched during glacials due to more arid conditions (or more precisely a higher ratio of evaporation to precipitation). In fact, many oxygen records from the Mediterranean region, including e.g. the Soreq and Piqiin cave speleothems in Israel (Bar-Matthews et al. 2003) show more enriched values (Fig. 14), which was originally interpreted to document more arid conditions (Roberts et al. 2008). However, doubts concerning this interpretation arose from lake level reconstructions of Lake Lisan, a glacial freshwater lake occupying the Dead Sea region (Lisker et al. 2009). As it turned out, the speleothem oxygen isotope records mainly followed the isotopic signal of the Mediterranean Sea, which serves as water source for regional precipitation and shows a pronounced enrichment during glacials (>3%) (Bar-Matthews et al. 2003; Almogi-Labin et al. 2009). This 'source effect' (translating into ~25‰ glacial-interglacial difference in δD of regional precipitation) is likely responsible for off-setting the expected temperature signal at Crvenka at least to some degree. Additionally, past changes in atmospheric circulation patterns and thus changing moisture source areas might have affected our record, though this effect is difficult to quantify.

It should be acknowledged at this point, that a detailed, robust deconvolution of all these factors is not trivial. Nevertheless, we would like to point to a second interesting feature of our record. The temperature difference between the Holocene and the Eemian basically accounts already for the differences in alkane δD. This might indicate that the Mediterranean source water effect, from which one would infer more positive isotope values during the Holocene, was offset by other factors, for example differences in aridity. If correct, this might document that the Eemian was more arid than the Holocene, an interpretation that would be in good agreement with the alkane patterns that have been used (further above) to infer more grass vegetation (steppe) during the Eemian.

We summarize that δD records from alkanes in LPS provide valuable information about past climatic and environmental changes, but that deconvolving the various factors influencing δD can be challenging. Apart from temperature, changes in precipitation, atmospheric circulation patterns and source effects should be taken into consideration.

3.5 Compound-specific $\delta^{18}O$-analyzes of monosaccharides

Similar to deuterium, the ^{18}O concentration in precipitation depends on climatic factors and therefore has high potential as paleoclimate proxy in appropriate archives. Likewise, however, bulk soil or sediment isotope analyzes using TC/EA-IRMS have the disadvantage that many different inorganic (carbonates, water from clay minerals) and organic pools contribute to the pyrolytically produced CO, which hence represents a mixed signal (see Fig. 3). Furthermore, not all oxygen pools in soils have a climate signal incorporated, as for instance oxygen in lignin does not derive from water, but from the atmosphere (Schmidt et al. 2001).

In loess research, attempts have been made to obtain $\delta^{18}O$ records from pedogenetic carbonates, mollusc shells, and crystal water in clay minerals (Kuleshov & Gavrilov 2001; Pustovoytov & Terhorst 2004). However, in contrast to carbonates from stalagmites, it is much more difficult to get well dated and continuous records, with potential recrystal-

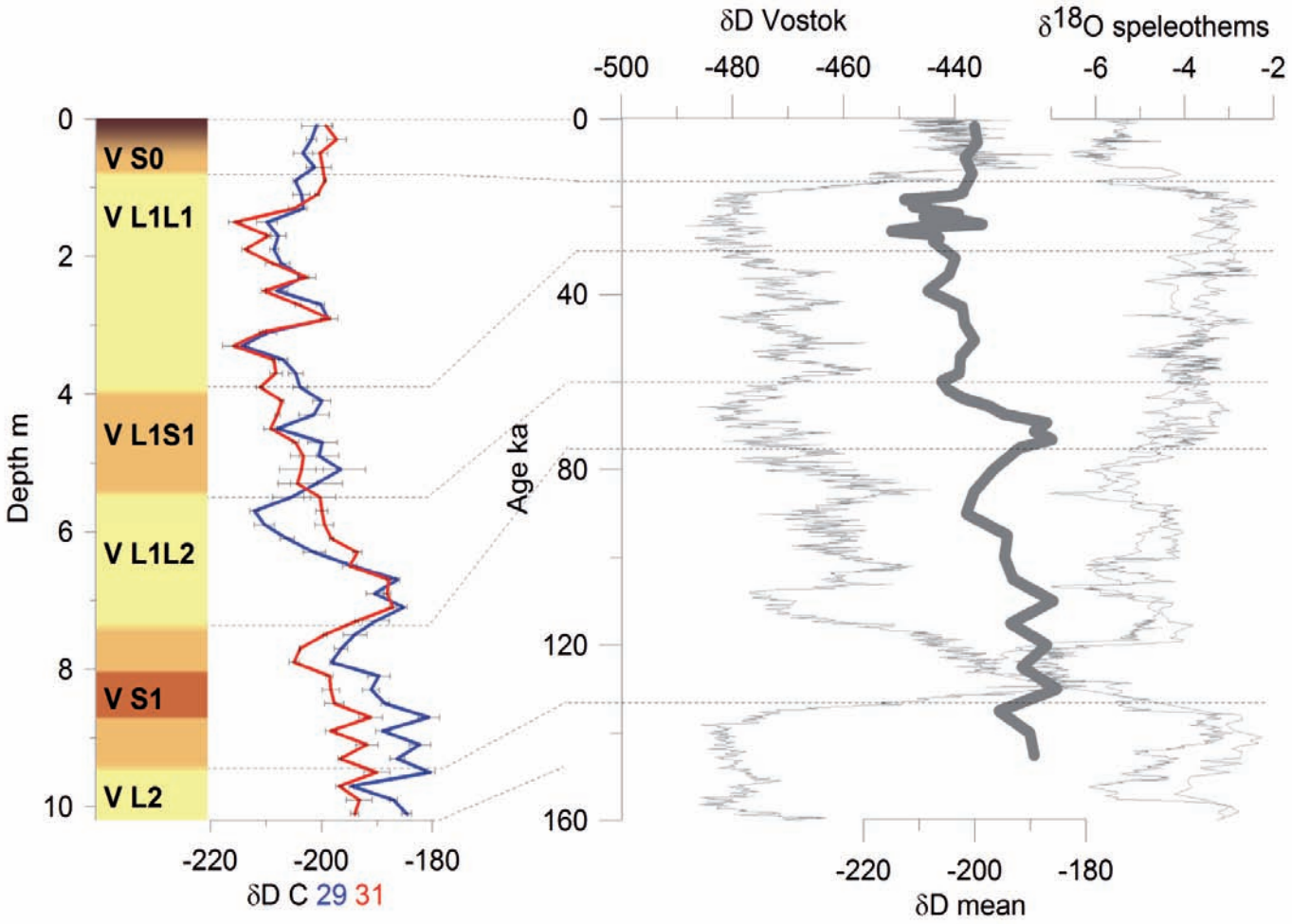

Fig. 14: Stratigraphy and δD of nC_{29} and nC_{31} from the Crvenka profile, compared to the δD record from Vostok and the $\delta^{18}O$ record from the Soreq/Piqiin speleothems (scaled to reflect respective δD changes based on the meteoric water line). Many factors, such as temperature, changes in precipitation, atmospheric circulation patterns, source effects and evaporative isotopic enrichment, need to be considered for the interpretation of the LPS δD-values.

Abb. 14: Stratigraphie und δD-Werte der n-Alkane nC_{29} und nC_{31} der LPS Crvenka. Im Vergleich dazu die δD-Kurve des Vostok Eisbohrkerns und die $\delta^{18}O$-Kurve der Soreq/Piqiin Speläothemen (umgerechnet auf entsprechende δD-Werte anhand der Meteoric Mater Line). Zahlreiche Faktoren, z.B. Temperatur, Niederschlagsmenge, Veränderungen der atmoshärischen Zirkukation, Quell-Effekte und Isotopenanreicherung durch Verdunstung müssen bei der Interpretation der LPS δD-Ergebnisse berücksichtigt werden.

E&G / Vol. 60 / No. 1 / 2011 / 170–187 / DOI 10.3285/eg.60.1.12

lisation presenting a major challenge. An alternative, more elegant approach might be to employ again compound-specific isotope methods (Fig. 15).

It is well known, for example, that hexoses (glucose, mannose and galactose), deoxyhexoses (fucose, rhamnose) and pentoses (xylose, arabinose) are plant and microbial biomarkers in soils (Gross & Glaser 2004; Sauheitl et al. 2005; Jia et al. 2008). Plant-derived monosaccharides could thus be measured in soils and sediments via GC-Py-IRMS (Fig. 15). Although the instrumental coupling of GC-Py-IRMS is commercially available for about 10 years, this method has hardly been adopted by researches so far (Hener et al. 1998; Jung et al. 2005; Jung et al. 2007; Greule et al. 2008). We think that the following $\delta^{18}O$ method may be most promising for loess research in the near future. More details are described in Zech & Glaser (2009):

- hydrolytic extraction of cellulose- or hemicellulose-derived neutral sugars, such as glucose, xylose, arabinose, fucose and rhamnose from soils/sediments
- purification of the monosaccharides using XAD- (remo-val of organic contaminants) and Dowex- (cation exchange resins)-columns
- derivatization of the monosaccharides in order to make them GC-amenable
- GC-separation of the individual monosaccharide-derivatives
- 'online' pyrolysis of the GC-eluates and quantitative conversion into carbon monoxide
- 'online' $\delta^{18}O$-determination for the CO in the IRMS.

As quality tests during the measurements, the authors recommend to regularly (i) co-analyze not only the masses m/z 28 and 30 ($C^{16}O$ and $C^{18}O$, respectively), but also the masses m/z 44 and 46 ($C^{16}O_2$ and $C^{16}O^{18}O$) in order to minimize isotope fractionation effects due to not quantitative CO-production (ii) co-analyze n-alkanes in order to check for oxygen contamination in the system, because alkanes contain no oxygen atoms and must not produce CO peaks in the chromatograms (iii) run batches of external monosaccharide standards with known $\delta^{18}O$ signatures and varying concentrations in order to check for amount-effects of the $\delta^{18}O$ measurements and to stick as close as possible to the 'Principle of Identical Treatment' of samples and standards.

Of course, when interpreting $\delta^{18}O$ records from LPS, one should keep in mind that the oxygen isotopic composition in plants (and preserved soil organic matter) does not only depend on $\delta^{18}O$ in precipitation/soil water, but is similar to δD controlled by evaporative enrichment and biophysiological fractionations, too (Scheidegger et al. 2000; Barbour 2007; Cuntz et al. 2007). Nevertheless, our proposed method might provide valuable new proxies from LPS, which could be directly correlated with other $\delta^{18}O$ records derived for instance from ice-cores, stalagmites or deep-sea sediments. Furthermore, the combination of δD- and $\delta^{18}O$-analyzes might help to assess the deuterium excess from LPS records and thus help to deconvolve in future the varying factors influencing the isotopic records. Zech & Glaser (2009) highlight that the new $\delta^{18}O$ method could potentially help to evaluate and improve paleolimnological and -climatic stud-

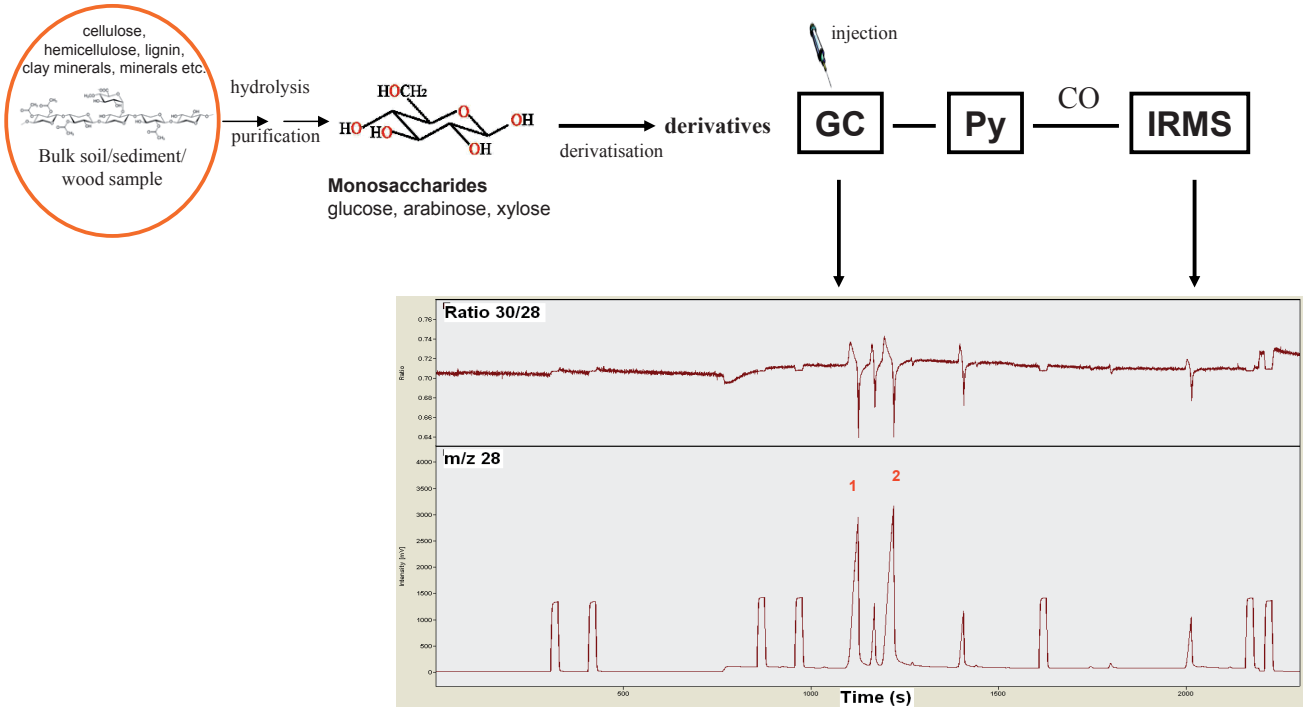

(1,2) = plant-derived sugars arabinose (1) and xylose (2)

Fig. 15: Principle of compound-specific $\delta^{18}O$ analyzes of plant-derived monosaccharides in soils. Monosaccharides are released hydrolytically from a soil/sediment/wood sample and derivatised after purification. The sugar-derivatives eluting successively from the GC-column are converted online to carbon monoxide (CO) and the $^{18}O/^{16}O$ isotopic composition of the gas is measured via a coupled IRMS.

Abb. 15: Prinzip der substanz-spezifischen $\delta^{18}O$-Analytik pflanzenbürtiger Einzelzucker in Böden. Einzelzucker werden hydrolytisch aus Boden/Sediment/Holz-Proben gewonnen und nach Aufreinigung derivatisiert. Die nacheinander von der GC-Säule eluierenden Zucker-Derivate werden im ‚online' Verfahren in Kohlenmonoxid-Gas (CO) umgewandelt und dessen $^{18}O/^{16}O$ Isotopenzusammensetzung in einem gekoppelten IRMS gemessen.

ies targeting lake cellulose for $\delta^{18}O$ analyzes (Wolfe et al. 2001; Wolfe et al. 2007; Wissel et al. 2008). Replacing the TC/EA-IRMS measurements on the extracted cellulose with GC-Py-IRMS measurements on the hydrolysed sugar monomers can overcome the common challenges of the current methods, namely purity after extraction and hygroscopicity of the cellulose.

Case study: Oxygen isotopic fractionation/exchange effects during litter decomposition?

In a first application of the above described method, Zech et al. (2011) used 5 different litter species (maple, beech, ash, pine and spruce), which were degraded in a 27 months field litterbag experiment in order to evaluate isotopic de-gradation effects during litter decomposition. While the bulk $\delta^{18}O$ values became systematically more negative due to relative mass increase of lignin (ranging from 145% in beech to 235% in pine litter) and relative mass decrease of (hemi-)cellulose (ranging from 31% in maple to 67% in ash), the compound-specific $\delta^{18}O$ values of the monosaccharides revealed no systematic trend over time (Fig. 16). This corroborates the general notion that isotopic signals of individual compounds are only negligibly affected during mineralisation, and it also indicates that oxygen exchange reactions of the hydroxyl-oxygen atoms do not occur.

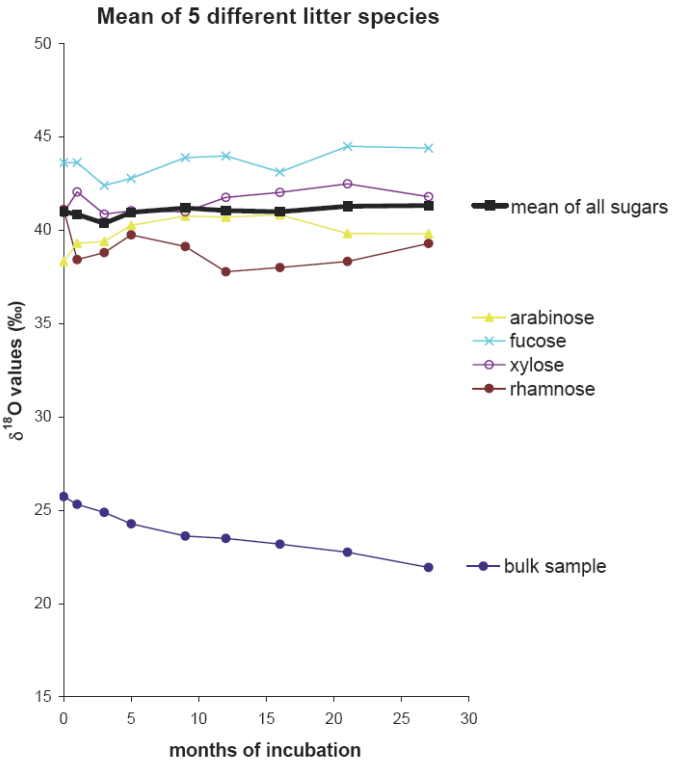

Fig. 16: Mean $\delta^{18}O$ values for 5 litter species during degradation in a 27 months field litterbag experiment (from Zech et al. 2011, submitted). While bulk litters are systematically depleted probably due to preferential degradation of cellulose (a relatively ^{18}O enriched organic pool) compared to lignin (a relatively ^{18}O depleted organic pool), $\delta^{18}O$ values of hemicellulose sugars remain virtually unchanged. This finding corroborates that oxygen exchange reactions and isotopic fractionation processes do not affect the $\delta^{18}O$ values of sedimentary sugar biomarkers.

Abb. 16: Gemittelte $\delta^{18}O$-Werte für 5 Streuproben eines 27-monatigen Freiland Streubeutel-Zersetzungs-Experiments (aus Zech et al. 2011, submitted). Während die Gesamtstreu vermutlich aufgrund des präferenziellen Abbaus von Zellulose (relativ ^{18}O-angereicherter organischer Pool) gegenüber bspw. Lignin (relativ ^{18}O-abgereicherter organischer Pool) systematisch isotopisch abgereichert wird, bleiben die $\delta^{18}O$-Werte der Hemizellulosen nahezu unverändert. Dieser Befund bestätigt, dass weder Sauerstoffaustausch-Reaktionen noch Isotopenfraktionierungsprozesse während der Degradation die $\delta^{18}O$-Werte der Hemizellulose-Biomarker beeinträchtigen.

Having demonstrated the absence of degradation effects on the ^{18}O-(hemi-) cellulose proxy, ongoing work focuses on (i) eliminating the oxygen atom in C1 position, which is prone to exchange reaction during analytical procedure and corrected mathematically, so far, (ii) calibrating the proxy with appropriate sample sets from climate chamber experiments and natural climate transects and on (iii) applying the proxy to promising LPS.

4 Concluding remarks

Given the meanwhile extremely wide range of very different analytical tools being employed in loess research, including numerical dating, micromorphology, mineralogy, elemental analysis, environmental and paleomagnetism, grain size analysis, and biomarker and isotope analyzes, we conclude that multi-disciplinary and multi-proxy approaches are most promising.

We hope that our review illustrated the fascinating potential of the selected novel methods in loess research, and also provided an overview over the current shortcomings and limitations. Ongoing joint research is required to further develop and apply the new methods.

Acknowledgements

The authors gratefully acknowledge the support provided by the many cooperation partners world-wide during the last few years. M. Zech and B. Buggle thank all members of the Soil Physics Department, University of Bayreuth, for the familial working atmosphere, A. Mergner and K Jeschke for laboratory assistance, PD Dr. M. Fuchs, Dr. U. Hambach and Dr. G. Wiesenberg for valuable discussions and Prof. B. Glaser, Prof. G. Gebauer, Prof. B. Huwe and Prof. S. Markovic for logistic support. B. Buggle appreciates the financial support given by the German Research Foundation (DFG GL 327/8–2) and M. Zech expresses gratitude for the financial support given by the Alexander von Humboldt-Foundation and the German Research Foundation (DFG ZE 844/1–1). R. Zech was supported by an SNF fellowship, and gratefully acknowledges the supervision and training by Prof. Y. Huang and his team at the Brown University over the last two years. We also thank Prof. M. Frechen for the editorial handling and proof-reading of our manuscript and an anonymous reviewer for valuable comments and suggestions.

References

Almogi-Labin, A., Bar-Matthews, M., Shriki, D., Kolosovsky, E., Paterne, M., Schilman, B., Ayalon, A., Aizenshtat, Z. & Matthews, A. (2009): Climatic variability during the last ~90 ka of the southern and northern Levantine Basin as evident from marine records and speleothems. - Quaternary Science Reviews, 28(25–26): 2882–2896.

Amelung, W. & Zhang, X. (2001): Determination of amino acid enantiomers in soils. – Soil Biology & Biochemistry, 33: 553–562.

Amelung, W. & Brodowski, S. (2002): In vitro quantification of hydrolysis-induced racemization of amino acid enantiomers in environmen-

tal samples using deuterium labeling and electon impact ionization mass spectrometry. – Analytical Chemistry, 74: 3239–3246.

Amelung, W. (2003): Nitrogen biomarkers and their fate in soil. – Journal of Plant Nutrition and Soil Science, 166: 677–686.

Amelung, W., Brodowski, S., Sandhage-Hofmann, A. & Bol, R. (2008): Combining Biomarker with Stable Isotope Analyses for Assessing the Transformation and Turnover of Soil Organic Matter. – In: D.L. Sparks (Editor), Advances in Agronomy. – Academic Press, Burlington, 155–250.

Araguas-Araguas, L., Froehlich, K. & Rozanski, K. (2000): Deuterium and oxygen-18 isotope composition of precipitation and atmospheric moisture. – Hydrological Processes, 14: 1341–1355.

Bada, J.L. (1985): Racemization of amino acids. – In: G.C. Barrett (Editor), Chemistry and Biochemistry of Amino Acids. – Chapman and Hall, London, New York, 399–414.

Bai, Y., Fang, X., Nie, J., Wang, Y. & Wu, F. (2009): A preliminary reconstruction of the paleoecological and paleoclimatic history of the Chinese Loess Plateau from the application of biomarkers. – Palaeogeography, Palaeoclimatology, Palaeoecology, 271: 161–169.

Balabane, M. (1983): Oxygen-18, deuterium and carbon-13 content of organic matter from litter and humus layers in podzolic soils. – Catena, 10: 159–166.

Bar-Matthews, M., Ayalon, A., Gilmour, M., Matthews, A. & Hawksworth, C.J. (2003): Sea-land oxygen isotopic relationships from planktonic foraminifera and speleothems in the Eastern Mediterranean region and their implication for paleorainfall during interglacial intervals. – Geochimica et Cosmochimica Acta, 67(17): 3181–3199.

Barbour, M. (2007): Stable oxygen isotope composition of plant tissue: a review. – Functional Plant Biology, 34: 83–94.

Bechtel, A., Smittenberg, R.H., Bernasconi, S.M. & Schubert, C.J. (2010): Distribution of branched and isoprenoid tetraether lipids in an oligotrophic and a eutrophic Swiss lake: Insights into sources and GDGT-based proxies. – Organic Geochemistry, 41(8): 822–832.

Blaga, C., Reichart, G.-J., Heiri, O. & Sinninghe Damsté, J. (2009): Tetraether membrane lipid distributions in water-column particulate matter and sediments: a study of 47 European lakes along a north–south transect. – Journal of Paleolimnology, 41(3): 523–540.

Bourbonniere, R.A., Telford, S.L., Ziolkowski, L.A., Lee, J., Evans, M.S. & Meyers, P.A. (1997): Biogeochemical marker profiles in cores of dated sediments from large North American lakes. – In: R.P. Eganhouse (Editor), Molecular Markers in Environmental Geochemistry, ACS Symposium Series. – American Chemical Society, Washington, DC, 133–150.

Boutton, T.W. (1996): Stable Carbon Isotope Ratios of Soil Organic Matter and Their Use as Indicators of Vegetation and Climate Change. – In: T.W. Boutton and S. Yamasaki (Editors), Mass Spectrometry of Soils. – Marcel Dekker, Inc., New York, 47–82.

Buggle, B., Wiesenberg, G. & Glaser, B. (2010): Is there a possibility to correct fossil n-alkane data for postsedimentary alteration effects? – Applied Geochemistry, 25(7): 947–957.

Burgoyne, T. & Hayes, J.M. (1998): Quantitative production of H2 by pyrolysis of gas chromatographic effluents. – Analytical Chemistry, 70: 5136–5141.

Craig, H. (1961): Isotopic variations in meteoric waters. – Science, 133: 1702–1703.

Cranwell, P.A. (1973): Chain-length distribution of n-alkanes from lake sediments in relation to post-glacial environmental change. – Freshwater Biology, 3: 259–265.

Cranwell, P.A. (1981): Diagenesis of free and bound lipids in terrestrial detritus deposits in a lacustrine sediment. – Organic Geochemistry, 3: 79–89.

Cuntz, M., Ogée, J., Farquhar, G., Peylin, P. & Cernusak, L. (2007): Modelling advection and diffusion of water isotopologues in leaves. – Plant, Cell and Environment, 30: 892–909.

Danis, P.A., Masson-Delmotte, V., Stievenard, M., Guillemin, M.T., Daux, V., Naveau, P. & von Grafenstein, U. (2006): Reconstruction of past precipitation $\delta^{18}O$ using tree-ring cellulose $\delta^{18}O$ and $\delta^{13}C$: a calibration study near Lac d'Annecy, France. – Earth and Planetary Science Letters, 243: 439–448.

Dansgaard, P. (1964): Stable isotopes in precipitation. – Tellus, 16: 436–468.

Dawson, D., Grice, K., Alexander, R. & Edwards, D. (2007): The effect of source and maturity on the stable isotopic compositions of individual hydrocarbons in sediments and crude oils from the Vulcan Sub-basin, Timor Sea, Northern Australia. – Organic Geochemistry, 38: 1015–1038.

Eganhouse, R.P. (Editor), (1997): Molecular Markers in Environmental Geochemistry. – ACS Symposium Series 671, Washington, DC.

Eglington, G. & Hamilton, R. (1967): Leaf epicuticular waxes. – Science, 156: 1322–1334.

Eglinton, T. & Eglinton, G. (2008): Molecular proxies for paleoclimatology. – Earth and Planetary Science Letters, 275: 1–16.

Feakins, S. & Sessions, A. (2010): Controls on the D/H ratios of plant leaf waxes in an arid ecosystem. – Geochimica et Cosmochimica Acta, 74: 2128–2141.

Ficken, K.J., Li, B., Swain, D.L. & Eglinton, G. (2000): An n-alkane proxy for the sedimentary input of submerged/floating freshwater aquatic macrophytes. – Organic Geochemistry, 31: 745–749.

Frechen, M. (2011): Loess in Eurasia. – Quaternary International, 234.

Gat, J.R. (1996): Oxygen and hydrogen isotopes in the hydrologic cycle. – Annual review of Earth and Planetary Sciences, 24: 225–262.

Gessler, A., Brandes, E., Buchmann, N., Helle, G., Rennenberg, H. & Barnard, R. (2009): Tracing carbon and oxygen isotope signals from newly assimilated sugars in the leaves to the tree-ring archive. – Plant, Cell and Environment, 32(7): 780–795.

Glaser, B. (2005): Compound-specific stable-isotope ($\delta^{13}C$) analysis in soil science. – Journal of Plant Nutrition and Soil Science, 168: 633–648.

Glaser, B. & Zech, W. (2005): Reconstruction of climate and landscape changes in a high mountain lake catchment in the Gorkha Himal, Nepal during the Late Glacial and Holocene as deduced from radiocarbon and compound-specific stable isotope analysis of terrestrial, aquatic and microbial biomarkers. – Organic Geochemistry, 36: 1086–1098.

Gocke, M., Kuzyakov, Y. & Wiesenberg, G. (2010): Rhizoliths in loess – evidence for post-sedimentary incorporation of root-derived organic matter in terrestrial sediments as assessed from molecular proxies. – Organic Geochemistry, 41: 1198–1206.

Greule, M., Hänsel, C., Bauermann, U. & Mosandl, A. (2008): Feed additives: authenticity assessment using multicomponent-/multielement-isotope ratio mass spectrometry. – European Food Research and Technology, 227: 767–776.

Gross, S. & Glaser, B. (2004): Minimization of carbon addition during derivatization of monosaccharides for compound-specific $\delta^{13}C$ analysis in environmental research. – Rapid Communications in Mass Spectrometry, 18: 2753–2764.

Hener, U., Brand, W.A., Hilkert, A.W., Juchelka, D., Mosandl, A. & Podebrad, F. (1998): Simultaneous on-line analysis of $^{18}O/^{16}O$ and 13C/12C ratios of organic compounds using GC-pyrolysis-IRMS. – Zeitschrift für Lebensmitteluntersuchung und -Forschung A, 206(3): 230–232.

Hilkert, A., Douthitt, C., Schlüter, H. & Brand, W. (1999): Isotope ratio monitoring gas chromatography/mass spectrometry of D/H by high temperature conversion isotope ratio mass spectrometry. – Rapid Communications in Mass Spectrometry, 13: 1226–1230.

Hou, J., D'Andrea, W., MacDonald, D. & Huang, Y. (2007): Hydrogen isotopic variability in leaf waxes among terrestrial and aquatic plants around Blood Pond, Massachusetts (USA). – Organic Geochemistry, 38: 977–984.

Huang, Y., Shuman, B., Wang, Y. & Webb III, T. (2004): Hydrogen isotope ratios of individual lipids in lake sediments as novel tracers of climatic and environmental change: a surface sediment test. – Journal of Paleolimnology, 31: 363–375.

Jia, G., Dungait, J.A.J., Bingham, E.M., Valiranta, M., Korhola, A. & Evershed, R.P. (2008): Neutral monosaccharides as biomarker proxies for bog-forming plants for application to palaeovegetation reconstruction in ombrotrophic peat deposits. – Organic Geochemistry, 39: 1790–1799.

Jung, J., Sewenig, S., Hener, U. & Mosandl, A. (2005): Comprehensive authenticity assessment of lavender oils using multielement/multicomponent isotope ratio mass spectrometry analysis and enantioselective multidimensional gas chromatography–mass spectrometry. – European Food Research and Technology, 220: 232–237.

Jung, J., Puff, B., Eberts, T., Hener, U. & Mosandl, A. (2007): Reductive ester cleavage of acyl glycerides–GC-C/P-IRMS measurements of glycerol and fatty alcohols. – European Food Research and Technology, 225: 191–197.

Kaufman, D. (2003): Amino acid paleothermometry of Quaternary ostracodes from the Bonneville Basin, Utah. – Quaternary Science Reviews, 22(8–9): 899–914.

Kim, J.-H., Schouten, S., Hopmans, E.C., Donner, B. & Sinninghe Damsté, J.S. (2008): Global sediment core-top calibration of the TEX86

paleothermometer in the ocean. – Geochimica et Cosmochimica Acta, 72(4): 1154–1173.

Kolattukudy, P.E. (1976): Biochemistry of plant waxes. – In: P.E. Kolattukudy (Editor), Chemistry and Biochemistry of Natural Waxes. – Elsevier, Amsterdam, 290–349.

Kornexl, B.E., Gehre, M., Höfling, R. & Werner, R.A. (1999): On-line d18O Measurement of Organic and Inorganic Substances. – Rapid Communications in Mass Spectrometry, 13: 1685–1693.

Kuleshov, V. & Gavrilov, Y. (2001): Isotopic composition (d13C, d18O) of carbonate concretions from terrigenous deposits in the Northern Caucasus. – Lithology and Mineral Resources, 36: 160–163.

Lichtfouse, E. (1998): Isotope and Biosynthetic Evidence for the Origin of Long-Chain Aliphatic Lipids in Soils. – Naturwissenschaften, 85: 76–77.

Lichtfouse, E., Chenu, C., Baudin, F., Leblond, C., Silva, M., Behar, F., Derenne, S., Largeau, C., Wehrung, P. & Albrecht, P. (1998): A novel pathway of soil organic matter formation by selective preservation of resistant straight-chain biopolymers: chemical and isotope evidence. – Organic Geochemistry, 28(6): 411–415.

Lisker, S., Vaks, A., Bar-Matthews, M., Porat, R. & Frumkin, A. (2009): Stromatolites in caves of the Dead Sea Fault Escarpment: implications to latest Pleistocene lake levels and tectonic subsidence. – Quaternary Science Reviews, 28(1–2): 80–92.

Liu, T., Ding, Z. & Rutter, N.W. (1999): Comparison of Milankovitch periods between continental loess and deep sea records over the last 2.5 Ma. – Quaternary Science Reviews, 18: 1205–1212.

Liu, W. & Huang, Y. (2005): Compound specific D/H ratios and molecular distributions of higher plant leaf waxes as novel paleoenvironmental indicators in the Chinese Loess Plateau. – Organic Geochemistry, 36: 851–860.

Liu, W., Huang, Y., An, Z., Clemens, S.C., Li, L., Prell, W.L. & Ning, Y. (2005): Summer monsoon intensity controls C4/C3 plant abundance during the last 35 ka in the Chinese Loess Plateau: Carbon isotope evidence from bulk organic matter and individual leaf waxes. – Palaeogeography, Palaeoclimatology, Palaeoecology, 220: 243–254.

Liu, W., Yang, H. & Li, L. (2006): Hydrogen isotopic compositions of n-alkanes from terrestrial plants correlate with their ecological life forms. – Oecologia, 150: 330–338.

Mahaney, W.C. & Rutter, N.W. (1989): Amino acid D/L ratio distribution in two Late Quaternary soils in the afroalpine zone of Mount Kenya, East Africa. – Catena, 16: 205–214.

Markovic, S., Smalley, I., Hambach, U. & Antoine, P. (2009): Loess in the Danube region and surrounding loess provinces: The Marsigli memorial volume. – Quaternary International, 198(1–2): 5–6.

Markovic, S. (2011): Loessfest 2. – special issue in QI, in press.

Mayer, B. & Schwark, L. (1999): A 15,000-year stable isotope record from sediments of Lake Steisslingen, Southwest Germany. – Chemical Geology, 161: 315–337.

Mügler, I., Sachse, D., Werner, M., Xu, B., Wu, G., Yao, T. & Gleixner, G. (2008): Effect of lake evaporation on dD values of lacustrine n-alkanes: A comparison of Nam Co (Tibetian Plateau) and Holzmaar (Germany). – Organic Geochemistry, 39: 711–729.

Novothny, A., Frechen, M., Horváth, E., Bradák, B., Oches, E., McCoy, W. & Stevens, T. (2009): Luminescence and amino acid racemization chronology of the loess–paleosol sequence at Süttő, Hungary. – Quaternary International, 198(1–2): 62–76.

Oches, E. & McCoy, W. (2001): Historical developments and recent advances in amino acid geochronology applied to loess research: examples from North America, Europe, and China. – Earth-Science Reviews, 54(1–3): 173–192.

Pagani, M., Pedentchouk, N., Huber, M., Sluijs, A., Schouten, S., Brinkhuis, H., Damste, J.S.S., Dickens, G. & Expedition 302 Scientists (2006): Arctic hydrology during global warming at the Palaeocene/Eocene thermal maximum. – Nature, 442: 671–675.

Pedentchouk, N., Freeman, K.H. & Harris, N. (2006): Different response of dD values of n-alkanes, isoprenoids, and kerogen during thermal maturation. – Geochimica et Cosmochimica Acta, 70: 2063–2072.

Penkman, K., Kaufman, D. & Collins, M. (2008): Closed-system behaviour of the intra-crystalline fraction of amino acids in mollusc shells. – Quaternary Geochronology, 3(1–2): 2–25.

Peterse, F., Kim, J.-H., Schouten, S., Kristensen, D.K., Koç, N. & Sinninghe Damsté, J.S. (2009a): Constraints on the application of the MBT/CBT palaeothermometer at high latitude environments (Svalbard, Norway). – Organic Geochemistry, 40(6): 692–699.

Peterse, F., Meer, M.T.J. v.d., Schouten, S., Jia, G., Ossebaar, J., Blokker, J. & Damste, J.S.S. (2009b): Assessment of soil n-alkane δD and branched tetraether membrane lipid distributions as tools for paleoelevation reconstruction. – Biogeosciences, 6: 2799–2807.

Powers, L., Werne, J.P., Vanderwoude, A.J., Sinninghe Damsté, J.S., Hopmans, E.C. & Schouten, S. (2010): Applicability and calibration of the TEX86 paleothermometer in lakes. – Organic Geochemistry, 41(4): 404–413.

Prügel, B., Loosveldt, P. & Garrec, J.P. (1994): Changes in the content and constituents of the cuticular wax of Picea abies (L.) Karst. in relation to needle ageing and tree decline in five European forest ageas. – Trees, 9: 80–87.

Pustovoytov, K. & Terhorst, B. (2004): Linking stable oxygen and carbon isotopes with stomatal conductance and photosynthetic capacity: a conceptual model. – Revista Mexicana de Ciencias Geológicas, 21(1): 88–93.

Roberts, N., Jones, M.D., Benkaddour, A., Eastwood, W.J., Filippi, M.L., Frogley, M.R., Lamb, H.F., Leng, M.J., Reed, J.M., Stein, M., Stevens, L., Valero-Garcés, B. & Zanchetta, G. (2008): Stable isotope records of Late Quaternary climate and hydrology from Mediterranean lakes: the ISOMED synthesis. – Quaternary Science Reviews, 27: 2426–2441.

Rudner, Z. & Sümegi, P. (2001): Recurring Taiga forest-steppe habitats in the Carpathian Basin in the Upper Weichselian. – Quaternary International, 76/77: 177–189.

Ruppenthal, M., Oelmann, Y. & Wilcke, W. (2010): Isotope ratios of nonexchangeable hydrogen in soils from different climate zones. – Geoderma, 155: 231–241.

Sachse, D., Radke, J. & Gleixner, G. (2004): Hydrogen isotope ratios of recent lacustrine sedimentary n-alkanes record modern climate variability. – Geochimical et Cosmochimica Acta, 68(23): 4877–4889.

Sauer, P.E., Eglinton, T., Hayes, J.M., Schimmelmann, A. & Sessions, A. (2001): Compound-specific D/H ratios of lipid biomarkers from sediments as a proxy for environmental and climatic conditions. – Geochimica et Cosmochimica Acta, 65(2): 213–222.

Sauheitl, L., Glaser, B. & Bol, R.A. (2005): Short-term dynamics of slurry-derived plant and microbial sugars in a temperate grassland soil as assessed by compound-specific $\delta^{13}C$ analyses. – Rapid Communications in Mass Spectrometry, 19: 1437–1446.

Schatz, A., Zech, M., Buggle, B., Gulyas, S., Hambach, U., Markovic, S., Sümegi, P. & Scholten, T. (2011): The Quaternary loess record of Tokaj, Hungary – reconstructing palaeoenvironment, vegetation and climate using stable C and N isotopes and biomarkers. – Quaternary International, doi:10.1016/j.quaint.2010.10.009.

Scheidegger, Y., Saurer, M., Bahn, M. & Siegwolf, R. (2000): Linking stable oxygen and carbon isotopes with stomatal conductance and photosynthetic capacity: a conceptual model. – Oecologia, 125: 350–357.

Schimmelmann, A., Sessions, A. & Mastalerz, M. (2006): Hydrogen isotopic (D/H) composition of organic matter during diagenesis and thermal maturation. – Annual Review of Earth and Planetary Sciences, 34: 501–533.

Schmidt, H.-L., Werner, R. & Rossmann, A. (2001): ^{18}O Pattern and biosynthesis in natural plant products. – Phytochemistry, 58: 9–32.

Schouten, S., Hopmans, E., Schefuss, E. & Sinninghe Damsté, J. (2002): Distributional variations in marine crenarchaeotal membrane lipids: a new tool for reconstructing ancient sea water temperatures? – Earth and Planetary Science Letters, 204: 265–274.

Schwark, L., Zink, K. & Lechtenbeck, J. (2002): Reconstruction of postglacial to early Holocene vegetation history in terrestrial Central Europe via cuticular lipid biomarkers and pollen records from lake sediments. – Geology, 30(5): 463–466.

Sessions, A., Burgoyne, T., Schimmelmann, A. & Hayes, J.M. (1999): Fractionation of hydrogen isotopes in lipid biosynthesis. – Organic Geochemistry, 30: 1193–1200.

Sessions, A., Sylva, S., Summons, R.E. & Hayes, J.M. (2004): Isotopic exchange of carbon-bound hydrogen over geologic timescales. – Geochimica et Cosmochimica Acta, 68(7): 1545–1559.

Shepherd, T. & Griffiths, D.W. (2006): The effects of stress on plant cuticular waxes. – New Phytologist, 171: 469–499.

Smith, F. & Freeman, K.H. (2006): Influence of physiology and climate on dD of leaf wax n-alkanes from C3 and C4 grasses. – Geochimica et Cosmochimica Acta, 70: 1172–1187.

Sternberg, L. (1988): D/H Ratios of environmental water recorded by D/H ratios of plant lipids. – Nature, 333: 59–61.

Tierney, J.E., Russell, J.M., Eggermont, H., Hopmans, E.C., Verschuren, D. & Sinninghe Damsté, J.S. (2010): Environmental controls on branched tetraether lipid distributions in tropical East African lake sediments. – Geochimica et Cosmochimica Acta, 74(17): 4902–4918.

Wagner, G.A. (1998): Racemization. – In: G.A. Wagner (Editor), Age determination of young rocks and artifacts. – Springer, Berlin, 339–355.

Wang, X., Auler, A.S., Edwards, R.L., Cheng, H., Ito, E. & Solheid, M. (2006): Interhemispheric anti-phasing of rainfall during the last glacial period. – Quaternary Science Reviews, 25(23–24): 3391–3403.

Weijers, J.W.H., Schouten, S., Donker, J.C.v.d., Hopmans, E.C. & Damste, J.S.S. (2007): Environmental controls on bacterial tetraether membrane lipid distribution in soils. - Geochimica et Cosmochimica Acta, 71: 703–713.

Weijers, J.W.H., Wiesenberg, G.L.B., Bol, R., Hopmans, E.C. & Pancost, R.D. (2010): Carbon isotopic composition of branched tetraether membrane lipids in soils suggest a rapid turnover and a heterotrophic life style of their source organism(s). – Biogeosciences, 7: 2959–2973.

Werner, R.A., Kornexl, B.E., Rossmann, A. & Schmidt, H.-L. (1996): On-line determination of $\delta^{18}O$ values of organic substances. – Analytica Chimica Acta, 319: 159–164.

Werner, R.A. (2003): The online $^{18}O/^{16}O$ analysis: development and application. – Isotopes in Environmental and Health Studies, 39(2): 85–104.

Wiesenberg, G.L.B., Schwark, L. & Schmidt, M.W.I. (2004): Improved automated extraction and separation procedure for soil lipid analyses. – European Journal of Soil Science, 55: 349–356.

Willis, K., Rudner, E. & Sümegi, P. (2000): The Full-Glacial Forests of Central and Southeastern Europe. – Quaternary Research, 53: 203–213.

Willis, K. & Andel, T. (2004): Trees or no trees? The environments of central and eastern Europe during the Last Glaciation. – Quaternary Science Reviews, 23: 2369–2387.

Wissel, H., Mayr, C. & Lücke, A. (2008): A new approach for the isolation of cellulose from aquatic plant tissue and freshwater sediments for stable isotope analysis. – Organic Geochemistry, 39: 1545–1561.

Wolfe, B.B., Edwards, T.W.D., Elgood, R.J. & Beuning, K.R.M. (2001): Carbon and Oxygen Isotope Analysis of Lake Sediment Cellulose: Methods and Applications. – In: W.M. Last and J.P. Smol (Editors), Tracking Environmental Change Using Lake Sediments, 2, Physical and Chemical Techniques. – Kluwer Academic Publishers, Dordrecht, The Netherlands, 1–28.

Wolfe, B.B., Falcone, M., Clogg-Wright, K., Mongeon, C., Yi, Y., Brock, B., Amour, N., Mark, W. & Edwards, T.W.D. (2007): Progress in isotope paleohydrology using lake sediment cellulose. – Journal of Paleolimnology, 37: 221–231.

Xie, S., Nott, C.J., Avsejs, L.A., Maddy, D., Chambers, F.M. & Evershed, R.P. (2004): Molocular and isotopic stratigraphy in an ombotrophic mire for paleoclimate reconstruction. – Geochimical et Cosmochimica Acta, 68(13): 2849–2862.

Zech, M. (2006): Evidence for Late Pleistocene climate changes from buried soils on the southern slopes of Mt. Kilimanjaro, Tanzania. – Palaeogeography, Palaeoclimatology, Palaeoecology, 242: 303–312.

Zech, M., Zech, R. & Glaser, B. (2007): A 240,000-year stable carbon and nitrogen isotope record from a loess-like palaeosol sequence in the Tumara Valley, Northeast Siberia. – Chemical Geology, 242: 307–318.

Zech, M., Buggle, B., Markovic, S., Lucic, T., Stevens, T., Gaudenyi, T., Jovanovic, M., Huwe, B. & Zöller, L. (2008a): First Alkane Biomarker Results for the Reconstruction of the Vegetation History of the Carpathian Basin (SE Europe). – In: J. Reitner, M. Fiebig, C. Neugebauer-Maresch, M. Pacher and V. Winiwarter (Editors), Veränderter Lebensraum – Gestern, Heute und Morgen, DEUQUA Symposium 2008. Abhandlungen der Geologischen Bundesanstalt 62, Wien, pp. 123–127.

Zech, M. & Glaser, B. (2008): Improved compound-specific $\delta^{13}C$ analysis of n-alkanes for application in palaeoenvironmental studies. – Rapid Communications in Mass Spectrometry, 22: 135–142.

Zech, M., Zech, R., Zech, W., Glaser, B., Brodowski, S. & Amelung, W. (2008b): Characterisation and palaeoclimate of a loess-like permafrost palaeosol sequence in NE Siberia. – Geoderma, 143(3–4): 281–295.

Zech, M., Buggle, B., Leiber, K., Markovic, S., Glaser, B., Hambach, U., Huwe, B., Stevens, T., Sümegi, P., Wiesenberg, G. & Zöller, L. (2009a): Reconstructing Quaternary vegetation history in the Carpathian Basin, SE Europe, using n-alkane biomarkers as molecular fossils: problems and possible solutions, potential and limitations. –Eiszeitalter und Gegenwart – Quaternary Science Journal, 85(2): 150–157.

Zech, M. & Glaser, B. (2009): Compound-specific $\delta^{18}O$ analyses of neutral sugars in soils using GC-Py-IRMS: problems, possible solutions and a first application. – Rapid Communications in Mass Spectrometry, 23: 3522–3532.

Zech, M., Zech, R., Morrás, H., Moretti, L., Glaser, B. & Zech, W. (2009b): Late Quaternary environmental changes in Misiones, subtropical NE Argentina, deduced from multi-proxy geochemical analyses in a palaeosol-sediment sequence. – Quaternary International, 196: 121–136.

Zech, M., Andreev, A., Zech, R., Müller, S., Hambach, U., Frechen, M. & Zech, W. (2010a): Quaternary vegetation changes derived from a loess-like permafrost palaeosol sequence in northeast Siberia using alkane biomarker and pollen analyses. – Boreas, 39: 540–550.

Zech, M., Werner, R., Juchelka, D., Buggle, B. & Glaser, B. (2011): Absence of oxygen isotope fractionation/exchange of (hemi-) cellulose-derived sugars during litter decomposition. – Organic Geochemistry, submitted.

Zech, R., Huang, Y., Zech, M., Tarozo, R. & Zech, W. (2010b): A permafrost glacial hypothesis to explain atmospheric CO2 and the ice ages during the Pleistocene. – Cimate of the Past Discussions, 6: 2199–2221.

Zhang, Z., Zhao, M., Eglington, G., Lu, H. & Huang, C. (2006): Leaf wax lipids as paleovegetational and paleoenvironmental proxies for the Chinese Loess Plateau over the last 170 kyr. – Quaternary Science Reviews, 20: 575–594.

Zöller, L., Oches, E. & McCoy, W. (1994): Towards a revised chronostratigraphy of loess in Austria with respect to key sections in the Czech Republic and in Hungary. – Quaternary Science Reviews, 13(5–7): 465–472.

Zöller, L. & Faust, D. (2009): Lower latitudes loess – Dust transport past and present. – Quaternary International, 196(1–3).

Zöller, L. (2010): New approaches to European loess: a stratigraphic and methodical review of the past decade. – Central European Journal of Geosciences, 2(1): 19–31.

E&G Quaternary Science Journal
Volume 60 / Number 1 / 2011 / 188–202 / DOI 10.3285/eg.60.1.13
www.quaternary-science.net

GEOZON SCIENCE MEDIA
ISSN 0424-7116

Late Pleistocene-Holocene History of Chaco-Pampa Sediments in Argentina and Paraguay

Wolfgang Kruck, Fabian Helms, Mebus A. Geyh, José M. Suriano, Hugo G. Marengo, Fernando Pereyra

Abstract: A substantially improved reconstruction of the Late Pleistocene-Holocene morphological and geological history of the Paraguayan Chaco and the Argentine Pampa Plain (Chaco-Pampa Plain) is presented. Due to the vast extension of the area, satellite images are the clue to synthesize previous and new multidisciplinary geoscientific results to set up a more reliable regional picture. For this synoptic view the interpretation of remote sensing data was complemented by ground investigation and physical age determinations. Luminescence ages (75 IRSL and 12 TL) of loess, loessoids and sands were determined to reconstruct the climatic history of the study area in the Marine Isotopic Stages (MIS) 3 to 1. Loess deposition dominated the period prior to MIS 2. For MIS 2 and MIS 1 the numerical ages of lacustrine and alluvial sediments intercalating the loess provide evidence for alternating humid and dry periods in the Chaco-Pampa Plain. Prevailing dry climate lasted from 8.5 to 3.5 ka (middle MIS 1) when sandy sediments deposited as dunes or filled palaeoriver beds. Temporarily limited phases of palaeoriver activity were related to sporadic torrential rainfall in the Andes Mountains.
Source regions of loess, loessoid and sandy deposits were localized in the south-western Pampa and the neighbouring Andean slopes and the Altiplano. These sediment were transported towards east and later northeast as reconstructed by the morphological features and remnants of past aeolian activity periods.

[Spätpleistozän-holozäne Geschichte der Chaco-Pampasedimente in Argentinien und Paraguay]

Kurzfassung: Eine erheblich verbesserte Rekonstruktion der spätpleistozänen/holozänen morphologischen und geologischen Geschichte des paraguayischen Chaco und der argentinischen Pampa Ebene wird vorgestellt. Wegen der großen Ausdehnung des Gebietes waren Satellitenbilder der Schlüssel, um frühere und neue interdisziplinäre geowissenschaftliche Ergebnisse zu einem verlässlicheren Bild zusammenzuführen. Für diesen synoptischen Überblick wurde die Interpretation von Fernerkundungsdaten durch Geländeuntersuchungen und physikalische Altersbestimmungen ergänzt. Viele Lumineszenzalter (75 IRSL und 12 TL) von Löß, lößähnlichen Sedimenten und Sanden wurden bestimmt, die bei der Rekonstruktion der Klimageschichte des Untersuchungsgebiets im Marinen Isotopen Stadium 3 bis 1 (MIS 3–1) beitragen.
Lößablagerungen überwiegen in der Zeit vor MIS 2. Die numerische Alter von lakustrinen und alluvialen Sedimenten, im Löß zwischengelagert, belegen wechselnde feuchte und trockene Perioden in der Chaco/Pampa-Ebene im MIS 2 und MIS 1. Überwiegend trockene Bedingungen herrschten von 8.5 bis 3.5 ka BP (mittleres MIS 1), als Sande in Form von Dünen oder in Paläoflussbetten abgelagert wurden. Zeitlich begrenzte Phasen extrem verstärkter Paläoflussaktivität im Mittelholozän wurden auf sporadische Starkregenereignisse in den Anden zurückgeführt.
Die Ursprungsgebiete des Löß, der lößartigen Sedimente und der sandigen Ablagerungen wurden in der südwestlichen Pampa, den benachbarten Andenabhängen und im Altiplano lokalisiert. Diese Sedimente wurden von dort nach Osten und später nach Nordosten transportiert, wie sich aus den morphologischen Mustern als Zeugnisse früherer äolischer Aktivität rekonstruieren ließ.

Key words: *Pampa, Chaco, morphology, chronology, Pleistocene, Holocene, Loess*

Addresses of authors: **W. Kruck**, Ginsterweg 16, D-29323 Wietze, Germany. E-Mail: w.kruck@t-online.de; **F. Helms**, BGR, Stilleweg 2, D-30655 Hannover, Germany. E-Mail: fabian-helms@gmx.de; **M.A. Geyh**, Rübeland 12, OT Bannetze, D-29308 Winsen, Germany. E-Mail: mebus.geyh@t-online.de; **J.M. Suriano**, **H.G. Marengo**, **F. Pereyra**, SEGEMAR, Avda.Roca 651, 1322 Buenos Aires, Argentina. E-Mail: canaleana@yahoo.com.ar, hugomarengo@gmail.com, fernap@mecon.gov.ar

1 Introduction

The Chaco-Pampa Plain extends from the central and northern lowlands of Argentina to the Paraguayan (and Bolivian) Chaco. It covers an area of more than 1 500 000 km^2 and stretches from the Paraguay-Bolivian border in the north to the Río Colorado in the south (southern border of the Buenos Aires Province), from the Andean foot in the west to the Río Paraná, Uruguay and the Atlantic coast in the east. The surface is generally dipping to the east and south-east.

The climate is controlled by both semi-permanent south-eastern Pacific anticyclones in the west and south-western Atlantic anticyclones in the east. Warm and humid air masses mainly originate from the Atlantic. Isohyets are nearly oriented north-northwest/south-southeast with decreasing rainfall to the west. Hence, the climate changes from subtropical to arid conditions from north-east to south-west. The north is affected by pronounced summer rainfall (October to March). In the south precipitation occurs almost the year around.

The knowledge on the Quaternary geology of the Chaco-Pampa Plain has increased during recent years, mainly due to the implementation of physical dating methods. However, a reasonable and consistent multidisciplinary overview on the morphological and geological development was still missing when SEGEMAR (Servicio Geológico Minero Argentino) assisted by BGR (Federal Institute for Geosciences and Natural Resources, Hannover, Germany) started a geological mapping project in the Chaco-Pampa Plain of the scale of 1:250 000. In the Paraguayan Chaco, the Geological Survey of Germany (BGR) and Paraguayan institutions (e.g. Ministerio de Agricultura) had already performed luminescence and radiocarbon datings within the frame of an environmental mapping program in the 1990s.

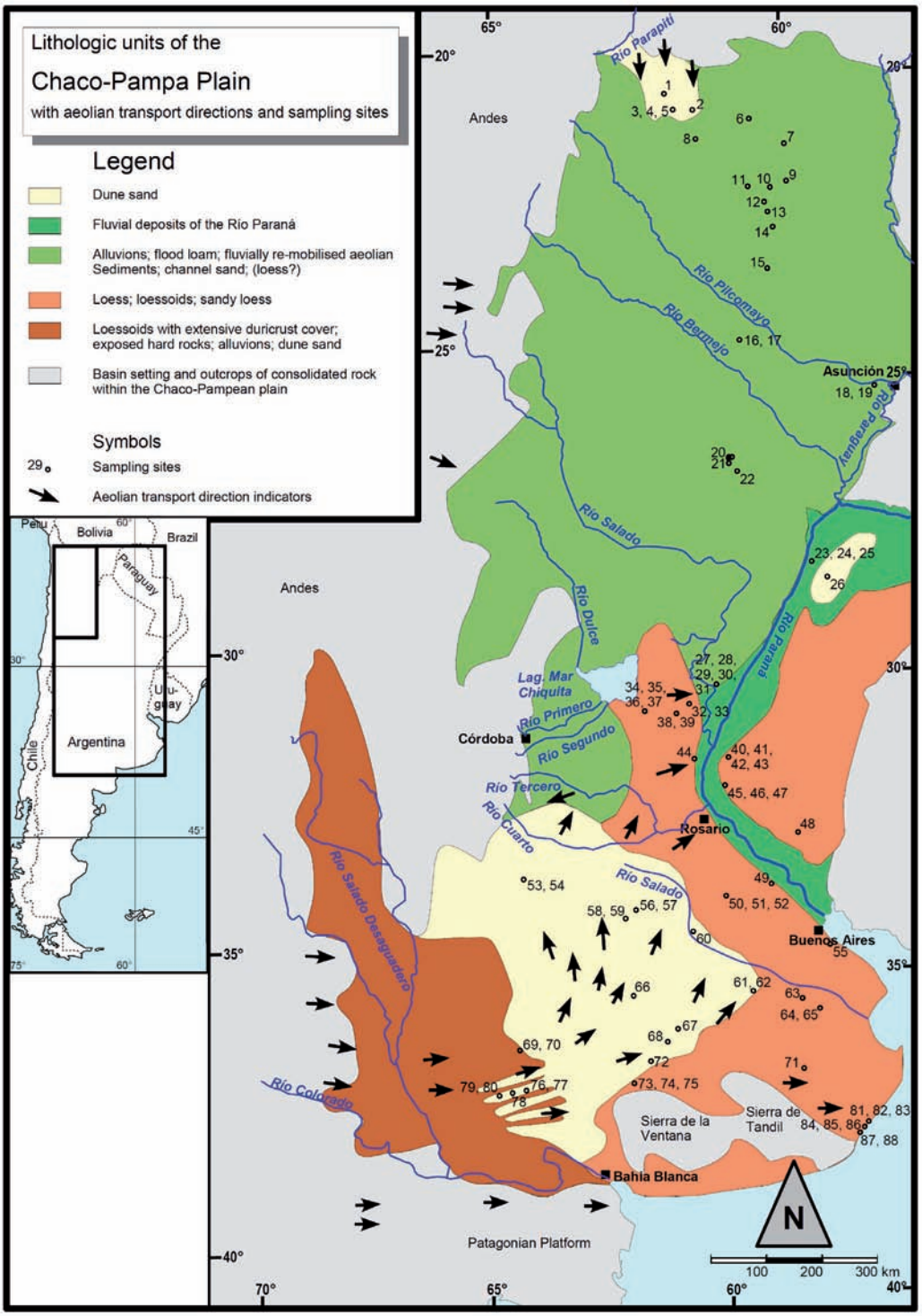

Fig. 1: The Chaco-Pampa Plain: Lithology sampling sites and aeolian transport directions. The map was elaborated by means of field observations, satellite image interpretation and information of the cited literature.

Abb. 1: Die Chaco-Pampa Ebene: Lithologie, Probenentnahmepunkte und äolische Transportrichtungen. Die Karte wurde mittels Geländebeobachtungen, Satellitenbildinterpretation und der zitierten Literatur erarbeitet.

2 Geological, Geomorphological and Climatological Setting

The Chaco-Pampa Plain is the southern part of the vast South American deposition trough. It extends from the Venezuelan plains in the north to the Río de la Plata Region in the south. The subsidence of this trough, located between the Andean chains and the Brazilian Shield, is related to the opening of the Atlantic and the up-folding of the Andes mountains.

The present topography of the Chaco-Pampa Plain was formed along general lines by the last regression of the Miocene Paranaense Sea. A new basin developed which successively filled with terrestrial sediments. In the south-western Pampa loessoid sediments built up an elevated peneplain dissected by erosion. The sediments are composed of silt and sand with embedded duricrust layers, siliceous/calcareous concretions and nodules. These sequences are palaeontologically assigned to the Upper Miocene (Melchor et al., 2000; Abello et al., 2002) and named Formación Cerro Azul.

In a great part of the Chaco-Pampa Plain Quaternary loess and loessoid deposits cover Pliocene fluvial sand. In present coastal areas marine deposits of the Pleistocene and Holocene ingressions intercalate the dominant terrestrial Quaternary sediments of the Argentine Pampa (Fig. 1).

Teruggi (1957) links the loess in the Pampa to the vol-

canism of the southern Andes, as it contains 20–60% of volcanic material. During volcanic eruptions the majority of ash was deposited on the foot of the volcanoes. From here the ashes were repeatedly deflated or fluvially removed (Inbar & Risso, 2000) and re-deposited further to the east in great fans. The volcanic activity is still going on. Ashes of the Quizapú eruption on 1932 reached Río de Janeiro (Kittl, 1933). This volcano belongs to the Descabezado Group situated on Chilean territory.

Meanwhile there is general agreement that the main source areas of the loess, loessoid sediments and sands of the Argentine Pampa are from the southwest of the Chaco-Pampa Plain, the flood plains of northern Patagonia and the piedmont of the Andes. Rivers transported material to the south and east, while southerly winds transported it to the north during dry and cold periods of the Pleistocene (e.g. Iriondo, 1990a; Zárate & Blasi, 1990). The wide SW-NE directed fan of loessoid deposits is covered by sand dunes in the southwest.

In the northern Chaco-Pampa Plain (northern part of Argentina and western part of Paraguay) the source area of aeolian and fluvial loessoid sediments are the Andine sierras in Argentina and Bolivia. The rivers (e.g. Río Pilcomayo, Río Bermejo, Río Salado) descend from there and flow to the east. They have developed extensive alluvial fans of several hundred kilometres width which are easily visible on satellite imagery. Iriondo (1990a) and Sayago (1995) have a deviating opinion on the proportions of alluvial and pristine loess in the sediments of the river fans. A comprehensive review about the associated problems arising from the distinction of pristine, reworked and fluvial dislocated loess is given by Zárate (2003).

In order to develop a regional lithostratigraphic concept of the Chaco-Pampa Plain numerous local studies were carried out. Formations were defined on the correlation of a small number of representative sites. But the result has still to be improved in order to sharpen the litho- and biostratigraphic as well as geochronologic statements.

The terrestrial Quaternary deposits are famous for their extraordinary richness of fossils at particular sites, which have been investigated very intensively since the 19th century. Ameghino (1908) established an evolutionary succession of the fauna which geologists have tried to correlate without success with lithostratigraphic sequences. Frenguelli (1957) tried to develop a lithostratigraphic sequence of the Pampa sediments by correlating alternating loess and loam sequences with the palaeoclimate of the northern hemisphere. He also failed, causing stratigraphic confusion. The inherent problems were seemingly solved by Pascual et al. (1965), who introduced the Edades Mamifero (mammal ages) without taking into account the geological conditions. Therefore, their investigations have not resulted in a clearly defined biostratigraphy. Fidalgo et al. (1975), Tonni et al. (1999) and others differentiate the Pleistocene loess (so-called Pampeano) into two units. The lower unit (Formación Ensenada – Ensenadense) consists of consolidated sediments. The upper unit contains less consolidated loess (Formación Buenos Aires-Bonaerense) and is intercalated by lacustrine and fluvial deposits (Formación Lujan-Lujanense). It is partly covered by Holocene aeolian, lacustrine, fluvial and near the coast by marine sediments. Tonni et al. (1999) differentiate the upper lithological unit in more detail using faunal elements and several radiocarbon dates. But the implementation of physical dating methods also did not overcome the lithostratigraphic problems. Due to the limited dating range of the ^{14}C method only minimum ages of the Pampeano sediments were obtained.

Based on locally restricted geochronological and geological information Iriondo (1999) developed an ambiguous and regionally questionable palaeoclimatic and palaeogeographic concept selectively adapted to the Marine Isotopic Stage (MIS) chronology of the northern hemisphere. The interpretation problems arising from too small or unreliable data base are demonstrated by Prieto (1996; 1997) criticizing the regional Holocene chronology by Iriondo (Iriondo, 1997). Iriondo (1999) and Kröhling (1999) assume wet and dry (or at least generally semiarid) climate for the periods between ca. 8500 yr cal BP and 3500 cal BP as well as between 3500 yr cal BP and 1000 yr cal BP, respectively. In opposite Geyh et al. (1996), Barboza et al. (2000) and Zech et al. (2008) provide evidence for dry and wet climate for the succeeding periods. After the predominantly dry mid-Holocene the climate changed to wet about 3500 yr cal BP with several short dry interruptions.

Palaeomagnetic studies in the eighties by e.g. Valencio and Orgeira (1983), Orgeira (1987), Bidegain (1991) and Nabel (1993) detected the Matuyama-Brunhes boundary in the upper part of the Formación Ensenada. This means that the Formación Buenos Aires must be considerably younger than 0.79 Ma. Kröhling (1999) and Kröhling and Iriondo (1999) published a small number of luminescence ages which was not sufficient to derive a reliable regional conception of the huge study area. Frechen et al. (2009) evaluated the data set of Kröhling (1999) and conclude that these reported TL age estimates should not be considered for further chronostratigraphic interpretation owing to the lack of methodological background information.

Kemp et al. (2006) describe the large variability of the micromorphological composition of loess and loess-like sediments. Arguello et al. (2010) demonstrate the dominance of loess-like sediments in one profile east of Córdoba which were transported and re-deposited by fluvial processes. As loess is usually diagenetically modified and dune sands are often re-deposited; then luminescence dates represent minimum ages of the associated morphological processes. Due to this situation many previous chronological classifications are misleading.

3 Material and Methods

The main lithostratigraphical and geomorphological problems of the previous studies arose from the uniformity of the sediments and the flatness of the huge study area with a few outcrops. This situation hampered the collection of samples suitable for luminescence dating. Luminescence dates are exaggerated if the samples were not completely bleached. Examples might be fluvial remobilized material.

In order to overcome these constrains we had to search for geoscientific methods which allow to join local multi-disciplinary information to a reliable regional geomorphological conception of global relevance. The most suitable method for this task has been found to be satellite remote sensing.

3.1 Remote sensing and sedimentological methods

Remote sensing techniques facilitated the identification of geomorphological and genetically comparable units over long distances. Due to the generous NASA information policy, most of the used satellite material could be obtained free of charge.

Samples of the following systems were downloaded and processed:

- Landsat 5 TM and Landsat 7 ETM+: These systems became the principal source of spectral data.
- SRTM (on Space Shuttle): The only available radar instrument which covered the entire investigated terrain delivered data which allowed an easy pre-processing for the Digital Elevation Model (DEM). The ground resolution is roughly comparable with that of the Landsat imagery. The altitude and spectral information could be evaluated.
- NOAA AVHRR: Its resolution allowed to localize the direction of aeolian sediment transport and deposition areas.
- After downloading the metadata and the single spectral band files in GeoTiff format, each file with single band information was processed as follows:
  Uncompressing and visualizing the data by bitmap processing software (GIMP 2.2 and COREL Photo Paint 11).
- Greyscale stretching the histogram without loss of information on the black/white side for contrast optimising (possible only for images without water, cloud cover or snow surfaces).
- Gradation curve adaptation for features on snow-free ground by compressing near the black and/or the white ends without loss of the grey tones.

The satellite image interpretation was important to reconstruct the palaeogeographic situation and deposition processes in the study area. Finally we ended up in a consistent and reasonable regional conception which was verified and refined by means of field studies. Key sites as coincidentally encountered outcrops at road cuts, river banks and excavations in the Argentine Chaco-Pampa Plain were localized for the collection of samples for luminescent dating.

Different types of involved diagenetic processes and the morphological conditions at the sampling sites allowed distinguishing sediments according to aeolian and/or fluvial transport, weathering, and remobilization. This classification was supported by grain size analysis.

3.2 Luminescence dating of sediments

Samples for luminescence dating (75 IRSL = infrared stimulated luminescence and 12 TL = thermoluminescence) were taken in the Pampa and the Chaco (Fig. 1). In the Paraguayan Chaco outcrops are so rare that in most cases small holes had to be excavated. The maximum and minimum sampling depth was between 7 and >0.3 m, the latter due to the requirements of luminescence dating. The luminescence ages and the relevant field and laboratory results are compiled in the Table 1 and 2, respectively. The luminescent ages are given in ka before present.

Samples for luminescence dating were collected between 1993 and 2006 during which luminescence dating techniques made considerable methodical progress (e.g. Preusser et al., 2008; Wintle, 2008). We applied the meanwhile antiquated dating techniques of the 1990s similar as it was done in almost all previous studies in the Chaco-Pampa Plain. The obtained luminescence dates and their confidence intervals may up to 30% older than the actual dates but are considered as sufficient reliable for the development of a raw synchronopsis. Three laboratories were involved.

The generalized procedure of collection, treatment and measurement of samples is given as follows: Each sample was taken in a light-tight cylinder from freshly exposed surfaces. The surface layer of the light-exposed part was removed under subdued red-light in the laboratories. Carbonate was removed by diluted hydrochloric acid before various grain-size and mineral fractions were separated by sieving. The 4–11 µm polymineral grain-size fraction was enriched according to Frechen et al. (1996). After this the fractions were treated with sodium oxalate solution and 30% hydrogen peroxide to remove clay coatings and organic matter. In case of luminescence dating of mono-mineral fractions potassium feldspar and quartz were separated from each other by heavy liquids, such as sodium polytungstate (2.58, 2.62 and 2.70 g/cm^3).

Between 1993–1996 IRSL and TL datings were carried out by the Archaeometry Research Group Heidelberg at the Max-Planck Institute of Nuclear Physics in Heidelberg (P. Kuhn). Polymineral fractions of 4–11 µm size and 100–200 µm quartz extracts were used. Details of the applied technique are given by Kuhn (2000).

Between 1999–2000 IRSL, GRSL (green light stimulated luminescence), and TL age determinations were performed at the Geological Institute of the University Cologne (F. Preusser). The 4–11 µm sized polymineral fraction and various coarse grain-size fractions between 63 and 200 µm of K-rich feldspars were used. For maintaining consistency only IRSL and TL ages were included in the interpretation though in several cases other kinds of luminescence ages were determined. This was justified because the corresponding ages agreed within a few millennia. Due to methodical reasons – higher probability for insufficient bleaching prior to deposition – exceptional TL ages overestimated the true sedimentation age. The reason is that TL traps require a longer light exposure time for total bleaching of the luminescence signal than luminescence traps (Godfrey-Smith et al., 1988). Details of his procedure are given by Fuller et al. (1994) and Preusser (1999).

Between 2001 and 2006 the Leibniz Institute for Applied Geosciences in Hannover carried out IRSL age determinations on 4–11 µm sized polymineral fractions and quartz extracts from loess, loessoids and dune sands. The sample preparation and measurement techniques of sands are described by Frechen et al. (2001) and of loess by Frechen et al. (2009). As the preparation and measurement techniques of the three involved laboratories differ only slightly it seemed to be justified that the reliability of the IRSL and TL ages within the investigated age range of maximum 60 ka is similar.

The multiple-aliquot regeneration and (total bleach) additive dose protocols were applied. The luminescence signal of K-feldspar samples was normalized by short shine measurements. At least six aliquots of the extracts were fixed on aluminium or stainless steel discs and irradiated at least 8-times with stepwise increasing doses using a calibrated ^{90}Sr/^{90}Y

beta source for mono-mineral extracts and calibrated ^{60}Co gamma sources for polymineral extracts. After the artificial irradiation, the samples were stored at room temperature for at least four weeks or at 70°C for one week. These experiments did not indicate anomalous fading after a delay of 4 weeks to 12 months after artificial irradiation. Several aliquots were exposed to a solar simulator lamp (dr hoenle Sol2) for several hours in order to determine the residual IRSL and TL signal.

The luminescence measurements were started with a subsequent pre-heating of the fine-grained aliquots at less than 200°C for at least 15 hours and of the feldspars fraction at more than 200°C for at least 1 minute in order to eliminate the unstable component induced by the artificial irradiation. The IRSL and TL signals were measured in commercial TL/OSL readers. Optical filter sets were placed between the sample and the photomultipliers in order to select the blue wavelength spectra for both IRSL and TL measurements. During 25–60 s exposure by IR diodes (880 ± 80 nm) the decay curve was recorded. The equivalent dose was integrated from the 10–25 s section.

From fine grains also TL ages were determined. The TL dose response curve was recorded at a heating rate of 5°C/s applied to 450°C. Second glow normalization was used to reduce the disc-to-disc scatter of the results. The 300–400°C region of the TL dose response curve yielded the equivalent dose. The TL signals of the stepwise irradiated samples were mathematically fitted to an exponential curve and extrapolated to the zero dose which yielded the equivalent dose of the natural luminescence signal.

Dose rates for all samples were calculated from the potassium concentration determined by AAS and the specific activities of potassium, uranium and thorium measured by gamma spectrometry (Table 2). The natural water content of the sediment was assumed to be in the range of 15-35 ± 5% in relation to the porosity of the sediment.

4 Results

Based on the results of geological field studies, sedimentological investigations and age determinations as well as morphological evaluations using satellite imagery a reconnaissance map was elaborated. It gives a general overview about the lithology, the main aeolian transport directions of sediments and the locality of the sampling sites (Fig.1).

Loess

We define the loess of the study area as non-stratified, loose and friable, yellowish brown and never dislocated windblown sediment with a grain size composition of predominantly coarse silt and a varying content of fine material (mainly due to weathering). Diagenetic changes do not affect this classification. A specific property of the loess in the Pampean Formation is its abundant volcanic components according to Teruggi (1957).

Teruggi (1957) and Zárate (2003) found that most sediments previously classified as loess of the Argentine Pampa had a strongly deviating grain size distribution. Our grain size analyses carried out in connection with OSL age determinations confirmed this statement. However, we found 10 sites with pristine loess in the Chaco-Pampa Plain. The grain size of the loess ranges from coarse silt to fine sand. Some clay is also present due to weathering of feldspars. Most loess samples yielded ages between 60 ka and 18 ka, two samples exceed these ages.

Loessoids

Loess dislocated by water or any other loess-like sediment with the appearance of loess independent of its origin are classified as loessoid. Material dislocated by water may yield overestimated luminescence ages due to incomplete bleaching.

The loessoid sediments of the Upper Miocene (Formación Cerro Azul) in the southwest are composed of silt and sand with embedded duricrust layers, siliceous/calcareous concretions and nodules (Grl. Acha , Nos. 76 and 77). A sample of a duricrust covering these sediments yielded a calibrated ^{14}C age of 25,800–24,500 cal BP (Hv 23 838). The actual age might be considerably older, as the samples might had been contaminated with secondary carbonates formed by repeated wetting and weathering

The facial similarity between this poorly sorted material of loessoid deposits in the east is obvious, where samples were taken at the slopes of elongated flat depressions. The samples consisted of silt (0.004–0.060 mm) and middle sand (0.20–0.63 mm). They often contained a large amount of clay, which is ascribed to weathering or a result of slope wash. The material is poorly sorted. Due to the topographic situation these sediments were transported only over short distances. OSL ages of 14 samples ranged from 60 ka to 6 ka and those of 9 samples from 32 ka to 18 ka. Five samples were older than 60 ka.

Dune sand

In the southern dune field (Pampean Sand Sea – PSS) 16 samples of dune sand were taken. They consisted of well-sorted fine to middle sand. The sites are distributed over the whole study area (Fig.1). Samples of the basal deposits which rest on loessoid sediments were taken along the western rim of the Pampean Sand Sea. At the eastern rim of the Pampean Sand Sea, sampling was done less than 2 meters above the base estimated from the topographic situation. Recent and old sands were found at the eastern and northern rim of the Pampean Sand Sea. The oldest determined OSL ages of sands are minimum ages in case the base of the outcrop was not the base of the sands. Older sands from the dune field northwest of the PSS with OSL ages of 33 ka to 23 ka are described by Tripaldi & Forman (2007). The thickness of the dune sand sequence is differing with maximum values estimated to about 20 to 30 m.

Five samples were dated from the northern dune field in the Paraguayan Chaco. They were collected between the central and south-eastern part. By topographic calculations their position is less than 3 meters above the dune basis. These sediments have mid-Holocene ages between 5 ka and 3 ka. One sample from another dune field located in the east of the Río Paraná is of modern age.

Channel sand

Satellite images of the northern part of the study area show a pattern of fluvial activity. The related field study confirmed that the corresponding sediments are channel sands from palaeorivers of the Río Pilcomayo-Bermejo-Salado

system (see also Section 5.2). They are very well sorted with grain sizes between silt and middle sand. Dating of 11 samples yielded OSL ages ranging from 12 ka to 3 ka which may be minimum ages, as the samples had to be collected above the unknown base of these deposits.

Fluvio-lacustrine sediments

The sampling sites are located near the still active water courses in the back water and flood plain areas. The sediments occur in lenses of clayey diamictit. They have a bimodal grain size distribution from fine to middle sands and clay to fine silt. Several samples contained a high proportion of clay. Two fluvio-lacustrine sediment samples (Nos. 24 and 25) with many fossils were taken from an outcrop at Bella Vista. They yielded OSL ages of 53 ka and 37 ka, respectively. These deposits belong palaeontologically to the Formación Toropí and Formación Yupoi (Tonni et al., 2005). At the Arroyo Barrenechea near Diamante, Entre Rios (No. 47) the sediments have an OSL age of 34 ka. They contain well preserved fossils, indicating a short transport distance and could belong to the Formación Arroyo Feliciano (Iriondo et al., 1985). According to the dates both the Formación Yupoi and Formación Arroyo Feliciano would be coeval. Luminescence dates of fluvio-lacustrine sediments obtained by the antiquated technique of 1990s might be exaggerated due to incomplete bleaching.

Flood loam

On satellite images of the northern Chaco-Pampa Plain macro and dense micro flow patterns are visible. The sediments are badly sorted and the grain sizes ranged from clay (<0.005 mm) to middle sand. One sample out of nine was older than 60 ka, the others were between 30 ka and 2 ka old. Similar to fluvio-lacustrine sediments luminescence ages of flood loam might also be exaggerated due to incomplete bleaching.

Not classified material

Sediments of unsorted grains and without any clear morphological relationship could not be classified. It is unknown whether they were weathered, bioturbated or fluvial re-mobilized loess. One sand sample taken near Bella Vista might have been of fluvial or aeolian origin. At Mar del Plata sandy sediments underlying marine deposits could have been shore or aeolian sands.

5 Origin and Fate of the Sediments

Satellite data evaluation provided evidence that westerly winds dominated in the Argentine Pampa during the Pleistocene. Indications are morphological stripes and furrows in the sedimentary and volcanic cover at the Andean foot-

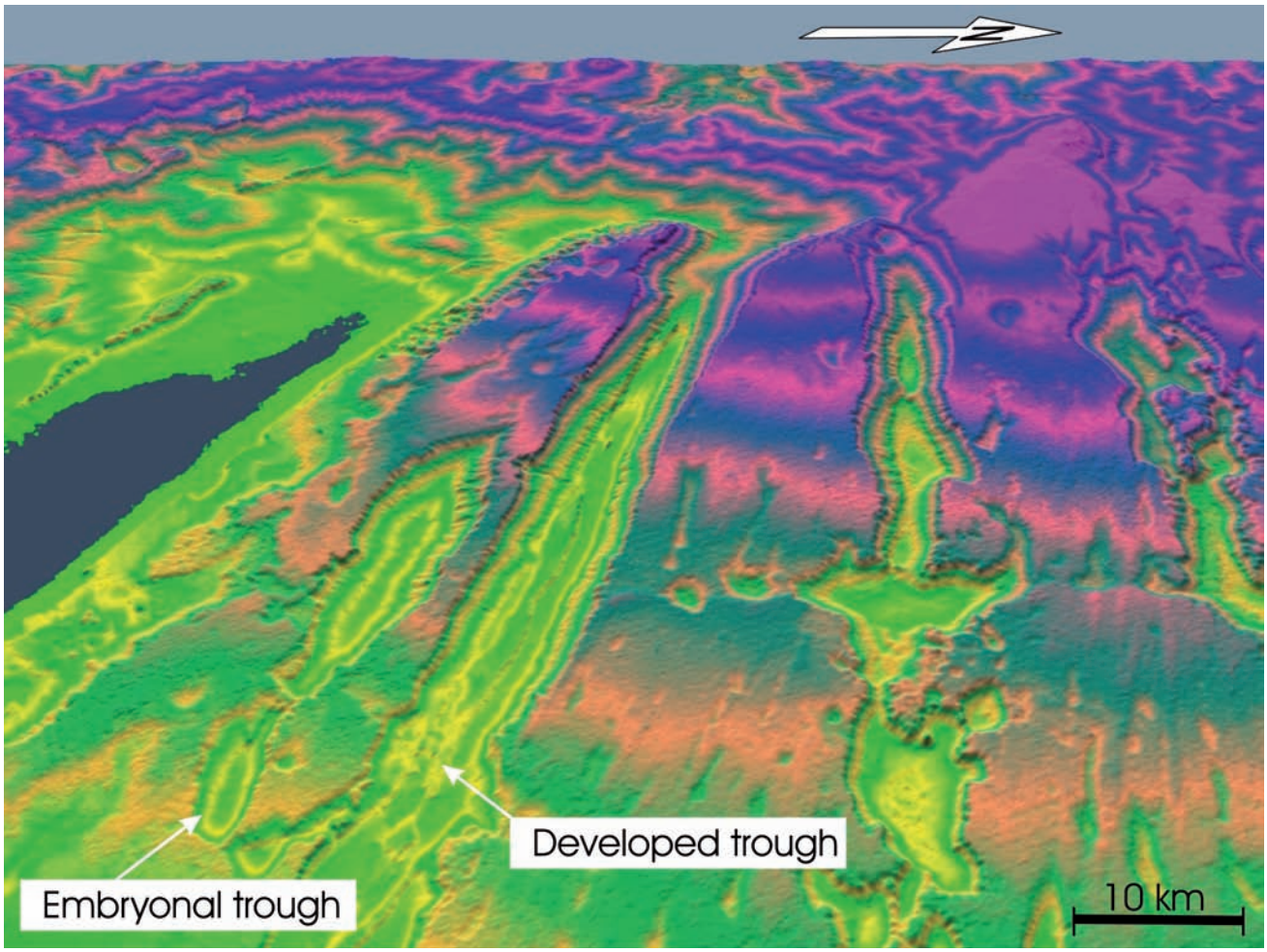

Fig. 2: Digital Elevation Model of the "Valles Grandes" area in the southwestern Pampa (see Fig.1), derived from SRTM data (SRTM tiles: 36S/64W to 39S/67W). Big and small troughs reflect different stages of aeolian valley evolution. Wind direction was to the east.

Abb. 2: Digitales Höhenmodell vom Gebiet der Valles Grandes in der südwestlichen Pampa (siehe Fig.1), erstellt aus SRTM Daten (SRTM tiles: 36S/64W to 39S/67W). Große und kleine Tröge stellen verschiedene Stadien der äolischen Talbildung dar. Der Wind kam aus dem Westen.

Tab. 1: Luminescence dates of sediments from the Chaco-Pampa Plain: site description, numerical dates with reference and climatic classification of the samples (Fig. 1 – sample numbers increase from N to S). Laboratory results of the luminescence dating are compiled in Table 2.

Tab. 1: Lumineszenz-Alter von Sedimenten aus dem Chaco und der Pampa: Angaben zu den Beprobungsorten und klimatische Klassifikation der Proben (Fig. 1 – die Probennummern steigen von S nach N). Laborergebnisse der Lumineszenzdatierung sind in Table 2 zusammengestellt

No.	material	location	depth m	latitude S	longitude W	method	lab.	age ka BP			climatic classification
Samples representing arid climate											
1	dune sand	Est. Calvet	1.00	20.6545°	61.9929°	TL	MPI K H	3.0	±	0.4	arid
2	dune sand	Tte. Enciso/Transchaco	0.50	20.9074°	61.5059°	TL	MPI K H	2.9	±	0.4	arid
3	dune sand	Tte. Enciso/Transchaco	0.45	20.9017°	61.8443°	TL	MPI K H	3.1	±	0.5	arid
4	dune sand	Tte. Enciso/Transchaco	0.65	20.9017°	61.8443°	TL	MPI K H	5.5	±	0.6	arid
5	dune sand	Tte. Enciso/Transchaco	0.75	20.9017°	61.8443°	TL	MPI K H	4.8	±	0.6	arid
26	dune sand	9 de Julio	1.40	28.8369°	58.8437°	IRSL	LIAG	modern			arid
27	loessoid	Autodromo Emilia	4.65	31.0501°	60.8176°	IRSL	LIAG	96.5	±	5.6	arid (?)
28	loessoid	Autodromo Emilia	5.10	31.0501°	60.8176°	IRSL	LIAG	91.6	±	7.6	arid (?)
29	loessoid	Autodromo Emilia	4.00	31.0501°	60.8176°	IRSL	LIAG	84.9	±	6.7	arid (?)
34	loessoid	Freyre	3.50	31.1743°	61.9812°	IRSL	LIAG	32.1	±	2.7	arid (?)
35	loessoid	Freyre	2.20	31.1743°	61.9812°	IRSL	LIAG	18.6	±	1.6	arid (?)
36	loessoid	Freyre	1.85	31.1743°	61.9812°	IRSL	LIAG	17.4	±	1.5	arid (?)
37	loessoid	Freyre	0.90	31.1743°	61.9812°	IRSL	LIAG	5.8	±	0.6	arid (?)
38	loessoid	Rafaela	1.30	31.2362°	61.4508°	IRSL	Uni Cologne	28.8	±	2.9	arid (?)
39	loessoid	Rafaela	2.50	31.2362°	61.4508°	IRSL	Uni Cologne	18.8	±	3.2	arid (?)
40	loessoid	Parana	2.55	31.7031°	60.4769°	IRSL	LIAG	56.6	±	5	arid (?)
41	loessoid	Paraná	0.65	31.7031°	60.4769°	IRSL	LIAG	28.3	±	2.4	arid (?)
42	loessoid	Paraná	1.40	31.7031°	60.4769°	IRSL	LIAG	26.9	±	2.3	arid (?)
43	loessoid	Paraná	2.65	31.7031°	60.4769°	IRSL	LIAG	23.2	±	1.8	arid (?)
46	loess	Diamante	1.90	32.0665°	60.6242°	IRSL	LIAG	17.8	±	1.3	arid
49	loessoid	Autodromo Barradero	2.30	33.8206°	59.4778°	IRSL	Uni Cologne	40.2	±	6.3	arid (?)
52	loess	Arrecifes	0.40	34.0644°	60.0616°	IRSL	LIAG	26.9	±	1.9	arid
53	dune sand	Vicuña Mackenna	3.15	33.9303°	64.3724°	IRSL	Uni Cologne	12.4	±	1.0	arid
54	dune sand	Vicuña Mackenna	1.35	33.9303°	64.3724°	IRSL	Uni Cologne	2.9	±	0.5	arid
56	loess	La Picasa N	1.30	34.3856°	62.2118°	GSA	LIAG	144 ± 16			arid
57	dune sand	La Picasa N	0.40	34.3856°	62.2118°	IRSL	LIAG	16.1	±	1.2	arid
58	loess	La Picasa S	1.50	34.4557°	62.3776°	IRSL	LIAG	26.4	±	1.9	arid
59	dune sand	La Picasa S	0.60	34.4557°	62.3776°	IRSL	LIAG	10.9	±	1.3	arid
60	dune sand	Junin	1.50	34.6614°	60.9861°	IRSL	Uni Cologne	7.3	±	1.4	arid
61	dune sand	Saladillo	1.40	35.5936°	59.7431°	IRSL	LIAG	14.2	±	3.2	arid
62	dune sand	Saladillo	0.40	35.5936°	59.7431°	IRSL	LIAG	modern			arid
63	dune sand	San Miguel del Monte	0.70	35.6602°	58.8016°	IRSL	Uni Cologne	9.8	±	1.2	arid
64	loess	Grl. Belgrano	1.50	35.8301°	58.4082°	IRSL	Uni Cologne	57.8	±	7.6	arid
65	loess	Grl. Belgrano	1.20	35.8301°	58.4082°	IRSL	Uni Cologne	17.9	±	3.2	arid
67	dune sand	San Carlos de Bolivar	1.40	36.2725°	61.2123°	IRSL	Uni Cologne	10.6	±	1.7	arid
68	dune sand	Pirovano	2.50	36.5069°	61.566°	IRSL	LIAG	6.7	±	1.3	arid
69	dune sand	Toay	5.50	36.6835°	64.4142°	IRSL	Uni Cologne	3.8	±	0.4	arid
70	dune sand	Toay	3.50	36.6835°	64.4142°	IRSL	Uni Cologne	0.3	±	0.1	arid
71	loess	Arroyo El Perdido	1.35	36.8104°	58.5675°	IRSL	Uni Cologne	13.1	±	1.8	arid
72	dune sand	Cochiso/Alsina	1.25	36.9138°	62.246°	IRSL	LIAG	5.0	±	1.7	arid
73	loessoid	Carhue W	1.24	37.2042°	62.8621°	GSA	LIAG	139	±	7	arid (?)
74	loessoid	Carhue W	3.15	37.2042°	62.8621°	GSA	LIAG	123	±	7	arid (?)
75	loessoid	Carhue W	0.85	37.2042°	62.8621°	IRSL	LIAG	21.6	±	2.2	arid (?)
78	dune sand	Grl. Acha N	2.80	37.3633°	64.5970°	IRSL	Uni Cologne	2.3	±	0.3	arid
79	dune sand	Grl. Acha W	3.50	37.3978°	64.8577°	IRSL	Uni Cologne	5.4	±	0.5	arid
80	dune sand	Grl. Acha W	4.50	37.3978°	64.8577°	IRSL	Uni Cologne	5.0	±	0.6	arid
82	loessoid	Mar del Plata Santa Clara d.M.	0.50	37.8602°	57.5082°	IRSL	LIAG	55.2	±	4.4	arid (?)
85	loess	Mar del Plata Camet	1.70	37.9084°	57.5215°	GSA	LIAG	103	±	140	arid
86	loess	Mar del Plata Camet	0.30	37.9084°	57.5215°	IRSL	LIAG	53.7	±	3.3	arid
88	loess	Mar del Plata	0.50	37.9577°	57.534°	IRSL	LIAG	45.7	±	2.9	arid

E&G / Vol. 60 / No. 1 / 2011 / 188–202 / DOI 10.3285/eg.60.1.13

No.	material	location	depth m	latitude S	longitude W	method	lab.	age		ka BP	climatic classification
Fluvial samples representing arid climate											
6	channel sand	Tte. Pico/Est. San Juan	0.60	21.0527°	60.5425°	TL	MPI K H	3.3	±	0.4	arid/palaeoriver
7	channel sand	Filadelfia/Madrejon	0.60	21.4390°	59.8682°	TL	MPI K H	7.7	±	0.9	arid/palaeoriver
10	channel sand	Campo Aroma	0.55	22.1692°	60.0714°	TL	MPI K H	4.6	±	0.6	arid/palaeoriver
13	channel sand	Neuland	0.60	22.5699°	60.0927°	TL	MPI K H	3.4	±	0.4	arid/palaeoriver
14	channel sand	Neuland	0.60	22.8689°	60.0205°	TL	MPI K H	4.5	±	0.7	arid/palaeoriver
15	channel sand	Pozo Col./Grl.Diaz	0.60	23.4882°	60.0696°	TL	MPI K H	6.4	±	0.9	arid/palaeoriver
16	channel sand	Las Lomitas	3.40	24.7416°	60.5512°	IRSL	Uni Cologne	12.4	±	2.2	arid/palaeoriver
17	channel sand	Las Lomitas	2.05	24.7416°	60.5512°	IRSL	Uni Cologne	11.8	±	0.8	arid/palaeoriver
18	channel sand	Clorinda W	1.80	25.2528°	58.0109°	IRSL	Uni Cologne	3.0	±	0.3	arid/palaeoriver
19	channel sand	Clorinda W	1.60	25.2528°	58.0109 °	IRSL	Uni Cologne	3.0	±	0.2	arid/palaeoriver
21	channel sand	7km N Napenay	0.50	26.6732°	60.6293°	IRSL	Uni Cologne	3.7	±	0.3	arid/palaeoriver
Samples representing humid climate											
8	flood loam	La Patria	1.00	21.4001°	61.4374°	IRSL	MPI K H	9.8	±	1.3	humid
9	flood loam	Tte. Montania	0.45	22.0523°	59.9282°	IRSL	MPI K H	2.1	±	0.2	humid
11	flood loam	Transchaco/Lag. Negra	2.00	22.1809°	60.4494°	TL	MPI K H	12.3	±	1.5	humid
12	flood loam	Transchaco/Fila.	1.00	22.4370°	60.1293°	IRSL	MPI K H	12.1	±	2.6	humid
20	flood loam.	7km N Napenay	1.20	26.6692°	60.6287°	IRSL	Uni Cologne	19.8	±	1.3	humid
22	flood loam	Grl. Roque Saenz Peña	2.75	26.7809°	60.4781°	IRSL	Uni Cologne	28.7	±	5.4	humid
23	well sorted sand	Bella Vista. Corrientes	0.50	28.5947°	59.0430°	GSA	LIAG	115	±	7	not classified
24	fluvio-lacustrine clayey diamict	Bella Vista/ Corrientes	6.50	28.5943°	59.0484°	IRSL	LIAG	53.2	±	3.9	humid
25	fluvio-lacustrine clayey diamict	Bella Vista/ Corrientes	2.00	28.5943°	59.0484°	IRSL	LIAG	36.7	±	2.2	humid
27	flood loam	Autodromo Emilia	4.65	31.0501°	60.8176°	IRSL	LIAG	96.5	±	5.6	humid
30	flood loam	Autodromo Emilia	5.05	31.0501°	60.8176°	IRSL	LIAG	46.5	±	3.2	humid
31	flood loam	Autodromo Emilia	1.80	31.0501°	60.8176°	IRSL	LIAG	25.8	±	2.2	humid
32	loessoid	Felicia	1.70	31.1891°	61.2153°	IRSL	LIAG	34.6	±	2.8	not classified
33	fluvio-lacustrine clayey diamict	Felicia	1.00	31.1891°	61.2153°	IRSL	LIAG	15.8	±	1.5	humid
44	fluvio-lacustrine clayey diamict	Arroyo Colastiné;Gessler	1.00	31.9148°	61.1204°	IRSL	LIAG	14.3	±	1.5	humid
45	clay with silt	Diamante/Camino al Balneario Valle María	1.90	32.0101°	60.6387°	GSA	LIAG	not datable saturation			humid (?)
47	fluvio-lacustrine clayey diamict	Diamante/Arr. Barrenechea	1.60	32.0729°	60.5594°	IRSL	LIAG	34.3	±	2.1	humid
48	fluvio-lacustrine clayey diamict	Larocca	1.90	33.0190°	59.0013°	IRSL	Uni Cologne	12.1	±	1.4	humid
50	clayey silt	Arrecifes	2.20	34.0644°	60.0616°	GSA	LIAG	207	±	11	not classified
51	fluvio-lacustrine clayey diamict	Arrecifes	4.65	34.0641°	60.0610°	GSA	LIAG	159	±	12	humid
55	clayey silt	La Plata	7.00	34.9082°	58.0111°	GSA	LIAG	>390			not classified
66	fluvio-lacustrine clayey diamict	Canal Jauretche	1.50	35.7216°	62.0808°	IRSL	Uni Cologne	8.2	±	0.7	humid
76	silty diamict	Grl. Acha E	3.80	37.3478°	64.2887°	GSA	Uni Cologne	not datable			humid (?)
77	silty diamict	Grl. Acha E	2.40	37.3478°	64.2887°	GSA	Uni Cologne	not datable			humid (?)
81	sand (shore sand?)	Mar del Plata Santa Clara d.M.	6.10	37.8602°	57.5082°	GSA	LIAG	104	±	6	not classified
83	fluvio-lacustrine clayey diamict	Mar del Plata Santa Clara d.M.	1.60	37.8602°	57.5082°	IRSL	LIAG	53.8	±	5.2	humid
84	fluvio-lacustrine clayey diamict	Mar del Plata Camet	0.50	37.9084°	57.5215°	GSA	LIAG	121	±	6	humid
87	clayey silt	Mar del Plata	1.80	37.9577°	57.5340°	GSA	LIAG				not classified

Abbreviations: lab – laboratory: UNI Cologne – University of Cologne (F. Preusser); LIAG – Leibniz Institute of Applied Geophysics, Hannover (M. Frechen); MPI K H – Max Planck Institute of Nuclear Physics, Heidelberg (R. Kuhn); method: IRSL – infrared-stimulated luminescence; TL – thermoluminescence; age; GSA – grain size analysis

Tab. 2: Dated fraction, analytical results, dose rate measurements and estimates, assumed moisture content and equivalent dose of sediments samples from the Chaco-Pampa Plain (see Table1 and Fig. 1 – sample numbers increase from N to S). Analytical data from the Max-Planck-Institute Heidelberg (MPI H) are missing.

Tab. 2: Datierter Sedimentextrakt, analytische Ergebnisse, angenommener Feuchtgehalt, gemessene und geschätzte Dosisraten und Äquivalenzdosis der Proben vom der Pampa und dem Chaco (s. Tabelle 1 und Fig. 1 – die Probenummern steigen von N nach S. Die Laborergebnisse der Lumineszenzalter vom Max-Planck-Institut Heidelberg liegen nicht vor.

No.	location	grain size mineral	K %	Th ppm	U ppm	water %	d_{cosm} mGy/a	d_{tot} mGy/a	D_{equ} Gy
Samples representing arid climate									
1	Est. Calvet	4-11 mm P							
2	Tte. Enciso/ Transchaco	90-200 mm Q							
3	Tte. Enciso/ Transchaco	90-200 mm Q							
4	Tte. Enciso/ Transchaco	90-200 mm Q							
5	Tte. Enciso/ Transchaco	90-200 mm Q							
26	9 de Julio	4-11 mm P	1.09 ± 0.02	4.55 ± 0061	0.35 ± 0.02	15 ± 5	182 ± 9	4.17 ± 0.33	133.9 ± 4.7
27	Autodromo Emilia	4-11 mm P	1.71 ± 0.08	5.29 ± 0.26	1.49 ± 0.07	15 ± 5	172 ± 9	2.68 ± 0.14	258.3 ± 5.8
28	Autodromo Emilia	4-11 mm P	1.82 ± 0.09	8.97 ± 0.54	1.62 ± 0.10	15 ± 5	178 ± 9	3.34 ± 0.24	305.5 ± 9.6
29	Autodromo Emilia	4-11 mm P	1.99 ± 0.10	8.66 ± 0.52	1.59 ± 0.19	15 ± 5	175 ± 9	3.44 ± 0.27	291.6 ± 5.2
34	Freyre	4-11 mm P	2.35 ± 0.12	10.20 ± 0.61	2.26 ± 0.14	15 ± 5	182 ± 9	4.17 ± 0.33	133.9 ± 4.7
35	Freyre	4-11 mm P	2.20 ± 0.11	9.72 ± 0.58	2.34 ± 0.14	15 ± 5	190 ± 10	4.03 ± 0.31	74.9 ± 2.6
36	Freyre	4-11 mm P	2.18 ± 0.11	10.30 ± 0.62	2.29 ± 0.14	15 ± 5	192 ± 10	4.06 ± 0.32	70.4 ± 2.3
37	Freyre	4-11 mm P	2.37 ± 0.12	8.75 ± 0.53	2.21 ± 0.13	15 ± 5	197 ± 10	4.03 ± 0.31	23.3 ± 1.4
38	Rafaela	4-11 mm P	1.97 ± 0.10	10.43 ± 0.52	2.20 ± 0.11	20 ± 5	145	3.40 ± 0.30	97.3 ± 7.8
39	Rafaela	4-11 mm P	1.90 ± 0.10	10.33 ± 0.52	2.32 ± 0.12	20 ± 5	125	3.50 ± 0.30	66.6 ± 13.0
40	Parana	4-11 mm P	2.89 ± 0.14	8.98 ± 0.54	1.51 ± 0.09	15 ± 5	209 ± 10	4.26 ± 0.32	241.1 ± 10.7
41	Paraná	4-11 mm P	2.28 ± 0.11	9.86 ± 0.59	1.77 ± 0.11	15 ± 5	207 ± 10	3.92 ± 0.30	111.0 ± 3.6
42	Paraná	4-11 mm P	2.57 ± 0.13	9.48 ± 0.57	1.61 ± 0.10	15 ± 5	201 ± 10	4.06 ± 0.31	109.2 ± 4.2
43	Paraná	4-11 mm P	3.33 ± 0.17	8.92 ± 0.54	1.42 ± 0.09	15 ± 5	193 ± 10	4.58 ± 0.35	106.3 ± 1.7
46	Diamante	4-11 mm P	1.54 ± 0.04	8.04 ± 0.40	1.69 ± 0.09	15 ± 5	192 ± 10	3.03 ± 0.16	54.0 ± 2.7
49	Autodromo Barradero	4-11 mm P	1.62 ± 0.08	10.30 ± 0.51	2.30 ± 0.12	20 ± 5	125	3.20 ± 0.20	128.5 ± 19.0
52	Arrecifes	4-11 mm P	1.92 ± 0.05	4.58 ± 0.23	1.64 ± 0.08	15 ± 5	202 ± 10	2.98 ± 0.15	80.0 ± 4.3
53	Vicuña Mackenna	100-150 mm F	1.79 ± 0.09	7.00 ± 0.35	1.83 ± 0.09	10 ± 5	110	3.10 ± 0.20	38.9 ± 1.9
54	Vicuña Mackenna	100-150 mm F	1.71 ± 0.09	7.11 ± 0.36	1.90 ± 0.10	10 ± 5	145	3.10 ± 0.20	9.0 ± 1.4
56	La Picasa N	4-11 mm P	1.80 ± 0.09	3.27 ± 0.17	1.92 ± 0.10	15 ± 5	193 ± 10	2.89 ± 0.15	416.0 ± 41.0
57	La Picasa N	4-11 mm P	1.90 ± 0.10	4.03 ± 0.24	1.91 ± 0.10	15 ± 5	206 ± 10	3.01 ± 0.16	48.4 ± 2.3
58	La Picasa S	4-11 mm P	2.07 ± 0.10	9.53 ± 0.48	1.89 ± 0.10	15 ± 5	190 ± 10	3.73 ± 0.20	98.5 ± 4.7
59	La Picasa S	4-11 mm P	1.98 ± 0.08	9.55 ± 0.48	1.88 ± 0.09	15 ± 5	202 ± 10	3.66 ± 0.20	40.0 ± 4.1
60	Junin	4-11 mm P	1.82 ± 0.09	7.02 ± 0.35	2.01 ± 0.10	20 ± 5	145	3.00 ± 0.20	12.45 ± 0.7
61	Saladillo	4-11 mm P	1.90 ± 0.05	3.44 ± 0.17	1.23 ± 0.06	15 ± 5	197 ± 10	2.68 ± 0.13	37.9 ± 8.5
62	Saladillo	4-11 mm P	1.09 ± 0.02	4.55 ± 0.06	0.35 ± 0.02	15 ± 5	193 ± 10	0	0
63	San Miguel del Monte	dune sand	1.81 ± 0.09	8.36 ± 0.42	2.09 ± 0.10	10 ± 5	145	3.40 ± 0.20	32.7 ± 3.3
64	Grl. Belgrano	4-11 mm P	1.53 ± 0.08	7.54 ± 0.38	1.99 ± 0.10	20 ± 5	145	2.80 ± 0.20	159.6 ± 16.4
65	Grl. Belgrano	4-11 mm P	1.85 ± 0.09	8.95 ± 0.45	1.87 ± 0.09	20 ± 5	150	3.10 ± 0.20	55.9 ± 8.8
67	San Carlos de Bolivar	100-150 mm F	1.72 ± 0.09	5.93 ± 0.30	1.58 ± 0.08	10 ± 5	145	3.00 ± 0.20	32.1 ± 4.5
68	Pirovano	4-11 mm P	1.74 ± 0.05	3.10 ± 0.15	1.19 ± 0.06	15 ± 5	192 ± 10	2.48 ± 0.14	16.6 ± 3.0
69	Toay	100-200 mm F	1.95 ± 0.10	6.97 ± 0.35	1.85 ± 0.09	10 ± 5	75	3.20 ± 0.20	12.8 ± 1.0
70	Toay	100-200 mm F	1.91 ± 0.10	6.57 ± 0.33	1.70 ± 0.09	10 ± 5	105	3.20 ± 0.20	1.1 ± 0.3
71	Arroyo El Perdido	4-11 mm P	1.58 ± 0.08	8.41 ± 0.42	1.92 ± 0.10	23	145	2.90 ± 0.20	37.5 ± 4.1

E&G / Vol. 60 / No. 1 / 2011 / 188–202 / DOI 10.3285/eg.60.1.13

No.	location	grain size mineral	K %	Th ppm	U ppm	water %	d_{cosm} mGy/a	d_{tot} mGy/a	D_{equ} Gy
72	Cochiso/ Alsina	4-11 mm P	1.84 ± 0.05	2.94 ± 0.15	1.31 ± 0.07	15 ± 5	201 ± 10	2.61 ± 0.15	13.0 ± 4.3
73	Carhue W	4-11 mm P	1.35 ± 0.06	7.04 ± 0.35	1.48 ± 0.04	15 ± 5	201 ± 10	2.75 ± 0.14	382.9 ± 6.0
74	Carhue W	4-11 mm P	1.49 ± 0.06	6.02 ± 0.30	1.53 ± 0.04	15 ± 5	188 ± 9	2.73 ± 0.14	334.4 ± 6.4
75	Carhue W	4-11 mm P	1.53 ± 0.04	6.12 ± 0.30	1.16 ± 0.05	15 ± 5	204 ± 10	2.63 ± 0.13	56.8 ± 5.1
78	Grl. Acha N	100-200 KF	1.67 ± 0.08	5.60 ± 0.28	1.46 ± 0.07	10 ± 5	115	2.90 ± 0.20	6.5 ± 0.6
79	Grl. Acha W	100-200 KF	1.82 ± 0.09	6.10 ± 0.31	1.71 ± 0.09	10 ± 5	105	3.20 ± 0.20	17.1 ± 1.2
80	Grl. Acha W	4-11 mm P	1.86 ± 0.09	6.67 ± 0.33	1.79 ± 0.09	10 ± 5	85	3-20 ± 0.20	16.3 ± 1.7
82	Mar del Plata Santa Clara d.M.	4-11 mm P	1.28 ± 0.06	5.92 ± 0.30	1.72 ± 0.04	15 ± 5	204 ±10	2.82 ± 0.14	155.4 ± 10.0
85	Mar del Plata Carnet	4-11 mm P	1.23 ± 0.06	5.70 ± 0.33	1.61 ± 0.04	15 ± 5	195 ± 10	2.67 ± 0.13	276.3 ± 33.7
86	Mar del Plata Carnet	4-11 mm P	1.45 ± 0.07	6.59 ± 0.33	1.64 ± 0.04	15 ± 5	200 ± 10	2.88 ± 0.14	154.7 ± 5.6
88	Mar del Plata	4-11 mm P	1.23 ± 0.06	6.55 ± 0.33	1.65 ± 0.04	15 ± 5	204 ± 10	2.81 ± 0.14	45.7 ± 2.7
Fluvial samples representing arid climate									
6	Tte. Pico/Est. San Juan	90-200 mm Q							
7	Filadelfia/ Madrejon	90-200 mm Q							
10	Campo Aroma	90-200 mm Q							
13	Neuland	90-200 mm Q							
14	Neuland	90-200 mm Q							
15	Pozo Col./ Grl.Diaz	90-200 mm Q							
16	Las Lomitas	150-200 KF	0.71 ± 0.04	3.55 ± 0.18	0.97 ± 0.05	15 ± 5	105	1.80 ± 0.10	21.8 ± 3.7
17	Las Lomitas	150-200 KF	0.82 ± 0.04	4.62 ± 0.23	1.24 ± 0.06	10 ± 5	130	2.00 ± 0.10	24.1 ± 0.8
18	Clorinda W	4-11 mm P	1.60 ± 0.08	17.71 ± 0.89	5.04 ± 0.25	15 ± 5	135	5.10 ± 0.40	14.4 ± 0.7
19	Clorinda W	4-11 mm P	1.37 ± 0.07	8.43 ± 0.42	2.22 ± 0.11	15 ± 5	140	2.80 ± 0.20	8.2 ± 0.4
21	7km N Napenay	4-11 mm P	2.07 ± 0.10	12.35 ± 0.62	3.14 ± 0.16	15 ± 5	150	4.30 ± 0.30	16.2 ± 2.4
Samples representing humid climate									
8	La Patria	90-200 mm Q							
9	Tte. Montania	4-11 mm P							
11	Transchaco/ Lag. Negra	4-11 mm P							
12	Transchaco/ Fila.	90-200 mm Q							
20	7km N Napenay	4-11 mm P	2.08 ± 0.10	10.07 ± 0.50	2.61 ± 0.13	15 ± 5	150	3.90 ± 0.30	87.1 ± 3.8
22	Grl. Roque Saenz Peña	4-11 mm P	2.38 ± 0.12	11.38 ± 0.57	2.49 ± 0.12	20 ± 5	120	3.90 ± 0.30	117.0 ± 27.5
23	Bella Vista Corrientes	4-11 mm P	1.04 ± 0.05	8.27 ± 0401	0.07 ± 0.02	15 ± 5	198 ± 10	2.09 ± 0.12	241.1 ± 4.1
24	Bella Vista Corrientes	4-11 mm P	1.39 ± 0.07	5.49 ± 0.27	1.18 ± 0.03	15 ± 5	161 ± 8	2.30 ± 0.12	122.4 ± 6.4
25	Bella Vista Corrientes	4-11 mm P	1.51 ± 0.06	2.31 ± 0.12	1.67 ± 0.06	15 ± 5	188 ± 9	2.45 ± 0.12	90.0 ± 3.2
27	Autodromo Emilia	4-11 mm P	1.71 ± 0.08	5.29 ± 0.26	1.49 ± 0.07	15 ± 5	172 ± 9	2.68 ± 0.14	258.3 ± 5.8
30	Autodromo Emilia	4-11 mm P	1.73 ± 0.08	8.17 ± 0.40	1.21 ± 0.06	15 ± 5	170 ± 9	2.75 ± 0.16	128.0 ± 4.7
31	Autodromo Emilia	4-11 mm P	1.44 ± 0.09	9.47 ± 0.57	2.14 ± 0.11	15 ± 5	182 ± 9	4.17 ± 0.33	133.9 ± 4.7
32	Felicia	4-11 mm P	2.02 ± 0.12	9.03 ± 0.54	2.20 ± 0.11	15 ± 5	190 ± 10	3.83 ± 0.30	132.7 ± 3.5
33	Felicia	4-11 mm P	3.82 ± 0.23	12.40 ± 0.74	2.93 ± 0.15	15 ± 5	195 ± 10	5.51 ± 0.52	86.9 ± 2.2
44	Arroyo	4-11 mm P	2.56 ± 0.12	4.02 ± 0.20	2.07 ± 0.10	15 ± 5	194 ± 10	3.38 ± 0.19	
45	Diamante/ Camino al Balneario Valle María	4-11 mm P				15 ± 5	192 ± 10		saturation

No.	location	grain size mineral	K %	Th ppm	U ppm	water %	d_{cosm} mGy/a	d_{tot} mGy/a	D_{equ} Gy
47	Diamante/ Camino al Balneario Valle María	4-11 mm P	3.18 ± 0.16	6.16 ± 0.30	1.15 ± 0.102	15 ± 5	192 ± 10	3.04 ± 0.18	104.3 ± 2.4
48	Larocca	4-11 mm P	1.28 ± 0.06	9.80 ± 0.49	1.91 ± 0.05	20 ± 5	135	2.70 ± 0.20	33.4 ± 2.9
50	Arrecifes	4-11 mm P	1.72 ± 0.09	7.79 ± 0.40	1.79 ± 0.06	15 ± 5	190 ± 10	3.23 ± 0.17	669.4 ± 8.5
51	Arrecifes	4-11 mm P	1.24 ± 0.06	4.20 ± 0.21	12706 ± 0.06	15 ± 5	174 ± 9	2.57 ± 0.13	408.0 ± 23.1
55	La Plata	4-11 mm P	1.22 ± 0.06	5.22 ± 0.25	1.73 ± 0.05	15 ± 5	163 ± 8	2.69 ± 0.13	1036 ± 16
66	Canal Jauretche	4-11 mm P	1.75 ± 0.09	7.51 ± 0.38	1.84 ± 0.09	20 ± 5	145	2.90 ± 0.20	23.0 ± 1.6
76	Grl. Acha E	4-11 mm P	1.26 ± 0.06	6.74 ± 0.34	1.73 ± 0.09	20 ± 5	100	2.30 ± 0.20	1400 ± 375
77	Grl. Acha E	4-11 mm P	1.33 ± 0.06	7.67 ± 0.38	1.40 ± 0.07	20 ± 5	125	2.40 ± 0.20	800 ± 130
81	Mar del Plata Santa Clara d.M.	4-11 mm P	1.30 ± 0.06	6.51 ± 0.33	1.61 ± 0.04	15 ± 5	168 ± 8	2.76 ± 0.14	148.4 ± 12.3
83	Mar del Plata Santa Clara d.M.	4-11 mm P	1.11 ± 0.06	4.45 ± 0.22	1.68 ± 0.04	15 ± 5	196 ± 10	2.55 ± 0.12	265.5 ± 8.0
84	Mar del Plata Camet	4-11 mm P	0.99 ± 0.05	4.56 ± 0.23	1.60 ± 0.04	15 ± 5	204 ± 10	2.46 ± 0.12	296.7 ± 7.5
87	Mar del Plata	4-11 mm P				15 ± 5	194 ± 10		saturation

Abbreviations: mineral P, F and Q: P = polymineral; F = feldspar; KF = potassium feldspar; Q = quartz; K – potassium concentration; U – uranium concentration: Th – thorium concentration; water – proposed water concentration of the samples; d_{cosm} – cosmic dose rate; d_{tot} – total dose rate (estimated values are given in italics); D_{equ} – equivalent dose

hills, parabolic dunes and windward hollows of associated dunes. In the southern and central part of the investigated area, aeolian sediments dominate originating from the south-western Andes and the Andes foreland (Fig.1). In the north alluvial loessoid sediments dominate in the extensive fans of the main rivers Río Pilcomayo, Río Bermejo, Río Salado and are often intersected by channel sands.

5.1 Southern region (Pampa)

In the south western part of the study area an extensive duricrust platform covers aeolian, fluvial and lacustrine deposits of Late Miocene age (Formación Cerro Azul). This duricrust is incised in east-westerly directions by elongated closed valleys of different extension and depth. Some of them are more than 100 km long, 10 km wide and 80 m deep. The bottom of the troughs is dipping to the east following the general morphological inclination of the surface. Several troughs contain Late Pleistocene (Tapia, 1935) and Holocene deposits.

According to our understanding they might have been formed by karstification and wind erosion (Lorenz, 2002). A Digital Elevation Model using SRTM data and visualizing the morphology of the valleys and their neighbouring areas is the basis for the reconstruction of these processes (Fig. 2).
These loessoid sediments originally extended further to the west and covered a wide area of the actual drainage system of the Río Salado Desaguadero. Accordingly, the karstification and erosion processes possibly already began in the early Pleistocene and has continued to the presence. The duricrust was partly decomposed under temporary humid conditions. Strings of small elongated depressions forming temporary lakes after rainfall were developed. Sediment was washed from the edges into the karst depressions. The lakes dried out during successive dry climatic conditions and accumulated material of the depressions. The exposed loose fine-grained loessoid sediments of the borders were blown out. The material was deposited further to the east as part of the loess cover. These repeated processes facilitated the longitudinal growth and the interconnection of the small blow-out depressions which consequently formed the "Valles Grandes". The direction of these troughs matches the direction of the deflation pattern at the eastern slope and the piedmont of the Andean chains.

In the west where sediments were already eroded, the Río Salado Desaguadero system developed in the late Pleistocene. This river lost its sandy sediment load in a resulting wide flat depression of the western Pampa between the Andean foothills and the duricrust platform. The sand was deflated from the bed of Río Salado Desaguadero system and formed a radial fan of mainly parabolic, linear and star dunes on top of the loessoids, duricrust and loess (Fig. 3).

This Pampean Sand Sea (Iriondo, 1990b) covers an area of more than 200 000 km^2. Estimates yielded a very variable thickness of the sand layers up to a maximum of 20 m. The transport was directed to the east turning over northeast to north or even northwest (Fig. 3). The Late Pleistocene-Holocene sediment ages increase with rising distance from the source areas. That means that the strength of the westerly winds was larger in the Pleistocene than in the Holocene.

Satellite images show lineations in the loess north of the Pampean Sand Sea which are elongated flat depressions called „bajos". The depressions are visible due to higher soil humidity and related denser vegetation cover or open water bodies after rainfall. They are important for rain water infiltration and recharge of fresh groundwater in the shallow aquifer which otherwise contains highly saline groundwater (Kruck, 1976). The depression pattern, morphology and ar-

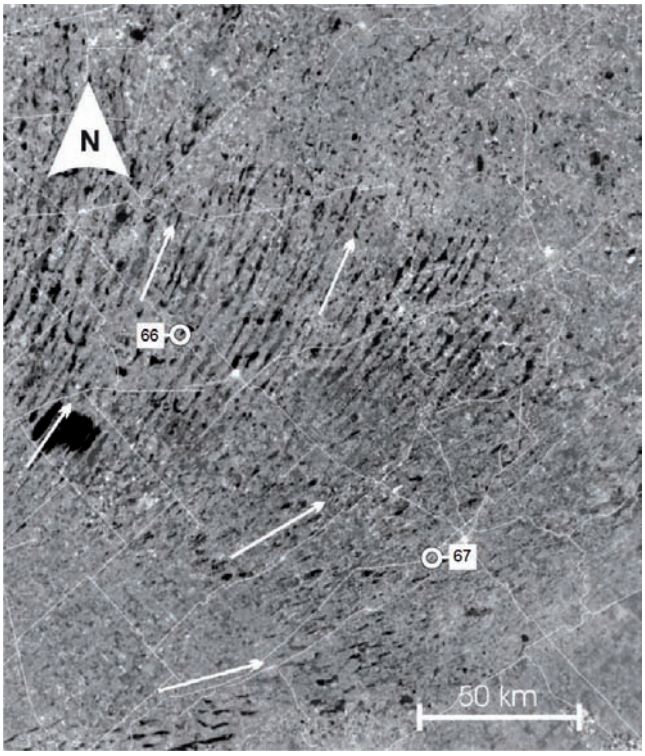

Fig. 3: South western dune field (Pampean Sand Sea; sampling sites Nos. 66 and 67 for orientation), transport direction from southwest; areas with open water due to high groundwater level are dark (Landsat 7 ETM+, true color composite, printed in black & white).

Abb. 3: Südwestliches Dünenfeld (Pampean Sand Sea – Beprobungsorte Nr. 66 und 67 zur Orientierung): Das Sediment kam von SW; Schwarz repräsentiert oberflächlich anstehende Grundwasser (Landsat 7 ETM+, Echtfarbenbild in schwarz/weiß).

rangement are similar to that of the dune field in the south indicating an aeolian origin. Most likely the „bajos" are interdune depressions of a "pre-Pampean Sand Sea" dune field. The dunes might have been covered by loess and later the morphology was flattened by erosion. The parallel structures of the "bajos" can be traced over many hundred kilometres in northern direction where they turn to approximately east-west (Fig. 1). As we did not find any sandy intercalations in the loess outcrops, the old dune system might consist of loess-like fine-grained material or is situated in large depth. Only Iriondo (1999) describes sand layers in two river valleys and related them to an old megadune system of MIS 4.

Our results support the previous sedimentological and geochemical conception by Teruggi (1957) that the loess generally originated from areas in the southwest or south of the Pampa. We more precisely localized the source in the high Andes (most probably for the finer material), the Andes foothills and the plain southwest of the loess area. All wind features in the southwest of the source area are relatively uniform oriented from west to east. Inbar & Risso (2000) describe yardang features by field observation of similar direction about 1000 years old in the Payun Matru volcanic field which we identified on satellite images.
Sedimentological indications of transport by water over longer distances are seldom in the southern part of the Chaco-Pampa Plain. Predominantly clayey lenticular intercalations are of fluvio-lacustrine origin due to their grain size composition and fossil content. Other sediments without gradation of the grain size were transported over short distances and became loessoids. Satellite images show that these sediments are located at slopes of elongated depressions without outlet or in floodplains of rivers. They provided evidence for the following diagenetic processes: During dry climate periods rainwater from rare storm events reworked sediments from the slopes of flat depressions. During humid periods this area became inundated and the water sapped new river beds in between. The Rio Salado south of Buenos Aires is such an example where several flat depressions became interconnected.

5.2 Northern region (Chaco)

In the northern Chaco-Pampa Plain (northern part of Argentina and western part of Paraguay) extensive alluvial fans of several hundred kilometres with a typical micro-flow pattern are visible on satellite images. The surface is slightly sloping towards the Rio Paraguay-Paraná which represents the base level of the rivers. Extended dark areas of the river fans represent flood loam (Fig. 4). Until recent times, the flood-loam areas hosted dense wood and bush which has been meanwhile widely cleared in order to expand the pasture area for extensive livestock farming.

Sandy river beds are visible as light broad strings on the satellite images as these sandy deposits have high reflection property (Fig. 4). Until recent times the sandy river beds were covered with grass and remote trees. Later on, they were used for agriculture. The pioneer vegetation has been only maintained in environmentally protected areas. In the northwest a dune field extends over more than 10 000 km^2 in the border region to Bolivia.

The flood loam was deposited by the Chaco rivers (Ríos Pilcomayo, Bermejo, Salado and other small rivers) originating in the Andes mountains. These rivers transported fine grained material and remobilized aeolian sediments from the upper courses. These processes are still going on. After excessive rainfall events in the 1980's, rivers in the Chaco inundated wide areas from the lower to the middle parts of the fans and flood loam was deposited. This material is unsorted due to short distance transport by water and re-deposition processes (flooding) in the flat area. The fine grained sediments sometimes block and displace the river courses. The Río Paraguay-Paraná base level system caused widely extended inundations due to backwater during periods with heavy rainfall as observed during the 1990s. Its tributaries retained more than 200 km upstream in the Chaco and formed temporary lakes and ponds. OSL ages of the corresponding sediments (Table 2) cluster around the humid Late Glacial-early Holocene period coinciding with the humid Tauca Phase in the High Andes.

In the Late Glacial-Early Holocene period torrential floods of rivers started to engrave the above mentioned channels into the flood loam after short and heavy rainfall events particularly during the long-lasting dry period between 6.4 and about 3.5 ka. The succeeding alternating humid and arid phases are well correlated with the up and down of the climate-controlled human settlement fluctuations in the High Andes (Grosjean et al. 2007).

The sand of the northern dune field near the Paraguayan-Bolivian border was dated to Mid-Holocene. It

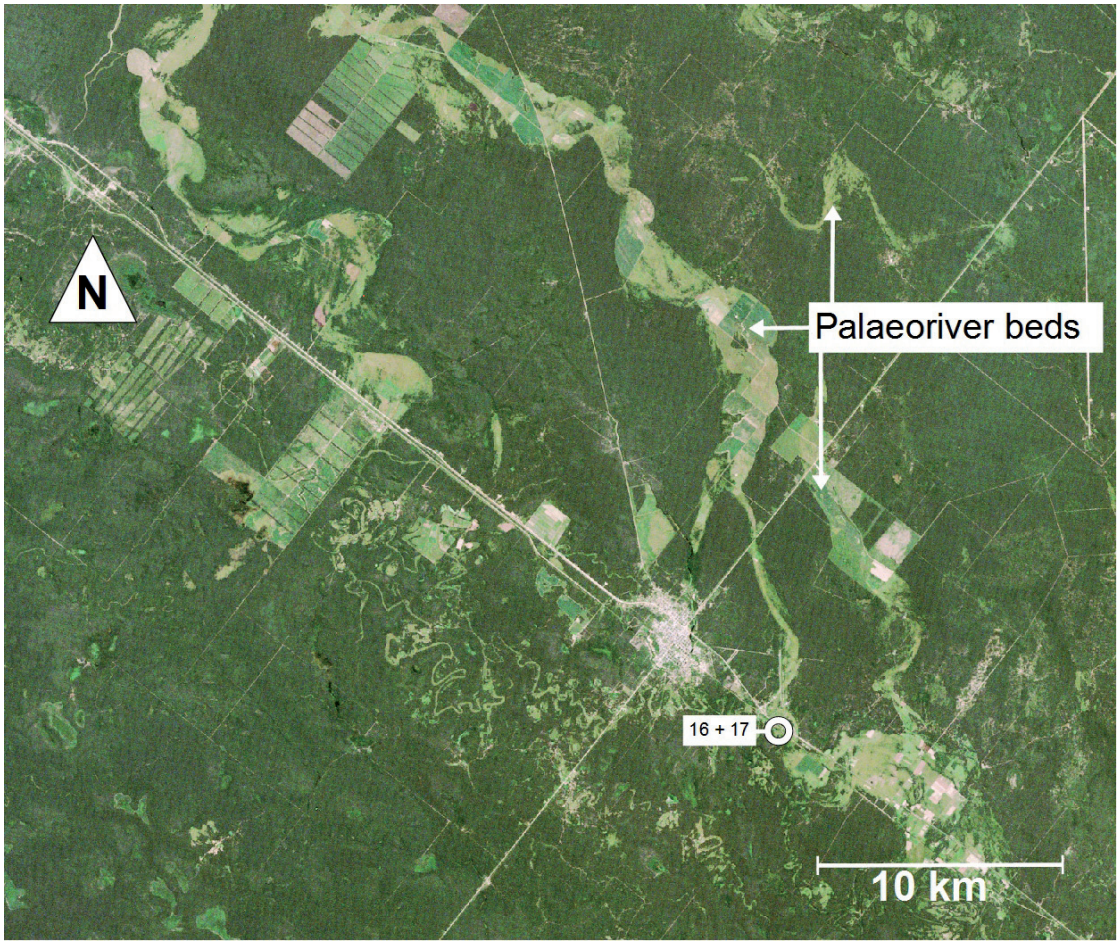

Fig. 4: Palaeoriver pattern of the Río Pilcomayo (sampling sites Nos. 16 and 17 for orientation): Sandy deposits incise flood loam recognizable by intense agricultural use (Landsat 5 TM, true colour composite, 321 RGB).

Abb. 4: Paläoflusssystem des Río Pilcomayo (Probenpunkte Nr. 16 und 17 zur Orientierung): Sandige Ablagerungen eingebettet in Hochflutlehm erkennbar an intensiver landwirtschaftlicher Nutzung (Landsat 5 TM, Echtfarbenbild, 321 RGB).

originates from the Río Parapití which transported sediments to the glacis of the eastern Andes (Servant et al. 1981). The river continuously dislocated to the north and the sandy deposits were blown out to the south by predominant northerly winds. This process was already recognized by Werding (1977) and is visible on satellite imagery (Barboza et al., 2000).

5.3 Modern and palaeowind directions

Aeolian activity is still going on in the Chaco-Pampa Plain. Heavy dust and sand storms and dune movements occurred in periods of pronounced drought in the 18th and 19th centuries and in the thirties and forties of the 20th century. Satellite images from Río Salado (Desaguadero) show recent dust and sand plumes, which provide evidence that the source locations of the dune sands did not change since long and dune formation was relatively continuous (Szelagowski et al., 2004).

The direction of the parabolic dunes of the Pampean Sand Sea in the south west and that of the "Valles Grandes" confirms that strong winds did not change their direction at least since the Pleistocene.

The detected transport and wind direction over the Chaco-Pampa region match with today's occasionally occurring sand and dust storms ("Pampero") in the southern part. They are named "Zonda" in the central and "Nordsturm" (a Mennonite expression in the Chaco) in the northern part, respectively. On June 21, 1993 a dust plume starting from the dry Parapití River bed extended several hundreds of kilometres to the south (NOAA-AVHHR satellite image, from 21st June 1993). A photo taken from a Space Shuttle and published by NASA shows a heavy dust storm over the Altiplano at 26.5°S, 66.5°W (1983-09-05; NASA photo ID:STS008-46-937). The dust is blown to the SE into the Chaco region.

Geochronology and palaeoclimate

We distinguished "arid", "humid" and "cataclysmic flood" samples based on the morphological situation at the sampling site, the facies of the deposits, the kind of fossils, the grain size analysis and the evaluation of satellite images. "Humid" samples are lacustrine, fluvial and loamy materials, fossil bearing deposits and groundwater (Pasig, 2005). Loessoids from the slopes of closed elongated depressions and dune sands represent "arid" periods. Cataclysmic floods during dry periods formed sandy channel deposits. Datable samples which refer to humid conditions were seldom. The reason is that they were deposited in shallow and narrow morphological depressions. Hence, fluvio-lacustrine deposits are generally thin lenticular layers and locally restricted. "Dry material" consists mainly of loessic sediments which

E&G / Vol. 60 / No. 1 / 2011 / 188–202 / DOI 10.3285/eg.60.1.13

Tab. 3: Climatic fluctuations in the Pampa-Chaco Plain during the last 60 ka.

Tab. 3: Klimatische Fluktationen im Pampa-Chaco-Gebiet während der letzten 60 ka.

Period (ka BP)	*Climatic change and corresponding datable material*
60–41	*Arid and humid phases (sub-periods cannot be substantiated)* Loess, fluvio-lacustrine deposits with bones of macrofauna low density of dates
41–28	*Predominant humid phase* Fluvio-lacustrine deposits with bones of macrofauna, flood loam, groundwater recharge
28–16	*Arid with very weak humid spells* Dunes, loess and flood loam moderate density of dates
16–8.5	*Humid with an arid interruption* Fluvio-lacustrine deposits, flood loam, channel sand and loess, dune sands moderate density of dates
8.5–3.5	*Arid period with several humid spells* Dune sand, channel sand and few soils high density of dates
3.5–0	*Dominant humid phase with arid spells* Soils and dune sand as well as channel sands high density of dates

usually contain short-distance transported material or is bioturbated. As a consequence the zeroing of the luminescence signal is not guaranteed. All these interferences complicate the non-ambiguous classification of such samples as "arid" material. Based on numerical ages (OSL and ^{14}C) between 60 ka and 0 ka (MIS 3 to MIS 1) determined within the frame of this study (Table 2) the geomorphological and sedimentological results were recapitulated for the reconstruction of the palaeogeographic and palaeoclimatic evolution of the Chaco-Pampa Plain. Due to the limited number of low precision dates older than 60 ka we omitted their palaeoclimatical interpretation though the corresponding grain size analysis yielded valuable information for the lithologic classification of the corresponding samples in Fig. 1.

The synopsis of the palaeoclimatic interpretation of published and the new dates (Table 3) are compiled in Table 2. The boundaries of the periods may be prone to corrections. Luminescence dates determined with the former conventional methods might be exaggerated due to incomplete bleaching.

6 Conclusions

Our interdisciplinary study in the Chaco-Pampa Plain was mainly based on the interpretation of satellite images and many new luminescence dates. It considerably improved the knowledge on the geomorphological, geological and climatic history since 60 ka.

The source areas of the loessoid and sandy sediments in the Andes piedmont were more precisely located by means of the wind erosion pattern. The „Valles Grandes" in the southwest were identified as supplementary source area of loess and loessoid material using the Digital Elevation Model. We deduced the genesis of these valleys from their shape and spatial arrangement. Their formation began with the local decomposition of the duricrust covering the whole area and the exposure of the underlying Upper Miocene loessoid sediments. The latter were mobilized by wind erosion and aeolian transport to the east and northeast. The topographic erosion pattern allowed to reconstruct the wind directions and transport routes of the sediments. Both seem not to have changed since the Pleistocene. In the western erosion areas, westerly winds dominated; further to the east also wind was active to the northeast, north and northwest. The morphology of the loess area is interpreted as covered old dune field consisting of fine sands or loess-like fine sediments. Luminescence dates were obtained from aeolian sandy and loessic sediments representing arid climate. Channel sands were another dated material deposited by cataclystic floods during dominant dry periods. Dunes in the southwest and northwest and channel sands are markers for an intensification of aridity between 8.5–3.5 ka accompanied by occasional sporadic torrential rainfalls in the mid Holocene.

Acknowledgements

Many colleagues supported the investigations. We thank V. Baumann, D. Budziak, R. Hoffmann and P. Tchilinguirian for sampling, soil identification and data processing in the frame work of the Segemar/BGR project. We appreciate the steady interest of the director O. Lapido who always supported our activities.

We gratefully acknowledge the constructive discussions and assistance in the selection of sampling sites and field work by J.C. Bertolini, A. Carlini, A. Cione, M.A. Gonzalez, J.I. Noriega, J. San Cristobal, E. Tonni and the assistance in luminescence dating by M. Frechen (Leibniz Institute of Geophysics, Hannover), F. Preusser (University of Cologne) and R. Kuhn (Max-Planck Institute of Nuclear Physics, Heidelberg). We are grateful to both reviewers G.L. Argüello and M. Frechen for valuable improvements.

References

Abello, A,, Montalvo, C,I,, & Goin, F.J. (2002): Marsupiales del Mioceno Superior de Caleufú (La Pampa, Argentina). – Ameghiniana, 39 (4): 433–422.

Ameghino, F. (1908): Las formaciones sedimentarias de la región litoral de Mar del Plata y Chapadmalán. – Anales del Museo Nacional de Historia Natural, X: 343–428.

Argüello, G,L,, Dohrmann, R., Sanabria, J.A. & Zahn, E. (2010): Genetic implications of a retransported loess profile near Córdoba, Argentina. – Journal of South American Earth Sciences, 29: 642–649; doi:10.1016/j.jsames.2009.12.003.

Barboza, F., Geyh, M., Hoffmann, R., Kruck, W., Medina Netto, A., Merkt, J. & Rojas, C. (2000): Soil Formation and Quaternary Geology of the Paraguayan Chaco - thematic Mapping. Geoscientific Cooperation with Latin America. – Zeitschrift für Angewandte Geologie, Sonderheft, 1: 49–54.

Bidegain, J.C. (1991): Sedimentary development, magnetostratigraphy and sequence of events of the Late Cenozoic in Entre Ríos and surrounding areas in Argentina. – Ph.-Thesis: 345 pp; Stockholm.

Fidalgo, F., de Francesco, F., Pascual, R. (1975): Geología superficial de la Llanura Bonaerense. – Relatorio del VI Congreso Geológico Argentino: 103–138; Bahia Blanca.

Frechen, M., Schweizer, U. & Zander, A.M. (1996): Improvements in sample preparation for the fine grain technique. – Ancient TL, 14: 15–17.

Frechen, M., Vanneste, K., Verbeeck, K., Paulissen, E. & Camelbeeck, T. (2001): The deposition history of the cover sands along the Bree Fault Escarpment, NE Belgium. – Netherlands Journal of Geosciences (Geologie en Mijnbouw), 80 (3-4): 171–185.

Frechen, M., Seifert, B., Sanabria, J. A. & Argüello, G.L. (2009): Chronology of late Pleistocene Pampa loess from the Córdoba area in Argentina. – Journal of Quaternary Science, 24: 761–772.

Frenguelli, J. (1957): Neozoico. – Sociedad Argentina de estudios geográficos GAEA, Tomo II (3): 1–218; Buenos Aires.

Fuller, I.C., Wintle, A.G. & Duller, G.A.T. (1994): Test of partial bleach methodology as applied to the infrared stimulated luminescence of alluvial sediment from the Danube. – Quaternary Geochronology, 13: 539–543.

Geyh, M.A., Grosjean, M., Kruck, W. & Schotterer,U. (1996): Síncronopsis del Desarrollo Morfológico y Climático del Chaco Boreal y de Atacama en los Últimos 35.000 años AP. – Memorias del XII Congreso Geológico de Bolivia, Tomo, III: 1267–1276; Tarija.

Godfrey-Smith, D.I., Huntley, D.J. & Chen, W.-H. (1988): Optical dating studies of quartz and feldspar sediment extracts. – Quaternary Science Reviews, 7: 373–380.

Grosjean, M., Calogero, M.S., Tompson, L.G., Nuñez, L. & Standen, V. G. (2007): Mid-Holocene climate and culture change in the South Central Andes. – In: Anderson, D.G., Masch, K.A & Sandweiss D.H. (eds.): Climate Change and Cultural Dynamics: A Global Perspective on Mid-Holocene Transitions: 51–153; Elsevier (Amsterdam)..

Inbar, M. & Risso, C. (2000): Holocene yardangs in volcanic terrains in the southern Andes, Argentina. – Earth Surface Processes and Landforms, 26 (6): 657–666.

Iriondo, M. (1990a): A late Holocene dry period in the Argentine plains. – Quaternary of South America and Antarctic Peninsula, 7: 197–218.

Iriondo, M. (1990b): Map of the South American plains-its present state. – Quaternary of South America and Antarctic Peninsula, 6: 297–308.

Iriondo, M. (1997): Letter to the Editor: Comment on A. Prieto's "Late Quaternary Vegetational and Climatic Changes in the Pampa Grassland of Argentina". – Quaternary Research, 48: 251–252.

Iriondo, M. (1999): Climatic changes in the South American plains: Records of a continent-scale oscillation. – Quaternary International, 57/58: 93–112.

Iriondo, M., Ceruti, C. &Tardivo, R. (1985): Geomorfología y Cuaternario del tramo inferior del Arroyo Feliciano. – Revista de la Asocación de Ciencias Naturales de Litoral, 16: 149–156.

Kemp, R.A., Zárate, M., Toms, P., King, M., Sanabria, J. & Arguello, G. (2006): Late Quaternary paleosols, stratigraphy and landscape evolution in the Northern Pampa, Argentina. – Quaternary Research, 66: 119–132.

Kittl, E. (1933): Sobre los fenómenos volcánicos y material caído durante la erupción del grupo del "Descabezado" en el mes de abril de 1932. – Anales del Museo de Ciencias Naturales, B. Anales, tomo XXXVII: 264–321; Buenos Aires.

Kröhling, D.M. (1999): Upper Quaternary geology of the lower Carcarañá Basin, North Pampa, Argentina. – Quaternary International, 57/58: 135–148.

Kröhling, D.M. & Iriondo, M. (1999): Upper Quaternary palaeoclimates of the Mar Chiquita area, North Pampa, Argentina. – Quaternary International, 57/58: 149–163.

Kruck, W. (1976): Hydrogeological investigations in the Argentine Pampa using satellite imagery. – Geologisches Jahrbuch, A 33: 145–159.

Kuhn, R. (2000): Vergleichende Untersuchungen der Optisch (Grün) Stimulierten Lumineszenz und der Thermolumineszenz von Quarz zum Zwecke der Altersbestimmung. – Ph.D.-Thesis, Heidelberg.

Lorenz, W. (2002): The Calcrete Principal (tosca) at the border of the province of La Pampa and Buenos Aires. – Zeitschrift für Angewandte Geologie, 1: 44–51.

Melchor, R., Visconti, G., Montalvo,C.I. (2000): Late Miocene calcic vertisols from Central La Pampa, Argentina. – Resúmenes del 2° Congreso Latinoamericano de Sedimentología y 8° Reunión Argentina de Sedimentología: 119–120; Mar del Plata, Argentina.

Nabel, P. (1993): The Brunhes-Matuyama Boundary in Pleistocene Sediments of Buenos Aires Province, Argentina. – Quaternary International, 17: 220–227.

Orgeira, M.J. (1987): Estudio paleomagnético de sedimentos del Cenozoico tardio de la costa atlántica bonaerense. – Revista de la Asociación Geológica Argentina, XLII: 362–376.

Pasig, R. (2005): Origen y Dinámica del Agua Subterranea en el noreste del Chaco Sudamericano. – Zeitschrift des Lehr- und Forschungsbereiches Hydrogeologie und Umwelt der Universität Würzburg, 34: 1–103.

Pascual, R., Ortega Hinojosa, E.J.,Gondar, D & Tonni, E. (1965): Las edades del Cenozoico mamalífero de la Argentina, con especial atención a aquellas del territorio bonaerense. – Anales de la Comisión de Investigaciones Científicas de la Provincia de Buenos Aires, 6: 165–193, La Plata.

Preusser, F. (1999): Lumineszenzdatierung fluviatiler Sedimente – Fallbeispiele aus der Schweiz und Norddeutschland. – Kölner Forum für Geologie und Paläontologie, 3: 1–62.

Preusser, F., Degering, D., Fuchs, M., Hilgers, A., Kadereit, A., Klasen, N., Krbetschek, M., Richter, D. & Spencer, J.Q.G. (2008): Luminescence dating: basics, methods and applications. – Eiszeitalter und Gegenwart Quaternary Science Journal, 57 (1–2): 95–149.

Prieto, A.R. (1996): Late Quaternary vegetational and climatic changes in the Pampa Grassland of Argentina. – Quaternary Research, 45 (1): 73–88.

Prieto, A.R. (1997): Reply to the letter to the editor on "Late Quaternary vegetational and climatic changes in the Pampa Grassland of Argentina" by M. Iriondo. – Quaternary Research, 48 (1): 253–256.

Sayago, J.M. (1995): The Argentinian neotropical loess: an overview. – Quaternary Science Reviews, 14: 755–766.

Servant, M., Fontes, J.-C., Rieu, M. & Saliège, X. (1981) : Phases climatiques arides holocènes dans le sud-ouest de l´Amazonie (Bolivie). – Compte Rendus de l'Académie des Sciences de Paris, Série II, 292: 1295–1297.

Szelagowski, M., Zárate, M. & Blasi, A.M. (2004): Aspectos sedimentologicos de arenas eolicas del Pleistoceno Tardio- Holoceno de la Provincia La Pampa. Latin America. – Journal of Sedimentology and Basin Analysis, 11 (2): 57–68.

Tapia, A. (1935): Causas geológicas y consecuencias políticas de los cambios del cauce del Pilcomayo en Formosa. – Anales de la Sociedad Argentina de Estudios Geográficos, IV (2): 235 pp; Buenos Aires, Argentina.

Teruggi, M.E. (1957) : The nature and origin of Argentine loess. – Journal of Sedimentary Petrology, 27 (3): 322–332.

Tonni, E.P., Cione, A.L. & Figini, A.J. (1999): Predominance of arid climates indicated in the pampas of Argentina during the Late Pleistocene and Holocene. – Palaeogeography, Palaeoclimatology, Palaeoecology, 147: 257–281.

Tonni, E. P., Carlini, A. A., Zurita, A., Frechen, M., Gasparini, G., Budziak, D. & Kruck, W. (2005): Cronología y bioestratigrafía de las unidades del Pleistoceno aflorantes en el Arroyo Toropí, provincia de Corrientes, Argentina. – Congreso Brasileiro de Paleontologia, 19. Congreso Latino-Americano de Paleontología de Vertebrados, 6: Edición electrónico de resúmenes; Rio de Janeiro, Brasil.

Tripaldi, A. & Forman, S.L. (2007): Geomorphology and chronology of Late Quaternary dune fields of western Argentina. – Palaeogeography Palaeoclimatology Palaeoecology, 251(2): 300–320.

Valencio, D.A. & Orgeira, M.J. (1983): La magnetostratigrafía del Ensenadense y Bonaerense de la ciudad de Buenos Aires. Parte II. – Revista de la Asociación Geológica Argentina, XXXVIII: 24–33.

Werding, L. (1977): Geomorphologie und rezente Sedimentation im Chaco boreal, Bolivien. – Gießener Geologische Schriften, 12: 429–446.

Wintle, A.G. (2008): Luminescence dating: where it has been and where it is going? – Boreas, 37: 471–482.

Zárate, M. (2003): The loess record of southern South America. – Quaternary Science Reviews, 22: 1987–2006.

Zárate, M. & Blasi, A. (1990): Consideraciones sobre el origen, procedencia y transporte del loess del sudoeste de la Provincia de Buenos Aires. – International Symposium on Loess, extended abstract: 15–20; Mar del Plata.

Zech, W., Zech, M., Zech,R., Peinemann, N., Morrás, H.J.M., Moretti, L., Ogle, N., Kalim, R.M., Fuchs, M., Schad, P., & Glaser, B. (2008): Late Quaternary palaeosol records from subtropical (38°S) to tropical (16°S) South America and palaeoclimatic implications. – Quaternary International, 196: 107–120.

AKTUELLE VERÖFFENTLICHUNGEN

Eiszeitlandschaften in Mecklenburg-Vorpommern

Exkursionsführer zur DEUQUA-Tagung 2010

Hrsg.: Reinhard Lampe, Sebastian Lorenz

DIN A4 / 164 Seiten / Softcover / 34,– € / 2010
ISBN: 978-3-941971-05-9

Zur Landschafts- und Gewässergeschichte der Müritz

Umweltgeschichtlich orientierte Bohrungen 2004–2006 zur Rekonstruktion der nacheiszeitlichen Entwicklung

Hrsg.: Nationalparkamt Müritz

DIN A4 / 94 Seiten + 1 Faltblatt / Softcover / 29,– € / 2010
ISBN: 978-3-941971-00-4

IN VORBEREITUNG

Die spätpleistozäne und holozäne Gewässernetzentwicklung im Bereich der Pommerschen Haupteisrandlage Mecklenburgs

Autor: Sebastian Lorenz

DIN A4 / Softcover / Vorbestellungen möglich
ISBN: 978-3-941971-03-5

BESTELLUNG

GEOZON

Geozon Science Media
Postfach 3245
D-17462 Greifswald
Germany

Tel. 03834-80 40 80
Fax 03834-80 40 81
E-Mail: info (at) geozon.net
www.geozon.net

Instruction to Authors

Basically the manuscript shall be submitted in electronic form and has to include the name and the address of the first author. Please use a standard word processor in .rtf, .odt or .doc-format (LaTeX files on request). As character set please use the standard fonts Times Roman, Helvetica or Courier with 1.5 line spacing.

For the submission please use our online system at *www.quaternary-science.net*. After the login you can upload your manuscript as well as separate figures and tables.

Manuscript style

The acceptable languages are English and German. Manuscripts in German have to contain an English subtitle, an abstract in English and English keywords. The rules of the new German spelling reform apply to German texts.

Manuscripts should be arranged in the following order:

I Short but concise title
II Full names, full address and e-mail
III 5 to 10 keywords that describe the contents of your paper
VI An abstract of up to 200 words in German and English. The translated abstract should carry the translated titel in square brackets,
V Clearly structured text. For chapter numbering use Arabic numerals.
VI The reference list has to be arranged alphabetically and should be conform to the examples given below.

References have to be insert in the text as brief quotations, the name of the author has to be set in small Capitals, the year of publication in brackets e.g. Müller (2006). If more than one publication of the same author in the same year is cited, identify each citation as follows: Müller (2006a, 2006b). Where three or more authors are listed in the reference list, please cite in the text as Müller et al. (2006). Papers with up to three authors should be cited as Müller & Meyer (2006) or Müller, Meyer & Schulz (2006). If a special page or figure of a paper should be cited, use following citation style: Müller (2006: 14) or Müller (2006, Fig. 14).

Scientific names of flora and fauna (*gender, sub-gender, species, sub-species*) have to be written in *italics*. Use small Capitals for the author (*Armeria maritima* Willd.)

Do not justify your text, use a ragged left alignment.
Do not use automatic hyphenation.
Do not use any automatic formatting.
Do not use pagination.

Do not insert images, tables and photos into the text, it should be added as separate files. Captions of figures and tables in German and English should be placed at the end of the manuscript.

Illustrations

Supply each figure as a separate file with the name of the author. Illustrations should be reducible to a column width (8.4 cm) or type area (17.2 x 26 cm). The lettering has to be easy readable after reduction. Where a key of symbols is required, include this in the figure, not in the caption of the figure. Avoid fine lines (hairlines) and grey-shading/halftones. All figures may be colored. There are no additional costs.

For printing all illustrations have to be supplied electronically. Please use for pixel-based images (photos) the .tif-format with a resolution of at least 450 dpi and for vector-based illustrations (graphs, maps, tables) the .eps-format. Greatly reduced .jpg-files or .pdf-files or figures included in word-documents are not accepted.

References (examples)

Papers:
Schwarzbach, M. (1968): Neue Eiszeithypothesen. – Eiszeitalter und Gegenwart, 19: 250–261.
Eissmann, L. & Müller, A. (1979): Leitlinien der Quartärentwicklung im norddeutschen Tiefland. – Zeitschrift für Geologische Wissenschaften, 7: 451–462.
Zagwijn, W.H. (1996): The Cromerian Complex Stage of the Netherlands and correlation with other areas in Europe. – In: Turner, C. (ed.): The Middle Pleistocene in Europe: 145–172; Rotterdam (Balkema).
Magny, M. & Haas, J.N. (2004): A major widespread climatic change around 5300 cal. yr BP at the time of the Alpine Iceman. – Journal of Quaternary Science, 19: 423–430. DOI: 10.1002/jqs.850

Books:
Ehlers, J. (1994): Allgemeine und historische Quartärgeologie. – 358 S.; Stuttgart (Enke).

Please do not use abbreviations of the journal names.

Specimen copies

Authors receive 2 printed specimen copies. The electronic version is available as download free.

For further questions about the submission of manuscripts please contact the production editor.

Autorenhinweise

Das Manuskript ist grundsätzlich in elektronischer Form einzureichen und muss mit Namen und Adresse des Erstautoren versehen sein. Bitte benutzen Sie eine Standard-Textverarbeitung im .rtf, .odt oder .doc-Format (LaTeX-Dateien auf Anfrage). Als Zeichensatz verwenden Sie bitte die Standard-Fonts Times Roman, Helvetica oder Courier mit einem 1,5-fachen Zeilenabstand.

Zur Einreichung nutzen Sie bitte unser Online Submission System unter *www.quaternary-science.net.* Nach dem Login steht Ihnen hier eine Upload-Funktion für das Manuskript und die Abbildungs-Dateien zur Verfügung.

Manuskriptform

Als Publikationssprachen sind Englisch und Deutsch zugelassen. Manuskripte in deutscher Sprache müssen einen englischen Untertitel tragen sowie eine englische Kurzfassung und englische Keywords beinhalten. Für die deutschen Texte gelten die Regeln der neuen Rechtschreibreform.

Die Manuskripte sollen folgendem Aufbau entsprechen:

I Kurze, aber prägnante Überschrift
II Ausgeschriebener Vor- und Nachname, Post- und E-Mail-Adresse
III 5 bis 10 englische Keywords, die den Inhalt des Manuskriptes widerspiegeln.
IV Deutsche und englische Kurzfassung des Textes mit einer Länge von bis zu 200 Wörtern. Der englische Untertitel des Manuskriptes ist der englischen Kurzfassung in eckigen Klammern voranzustellen.
V Klar gegliederter Text. Kapitelnummerierungen sind mit arabischen Ziffern zu versehen.
VI Alphabetisch geordnete Literaturliste. Die Zitierweise muss der unten angegebenen Form entsprechen.

Im fortlaufenden Text sind Literaturhinweise als Kurzzitate einzufügen, der oder die Autorennamen sind in Kapitälchen-Schrift zu setzen, das Erscheinungsjahr in Klammern, z. B. Müller (2006). Werden von einem Autor mehrere Arbeiten aus einem Jahr zitiert, so sind diese durch Buchstaben zu unterscheiden: Müller (2006a, 2006b). Bei mehr als drei Autoren kann et al. verwendet werden: Müller et al. (2006). Arbeiten mit bis zu drei Autoren werden folgendermaßen zitiert: Müller & Meyer (2006) oder Müller, Meyer & Schulz (2006). Sind mit der Zitierung bestimmte Seiten oder Abbildungen gemeint, müssen diese genau angegeben werden: Müller (2006: 14) oder Müller (2006: Fig. 14).

Die wissenschaftlichen Namen von Pflanzen und Tieren (*Gattungen*, *Untergattungen*, *Arten*, *Unterarten*) sind kursiv zu schreiben. Die den biologischen Namen folgenden Autoren werden in Kapitälchen gesetzt (*Armeria maritima* Willd.).

Bitte keinen Blocksatz verwenden, sondern linksbündigen Satz.
Bitte keine automatische Silbentrennung verwenden.
Bitte alle automatischen Formatierungen in Ihrer Textbearbeitung deaktivieren.
Bitte keine Seitenzählung.

Abbildungen, Tabellen und Fotos nicht in den Text einbauen, sondern separat als Datei beifügen. Abbildungsunterschriften in Deutsch und Englisch am Ende des Manuskripttextes platzieren.

Abbildungen

Bitte fügen Sie jede Abbildung als separate Datei mit einem eindeutigen Namen bei. Alle Grafiken müssen eine Verkleinerung auf Spaltenbreite (= 8,4 cm) oder Satzspiegel (= 17,2 x 26 cm) zulassen. Die Beschriftung muss nach der Verkleinerung noch gut lesbar sein. Sollte eine Legende nötig sein, so binden Sie diese in die Abbildung ein. Bitte vermeiden Sie Haarlinien oder Grauwerte. Alle Abbildungen können farbig sein. Es entstehen keine Mehrkosten.

Für die Drucklegung müssen alle Abbildungen in elektronischer Form eingereicht werden. Bitte verwenden Sie für pixelbasierte Abbildungen (Fotos) das .tif-Format mit einer Auflösung von mindestens 450 dpi und für vektorbasierte Abbildungen (Diagramme, Maps, Tabellen) das .eps-Format. Stark reduzierte .jpg oder .pdf-Dateien sowie in Text-Dokumente eingebundene Abbildungen werden nicht akzeptiert.

Zitierweise (Beispiele)

Aufsätze:

Schwarzbach, M. (1968): Neue Eiszeithypothesen. – Eiszeitalter und Gegenwart, 19: 250–261.

Eissmann, L. & Müller, A. (1979): Leitlinien der Quartärentwicklung im norddeutschen Tiefland. – Zeitschrift für Geologische Wissenschaften, 7: 451–462.

Zagwijn, W.H. (1996): The Cromerian Complex Stage of the Netherlands and correlation with other areas in Europe. – In: Turner, C. (ed.): The Middle Pleistocene in Europe: 145–172; Rotterdam (Balkema).

Magny, M. & Haas, J.N. (2004): A major widespread climatic change around 5300 cal. yr BP at the time of the Alpine Iceman. – Journal of Quaternary Science, 19: 423–430. DOI: 10.1002/jqs.850

Monographische Werke, Bücher:

Ehlers, J. (1994): Allgemeine und historische Quartärgeologie. – 358 S.; Stuttgart (Enke).

Bitte keine Abkürzungen der Zeitschriftentitel verwenden.

Belegexemplare

Autoren erhalten 2 gedruckte Belegexemplare. Die elektronische Version steht zum kostenlosen Download zur Verfügung.

Bei weiteren Fragen zur Manuskripteinreichung wenden Sie sich bitte an die technische Redaktion (s. Impressum).

DEUQUA

German Quaternary Association

The German Quaternary Association (DEUQUA) eV is an association of German-speaking Quaternary Scientists. The aim of the association is to promote the Quaternary Science, to represent it in public, to intensify the contact to applied science as well as to advice public and political boards in quaternary issues.

Furthermore, the association has set itself the task of operating the contacts between the Quaternary Scientists and related organizations at home and abroad.

The DEUQUA published annually several editions of "E&G – Quaternary Science Journal". In that journal research results from the field of Quaternary Science are published. In addition, developments in the DEUQUA are announced in the "Geoscience messages" (GMIT). GMIT is published quarterly.

Every two years, the German Quaternary Association held the DEUQUA-Conference. At this conference the latest research results of the Quaternary Science are presented and discussed.

Deutsche Quartärvereinigung

Die Deutsche Quartärvereinigung (DEUQUA) e.V. ist ein Zusammenschluss deutschsprachiger Quartärwissenschaftler und wurde 1949 gegründet. Der Verein hat zum Ziel die Quartärwissenschaft zu fördern, sie in der Öffentlichkeit zu vertreten, den Kontakt zu angewandter Wissenschaft zu intensivieren sowie öffentliche und politische Gremien in quartärwissenschaftlichen Fragestellungen zu beraten. Desweiteren hat der Verein sich zur Aufgabe gemacht, die Kontaktpflege der Quartärforscher untereinander und zu verwandten Organisationen im In- und Ausland zu betreiben.

Die DEUQUA veröffentlicht jährlich mehrere Ausgaben von „E&G – Quaternary Science Journal". Dort werden Forschungserkenntnisse aus dem Bereich der Quartärwissenschaft publiziert. Zusätzlich werden Entwicklungen in der DEUQUA vierteljährlich in den Geowissenschaftlichen Mitteilungen (GMIT) bekannt gemacht.

Im zweijährigen Turnus veranstaltet die Deutsche Quartärvereinigung e.V. die DEUQUA-Tagung. Diese bietet ein Forum, in welchem aktuelle Forschungsergebnisse aus dem Bereich der Quartärwissenschaften vorgestellt und diskutiert werden.

Committee / Vorstand

PRESIDENT / PRÄSIDENTIN
PROF. DR. MARGOT BÖSE
Freie Universität Berlin
Malteserstr. 74–100
D-12249 Berlin, Germany
Tel.: +49 (0)30-838-70 37 3
E-Mail: m.boese (at) fu-berlin.de

VICE PRESIDENTS / VIZEPRÄSIDENTEN
UNIV.-PROF. MAG. DR. CHRISTOPH SPÖTL
Institut für Geologie und Paläontologie
Universität Innsbruck
Innrain 52
A-6020 Innsbruck, Österreich
Tel.: +43 (0)512-507-5593
Fax: +43 (0)512-507-2914
E-Mail: christoph.spoetl (at) uibk.ac.at

PROF. DR. LUDWIG ZÖLLER
Fakultät II – Lehrstuhl für Geomorphologie
Universität Bayreuth
Universitätsstrasse 30
D-95440 Bayreuth, Germany
Tel.: +49 (0)921-55 2266
Fax: +49 (0)921-55 2314
E-Mail: ludwig.zoeller (at) uni-bayreuth.de

TREASURER / SCHATZMEISTER
DR. JÖRG ELBRACHT
Landesamt für Bergbau, Energie und Geologie
Stilleweg 2
D-30655 Hannover, Germany
Tel.:+49 (0)511-643-36 13
E-Mail: joerg.elbracht (at) lbeg.niedersachsen.de

EDITOR-IN-CHIEF / SCHRIFTLEITUNG (E&G)
PD DR. HOLGER FREUND
ICBM – Geoecology
Carl-von-Ossietzky Universitaet Oldenburg
Schleusenstr 1
D-26382 Wilhelmshaven, Germany
Tel.: +49 (0)4421-94 42 00
E-Mail: holger.freund (at) uni-oldenburg.de

ARCHIVIST / ARCHIVAR
DR. STEFAN WANSA
Landesamt für Geologie und Bergwesen
Sachsen-Anhalt
Postfach 156
D- 06035 Halle, Germany
Tel. +49 (0)345-5212-12 7
E-Mail: wansa (at) lagb.mw.sachsen-anhalt.de

ADVISORY BOARD / BEIRAT
DR. CHRISTIAN HOSELMANN
Hessisches Landesamt für Umwelt und Geologie
Postfach 3209
D-65022 Wiesbaden, Germany
Tel.: +49 (0)611-69 39 92 8
E-Mail: christian.hoselmann (at) hlug.hessen.de

DR. DANIELA SAUER
Institut für Bodenkunde und Standortslehre
Universität Hohenheim
Emil-Wolff-Str. 27
D-70593 Stuttgart, Germany
Tel.: +49 (0)711-459-22 93 5
E-Mail: d-sauer (at) uni-hohenheim.de

DR. FRANK PREUSSER
Geologisches Institut
Universität Bern
Baltzerstr. 1–3
CH-3012 Bern, Switzerland
Tel.: +41-31-631 87 70
E-Mail: preusser (at) geo.unibe.ch

PROF. DR. REINHARD LAMPE
Institut für Geographie und Geologie
Ernst-Moritz-Arndt-Universität Greifwald
Friedrich-Ludwig-Jahn-Strasse 16
D-17487 Greifswald, Germany
Tel: +49 (0)3834-86-45 21
E-Mail: lampe (at) uni-greifswald.de

PROF. DR. BIRGIT TERHORST
Geographisches Institut
Universität Würzburg
Am Hubland
D-97074 Würzburg, Germany
Deutschland
Tel. +49 (0)931-88 85 58 5
E-Mail: birgit.terhorst (at) uni-wuerzburg.de

Reorder / Nachbestellung

The volumes 6–7, 11–17, 19–28 and 30–58 are currently available. All other volumes are sold out. A reduced special price of 10,– € per edition is up to and including volume 55. The regular retail price applies from vol. 56/1–2. A complete table of contents is downloadable at *www.deuqua.org*.

1951–2006

Vol. 6–7, 11–17, 19–28, 30–55	each volume 10,– €

2007	Topics	Price
Vol. 56 No 1–2	Special issue: Startigraphie von Deutschland – Quartär	54,– €
Vol. 56 No 3	Pfälzerwald, pollen types and taxa, Oberösterreich, Riß-Iller, Schatthausen	27,– €
Vol. 56 No 4	Nußloch, Rangsdorfer See, Lieth/Elmshorn, Gardno Endmoräne/Debina Cliff	27,– €

2008	Topics	Price
Vol. 57 No 1–2	Special issue: Recent progress in Quaternary dating methods	54,– €
Vol. 57 No 3–4	Special issue: The Heidelberg Basin Drilling Project	54,– €

2009	Topics	Price
Vol. 58 No 1	Surface Exposure Dating, Bodensee, Living Fossil, Hochgebirgsböden	27,– €
Vol. 58 No 2	Special issue: Changing environments – Yesterday, Today, Tomorrow	27,– €

2010	Topics	Price
Vol. 59 No 1–2	Baltic Sea Coast, Rodderberg Crater, Geiseltal, Wettersteingebirge, Møn, Argentina	54,– €

2011	Topics	Price
Vol. 60 No 1	Special issue: Loess in Europe	27,– €

The prices are understood plus shipping costs. VAT is included.

Subscription / Abonnement

Title: E&G – Quaternary Science Journal
Print-ISSN: 0424-7116
Issues per volume: 4

Prices (EUR) print per volume

End customers: 100,92 € (Free for DEUQUA-Members)
Wholesalers, booksellers: 65,60 €
Scientific libraries: 95,87 €

VAT is not included.

Postage (EUR) per volume

within Germany: 5,00 €
Europe (Surface): 12,40 €
Europe (Airmail): 15,20 €
World (Surface): 20,80 €
World (Airmail): 25,60 €

Special offer

Libraries which subscribe our journal can receive the volumes 1951–2006 for free. Only shipping costs have to be paid.

Order address

Geozon Science Media
po box 3245
D-17462 Greifswald
Germany

tel.: +49 (0)3834-80 40 80
fax: +49 (0)3834-80 40 81

e-mail: info (at) geozon.net
web: www.geozon.net

E&G Quaternary Science Journal
Volume 60 / Number 1 / 2011 / ISSN 0424-7116 / DOI 10.3285/eg.60.1
www.quaternary-science.net

Contents

GEOZON SCIENCE MEDIA
www.geozon.net